ACTA PHYSICA

ACADEMIAE SCIENTIARUM HUNGARICAE

TOMUS XLVIII FASCICULUS 1

AKADÉMIAI KIADÓ, BUDAPEST

1980

ACTA PHYS. HUNG. APAHAQ 48 (1) 3—118 (1980)

ACTA PHYSICA

ACADEMIAE SCIENTIARUM HUNGARICAE

SZERKESZTI

KOVÁCS ISTVÁN

Az *Acta Physica* angol, német, francia vagy orosz nyelven közöl értekezéseket. Évente két kötetben, kötetenként 4—4 füzetben jelenik meg. Kéziratok a szerkesztőség címére (1521 Budapest XI., Budafoki út 8.) küldendők.

Megrendelhető a belföld számára az Akadémiai Kiadónál (1363 Budapest Pf. 24. Bankszámla 215-11488), a külföld számára pedig a „Kultura" Külkereskedelmi Vállalatnál (1389 Budapest 62, P.O.B. 149. Bankszámla 217-10990), vagy annak külföldi képviseleteinél.

The *Acta Physica* publish papers on physics in English, German, French or Russian in issues making up two volumes per year. Distributor: "Kultura" Foreign Trading Company (1389 Budapest 62, P.O. Box 149) or its representatives abroad.

Die *Acta Physica* veröffentlichen Abhandlungen aus dem Bereich der Physik in deutscher, englischer, französischer oder russischer Sprache, in Heften, die jährlich zwei Bände bilden.

Bestellbar bei »Kultura« Außenhandelsunternehmen (1389 Budapest 62, Postfach 149) oder seinen Auslandsvertretungen.

Les *Acta Physica* publient des travaux du domaine de la physique en français, anglais, allemand ou russe, en fascicules qui forment deux volumes par an.

On peut s'abonner à l'Entreprise du Commerce Extérieur «Kultura» (1389 Budapest 62, P.O.B. 149) ou chez représentants à l'étranger.

«*Acta Physica*» публикуют трактаты из области физических наук на русском, немецком, английском и французском языках.

«*Acta Physica*» выходят отдельными выпусками, составляющими два тома в год.

Заказы принимает предприятие по внешней торговле «Kultura» (1389 Budapest 62, P.O.B. 149) или его заграничные представительства.

ACTA PHYSICA

ACADEMIAE SCIENTIARUM HUNGARICAE

TOMUS XLVIII

AKADÉMIAI KIADÓ, BUDAPEST
1980

INDEX

Tomus 48

FLUIDS, PLASMAS AND ELECTRIC DISCHARGES

PHYSICS OF CONDENSED MATTER

INTERDISCIPLINARY

ASTROPHYSICS

CLASSICAL AND APPLIED PHYSICS

ACTA PHYSICA

ACADEMIAE SCIENTIARUM HUNGARICAE

REDIGIT
I. KOVÁCS

TOMUS XLVIII FASCICULUS 1

AKADÉMIAI KIADÓ, BUDAPEST
1980

ACTA PHYS. HUNG.

INDEX

Acta Physica Academiae Scientiarum Hungaricae, Tomus 48 (1), pp. 3—17 (1980)

MATHEMATICAL MODELLING OF DIFFUSE LIGHT SCATTERING

By

GY. MAJOR

SPECTROSCOPIC LABORATORY, MINISTRY OF THE INTERIOR, BUDAPEST, HUNGARY

(Received in revised form 12. VI. 1979)

A simplified model is proposed and mathematically simulated on a computer by the Monte-Carlo method to study the phenomenon of diffuse light scattering. The data of simulation yield the density functions of the pathlength distribution of light and several graphical relations for the reflection and transmission of light against the layer thickness and the absorptivity of the sample, respectively. The character of these graphical relations is in good agreement with experimental data.

1. Introduction

In the past few decades there has been growing interest in the spectrophotometric investigation of diffuse light scattering systems. The intricacy of the phenomenon is shown by the great number of different theories attempting its formulation, none of which, however, has so far given a satisfactory answer to all problems which have emerged.

Of the proposed theories the one most widely used is the KUBELKA—MUNK—GUREVITSCH theory [1, 2], assuming two constants, absorption k and scattering s, which characterize the respective processes taking place in the layer. The function

$$\frac{k}{s} = \frac{(1 - R_\infty)^2}{2R_\infty} \tag{1}$$

according to KORTÜM [3, 4, 5], however, also shows the relation between the absorption coefficient of the material and reflectance (R_∞) as k corresponds to the absorption coefficient and s is independent of wavelength.

Since experimental data failed to give satisfactory agreement between the absorption coefficient and the so-called k/s function of the KUBELKA—MUNK—GUREVITSCH theory, SCHREYER [6, 7, 8] introduced, in addition to the scattering constant, a scattering coefficient, assuming both to be independent of wavelength.

Starting from a simple model BODÓ and others [9, 10, 11] assumed that the sample consists of thin plane-parallel layers. Thus, by using the surface

reflection and absorption coefficients the path covered by the light multiply reflected by and passing through the layers can be described by two arithmetical progressions. According to the theory the sum of these two progressions gives the quantity of light passing through and reflected by the sample.

GILES and others [12] assumed that the rays of the beam passing through and reflected by the sample emerge from the sample after covering different pathlengths. The absorption of the individual rays deviated to identical pathlengths can, however, be calculated by the Bouguer—Lambert—Beer law (in the following referred to as BLB law)

$$I_{r_i a_i} = a_i \cdot I_0 \cdot 10^{-\varepsilon c l_i}, \tag{2}$$

where I_0 is the intensity of incident light, a_i is the portion of light deviated to pathlength l_i, l_i is the pathlength, ε the molar extinction coefficient, and c the concentration.

The total flux of reflected light is

$$I_r = \sum_{i=1}^{n} a_i I_0 10^{-\varepsilon c l_i}. \tag{3}$$

GILES et al assumed that equal light portions a_i are deviated to the different pathlengths. The equation so obtained, however, did not perfectly agree with the experimental data, so a correction factor had to be introduced. SID'KO and TERSKOV [13] assumed a as an exponential function; consequently, the relation obtained for concentration dependence shows linear dependence for an extended concentration range.

These theories fail to account for the complexity of the phenomenon.

For measurement-technical reasons, the spectra of diffuse scattering samples may only be recorded with reference to some standard. Various standards are used, such as magnesium oxide, potassium bromide, barium sulphate, opaque glass, etc.

To record the spectrum of a coloured substance deposited on the surface of a carrier, it is often the unstained carrier that is used as reference standard. Some experiments, however, show that the comparative measurement does not fully compensate for the spectral characteristics of the carrier.

For studying the above problems a mathematical model has been developed [16], which seems to be suitable to formulate the relations describing the phenomenon of diffuse light scattering.

2. Starting points for modelling

The fundamental equation of absorption spectrophotometry is given by the BLB law as

$$I = I_0 e^{-\varepsilon c l}, \tag{4}$$

where I_0 and I are the intensities of incident and transmitted light, respectively, ε is the molar extinction coefficient, c is the concentration and l is the layer thickness.

The basic requirement regarding the performance of the measurement is that the beam should pass perpendicularly through a homogeneous, non-scattering medium confined between plane-parallel layers. In the law of absorption this is expressed by the layer thickness, since the probability for each photon to enter into interaction with the absorbing medium is the same while passing through it in a straight line along a pathlength corresponding to the thickness of the layer. This does not mean, of course, that every photon covers the same pathlength, because absorption may occur anywhere inside the layer, but the logarithm of loss is proportional to the pathlength.

This relation cannot be applied to characterize the spectrophotometric properties of diffuse scattering media, as they differ from solutions (non-scattering media) in many respects.

The essential property of a diffuse light-scattering medium giving rise to the phenomenon of scattering is that it contains substances of different refractive indices in one or more phases in the form of droplets or particles and so it has inside surfaces.[1]

The rays of light do not travel in parallel inside the sample, but they are multiply deviated. The different portions of the beam are multiply reflected and refracted by the inside surfaces. In the course of this process he photons are deviated to different directions to cover various pathlengths. This is the phenomenon generally termed scattering in reflection spectrophotometry. Scattering in itself does not actually mean a loss of light, i.e. absorption. A real loss of light is due to the absorption process according to BLB law, in proportion to the absorptivity, concentration and the pathlength covered by the beam in the absorbing medium.

It can be assumed that for a small portion of the beam deviated to the same pathlength and so passing through the same quantity of absorbing medium, the BLB law may be written as

$$dI = dI_0 \, e^{-\alpha\gamma u}, \tag{5}$$

where dI_0 is a small portion of the beam passing through a quantity of material $\gamma \cdot u$ (g/cm^2) (γ = specific gravity, u = pathlength), attenuated according to absorptivity (α) and emerging from the medium as a quantity dI. It is to be noted that the total quantity dI_0 of the light beam does not cover the pathlength u but it is this quantity, according to assumption, that is deviated to pathlength u.

[1] We do not discuss the extreme case, where the sample is homogeneous, continuous and it is only the coarse, unpolished surface that causes light scattering.

To determine the total portion of reflected light all rays of the beam emerging from the sample after covering different pathlengths must be added. But this requires the knowledge of the portions of light having covered the different pathlengths. In other words we have to know the density function of the pathlength distribution of light. Since the portions of beam may cover very different pathlengths when passing through the particles, the density function may be considered as a continuous one. Supposing that the density function is

$$dI_0 = I_0 f_R(u) du \tag{6}$$

and substituting it into Eq. (5)

$$dI = I_0 f_R(u)\, e^{-\alpha\gamma u}\, du\,, \tag{7}$$

so the total quantity of reflected light is obtained by integration

$$I = I_0 \int_0^\infty f_R(u)\, e^{-\alpha\gamma u}\, du\,. \tag{8}$$

If the layer is thin, a small portion of the beam may emerge on the other side. This portion of light — similarly to reflected light — emerges from the sample after a multiple repetition of the three elementary processes: refraction, reflection and absorption. This means, of course, that the individual rays of the beam traverse different pathlengths inside the absorbing medium. So to describe the light passing through a diffuse scattering medium we have to apply similar methods as for reflection. We have to find the density function of pathlength distribution also for the transmitted light.

More precisely, the incident light is divided into 3 parts in the sample:

$$I_0 = I_R + I_T + I_L\,, \tag{9}$$

where I_0, I_R and I_T mean the intensity of incident, reflected and transmitted light, respectively, and I_L is the intensity of light transversely deviated to a long path inside the sample, meanwhile not crossing any of the boundary surfaces.

According to present-day knowledge the density function of pathlength distribution cannot be determined either by direct or by indirect measurement. All measurements supply integrated data. Mathematical modelling (simulation) by using a modified Monte-Carlo method makes it possible to investigate the phenomenon, and to get the density functions for the reflection and transmission of light for different layer thicknesses. The Monte-Carlo method is very widely used for the investigation of several scattering processes [18], first of all for the investigation of neutron scattering. In the present case,

however, we use it for the solution of a different problem, i.e. to get the density function of the distribution of the pathlengths covered.

To construct our model the task had obviously to be restricted and simplified. We have assumed that the material is homogeneous, compact, but has phase bounds along which the refractive indices differ. Rays of light travel in straight line between the phase bounds: at the boundary surface, however, they may proceed in any direction, due to the irregular shape of the particles. After the change of direction they proceed straight until reaching the next surface. The model simulates a sample consisting of particles embedded in air but the path traversed in the air can be neglected because of the small absorptivity. Since our aim was primarily to draw general conclusions from the model concerning the spectroscopical behaviour of diffuse scattering systems, we considered these assumptions and simplifications permissible.

As no mathematical derivation could be found, we expected the model to provide information on the mathematical relations between reflection and transmission data on the one hand and absorptivity, scattering properties, layer thickness, concentration, on the other, in graphical form, which may be suitable to interpret the essential features of the phenomenon.

3. Modelling of light scattering by the Monte-Carlo method

Our primary aim in constructing the model was to derive the density function of pathlength distribution of the incident light beam but at the same time we carried out the integration of Eq. (8).

We chose for the investigation the following simplified model.

The rays of light are incident at point O at right angles unto the surface of a layer of thickness L (Fig. 1). The other two dimensions of the layer (along the Y, Z axes) are infinite.

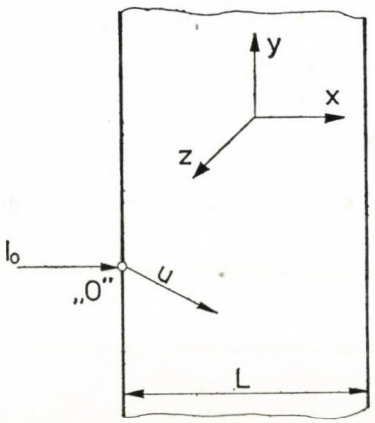

Fig. 1. Diagram of the model

The photons may make steps in any direction inside the layer. The direction and size of the steps (in arbitrary units) were calculated from three random numbers considered as projections of the X, Y, Z axes. Each step means the path of a photon from one surface to the other of a particle. The random numbers were produced by a random number generator of uniform distribution over the range $-1 \div +1$. Accordingly, the length of the largest possible step is

$$u = \sqrt{x^2 + y^2 + z^2} = \sqrt{1^2 + 1^2 + 1^2} = 1.73. \tag{10}$$

The steps are repeated until the ray emerges from the layer. The generation of three random numbers in the program gives the possibility for more detailed investigations on the structure of the layer.

Traversing the plane $X = 0$ in negative direction means reflection, traversing the plane $X = L$ in positive direction means transmission. The photons emerging either from the illuminated or from the opposite surface of the sample were counted separately according to the pathlength covered, rounded off to integers. Rays which have travelled pathlengths over 100 units were considered lost.

To construct our model we had to choose parameters suitable to describe the most important features of the phenomenon. The variation of value L directly simulates the layer thickness, which considerably affects in particular the amount of transmitted light.

The variation of the step length by a multiplicative factor corresponds to the change of particle size. It is much more difficult to find a convenient parameter for modelling the refractive index, which affects the ratio of reflected to transmitted light by the surfaces of the particles as well as the angle of refraction. Its value determines on the one hand the pathlength of light inside the sample and on the other the ratio of pathlengths covered in the different media. In view of the statistical character of the phenomenon we may suppose that inside the sample its effect is similar to that of particle size, and can be modelled by a common parameter.

The effect of refractive index is substantially different on the illuminated surface of the sample. This follows from the fact that the portion of light beam reflected directly from the surface does not pass through absorbing material, thus it is not attenuated. Its quantity depends on the value of refractive indices (sample, air). In the literature this quantity of light is called the external component [14, 3, 4].

In modelling the density function of pathlength distribution the material was regarded as a non-absorbing one. Absorption was taken into account only in the integration on the basis of Eq. (8).

Accordingly, we applied two basic parameters for the computer modelling of pathlength distribution: layer thickness L and particle size F. The effect

of the refractive indices could be taken into account by the subsequent calculation of the quantity of light reflected from the surface whereby computer time was considerably reduced.

In the course of modelling we desired to get an answer also to the question to what degree the result depends on the selected model. Therefore we examined various particle shapes and step lengths along the X, Y, Z axes:

1. Cubic particle: the maximum step length is the same along all three axes.
2. Prismatic particle: the value of component X was multiplied by 2.
3. Prismatic particle: the value of components Y, Z was multiplied by 2.
4. Prismatic particle: the value of components Y, Z was multiplied by 3.

These variations simulate on the one hand the different particle shapes and on the other hand they modify the distribution function of the single steps, i.e. the probability for the light beam to cover a shorter or longer pathlength inside a particle.

In the second part of the program we carried out the integration of Eq. (8) over the different values of the third parameter, absorptivity Z. The number of photons launched was 10 000 for each version. The layer thickness was varied from 1 to 20 units by one unit and the absorptivity from 0.05 to 1.00 by 0.05 steps. The computations were peformed on an ICL 1905 type computer, using an Algol program.

4. Graphical relations obtained from the model

The data obtained from modelling were plotted graphically against different parameters. The graphs make the evaluation of the relations and their comparison with the measured data possible.

Table I and Fig. 2 show the density function of the pathlength distribution of reflected light, i.e. the quantity of photons RI emerging on the side of illumination after covering different pathlengths u. The curves (R_1, R_2, R_∞) represent the different layer thicknesses ($L = 1, 2$) and the so-called infinite layer thickness. The curves have a maximum, which means that the greater part of the rays emerge from the medium after covering relatively short pathlengths. With increasing layer thickness the quantity of rays reflected after traversing longer pathlengths also increases. Over a certain layer thickness, however, the function does not change any more, that is the quantity of reflected light becomes constant. This corresponds to the fact that, by increasing the layer thickness, remission approaches a boundary value (R_∞).

The density function of the pathlength distribution of transmitted light (Fig. 3) also shows a maximum, which is shifted with increasing layer thickness, the curve becomes flatter and takes a prolated shape.

Table I

Density function of the pathlength distribution of reflected light for different layer thicknesses for the cubic particle shape version

Layert hickness	1	2	3	5	10	15
Pathlength						
0	1	1	1	1	1	1
1	366	366	366	366	366	366
2	2268	2268	2268	2268	2268	2268
3	1179	1192	1192	1192	1192	1192
4	653	782	782	782	782	782
5	284	518	518	518	518	518
6	140	424	427	427	427	427
7	71	303	317	317	317	317
8	23	216	246	247	246	246
9	14	201	237	237	237	237
10	4	136	178	179	179	179
11	0	104	167	172	172	172
12	0	82	148	151	151	151
13	1	53	98	108	108	108
14	0	48	103	115	115	115
15	0	32	80	94	94	94
16	0	17	74	93	93	93
17	0	17	63	75	75	75
18	0	28	58	74	74	74
19	0	14	50	70	70	70
20	0	18	44	66	66	66
21	0	8	42	61	61	61
22	0	5	33	63	63	63
23	0	3	30	58	58	58
24	0	1	17	37	38	38
25	0	4	28	50	52	52

Different models yielded relations of identical type, whereas the location and height of maxima were different. Since these functions could not be checked directly by experiments, therefore the results of integration comparable with the experimental data are particularly interesting.

Figure 4 shows the proportion (in percentages) of reflectance and transmittance vs layer thickness. With the increase of the layer thickness reflectance increases up to R_∞, with increasing absorptivity Z it decreases. Transmission decreases with increasing layer thickness and absorptivity.

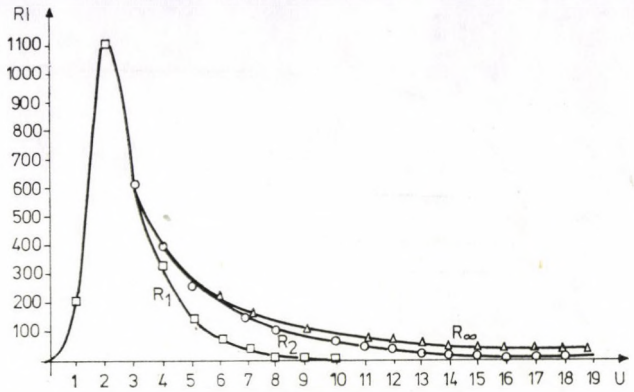

Fig. 2. Density function of the pathlength distribution of reflected light for different layer thicknesses for the cubic particle shape version (u = pathlength, RI = number of reflected photons)

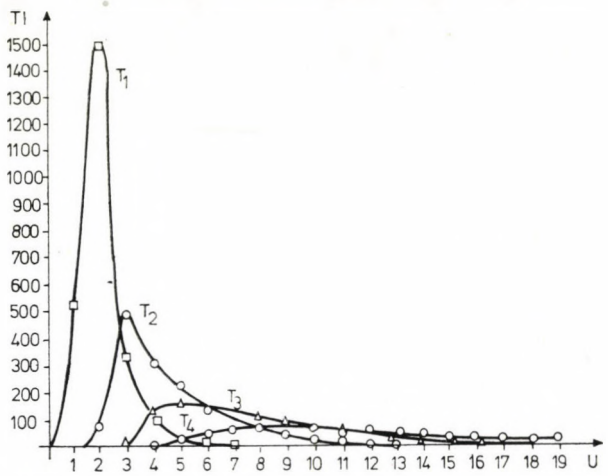

Fig. 3. Density function of the pathlength distribution of transmitted light for different layer thicknesses for the cubic particle shape version (u = pathlength. TI = number of transmitted photons)

The character of the obtained data is in full agreement with experiments (Fig. 5). The Figure shows the dependence of transmittance and reflectance of Wattman No. 1 filter-paper on layer thickness at 3 different wavelengths, corresponding to different absorptivities.

The parameter effect of particle size corresponds to experimental observations. If it decreases, reflection increases and transmission decreases. We want to emphasize that the variation of particle size and absorptivity equally change the so-called infinite layer thickness in agreement with the experimental data.

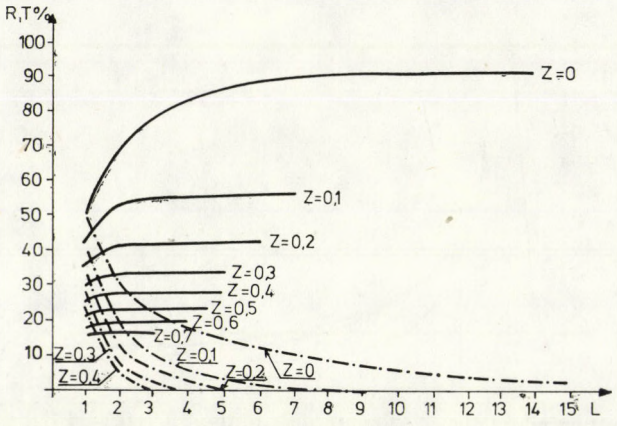

Fig. 4. Intensity of reflected and transmitted light, respectively, vs layer thickness for different values of absorptivity
Continuous line = reflection, dots and dashes = transmission, Z = absorptivity, L = layer-thickness

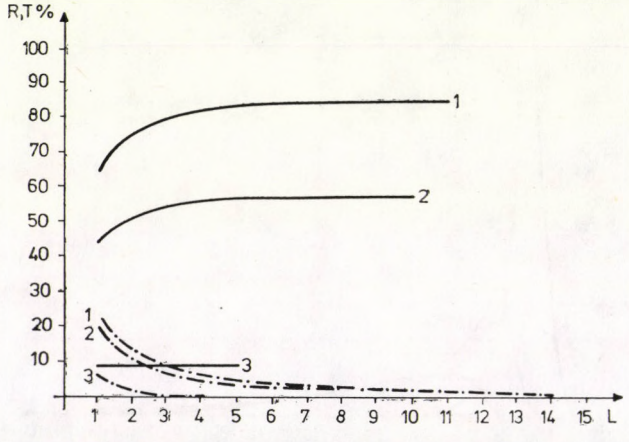

Fig. 5. Dependence of reflection and transmitted light, respectively, on layer thickness for Wattman No. 1 filter-paper at 3 different wavelengths:
1 = 1000 nm: 2 = 667 nm: 3 = 250 nm.
Continuous line = reflection, dots and dashes: transmission: L = layer thickness

The data of modelling were compared with the data obtained by applying the KUBELKA—MUNK—GUREVITSCH theory. On the basis of the relations given by JUDD [15] we have calculated and plotted the dependence of reflection and transmission on layer thickness

$$R = \frac{1}{V + W \coth (W \cdot s \cdot l)} \tag{11}$$

$$T = [(V + R)^2 - W^2]^{1/2}, \tag{12}$$

where

$$V = \frac{s+k}{s} = \frac{1}{2}\left(\frac{1}{R_\infty} + R_\infty\right), \tag{13}$$

$$W = \frac{1}{2}\left(\frac{1}{R_\infty} - R_\infty\right), \tag{14}$$

k and s are the constants of absorption and scattering, respectively, and l is the layer thickness.

The value of s was chosen to be 0.1.

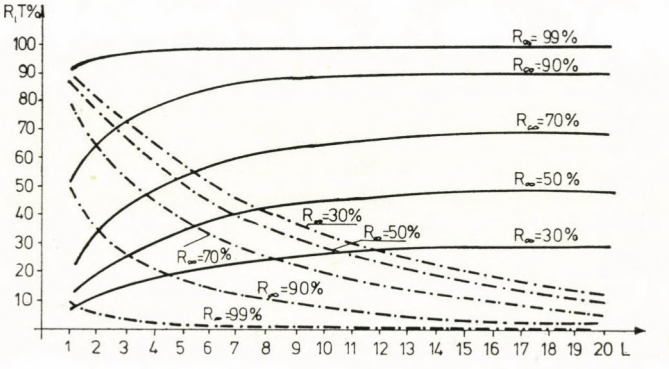

Fig. 6. Reflection (continuous line) and transmission (dots and dashes) calculated on the basis of the KUBELKA—MUNK—GUREVITSCH theory vs layer thickness for samples of different absorptivity. R is the reflectance of the infinite layer.

On the diagrams plotted on the basis of the KUBELKA—MUNK—GUREVITSCH theory (Fig. 6) a small absorption coefficient would correspond to a small infinite layer thickness and small transmittance, which, however, contradicts the experimental observations.

Reverting to the data of modelling, the diagram (Fig. 7) obtained by plotting the reflection of an infinite layer vs absorptivity yields a relation

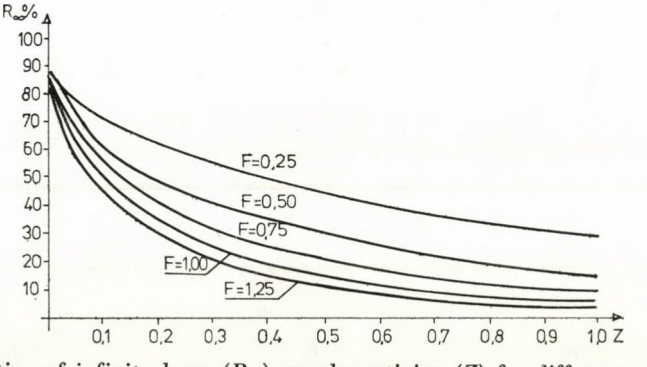

Fig. 7. Reflection of infinite layer (R_∞) vs absorptivity (Z) for different particle sizes (F)

analogous to BLB law for the scattering system. As may be seen in Fig. 7 the decrease of particle size increases reflection that means that a greater portion of light emerges after traversing a shorter pathlength. The essential difference as compared to the non-scattering system is that the function is not logarithmic. A similar relation is obtained by plotting transmittance against absorptivity. In this case the role of particle size is different, with its decrease the quantity of the transmitted light is also reduced.

The light reflected from the surface without absorption can be taken into account by the simple equations:

$$R_N = R + N \cdot R, \tag{15}$$

$$T_N = T \cdot (1 - N). \tag{16}$$

The portion of light reflected directly from the surface increases reflection and decreases transmission. With increasing absorptivity Z the proportion of light reflected directly from the surface increases (Fig. 8). N is the proportion of light reflected from the surface.

Setting up the model we assumed that each ray of the light beam covers a different pathlength in the scattering system. For the light beam as a whole, however, a so-called equivalent average pathlength may be calculated on the basis of the following equations:

$$R = 10^{-Z \cdot \gamma \cdot l_{e,R}}, \tag{17}$$

$$T = 10^{-Z \cdot \gamma \cdot l_{e,T}} \tag{18}$$

l_e is not the average of pathlengths, but a calculated value expressing the layer thickness at which, in a non-scattering medium, the transmittance of the substance of identical absorption coefficient equals R or T.

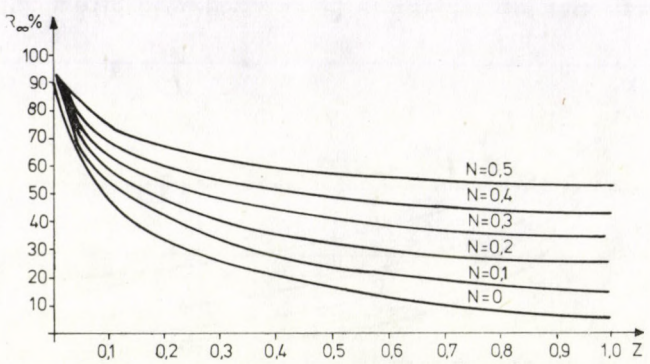

Fig. 8. Reflection of the infinite layer (R_∞) vs absorptivity (Z) for different surface reflections (N)

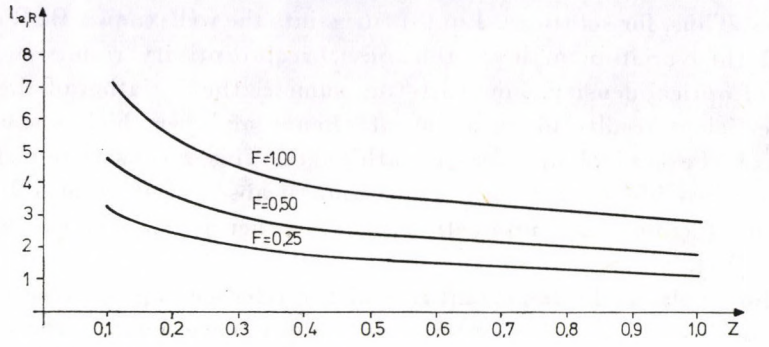

Fig. 9. Equivalent average pathlength (l_e) vs absorptivity (Z) for reflection measurement with different particle sizes (F)

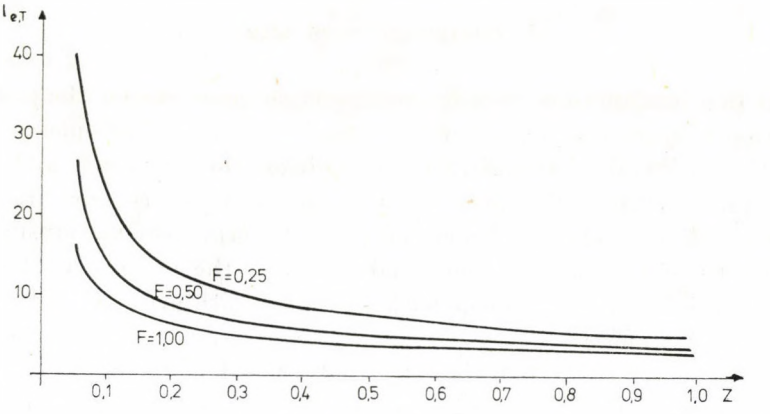

Fig. 10. Equivalent average pathlength (l_e) vs absorptivity (Z) for transmission measurement with different particle sizes (F)

Fig. 9 and Fig. 10, respectively, show the values of l_e calculated from the model for reflection for transmission measurement as a function of absorptivity Z. From the comparison of the data the following conclusions can be drawn: the increase of absorptivity decreases l_e both for reflection and transmission. The effect of various particle sizes, however, is different, with decreasing particle size the equivalent reflection pathlength decreases and that of transmission increases. For both measuring arrangements the efficiency of absorption is a number of times higher than for non-scattering media. According to the Figure the difference is greatest for small layer thicknesses in transmission measurement.

These relations show the essential difference between scattering and nonscattering media in respect of spectrophotometry. Solutions (nonscattering media) are a limit case of the more general scattering system, where the density function of pathlength distribution approaches a given pathlength, i.e. layer

thickness. Thus, for solutions, Eq. (8) turns into the well-known BLB equation (4), and the variation of layer thickness or absorptivity results in a linear change of optical density. For scattering samples the variation of the absorption coefficient results in an apparent change of layer thickness, and in a change of the equivalent average pathlength. This means that if all other parameters are identical, with the variation of absorptivity l_e also varies and so the light enters into interaction with another portion of the absorbing medium [17].

This explains the important role of the reference applied (the unstained carrier) in diffuse scattering systems, as the difference between the real pathlengths covered by light in an absorbing and in a very slightly absorbing medium is very remarkable.

5. Interpretation of data

The density functions may be considered as solutions for the pathlength distribution of three-dimensional wandering in a layer of half-space when the steplength and direction are arbitrary. According to the BODÓ and the KUBELKA—MUNK—GUREVITSCH theories the motion of light is one-dimensional, with fixed (BODÓ) and arbitrary (KUBELKA—MUNK—GUREVITSCH) steplength. GILES selects the pathlength covered and the process of absorption, but the unsatisfactory agreement with experimental data shows the need of further investigations.

According to our present-day knowledge the density functions obtained from our model cannot be written down in closed form equations and are not identical with the density functions used by the Theory of Probability.

This can be explained by the following considerations: for a small number of steps in the pathlength distribution the one steplength distribution function depending on the shape of the particle predominates. Over a certain number of steps it is the distribution function of the step numbers that prevails. For small layer thicknesses the mathematical description of the break in the density function of reflection pathlength distribution is conceivable only in very complicated form.

The density function of reflection, or transmission pathlength distribution may be considered the fundamental characteristic of light scattering. Relations obtained from the simulation yield the dependence of reflection and transmission on different parameters.

Fig. 7 may be regarded as the graphical analogue of the BLB law concerning the dependence of reflection on absorptivity. A similar relation may be derived for transmission. Fig. 5 shows the dependence on layer thickness. The character of the above relations is in good agreement with the experimental data.

Since the reflection and transmission of the scattering medium depend on several parameters (absorptivity, particle size, refractive index, etc.) it is impossible to draw conclusions for the absorption coefficient from one measured value. The graphical relations plotted here, however, describe and explain various properties of diffuse scattering systems. Further investigations may lead to the direct determination of the absorption coefficient.

REFERENCES

1. P. KUBELKA and F. MUNK, Z. Techn. Phys., **12**, 593, 1931.
2. M. GUREVITSCH, Phys. Zs., **31**, 753, 1930.
3. G. KORTÜM, Revue Univ. des Mines, 9e Serie I. XV N° 5, 1959.
4. G. KORTÜM and W. BRAUN, Angew. Chem., **75**, 653, 1963.
5. G. KORTÜM and W. BRAUN, Liebigs Ann. **632**, 104, 1960.
6. G. SCHREYER, Z. Phys. Chem., **12**, 359, 1957.
7. G. SCHREYER, Z. Phys. Chem., **12**, 375, 1957.
8. G. SCHREYER, Z. Phys. Chem., **18**, 123, 1958.
9. Z. BODÓ, Acta Phys. Hung., **1**, 135, 1951.
10. Z. BODÓ, Acta Phys. Hung., **2**, 5, 1952.
11. Ю. И. Чекалинская, Изв. АН. СССР сер. физ. **11**, 1494, 1957.
12. C. H. GILES, S. H. K. RAHMAN and D. SMITH, Textile Research J., **31**, 679, 1961.
13. Ф. Я. Сидько, И. А. Терсков, Изв. Сиб. отд. АН. СССР, 78, 1961.
14. M. B. Савостьянова, Спектроскопия светорассеивающих сред. Сборник, Минск, 179, 1963.
15. D. B. JUDD, J. Res. Nat. Bureau of Stand., **19**, 288, 1937.
16. GY. MAJOR, Dissertation, Leningrad, 1968.
17. J. HUSZÁR, Dissertation, Budapest, 1968.
18. Г. И. Марчук: Метод Монте-Карло в проблеме переноса излуечний. Сборник, Москва, 1967.

Acta Physica Academiae Scientiarum Hungaricae, Tomus 48 (1), pp. 19—30 (1980)

TACHYONS IN THE FRAMEWORK OF THE TWO CENTRES PARTICLES

By

E. BASSILA

FACULTY OF SCIENCES, LEBANESE UNIVERSITY, HADATH, BEIRUT, LEBANON

(Received 30. VIII. 1979)

Using the fluid droplet model of elementary particles, we propose to introduce two spinor fields φ and χ in order to define two centres. We introduce a new concept of invariance in connection with the possibility that the particle may have a velocity larger than the velocity of light without the need to introduce imaginary proper masses, proper time and proper length. To this new concept, we attach new invariance groups that we interpret physically. In a simple case, we propose a dynamical equation for tachyons.

I. Introduction

In the study of elementary particles, new models and new concepts have been introduced. One of them is the fluid droplet model proposed by WEYSSENHOFF [1] and studied in detail by MÖLLER [2], BOHM and VIGIER [3].

A spinor field defines the motion of a particle considered as a point [4]. In order to introduce two centres for the particle, we propose [6] to introduce two spinor fields φ and χ, whose transformation under Tousheck group is:

$$\begin{aligned} \varphi' &= e^{i\alpha\gamma_5}\varphi\,, \\ \chi' &= e^{-i\alpha\gamma_5}\chi\,. \end{aligned} \tag{1}$$

In this way the two spinor fields φ and χ define two space-time points that we consider as the two centres of the particle. Instead of the two four-spinors, φ_4 and χ_4 we introduce the 2-spinors $\varphi + j\chi$ twice—complex in i and j where i and j are two imaginary numbers:

$$\varphi = j\chi = \begin{pmatrix} [\varphi_{11} + i\varphi_{12}] + j\,[\chi_{11} + i\chi_{12}] \\ [\varphi_{21} + i\varphi_{22}] + j\,[\chi_{21} + \chi_{22}] \end{pmatrix}, \tag{2}$$

Note that there are two possibilities to take the conjugate of a 2-spinor:

a) The complex conjugate with respect to i:

$$\varphi^* + j\,\chi^*; \tag{3}$$

b) The complex conjugate with respect to j:

$$\varphi - j\chi \,. \tag{4}$$

Thus, in the 2-spinor formalism, it is possible to introduce two centres with two new invariance groups that we study in Section II. In Section III, we show the possibility of having velocities larger than the velocity of light c, without the need of imaginary proper masses, proper time and proper length we propose a physical interpretation of these invariance groups. Using these concepts, a new model of tachyons is introduced in Section IV. In Section V a dynamical equation for tachyons is proposed.

II. Invariance groups

a) *The four-spinor formalism*

Consider the four-spinor φ_4. An example of the 4-spinor χ_4 associated to φ_4 is:

$$\frac{1}{m_0}\gamma^\mu \frac{\partial}{\partial \chi\mu}\alpha_4 \,. \tag{5}$$

The four-spinor φ_4 defines the first centre through the four-vector:

$$X^\mu = \bar{\varphi}_4 \gamma^\mu \varphi_4 \tag{6}$$

and the second four-spinor χ_4 defines the second centre through the four-vector

$$Y^\mu = \bar{\chi}_4 \gamma^\mu \chi_4 \,. \tag{7}$$

Thus we have the two centres:

$$\begin{aligned} X^\mu &= \bar{\varphi}_4 \gamma^\mu \varphi_4 \,, \\ Y^\mu &= \bar{\chi}_4 \gamma^\mu \chi_4 \,. \end{aligned} \tag{8}$$

The two invariance groups leave invariant the quantities A and B:

$$\begin{aligned} A &= \mathbf{X}^2 - (X^0)^2 \,, \\ B &= \mathbf{Y}^2 - (Y^2)^0 \,. \end{aligned} \tag{9}$$

b) 2-*spinor formalism*

Instead of the four-spinors φ_4 and χ_4 we introduce the two 2-spinors φ and χ. Let us introduce an imaginary number j independent of i, in the sense that we may take separately the complex conjugate with respect to i and j.

Let us construct the 2-spinor $\varphi + j\chi$ twice complex in i and j:

$$\varphi + j\chi = \begin{pmatrix} [\varphi_{11} + i\varphi_{12}] + j\,[\chi_{11} + i\chi_{12}] \\ [\varphi_{21} + j\varphi_{22}] + j\,[\chi_{21} + i\chi_{22}] \end{pmatrix}, \tag{10}$$

σ^μ being the Pauli matrices. Let us define:

$$Z^\mu = (\bar{\varphi} + j\bar{\chi})\,\sigma^\mu(\varphi + j\chi)\,. \tag{11}$$

We set:

$$\begin{aligned} X^\mu &= \bar{\varphi}\sigma^\mu\varphi - \bar{\chi}\sigma^\mu\chi\,, \\ Y^\mu &= \bar{\varphi}\sigma^\mu\chi + \bar{\chi}\gamma^\mu\varphi\,. \end{aligned} \tag{12}$$

Thus:

$$Z^\mu = X^\mu + jY^\mu. \tag{13}$$

We enlarge the two invariance groups by requiring the invariance of the quantity:

$$\mathbf{Z}^2 - (Z^0)^2.$$

This implies that the two quantities C and D:

$$\begin{aligned} C &= [\mathbf{X}^2 + (Y^0)^2] - [\mathbf{Y}^2 + (X^0)^2]\,, \\ D &= \mathbf{XY} - X^0\,Y^0 \end{aligned} \tag{14}$$

remain invariant. We may consider four types of invariance groups.

1. *Group of first kind.* This group is associated with the transformation:

$$(\varphi + j\chi)' = e^{\frac{\alpha}{2}\sigma^k}(\varphi + j\chi)$$

which means that:

$$\begin{aligned} \varphi' &= \left(\mathrm{ch}\,\frac{\alpha}{2} + \mathrm{sh}\,\frac{\alpha}{2}\sigma^k\right)\varphi, \\ \chi' &= \left(\mathrm{ch}\,\frac{\alpha}{2} + \mathrm{sh}\,\frac{\alpha}{2}\sigma^k\right)\chi\,. \end{aligned} \tag{15}$$

This implies the following transformation law for X^μ and Y^μ:

$$\left|\begin{aligned} X^{l'} &= X^l\,, \\ X^{k'} &= X^k\,\mathrm{ch}\,\alpha + X^0\,\mathrm{sh}\,\alpha\,, \\ X^{0'} &= X^k\,\mathrm{sh}\,\alpha + X^0\,\mathrm{ch}\,\alpha\,, \end{aligned}\right| \qquad \left|\begin{aligned} Y^{l'} &= Y^l\,\mathrm{ch}\,, \\ Y^{k'} &= Y^k\,\mathrm{ch}\,\alpha + Y^0\,\mathrm{sh}\,\alpha\,, \\ Y^{0'} &= Y^k\,\mathrm{sh}\,\alpha + Y^0\,\mathrm{ch}\,\alpha\,, \end{aligned}\right.$$

where

$$k = 1 \text{ or } 2 \text{ or } 3,$$

$$l \neq k\,.$$

This is the special Lorentz transformation along the axis (k) of velocity:

$$v = c \operatorname{th} \alpha$$

2. *Group of second kind.* This group is associated with the transformation:

$$(\varphi + j\chi)' = e^{i\frac{\beta}{2}\sigma^k}(\Phi + j\chi)', \tag{16}$$

which means that:

$$\varphi' = \left(\cos\frac{\beta}{2} + i\sin\frac{\beta}{2}\sigma^k\right)\varphi\,, \qquad \chi' = \left(\cos\frac{\beta}{2} + i\sin\frac{\beta}{2}\sigma^k\right)\chi\,. \tag{17}$$

This implies the following transformation law for X^μ and Y^μ:

$$\left|\begin{array}{ll} X^{k'} = X^k, & Y^{k'} = Y^k, \\ X^{0'} = X^0, & Y^{0'} = Y^0, \\ X^{l'} = X^l\cos\dfrac{\beta}{2} + X^m\sin\dfrac{\beta}{2}, & Y^{l'} = Y^l\cos\beta + Y^m\sin\beta\,, \\ X^{m'} = -X^l\sin\dfrac{\beta}{2} + X^m\cos\dfrac{\beta}{2}, & Y^{m'} = Y^l - \sin\beta + Y^m\cos\beta\,, \end{array}\right. \tag{18}$$

where $k = 1$ or 2 or 3 $(l \neq m \neq k)$.

This is a space rotation of angle β about the (k) axis.

3. *Group of third kind.* This group leaves invariant the quantities E, F and D:

$$E = \mathbf{X}^2 + (Y^0)^2,$$
$$F = \mathbf{Y}^2 + (X^0)^2,$$
$$G = XY - X^0Y^0.$$

The corresponding transformation law for the spinors φ and χ is

$$(\varphi + j\chi)' = e^{j\frac{\gamma}{2}\sigma^k}(\varphi + j\chi)\,,$$

which means that:

$$\varphi' = \cos\frac{\gamma}{2}\varphi - \sin\frac{\gamma}{2}\gamma^k\chi\,, \quad \chi' = \cos\frac{\gamma}{2}\chi + \sin\frac{\gamma}{2}\sigma^k\varphi \tag{19}$$

and the corresponding transformation law for X^μ and Y^μ:

$$\left|\begin{array}{l} X^{k'} = X^k \cos\gamma - Y^0 \sin\gamma\,, \\ Y^{0'} = X^k \sin\gamma + Y^0 \cos\gamma\,, \\ X^{l'} = X^l\,, \end{array}\right. \qquad \left|\begin{array}{l} Y^{k'} = Y^k \cos\gamma + X^0 \sin\gamma\,, \\ X^{0'} = -Y^k \sin\gamma + X^0 \cos\gamma\,, \\ Y^{l'} = Y^l\,, \end{array}\right. \tag{20}$$

where

$$k = 1 \text{ or } 2 \text{ or } 3,\ \omega l = k.$$

In the case: $X^0 = Y^0$, in order to satisfy Eqs. (20), we must take:

$$Y^k = -X^k,\ k = 1, 2, 3.$$

Indeed, let us set $X^0 = Y^0$, we find:

$$X^{0'} = Y^{0'} = -Y^k \sin\gamma + X^0 \cos\gamma = X^k \sin\gamma + X^0 \cos\gamma\,,$$

which gives: $Y^k = -\chi^k$, $k = 1, 2, 3$.

4. *Group of fourth kind.* This group leaves the quantities

$$\mathbf{X}^2 - \mathbf{Y}^2,$$
$$\mathbf{XY}$$

invariant.

The corresponding transformation law for the spinors φ and χ is:

$$(\varphi + j\chi)' = e^{i\gamma \frac{\delta}{2} \sigma^k} (\Phi + j\chi)\,,$$

which means that:

$$\begin{aligned} \varphi' &= \operatorname{ch}\frac{\delta}{2}\varphi - i \operatorname{sh}\frac{\delta}{2}\sigma^k \chi\,, \\ \chi' &= \operatorname{ch}\frac{\delta}{2}\chi + i \operatorname{sh}\frac{\delta}{2}\sigma^k \varphi'\,. \end{aligned} \tag{21}$$

The transformation law of the coordinates X^μ and Y^μ is:

$$\begin{aligned} X^{k'} &= X^k, & X^{l'} &= X^l \operatorname{ch}\delta - Y^m \operatorname{sh}\delta\,, \\ X^{0'} &= X^0, & Y^{m'} &= -X^l \operatorname{sh}\delta + Y^m \operatorname{ch}\delta\,, \\ Y^{k'} &= Y^k, & X^{m'} &= X^m \operatorname{ch}\delta + Y^l \operatorname{sh}\delta\,, \\ Y^{0'} &= Y^0\,, & Y^{l'} &= X^m \operatorname{sh}\delta + Y^l \operatorname{ch}\delta\,, \end{aligned}$$

$$k = 1 \text{ or } 2 \text{ or } 3,\ l \neq m \neq k.$$

III. Physical interpretation of the invariance groups

To the spinors transformations φ and χ:

$$(\varphi + j\chi)' = e^{\frac{1}{2}(\alpha+j\gamma)\sigma^k}(\varphi + j\chi)$$

corresponds the transformation of Z^μ:

$$Z^{k'} = Z^k \operatorname{ch}\Theta + Z^0 \operatorname{sh}\Theta,$$
$$Z^{0'} = Z^s \operatorname{sh}\Theta + Z^0 \operatorname{ch}\Theta,$$
$$Z^{l'} = Z^l,$$

where

$$k = 1 \text{ or } 2 \text{ or } 3,$$
$$l \neq k,$$
$$\Theta = (\alpha + j\gamma),$$

which is called the generalized Lorentz transform. In the case where the particle is considered as a point determined by $Z^\mu = X^\mu$, the Lorentz transform introduces a real angle $\Theta = \alpha$ attached to the velocity v of the origin of the mobile frame. In the case where the particle is considered as a fluid droplet [1, 2, 3], the position of the praticle is defined by two points M and N corresponding to the two centres attached to the fluid droplet. The generalized Lorentz transforms introduce a complex angle $\theta = \alpha + j\gamma$, with two real parameters α and γ attached to the two velocities of the mobile frame of reference. Thus, the origin of this system introduces two velocities $\mathbf{v}_1$ and $\mathbf{v}_2$ which are determined from α and γ and vice versa. This leads us to consider the origin of the mobile frame as formed by two points O_1 and O_2 and the frame of reference becomes the set of the two frames $O_1 X^1 X^2 X^3 X^0$ and $O_2 Y^1 Y^2 Y^3 Y^0$, of origins O_1 and O_2 which possess the velocities $\mathbf{v}_1$ and $\mathbf{v}_2$. This interpretation faces a serious difficulty when O_1 and O_2 are completely unknown. But a frame of reference is associated with an observer, hence with a material object determined according to the model of the fluid droplet by two centres. Hence, the points O_1 and O_2 are the two centres associated with the mobile frame. In this case, the distance O_1O_2 is very small, that is of the order of 10^{-17} cm: we assume here that the distance of the two centres is of the order of $10^{-4}\, l_0$, where l_0 is the fundamental distance 10^{-13} cm.

The mobiled frame is then composed of two mobile frames S_1 and S_2 attached to the two centres O_1 and O_2 of the material observer O. O_1 indicates the centre of mass of the observer. O_2 indicates the centre of matter of the observer.

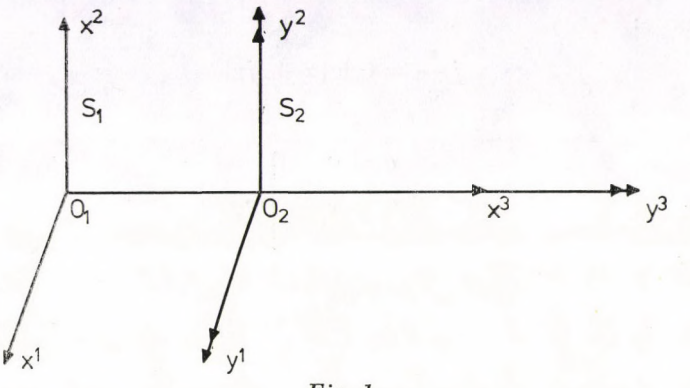

Fig. 1

Consider a particle P. It is determined by its two centres M an N, where M indicates the centre of mass of P, and N the centre of matter of P. The coordinates X^μ and Y^μ are then the coordinates of M and N, respectively with respect to the frames O_1S_1 and O_2S_2: X^μ indicates the coordinates of M with respect to S_2, Y^μ indicates the coordinates of N with respect to S_2.

In the common case where X^μ and Y^μ are of the order of 1 cm, X^μ and Y^μ are nearly equal (with an error equal to 10^{-17} cm) which is a good approximation, and we notice that the difference used is physically not appreciable. Whereas if we imagine the case where $X^k \neq -Y^k$, something new would be introduced.

The position of the particle determined by the two centres M and N, is given from X^μ and Y^μ by the complex quantity:

$$Z^\mu = X^\mu + jY^\mu . \tag{22}$$

The case $X^k = -Y^k$ corresponds to $X^0 = Y^0$ there:

$$Z^k = X^k(1 - j), \qquad T = t(1 + j) \tag{23}$$

and

$$\frac{dZ^k}{dt} = -j\frac{dX^k}{dt} .$$

The velocity of a particle P in this case

$$(X^k = -Y^k \text{ and } X^0 = Y^0) \quad \text{is} \quad j\frac{dY^k}{dt} .$$

The origin (O_1, O_2) of the mobile frame of reference has a velocity:

$$jv \text{ then: } -\mathbf{v}_1 = \mathbf{v}_2 = v\mathbf{e} \tag{24}$$

we must have:

$$j\frac{v}{c} = \operatorname{tgh}(\alpha + j\gamma)^{1}.$$

Hence,

$$\left.\begin{aligned} a &= 0 \\ \frac{v}{c} &= \operatorname{tg}\gamma \end{aligned}\right\}, \tag{25}$$

which gives:

$$\cos^2\gamma = \frac{\dfrac{v^2}{c^2}}{1+\dfrac{v^2}{c^2}}, \qquad \sin^2\gamma = \frac{1}{1+\dfrac{v^2}{c^2}}, \tag{26),(27}$$

Therefore, the suggestion of taking complex and equal to $\alpha + j\gamma$ is a generalization of the Lorentz transform. The introduction of γ is linked to the introduction of Y^{μ} and to the frame of origin O_2 and of velocity $\mathbf{v}_2$. The frame of reference is itself a set of two frames linked to the two centres O_1 and O_2 of the mobile observer and having the velocities $\mathbf{v}_1$ and $\mathbf{v}_2$. We have examined the case when $\mathbf{v}_1 = -\mathbf{v}_2$ (opposed velocities for the two frames). The origins O_1 and O_2 of the observer move such that their distance O_1O_2 increases rapidly and reaches the value of 10^{-17} cm in a very short time:

$$\frac{10^{-10}}{310^{10}} = 3.3 \cdot 10^{-27}\,\mathrm{s}. \tag{28}$$

Since

$$\frac{v}{c} = \operatorname{tg}\gamma,$$

we see that it is possible to have a frame of reference linked to the observer (O_1, O_2), whose velocities $\mathbf{v}_1$ and $\mathbf{v}_2$ $(\mathbf{v}_1 = -\mathbf{v}_2)$ have a modulus greater than the velocity of light.

Let us examine in this case the ds^2:

$$\begin{aligned} ds^2 &= (dZ^0)^2 - d\mathbf{Z}^2\,, \\ dZ^0 &= Cdt(1+j)\,, \\ dZ^k &= dx^k(1-j)\,, \\ \frac{d\mathbf{X}}{dt} &= -\frac{d\mathbf{Y}}{dt}\,, \end{aligned}$$

then:

$$\begin{aligned} ds^2 &= C^2\,dt^2(1+j)^2 - d\mathbf{X}^2(1-j)^2\,, \\ ds^2 &= C^2dt^2(1+j)^2\left[1+\left(\frac{d\mathbf{X}}{dt}\right)^2\right]\Big/C^2\,, \end{aligned} \tag{29}$$

ds^2 is not negative any longer, even when

$$\left|\frac{d\mathbf{X}}{dt}\right| > C\,.$$

The formula (29) expresses the fact that the ds^2 is the same with respect to the two fraes S_1 and S_2, it is equal to:

$$dt^2\left[C^2 + \left[\frac{d\mathbf{X}}{dt}\right]^2\right].$$

Hence for a particle, having a modulus of velocity of its two centres:

$$\left|\frac{d\mathbf{X}}{dt}\right| > C$$

greater than the velocity of light, we have:

$$ds^2 \geq 0.$$

IV. Towards a new model of tachyons

The idea of having particles with velocities greater than the velocity of light has been suggested by TANALEA [7], BILIANIUK, DESHPANDE and SUDARSHAN [8], BASSILA [6] and FEINBERG [9].

In the simple model where a particle is considered as a point of mass m and velocity v, it is difficult to consider velocities greater than c without running into serious difficulties. Indeed, we have:

$$m = \frac{m_0}{\sqrt{1 - \frac{v^2}{c^2}}} \tag{30}$$

and if $v > c$, then we must have $m_0 = i\mu_0$, and the mass at rest would be imaginary. We assume also that the intrinsic length and time are also imaginary.

We start from a new model of particles. This model is mainly studied in [1], [2], [3]. The particle is essentially considered as a fluid droplet having two centres: centre of mass and centre of matter. Thus, in this model, a particle is represented by two points M and N. The frame of reference itself is considered to be formed by two frames $O_1X^1X^2X^3X^0$ and $O_2Y^1Y^2Y^3Y^0$. The velocities $\mathbf{v}_1$ of O_1 and $\mathbf{v}_2$ of O_2 are colinear and can exceed the speed of light. The most

general coordinate transformation is that represented by a transformation on the spinors $(\varphi + j\chi)$ given by

$$(\varphi + j\chi)' = e^{\frac{1}{2}\Theta\sigma^k}(\varphi + j\chi)\,,$$

where $\theta = \alpha + i\beta + j\gamma + ij\delta$.

Consider the particular case $\alpha = \beta = \gamma = 0$. This corresponds to the case:

$$\mathbf{v}_1 = -\mathbf{v}_2 = \mathbf{v}.$$

This is equivalent to taking a set of two frames of opposite velocities with these velocities being both greater than c. A particle in this model has a lifetime related to the spreading of the droplet, the distance between its centres not exceeding 10^{-17} cm.

Consider the formula which relates the mass to the velocity in the case of $\mathbf{v}_1 = -\mathbf{v}_2 = \mathbf{v}$. We have the expression for the mass of the particle, its velocity, its mass at rest and the speed of the light as follow:

$$M = m(1 \times j)\,,$$

$$V = vhj\,,$$

$$M_0 = m0(1 + j)\,,$$

$$C = C\,.$$

Hence we write:

$$(MC)^2 - (MV)^2 = (M_0 C)^2\,,$$

$$(1 + j)^2 m^2 c^2 + (1 + j)^2 m^2 v^2 = m_0 c^2 (1 + j)^2,$$

with

$$m = \frac{m_0}{\sqrt{1 + \dfrac{v^2}{c^2}}}\,. \tag{31}$$

v can be greater than c and m_0 is not imaginary. This new model rejects all the objections to the tachyons: in particular, intrinsic length and intrinsic imaginary time.

In the case where the velocities of the centres are opposite to each other, the lifetime of the tachyons is very short, shorter than:

$$\frac{10^{-11}}{3.10^{10}} \# 3.3 \cdot 10^{-27}\ \text{s}.$$

V. Dynamic equation of the tachyon in the special case ($x^0 = y^0$, $x^k = -y^k$)

In the special case when ($x^0 = y^0$, $x^k = -y^k$) the quadrivector impulsion can be written:

$$p^k(1 - j), \quad mc(1 + j)$$

to which corresponds the operator

$$\left(\frac{\partial}{\partial x^k}(1 + j), \; -\frac{\partial}{\partial x^0}(1 + j)\right).$$

In the formalism of the 2-spinor the dynamic equation can be written: if we replace P_μ by the operators

$$\sigma^\mu P_\gamma(\Phi + j\chi) = m_0 cj(1 + j)(\varphi - j\chi) = 0 .$$

In the formalism of the 2-spinor the dynamic equation can be written: if we replace P_μ by the operators

$$\frac{\partial}{\partial x^k}(1 - j), \; -\frac{\partial}{\partial x^0}(1 + j) ,$$

we have

$$\sigma^k \frac{\partial}{\partial x^k}(1 - j)(\varphi + j\chi) - \sigma^0 \frac{\partial}{\partial x^0}(1 + j)(\Phi + j\chi) - m_0 cj(1 + j)(\chi - j\chi) = 0 ,$$

$$\sigma^k \frac{\partial}{\partial x^k}(\varphi + j\chi) - \sigma^0 \frac{\partial}{\partial x^0} j(\varphi + j\chi) + m_0 c(\Phi - j\chi) = 0 ,$$

which we can decompose into two equations

$$\sigma^k \frac{\partial}{\partial x^k}\varphi + \sigma^0 \frac{\partial}{\partial x^0}\chi + m_0 c\varphi = 0 ,$$

$$-\sigma^k \frac{\partial}{\partial x^k}\chi + \sigma^0 \frac{\partial}{\partial x^0}\varphi + m_0 c\chi = 0 .$$

By using the ϱ^k matrix we can rewrite these equations in one:

$$\left[\varrho^3 \, \theta \, \sigma^k \frac{\partial}{\partial x^k} + \varrho^1 \theta \sigma^0 \frac{\partial}{\partial x^0} + m_0 c\right]\psi = 0$$

with

$$\psi = \begin{pmatrix} \varphi \\ \chi \end{pmatrix} .$$

REFERENCES

1. J. Weyssenhoff, Acta Phys. Pol., **9**, 8, 1947.
2. C. Möller, Ann. Inst. H. Poincaré, **11**, 251, 1949.
3. D. Bohr and J. P. Vigier, Phys. Rev., **109**, 1882, 1958.
4. F. Gürsey, Nuov. Cim., **4**, 784, 1957.
   A. Proca, Journ. Phys. Rad., **2**, 65, 1954.
5. A. Proca, Journ. Phys. Rad., **17**, 83, 1956.
6. E. Bassila, Thèse de Doctorat des Sciences.
7. S. Tanaka, Progr. Theor. Phys., **24**, 171, 1960.
8. O. M. P. Bilianiuk, V. K. Deshpande, E. C. G. Sudarshan, Am. J. Phys., **30**, 718, 1962.
9. G. Feinberg, Phys. Rev., **159**, 1089, 1967.
10. A. Einstein, Ann. Physik, **17**, 891, 1905.

Acta Physica Academiae Scientiarum Hungaricae, Tomus 48 (1), pp. 31—42 (1980)

FURTHER INVESTIGATIONS FOR THE LEAST-SQUARES METHOD

By

M. A. ABDEL-RAOUF

INSTITUTE FOR THEORETICAL PHYSICS, TÜBINGEN UNIVERSITY, D-7400 TÜBINGEN 1, FRG*

(Received 30. VIII. 1979)

The least-squares S-wave phase shifts of the scattering of electrons by simple, Yukawa and static potentials are compared with the exact phases. Additionally, KOHN's, RUBINOW's and the least-squares methods (LSM) are used for calculating the S-wave phase shifts of e^+ — H elastic scattering by employing trial and test-function spaces which allow for virtual positronium excitation. The results are in good agreement with those of other authors.

Introduction

The LSM has been originally suggested by LADANYI and SZONDY [1, 2], SCHMID and HOFFMANN [3], SCHMID and SCHWAGER [4], SCHMID [5, 6] and WLADAWSKY [7] for treating the scattering processes. SCHWAGER and SCHMID [8], SCHWAGER [9] and MADER [10] used SCHMID's version for dealing with different three body problems. They showed that the LSM is free of any traces of the phenomenon of pseudoresonances which appears in the classical variational methods [11—13]. ABDALLAH and TRUHLAR [14] investigated WLADAWSKY's technique in e^-—H inelastic scattering and emphasized that the method is more effective than the minimum norm method of HARRIS and MICHELS [15, 16] and the anomaly-free methods of NESBET [17—20]. ABDEL-RAOUF and BELSCHNER [21] pointed out that the LSM yields approximative phase shifts which converge steadily to certain values and the norm of the vector $(E - H)|\psi_n\rangle$ becomes smaller by enlarging the trial and test-function spaces.

In this paper we show that the convergence of the S-phase shifts of the scattering of electrons by simple, Yukawa and static potentials is always towards the exact phases. The exact solutions of the S-wave scattering of electrons by other exponential potentials using the procedure of KANELLOPOULOS et al [22] are also given in Tables. Finally, we carry out calculations for the S-phases of e^+ — H elastic scattering by adding positronium vectors to trial expansion and test-function spaces. In this case we use the variational methods of KOHN, RUBINOW and the LSM. The whole results will be compared with those of other authors.

* Present address: Faculty of Physics, Freiburg University, D—7800 Freiburg, FRG

Variational methods

The S-wave elastic scattering of a projectile by atomic target can be expressed, approximately, by the trial expansion space

$$|\psi_n\rangle = a\,|S\rangle + b|C\rangle + |\Phi_n\rangle\,, \tag{1}$$

where the vectors $|S\rangle$ and $|C\rangle$ describe, asymptotically, the final state of the scattering system, while $|\Phi_n\rangle$ spans the domain of interaction. It is then the superposition of Hilbert-space vectors $\{|\chi_i\rangle;\ i = 1, 2, \ldots, n\}$, i.e.

$$|\Phi_n\rangle = \sum_{i=1}^{n} d_i\,|\chi\rangle\,. \tag{2}$$

The adjustable parameters a, b and d_i's are subjected to the variational procedures.

Since the principal idea behind the whole variational method [23] is to demand that the projections of Schrödinger's vector $(E - H)|\psi_n\rangle$ into a test-function space $\{|\varphi_j\rangle;\ j = 1, 2, \ldots, m;\ m \geqslant n + 1\}$ are zero (if $m = n + 1$) or of minimum lengths (if $m > n + 1$), one can simply formulate these methods by the following equations:

$$\langle\varphi_j|E - H|\psi_n\rangle = V_j, \quad j = 1, 2, \ldots, m\,, \tag{3a}$$

$$\delta \sum_{j=1}^{m} V_j^2 = 0\,. \tag{3b}$$

The case $m = n + 1$ corresponds to the methods of HULTHEN [11], KOHN [12], MALIK [24], HARRIS and MICHELS [15, 16], NESBET [17—20], TAKATSUKA and FUENO [25] as well as the quadratic HULTHEN, quadratic KOHN and quadratic RUBINOW methods [23]. The case $m > n + 1$ delivers the LSM and the quadratic least-squares method [23]. All the previous methods can be additionally distinguished through their choices of the test-function space $|\varphi_j\rangle$.} In the present work we restricted ourselves to the following choices, corresponding to the methods of KOHN, RUBINOW and the LSM, respectively:

$$\begin{aligned}
|\varphi\rangle_{\text{Kohn}} &\equiv (|C\rangle,\ |\chi_i\rangle\ ;\ i = 1, 2, \ldots, n)\,,\\
|\varphi\rangle_{\text{Rubinow}} &\equiv (|S\rangle,\ |\chi_i\rangle\ ;\ i = 1, 2, \ldots, n)\,,\\
|\varphi\rangle_{\text{LSM}} &\equiv (|S\rangle,\ |C\rangle,\ |\chi\rangle_i;\ i = 1, 2, \ldots, n).
\end{aligned}$$

Consequently, it is easy to prove that if $x_n = \tan(\xi_n)/k$, where ξ_n is the S-wave phase shift and k^2 is the energy of the incident projectiles, then x_n takes the following forms, respectively:

$$x_{\text{nKohn}} = b/a = -\,\Delta_n^{(C|S)}/\Delta_n^{(C|C)}\,, \tag{4}$$

$$x_{\text{nRubinow}} = b/a = -\,\Delta_n^{(S|S)}/\Delta_n^{(S|C)}\,, \tag{5}$$

$$x_{\text{nLSM}} = b/a = -\,\Delta_n^{(C;S)}/\Delta_n^{(C;C)}\,, \tag{6}$$

where

$$\Delta_n^{(g|f)} = \begin{vmatrix} (g|f) & (g|1) & (g|2) & \dots & (g|n) \\ (1|f) & (1|1) & (1|2) & \dots & (1|n) \\ \vdots & & & & \\ (n|1) & (n|f) & (n|2) & \dots & (n|n) \end{vmatrix}, \tag{7}$$

$$(g|f) = \langle g \,|\, E - H|f\rangle,$$
$$(i|j) = (\chi_i/\chi_j),\ i, j = 1, 2, \dots, n,,$$
$$(g{:}f) = \langle g|(E - H)^{+}P(E - H)|f\rangle$$

and the operator P is defined by

$$P = \sum_{i=-1}^{n} |\chi_i\rangle \langle {}_i\chi \,|\,,$$

with $|\chi_{-1}\rangle = |S\rangle$, and $|\chi_0\rangle = |C\rangle$. The determinants of Eq. (6) can be obtained from Eq. (7) by replacing the elements $(g|f)$ by $(g{:}f)$.

The corrected value of each x_n is given by:

$$[x_n] = x_n + \frac{1}{k}(\psi_n|\psi_n)\,. \tag{8}$$

Components of the trial expansion and test-function spaces

The vectors $|S\rangle$, $|C\rangle$ and $|\chi_i\rangle$'s take, in the scattering of electrons by exponential potentials, the following forms, respectively:

$$S = \sin(kr)/k,\ C = (1.0 - e^{-\alpha r})\cos(kr) \text{ and } \chi_i = r^i e^{-\alpha r}, \tag{9}$$

where r is the distance between the incident electrons and the scattering centre.

In case of e^+ — H elastic scattering, $|S\rangle$ and $|C\rangle$ are chosen to be

$$S = e^{-r_1}\sin(kr_2)/k\,, \tag{10a}$$
$$C = e^{-r_1}(\cos(kr_2) - e^{-\alpha r_2})\,, \tag{10b}$$

where r_1 and r_2 are the position vectors of the bounded electron and the incident positron, respectively. The truncated Hilbert-space $|\Phi_n\rangle$ of Eq. (1) is expressed by

$$|\Phi_n\rangle = a_0|\Phi_0\rangle + \sum_{i=1}^{n} a_i\,|\chi_i\rangle\,, \tag{10c}$$

where $|\Phi_0\rangle$ describes the positronium atom and its motion relative to the proton (26, 27), i.e.

$$\Phi_0 = e^{-\gamma_1 r_{12}} e^{-\gamma_2 |+r_2|}, \tag{10d}$$

with $\gamma_1 = 0.5$ and $\gamma_2 = (|1.0 - 2k^2|)^{1/2}$.

The $|\chi_i\rangle$'s of Eq. (10c) are given by

$$\chi_i = r_1^p r_2^s r_{12}^l e^{(-\alpha_1 r_1 + \alpha_2 r_2 + \beta r_{12})}, \tag{10e}$$

where r_{12} is a Hylleraas' vector. The parameters α_i and β of Eqs. (9), (10b) and (10e) are free parameters and the indices p, s, l are adjusted to satisfy the relation $p + s + l \leqslant M + 1$, where $M = 1, 2, 3, 4, 5, 6$ corresponding to $n = 3, 7, 13, 22, 34, 50$, respectively.

The operator E—H

The previous forms of $|S\rangle$ and $|C\rangle$ reduce the operator $E - H$, in e^- — exponential potential scattering, to the form:

$$E - H = d^2/dr + k^2 + V(r)\,, \tag{11a}$$

k^2 is the scattering energy and $V(r)$ is the considered potential. It is defined by

$$V(r) = A\, e^{-\xi r} \sin(\Theta_1 r) \cos(\Theta_2 r)\,, \tag{11b}$$

$$V(r) = \frac{A}{r} e^{-\xi r} \sin(\Theta_1 r) \cos(\Theta_2 r)\,, \tag{11c}$$

and

$$V(r) = \left(A + \frac{B}{r}\right) e^{-\xi r} \tag{11d}$$

corresponding to the simple, Yukawa and static potentials, respectively. The parameters A, B, ξ, Θ_1 and Θ_2 are free parameters.

Similarly, the operator $E - H$ can be written, in case of $e^+ - H$ elastic scattering, in the following form:

$$E - H = (d^2/dr_1^2) + (d^2/dr_2^2), + (2/r_1) - (2/r_2) + (2/r_{12}) + k^2 - 1.0\,. \tag{12}$$

Results and discussion

The LSM which has been employed in the peresent work is given by Eqs. (3a, b) with $m = n$ and $|\varphi_i\rangle \equiv |\varphi\rangle_{LSM}$.

The vectors $|S\rangle$, $|C\rangle$ and $|\chi_i\rangle$'s are defined, for the scattering of electrons by exponential potentials, by Eqs. (9). In Figs. 1, 2 and 3 we give three examples

for the variation of x_{nLSM} with the free parameter α at different values of n. The Figures correspond to the scattering of electrons by the potentials $2e^{-2r}$, $2/r\, e^{-2r}$ and $2(1 + 1/r)e^{-2r}$, respectively, at $k = 0.2$. It is clear that the relation (x_{nLSM}, α) leads to smooth plateaux which become wider by increasing n. The best η_n are given in Table I, columns 3, 5 and 7, respectively. The same Table

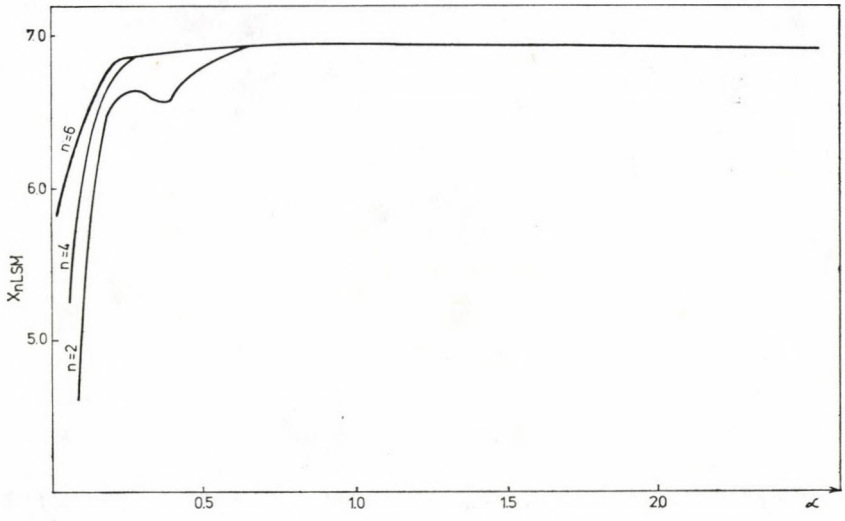

Fig. 1. Scattering of electrons by the potential $2\ e^{-2r}$ at $k = 0.2$ using the LSM

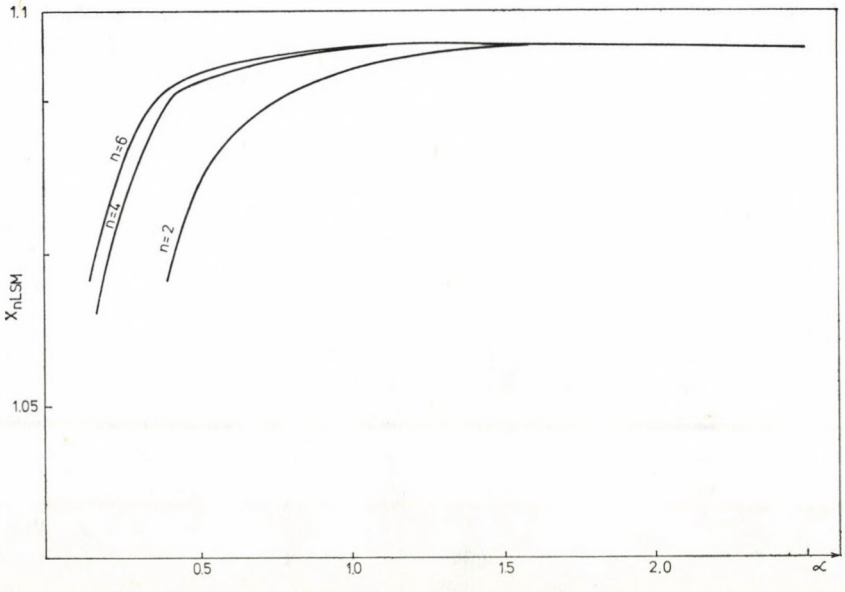

Fig. 2. Scattering of electrons by the potential $2/r\ e^{-2r}$ at $k = 0.2$ using the LSM

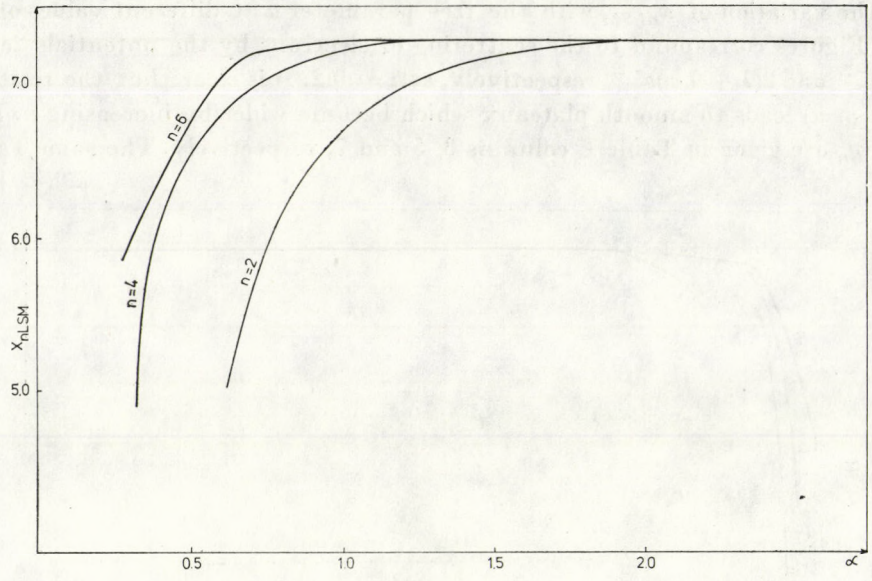

Fig. 3. Scattering of electrons by the potential $2\,(1 + 1/r)\,e^{-2r}$ at $k = 0.2$ using the LSM

contains the corresponding exact phase shifts obtained by KANELLOPOULOS et al procedure [22]. The comparison shows that the phases of the LSM are always very close to the exact ones. Tables II, III, IV involve the exact phase shifts for the scattering of electrons by the potentials of Eqs. (11b), (11c) and (11d) for different values of A, B, ξ, Θ_1 and Θ_2 at $k = 0.1-1.0$.

Table I

The exact and approximative phase shifts for the scattering of electrons by different exponential potentials

k (au)	$V(r) = 2e^{-2r}$		$V(r) = \frac{2}{r}e^{-2r}$		$V(r) = 2\left((1 + \frac{1}{r}\right))e^{-2r}$	
	exact	LSM	exact	LSM	exact	LSM
0.1	0.07242323	0.072423	0.10873179	0.10873	0.72220647	0.72221
0.2	0.13745234	0.13745	0.20849988	0.20849	0.97251122	0.97252
0.3	0.19021111	0.19021	0.29324701	0.29325	1.04554569	1.0455
0.4	0.2291750	0.22916	0.36088918	0.36089	0.05749069	1.0575
0.5	0.25537310	0.25537	0.41228775	0.41228	1.04465582	1.04466
0.6	0.27108001	0.27108	0.44982184	0.44982	1.02102781	1.0210
0.7	0.27881199	0.27881	0.47624339	0.47624	0.99289911	0.99290
0.8	0.2808053	0.28080	0.49408938	0.48405	0.96335331	0.96336
0.9	0.27884234	0.27884	0.50546212	0.50546	0.93396336	0.93397
1.0	0.27425763	0.27426	0.51201416	0.51201	0.90552018	0.90554

The above procedure has been used for calculating the best phase shifts for the scattering of positrons by atomic hydrogen. The asymptotic components of $|\psi_n\rangle$ and $|\varphi\rangle_{LSM}$ are defined at Eqs. (10a) and (10b) and their Hilbert-space parts are presented at Eq. (10c). Two different investigations are considered: In the first we put $\beta = 0$ at Eq. (10e), i.e. the Hilbert-space is the

Table II

The exact phase shifts for the scattering of electrons by potentials of the form (11b)

$$A = \xi = 2$$

k (au)	$\Theta_2 = 0$ $\Theta_1 = 2$	$\Theta_2 = 2$ $\Theta_1 = \pi/2$
0.1	0.01676480	3.130391144
0.2	0.03388021	3.119467854
0.3	0.05163694	3.109141154
0.4	0.07018207	3.099803204
0.5	0.08944334	3.091942024
0.6	0.10905836	3.086135724
0.7	0.12834385	3.083004434
0.8	0.14635006	3.086740454
0.9	0.16201812	3.086793584
1.0	0.17441485	3.094045734

Table III

The exact phase shifts for the scattering of electrons by potentials of the form (11c)

$$A = B = \xi = 2$$

k (au)	$\Theta_2 = 0$ $\Theta_1 = 2$	$\Theta_2 = 2$ $\Theta_1 = \pi/2$
0.1	0.03978666	0.00465102
0.2	0.07902021	0.00974087
0.3	0.11712903	0.01570883
0.4	0.15351222	0.02299087
0.5	0.18754196	0.03200157
0.6	0.21858601	0.04310217
0.7	0.24605180	0.05654735
0.8	0.26944805	0.07242272
0.9	0.28845132	0.09058264
1.0	0.3029587	0.11062016

Table IV

The exact phase shifts for the scattering of electrons by static potentials, form (11d) at different values of the free parameters A, B and ξ

k (au)	$A = B = \xi = 1.0$	$A = B = \xi = 0.5$	$A = B = \xi = 0.1$
0.1	2.304578624	2.466112824	0.26449940
0.2	1.845549364	1.977950204	2.326883504
0.3	1.57820334	1.65403821	1.753756304
0.4	1.39754726	1.42933669	1.40358733
0.5	1.26426334	1.26386286	1.16936385
0.6	1.16052780	1.13650917	1.00228832
0.7	1.07674261	1.03478157	0.87732804
0.8	1.00716174	0.95144158	0.78042266
0.9	0.94811021	0.88174543	0.70310366
1.0	0.89712392	0.82243427	0.6399841

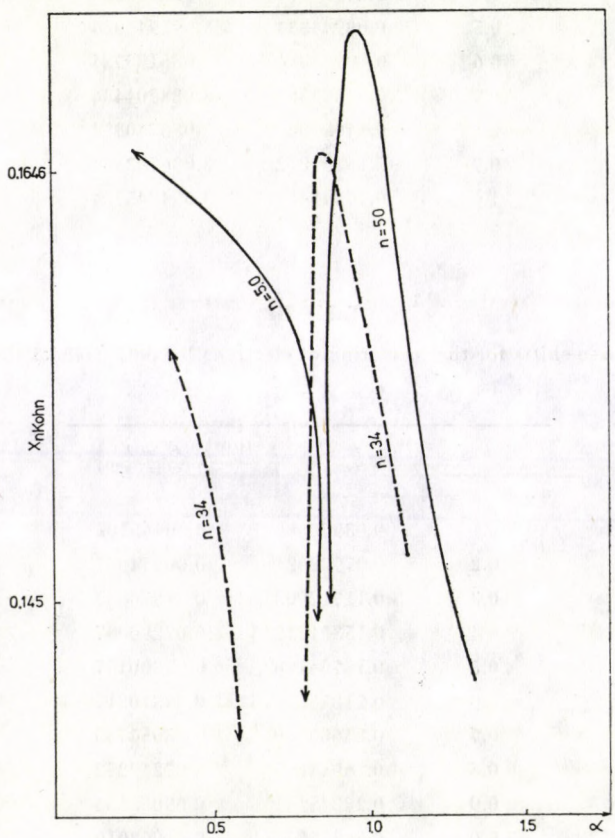

Fig. 4. e^+ — H elastic scattering using the LSM (first investigation), at $k = 0.3$

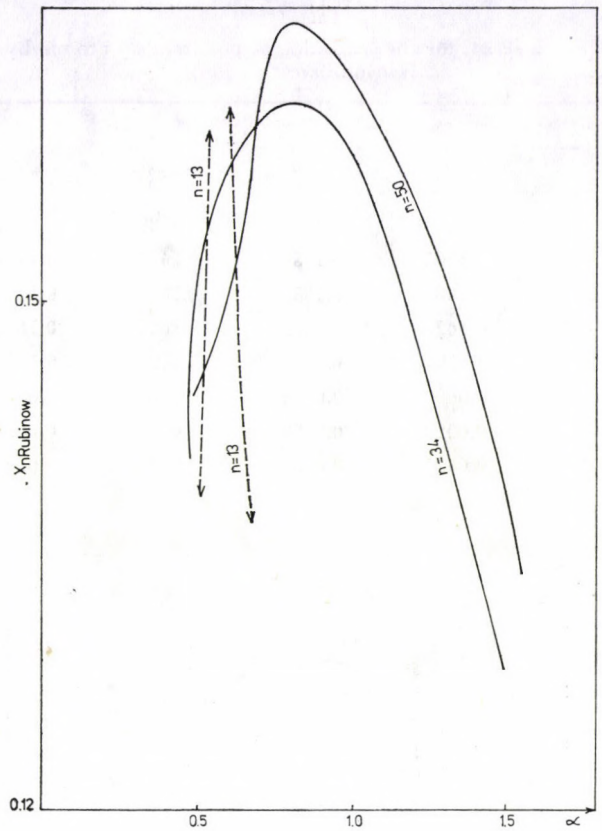

Fig. 5. e^+ — H elastic scattering using the KOHN method (first investigation), at $k = 0.3$

Table V

η_n and $[\eta_n]$, $n = 50$, for the scattering of positrons by atomic hydrogen (first investigation)

k (au)	LSM		KOHN's method		RUBINOW's method		BHATIA [30]
	η_n	$[\eta_n]$	η_n	$[\eta_n]$	η_n	$[\eta_n]$	$[\eta_n]$
0.01	0.01852	0.018522	0.01867	0.01867	0.01861	0.01861	
0.1	0.14591	0.14577	0.14561	0.14567	1.1488	0.14848	0.1483
0.2	0.1856	0.1849	0.18567	0.18563	0.1829	0.18349	0.1877
0.3	0.1651	0.1649	0.1694	0.1681	0.1693	0.16806	0.1677
0.4	0.11793	0.11746	0.11784	0.1177	0.1247	0.1219	0.1201
0.5	0.06649	0.0597	0.0601	0.0592	0.06074	0.05989	0.0624
0.6	0.020977	0.00125	0.00323	0.03766	0.0019	0.0077	0.0039
0.7	0.05329	−0.05339	−0.5399	−0.05359	−0.0569	−0.055	−0.0512

Table VI

η_n and $[\eta_n]$, $n = 34$, for the scattering of positrons by atomic hydrogen (second investigation)

k (au)	Kohn's method		Rubinow's method		LSM	
	η_n	$[\eta_n \cdot 09]$	η_n	$[\eta_n]$	η_n	$[\eta_n]$
0.01	0.01627	0.01629	0.0184	0.0189	0.0189	0.0188
0.1	0.1514	0.1505	0.1456	0.1457	0.1446	0.1428
0.2	0.1898	0.1883	0.1857	0.1856	0.1831	0.1800
0.3	0.1627	0.1622	0.1682	0.1627	0.1631	0.1529
0.4	0.1284	0.1290	0.1177	0.1129	0.1133	0.1085
0.5	0.0682	0.0602	0.0599	0.0546	0.0568	0.05054
0.6	0.0039	0.0029	0.0038	0.006	0.00374	0.00347
0.7	−0.065	−0.0621	−0.0533	−0.0614	−0.0622	−0.0719

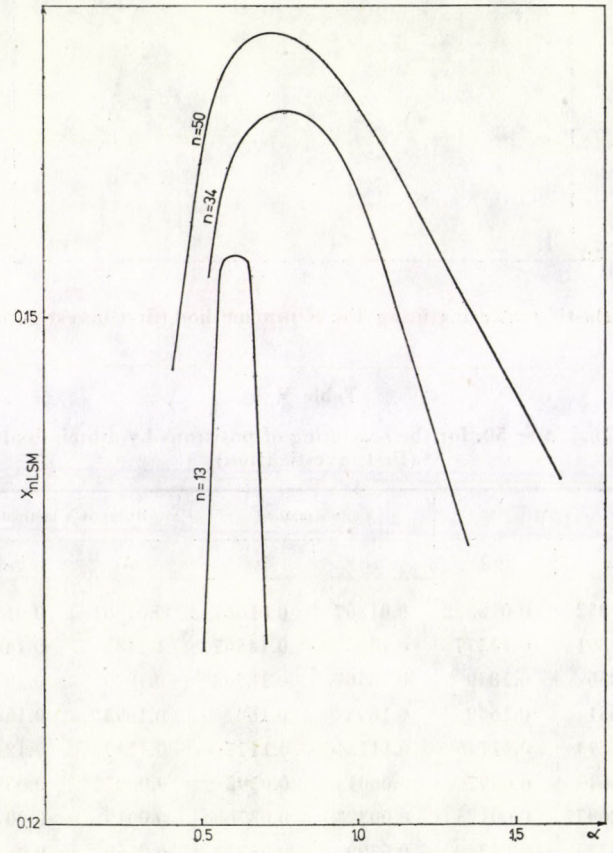

Fig. 6. e^+—H elastic scattering using the Rubinow method (first investigation), at $k = 0.3$

superposition of Φ_0 and the usual components of SCHWARTZ [28]. In the second investigation we chose $a_0 = \alpha_2 = 0$. Formulae (4), (5) and (6) are used for determining the x_n's corresponding to the methods of KOHN, RUBINOW and the LSM, respectively. The corrected phase shifts are obtained from Eq. (8).

The results of the above mentioned two investigations can be summarized in the following points:

1) The distortion* in the trial expansion and test-function spaces due to Φ_0 leads to large contribution and is enough for $k \leq 0.3$ to change x_n from negative to positive (compare with MOTT and MASSEY [29], p. 552). On adding more Hilbert-space vectors $|\chi_i\rangle$'s the effect of this distortion diminishes and the results converge to those of BHATIA et al [30].

2) The variation of x_n with $\alpha(\alpha = \alpha_1 = \alpha_2$, in the first investigation and $\alpha = \alpha_1$ in the second) yields in the LSM, at different values of n, smooth curves which show a monotonic convergence to certain value. The conventional pseudoresonances of KOHN's and RUBINOW's methods appear at different conditions. (In Figs. 4, 5 and 6 we demonstrate this variation for $k = 0.3$).

3) The best value of β (Eq. 10e, corresponding to the second investigation) is found to be $\beta \sim 0.5$, i.e. when $e^{-\beta r_{12}}$ is very close to the ground-state wave function of the positronium.

4) The best phase shifts of the present work (see Tables V and VI) are close to those of BHATIA et al. [30]. They emphasize the use of positronium function for dealing with e^+ — atom scattering processes.

Acknowledgement

I am very grateful to Prof. Dr. K. WILDERMUTH, Prof. Dr. E. SCHMID and Prof. Dr. TH. KANELLOPOULOS for generous help and kind guidance. I am also very indebted to Fr. Dr. E. KANELLOPOULOS for valuable communications.

REFERENCES

1. K. LADANYI and T. SZONDY, Nuovo Chim., **B5,** 70, 1971.
2. K. LADANYI, V. LENGYEL and T. SZONDY, Theor. Chim. Acta, **21,** 176, 1971.
3. E. SCHMID and K. HOFFMANN, Nucl. Phys., **A175,** 443, 1971.
4. E. SCHMID and J. SCHWAGER, Nucl. Phys., **A180,** 434, 1972.
5. E. SCHMID, Acta Phys. Austr. Suppl., IX, 44.
6. E. SCHMID, Nuovo Cim., **A18,** 771, 1973.
7. I. WLADAWSKY, J. Chem. Phys., **58,** 1826, 1973.
8. J. SCHWAGER and E. SCHMID, Nucl. Phys., **205A,** 168, 1973.
9. J. SCHWAGER, Nuovo Cim., **18A,** 787, 1973.
10. R. MADER, Ph. D. Thesis, Inst. f. Theor. Physik, Tübingen Univ., FRG.
11. L. HULTHEN, K. Fysiogr. Sallsk. Lund Förh, **14,** 257, 1944.
12. W. KOHN, Phys. Rev., **74,** 1763, 1948.
13. S. RUBINOW, Phys. Rev., **98,** 183, 1955.

* All integrals which involve Φ_0 have been carried out numerically with an accuracy of the order of 10^{-8}.

14. J. ABDALLAH and D. TRUHLAR, J. Chem. Phys., **60**, 4670, 1974.
15. F. HARRIS and H. MICHELS, Phys. Rev. Lett., **22**, 1036, 1969.
16. F. HARRIS and H. MICHELS, Meth. Comput. Phys., **10**, 143, 1971.
17. R. NESBET, Phys. Rev., **A175**, 134, 1968.
18. R. NESBET, Phys. Rev., **A179**, 60, 1969.
19. R. NESBET and E. OBEROI, Phys. Rev., **A6**, 1855, 1972.
20. R. OBEROI and R. NESEBT, Phys. Rev., **A8**, 215, 1973.
21. M. A. ABDEL-RAOUF and D. BELSCHNER, J. Phys., **B11**, 3677, 1978.
22. E. KANELLOPOULOS, TH. KANELLOPOULOS and K. WILDERMUTH, Com. math. Phys., **24**, 233, 1972.
23. M. A. ABDEL-RAOUF, J. Phys., **B12**, (to be published).
24. F. MALIK, Ann. Phys. (N. Y.), **20**, 464, 1962.
25. K. TAKATSUKA, and T. FUENO, Phys. Rev., **A19**, 1011, 1979.
26. A. H. MOUSSA, Proc. Phys. Soc., **74**, 101, 1959.
27. A. H. MOUSSA and M. A. ABDEL-RAOUF, Physica, **68C**, 195, 1973.
28. C. SCHWARTZ, Phys. Rev., **124**, 1468, 1961.
29. N. MOTT and H. MASSEY, The Theory of Atomic Collisions, 3*d* Ed., Oxford University Press, Oxford, 1965.
30. A. BHATIA, A. TEMKIN, F. DRACHMAN and H. EISERIKE, Phys. Rev., **A3**, 1328, 1971.

Acta Physica Academiae Scientiarum Hungaricae, Tomus 48 (1), pp. 43—55 (1980)

PHOTOGENERATION OF CHARGE CARRIERS IN ORTHORHOMBIC SULPHUR

By

M. SALEH

DEPARTMENT OF PHYSICS, UNIVERSITY OF SANA'A, SANA'A, YEMEN ARAB REPUBLIC

(Received in revised form 9. X. 1979)

The photogeneration efficiency of electrons and holes has been studied in orthorhombic sulphur crystals using fast excitation light pulses in the range of 2.0 to 6.0 eV. At photon energies below 3.6 eV, electron and hole generation is confined to the surface region. It may be associated with discrete centres and exciton diffusion. At photon energies above 3.6 eV, electron and hole generation rises sharply and tends towards unit quantum efficiency near 4.9 eV. Detailed measurements of the absorption coefficient at photon energies in the range from 2.0 to 3.9 eV and the reflectivity up to photon energies of 6.0 eV have also been made. The results are interpreted by a model in which two components, a photoconductive and a non-photoconductive one contribute to the optical properties. It is suggested that the Gaussian band characterizing the non-photoconductive process is associated with localized excitons which are formed by electronic transitions coupled linearly to the vibrational modes. The photoconductive component of the absorption, as well as photogeneration and reflectivity data place the onset of direct transition near 4.2 eV, and suggest that the previously assigned value of 2.5 eV is incorrect.

1. Introduction

The spectral dependence of the photoconductivity of orthorhombic sulphur has been investigated by KURRELMEYER [1] in the spectral range between 1.9 and 3.0 eV. He found that the steady photocurrent was ohmic up to the maximum applied field of 15 kV cm^{-1} and directly proportional to the intensity of illumination. He obtained a smooth response curve with a maximum at 2.63 eV, but estimated that even at the peak, the quantum efficiency of carrier generation was far below unity. The experiments of TARTAKOVSKY and REKALOVA [2] led to substantially similar results. On the basis of these results, and of resistivity measurements, MOSS [3] concluded that a value of about 2.5 eV should be assigned to the intrinsic band gap of orthorhombic sulphur. MEAD [4] concluded from his experimental results that the intrinsic band gap for orthorhombic sulphur was 3.82 eV.

A detailed interpretation of steady photoconductivity measurements on a highly insulating material such as orthorhombic sulphur is often complicated by the build-up of internal space charge and by electrode effects. These difficulties are largely overcome by the use of drift method [5, 6] in which the carriers produced by a fast excitation pulse are separated by a bias field and collected at external electrodes (see Section 2).

Absorption and reflectivity measurements have also been made on orthorombic sulphur in order to obtain further information about the mechanism of photogeneration (see Sections 3.2 and 3.3).

2. Experimental

2.1 *Preparation of specimens*

The crystals for investigation were grown from a solution of sulphur in CS_2, using both analytical grade and reagent grade laboratory reagents. Platelets with natural (111) faces of about 1 cm^2 area and thickness varying between 200 μm and 600 μm were obtained from a shallow pool of the solution on a horizontal glass plate. Thin specimens were also cut from large crystals of the bi-pyramidal habit grown by normal crystallization from volume. All the results for single crystals given in the following sections refer to platelets with (111) faces.

Specimens were prepared for the photoconductive measurements by evaporating either circular semi-transparent gold electrodes or a number of thin, closely spaced gold strips, onto each face in turn. The transmission of the semi-transparent gold was measured on a dummy layer produced on a glass slide in the same evaporation, so that in the subsequent experiments the absorption and reflection at the electrode could be allowed for. An appropriate correction was also applied in the case of the strip electrode.

2.2 *Apparatus and method*

A schematic diagram of the experimental arrangement is shown in Fig. 1. Both steady and transient photoconductive measurements were made with an Optica grating monochromator in the range of photon energies from 2.0 to 6.0 eV. For the transient measurements the steady sources were replaced by a Xenon flash tube for work in the visible region, and by a spark gap or mercury flash tube for the ultra violet. The number of photons per pulse (or per sec) indicent on the specimen was determined at each wavelength by means of a calibrated vacuum photocell.

Suppose electron-hole pairs are generated in a thin region close to the front electrode by a strongly absorbed light pulse. Depending on the polarity of the applied field F, either holes or electrons can be drawn across the specimen. The method of measurement used in the following experiments depended on the type of carrier under investigation. For holes, the transit times were of the order of a few μs, and it was more convenient to integrate the charge displacement of the hole carriers drifting towards the back electrode. A typical oscilloscope trace is shown in Fig. 2(a) which gives directly the transit time t_h. This shape is consistent with the excitation and subsequent drift of a domain

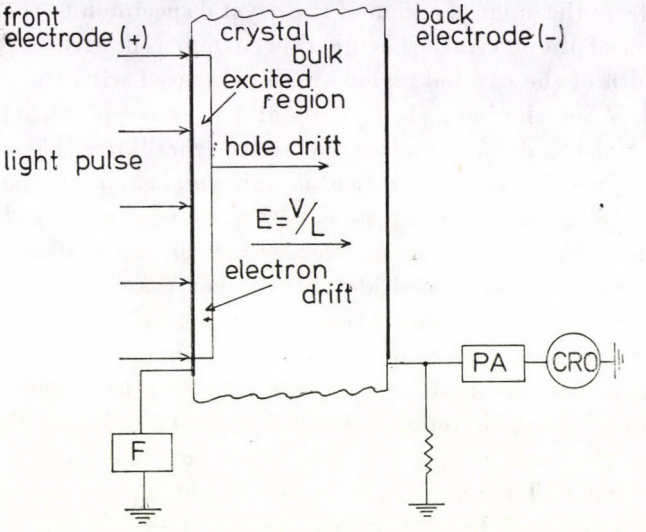

Fig. 1. Experimental arrangement for the determination of carrier mobilities and the number of photo-excited carriers in orthorhombic sulphur crystal. F provides steady or pulsed fields and the transit of generated carriers is observed on the oscilloscope. P.A. is preamplifier.

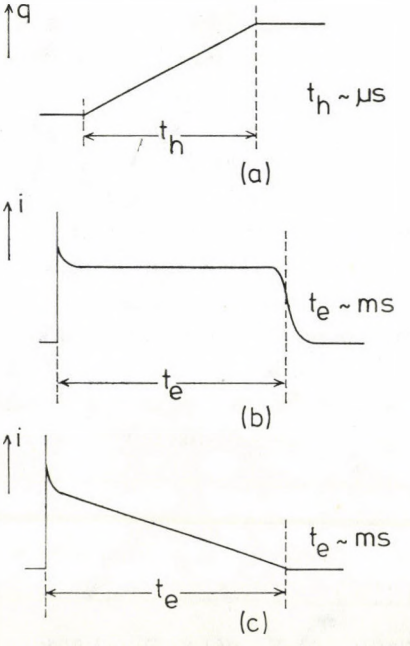

Fig. 2. (a) Integrated transit for generated holes. t_h is the observed transit time, (b) Current pulse showing transit of electrons generated near the front electrode, (c) Expected electron signal when carriers are generated uniformly throughout the crystal specimen volume

of carriers from the excited region of the crystal specimen to the back electrode, the duration of the excitation being short compared with the transit time t_h, and the width of the excited region small compared with the crystal specimen thickness d. When the back electrode is at a negative potential V with respect to the front electrode, the end of the ramp (the "knee") corresponds to the hole transit time. Providing the field is uniform, i.e. space charge is negligible, the hole mobility is given by $\mu_h = d^2/Vt_h$. t_h was always found inversely proportional to V, thus confirming the assumption of a uniform field. Moreover, as the lifetime of holes is considerably longer than t_h, the total number of holes drawn out of the generation region near front electrode can be determined directly from the pulse height at $t \geqslant t_h$ and the charge sensitivity of the detecting equipment. In the case of electrons, transit times were of the order of ms range, and it was, therefore, more convenient to display the current signal Fig. 2(b) on the oscilloscope. Fig. 2(b) represents the current flowing during the transit time t_e. The sharp spike at the beginning of the pulse is due to the reverse movement of holes towards the front electrode. From the steady current level and the transit time t_e the total number of electrons drawn out of the generation region can be obtained and also the electron mobility $\mu_e = d^2/Vt_e$, where the back electrode is at a positive potential V with respect to the front electrode.

To determine the quantum efficiency of carrier generation it was essential to work under saturation conditions, so that it could be assumed that every carrier generated in the region near front electrode had been drawn out of the specimen. Pulse measurements at saturation field strengths $\sim$75 kV cm^{-1} tended to be rather noisy on most specimens and the following experiments were normally made at about 15 kV cm^{-1} and then corrected to the saturation value. It was also found that in both the visible and ultra-violet spectral regions the number of carriers generated was directly proportional to the number of photons in the flash and all measurements were normalized to the photoresponse per incident photon (see Section 3). Moreover, in these experiments, an effective precaution was taken to keep the number of carriers generated per pulse below 10^8 in order to prevent the build-up of an appreciable trapped space charge. In case of a steady flash rate, the field pulses were synchronized to allow several discharge flashes at zero field between successive transits.

3. Results

3.1 *Photogeneration of charge carriers*

The spectral dependence of photogeneration of charge carriers has been investigated by the methods described in Section 2 and the experimental results for one of the specimens are shown in Fig. 3. The logarithmically

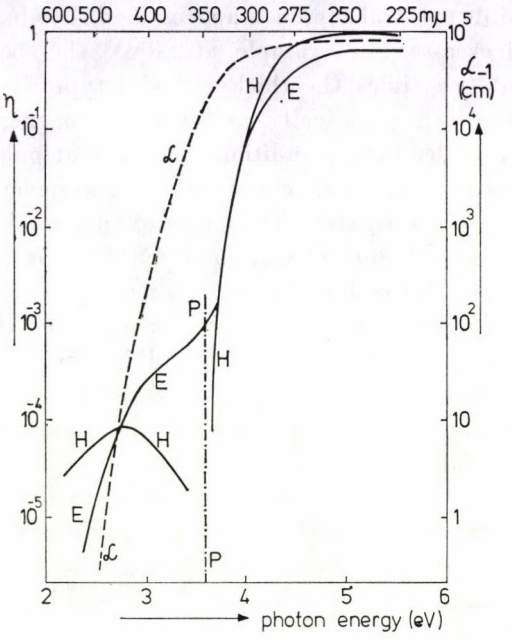

Fig. 3. Spectral dependence of the photogeneration of electrons (curve E) and holes (curve H) The dotted line represents the absorption coefficient (see right hand ordinate).

plotted ordinate η represents the quantum efficiency of carrier generation and is defined as the number of electrons (curve E) and holes (curve H) produced per incident photon, allowing for reflection and absorption at the semitransparent front electrode. The absorption coefficient α at various photon energies (dotted curve) is also shown in Fig. 3.

The characteristic features of the experimental results may be summarized as follows:

(a) The electron and hole mobilities for the spectral range investigated are 5.5×10^{-4} cm^2 s^{-1} V^{-1} and 4.5 cm^2 s^{-1} V^{-1} respectively at room temperature.

(b) It is evident, particularly from the results for holes, that there are at least two distinct carrier generation mechanisms. This is shown in Fig. 3 by the dotted line *P*, the transition occurs near 3.6 eV. To the left of *P*, for photon energies below 3.6 eV, the results suggest that fundamentally different generation mechanisms occur. However, for photon energies greater than 3.6 eV, the efficiency of both the electrons and hole generation rises sharply and approaches unit quantum efficiency at about 4.9 eV. The experimental difference between the *E* and *H* curves in that range has been found with most of the specimens. This may be partly due to the saturation correction, which in the case of electrons was less certain than for holes.

(c) As the visible spectral region is approached the absorption within the specimen rapidly decreases. For example, at 2.8 eV, the absorption depth can be seen to be about five times the thickness of a typical specimen (210 μm) and one would expect a practically uniform photogeneration throughout the crystal volume. Under these conditions the current pulse response should have the shape shown in Fig. 2 (c). However, this has never been observed on any of the specimens investigated. The pulse shapes for electrons were still like those of Fig. 2(b) and showed convincingly that the photogeneration at energies below that of P is confined to a region near the front electrode having a depth small compared to the specimen thickness. The same conclusion was reached for the hole generation. It was found in experiments with weakly absorbed light that the efficiency of photogeneration of electrons and holes near the front and back surface was practically the same, provided a platelet with two natural surfaces was used. If one of the surfaces was now ground with fine carborundum powder and the electrode re-evaporated, the photoresponse from this surface disappeared almost completely. For instance, in one experiment this treatment of the back surface of the specimen reduced the electron and hole generation near the back electrode by factors of 4 and of 50, respectively.

(d) Electrons and holes appear to be generated in this spectral region by different mechanisms. Fig. 3 shows that η for electrons at low photon energies rises nearly parallel to the absorption curve for over an order of magnitude. On the other hand, there appears to be little correlation between the hole response and the absorption curve in this spectral range. At energies below 2.8 eV, hole generation remains considerably more efficient than electron generation. But, above 2.8 eV, it actually decreases with increasing absorption. η values for holes in the region of P lay below the limit of detection of the measuring equipment.

3.2 *Absorption measurements*

In order to obtain further information about the mechanism of photogeneration, a fairly detailed investigation of the absorption coefficient of orthorhombic sulphur in the spectral range from 2.0 to 3.9 eV has been made. In these experiments the Optica grating monochromator was used in conjunction with an 11-stage E.M.I. photomultiplier. The experimental results for 6 of the specimens are shown in Fig. 4. Single crystals within a thickness ranging from 85 μm to 2.55 cm were used for these measurements up to photon energies of 3.2 eV, where $\alpha \sim 10^3$ cm^{-1}. At the lower photon energies a reflectivity correction was applied. Above 3.2 eV, even the thinnest crystal became too opaque for reliable measurements and, therefore, the range was extended using

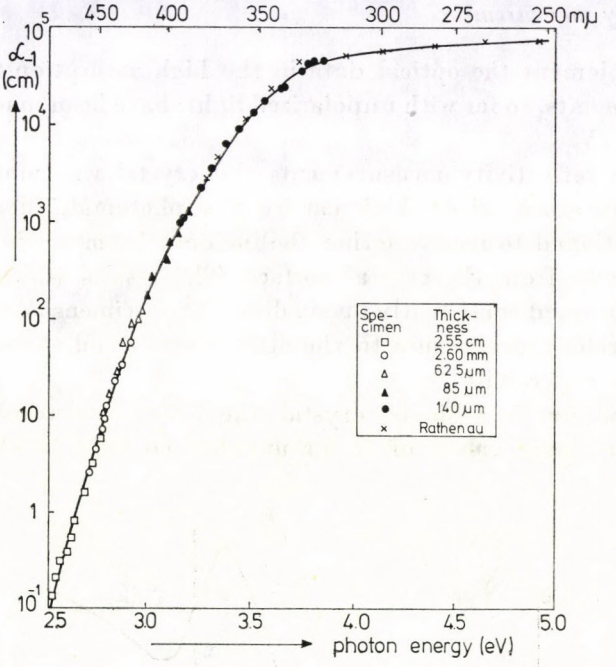

Fig. 4. Absorption coefficient for six of the specimens investigated. For $\alpha > 10^3$ cm^{-1} polycrystalline layers were used. The results of RATHENAU [7] have been fitted to the curve at higher photon energies

thin polycrystalline layers. These were produced by pressing a molten globule of sulphur between two thin, cleaved mica sheets. Since the thickness of the sulphur layer was unknown, the relative absorption values were fitted to single crystal values around 3.2 eV which resulted in a smooth transition between the two sets of points. In this way, the measurements were extended up to absorption levels of 5×10^4 cm^{-1}.

The only other experimental work in this spectral range is that of RATHENAU [7], who obtained by a photographic method the relative absorption constant of evaporated sulphur films up to 1600 Å. A number of his points, fitted to the results at 3.27 eV, are shown in Fig. 4. It is obvious from Fig. 4 that these points are in fair agreement with the measurements and confirm the levelling out of the curve between 3.76 eV and 3.86 eV. It seemed, therefore, reasonable to extend the absorption curve towards higher photon energies on the basis of RATHENAU's experimental results. It is of interest to note that his curve shows a further sharp rise in absorption near 7.0 eV.

A number of absorption runs up to $\alpha \sim 10$ cm^{-1} were made on single crystals at a temperature of 85 K. The absorption curve was found to shift towards the higher photon energies, but no structure could be detected.

3.3 *Reflectivity measurements*

To supplement the optical data in the high absorption region, reflectivity measurements, so far with unpolarized light, have been made up to photon energies of 6 eV.

For the reflectivity measurements the crystal was mounted near the centre of a rotating table which carried the photomultiplier. The detector could be positioned to receive either the incident beam or the light reflected almost normally from the crystal surface. The results which are shown in Fig. 5 were obtained consistently on six different specimens and did not change with time. Prolonged exposure to the atmosphere could therefore have little effect on the reflectivity.

Since sulphur is a biaxial crystal, the reflectivity results can only be regarded as average values of R for unpolarized light incident on a (111)

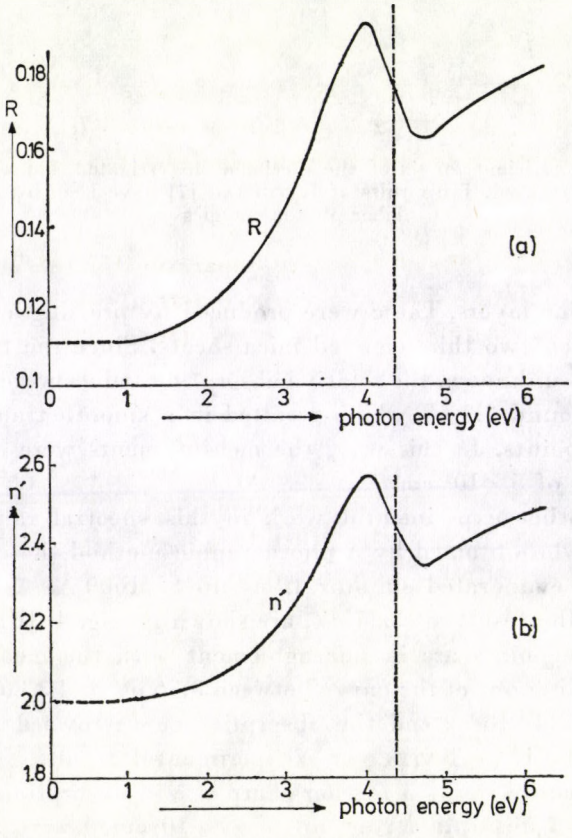

Fig. 5. (a) Reflectivity coefficient for unpolarized light incident on a (111) plane, (b) Average value of the refractive index in the (111) plane as calculated from reflectivity and absorption results

plane. An approximate value of the refractive index n' has been calculated from the reflectivity by the relation

$$R = \frac{(n' - 1)^2 + k^2}{(n' - 1)^2 + k^2},$$

where $k = \alpha\lambda/4\pi$ denotes the extinction coefficient.

Fig. 5(a) shows the reflectivity coefficient R for unpolarized light incident on a (111) plane and Fig. 5 (b) represents the average value of the refractive index n' in the (111) plane as calculated from reflectivity and absorption results. Both the R and n' curves possess a similar shape and show a typical anomalous dispersion curve superimposed on a rising background. The latter would be consistent with the presence of a second absorption band at higher photon energies. RATHENAU's results suggests that this could well be the band beyond 7.0 eV. The dispersion curve is centred at 4.35 eV (see Fig. 5) and an estimate based on dispersion theory suggests that the oscillator giving rise to the transition should be located close to this energy.

4. Discussion

To understand the mechanism of photogeneration and absorption in orthorhombic sulphur, let us consider the two related characteristics of the results mentioned in Section 3 which are of central importance. The first is the surprising width in energy of the absorption edge. That is, around $\alpha \sim 10^3 \text{cm}^{-1}$ the absorption increases by a factor e for an increase in photon energy of over 2 kT. The second is the pronounced separation in energy between the photoconductive and the absorption edge. Referring to Fig. 3, appreciable photoconductivity can be observed only at absorption levels above 10^4 cm^{-1}. The same two features have been observed in the case of vitreous Se by HARTKE and REGENSBURGER [8].

The interpretation regarding the above mentioned results is based on a model in which two independent absorption processes contribute to the optical properties. One is attributed to a photoconductive process which is represented by the superscript P, and the other to a non-photoconductive process denoted by the superscript N. A convenient optical constant to consider in this connection is the imaginary part of the complex dielectric constant, $\varepsilon_2 = 2nk$. The reason si that absorption processes expressed in terms of ε_2 are additive, a property which the coefficient α does not possess. According to HARTKE and REGENSBURGER [8], the P and N processes can be related to the photoconductive property η by

$$\varepsilon_2^P = \eta\varepsilon_2$$

and

$$\varepsilon_2^N = (1 - \eta)\,\varepsilon_2\,,$$

where ε_2 represents the measured value.

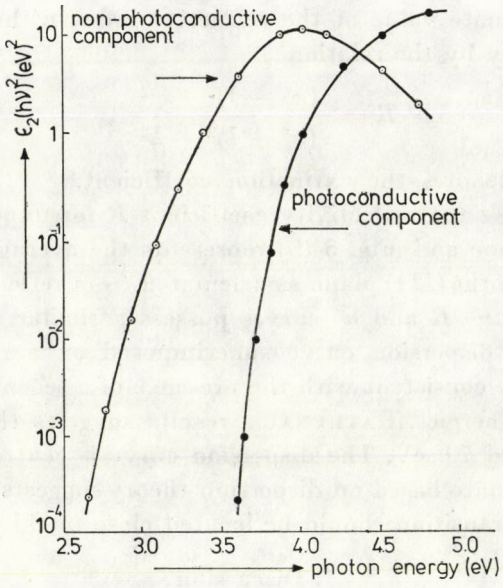

Fig. 6. **Photoconductive and non-photoconductive components of the absorption. The plotted ordinate is proportional to the transition probability and has been calculated from the experimental data. Points represent a Gaussian curve of half width 0.75 eV.**

Using the values of η (for holes), α and n' obtained in Section 3, the dependence of ε_2^P and ε_2^N on photon energy has been calculated. The normalized transition probability is proportional to $\varepsilon_1(h\nu)^2$ and in Fig. 6 this parameter is plotted against photon energy for both the P and N processes. The non-photoconductive absorption leads to a broad band centred about 4.02 eV with a half width of 0.75 eV. It should be noted that within experimental error it possesses a Gaussian distribution shape for over 5 orders of magnitude as is shown by the calculated points in Fig. 6. The measured absorption edge does not, therefore, satisfy URBACH's Rule [9]. This empirical relation predicts the typical exponential edge which represents with remarkable accuracy the absorption edges of alkali halides [10] and also of vitreous Se [8]. Apart from this difference, the results shown in Fig. 6 for the P and N components resemble closely those of HARTKE and REGENSBURGER for vitreous Se [8].

It is suggested that the band found here is associated with localized excitons which are momentarily 'self-trapped', most likely on an S_8 ring. The width of the band requires fairly strong exciton-phonon coupling. If the exciton is formed predominantly by the interaction of vibrational modes coupled linearly to the electronic transition, then the strictly Gaussian shape would be explainable [10]. In the model developed by TOYOZAWA [11], additional quadratic coupling is assumed, which then leads to an exponential band edge at lower absorption levels, in agreement with URBACH's Rule [9]. It appears on the

basis of the present results that the quadratic coupling is small as compared to the linear one.

The curve marked P in Fig. 6 represents the absorption leading to the photogeneration of holes. The square of the ordinate $[\varepsilon_2^P(h\nu)^2]^2$, has been plotted in Fig. 7 on a linear scale against photon energy for values in the highly absorbed region between 4.0 and 4.8 eV. It can be seen that above 4.3 eV the experimental points lie on a straight line which, when extrapolated, gives a photon energy of 4.22 eV. Although there exists some uncertainty about the fitted absorption data used in this range, it nevertheless seems reasonable to identify the above energy with the onset of allowed direct transitions.

It is obvious that the model used by HARTKE and REGENSBURGER [8] leads to a consistent, though still somewhat tentative, interpretation of photogeneration and absorption in orthorhombic sulphur. The onset of direct transition (Fig. 7), the information from the reflectivity measurements (Fig. 5) and the value of $1/2\eta$ (Fig. 3), all lead to activation energies between 4.2 and 4.3 eV for the intrinsic photogeneration mechanism.

It is, therefore, suggested that the value of 2.5 eV deduced by Moss [3] for the intrinsic edge of crystalline sulphur is incorrect. Steady photoconductive measurements on sulphur in the visible region by KURRELMEYER and TARTAKOVSKY [1, 2] are substantially in agreement with the hole response peak shown in Fig. 3 and correspond to quantum efficiencies below 10^{-4}.

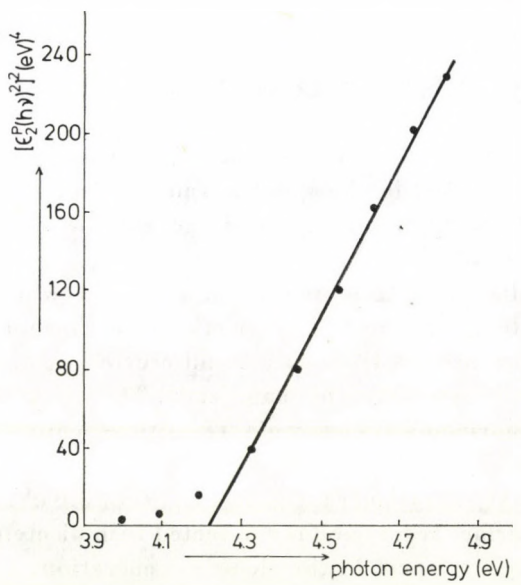

Fig. 7. Square of transition probability for photoconductive process plotted against photon energy

Finally, the carrier generation in the spectral range below 3.6 eV (see Fig. 3) will be discussed. Since an intrinsic mechanism can be excluded in this spectral range, the generation is likely to be associated with discrete centres. This is not in contradiction with the experimental results summarized under (*c*) in Section 3.1, for the density of imperfection centres is generally higher near the surface than in the crystal volume and, in addition, surface states may be present. It is suggested that at the smallest photon energies where only holes are generated, the radiation causes a transition from the valence band into discrete states which occur in sufficient density only near the surface. This leads to a free hole and a trapped electron.

It is possible that the correlation between the E and α curves below 2.7 eV might imply a connection between electron and excitation generation. The excited molecular state can diffuse during its lifetime and may interact with an electron trapped in the surface region. The energy transferred could raise the electron into a conducting state, so that such a mechanism would be consistent with the simultaneous rise of absorption and electron response, and also with the low efficiency of the latter.

A considerable amount of evidence exists in the case of organic molecular crystals, particularly anthracene, that the surface region is the predominant site of carrier generation [12]. Electron bombardment studies by SALEH [6, 13, 14] showed that exciton diffusion plays an important part in this process. However, there is still inadequate evidence for such a mechanism in the case of orthorhombic sulphur and it is desirable to take the above suggestion in a qualified way.

5. Conclusions

(a) An analysis based on photogeneration, absorption and reflectivity data orthorhombic sulphur in the spectral range from 2.0 to 6.0 eV indicates that the activation energy for an intrinsic generation of electrons and holes lies between 4.2 and 4.3 eV.

(b) The results are interpreted by a model in which two absorption processes contribute to the optical properties of orthorhombic sulphur. The non-photoconductive process leads to a band centred at 4.02 eV possessing a Gaussian shape over five orders of magnitude. This may be associated with localized excitons formed by electronic transitions coupled linearly to the vibrational modes.

(c) In the weakly absorbed range, that is, below 3.6 eV, carrier generation is confined to the surface region and is connected with discrete centres. Exciton diffusion seems to play a part in the electron generation.

Acknowledgement

Dr. M. SALEH wishes to thank the Chairman, Department of Physics, University of Multan, Multan, Pakistan for providing him with the facilities for conducting the experimental work.

REFERENCES

1. B. KURRELMEYER, Phys. Rev., **30**, 893, 1927.
2. P. TARTAKOVSKY and G. REKALOVA, J. Exp. Theor. Phys., **10**, 1025, 1940.
3. T. S. MOSS, Photoconductivity in the Elements, pp. 180—184. Butterworths, London, 1952.
4. C. A. MEAD, Phys. Lett., **11**, 212, 1964.
5. W. E. SPEAR, Proc. Phys. Soc., **B70**, 669, 1957; J. Non Cryst. Solids, **1**, 197, 1969.
6. M. SALEH, J. Phys. C.: Solid State Phys., **9**, 4165, 1976.
7. G. RATHENAU, Physica, Eindhoven, **3**, 42, 1936.
8. J. L. HARTKE and P. J. REGENSBURGER, J. Phys. Rev., **139**, A970, 1965.
9. F. URBACH, Phys. Rev., **92**, 1324, 1953.
10. H. MAHR, Phys. Rev., **132**, 1880, 1963.
11. Y. TOYOZAWA, Progr. Theor. Phys. (Kyoto), Suppl., **12**, 111, 1959; Tech. Report Inst. Solid St. Phys. (Univ. of Tokyo) Ser. A., No. 119, 1964.
12. M. SALEH and M. S. ZAFAR, Acta Phys. Hung., **45**, 233, 1978.
13. M. SALEH, Japanese Journal of Applied Phys., 17, No. 6 (June), 1978.
14. M. SALEH, Physica Scripta (Sweden), **19**, 54, 1979.

Acta Physica Academiae Scientiarum Hungaricae, Tomus 48 (1), pp. 57—67 (1980)

EXPERIMENTAL INVESTIGATION OF ANOMALOUS MAGNETORESISTANCE IN MONOCRYSTALLINE LEAD SULPHIDE

By

T. PORJESZ, I. KIRSCHNER, M. F. KOTKATA,*
M. S. ZAGHLOUL,** G. KOVÁCS and P. DEBRECENI
DEPARTMENT FOR LOW TEMPERATURE PHYSICS, ROLAND EÖTVÖS UNIVERSITY, BUDAPEST, HUNGARY

(Received in revised form 16. X. 1979)

Investigation of galvanomagnetic effects was carried out in the temperature range of 1.5—350 K. The samples were made of *n*- and *p*-type PbS, cut off in different orientations and rotated in the magnetic field.

The reproducibility of the measurement and the stability of the temperature was better than 0.1 %.

The results show in the entire temperature range that the magnetoresistance contrary to accepted assumptions cannot be expressed in terms of only even powers of the magnetic field strength and a negative change appears as well.

Calculating the electron effective mass more precisely considering the electron motion in the *k*-space the experimental results could be explained in a simple way in the whole temperature range.

1. Introduction

PEIERLS [1] pointed out that magnetoresistance (MR) effects were essentially due to departure from the isotropic free electron model. Later NORDHEIM [2] and JONES [3] reported that MR is nonnegative and depends only on even powers of applied magnetic field which we call "the normal effect". However, SASAKI et al [4] found negative MR in heavily doped *n*-type Ge and also the non-even power dependence of MR on B for dilute-alloys and in heavily doped semiconductors at low temperature was observed [5—8]. This is the "anomalous MR".

The above mentioned anomalies are explained by different transport mechanisms taking into account impurity band conduction [5, 9], the hopping process [10, 11] and the localized spin model of TOYOZAWA [13—12]. In some cases different models are used simultaneously trying to avoid discrepancies between experiments and calculations. None of these models are capable to cover the observed effects in the entire temperature range i.e. the departure from the quadratic dependence of MR on B, and even its negativity appearing in special cases. Nevertheless, they complete the picture of electron transport in certain cases mainly at low temperatures.

* Physics Department, Faculty of Science, Ain-Shams University, Cairo, Egypt
** Physics Department, Faculty of Science, Al-Azhar University, Cairo, Egypt

We carried out our measurements on heavily doped PbS samples and got the anomalous MR as mentioned above. To explain the facts we used a simple band structure but we took into consideration the anisotropy of the effective mass of electrons consistently. In this way we could give an explanation for a permanently appearing part of the anomaly and this applies to the whole measurements range. For this we considered the electron motion in the real space and the k-space at the same time in the solutions of the Boltzman equations [14].

2. Experimental details

n- and p-type PbS crystals with carrier concentrations of 1.3×10^{19} and 1.6×10^{19} cm^3 respectively were used. (They had been grown at the Department of Semiconductor Physics of the Leningrad State University.) The shapes of the samples were the conventional bridgeform, and of dimensions of $10\times1.5\times0.6$ mm. They were cut off ultrasonically from the monocrystalline material into different orientations.

Surfaces were prepared with great care, and the contacts were made by different techniques. However, we did not find any effect of the contacts on the measurements as ANDRONIK et al [6] did.

We measured the Hall voltage and MR in the temperature range of 1.5—350 K. For doing this two types of cryostats were used. One of them was an Oxford Instruments type, CF 100, Variable Temperature Cryostat. The second one was built by us for the very low temperatures and with superconducting magnets.

In the cryostats the temperature was controlled and regulated by a high precision equipment made by us [15]. The stability of the temperature was better than 10^{-4} grad.

The magnetic field was measured by Hall-probe formerly calibrated with proton resnonance, to an accuracy of 0.5% and with homogeneity and reproducibility of 10^{-4}. Rorating the sample, the accuracy of determining the angle was 0.1 grad.

The resistivity was measured as a function of current at zero magnetic field, to control the ohmic character of the contact. The measurable voltage drops were in the order of 10 mV because of the high conducitvity of the heavily doped samples. The variation of the resistivity was in the order of 1%. Therefore, to distinguish the normal and anomalous magnetoresistivity, we had to measure a change less than 0.1%. This was 10^{-8} V in the worst case. These measurements were carried out by the d.c. method and with the aid of a Keithley 180 Digital Nanovoltmeter.

3. Experimental results

3.1. *Temperature dependence of* ϱ, R_H *and* μ_H

In Fig. 1 there are two sets of curves of resistivity ϱ, Hall coefficient R_H and Hall mobility μ_H corresponding to *n*- and *p*-type PbS specimens plotted as a function of temperature. It shows no variation in the Hall coefficient in the investigated temperature range of 1.5—300 K. This indicates that the concentration of the charge carriers does not depend on temperature. Such apparent constancy of R_H is confirmed by the earlier measurements of FINLAYSON and GREIG [16] made on *n*-PbS and shows the Hall coefficient to be roughly constant below the intrinsic range.

Quite recently FINLAYSON and JOHNSON [17] observed no significant change either in R_H on their *n*-type (10^{16}—10^{17} cm^{-3}) natural PbS crystals. Further, FINLAYSON and MATTHEWSON [18] gave 3.8×10^{-5} eV for the ionization energy, consequently, the observed decrease of ϱ and the constancy of R_H should be accompanied by a comparable increase in the mobility with decreasing temperature which is the present case in the graph of Fig. 1.

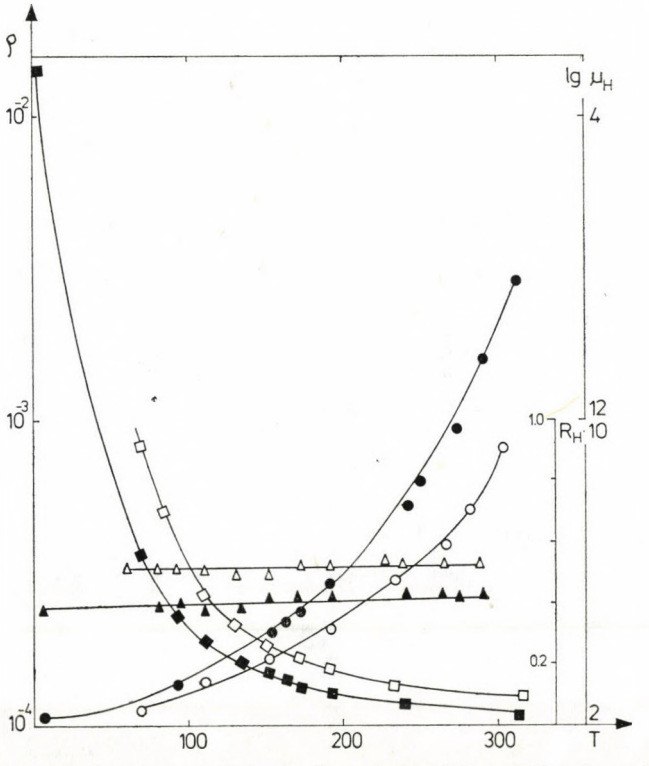

Fig. 1. Dependence of electric resistivity in Ω cm (○), Hall mobility in cm^2 V^{-1} sec^{-1} (□) and Hall coefficient in Coul cm^{-3} (△) on temperature. *Open symbols* *n*-PbS (1.3×10^{19} cm^{-3}), *Filled symbols*; *p*-PbS (1.6×10^{19} cm^{-3})

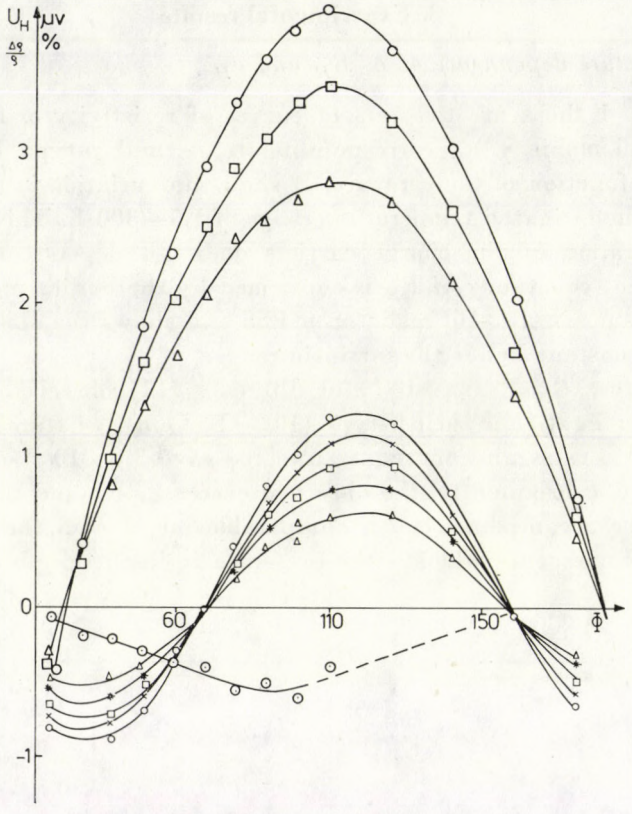

Fig. 2. The measured planar Hall voltage (U_H) and the calculated components of magnetoresistance $\Delta\varrho/\varrho_0$ as a function of angle between magnetic field and current direction for different field strengths. Symbols for calculated normal MR; ○ $B = 12$ kG, × $B = 11$ kG, □ $B = 10$ kG, ∗ $B = 9$ kG, △ $B = 8$ kG, ⊙ $B = 10$ kg calculated anomalous component Symbols for measured Hall field (U_H), ○ $B = 12$ kG, □ $B = 10$ kG, △ $B = 8$ kG

3.2. *Planar magnetoresistance and Hall effect*

The planar Hall voltage U_H as a function of the rotating angle Φ between B and I is given in Fig. 2. The measurements were made at 96 K and at different magnetic field strengths. Considering that

$$U_H = GIB^2 \sin(2\Phi - \vartheta)\,, \tag{1}$$

where G is the planar Hall coefficient. Fitting the experimental data, we got

$$U_H = 4.18 \sin(2\Phi - 15)\,, \tag{2}$$

where Φ and ϑ are measured in degree, and U_H in μV. We had to use for the fitting a phase angle ϑ in the above expressions to take into account the deviation of the current flow direction from the symmetry axis. We measured also

the MR in the same arrangement. It appeared from the Fourier analysis that the even terms of the series cannot describe the effect, inspite of the generally accepted theory, but the first two terms (not neglecting the first odd one) give a fairly good agreement. These two terms are drawn in Fig. 2 as well. The anomaly represented by the odd term is rather large. Moreover, from the planarly arranged measurements we concluded that the longitudinal MR and Hall effect are well measurable. It can be seen in Fig. 2 that the Hall voltage has a relatively high value. It shows at last that neither the conduction band nor the impurity band can be regarded as spherical. Measurements of the angular variation seem to indicate that the energy surfaces consist of ellipsoids of revolution along each cube axis. Since the normal component of $\Delta\varrho/\varrho_0$ must be symmetrical this MR is not affected by the reverse of the direction of the fields. Fig. 3 displays $\Delta\varrho/\varrho_0$ versus Φ for different field strengths.

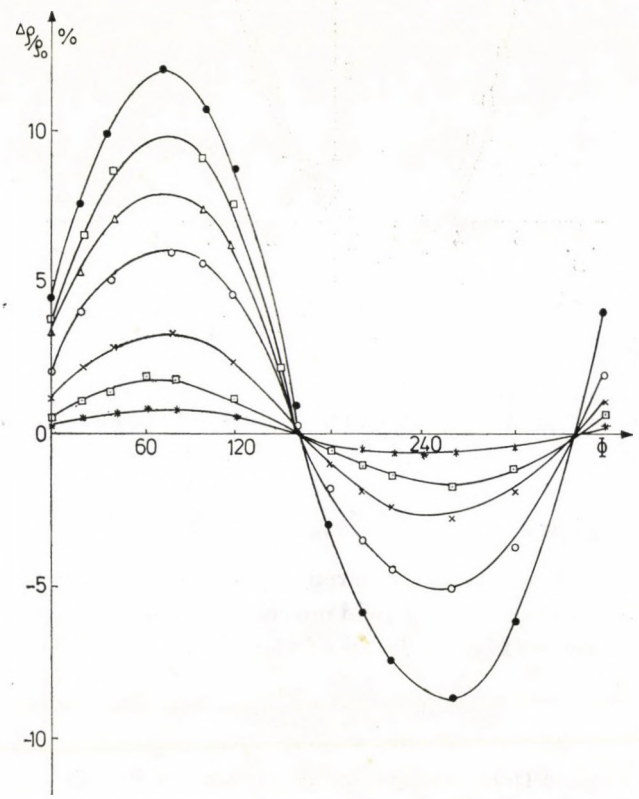

Fig. 3. Angular dependence of longitudinal magnetoresistivity at different field strengths for a temperature 96 K and 100 mA current passing through PbS sample of a resistance $9.7 \times 10^{-4} \pm 0.2\ \Omega$

Symbols: ● $B = 12$ kG, □ $B = 10$ kG, △ $B = 8$ kG, ○ $B = 6$ kG, × $B = 3$ kG, ⊡ B = 1.6 kG, ∗ B = 0.7 kG

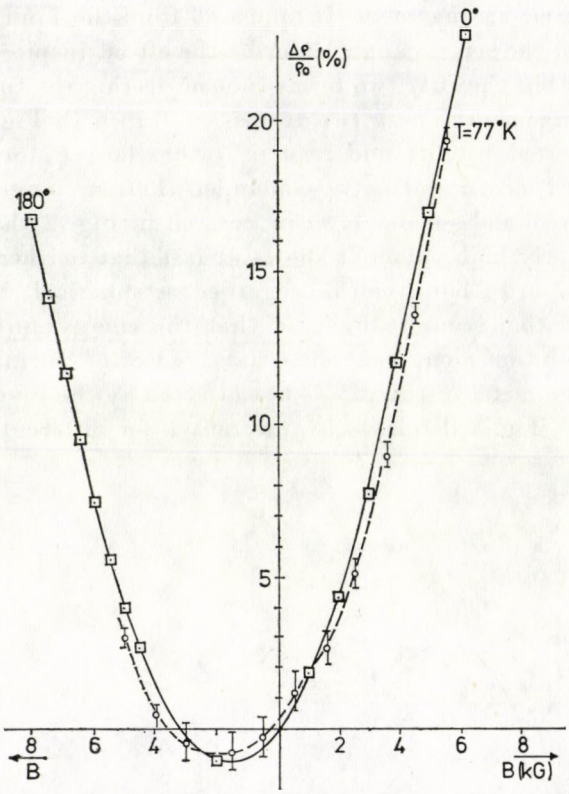

Fig. 4. Magnetoresistivity as a function of B, at a temperature of 77 K; ○ measured, ⊡ calculated

From this set of curves it is evident that the longitudinal Hall effect is affected by the reverse of B.

3.3. *Transversal effects*

Transversal MR was also measured for both n- and p-type PbS samples. In this arrangement the magnetic field moves in the plane perpendicular to the current density vector (Fig. 4). In all of the measurements we also examined the function of

$$\Delta\varrho/\varrho_0 = \Delta\varrho/\varrho_0(\Phi) \tag{3}$$

keeping the magnetic field strength as a parameter in this case. The results are shown in Fig. 5.

4. Discussion

To evaluate the data of the magnetic field dependence of MR, we used the following approximate expression

$$\Delta\varrho/\varrho_0(B) = a_0 + a_1 B + a_2 B^2 \tag{4}$$

and for the dependence of magnetoresistivity on the angle between the normal of the sample plane and **B** in the case of transverse MR and between **B** and **I** in the planar case we tried to fit Fourier series of the form:

$$\Delta\varrho/\varrho_0(\Phi_{\mathbf{B},\mathbf{I}}) = A_0 + A_1 \sin(\Phi + \vartheta_1) + A_2 \sin(2\Phi + \vartheta_2) \,. \tag{5}$$

By the terms with a_1, a_2, A_1, A_2 the experimental data could be represented within the experimental standard deviations. The a_1, $A_1 \sin(\Phi + \vartheta_1)$ terms show the anomalous character of the MR effect, and it was a surprise that

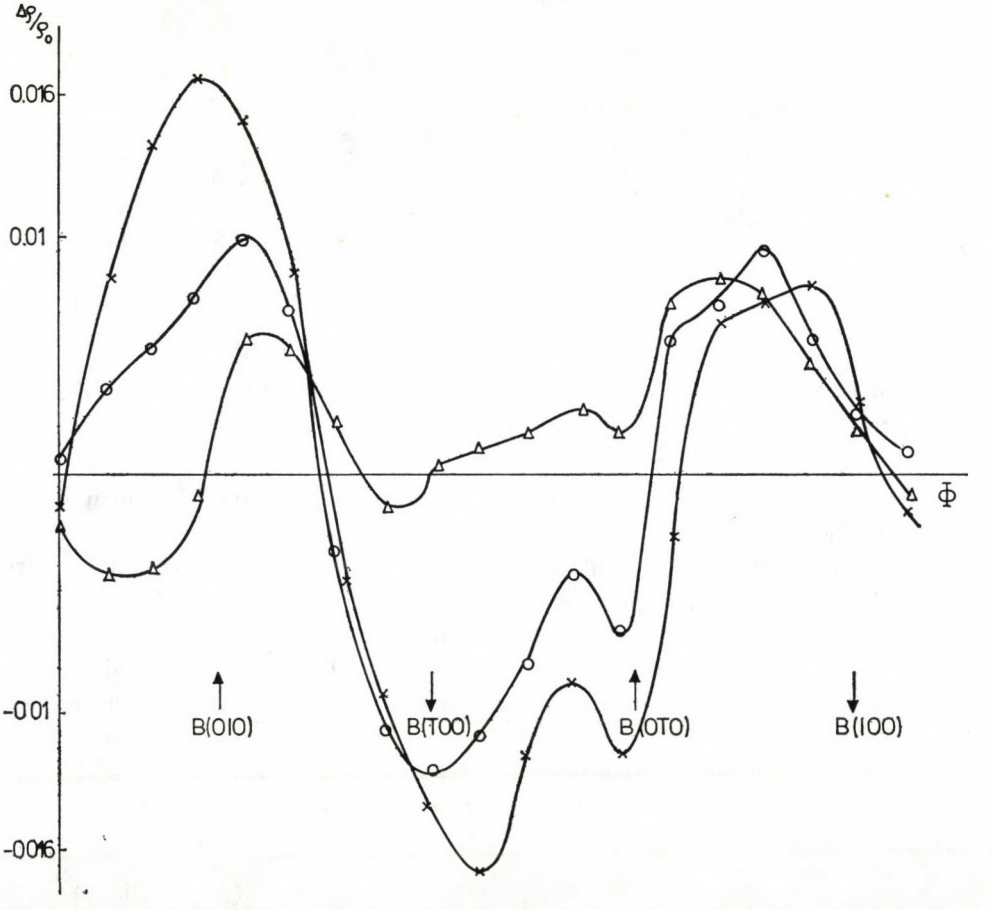

Fig. 5. Magnetoresistivity as a function of $\Phi_{\mathbf{B},\mathbf{I}}$, for $B = 5.6$ kG at temperatures: 133 K (×) 120 K (○) and 108 K (△)

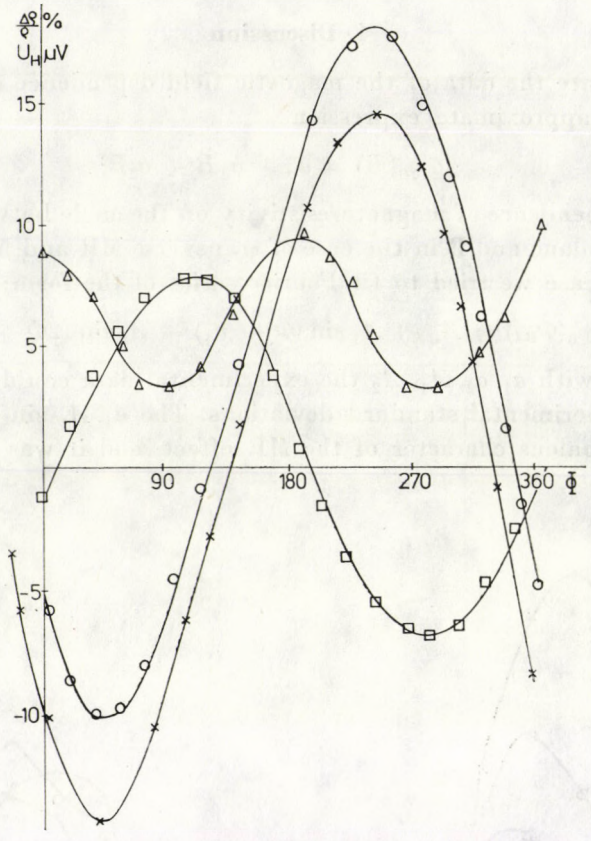

Fig. 6. Dependence of the measured magnetoresistivity (○) and Hall voltage (□) on the angle φ at 4.2 K, 100 mA current (1 ,0, 0) through PbS sample with $B = 3.2$ kG. The calculated anomalous $\Delta\varrho/\varrho_0(B)$ and the normal $\Delta\varrho/\varrho_0(B^2)$ components of magnetoresistance are represented by symbols (×) and (△), respectively

these anomalous odd terms turned out to be much higher than the normal ones in certain cases.

The measured and calculated curves for $\Delta\varrho/\varrho_0\,(B)$ and $\Delta\varrho/\varrho_0(\Phi_{B,I})$ are drawn in Figs. 4, 5, 6, respectively. We tried to explain the above mentioned features by considering the dynamical behaviour of the carriers. Therefore we looked up the motion of the carriers in the k-space, and took into consideration the effective-mass variation depending on the actual direction of the carrier motion.

The applied electric field and the Hall field cause a resultant drift field in the k-space, because of the effective-mass dependence on the direction as it can be seen from the equation for the effective-mass tensor elements

$$m_{ij}^{-1} = \frac{1}{\hbar^2} \frac{\partial^2 E}{\partial K_i \partial K_j} . \tag{6}$$

From the geometrical representation of a tensor we know that the actual value of the effective mass is the intersection of the direction of motion with the ellipsoid representing band minima. (This may be clarified by means of Figs. 7, 8, where we drew six ellipsoids of minimum energy, but we calculated for eight.) For the four-types of the eight ellipsoids we calculated separately the effective mass and in this way the mobility change, then we summed them up ($\mu_{\text{meff.}}(B, T) = \mu$):

$$\frac{1}{\mu} = \frac{1}{\mu_{[I,I,I]}} + \frac{1}{\mu_{[T,I,I]}} + \frac{1}{\mu_{[I,T,I]}} + \frac{1}{\mu_{[I,I,T]}} . \tag{7}$$

(One can mention that for example if the current flows along the bisector of the [1, 0, 0] and [1, 1, 0] orientations, in the plane (0, 0, 1) at a magnetic field strength of 1 kG the anisotropy for the effective mass will change by 15%.)

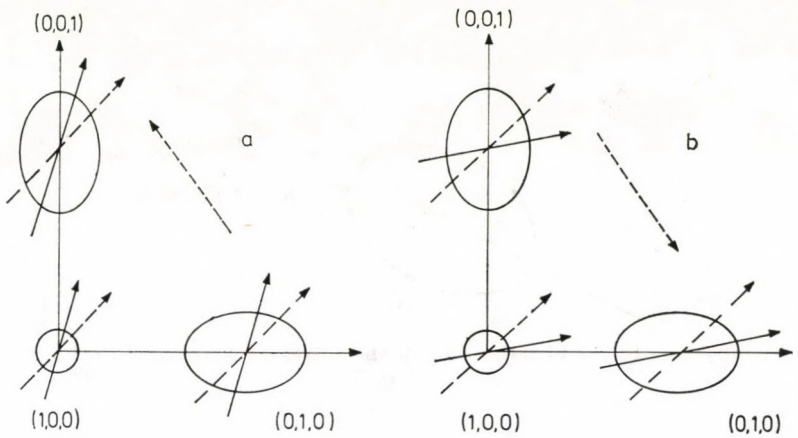

Fig. 7. Schematic demonstration of the drifting fields for the charge carriers with reversing the magnetic field. ——→ applied electric field, -----→ Hall field, ——→ direction of carrier motion along the ellipsoids

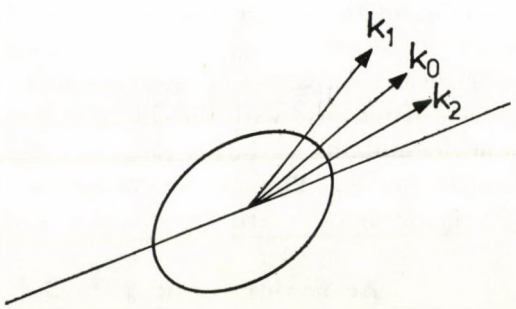

Fig. 8. The direction of the drifting field at different magnetic fields
k_0 corresponds to $I_{B(0)}$, k_1 corresponds to $I_{B(\Phi)}$, k_2 corresponds to $I_{B(\Phi+180°)}$

The drawing in Fig. 7 is of course a simplified one because we must sum up for the whole set of ellipsoids, and the case in the Figure is valid only for the resultant vector. From Fig. 7 we evidently get

$$\Delta\varrho/\varrho^0(\Phi) \neq \Delta\varrho/\varrho_0(\Phi + 180\,) \tag{8}$$

as it was mentioned in Part 3.2 referring to the measurements (Fig. 3). If the current flows along any of the symmetry axes related to the set of the ellipsoids the anomaly vanishes.

Remarks

1. On the basis of our model, the MR depends on the slope of the band taking part in the conduction process. Since the band has not changed, the anomalous component of MR must not change either. According to our measure-

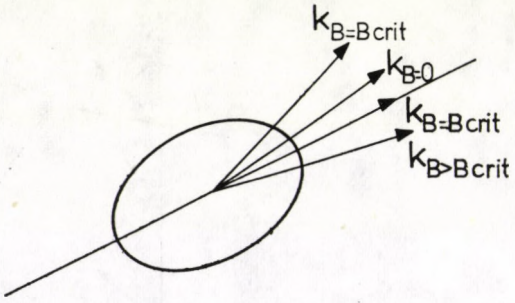

Fig. 9. The decrease of the bisection due to the increase of magnetic field above a critical value, $B_{crit.}$

ments the absolute value of the anomalous component does not show temperature dependence, in contrast to the relative change at low temperatures, because of the decreasing of ϱ_0. (The mean free path increases).

2. When the direction of the carrier motion is close to a symmetry axis, then even a low magnetic field called $B_{crit.}$ can cause the carriers move into a symmetry direction. Further increasing of the magnetic field, also acts so that the bisection of the drifting field with the ellipsoid starts to decrease once more, and the trend in the mobility variation turns out to be normal (Fig. 9).

3. It is worth to mention that PbS and Ge have a similar band structure. From this fact follows the prediction of the similar effects in Ge as well.

Acknowledgement

We are extremely grateful to Dr. G. REMÉNYI for providing us with the data measured at very low temperature.

REFERENCES

1. R. Peierls, Leipziger Vorträge p. 75, Leipzig, 1930.
2. L. Nordheim and D. Blohincev, Z. Phys., **84**, 168, 1933.
3. H. Jones and C. Zener, Proc. Roy. Soc., A **144**, 10, 1934.
4. W. Sasaki and Debruyn Ouboter, Physica, **27**, 877, 1961.
5. J. F. Woods and C. H. Chen, Phys. Rev., **125 A**, 1962, 1964.
6. I. K. Andronik, E. K. Arushan, O. V. Emelyanenko and D. N. Nasledov, Phys. Stat. Sol., **27**, 45, 1968.
7. O. V. Emelyanenko, T. C. Lagunova, A. N. Nasledov and R. N. Talankin, FTT, **7**, 1315, 1965.
8. O. V. Emelyanenko, E. E. Klotunus, T. C. Lagunova and A. N. Nasledov, FTP, **1**, 933, 1967.
9. W. Sasaki, Proc. Int. Conf. Phys. Semicond. Kyoto, p. 543, 1966.
10. R. J. Sladek and R. W. Keyes, Phys. Rev., **122**, 437, 1961.
11. N. Mikoshiba, Phys. Rev., **127**, 1962, 1962.
12. Y. Toyozawa, J. Phys. Soc. Jap., **17**, 986, 1962.
13. Y. Tokozawa, Proc. Int. Conf. Semicond. Phys. Exeter, 104, 1962.
14. T. Porjesz, Phys. Stat. Sol., **22**, K145, 1974.
15. I. Kirschner, T. Porjesz, P. Zentai, G. Kiss and G. Remenyi, Cryogenics, **14**, 559, 1974.
16. D. M. Finlayson and D. Greig, Proc. Phys. Soc., **B69**, 796, 1956.
17. D. M. Finlayson and I. A. Johnson, Phys. Stat. Sol., (b) **71**, 395, 1975.
18. D. M. Finlayson and A. G. Matthewson, J. Phys. Chem. Solids, **28**, 1501, 1967.
19. Ravits, Efimova and Smirnov, Moskva Izd. Nauka, 1968.

Acta Physica Academiae Scientiarum Hungaricae, Tomus 48 (1), pp. 69—76 (1980)

LA FORMULE RELATIVISTE DE L'EFFET DOPPLER DANS UNE THÉORIE D'ÉTHER

Par

M. F. PODLAHA et T. SJÖDIN

PHILOSOPHISCHES SEMINAR, NIKOLAUSBERGERWEG 9c, GÖTTINGEN, BRD

(Reçu 24. X. 1979)

La formule "relativiste" Doppler est déduite pour une classe de théories d'éther caractérisée par le fait que la relation entre la contraction longitudinale et transversale des corps en mouvement est exprimée par $\sqrt{1 - w^2/c^2}$. La formule déduite est comparée avec le résultat des expériences de rotor et on trouve que le ralentissement des horloges en mouvement est donné par $\Omega(w) = \sqrt{1 - w^2/c^2}$. Avec ces expériences on ne decide pas la fonction Ψ: cela signifie que la vitesse de la lumière pourrait être différente dans de différentes systèmes d'inertie. Une expérience est proposée pour démontrer l'indépendance de la fonction $\Omega(w)$ de l'accélération.

1. Introduction

La formule relativiste de l'effet Doppler est substantiellement différente de la formule classique valable par exemple pour les ondes sonores. Influencés par cette différence, beaucoup de gens sont convaincus qu'une théorie de la lumière contenant le concept de porteur d'ondes électromagnétiques ne puisse pas — contrairement à la théorie d'Einstein — expliquer exactement l'effet mesuré (voir par ex. [1]). S'il en était ainsi, en effet, il serait possible d'éliminer les théories fondées sur le concept d'éther — telles que la théorie de Lorentz—Larmor — sur des bases expérimentales.

L'intention principale de ce travail est de démontrer qu'il n'en est pas ainsi, mais nous espérons aussi que le lecteur se convaincra du fait que notre déduction de la formule Doppler est plus naturelle du point du vue physique et permet une compréhension meilleure des causes physiques de l'effet que la déduction relativiste habituelle. A cette fin nous ne nous limitons pas à *une* théorie d'éther (celle de Lorentz—Larmor) mais nous déduisons la formule Doppler pour une entière classe de théories d'éther (caracterisée par le fait que la relation entre la contraction longitudinale et transversale des corps en mouvement est exprimée par $\sqrt{1 - w^2/c^2}$.) Cela présente aussi l'avantage de pouvoir plus facilement décider dans quelle mesure de différentes expériences confirment les valeurs présumées dans la théorie de Lorentz—Larmor pour le ralentissement des horloges et pour la contraction longitudinale et transversale des corps en mouvement (voir aussi [2].)

D'habitude on tire la déduction relativiste de la formule Doppler d'une façon mathématique abstraite qui n'apporte aucune lumière sur les causes physiques de l'effet. On prend en considération deux systèmes de référence (c'est-à-dire deux différents observateurs) et la formule résulte presque immédiatement du postulat de l'invariance des lois physiques. C'est un moyen très utile de *trouver* des formules relativistes, mais à notre avis, il ne constitue pas une réelle explication physique de l'effet.

Nous exigeons d'une théorie physique qu'elle puisse résoudre tout problème physique justement dans *un* système de référence. Le fait est que nous nous refusons de réduire la physique en mathématique, mais considérons plutôt tout processus physique comme quelque chose de réel.

Compte tenu de cette exigence, on va tout d'abord déduire la formule Doppler dans le système de l'éther. Ensuite on va la transformer en un autre système moyennant une transformation générale. Enfin on va la comparer avec l'expérience (et avec la formule relativiste) et on va voir comment cela limite la généralité de la transformation. Nous tenons à souligner qu'on ne quitte jamais le concept d'éther, suivant une conception d'éther non pas en son sens "ancien", mais seulement au sens d'un *système de référence préféré.*

2. Notre approche

Nour présumons que les fréquences des oscillateurs et les dimensions des corps changent quand ils bougent par rapport à l'éther. Ensuite nous présumons que ces changements sont indépendants des coordonnées de l'espace et du temps (homogénéité de l'espace et du temps) et aussi indépendants de la direction du mouvement (isotropie de l'espace). Finalement nous présumons que le changement est indépendant de l'accélération. (Dans la section 5 nous proposerons une expérience pour tester cette dernière supposition.) Sur la base de cettes suppositions nous pouvons écrire le changement de la fréquence comme $\Omega = \Omega(w)$, et les changements des dimensions longitudinales et transversales comme respectivement $\Phi = \Phi(w)$ et $\Psi = \Psi(w)$, où w est un paramètre caractérisant l'état de mouvement dans l'éther de l'objet consideré.

Comme déjà Fresnel (1828), nous présumons que la vitesse de la lumière est indépendante de l'état de mouvement de la source dans l'éther (propriété d'onde) et qu'elle se propage dans l'éther avec la vitesse c dans toutes les directions. Pour simplifier le calcul nous considérons par la suite un espace à deux dimensions.

Comme connu, l'effet Doppler n'existe pas seulement pour la lumière, mais est importante pour toutes les ondes. La différence essentielle entre la lumière et les autres ondes en ce qui concerne l'effet Doppler n'est pas dans la nature des ondes, mais seulement dans le fait que les fréquences des oscilla-

teurs changent quand ils bougent par rapport à l'éther: la fréquence de la source avec le facteur $\Omega(w_S)$ et la fréquence du standard de fréquence de l'observateur avec le facteur $\Omega(w_B)$. Par conséquent, il faut multiplier l'expression classique pour l'effect Doppler (valable par exemple pour les ondes sonores) par $\Omega(w_S)/\Omega(w_B)$, et on obtient une équation semblable à celle de IVES [3]:

$$\nu = \frac{1 - \frac{w_B}{c}\cos\beta}{1 - \frac{w_S}{c}\cos\alpha} \frac{\Omega(w_S)}{\Omega(w_B)} \nu_0, \tag{1}$$

ou ν_0 est la fréquence propre de la source (la fréquence en repos), ν la fréquence mesurée par l'observateur, c une constante caractérisant la vitesse de la lumière dans l'éther, w_S et w_B sont des paramètres caractérisant l'état de mouvement dans l'éther de la source et de l'observateur respectivement, et α, β les angles entre les vecteurs de la vitesse et la ligne droite qui relie la source et l'observateur, mesurée dans l'éther (voir Fig. 1).

En tenant compte des changements de fréquence des oscillateurs en mouvement nous avons obtenu la formule Doppler dans le système d'éther. Comme un cas spécial — le cas $\Omega \equiv 1$ — elle contient la formule classique. Malheureusement la formule (1) est en général valable seulement dans le système de référence préféré. Pour obtenir la formule Doppler dans un autre système de référence il faut qu'on emploie une transformation de coordonnées. Ici nous voulons utiliser la transformation suivante (voir [4], où $\Psi = A_{R_0}$):

$$\begin{cases} x = \Psi \dfrac{x' + \dfrac{c'}{c} w t'}{\sqrt{1 - w^2/c^2}}, \\ y = \Psi y', \\ t = \Psi \dfrac{\dfrac{w}{c^2} x' + \dfrac{c'}{c} t'}{\sqrt{1 - w^2/c^2}}, \end{cases} \tag{2}$$

pour démontrer que la formule Doppler dans le système d'inertie de l'observateur est donnée par l'équation

$$\nu = \frac{\sqrt{1 - v^2/c'^2}}{1 - \frac{v}{c'}\cos\Theta_B} \Gamma \nu_0, \tag{3}$$

où

$$\Gamma = \frac{\sqrt{1 - w_B^2/c^2}}{\sqrt{1 - w_S^2/c^2}} \frac{\Omega(w_S)}{\Omega(w_B)},$$

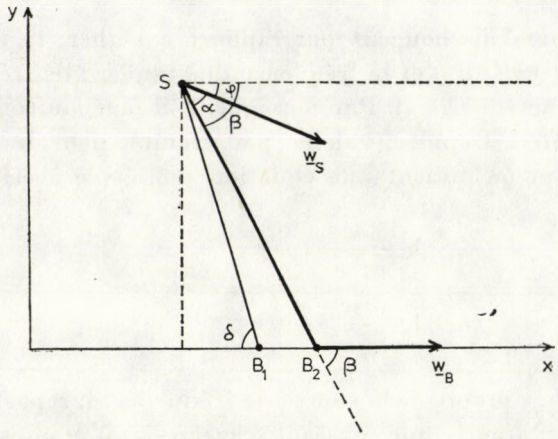

Fig. 1

et

$$c' = \frac{\sqrt{1 - w_B^2/c^2}}{\Psi\Omega}\, c\,.$$

Ici c' signifie la vitesse de la lumière dans le système d'inertie de l'observateur, v la vitesse de la source, et Θ_B est l'angle entre le vecteur de vitesse de la source et la ligne droite qui relie la source et l'observateuré, mesuré par l'observateur.*

La transformation (2) est caracterisée par la relation $\Phi = \Psi\sqrt{1 - w^2/c^2}$ et le choix de la synchronisation standard [2] dans le système d'inertie R'. Comme connu, cette relation résulte de l'indépendance d'orientation dans l'expérience de Michelson—Morley (ou de Kennedy—Thorndike) [6]. On souligne que selon cette transformation la loi de la transformation des angles est la même qu'en relativité, et la loi de la transformation des vitesses prend la forme suivante:

$$\begin{cases} w_x = \dfrac{v_x + uc'/c}{c'/c + uv_x/c^2}\,, \\ w_y = \dfrac{v_y\sqrt{1 - u^2/c^2}}{c'/c + uv_x/c^2}\,, \end{cases} \tag{4}$$

$\mathbf{w}$ et $\mathbf{v}$ étant les vitesses d'un objet par rapport à respectivement R et R', et $\mathbf{u} = (u, 0)$ la vitesse de R' par rapport à R.

* L'équivalence entre (1) et (3) pour le cas $c' = c$, $\alpha = \beta$ et $\Omega = \sqrt{1 - w^2/c^2}$ a été déjà affirmée par BUONOMANO et MOORE [5].

3. Déduction

La preuve de l'équivalence des formules (1) et (3) procède par les étapes suivantes:

a) On exprime α à l'aide de β et φ (voir Fig. 1):

$$\alpha = \beta - \varphi,$$

$$\cos\alpha = \cos\varphi\cos\beta + \sin\varphi\sin\beta\,. \tag{5}$$

b) On prend en considération le phénomène d'aberration indiqué par le triangle SB_1B_2. On obtient

$$\overline{B_1B_2}/\overline{SB_2} = w_B/c\,. \tag{6}$$

Il résulte de la géométrie (voir Fig. 1)

$$\overline{SB_1}\sin\delta = \overline{SB_2}\sin\beta\,,$$

$$\overline{SB_1}^2 = \overline{B_1B_2}^2 + \overline{SB_2}^2 - 2\,\overline{B_1B_2}\;\overline{SB_2}\cos\beta\,,$$

et par conséquent

$$\cos\beta = \frac{w_B}{c}\sin^2\delta + \sqrt{1 - w_B^2\,c^{-2}\sin^2\delta}\cos\delta\,. \tag{7}$$

En considérant les formules de la transformation des angles

$$\sin\delta = \sin\delta_B(1 - w_B^2\,c^{-2}\cos^2\delta_B)^{-1/2}, \tag{8a}$$

$$\cos\delta = \cos\delta_B(1 - w_B^2\,c^{-2})^{1/2}(1 - w_B^2\,c^{-2}\cos^2\delta_B)^{-1/2}, \tag{8b}$$

(δ_B est l'angle mesuré dans le système de référence de l'observateur), et insérant celles-ci et (7) dans (6), on obtient le résultat

$$\cos\beta = (1 + w_B\,c^{-1}\cos\delta_B)^{-1}(w_B/c + \cos\delta_B), \tag{9a}$$

$$\sin\beta = (1 + w_B\,c^{-1}\cos\delta_B)^{-1}(1 - w_B^2/c^2)^{1/2}\sin\delta_B\,. \tag{9b}$$

c) En exprimant $\cos\varphi$ et $\sin\varphi$ à l'aide du vecteur $\mathbf{w}_S$

$$\cos\varphi = w_{S_x}/w_S\,, \qquad \sin\varphi = w_{S_y}/w_S\,, \tag{10}$$

et en insérant ce résultat (9a, b) et (4) dans (5), et ensuite le résultat de cette opération (9a), (6) et (4) dans (1), on obtient:

$$v = \frac{\sqrt{1 - v^2/c'^2}}{1 - \dfrac{v_x}{c'}\cos\delta_B - \dfrac{v_y}{c'}\sin\delta_B}\,\Gamma v_0\,. \tag{11}$$

d) Pour finir on exprime δ_B à l'aide de Θ_B et φ_B, où φ_B est défini par les équations

$$\cos \varphi_B = v_x/v, \quad \sin \varphi_B = v_y/v, \quad \delta_B = \Theta_B + \varphi_B .$$

Les équations suivantes sont valables:

$$\cos \delta_B = (v_x \cos \Theta_B - v_y \sin \Theta_B)/v , \tag{12a}$$

$$\sin \delta_B = (v_x \cos \Theta_B + v_x \sin \Theta_B)/v . \tag{12b}$$

Insérant (12a, b) dans (11) on obtient finalement la formule (3).**

4. L'estimation expérimentale de Γ

La meilleure façon connue d'estimer expérimentalement Γ est celle fondée sur les expériences relativistes de rotor [8]. Le principe de ces expériences est illustré par la Fig. 2. Sur le cercle C_1 avec le rayon r_1 il est placé du matériel radiant. Le cercle C_1 tourne à la vitesse angulaire ω_1 et par conséquent la vitesse de la source de rayonnement est $v_1 = r_1\omega_1$. Un rayon est émis dans la direction SB.

Sur un autre cercle avec le rayon r_2 il est placé du matériel absorbant. Ce cercle tourne à la vitesse angulaire ω_2, et par conséquent la vitesse de l'absorbeur A est $v_2 = r_2\omega_2$. Il s'agit de calculer la différence $\Delta\nu$ de la fréquence de la radiation émise par la source S placée sur le cercle C_1 et la fréquence mesurée par l'observateur A placé sur le cercle C_2.

Suivant notre théorie d'éther nous voulons employer pour la solution la formule (3). Pour obtenir cette formule on n'a imposé aucune restriction à l'état de mouvement de la source S. Par conséquent le fait que la source est en mouvement circulaire n'a pas d'importance pour le calcul.

Mais dans les expériences du rotor l'observateur A n'est pas inertiel. On ne peut donc pas appliquer la formule (3) directement. Pour éviter cette difficulté nous allons rapporter toutes les calculations à un observateur B, qui est inertiel. Par conséquent il est nécessaire d'appliquer la formule (3) deux fois:
i) Pour estimer la fréquence de la radiation de la source S observée par B: ν_{BS}.
ii) Pour estimer la fréquence "absorbante" de l'observateur A observée par B: ν_{BA}.

** Des mesurages de l'effet Doppler dans *un* système de référence ne peuvent donc donner — compte tenu de l'invariance de forme de la formule Doppler — aucune information sur le rapport $c' - c$. Des mesurages précis dans des systèmes d'inertie différents décideraient toutefois la question. Dans la deuxième partie de l'expérience de Kennedy—Thorndike, dans laquelle les mesurages sont effectués pendant une partie considérable de l'année, on a trouvé que $c' = c$ [6, 7].

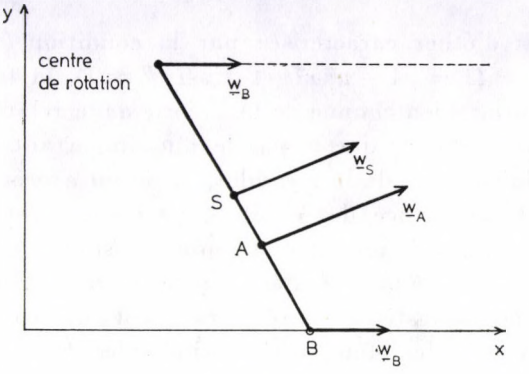

Fig. 2

Pour le cas $\Theta_B = \pi/2$ on obtient:

$$\Delta\nu = \nu_{BS} - \nu_{BA} = \left(\sqrt{1 - v_S^2/c'^2}\,\frac{\Omega(w_S)}{\sqrt{1 - w_S^2/c^2}} - \right.$$
$$\left. - \sqrt{1 - v_A^2/c'^2}\,\frac{\Omega(w_A)}{\sqrt{1 - w_A^2/c^2}}\right)\left(\frac{\sqrt{1 - w_B^2/c^2}}{\Omega(w_B)}\,\nu_0\right). \tag{13}$$

Dans le cas spécial des expériences de CHAMPENEY et MOON on avait: $r_1 = -r_2$, $\omega_1 = \omega_2$, c'est-à-dire $v_1^2 = v_2^2$. On n'a observé aucun changement des lignes spectroscopiques, c'est-à-dire on a trouvé $\Delta\nu = 0$. Il s'ensuit que $\Omega(w) = \sqrt{1 - w^2/c^2}$, et donc $\Gamma = 1$.***

5. L'indépendance de l'effet d'accélération

La formule (13) peut être utilisée pour une simple expérience démontrant l'indépendance de $\Omega(\mathbf{w})$ de l'accélération. En fixant r_2, ω_2 et la relation $r_1\omega_1 = r_2\omega_2$ mais variant r_1 et $w_1 \neq w_2$ on obtient de différentes accélérations de la source. Comme l'indique aussi l'expérience de Hafele et Keating, cela ne doit pas influencer le ralentissement des horloges [9]; la formule (13) dans ce cas aussi prévoit $\Delta\nu = 0$.

6. Conclusion

En départ de la formule classique pour l'effet Doppler nous avons déduit, en tenant compte des changements de fréquence des oscillateurs et des dimensions des corps, la formule (3), qui est la formule généralement valable pour la

*** Il faut observer que les expériences du rotor, malgré qu'elles déterminent complètement la fonction $\Omega = \Omega(w)$, ne donnent aucune information au sujet de la relation entre Ω et respectivement Φ ou Ψ.

classe des théories d'éther, caracterisée par la condition $\Phi = \Psi\sqrt{1-w^2/c^2}$. Dans le cas ou $\Phi = \Omega = \sqrt{1-w^2/c^2}$ (et ainsi $\Psi \equiv 1$), la formule (3) prend naturellement sa forme bien connue de la théorie de la relativité.

Nous voulons souligner que le pas le plus important du point de vue physique est l'établissement de la formule (1), où on a pris en considération les changements de fréquence des oscillateurs à cause du mouvement par rapport à l'éther. Jusqu'ici tous les phenomènes sont considérés seulement dans le système de référence préféré. Par la suite on transforme la formule déjà obtenue dans un autre système de référence, notamment dans le système d'inertie de l'observateur. Ici il faut aussi considérer les changements des dimensions des corps en mouvement et la synchronisation dans le système de référence de l'observateur.

La formule (3) a une application très importante: elle nous rend possible d'estimer le facteur $\Omega(w)$. La première expérience pour estimer ce facteur fut faite par IVES et STILWELL, qui mesurèrent la fréquence de la radiation des atomes en mouvement [10]. Ici nous avons décrit une autre expérience — notamment celle du rotor — qui représente la meilleure méthode connue pour estimer Ω. Cependent, avec ces expériences on ne décide pas la fonction Ψ; cela signifie que la vitesse de la lumière pourrait être différente dans de différents systèmes d'inertie (bien que isotrope dans chacun). Heureusement, de la deuxième partie de l'expérience de Kennedy—Thorndike [6, 7] on peut conclure que $\Psi\Omega = \sqrt{1-w^2/c^2}$, et donc $\Psi \equiv 1$.

Enfin nous avons proposé une expérience pour démontrer l'indépendance de la fonction Ω de l'accélération. Cette expérience devrait définitivement démontrer que la cause des effets observés dans les expériences du rotor et de Hafele—Keating n'est pas l'accélération, mais l'état de mouvement des horloges dans l'éther.

RÉFÉRENCES

1. A. MILLER, British Journ. Phil. Sci. **25,** 29, 1974.
2. T. SJÖDIN, Il Nuovo Cim., **51B,** 229, 1979.
3. H. E. IVES, Journ. Opt. Soc. Amer., **27,** 389, 1937.
4. T. SJÖDIN, Lettere al Nuovo Cimento, **18,** 241, 1977.
5. V. BUONOMANO et J. E. MOORE, American Journal of Physics, **42,** 1021, 1974.
6. M. F. PODLAHA, Il Nuovo Cim., **64B,** 181, 1969; Indian Journ. of Theoret. Phys., **26,** 189, 1978.
7. H. P. ROBERTSON, Rev. Mod. Phys., **21,** 378, 1949.
8. H. J. HAY, J. P. SCHIFFER, T. E. CRANSHAW et P. A. EGELSTAFF, Phys. Rev. Letters, **4,** 165, 1960; D. C. CHAMPENEY et P. B. MOON, Proc. Phys. Soc., **77,** 350, 1961; D. C. CHAMPENEY et G. R. ISAAK, Rev. Mod. Phys., **36,** 469, 1964; D. C. CHAMPENEY, G. R.ISAAK et A. M. KHAN, Proc. Phys. Soc., **85,** 583, 1965; W. KÜNDIG, Phys. Rev., **129,** 2371, 1963.
9. M. F. PODLAHA et T. SJÖDIN, Lettere al Nuovo Cimento, **20,** 593, 1977.
10. H. E. IVES et G. R. STILWELL, Journ. Opt. Soc. Amer., **28,** 215, 1938.

Acta Physica Academiae Scientiarum Hungaricae, Tomus 48 (1), pp. 77—84 (1980)

POWER REFLECTION, TRANSMISSION AND ABSORPTION COEFFICIENTS FOR A MOVING PLASMA SLAB IN A RECTANGULAR WAVEGUIDE

By

D. R. PHALSWAL, Y. P. SINGH and N. L. VARMA

DEPARTMENT OF PHYSICS, UNIVERSITY OF RAJASTHAN, JAIPUR-302004, INDIA

(Received 24. X. 1979)

Expressions for power reflection (R), transmission (T) and absorption (A) coefficients for TE modes for a homogeneous and collisional plasma slab (with sharp boundaries and thickness d_0) which is moving with a constant velocity (v) inside an infinitely long rectangular waveguide are investigated. The effects of slab velocity ($\beta = v/c$) and electron density $(\omega_p/\omega)^2$ on reflection, transmission and absorption coefficients are discussed numerically. It is observed that at low plasma density $(\omega_p/\omega)^2 = 0.5$, T and A are minimum, whereas R is maximum at $\beta = 0$. In case of high plasma density $(\omega_p/\omega)^2 = 1.5$, for high collision frequency, R and A; and for low collision frequency, R and T are more than unity in the limit $-0.5 < \beta < -0.2$.

1. Introduction

The problems of reflection, transmission and absorption of electromagnetic wave by moving plasma are of significant use in the fields of ionospheric studies, re-entry communications, plasma diagnostic technique and plasma heating devices, and have received considerable attention of many workers including YEH [1], JAIN et al [2], TIWARI et al [3], TAI [4] and PHALSWAL and VARMA [5]. A survey of the literature reveals that hardly any work has been reported so far on the reflection, transmission and absorption power coefficients for a rectangular waveguide containing a moving plasma slab. However, similar studies are available for a moving dielectric half-space (YEH, [1]) and moving plasma half-space (PHALSWAL and VARMA [5]).

The object of the present paper is to provide a theoretical expression for the power reflection, transmission and absorption coefficients for TE modes in rectangular waveguide containing a moving, homogeneous and collisional plasma slab, by solving the Maxwell's equations under necessary boundary conditions. The effects of slab velocity (β) and electron density $(\omega_p/\omega)^2$ have been studied numerically. The reflected and transmitted fields have also been calculated.

2. Formulation of the problem

An infinitely long rectangular waveguide having perfectly conducting walls contains a homogeneous, collisional plasma slab (with sharp boundaries at $Z = 0$ and $Z = d_0$). The slab in the waveguide can move with any velocity

(v) along its axis. Let us also consider two reference frames S and S' where Z axes coincide with the axis of the waveguide of cross-section area ab (where, a and b are the width and height of the waveguide). The primed frame is fixed in the slab and the unprimed frame is attached to the waveguide. Thus, the two reference frames are in relative motion along their Z axes. Following SOMMERFELD [6] the field expressions for s-polarized waves in a rectangular waveguide having perfectly conducting walls, the incident fields in the unprimed system are

$$\begin{aligned} E_y &= E_0 \sin\left(\frac{m\pi}{a}x\right) \exp\left[-i(kz - \omega t)\right], \\ B_y &= 0, \end{aligned} \tag{1}$$

where E_0, m, k and ω are respectively the amplitude of the incident electric field, an integer which corresponds to the order of mode, wave vector in positive direction of Z axis and the angular frequency of the wave.

The field equations for incident, reflected and transmitted TE modes in the primed frame at two interfaces of the plasma slab are given by

At $Z = 0$ interfaces:

Incident fields:

$$\begin{aligned} E'_y &= E'_0 \sin\left(\frac{m\pi}{a}x'\right) \exp\left[-i(k'z' - \omega' t')\right], \\ B'_y &= 0. \end{aligned} \tag{2}$$

Reflected fields:

$$\begin{aligned} E_y^{(r_1)'} &= A'(r_1) \sin\left(\frac{m\pi}{a}x'\right) \exp\left[i(k'z' + \omega' t')\right], \\ B_y^{(r_1)'} &= 0. \end{aligned} \tag{3}$$

Transmitted fields:

$$\begin{aligned} E_y^{(t_2)'} &= G'_{(t_1)} \sin\left(\frac{m\pi}{a}x'\right) \exp\left[-i(k'_s z' - \omega' t')\right], \\ B_y^{(t_2)'} &= 0. \end{aligned} \tag{4}$$

At $z = d' = d_0$ interface, the incident fields will be the same as given by Eq. (4) and reflected and transmitted fields are given by

$$\begin{aligned} E_y^{(r_2)'} &= A'_{(r_2)} \sin\left(\frac{m\pi}{a}x'\right) \exp\left[i(k'_s z' + \omega' t')\right], \\ B_y^{(r_2)'} &= 0 \end{aligned} \tag{5}$$

and

$$\begin{aligned} E_y^{(t_2)'} &= G'_{(t_2)} \sin\left(\frac{m\pi}{a}x'\right) \exp\left[-i(k'z' - \omega' t')\right], \\ B_y^{(t_2)'} &= 0, \end{aligned} \tag{6}$$

respectively, where E_0', $A'_{(r_1)}$, $G'_{(t_1)}$, $A'_{(r_2)}$ and $G'_{(t_2)}$ are the arbitrary constants. ω' is the frequency of the wave in the primed frame and k' and k_s' are the wave vectors in free space and plasma slab respectively, given by

$$k' = \left[\left(\frac{\omega'}{c}\right)^2 - \left(\frac{m\pi}{a}\right)^2\right]^{1/2},$$
$$k_s' = \left[\left(\frac{\omega'}{c}\right)^2 \frac{\varepsilon_p'}{\varepsilon_0} - \left(\frac{m\pi}{a}\right)^2\right]^{1/2}, \tag{7}$$

where ε_0 is the permittivity of free space and

$$\varepsilon_p' = \varepsilon_0\left[1 - \frac{\omega_p^2}{\omega'(\omega' - i\nu')}\right]$$

is the permittivity of the warm and collisional plasma slab in the primed frame (BACHYNSKI [7]); with ω_p the plasma frequency and ν' the collision frequency.

From Eqs. (1)—(6), matching the tangential electric and magnetic fields at the boundary $Z = 0$, we obtain (HEALD and WHARTON [8]) the average power reflection, transmission and absorption coefficients as

$$R' = \frac{r_p'\left[1 + (1 - 2r_p')\exp\left(-\frac{4\omega'}{c} k_i' d'\right)\right]}{1 - r_p'^2 \exp\left(-\frac{4\omega'}{c} k_i' d'\right)},$$

$$T' = \frac{(1 - r_p')^2 \exp\left(-\frac{2\omega'}{c} k_i' d'\right)}{1 - r_p'^2 \exp\left(-\frac{4\omega'}{c} k_i' d'\right)},$$

$$A' = \frac{(1 - r_p')\left[1 - \exp\left(-\frac{2\omega'}{c} k_i' d'\right)\right]}{1 - r_p' \exp\left(-\frac{2\omega'}{c} k_i' d'\right)}, \tag{8}$$

where

$$r_p' = \left|\frac{A'(r)}{E_0'}\right|^2 = \frac{(1 - k_r')^2 + k_i'^2}{(1 + k_r')^2 + k_i'^2}, \tag{9}$$

and k_r' and k_i' are the real and imaginary parts of k_s'/k' and have the form

$$k_r' = \left[\frac{1}{2}\left\{\sqrt{h_1'^2 + h_2'^2} + h_1'\right\}\right]^{1/2} \Big/ \left[\left(\frac{\omega'}{c}\right)^2 - \left(\frac{m\pi}{a}\right)^2\right]^{1/2},$$

$$k' = \left[\frac{1}{2}\left\{\sqrt{h_1'^2 + h_2'^2} - h_1'\right\}\right]^{1/2} \Big/ \left[\left(\frac{\omega'}{c}\right)^2 - \left(\frac{m\pi}{a}\right)^2\right]^{1/2},$$

with

$$h_1' = \left(\frac{\omega'}{c}\right)^2 \left(1 - \frac{\omega_p^2}{\omega'^2}\right) - \left(\frac{m\pi}{a}\right)^2,$$

$$h_2' = + \frac{v' \omega_p^2}{\omega' c^2} . \tag{10}$$

If in the unprimed frame, the reflected and transmitted fields at the two interfaces of the slab are

At first interface

$$E_y^{(r_1)} = A_{(r_1)} \sin\left(\frac{m\pi}{a} x\right) \exp\left[i(k^{(r_1)} z + \omega^{(r_1)} t)\right], \tag{11}$$
$$B_y^{(r_1)} = 0 ,$$

$$E_y^{(t_1)} = G_{(t_1)} \sin\left(\frac{m\pi}{a} x\right) \exp\left[-i(k_s^{(t_1)} z - \omega^{(t_1)} t)\right], \tag{12}$$
$$B_y^{(t_1)} = 0 .$$

At second interface

$$E_y^{(r_2)} = A_{(r_2)} \sin\left(\frac{m\pi}{a} x\right) \exp\left[i(k_s^{(r_2)} z + \omega^{(r_2)} t)\right], \tag{13}$$
$$B_y^{(r_2)} = 0 ,$$

$$E_y^{(t_2)} = G_{(t_2)} \sin\left(\frac{m\pi}{a} x\right) \exp\left[-i\,(k^{(t_2)} z - \omega^{(t_2)} t)\right], \tag{14}$$
$$B_y^{(t_2)} = 0 ,$$

where $A_{(r_1)}$, $G_{(t_1)}$, $A_{(r_2)}$ and $G_{(t_2)}$ are the arbitrary constants, $k^{(r_1)}$, $k_s^{(t_1)}$, $k_s^{(r_2)}$, $k_s^{(t_2)}$ and $\omega^{(r_1)}$, $\omega^{(t_1)}$, $\omega^{(r_2)}$, $\omega^{(t_2)}$ are the wave vectors and angular frequencies of the reflected and transmitted fields at the two interfaces of the slab, respectively.

Now, making use of phase invariance (PAULI [9]), the covariance of Maxwell's equations with respect to the Lorentz transformation (SOMMERFELD [6]) and satisfying the boundary conditions, we obtain

$$\omega' = \alpha\,(\omega - vk) = \alpha\omega(1 - \beta); \; k' = \alpha\left(k - \frac{\omega v}{c^2}\right) = \alpha k(1 - \beta) ,$$

$$k^{(r_1)} = \alpha\left(k' - \frac{\omega'\beta}{c}\right) = \alpha^2 k(1 - \beta)^2 ,$$

$$k_s^{(r_2)} = \alpha\left(k_8' - \frac{\omega'\beta}{c}\right) = \alpha^2 k(1 - \beta)(Q - \beta) = k_s^{(t_1)} ,$$

$$k^{(t_2)} = \alpha\left(k' + \frac{\omega'\beta}{c}\right) = \alpha^2 k(1-\beta)^2 ,$$

$$\omega^{(r_1)} = \alpha(\omega' - k'\beta c) = \alpha^2\omega(1-\beta)^2 ,$$

$$\omega^{(r_2)} = \alpha(\omega' - k_s'\beta c) = \alpha^2\omega(1-\beta)(1-Q\beta) = \omega^{(t_1)} ,$$

$$\omega^{(t_2)} = \alpha(\omega' + k'\beta c) = \alpha^2\omega(1-\beta^2), r_p = r_p'\left[\frac{1-\beta}{1+\beta}\right]^2,$$

$$r_p = \left(\frac{1-\beta}{1+\beta}\right)^2\left[\frac{(1-k_r)^2 + k_i^2}{(1+k_r)^2 + k_i^2}\right], \; d = \frac{d'}{\alpha} = \frac{d_0}{\alpha}, \; v' = \alpha v ,$$

$$k_r = \frac{\left[\frac{1}{2}\{(h_1^2 + h_2^2)^{1/2} + h_1\}\right]^{1/2}}{D}, \; k_i = \frac{\left[\frac{1}{2}\{(h_1^2 + h_2^2)^{1/2} - h_1\}\right]^{1/2}}{D}, \quad (15)$$

where $\alpha = (1-\beta^2)^{-1/2}$, $\beta = v/c$, d_0 is the proper thickness of the slab,

$$Q = \left[1 - \frac{\omega_p^2}{\omega^2\alpha^2(1-\beta)^2}\left(1 - \frac{iv}{\omega(1-\beta)}\right)\right]^{1/2};$$

$$h_1 = \frac{a^2\omega^2(1-\beta)^2}{c^2} - \left(\frac{\omega_p}{c}\right)^2 + \left(\frac{m\pi}{a}\right)^2,$$

$$h_2 = \frac{v\omega_p^2}{\omega c^2(1-\beta)}; \; D = \left[\frac{\alpha^2\omega^2(1-\beta)^2}{c^2} - \left(\frac{m\pi}{a}\right)^2\right]^{1/2}, \quad (16)$$

Substituting the values of $\omega^{(r_1)}$, $\omega^{(r_2)}$, $k^{(r_1)}$, $k^{(r_2)}$ and $\omega^{(t_1)}$, $\omega^{(t_2)}$, $k^{(t_1)}$, $k^{(t_2)}$ from Eq. (15) in Eqs. (11)—(14), we can obtain the field equations for TE modes.

3. Reflection, transmission and absorption coefficients

To calculate the reflection, transmission and absorption power coefficients in the unprimed frame, the transforms of parameters, given in Eq. (15) are used in Eq. (8) and after solving we obtain

$$R = \frac{r_p\left[1 + (1-2r_p)\exp\left(-\frac{4\omega k_i d_0}{c\alpha}\right)\right]}{1 - r_p^2\exp\left(-\frac{4\omega k_i d_0}{\alpha c}\right)},$$

$$T = \frac{(1-r_p)^2\exp\left(-\frac{2\omega k_i d_0}{c\alpha}\right)}{1 - r_p^2\exp\left(-\frac{4\omega k_i d_0}{c\alpha}\right)},$$

$$A = \frac{(1 - r_p)\left[1 - \exp\left(-\frac{2\omega k_i d_0}{c\alpha}\right)\right]}{1 - r_p \exp\left(-\frac{2\omega k_i d_0}{c\alpha}\right)}. \tag{17}$$

For $\omega_p = 0$ the TE_{10} modes in the rectangular waveguide are the same as that of plasma free waveguide, which is obvious. In case of collisional plasma (i.e. $\nu \neq 0$) and $a = \infty = d_0$, the reflection coefficient (R) in the Eq. (17) reduces similar to the one obtained by PHALSWAL and VARMA [5] for moving plasma half-space. In Figs. 1 and 2 the Eqs. (17) are plotted with respect to slab velocity ($\beta = v/c$) with $d_0 = 10$ cm; $\pi/a = 1.0$ cm^{-1} for $\nu/\omega_p = 0.001, 1.0$ at plasma density $(\omega_p/\omega)^2 = 0.5$ and 1.5, respectively. It is clear from Fig. 1 that at low plasma density $[(\omega_p/\omega)^2 = 0.5]$ and low collision frequency ($\nu/\omega_p = 0.001$), T and A are minimum when the slab remains stationary (i.e. $\beta = 0$) and by increasing the slab velocity in $\pm Z$ direction the value of T and A also increases, whereas R just shows the reverse effect. At high collision frequency

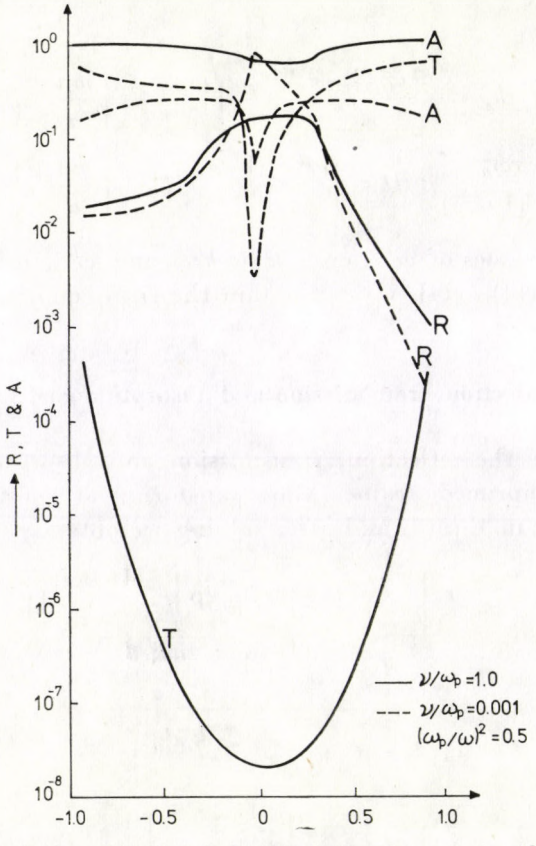

Fig. 1. Variation of R, T and A with plasma slab velocity ($\beta = v/c$)

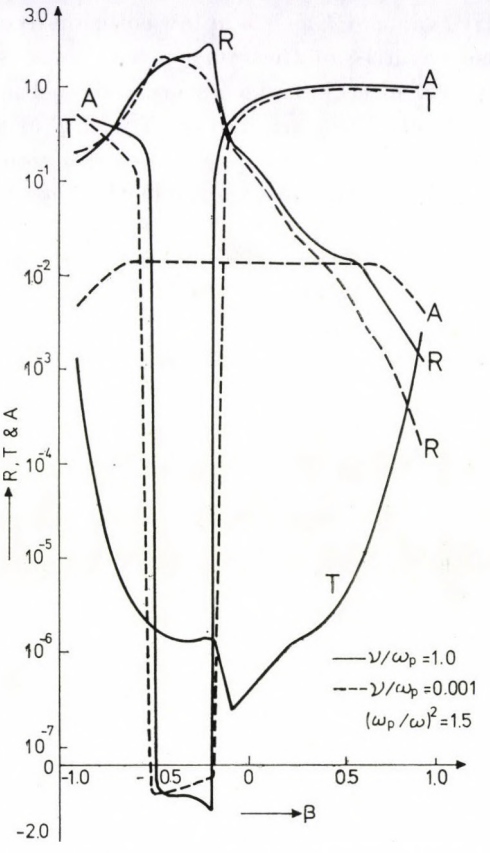

Fig. 2. Variation of R, T and A with plasma slab velocity ($\beta = v/c$)

(i.e. $v/\omega_p = 1.0$) the variations of R, T and A are similar as at low collision frequency, but at high collision frequency the transmission coefficient decreases, whereas the absorption coefficient increases. In the region $-0.1 < \beta < 0.4$ by increasing the collision frequency the reflection coefficient decreases but in the range $\beta < -0.1$ and $\beta > 0.4$, R shows reverse effect.

We conclude from Fig. 2 that at high plasma density $(\omega_p/\omega)^2 = 1.5$ and low collision frequency ($v/\omega_p = 0.001$) in the limit $-0.5 < \beta < +0.5$ the absorption coefficient nearly remains constant but in the range $\beta < -0.5$ and $\beta > 0.5$, A decreases by increasing the slab velocity in $\pm Z$ direction. The reflection coefficient is maximum at $\beta = -0.5$ and it decreases in the limit $\beta > -0.5$ and $\beta < -0.5$. The transmission coefficient is negative and more than unity in the range $-0.5 < \beta < -0.2$, but it increases with slab velocity in the limit $\beta > -0.2$ and $\beta < -0.5$.

At high collision frequency (i.e. $v/\omega_p = 1$) the transmission coefficient is minimum at $\beta = -0.1$ and it increases in the range $\beta > -0.1$ and $\beta < -0.1$

and there is no negative value of T as it is at low collision frequency. The absorption coefficient is also negative in the range $-0.5 < \beta < -0.2$ by increasing the slab velocity in $\pm Z$ direction the absorption coefficient increases and approaches unity as $\beta \to 1$. The variation of R with β at $\nu/\omega_p = 1$ and 0.001 is similar but in the range $-0.5 < \beta < -0.2$ the reflection coefficient is more than unity. With collision frequency the reflection coefficient increases a s shown in Fig. 2.

REFERENCES

1. C. YEH, J. Appl. Phys., **36**, 3513, 1965.
2. P. K. JAIN, D. SINGH, P. N. GUPTA and S. K. TALPADI, IEEE Trans., A P-21, 743, 1973.
3. G. N. TIWARI and S. K. TALPADI, Indian J. Radio and Space Phys., **6**, 114, 1977.
4. C. T. TAI, J. Math. Phys., **8**, 646, 1967.
5. D. R. PHALSWAL and N. L. VARMA, Indian J. Radio and Space Phys., **7**, 182, 1978.
6. A. SOMMERFELD, Electrodynamics, Academic Press Inc. N. Y. 280, 1952.
7. M. P. BACHYNSKI, T. W. JOHNSTON and I. P. SHKAREFAKY, Proc. Instn. Radio Engrs., **47**, 347, 1960.
8. M. A. HEALD and C. B. WHARTON, Plasma Diagnostics with Microwaves, John Wiley and Sons Inc., N. Y., 130, 1965.
9. W. PAULI, Theory of Relativity, Pergamon Press Inc. N. Y., 94, 1958.

Acta Physica Academiae Scientiarum Hungaricae, Tomus 48 (1), pp. 85—92 (1980)

A NEW VARIATIONAL TECHNIQUE TO FREE CONVECTION BOUNDARY LAYER FLOW AND HEAT TRANSFER

By

P. SINGH

DEPARTMENT OF MATHEMATICS, INDIAN INSTITUTE OF TECHNOLOGY, KANPUR, INDIA

and

D. K. BHATTACHARYA

DEPARTMENT OF MATHEMATICS, INDIAN INSTITUTE OF TECHNOLOGY, KHARAGPUR, INDIA

(Received 31. X. 1979)

A new variational method based on the governing principle of dissipative processes is developed for the solution of coupled non-linear equations arising in free convection boundary layer flow and heat transfer. The method is applied to get the approximate solution of free convection flow along a semi-infinite vertical plate. It is found that the rate of heat transfer computed for various Prandtl numbers using the present variational approach is quite close to exact known results. The result of present investigation is found to be better than that of well-known Karman-Pohlhausen integral method.

Introduction

The main aim of the present investigation is to introduce a variational technique to get the solution of free convection boundary layer equations. The method is based on the governing principle of dissipative processes which is developed by GYARMATI [1, 2] using the generalized linear constitutive equations and the famous reciprocal relations established by ONSAGER in 1931 [3, 4]. In its most general form, the governing principle is written as

$$\delta \int_V [\sigma - \Psi - \Phi] dV = 0 \,. \tag{1}$$

This principle describes the evolution of dissipative processes at any instant of time under the constraint that the general balance equations

$$\varrho \dot{a}_i + \nabla \cdot J_i = \sigma_i \quad (i = 1, 2, \ldots, f) \tag{2}$$

are satisfied. Here σ denotes the entropy production of the system and Ψ and Φ are the local dissipation potentials. It is well-known that the entropy production σ is a positive definite quantity and it is a bilinear function of f independent current densities J_i and the thermodynamic forces $\mathbf{X}_i$, i.e.,

$$\sigma(\mathbf{J}, \mathbf{X}) = \sum_{i=1}^{f} \mathbf{J}_i \cdot \mathbf{X}_i \geq 0 \,. \tag{3}$$

ϱ is the density of the continua, a_i is the specific value of the extensive transport quantity and σ_i is the source density of a_i. In the Onsager theory the fluxes are linear functions of the forces, i.e.

$$\mathbf{J}_i = \sum_{k=1}^{f} L_{ik}\mathbf{X}_k, \text{ or } \mathbf{X}_i = \sum_{k=1}^{f} R_{ik}\mathbf{J}_k \quad (i = 1, 2, \ldots, f). \tag{4}$$

In the linear laws the constant coefficients L_{ik} are conductivities while R_{ik} are resistances. These coefficients satisfy the famous Onsager's reciprocal relations:

$$L_{ik} = L_{ki}, \; R_{ik} = R_{ki} \; (i, k = 1, 2, \ldots, f). \tag{5}$$

he local dissipation potentials Ψ and Φ are defined as [1, 2]:

$$\Psi(\mathbf{X}, \mathbf{X}) \equiv \frac{1}{2} \sum_{i,k=1}^{f} L_{ik}\mathbf{X}_i \cdot \mathbf{X}_k \geq 0, \tag{6}$$

$$\Phi(\mathbf{J}, \mathbf{J}) \equiv \frac{1}{2} \sum_{i,k=1}^{f} R_{ik}\mathbf{J}_i \cdot \mathbf{J}_k \geq 0. \tag{7}$$

In the case of constant conductivities and the resistances

$$\Psi = \Phi = \sigma/2$$

and hence Ψ and Φ are the local measure of irreversibility. Principle (1) can now be written as

$$\delta \int_V \left[\sum_{i=1}^{f} \mathbf{J}_i \cdot \nabla \Gamma_i - \frac{1}{2} \sum_{i,k=1}^{f} L_{ik} \nabla\Gamma_i \cdot \nabla\Gamma_k - \frac{1}{2} \sum_{i,k=1}^{f} R_{ik}\mathbf{J}_i \cdot \mathbf{J}_k \right] dV = 0. \tag{8}$$

In the above formulation, the thermodynamic forces $\mathbf{X}_i$ are substituted by $\nabla\Gamma_i$, i.e.

$$\mathbf{X}_i \equiv \nabla \Gamma_i, \tag{9}$$

since in the case of transport processes the dissipative forces can always be generated as the gradient of certain 'Γ' variables which are state parameters and simultaneously internal parameters. It should be noted that the variational principle (8) is operative if and only if the balance equations (2) are regarded as auxiliary conditions and for their variation the following restrictions hold:

$$\delta[\varrho\dot{a}_i - \sigma_i] = -\delta\nabla \cdot \mathbf{J}_i = -\nabla \cdot (\delta\mathbf{J}_i), \tag{10}$$
$$(i = 1, 2, \ldots, f).$$

It is remarkable here that the simultaneous variation of the principle (8) with respect to forces $\nabla \Gamma_i$ and the fluxes $\mathbf{J}_i$ results in the universal form of GYARMATI's principle which is a genuine variational formulation [1, 2]. However, the restricted variations of the principle with respect to one of these two independent functions give two partial forms of the principle. The variation with respect to currents only, i.e. $\delta \mathbf{J}_i \neq 0$ but $\delta \nabla \Gamma_i = 0$ yields the flux representation of the principle which is equivalent to the Lagrangian thermodynamics of BIOT [5,6]. The variation of the principle with respect to forces only i.e. $\delta \nabla \Gamma_i \neq 0$ but $\delta \mathbf{J}_i = 0$ results in the force representation of the principle which is equivalent to the local potential method of GLANSDORFF and PRIGOGINE [2, 5]. It has also been proved by GYARMATI [2] that flux representation is a generalization of Onsager's principle of least dissipation of energy.

It should be noted that the formulation (1) or (8) is the most general principle of the dissipative processes which is valid for linear and quasilinear cases. The validity of the principle for quasi-linear cases (when L_{ik} and R_{ik} are functions of Γ_i variables) is guaranteed due to the following supplementary theorem of GYARMATI [1, 2]

$$\delta_\Gamma [\Psi + \Phi] = 0 ,$$

that is, in case of quasilinear constitutive equations the variation of the universal dissipation potential $(\Psi + \Phi)$ with respect to parameters, Γ_i, vanishes.

The governing principle of dissipative processes has already been applied to the various dissipative processes of macroscopic continuum systems. The equations of thermo-hydrodynamical systems were derived by VINCZE [7], while the principle was used to get the approximate solution of thermohydrodynamic stability by SINGH [5, 8, 9]. In the present analysis we have obtained the variational solution of free convection boundary layer along a vertical plate when the plate temperature T_w is higher than the temperature T_∞ of the ambient fluid. It is shown that the rate of heat transfer from the plate to the fluid is quite close to the exact result given by SCHLICHTING [10]. The results of the present investigation are found to be better than that of the Kármán—Pohlhausen integral method.

General formulation

In the usual boundary layer approximation the two-dimensional steady incompressible fluid flow along a vertical hot plate is described by the following equations of mass, momentum and energy conservation

$$\frac{\partial u}{\partial x} + \frac{\partial v}{\partial y} = 0 , \tag{11}$$

$$u\frac{\partial u}{\partial x}+v\frac{\partial u}{\partial y}=\nu\frac{\partial^2 u}{\partial y^2}+g\frac{T_w-T_\infty}{T_\infty}T, \tag{12}$$

$$u\frac{\partial T}{\partial x}+v\frac{\partial T}{\partial y}=\alpha\frac{\partial^2 T}{\partial y^2}, \tag{13}$$

where ν and α are the kinematic viscosity and thermal diffusivity, respectively, x and y are the coordinates along and normal to the plate while u and v are the velocity components along x and y directions, respectively. T denotes the dimensionless local temperature of the fluid inside the boundary layer.

It is well known that in the treatment of the fluid flow with heat transfer phenomenon, the energy picture of GYARMATI's principle is more convenient than the entropy picture [2]. Therefore we consider here the energy dissipation $T\sigma$ instead of entropy production σ. In the energy picture, the proper state vairable is $\ln T$ instead of T. Thus the above transport equations can be written as

$$u\frac{\partial u}{\partial x}+v\frac{\partial u}{\partial y}=\nu\frac{\partial^2 u}{\partial y^2}+g\frac{T_w-T_\infty}{T_\infty}\ln T, \tag{14}$$

$$u\frac{\partial}{\partial x}\ln T+v\frac{\partial}{\partial y}\ln T=\alpha\frac{\partial^2}{\partial y^2}\ln T. \tag{15}$$

The energy dissipation $T\sigma$ is given by

$$T\sigma=-J_q\frac{\partial}{\partial y}\ln T-P_{12}\frac{\partial u}{\partial y}, \tag{16}$$

and the constitutive equations are

$$J_q=-\lambda\frac{\partial}{\partial y}\ln T, \tag{17}$$

$$P_{12}=-\mu\frac{\partial u}{\partial y}, \tag{18}$$

where J_q denotes the heat flux and P_{12} is the viscous part of the pressure tensor. λ and μ are the thermal conductivity and the coefficient of shear viscosity, respectively. The dissipation potentials in energy picture are

$$\Psi^*=T\Psi=\frac{1}{2}\left[\lambda\left(\frac{\partial\ln T}{\partial y}\right)^2+\mu\left(\frac{\partial u}{\partial y}\right)^2\right], \tag{19}$$

$$\Phi^*=T\Phi=\frac{1}{2}\left[\frac{1}{\lambda}J_q^2+\frac{1}{\mu}P_{12}^2\right]. \tag{20}$$

Finally GYARMATI's principle in energy picture

$$\delta \int_V [T\sigma - \Psi^* - \Phi^*]\, dV = 0$$

takes the form

$$\delta \int_V \left[-J_q \frac{\partial}{\partial y} \ln T - P_{12} \frac{\partial u}{\partial y} - \frac{\lambda}{2} \left(\frac{\partial}{\partial y} \ln T \right)^2 - \frac{\mu}{2} \left(\frac{\partial u}{\partial y} \right)^2 - \right.$$
$$\left. - \frac{1}{2\lambda} J_q^2 - \frac{1}{2\mu} P_{12}^2 \right] dV = 0 \,. \tag{21}$$

Method of solution

It is clear that the principle (21) contains two sets of variables: currents J_q and P_{12} and state variables $\ln T$ and u. These variables are connected by the exact constitutive equations (17) and (18). In the dual field method, we replace the thermodynamic currents with approximate state variables which are connected with the approximate constitutive relations [5, 8]. Let us denote the approximate state variables by $\ln T^*$ and u^*. The constitutive equations are

$$J_q = -\lambda \frac{\partial \ln T^*}{\partial y} \,, \tag{22}$$

$$P_{12} = -\mu \frac{\partial u^*}{\partial y} \,. \tag{23}$$

Further it is assumed that temperature $\ln T^*$ and velocity u^* satisfy the same conditions as $\ln T$ and u. Replacing J_q and P_{12} in (14), (15) and (21) with the help of (22) and (23), we have

$$u \frac{\partial u}{\partial x} + v \frac{\partial u}{\partial y} = \nu \frac{\partial^2 u^*}{\partial y^2} + g \frac{T_w - T_\infty}{T_\infty} \ln T \,, \tag{24}$$

$$u \frac{\partial \ln T}{\partial x} + v \frac{\partial}{\partial y} \ln T = \alpha \frac{\partial^2}{\partial y^2} \ln T^* , \tag{25}$$

$$\delta \int_0^\infty \int_0^\infty \left[\lambda \left\{ \frac{\partial \ln T}{\partial y} \frac{\partial \ln T^*}{\partial y} - \frac{1}{2} \left(\frac{\partial \ln T}{\partial y} \right)^2 - \frac{1}{2} \left(\frac{\partial \ln T^*}{\partial y} \right)^2 \right\} + \right.$$
$$\left. + \mu \left\{ \frac{\partial u^*}{\partial y} \frac{\partial u}{\partial y} - \frac{1}{2} \left(\frac{\partial u}{\partial y} \right)^2 - \frac{1}{2} \left(\frac{\partial u^*}{\partial y} \right)^2 \right\} \right] dx\, dy = 0 \,. \tag{26}$$

Using the similarity transformations

$$\eta = cyx^{1/4}, \ln T = G(\eta) \,,$$
$$u = 4\nu c^2 \sqrt{x} f'(\eta) \,, \; v = \nu c\, x^{-1/4} (\eta f' - 3f) \,, \tag{27}$$

the Eqs. (24), (25) and the principle (26) become

$$f^{*'''} + 3ff'' - 2f'^2 + G = 0\,, \tag{28}$$

$$G^{*''} + 3P_r f G' = 0\,, \tag{29}$$

$$\delta \int_0^\infty \int_0^\infty \frac{c^2}{\sqrt{x}} \{[2G'G^{*'} - (G')^2 - (G^{*'})^2] + P_r[2f''f^{*''} - f''^2 - (f^{*''})^2]\}\, dxdy = 0\,, \tag{30}$$

where

$$c = \left[\frac{g(T_w - T_\infty)}{4\nu^2 T_\infty}\right]^{1/4} \text{ and } P_r(=\nu/\alpha) \text{ is the Prandtl number.}$$

G^* and f^* correspond to $\ln T^*$ and u^*, respectively. Consistent with the boundary conditions

$$\begin{aligned} &G = 1,\ f = 0,\ f' = 0 \text{ at } \eta = 0\,; \\ &G = 0,\ G' = 0,\ f' = 0 \text{ at } \eta = d_2\,; \end{aligned} \tag{31}$$

we assume the following simple expressions for velocity and temperature profiles [10]

$$f' = a\left[\frac{\eta^3}{d_1^3} - \frac{2\eta^2}{d_1^2} + \frac{\eta}{d_1}\right], \tag{32}$$

$$G = \left(1 - \frac{1}{d_2}\eta\right)^2, \tag{33}$$

where d_1 and d_2 are the boundary layer thicknesses which are considered to be equal in the present investigation. Here a and d_2 are considered as variational parameters and after variation d_1 and d_2 are taken to be equal to d. Using (32) and (33) in (24) and (25), we get

$$f^{*''} = -\frac{a^2}{6d_1^2}\left(\frac{3}{14d_1^4}\eta^4 - \frac{1}{d_1^3}\eta^3 + \frac{3}{2d_1^2}\eta^2 - 1\right)\eta^3 + \frac{\eta^2}{d_2} - \frac{\eta^3}{3d_2^2} - \eta - \frac{d_1 a^2}{21} + d_1 - \frac{d_1^2}{d_2} + \frac{d_1^3}{3d_2^2}\,, \tag{34}$$

$$G^{*'} = -6aP_r\left[\frac{\eta^6}{24d_1^3d_2^2} - \frac{2\eta^5}{15d_1^2d_2^2} - \frac{1}{20}\frac{\eta^5}{d_1^3d_2} + \frac{\eta^4}{8d_1d_2^2} + \frac{1}{6}\frac{\eta^4}{d_1^2d_2} - \frac{\eta^3}{6d_1d_2} + \frac{d_2^4}{120d_1^3} - \frac{d_2^3}{30d_1^2} + \frac{d_2^2}{24d_1}\right]. \tag{35}$$

Evaluating now the principle (30) with the help of (32), (33), (34) and (35), we get

$$\delta\int_0^\infty \frac{c^2}{\sqrt{x}}\left[a\left(-0.089\,\frac{d_2^4}{d_1^3}+0.343\,\frac{d_2^3}{d_1^2}-0.400\,\frac{d_2^2}{d_1}\right)+\frac{4}{3\,d_2\,P_r}+\right.$$

$$+P_r\,a^2\left(0.002\,\frac{d_2^9}{d_1^6}-0.012\,\frac{d_2^8}{d_1^5}+0.036\,\frac{d_2^7}{d_1^4}-0.052\,\frac{d_2^6}{d_1^3}+0.030\,\frac{d_2^5}{d_1^2}\right)+$$

$$+0.008\,a^3 d_1-0.033\,\frac{a d_1^3}{d_2^2}+0.133\,\frac{a d_1^2}{d_2}-0.166\,a d_1+\frac{2}{15}\,\frac{a^2}{d_1}+$$

$$+0.001\,a^4 d_1^3-0.038\,a^2 d_1^3-0.017\,\frac{a^2 d_1^5}{d_2^2}+0.048\,\frac{a^2 d_1^4}{d_2}+0.833\,\frac{d_1^5}{d_2^2}+$$

$$\left.+0.071\,\frac{d_1^7}{d_2^4}-0.389\,\frac{d_1^6}{d_2^3}+\frac{d_1^3}{3}-0.833\,\frac{d_1^5}{d_2}\right]dx=0. \tag{36}$$

Taking variations of (36) w.r. to d_2 and a we get

$$[(Pr-1.050552)\,a^2+4.225683]\,d^4-17.324281\,ad^2-\frac{118.329162}{Pr}=0. \tag{37}$$

$$[a^2+(1.869485Pr-3.382352)]\,d^4+[5.744944\,a^2-$$

$$-48.963694]\,d^2+61.274356a=0. \tag{38}$$

Eliminating d from (37) and (38) we get a sixth degree algebraic equation in a, which we have solved by Bairstow method. Out of six roots only one root is positive and real and substituting of this in any one of Eqs. (37) and (38) we determined the boundary layer thickness d.

Table I

Rate of heat transfer $\left(\frac{dG}{d\eta}\right)_{\eta=0}$

Pr	Approximate value from G.P.D.P.	Computer value	KÁRMÁN–POHLHAUSEN
0.5	0.442	0.442	0.462
0.773	0.528	0.507	0.540
1.0	0.609	0.567	0.607

For comparison we calculate an important characteristic of the problem, that is, the rate of heat transfer from plate to the fluid. From (33), we get

$$\left(\frac{dG}{d\eta}\right)_{\eta=0} = -\frac{2}{d}. \tag{39}$$

Inspection of Table I reveals that the rate of heat transfer obtained with the help of G.P.D.P. is quite close to the exact solution [11]. The present result is better than that of integral method of Karman—Pohlhausen.

Acknowledgement

Our thanks are due to Prof I. GYARAMATI for many useful suggestions. One of the authors (D. K. B.) is thankful to C. S. I. R., New Delhi for financial assistance.

REFERENCES

1. I. GYARMATI, Ann. Physik., **23**, 353, 1969.
2. I. GYARMATI, Non-Equilibrium Thermodynamics, Field Theory and Variational Principles, Springer, Berlin 1970.
3. L. ONSAGER, Phys. Rev., **37**, 405, 1931.
4. L. ONSAGER, Phys. Rev., **38**, 2265, 1931.
5. P. SINGH, Application of G.P.D.P. to Thermohydrodynamic Stability, D.Sc., Dissertation, Hungarian Academy of Sciences, Budapest, 1973.
6. P. SINGH, Acta Phys. Hung., **43**, 133, 1977.
7. GY. VINCZE, Ann. Physik, **27**, 225, 1971.
8. P. SINGH, Int. J. Heat Mass Transfer, **19**, 581, 1976.
9. P. SINGH, J. Non-equilib. Thermodyn. **1**, 105, 1976.
10. H. SCHLICHTING, Boundary Layer Theory, McGraw Hill, New York, 1968.
11. A. J. EDE, Advances in Heat Transfer, Vol. 4 (ed. by T. F. Irvine and J. P. Hartnet), Academic Press, 1967.

Acta Physica Academiae Scientiarum Hungaricae, Tomus 48 (1), pp. 93—102 (1980)

UTILIZATION OF TUNABLE INFRARED DIODE LASERS FOR THE DETERMINATION OF LABELLED MOLECULES IN GAS MIXTURES

By

G. J. KEMENY

OHIO UNIVERSITY, ATHENS, OH USA 45701*

R. S. ENG and A. W. MANTZ

LASER ANALYTICS, INC. 25 WIGGINS AVENUE, BEDFORD, MA USA 01730

(Received 16. XI. 1979)

The high resolution of a tunable diode laser spectrometer is combined effectively with a 100 m multiple pass cell to achieve a very high detection sensitivity for weak absorption lines of CO_2. Regular absorption, first derivative and second derivative techniques are discussed. It shows that the second derivative technique can be used for determining the concentration of labelled molecules in gas mixtures.

Introduction

It has long been a desire of spectroscopists to obtain a tunable infrared source which offers its total output energy in a narrow frequency range, and the energy of which can fully be utilized in a spectrometer. The advantages of a simple source, sample, detector arrangement are obvious as monochromators not only have a 30—70% throughput, depending on their quality and their optical layout, but the practice of splitting the energy emitted by a blackbody source into spectral elements decreases the energy falling onto the detector drastically as the resolution is increased. The detector sensitivity is one of the main factors limiting the highest achievable resolution in dispersive infrared instruments. With the most sensitive detectors and custom built gratings, the ultimate resolution can approach 10^{-3} cm^{-1}. However, the scanning of this type of instrument is usually extremely slow and it is very impractical in analytical applications.

Fourier transform spectrometers have several advantages over dispersive monochromators, as interferometers modulate the full spectrum of inci dent light instead of rejecting all but one narrow frequency band. There is no need for slits in an interferometer, and increased resolution does not drastically reduce the infrared light incident on the detector. The resolution of an interferometer is [1]

$$RES = 1/X, \tag{1}$$

* Present address: Institute of Isotopes, 1525 Budapest 114. P.O. Box 77, Hungary

where RES is the resolution in cm^{-1} and X is the mirror travel in cm. In order to achieve a resolution such as 10^{-4} cm^{-1}, the moving mirror should travel 100 m without even taking into account the apodisation function and other effects that reduce the ultimate resolution. A stroke length equivalent to 30 meters is currently feasible by operating the 10 m Michelson interferometer at the University of Paris [2] at triple pass. Physical requirements preclude this from being a practical and routine device.

Thus it appears that in order to achieve a spectral resolution significantly in excess of 10^{-3} cm^{-1} one has to resort to the use of suitable tunable sources. There have been numerous attempts to tune various infrared light emitting sources, mainly gas lasers, by electrical, electromagnetic, thermal, optical and other methods, but practically none of these devices operate over a wide enough range to cover the complete mid-infrared region. The various tunable infrared devices are summarized [3] in Table I. The wavelength coverage region as stated in the Table does not imply that the whole range can be tuned with one crystal (OPO) or one semiconductor (SDL). Although the four photon mixer is capable of tuning over a relatively wide range, the fact that a complete system requiring two nitrogen-laser-pumped dye lasers which are used in turn to optically pump potassium vapour makes this spectral source too expensive and complicated to use.

Among the tunable sources, the infrared diode laser offers the best overall parameters and promises a relative simplicity to users. Laser linewidths of 10^{-6} cm^{-1} have been achieved depending on the wavelength and operating

Table I

Properties of infrared tunable lasers*

Type	Symbol	Wavelength coverage (μm)	Highest resolution obtained (cm^{-1})
Semiconductor diode laser	DSL	<1—34	3×10^{-6}
Spin-flip Raman laser	SFR	5—6	3×10^{-5}
Nonlinear optical devices			
Optical parametric oscillator	OPO	<1—11	3×10^{-2}
Difference frequency generator	DFG	3—6	2×10^{-3}
Two-photon mixer	TPM	9—11	3×10^{-5}
Four-photon mixer	FPM	2—24	1×10^{-1}
Gas lasers			
Zeeman-tuned	ZTG	3—9	3×10^{-3}
High pressure CO_2	HPG	9—11	3×10^{-2}
F-center laser	FCL	2.2—3.3	3×10^{-5}

* After [3] with the addition of the F-center lasers.

environment. The brightness of the laser source (usually in the order of 0.5 mW) makes possible the use of very long gas cells with pathlength up to 500 m [4]. Diode lasers are available in the 300—3600 cm^{-1} region and their output frequency is tuned in general and most conveniently by bias current and temperature, although both magnetic and pressure tunings are possible. In this paper we selected a narrow region of the infrared spectrum, where only very weak CO_2 absorptions occur, to demonstrate the sensitivity of a proposed system to measure various species in the gas phase.

Measurements of CO_2 isotopic ratios have recently been performed in the ν_3 band using tunable diode laser technique. In that work the authors [5, 6] used only enriched $^{14}CO_2$ samples rather than natural CO_2 samples. Therefore, they were able to employ convenient absorption paths in the measurements of the isotopic ratios $^{14}CO_2 : {}^{13}CO_2 : {}^{12}CO_2$ without even using the derivative technique. Based on their strength measurements on the strong $^{14}CO_2$ ν_3 band lines, these authors claimed a sensitivity of 2.6×10^4 $^{14}CO_2$ molecules/cm^3 could be achieved using the second derivative technique at a reduced total pressure of 7.6 Torr.

Experimental details

The heart of our experimental setup was a modular version of the LS-3 Laser Source Spectrometer (Laser Analytics, Inc., Bedford, MA). In this system the source is a PbSnSe or PbCdSe tunable diode laser, which is mounted on a liquid He cooled cold finger (CTI Cryogenics, Inc). Since the closed cycle cooling pump is near the diode head, the latter is vibrationally isolated from the former.

The temperature of the diodes, two of which can be mounted in the same head, is controlled by the Cryogenic Temperature Stabilizer (Laser Analytics, Inc.) to better than 0.0003 K in the 10—100 K range. The laser bias current is controlled to better than 0.0001 mA by the Laser Control Module, LCM, (Laser Analytics, Inc.).

Fig. 1 shows the experimental arrangement. The light emerging from the diode is collimated by a ZnSe lens that is attached to an $x—y—z$ adjustable optical mount. A Ge etalon (2.5905 cm or 7.6505 cm thick at $T = 296$ K) or a 16 cm gas absorption cell can be pulled into the beam for calibration purposes. The source frequency can be modulated either sinusoidally, or by a positive-slope or negative-slope sawtooth voltage. The output beam intensity can be modulated using the 400 Hz mechanical chopper, which is located next to the entrance slit of the grating monochromator. To separate the longitudinal modes of the laser, a 1/2 m grating spectrometer arrangement is used before the infrared detector. A liquid nitrogen cooled mercury-cadmium-telluride

(HgCdTe) photoconductive detector with spectral response from 3 to 16 μm is used (Santa Barbara Research, Inc.). The D* of the detector is typically 2×10^{10} cm $(Hz)^{0.5}/W$.

Fig. 2 shows the outline of the adjustable pathlength White cell that was attached to the optical unit of the LS-3 laser spectrometer. The base

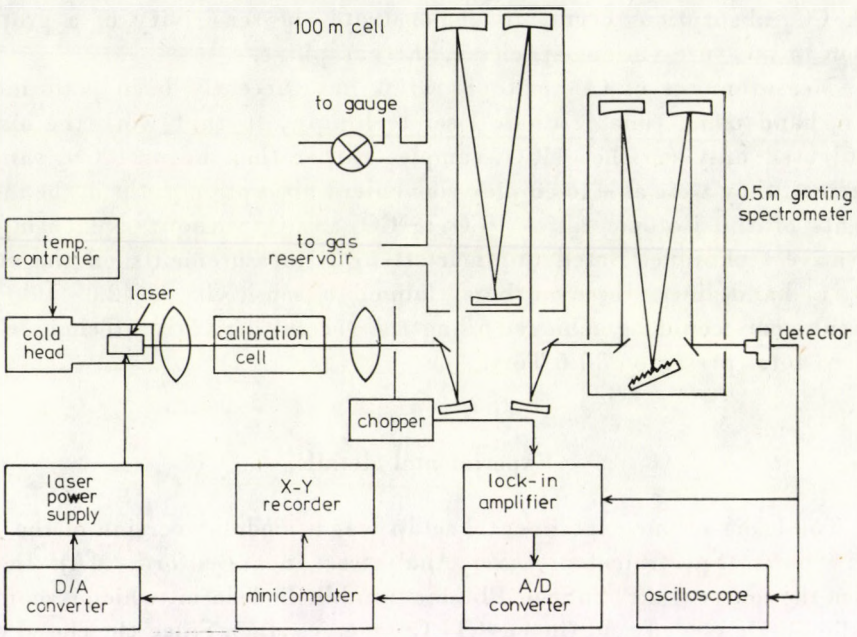

Fig. 1. Schematic diagram of experimental arrangement for the determination of labelled species in gas mixtures

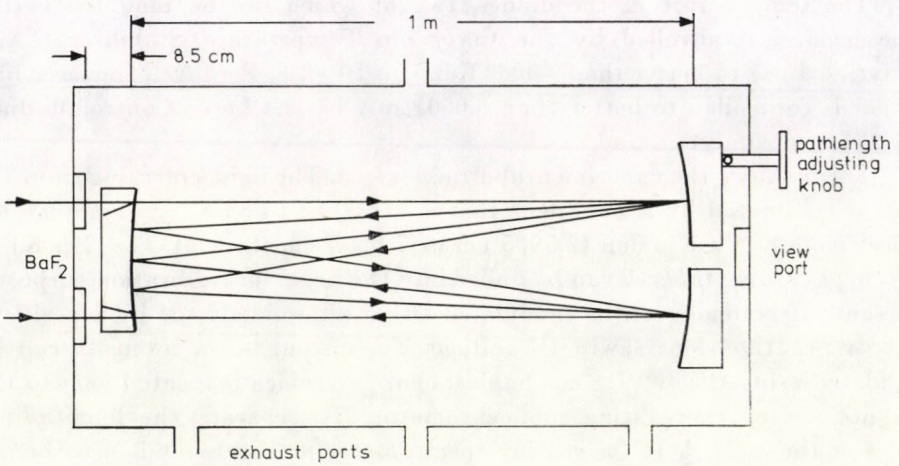

Fig. 2. Outline of the adjustable pathlength White cell showing the beam paths for eight passes

length is 1 m and the cell is adjustable in steps of 4 m. With a good alignment, a pathlength of 152 cm can be achieved. For a precise optical alignment, a He—Ne laser (Spectra-Physics Model 155) was added to the system. If the alignment is appropriate, the 0.5 mm input and output alignment pinholes of the White cell decrease the total throughput by only about 50%. The cell itself is specified to have a 100 m optical path when the first image is the same distance from the edge of the field mirror as the alignment pinhole.

The stainless steel White cell can be heated with its temperature monitored to ± 0.1 °C at four points along the cell wall by a Fluke Model 2100 A digital thermometer. The cell has been used to obtain water vapor continuum absorption data at temperatures of 60 °C. A mechanical vacuum pump is used for evacuation, vacuum testing and gas handling. Total pressure is measured on an MKS Instruments Model 22A pressure gauge with a precision of about 1%. The detector signal is first amplified by an FET preamplifier then by an Ortec Brookdeal Model 9503 precision lock-in amplifier. The reference for the lock-in amplifier is either the modulating voltage used for internal modulation or the chopper reference signal, i.e., a signal generated by the mechanical tuning fork chopper. The analog output of the lock-in amplifier is sampled by a Hewlett—Packard 9825A desk-top computer. The computer has a 23k-byte memory for data with an 8-byte data word structure. The program in HP-L occupies 3k bytes of memory. In addition to the collection of the sample and reference spectra, it is possible to correct for background spectra. Data can be stored on magnetic cassette or plotted through the multiprogrammer to the HP 9872A plotter. The computer also controls the current drive reference of the laser control module LCM through an 11-bit D/A channel of the multiprogrammer. 300 and 600 ms/data point scan speeds were used and a settling time of at least 2 minutes was allowed between consecutive scans. The ratioed spectra are plotted in either transmittance or absorbance.

Results and discussion

The first salient feature of a diode laser single beam absorption spectrum is the broad envelope across the spectral range, which is introduced by the slit response of the monochromator used to isolate the desired mode of the laser. The single beam spectrum (Fig. 3 curve B) should be ratioed against the background (Fig. 3 curve A) to result in a transmittance plot (Fig. 3 curve C). Fig. 3 is a part of the spectrum of CO_2, in the 996 cm^{-1} region. An etalon trace obtained with a 2.5905 cm long Ge etalon serves as a relative wavenumber reference (Fig. 3 curve D). The line at 996.6646 cm^{-1} is the R(60) line of the $00^01 \leftarrow (10^00.02^00)_I$ band of $^{12}C^{16}O_2$; the higher frequency line at 996.90089 cm^{-1} is the P(24) line of the $00^01 \leftarrow (10^00.02^00)_{II}$ band of $^{13}C^{16}O_2$. The line positions

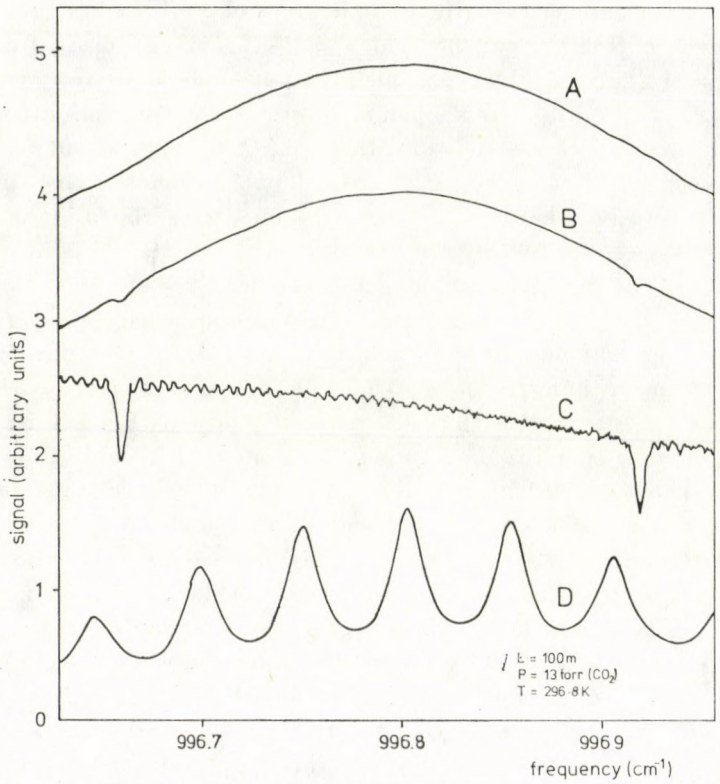

Fig. 3. Single beam spectra normally taken in diode laser absorption spectroscopy. Curve A is a background scan with the cell evacuated. Curve B is the absorption spectra. Curve C is the ratio of curve B to curve A. Curve D is the Ge etalon trace with a 0.04815 cm^{-1} free spectral range

given here are calculated using the very accurate molecular constants reported by FREED et al [7]. Beside the relatively high noise level, there is a systematic fringe-type noise that corresponds to an interference length of 9.17 cm.

In order to reduce noise and be able to detect weak absorption, derivative type detection schemes are used [8, 9]. The first derivative of the spectrum can be obtained if the source signal is frequency modulated electronically with a frequency deviation smaller than the width of the line to be detected. Curve A in Fig. 4 shows a typical first derivative spectrum. The first derivative signal enhances the signal at a region of rapidly changing amplitude (with respect to laser frequency) such as that near the line center of an absorption line at low gas pressures. Therefore, the derivative spectrum in such cases offers a higher signal-to-noise ratio when the background is smooth and slow varying. The second derivative detection utilizes the same modulation, but the second harmonic of the modulation is used as the reference for the lock-in amplifier.

Curve B in Fig. 4 is a second derivative scan, which shows an enhanced signal-to-noise ratio over the transmittance spectrum and has also a flat baseline. Recently GRIFFITHS et al [10] have investigated the quantitative aspects of the second derivative laser spectroscopy and suggested a simple method to determine the intensity and halfwidths of a line from readily measurable features of the derivative contours. If the lines are very close to each other, it is sometimes more difficult to separate them even on the second derivative spectrum. This happens to be the case for the scan in Fig. 5, where in order to separate the two strong lines (the P(22) line of the $00^01 \leftarrow (10^00,02^00)_{II}$ band of $^{13}C^{16}O_2$ at 998.78808 cm^{-1} and the R(66) line of the $00^01 \leftarrow (10^00,02^00)_I$ band of $^{12}C^{16}O_2$ at 998.9322 cm^{-1}), one has to apply a much narrower frequency modulation. The weak line at 998.8565 cm^{-1} is the P(28D) line of the $01^11 \leftarrow 11^10$ hot band of $^{13}C^{16}O_2$. Its intensity is 1.02×10^{-26} cm^{-1} molecule^{-1} cm^2. The assignment of these lines was made using the Air Force Geophysics Laboratory Line Parameter Listing [11]. The position of the line at 998.78808 cm^{-1} is from [7]; the positions of the other two lines are as measured. It is worth noting that the P(28D) line as reported in [11] is at 998.905 cm^{-1}, a discrepancy of about 0.050 cm^{-1} from the present value. This very weak line is clearly

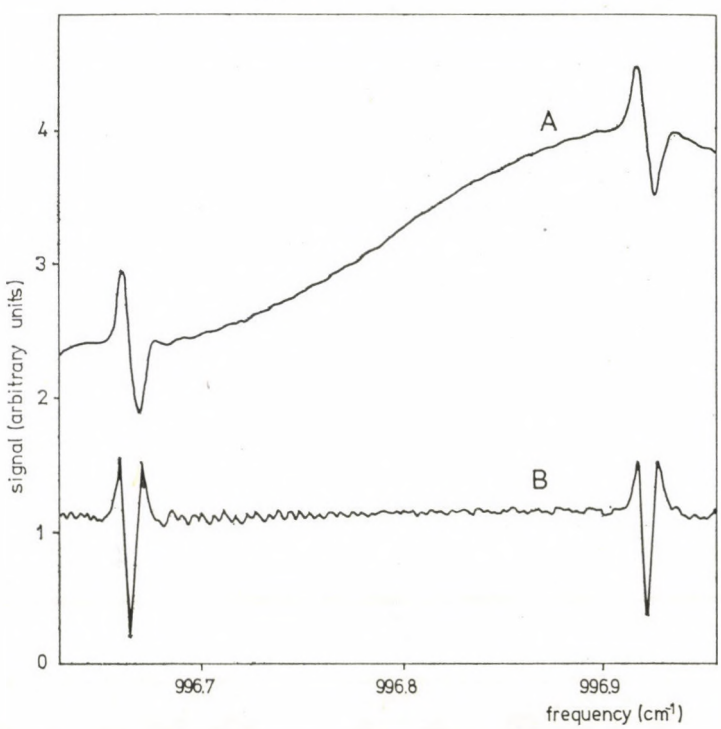

Fig. 4. Curve A is the first derivative scan and Curve B is the second derivative scan. The experimental conditions and absorption lines are the same as those shown in Fig. 3

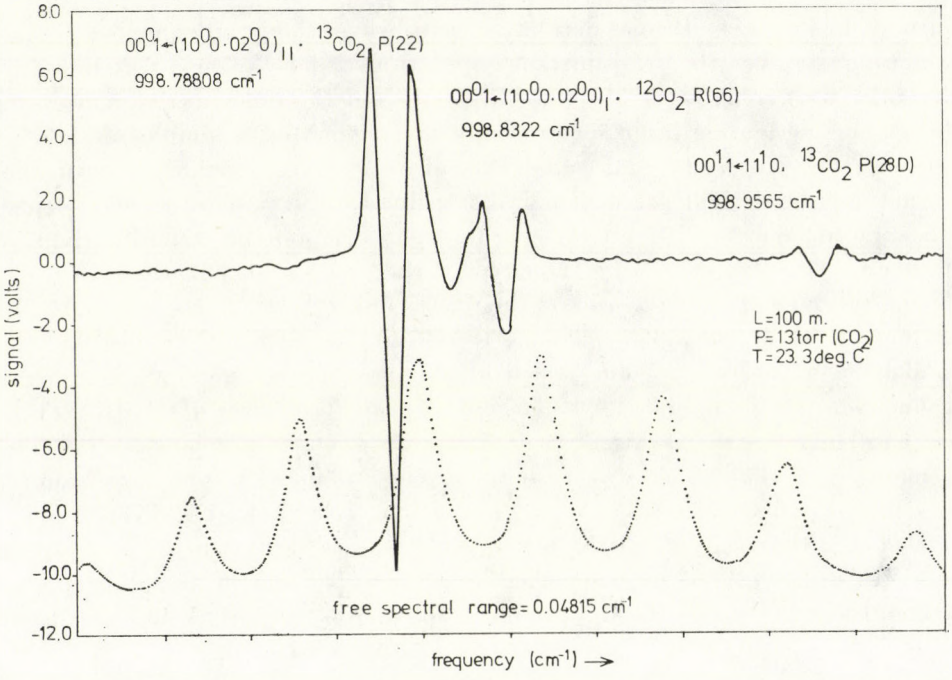

Fig. 5. A second derivative scan near 999 cm^{-1} (top curve) and the Ge etalon transmission curve (bottom curve)

seen under our experimental conditions, and if we compare this very weak absorption to a strong analytical line of CO_2, the sensitivity of our system can be estimated without having to use calibrated ppm concentration gases, or having to purge the optical path to a technically unreasonable limit.

The R(14) line of the fundamental v^3 vibrational band in the 4.3 μm region has an intensity of 3.5×10^{-18} cm^{-1} molecule^{-1} cm^2, which is 3.43×10^8 times stronger than the weakest line we just measured. A rough estimate shows that the R(14) line of the v^3 fundamental band should be detectable even at 3×10^{-8} Torr of partial pressure. This sensitivity is high enough for detecting traces of isotopically labelled molecules. For the White cell used here, it is possible to increase the number of passes and thus the optical pathlength, however there is a tradeoff between increasing the pathlength, absorption and the transmittance of the cell.

The absorption at line center for an unknown gas in a gas mixture cannot be related directly to the concentrations or the partial pressures of the absorbing species because the absorption coefficient is a function of line strength, linewidth and lineshape. These absorption line parameters are temperature, pressure and collision-species dependent. Many authors [12—16] have investigated the effects of foreign and self-broadening on the high reso-

lution spectra of various simple gases as a function of temperature and pressure. The results for the linewidth are given by the following formula:

$$\Delta\nu = \Delta\nu_0(T/T_0)^{-\alpha}(P/P_0), \tag{2}$$

where $\Delta\nu$ ($\Delta\nu_0$) is the linewidths at half absorption coefficient maximum at temperature $T(T_0)$ and pressure $P(P_0)$, and α is a constant with a value in the range 0.5 to 1.5. Eq. (2) is valid for pressure in excess of 100 Torr. The lineshape is also pressure dependent. In general, at pressures greater than 100 Torr, the lineshape is Lorentzian. At low pressures ($\leq$2 Torr), the lineshape is Gaussian. At pressures between 2 Torr and 100 Torr, the lines have in general the Voigt shape. Finally, the intensity S is a function of the temperature only. The temperature dependence of intensity is given by

$$S = S_0 \frac{Q_{R_0} Q_{V_0}(1 - ge^{-h\nu/kT})\, e^{-E''/kT}}{Q_R Q_V(1 - ge^{-h\nu/kT_0})\, e^{-E''/kT_0}}, \tag{3}$$

where S, (S_0) is the line intensity at temperature T, (T_0), Q_R (Q_{R_0}) and Q_V, (Q_{V_0}) are the rotational and vibrational partition functions at T (T_0) respectively, h and k are Planck's constant and Boltzmann constant, respectively, ν is the transition or line frequency, E'' is the lower-state energy and g is the ratio of the lower state rotational level degeneracy to the upper-state rotational level degeneracy.

The investigation of the line parameters [17] is one of the key issues for the utilization of the diode lasers for direct analytical and environmental measurements.

Conclusion

We have examined the practical side of various analytical instruments with respect to spectral resolution and detection sensitivity. The combination of a tunable diode laser spectrometer and a multiple pass cell offers the best in both resolution and sensitivity. Using this combination and employing the second derivative technique, we have demonstrated the high sensitivity by detecting very weak CO_2 absorption lines. Our results indicate that this technique is readily applicable to the determination of labelled species in gas mixtures.

REFERENCES

1. P. R. Griffiths, Chemical Infrared Fourier Transform Spectroscopy, John Wiley & Sons, New York—London—Sydney—Toronto, 1975.
2. A. Henry, private communications.
3. E. D. Hinkley, K. W. Nill and F. A. Blum, in Topics in Applied Physics, Laser Spectroscopy of Atoms and Molecules, H. Walther, Editor, Springer-Verlag, Berlin, 1974, Vol. 2. p. 125.

4. J. Reid, private communications.
5. M. Wahlen, R. S. Eng and K. W. Nill, Appl. Opt., **16**, 2350, 1977.
6. R. S. Eng, K. W. Nill and M. Wahlen, Appl. Opt., **16**, 3072, 1977.
7. C. Freed, A. H. M. Ross and R. G. O'Donnell, J. Mol. Spectrosc., **49**, 439, 1974.
8. J. Reid, J. Shewchun, B. K. Garside and E. A. Ballik, Appl. Opt. **17**, 300, 1978.
9. J. Reid, B. K. Garside, J. Shewchun, M. El-Sherbiny and E. A. Ballik, Appl. Opt., **17**, 1806, 1978.
10. P. R. Griffiths and M. L. Olson, to be published.
11. R. A. McClatchey, W. S. Benedict, S. A. Clough, D. E. Burch, R. F. Calfee, K. Fox, L. S. Rothman and J. C. Garing, AFCRL Atmospheric Absorption Line Parameters Compilation, AFCRL-TR-73-0096, January, 1973.
12. R. S. Eng and A. W. Mantz, J. Mol. Spectrosc., **74**, 331, 1979 (and references cited therein).
13. R. S. Eng and A. W. Mantz, J. Mol. Spectrosc., **74**, 338, 1979.
14. R. W. Davies and B. A. Oli, J. Quant. Spectrosc. Radiat. Transfer, **20**, 95, 1978 (and references cited therein).
15. W. G. Planet, G. L. Tettemer and J. S. Knoll, J. Quant. Spectrosc. Radiat. Transfer, **20**, 547, 1978.
16. W. G. Planet and G. L. Tettemer, to be published.
17. R. S. Eng and K. W. Nill, "Tunable Laser Measurements of Atmospheric Infrared Absorption Parameters", Applications of Laser Spectroscopy, a digest of technical papers presented at the Spring Conference sponsored by Optical Society of America, March 1975.

Acta Physica Academiae Scientiarum Hungaricae, Tomus 48 (1), pp. 103—108 (1980)

KELVIN—HELMHOLTZ INSTABILITY THROUGH POROUS MEDIUM OF TWO SUPERPOSED PLASMAS

By

R. C. SHARMA, H. SINGH and K. P. THAKUR

DEPARTMENT OF MATHEMATICS, HIMACHAL PRADESH UNIVERSITY, SIMLA-171005, INDIA

(Received 22. XI. 1979)

A study has been made of the effects of collisions with neutral particles on the stability of the plane interface separating two streaming superposed plasmas of uniform densities through porous medium. The instability criterion is found to be independent of the permeability of the medium and the collisional effects with neutral particles. The criterion determining stability does not depend on permeability of the medium but depends on the density of neutral particles. The growth rates both increase or decrease with the increase in collisional frequency as well as with the increase in permeability of the medium.

1. Introduction

The instability of the plane interface separating two uniform superposed streaming fluids, under varying assumptions of hydrodynamics and hydromagnetics, has been discussed in a treatise by CHANDRASEKHAR [2]. SHARMA and SRIVASTAVA [4] have studied this stability problem for general perturbations in hydromagnetics The effects of collisions with neutral particles on the stability of the interface which separates two uniform superposed composite hydromagnetic streaming systems have been studied by HANS [3], for transverse propagation, and by BHATIA and STEINER [1], for general perturbations. In all the above studies, the medium has been considered to be non-porous.

The flow through porous medium has been of considerable interest in recent years particularly among geophysical fluid dynamicists. The gross effect, as the fluid slowly percolates through the pores of the rock, is represented by Darcy's law which states that the usual viscous term in the equations of fluid motion will be replaced by the resistance term $(\mu/k_1)\mathbf{q}$, where μ is the viscosity of the fluid, k_1 the permeability of the medium (which has the dimension of length squared), and $\mathbf{q}$ the velocity of the fluid. The Rayleigh instability of a thermal boundary layer in flow through a porous medium has been considered by WOODING [5].

In the present paper we study the effects of collisions with neutral particles and medium porosity on the stability of the plane interface separating two streaming superposed composite plasmas of uniform densities through porous medium.

2. Perturbation equations

We consider the motion of the mixture of an infinitely conducting, incompressible and hydromagnetic (ionized) fluid and a neutral gas through porous medium, acted on by magnetic field $\mathbf{H}$ $(H_x, H_y, 0)$, gravity force $\mathbf{g}(0, 0, -g)$ and streaming velocity $\mathbf{U}(U, 0, 0)$. We assume that both the conducting fluid and neutral gas behave like continuum fluids and that the effects on the neutrals resulting from the presence of a magnetic field and the fields of gravity and pressure are neglected.

Let $\mathbf{q}(u, v, w)$, $\mathbf{h}(h_x, h_y, h_z)$, $\delta\varrho$ and δp denote respectively the perturbations in velocity, magnetic field $\mathbf{H}$, density ϱ and pressure p of the conducting fluid while ϱ_d, v_c, $\mathbf{q}_d$ and ν denote the density of the neutrals, the collisional (frictional) frequency between the two components of the composite medium, the velocity of the neutral component and the kinematic viscosity of the conducting fluid, respectively. Then, the linearized perturbation equations governing the motion of the composite medium are

$$\varrho\left(\frac{\partial}{\partial t} + \mathbf{U}\cdot\nabla\right)\mathbf{q} = -\nabla\delta p + \frac{1}{4\pi}(\nabla\times\mathbf{h})\times\mathbf{H} + \mathbf{g}\,\delta\varrho - \frac{\varrho\nu}{k_1}\varrho + \varrho_d v_c(\mathbf{q}_d - \mathbf{q}), \tag{1}$$

$$\left(\frac{\partial}{\partial t} + \mathbf{U}\cdot\nabla\right)\mathbf{q}_d = -v_c(\mathbf{q}_d - \mathbf{q}), \tag{2}$$

$$\nabla\cdot\mathbf{q} = 0,\ \nabla\cdot\mathbf{h} = 0, \tag{3}$$

$$\frac{\partial\mathbf{h}}{\partial t} + (\mathbf{U}\cdot\nabla)\,\mathbf{h} = \nabla\times(\mathbf{q}\times\mathbf{H}), \tag{4}$$

$$\left(\frac{\partial}{\partial t} + \mathbf{U}\cdot\nabla\right)\delta\varrho + (\mathbf{q}\cdot\nabla)\varrho = 0. \tag{5}$$

We analyse the disturbances into normal modes by seeking solutions of the above equations, whose dependence on x, y and t is of the form:

$$\exp(ik_x x + ik_y y + nt), \tag{6}$$

where n is the frequency of the harmonic disturbance and k_x, k_y $(k^2 = k_x^2 + k_y^2)$ are the horizontal wave numbers.

Eliminating $\mathbf{q}_d$ between Eqs. (1) and (2) and using the form (6), Eqs. (1)—(5) give

$$\varrho\left\{n + ik_x U + \frac{\nu}{k_1} + \frac{(n + ik_x U)\,\beta v_c}{n + ik_x U + v_c}\right\}u = \\ = -ik_x\,\delta p + \frac{H_y}{4\pi}(ik_y h_x - ik_x h_y), \tag{7}$$

$$\varrho\left\{n + ik_x U + \frac{\nu}{k_1} + \frac{(n + ik_x U)\beta\nu_c}{n + ik_x U + \nu_c}\right\} v = \\ = -ik_y \delta p + \frac{H_x}{4\pi}(ik_x h_y - ik_y h_x)\,, \tag{8}$$

$$\varrho\left\{n + ik_x U + \frac{\nu}{k_1} + \frac{(n + ik_x U)\beta\nu_c}{n + ik_x U + \nu_c}\right\} w = \\ = -D\delta p - g\delta\varrho + \frac{H_x}{4\pi}(ik_x h_z - Dh_x) + \frac{H_y}{4\pi}(ik_y h_z - Dh_y), \tag{9}$$

$$(n + ik_x U)\,\mathbf{h} = (ik_x H_x + ik_y H_y)\,\mathbf{q}, \tag{10}$$

$$(n + ik_x U)\,\delta\varrho = -wD\varrho\,, \tag{11}$$

$$ik_x u + ik_y v + Dw = 0,\ ik_x h_x + ik_y h_y + Dh_z = 0\,, \tag{12}$$

where

$$\beta = \frac{\varrho_d}{\varrho} \quad \text{and} \quad D = \frac{d}{dz}\,.$$

Multiplying Eqs. (7) and (8) by $-ik_x$ and $-ik_y$ and adding the results, and also using Eqs. (9)—(12) we obtain

$$\left\{n + ik_x U + \frac{\nu}{k_1} + \frac{(n + ik_x U)\beta\nu_c}{n + ik_x U + \nu_c}\right\}[D(\varrho Dw) - k^2\varrho w] + \\ + \frac{(k_x H_x + k_y H_y)^2}{4\pi(n + ik_x U)}(D^2 - k^2)w + \frac{gk^2(D\varrho)}{n + ik_x U} w = 0\,. \tag{13}$$

3. Two uniform superposed composite media separated by a horizontal boundary

We consider the case that the two superposed composite media, in which the densities ϱ_1 and ϱ_2 (and also ϱ_d), are assumed to be uniform, are streaming past each other with uniform streaming velocities U_1 and U_2 and are separated by a horizontal boundary at $z = 0$. Then in each region of constant ϱ (and the same kinematic viscosity ν, as in CHANDRASEKHAR [2], p. 443), Eq. (13) becomes

$$(D^2 - k^2)w = 0\,. \tag{14}$$

Since w must be bounded both when $z \to +\infty$ (in the upper fluid) and $z \to -\infty$ (in the lower fluid), the appropriate solutions of w can be written as

$$w_1 = A(n + ik_x U_1)\exp(kz),\ z < 0\,, \tag{15}$$

$$w_2 = A(n + ik_x U_2)\exp(-kz),\ z > 0\,, \tag{16}$$

where the same constant A has been chosen to ensure the continuity of $\left(\frac{w}{n+ik_xU}\right)$. The subscripts 1 and 2 distinguish the quantities for the lower ($z<0$) and upper ($z>0$) media, respectively.

Integrating Eq. (13) across the interface at $z=0$, we obtain

$$\Delta_0\left[\left\{n+ik_xU+\frac{\nu}{k_1}+\frac{(n+ik_xU)\beta\nu_c}{n+ik_xU+\nu_c}\right\}\varrho Dw\right]+$$
$$+\frac{k_x^2H_x^2}{4\pi}\Delta_0\left(\frac{Dw}{n+ik_xU}\right)+\frac{k_y^2H_y^2}{4\pi}\Delta_0\left(\frac{Dw}{n+ik_xU}\right)+$$
$$+\frac{k_xk_yH_xH_y}{2\pi}\Delta_0\left(\frac{Dw}{n+ik_xU}\right)+gk^2\Delta_0(\varrho)\left(\frac{w}{n+ik_xU}\right)_0=0, \quad (17)$$

where $\Delta_0(f)$ is the jump that a quantity f experiences at $z=0$ and $\left(\frac{w}{n+ik_xU}\right)_0$ is the unique value that this quantity has at $z=0$.

Substituting the values of w_1 and w_2 from Eqs. (15) and (16) in Eq. (17), we obtain the dispersion relation

$$(n+ik_xU_2)\left(n+ik_xU_2+\frac{\nu}{k_1}\right)\alpha_2+(n+ik_xU_1)(n+ik_xU_1+\frac{\nu}{k_1})\alpha_1+$$
$$+\frac{\alpha_2\beta_2\nu_c(n+ik_xU_2)^2}{n+ik_xU_2+\nu_c}+\frac{\alpha_1\beta_1\nu_c(n+ik_xU_1)^2}{n+ik_xU_1+\nu_c}-$$
$$-gk(\alpha_2-\alpha_1)+2(k_xV_A+k_yV_B)^2=0\,, \quad (18)$$

where

$$\alpha_{1,2}=\frac{\varrho_{1,2}}{\varrho_1+\varrho_2}\,,\quad \beta_{1,2}=\frac{\varrho_d}{\varrho_{1,2}}\,,\quad V_{A,B}^2=\frac{H_{x,y}^2}{4\pi(\varrho_1+\varrho_2)}\,,$$

4. Discussion

The dispersion relation (18), in its present form, is quite complex. We therefore consider a simple model in which the two media of the same density ($\alpha_1=\alpha_2$) are flowing across each other with streaming velocities U, $-U$. This model was also used by HANS [3]. Thus putting

$$\alpha_1=\alpha_2=\alpha,\ U_1=U,\ U_2=-U,\ \beta_1=\beta_2=\frac{\varrho_d}{\varrho}=\beta,$$

the dispersion relation (18) reduces to

$$n^4 + \left[\nu_c(2+\beta) + \frac{\nu}{k_1}\right] n^3 + \left[2(k_x V_A + k_y V_B)^2 + \nu_c^2(1+\beta) + 2\nu_c\left(\frac{\nu}{k_1}\right)\right] n^2 +$$
$$+ \left[\beta\nu_c k_x^2 U^2 + \frac{\nu}{k_1}(\nu_c^2 + k_x^2 U^2) + 2\nu_c\{2(k_x V_A + k_y V_B)^2 - k_x^2 U^2\}\right] n +$$
$$+ \left[\nu_c^2\{2(k_x V_A + k_y V_B)^2 - k_x^2 U^2(1+\beta)\} + \right.$$
$$\left. + k_x^2 U^2\{2(k_x V_A + k_y V_B)^2 - k_x^2 U^2\}\right] = 0 . \qquad (19)$$

It is evident from Eq. (19) that if

$$2(k_x V_A + k_y V_B)^2 > k_x^2 U^2(1+\beta) , \qquad (20)$$

there is no change of sign in the quartic equation in n. Eq. (19) therefore cannot allow any positive root meaning thereby that the system is stable.

If

$$2(k_x V_A + k_y V_B)^2 < k_x^2 U^2 , \qquad (21)$$

there is one change of sign in Eq. (19). Eq. (19) therefore allows one positive root and so the system is unstable. In inequalities (20) and (21), the permeability of the medium k_1 and collisional frequency ν_c do not come into picture. The instability criterion (21) is independent of the permeability of the medium and the collisional effects with neutral particles. The criterion (20) determining stability does not depend on permeability of the medium but depends on the density of neutral particles.

If the inequality (21) is satisfied, Eq. (19) possesses one positive root implying thereby that the system is unstable. Let n_0 denote the positive root of Eq. (19). Then

$$n_0^4 + \left[\nu_c(2+\beta) + \frac{\nu}{k_1}\right] n_0^3 + \left[2(k_x V_A + k_y V_B)^2 + \nu_c^2(1+\beta) + 2\nu_c\left(\frac{\nu}{k_1}\right)\right] n_0^2 +$$
$$+ \left[\beta\nu_c k_x^2 U^2 + \frac{\nu}{k_1}(\nu_c^2 + k_x^2 U^2) + 2\nu_c\{2(k_x V_A + k_y V_B)^2 - k_x^2 U^2\}\right] n_0 +$$
$$+ \left[\nu_c^2\{2(k_x V_A + k_y V_B)^2 - k_x^2 U^2(1+\beta)\} + \right.$$
$$\left. + k_x^2 U^2\{2(k_x V_A + k_y V_B)^2 - k_x^2 U^2\}\right] = 0 . \qquad (22)$$

To find the role of permeability of the medium on the growth rate of unstable modes, we examine the nature of dn_0/dk_1. It follows from Eq. (22)

that

$$\frac{dn_0}{dk_1} = \frac{\left(\frac{v}{k_1^2}\right)\left[n_0^3 + 2v_c n_0^2 + (v_c^2 + k_x^2 U^2) n_0\right]}{4n_0^3 + 3\left[v_c(2+\beta) + \frac{v}{k_1}\right] n_0^2 + 2En_0 + F}, \tag{23}$$

where E, F are the coefficients of n_0^2 and n_0 respectively in Eq. (22). It is clear from Eq. (23) that the growth rates may be both increasing or decreasing with the increase in permeability of the medium, as dn_0/dk_1 may be both positive or negative depending on the coefficients E and F.

Eq. (22) yields

$$\frac{dn_0}{dv_c} = -\frac{\begin{array}{l}(2+\beta)n_0^3 + 2\left\{v_c(1+\beta) + \frac{v}{k_1}\right\} n_0^2 + \left[\beta k_x^2 U^2 + \right. \\ \left. + 2v_c\left(\frac{v}{k_1}\right) + 2\left\{2(k_x V_A + k_y V_B)^2 - k_x^2 U^2\right\}\right] n_0 + \\ + 2v_c\left[2(k_x V_A + k_y V_B)^2 - k_x^2 U^2(1+\beta)\right]\end{array}}{4n_0^3 + 3\left\{v_c(2+\beta) + \frac{v}{k_1}\right\} n_0^2 + 2En_0 + F}. \tag{24}$$

It is also evident from Eq. (24) that the growth rates may be both increasing or decreasing with the increase in the collisional frequency.

REFERENCES

1. P. K. Bhatia and J. M. Steiner, Aust. J. Phys., **27**, 53, 1974.
2. S. Chandrasekhar, Hydrodynamic and Hydromagnetic Stability, Chap. XI, Oxford University Press, London, 1961.
3. H. K. Hans, Nucl. Fusion, **8**, 89, 1968.
4. R. C. Sharma and K. M. Srivastava, Aust. J. Phys., **21**, 917, 1968.
5. R. A. Wooding, J. Fluid Mech., **9**, 183, 1960.

Acta Physica Academiae Scientiarum Hungaricae, Tomus 48 (1), pp. 109—116 (1980)

TEMPERATURE VARIATION OF GRÜNEISEN PARAMETER IN ALKALI METALS

By

L. P. PATHAK, B. P. SINGH and M. P. HEMKAR

DEPARTMENT OF PHYSICS, ALLAHABAD UNIVERSITY, ALLAHABAD, INDIA

(Received 22. XI. 1979)

The temperature variation of the GRÜNEISEN parameter $\gamma_G(T)$ for alkali metals is computed from the observed pressure derivatives of elastic constants using a modified angular force model. Mode GRÜNEISEN parameters, $\gamma_{\mathbf{q},j}$ are calculated as a function of the wave vector $\mathbf{q}$ along the six directions in reciprocal space and are averaged by a modification of HOUSTON's six term integration procedure. The values of $\gamma_G(T)$ are in reasonable agreement with the experimental data.

I. Introduction

The thermal expansion of a crystal is inherently linked with the anharmonic effects of lattice vibrations. The effect of anharmonicity on thermal crystal is described in terms of a dimensionless parameter γ_G known as GRÜNEISEN parameter. The coefficient of volume thermal expansion (α) of the crystal is expressed as

$$\alpha = \gamma_G C_v / B_r V, \tag{1}$$

where V is the crystal volume, C_v is the heat capacity at constant volume and B_T is the isothermal bulk modulus.

According to the GRÜNEISEN [1] theory, γ_G is assumed to be a constant and quite independent of temperature and frequency with a numerical value ~ 2. In recent past, a considerable progress has been achieved in theoretical [2—5] and experimental [6—8] investigations on thermal expansions. It is now well established that γ_G depends both on the temperature and frequencies of the crystal.

In the present communication, we report an interpretation of GRÜNEISEN parameter on the basis of a modified angular force model [9] which had already proved its adequacy in explaining various lattice-dynamical properties [10—13] quite satisfactorily. This work further provides a check on the validity of the lattice dynamical theories of cubic crystals.

II. Theoretical formulation

In the quasi-harmonic approximation, the free energy F of a crystal is expressed by SLATER [14] as

$$F = U_0 + k_B T \sum_{\mathbf{q},j} \ln \left[1 - \exp\left(-h\nu_{\mathbf{q},j}/k_B T\right)\right], \tag{2}$$

where U_0 is the internal plus zero point energy of the crystal at absolute zero, $\nu_{\mathbf{q},j}$ is the frequency of normal mode of wave-vector $\mathbf{q}$ and polarisation j, k_B is the Boltzmann constant. The Eq. (2) with the help of the thermodynamic relation

$$\alpha = \frac{1}{V}\left(\frac{\partial V}{\partial T}\right)_P = \frac{1}{B_T}\left(-\frac{\partial^2 F}{\partial V \partial T}\right)$$

gives the relation (1), where γ_G is the mean value $\gamma_{\mathbf{q},j}$ defined by

$$\gamma_G = \frac{\sum_{\mathbf{q},j} \gamma_{\mathbf{q},j} E(x)}{\sum_{\mathbf{q},j} E(x)}, \tag{3}$$

where $\mathbf{E(x)}$ is the Einstein specific heat function and is expressed as

$$E(x) = \frac{x^2 e^x}{(e^x - 1)^2} \quad \text{with} \quad x = h\nu_{\mathbf{q},j}/k_B T$$

and microscopic GRÜNEISEN parameter $\gamma_{\mathbf{q},j}$ is defined by the relation

$$\gamma_{\mathbf{q},j} = -\left(\frac{\ln \omega_{\mathbf{q},j}}{\ln V}\right)_T, \tag{4}$$

where

$$\omega_{\mathbf{q},j} = 2\pi\nu_{\mathbf{q},j}.$$

Now replacing the summation over $\mathbf{q}$ by an integration over the allowed values of $\mathbf{q}$ within the first Brillouin zone (BZ), Eq. (3) can be written as

$$\gamma_G(T) = \frac{\sum_j \int_0^{q_{\max}} \int_\Omega \gamma_j(\mathbf{q})\, E(x)\, q^2 dq\, d\Omega}{\sum_j \int_0^{q_{\max}} \int_\Omega E(x)\, q^2\, dq\, d\Omega}. \tag{5}$$

Here Ω is the solid angle in the wave vector space.

III. Numerical computation

The GRÜNEISEN parameter (γ_G) for lithium, sodium, potassium and rubidium have been computed at different temperatures from Eq. (5) by using HOUSTON's [15] method for evaluation of integrals. At low temperatures where the lower frequencies have a predominating influence, HOUSTON's method will yield more reliable values of γ_G. The integration over $\mathbf{q}$ is performed numerically and the angular integration over Ω is carried by using a modified HOUSTON's spherical six-term integration procedure as elaborated by BETTS et al [16]. The six directions used for $\mathbf{q}$ are [100], [110], [111], [210], [211] and [221]. Their solutions are given in Appendix.

Normally a three parameter force model is usually employed to evaluate γ_G in which interatomic interactions are confined to nearest-neighbours only. It is worth mentioning that we have used here a five force constants model (β_1, β_2, r_1, r_2 and ak_e). The bulk modulus k_e is determined by GELLMANN—BRUCKNER [17] method. Its pressure derivatives are determined theoretically. The remaining four disposable force constants have been reduced to three by taking a suitable ratio of r_1/r_2 which gives a better fit to phonon dispersion curves with experimental data. Thus $\gamma_{\mathbf{q},j}$ are calculated in terms of observed values of adiabatic elastic constants C_{ij} and their pressure derivatives. These values are averaged over the wave vector space in the first BZ using the HOUSTON's six-term integration method. The sources of the temperature

Table I

Pressure derivatives and temperature variation of elastic constants for alkali metals

Metal	Pressure derivatives			Source	Elastic constants data
	$\partial C_{11}/\partial P$	$\partial C_{12}/\partial P$	$\partial C_{44}/\partial P$		
Lithium	3.286	3.116	1.034	a)	d)
Sodium	3.931	3.479	1.567	a)	e)
	3.901	3.444	1.630	b)	e)
Potassium	4.156	3.650	1.539	a)	f)
	4.305	3.803	1.630	c)	f)
Rubidium	4.169	3.663	1.565	a)	g)

a) T. SUZUKI, A. V. GRANATO and J. F. THOMAS, Phys. Rev., **175**, 766, 1968.
b) W. B. DANIELS, Phys. Rev., **119**, 1246, 1960.
c) P. A. SMITH and C. S. SMITH, J. Phys. Chem. Solids, **26**, 279, 1965.
d) H. C. NASH and C. S. SMITH, J. Phys. Chem. Solids, **9**, 113, 1959.
e) M. E. DIEDERICH and J. TRIVISONNO, J.Phys. Chem. Solids, **27**, 637, 1966.
f) W. R. MARQUARDT and J. TRIVISONNO, J. Phys. Chem. Solids, **26**, 273, 1965.
g) C. A. ROBERTS and R. MEISTER, J. Phys. Chem. Solids, **27**, 1401, 1966.

variation of the elastic constants together with their pressure derivatives at room temperature are given in Table I. For sodium and potassium, we have used two sets of pressure derivatives.

IV. Results and discussion

The calculated results of temperature variation of γ_G for alkali metals are plotted in Figs. 1—4 along with the observed values. For lithium, the calculated $\gamma_G - T/\Theta_0$ curve (Θ_0 = Debye temperature) is shown in Fig. 1. Our curve

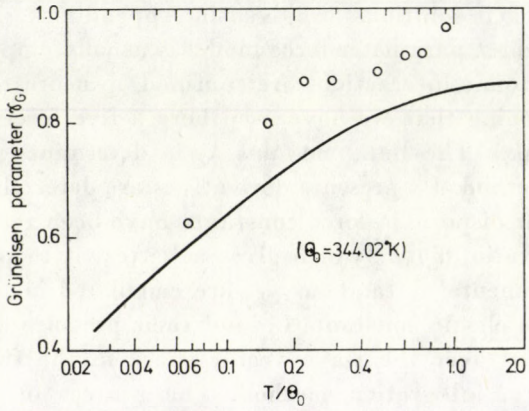

Fig. 1. Temperature variation of GRÜNEISEN parameter of lithium. Solid curve corresponds to the computed values. Experimental points (○) are of SWENSON [18].

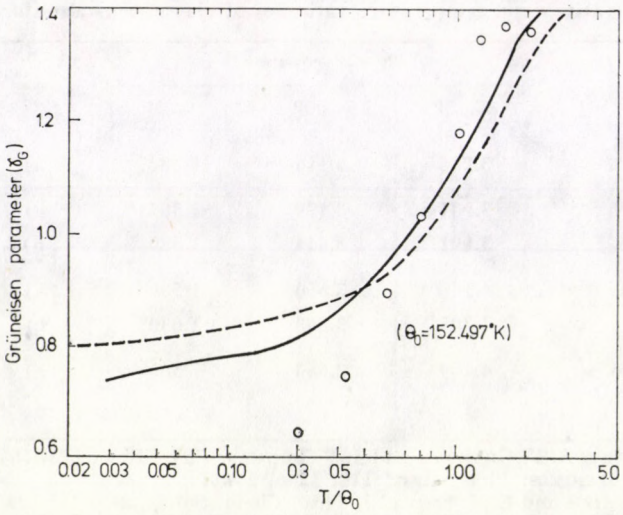

Fig. 2. Temperature variation of GRÜNEISEN parameter of sodium. The dashed curve corresponds to the experimental pressure derivative data and solid curve corresponds to the theoretical pressure derivative data. Experimental points (○) are due to SIEGEL and QUIMBY [19].

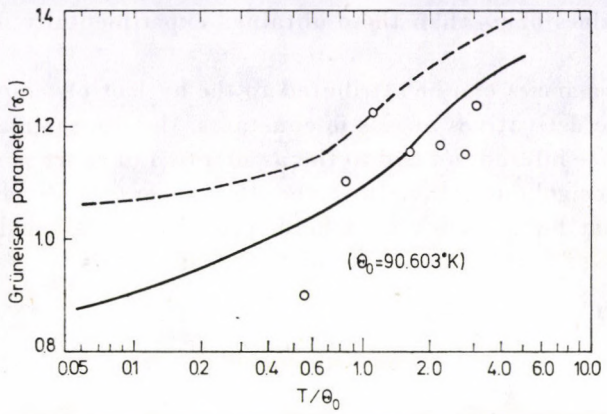

Fig. 3. Temperature variation of GRÜNEISEN parameter of potassium. Solid curve corresponds to the theoretical pressure derivative data and dashed curve corresponds to experimental pressure derivative data. Experimental points (○) are of MONFORT and SWENSON [20].

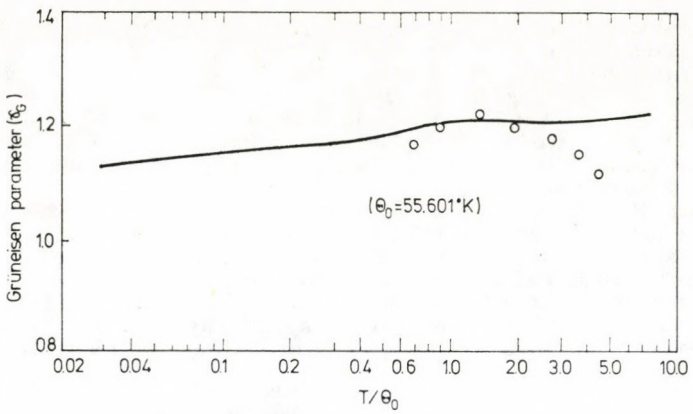

Fig. 4. Temperature variation of GRÜNEISEN parameter of rubidium. Solid curve corresponds to the computed values from theoretical pressure derivative data. Experimental points (○) are of KELLY and PEARSON [21].

is systematically lower than the observed data of SWENSON [18] and the deviation varies with the rise of temperature. For sodium our curve is in a tolerable agreement with the experimental data of SIEGEL and QUIMBY [19] as is evident from Fig. 2. In the case of potassium, as is shown in Fig. 3, it is not possible to find deviation between calculated and scattered observed value of MONFORT and SWENSON [20]. The calculated curve based on experimental pressure derivatives data exhibits inferior agreement than that with theoretical $\partial C_{ij}/\partial p$ for both metals sodium and potassium. For rubidium the computed curve is shown in Fig. 4. As is quite obvious, our calculated curve gives

a bit higher values of γ_G than those obtained experimentally by KELLY and PEARSON [21].

The discrepancies can be attributed to the neglect of temperature variation of pressure derivatives of elastic constants, the approximate description of electron-lattice interaction and to the assumption of short range interaction up to second neighbours only. However, the present study shows that the modified angular force model, used here, provides a reasonably satisfactory description of GRÜNEISEN parameter of the alkali metals.

Acknowledgement

The authors are grateful to Prof. VACHASPATI for providing the facilities in the Department. One of us (B.P.S.) records his sincere thanks to University Grants Commission, New Delhi, for the award of "Teacher Fellowship".

REFERENCES

1. E. GRÜNEISEN, in Hdb. Phys. Vol. 10, ed. S. Flügge, Springer-Verlag, Berlin 1928, p. 1.
2. T. H. K. BARRON, Ann. Phys. (Germany), **1**, 77, 1957.
3. M. BLACKMAN, Proc. Phys. Soc. (London), **74B**, 17, 1959.
4. F. W. SHEARDS, Phil. Mag. **3**, 1381, 1958.
5. T. TOYA, J. Res. Inst. Catalysis, Hokkaido Univ., **9**, 1778, 1961.
6. T. RUBIN, H. W. ALTMAN and H. L. JOHNSTON, J. Phys. Chem., **65**, 65, 1961.
7. G. K. WHITE, Proc. VIII International Conference on Low Temperature Physics, Butterworth, London, 1963, p. 394.
8. R. H. CARR, R. D. MC COMMON and G. K. WHITE, Proc. Roy. Soc., **A280**, 72, 1964.
9. J. BEHARI and B. B. TRIPATHI, Phys. Letters, **29A**, 313, 1969.
10. J. PRAKASH, L. P. PATHAK and M. P. HEMKAR, J. Phys., **F4**, 1107, 1974.
11. L. P. PATHAK and M. P. HEMKAR, Ind. J. Phys., **51A**, 282, 1977.
12. L. P. PATHAK, R. C. RAI and M. P. HEMKAR, J. Phys. Soc. Japan, **44**, 1834, 1978.
13. L. P. PATHAK, B. P. SINGH and M. P. HEMKAR, Acta Phys. Pol., **56A**, 189, 1979.
14. J. C. SLATER, Introduction to Chemical Physics, McGraw-Hill Publ. Comp., New York, 1939, p. 219.
15. W. V. HOUSTON, Rev. Mod. Phys., **20**, 161, 1948.
16. D. D. BETTS, A. B. BHATIA and M. WYMAN, Phys. Rev., **10**, 37, 1956.
17. M. GELLMANN and K. A. BRUCKNER, Phys. Rev., **106**, 364, 1957.
18. C. A. SWENSON, J. Phys. Chem. Solids, **27**, 33, 1967.
19. S. SIEGEL and S. L. QUIMBY, Phys. Rev., **54**, 76, 1938.
20. C. E. MONFORT and C. A. SWENSON, J. Phys. Chem. Solids, **26**, 291, 1965.
21. F. M. KELLY and W. B. PEARSON, Canad. J. Phys., **33**, 17, 1955.

Appendix

Direction [100]

$$m\omega_L^2 = 16(\beta_1 + 2r_1 + 3r_2)\sin^2\frac{aq}{4} + 4(\beta_2 + 4r_1)\sin^2\frac{aq}{2} + 1/2\, a^2 q^2 g^2 (x) a k_e .$$

$$m\omega_T^2 = 16(\beta_1 + 2r_1 + 3r_2)\sin^2\frac{aq}{4} + 2(3r_2 - 2r_1)\sin^2\frac{aq}{2} .$$

Direction [110]

$$m\omega_L^2 = 2(8\beta_1 + 2\beta_2 + 10r_1 + 21r_2)\sin^2\frac{aq}{2\sqrt{2}} + 1/2\, a^2 q^2 g^2(x)\, ak_e .$$

$$m\omega_{T_1}^2 = 2(2\beta_2 + 18r_1 + 9r_2)\sin^2\frac{aq}{2\sqrt{2}} .$$

$$m\omega_T^2 = 4(2\beta_1 + 2r_1 + 9r_2)\sin^2\frac{aq}{2\sqrt{2}} .$$

Direction [111]

$$m\omega_L^2 = 4(\beta_1 + 8r_1 + 6r_2)\sin^2\frac{aq}{4\sqrt{3}} + 12(\beta_1 + 2r_2)\sin^2\frac{aq\sqrt{3}}{4} +$$
$$+ 4(\beta_2 + 2r_1 + 3r_2)\sin^2\frac{aq}{2\sqrt{3}} + 1/2\, a^2 q^2 g^2(x)\, ak_e .$$

$$m\omega_T^2 = 2(8\beta_1 + 10\, r_1 + 21r_2)\sin^2\frac{aq}{4\sqrt{3}} + 6(2r_1 + r_2)\sin^2\frac{aq\sqrt{3}}{4} +$$
$$+ 4(\beta_2 + 2r_1 + 3\, r_2)\sin^2\frac{aq}{2\sqrt{3}} .$$

Direction [210]

$$m\omega^2 = 8(\beta_1 + 2r_1 + 3r_2)\left[\sin^2\left(\frac{3aq}{4\sqrt{5}}\right) + \sin^2\left(\frac{aq}{4\sqrt{5}}\right)\right] +$$
$$+ 2(3r_2 - 2r_1)\left[\sin^2\left(\frac{aq}{\sqrt{5}}\right) + \sin^2\left(\frac{aq}{2\sqrt{5}}\right)\right] .$$

$$m\omega_{\pm}^2 = 8(\beta_1 + 2r_1 + 3r_2)\left[\sin^2\left(\frac{3aq}{4\sqrt{5}}\right) + \sin^2\left(\frac{aq}{4\sqrt{5}}\right)\right] +$$
$$+ (2\beta_2 + 6\, r_1 + 3r_2)\left[\sin^2\left(\frac{aq}{\sqrt{5}}\right) + \sin^2\left(\frac{aq}{2\sqrt{5}}\right)\right] + 1/4\, a^2 q^2 g^2(x)\, ak_e +$$
$$+ \left[\left\{(2\beta_2 + 10r_1 - 3r_2)\left[\sin^2\left(\frac{aq}{\sqrt{5}}\right) - \sin^2\left(\frac{aq}{2\sqrt{5}}\right)\right] +\right.\right.$$
$$\left. + \frac{3}{20}\, a^2 q^2 g^2(x)\, ak_e\right\}^2 + 16\left\{(2\beta_1 - 2r_1 + 3r_2)\left[\sin^2\left(\frac{3aq}{4\sqrt{5}}\right) -\right.\right.$$
$$\left.\left. - \sin^2\left(\frac{aq}{4\sqrt{5}}\right)\right] + \frac{1}{20}\, a^2 q^2 g^2(x)\, ak_e\right\}^2\Bigg]^{1/2} .$$

Direction [211]

$$m\omega^2 = 2(8\beta_1 + 2\beta_2 + 10r_1 + 21r_2)\sin^2\frac{aq}{2\sqrt{6}} + 4(2r_1 + 3r_2)\sin^2\frac{aq}{\sqrt{6}} .$$

$$m\omega^2_{\pm} = 2(3\beta_1 + \beta_2 + 6r_1 + 9r_2)\sin^2\frac{aq}{\sqrt{6}} + (4\beta_1 + 2\beta_2 + 22r_1 + 27r_2)\sin^2\frac{aq}{2\sqrt{6}} +$$
$$+ 1/4\, a^2q^2g^2(x)\, ak_e \pm \Bigg[\Bigg\{(2\beta_2 - 2\beta_1 + 12r_1 - 6r_2)\sin^2\left(\frac{aq}{\sqrt{6}}\right) +$$
$$+ (4\beta_1 - 2\beta_2 - 14r_1 + 9r_2)\sin^2\left(\frac{aq}{2\sqrt{6}}\right) + \frac{1}{12}a^2q^2g^2(x)\, ak_e\Bigg\}^2 +$$
$$+ 8\left\{(2\beta_1 - 2r_1 + 3r_2)\sin^2\left(\frac{aq}{\sqrt{6}}\right) + \frac{1}{12}a^2q^2g^2(x)\, ak_e\right\}^2\Bigg]^{1/2} .$$

Direction [221]

$$m\omega^2 = 4(4\beta_1 + 2r_1 + 9r_2)\sin^2\left(\frac{aq}{12}\right) + 2(2\beta_2 + 6r_1 + 3r_2)\sin^2\left(\frac{aq}{3}\right) + 6(2r_1 + r_2) \times$$
$$\times\left[\sin^2\left(\frac{5aq}{12}\right) + \sin^2\left(\frac{aq}{4}\right)\right] + 2(3r_2 - 2r_1)\sin^2\left(\frac{aq}{6}\right) .$$

$$m\omega^2_{\pm} = 3(2\beta_1 + 2r_1 + 5r_2)\left[\sin^2\frac{5aq}{12} + \sin^2\frac{aq}{4}\right] + 2(2\beta_1 + 10r_1 + 9r_2)\left(\sin^2\frac{aq}{12}\right) +$$
$$+ (2\beta_2 + 6r_1 + 3r_2)\sin^2\frac{aq}{6} + (2\beta_2 + 2r_1 + 9r_2)\sin^2\frac{aq}{3} +$$
$$+ 1/4\, a^2q^2g^2(x)\, ak_e \pm \Bigg[\Bigg\{(2\beta_1 + 3r_2 - 2r_1)\left[\sin^2\left(\frac{5aq}{12}\right) +\right.$$
$$\left. + \sin^2\left(\frac{aq}{4}\right) - 2\sin^2\left(\frac{aq}{12}\right)\right] + (2\beta_2 + 10r_1 - 3r_2) \times$$
$$\times\left[\sin^2\left(\frac{aq}{3}\right) - \sin^2\frac{aq}{6}\right] + \frac{7}{36}a^2q^2\, g^2(x)\, ak_e\Bigg\}^2 +$$
$$+ 8\Bigg\{(2\beta_1 - 2r_1 + 3r_2) \times\left[\sin^2\left(\frac{5aq}{12}\right) -\right.$$
$$\left. - \sin^2\left(\frac{aq}{4}\right)\right] + \frac{1}{18}a^2q^2g^2(x)\, ak_e\Bigg\}^2\Bigg]^{1/2} .$$

RECENSIONES

The Neutron (Prehistory, Discovery, Consequences)

Edited by B. M. Kedrov, Akademie Verlag Berlin, 1975
German translation of the Russian original published by Nauka, Moscow, 1971

This book contains relatively little concrete information on neutron physics itself, its value is rather in the analysis of the discovery of the neutron and the development of neutron physics. The book traces the influence of neutron physics on the further development of nuclear physics, primarily from the science historical and methodological points of view.

The book can be divided into three Parts:

The first quotes such well-known scientists as CHADWICK, IVANENKO, AMALDI and GERLACH on the circumstances of discovering the neutron.

The second Part contains a detailed discussion by WJALZEW and KEDROV on the science historical and metodological aspects of the discovery of the neutron.

In the third Part (actually an Appendix) there are brief original extracts from works of famous physicists including RUTHERFORD, CURIE, JOLIOT, HEISENBERG, FERMI, TAMM, YUKAWA and others.

Stress is placed on the early thirties, years of decisive importance in the development of nuclear physics. Topical questions are discussed, e.g. the kind of conclusions that can be drawn from this period for planning, organizing and developing the physical research of today.

As a highly useful reading for physicists, science historians, teachers and students alike, the book is likely to interest a very wide audience.

D. KISS

Advances in Nuclear Physics, Volume 10

Edited by Michel Baranger and Erich Vogt
Plenum Publishing Corporation, New York— London, 1978, pp. 336

This volume of the well-known series contains three articles. The first, "*Phenomena in fast rotating heavy nuclei*" by R. M. LIEDER and H. RYDE gives an account of a rapidly developing field in nuclear physics: the properties of high-spin nuclear states. The authors follow a natural way in the presentation of nuclear structure at high angular moments: they discuss the different regions of the yrast-line (Section 2). At low spin values almost all the energy is used to generate angular momentum, the strongly deformed nuclei have in their ground state the well-known prolate and symmetrical shape with a deformation of $\beta \approx 0.3$. When the nucleus rotates, the individual nucleons are affected by centrifugal and Coriolis forces, which tend to counteract the pairing force: this effect has been called the Coriolis antiparing (CAP) effect. At a critical angular momentum ($I \approx 20$), a transition from the superfluid to the normal phase occurs; this manifests itself in the drastic change in the moment of inertia. These changes are often referred to as the "backbending" effect. Particles with large angular momenta are affected by the Coriolis force most strongly, and the breaking of one of those pairs generally seems to be sufficient to explain the experimentally observed increase of the moment of inertia with increasing rotational frequency. The backbending effect is the main subject of the first part of this article (Section 3). With increasing angular momentum, the centrifugal forces produce effects comparable in strength to the shellstructure effects and gradually drive the prolate nuclei into triaxial shapes, which in turn lead to alterations among the single particle orbitals. These changes in the yrast region result in a crossing band structure. For still larger angular momenta the nucleus acquires an oblate deformation; the total angular momentum is aligned along the symmetry axis and not perpendicular to it, as is the case in low-spin region. The states along the yrast line do not form collective rotational bands, but the energy differences between adjacent states vary statistically, and the transition matrix elements adopt single-particle values. When going away from the yrast line towards higher energies, we gradually leave the "cold nucleus" and enter the statistical region; attention has recently been focused on this statistical region (Section 4).

The second article is "*Valence and doorway mechanism in resonance neutron capture*" by B. J. ALLEN and A. R. de L. MUSGROVE. At low neutron energiès, Bohr's compound nucleus model was initially considered to provide an adequate description of the neutron interaction

exhibiting narrow resonances in the scattering and capture cross sections. However, the observation in thermal capture spectra of correlations between the reduced γ-ray intensities and the spectroscopic factors of final states led to the proposal of a direct capture mechanism. For neutron energies in the giant dipole resonance (GDR) region, the direct and compound-nucleus components could not account for the measured capture cross sections, and a collective semidirect capture mechanism was introduced to account for the data. This theory assumes that the incident nucleon is captured into a lower orbit, exciting the target nucleus into its giant dipole resonance. This intermediate state subsequently decays by enhancend γ-ray emission. The resonance capture reaction can be pictured as a series of two-body interactions beginning with the entrance channel valence (1p-0h) state, exciting doorway states (2p-1h or collective modes) and through a succession of more complex p-h interactions, leading ultimately to the statistical interaction of many nucleons. Statistical interactions are reviewed in Section 2. A brief discussion of nonresonant neutron capture is given in Section 3 together with effects of interference between resonant and nonresonant capture amplitudes. The theoretical description of valence neutron transitions is presented in Section 4, where it is shown that enhanced E1 transitions can occur in the regions of maxima of the 2p, 3s and 3p neutron strength functions. Reduced valence widths are calculated using optical model wave functions in Section 5. Measured and calculated radiative widths are compared, and the role of excited target states and the giant dipole resonance in valence capture is considered. In Section 6, the experimental values for initial and final state correlations are tabulated and the results are used to delineate the role of further nonstatistical mechanisms in resonance neutron capture. The relationship between valence and doorway interactions and the correlation coefficients is formalized in Section 6, and in Section 8 the role of 3-quasiparticle and phonon excitations is reviewed. The general conclusions regarding the neutron capture mechanism are summarized in Section 9.

In the third article *"Lifetime measurements of excited nuclear levels by Doppler-shift methods"* by T. K. ALEXANDER and J. S. FORSTER, the authors discuss the two Doppler-shift methods: the recoil distance plunger method (RDM) and the Doppler-shift attenuation method (DSAM), which cover the time scale of 10^{-15}—10^{-9} s. The two techniques are rather different, but both rely on the Doppler effect, i.e. the shift in the energy of a γ-ray when it is emitted from a moving source. In the RDM the nuclei excited by a reaction recoil freely in a vacuum until they are quickly stopped by a movable plunger. It is possible to obtain lifetimes in the range 10^{-9}—10^{-12} s. The DSAM makes use of the slowing down time in a solid material: a range of lifetimes from 10^{-11} to about 10^{-15} s can be determined in this way. In Section 1, some general background relevant to the discussion of Doppler-shift methods is represented. In Sections 2 and 3, the two methods are discussed in detail; these Sections will be useful for experimental design as well as data analysis. In Section 4 some complemetary techniques are briefly discussed. Finally, in Section 5, some lifetime data obtained by the various techniques are compared and some conclusions drawn about the Doppler-shift methods.

The three articles of this volume of Advances in Nuclear Physics are intended for a wide audience, from research students to active research workers. The basic viewpoint of the treatment is pedagogical; therefore, the volume is highly recommended to those wishing to start research work in one of these promising fields of nuclear physics.

I. ANGELI

A. MERCIER, H.-J. TREDER and W. YOURGRAU: On General Relativity

Akademie-Verlag, Berlin, 1979, pp. 154

This small book is written about Einstein's general relativity. Its seven chapters follow a conventional path: differential geometry (a rather out-of-date account), gravitational equations, experimental tests and cosmology. A late chapter is devoted to the principle of equivalence. Finally, under the heading "Future of GRG" the reader actually finds an account of some past attempts like Rainich geometry or Finsler spaces. On p. 145, complex manifolds are introduced where "complex" means Kählerian (in Einstein's unified theory).

An illuminating excerpt (from p. 19) may help the reader to taste the spirit of this volume: "GRG theory . . . must be submitted to further generalizations or unifications which never get to an end".

Z. PERJÉS

Printed in Hungary

A kiadásért felel az Akadémiai Kiadó igazgatója **Műszaki szerkesztő:** Botyánszky Pál
A kézirat a kiadóba érkezett 1979. XII. 27. **A kézirat nyomdába érkezett:** 1980. I. 15. — **Terjedelem:** 10,5 (A/5) ív, 46 ábra

80.7897 **Akadémiai Nyomda, Budapest — Felelős vezető:** Bernát György

NOTES TO CONTRIBUTORS

I. PAPERS will be considered for publication in Acta Physica Hungarica, only if they have not previously been published or submitted for publication elsewhere. They may be written in English, French, German or Russian.

Papers should be submitted to

Prof. I. Kovács, Editor
Department of Atomic Physics, Technical University
1521 Budapest, Budafoki út 8, Hungary

Papers may be either articles with abstracts or short communications. Both should be as concise as possible, articles in general not exceeding 25 typed pages, short communications 8 typed pages.

II. MANUSCRIPTS

1. Papers should be submitted in five copies.

2. The text of papers must be of high stylistic standard, requiring minor corrections only.

3. Manuscripts should be typed in double spacing on good quality paper, with generous margins.

4. The name of the author(s) and of the institutes where the work was carried out should appear on the first page of the manuscript.

5. Particular care should be taken with mathematical expressions. The following should be clearly distinguished, e.g. by underlining in different colours: special founts (italics, script, bold type, Greek, Gothic, etc.); capital and small letters; subscripts and superscripts, e.g. x^2, x_3; small l and 1; zero and capital O; in expressions written by hand: e and l, n and u, v and v, etc.

6. References should be numbered serially and listed at the end of the paper in the following form: J. Ise and W. D. Fretter, Phys. Rev., *76*, 933, 1949.

For books, please give the initials and family name of the author(s), title, name of publisher, place and year of publication, e.g.: J. C. Slater, Quantum Theory of Atomic Structures, I. McGraw-Hill Book Company, Inc., New York, 1960.

References should be given in the text in the following forms: Heisenberg [5] or [5].

7. Captions to illustrations should be listed on a separate sheet, not inserted in the text.

8. As per lst January 1980 the use of SI units has been made compulsory for all publications issued in Hungary. Please note that in papers submitted to Acta Physica after that date all measures should be expressed in SI units.

III. ILLUSTRATIONS AND TABLES

1. Each paper should be accompanied by five sets of illustrations, one of which must be ready for the blockmaker. The other sets attached to the copies of the manuscript may be rough drawings in pencil or photocopies.

2. Illustrations must not be inserted in the text.

3. All illustrations should be identified in blue pencil by the author's name, abbreviated title of the paper and figure number.

4. Tables should be typed on separate pages and have captions describing their content. Clear wording of column heads is advisable. Tables should be numbered in Roman numerals. (I, II, III, etc.).

IV. MANUSCRIPTS not in conformity with the above Notes will immediately be returned to authors for revision. The date of receipt to be shown on the paper will in such cases be that of the receipt of the revised manuscript.

Reviews of the Hungarian Academy of Sciences are obtainable at the following addresses:

AUSTRALIA
C.B.D. LIBRARY AND SUBSCRIPTION SERVICE, Box 4886, G.P.O., *Sydney N.S.W.2001*
COSMOS BOOKSHOP, 145 Ackland Street, *St. Kilda (Melbourne), Victoria 3182*

AUSTRIA
GLOBUS, Höchstädtplatz 3, *1200 Wien XX*

BELGIUM
OFFICE INTERNATIONAL DE LIBRAIRIE, 30 Avenue Marnix, *1050 Bruxelles*
LIBRAIRIE DU MONDE ENTIER, 162 Rue du Midi, *1000 Bruxelles*

BULGARIA
HEMUS, Bulvar Ruszki 6, *Sofia*

CANADA
PANNONIA BOOKS, P.O. Box 1017, Postal Station "B", *Toronto, Ontario M5T 2T8*

CHINA
CNPICOR, Periodical Department, P.O. Box 50, *Peking*

CZECHOSLOVAKIA
MAD'ARSKÁ KULTURA, Národní třida 22, *115 66 Praha*
PNS DOVOZ TISKU, Vinohradská 46, *Praha 2*
PNS DOVOZ TLAČE, *Bratislava 2*

DENMARK
EJNAR MUNKSGAARD, Norregade 6, *1165 Copenhagen*

FINLAND
AKATEEMINEN KIRJAKAUPPA, P.O. Box 128, *SF-00101 Helsinki 10*

FRANCE
EUROPERIODIQUES S. A., 31 Avenue de Versailles, *78170 La Celle St.-Cloud*
LIBRAIRIE LAVOISIER, 11 rue Lavoisier, *75008 Paris*
OFFICE INTERNATIONAL DE DOCUMENTATION ET LIBRAIRIE, 48 rue Gay-Lussac, *75240 Paris Cedex 05*

GERMAN DEMOCRATIC REPUBLIC
HAUS DER UNGARISCHEN KULTUR, Karl-Liebknecht-Strasse 9, *DDR-102 Berlin*
DEUTSCHE POST ZEITUNGSVERTRIEBSAMT, Strasse der Pariser Kommüne 3—4, *DDR-104 Berlin*

GERMAN FEDERAL REPUBLIC
KUNST UND WISSEN ERICH BIEBER, Postfach 46, *7000 Stuttgart 1*

GREAT BRITAIN
BLACKWELL'S PERIODICALS DIVISION, Hythe Bridge Street, *Oxford OX1 2ET*
BUMPUS, HALDANE AND MAXWELL LTD., Cowper Works, *Olney, Bucks MK46 4BN*
COLLET'S HOLDINGS LTD., Denington Estate, *Wellingborough, Northants NN8 2QT*
W.M. DAWSON AND SONS LTD., Cannon House, *Folkestone, Kent CT19 5EE*
H. K. LEWIS AND CO., 136 Gower Street, *London WC1E 6BS*

GREECE
KOSTARAKIS BROTHERS, International Booksellers, 2 Hippokratous Street, *Athens-143*

HOLLAND
MEULENHOFF-BRUNA B.V., Beulingstraat 2, *Amsterdam*
MARTINUS NIJHOFF B.V., Lange Voorhout 9—11, *Den Haag*
SWETS SUBSCRIPTION SERVICE, 347b Heereweg, *Lisse*

INDIA
ALLIED PUBLISHING PRIVATE LTD., 13/14 Asaf Ali Road, *New Delhi 110001*
150 B-6 Mount Road, *Madras 600002*
INTERNATIONAL BOOK HOUSE PVT. LTD., Madame Cama Road, *Bombay 400039*
THE STATE TRADING CORPORATION OF INDIA LTD., Books Import Division, Chandralok, 36 Janpath, *New Delhi 110001*

ITALY
EUGENIO CARLUCCI, P.O. Box 252, *70100 Bari*
INTERSCIENTIA, Via Mazzé 28, *10149 Torino*
LIBRERIA COMMISSIONARIA SANSONI, Via Lamarmora 45, *50121 Firenze*
SANTO VANASIA, Via M. Macchi 58, *20124 Milano*
D. E. A., Via Lima 28, *00198 Roma*

JAPAN
KINOKUNIYA BOOK-STORE CO. LTD., 17-7 Shinjuku-ku 3 chome, Shinjuku-ku, *Tokyo 160-91*
MARUZEN COMPANY LTD., Book Department, P.O. Box 5050 Tokyo International, *Tokyo 100-31*
NAUKA LTD. IMPORT DEPARTMENT, 2-30-19 Minami Ikebukuro, Toshima-ku, *Tokyo 171*

KOREA
CHULPANMUL, *Phenjan*

NORWAY
TANUM-CAMMERMEYER, Karl Johansgatan 41—43, *1000 Oslo*

POLAND
WĘGIERSKI INSTYTUT KULTURY, Marszalkowska 80, *Warszawa*
CKP I W ul. Towarowa 28 *00-958 Warsaw*

ROMANIA
D. E. P., *Bucureşti*
ROMLIBRI, Str. Biserica Amzei 7, *Bucureşti*

SOVIET UNION
SOJUZPETCHATI — IMPORT, *Moscow* and the post offices in each town
MEZHDUNARODNAYA KNIGA, *Moscow G-200*

SPAIN
DIAZ DE SANTOS, Lagasca 95, *Madrid 6*

SWEDEN
ALMQVIST AND WIKSELL, Gamla Brogatan 26, *101 20 Stockholm*
GUMPERTS UNIVERSITETSBOKHANDEL AB, Box 346, *401 25 Göteborg 1*

SWITZERLAND
KARGER LIBRI AG, Petersgraben 31, *4011 Basel*

USA
EBSCO SUBSCRIPTION SERVICES, P.O. Box 1943, *Birmingham*, Alabama 35201
F. W. FAXON COMPANY, INC., 15 Southwest Park, *Westwood*, Mass. 02090
THE MOORE-COTTRELL SUBSCRIPTION AGENCIES, *North Cohocton, N. Y. 14868*
READ-MORE PUBLICATIONS, INC., 140 Cedar Street, *New York, N. Y. 10006*
STECHERT-MACMILLAN, INC., 7250 Westfield Avenue, *Pennsauken* N. J. 08110

VIETNAM
XUNHASABA, 32, Hai Ba Trung, *Hanoi*

YUGOSLAVIA
JUGOSLAVENSKA KNJIGA, Terazije 27, *Beograd*
FORUM, Vojvode Mišiča 1, *21000 Novi Sad*

Acta Phys. Hung. Tom. 48. No. 1. Budapest, 30. VII. 1980

Index: 26.022
HU-ISSN 0001-6705

ACTA PHYSICA

ACADEMIAE SCIENTIARUM HUNGARICAE

TOMUS XLVIII FASCICULI 2–3

AKADÉMIAI KIADÓ, BUDAPEST

1980

ACTA PHYS. HUNG. APAHAQ 48 (2–3) 119–336 (1980)

ACTA PHYSICA

ACADEMIAE SCIENTIARUM HUNGARICAE

SZERKESZTI
KOVÁCS ISTVÁN

Az *Acta Physica* angol, német, francia vagy orosz nyelven közöl értekezéseket. Évente két kötetben, kötetenként 4—4 füzetben jelenik meg. Kéziratok a szerkesztőség címére (1521 Budapest XI., Budafoki út 8.) küldendők.

Megrendelhető a belföld számára az Akadémiai Kiadónál (1363 Budapest Pf. 24. Bankszámla 215-11488), a külföld számára pedig a „Kultura" Külkereskedelmi Vállalatnál (1389 Budapest 62, P.O.B. 149. Bankszámla 217-10990), vagy annak külföldi képviseleteinél.

The *Acta Physica* publish papers on physics in English, German, French or Russian, in issues making up two volumes per year. Distributor: "Kultura" Foreign Trading Company (1389 Budapest 62, P.O. Box 149) or its representatives abroad.

Die *Acta Physica* veröffentlichen Abhandlungen aus dem Bereich der Physik in deutscher, englischer, französischer oder russischer Sprache, in Heften, die jährlich zwei Bände bilden.

Bestellbar bei »Kultura« Außenhandelsunternehmen (1389 Budapest 62, Postfach 149) oder seinen Auslandsvertretungen.

Les *Acta Physica* publient des travaux du domaine de la physique en français, anglais, allemand ou russe, en fascicules qui forment deux volumes par an.

On peut s'abonner à l'Entreprise du Commerce Extérieur «Kultura» (1389 Budapest 62, P.O.B. 149) ou chez représentants à l'étranger.

«*Acta Physica*» публикуют трактаты из области физических наук на русском, немецком, английском и французском языках.

«*Acta Physica*» выходят отдельными выпусками, составляющими два тома в год.

Заказы принимает предприятие по внешней торговле «Kultura» (1389 Budapest 62, P.O.B. 149) или его заграничные представительства.

ACTA PHYSICA

ACADEMIAE SCIENTIARUM HUNGARICAE

TOMUS XLVIII

AKADÉMIAI KIADÓ, BUDAPEST
1980

INDEX

Acta Physica Academiae Scientiarum Hungaricae, Tomus 48 (2—3), pp. 119—130 (1980)

CHARACTERIZATION OF HIGHLY COMPENSATED SEMI-INSULATED GaAs SUBSTRATES*

By

L. GÚTAI

RESEARCH INSTITUTE FOR TECHNICAL PHYSICS OF THE HUNGARIAN ACADEMY OF SCIENCES
H-1325 BUDAPEST, ÚJPEST 1, P.O.B. 76, HUNGARY

(Received 29. XI. 1979)

In recent years semi-insulating GaAs bulk material has been used as a substrate material in the production of many microwave devices. Compensating the shallow energy levels with deep centres of opposite type the specific resistivity of 10^8 ohmcm can easily be obtained.

The effect of SI substrate on the device performance, theoretical models for electrical compensation in the case of one and two deep levels and the different methods of compensation ratio determination are discussed. The widely used galvanomagnetic methods and the promising luminescent spectra analysis compared to other methods are investigated in detail.

1. Introduction

In recent years semi-insulating (SI) gallium arsenide bulk material with nearly intrinsic carrier concentration has come to be used as a substrate material for the fabrication of microwave field-effect transistors and Gunn effect digital devices or as a window material for high sensitivity infra-lasers. At the present stage of bulk crystal growing techniques intrinsic purity is out of the reach, so there is a necessity of using semi-insulating GaAs crystals of low free-carrier concentrations. The usual way is to compensate the shallow energy levels with deep centres of opposite type. Using chromium as a deep level impurity gallium arsenide with specific resistivity of 10^8 ohmcm at room temperature can easily be obtained [1, 2, 3, 4].

In the early stages of development of semi-insulating GaAs, before Cr doping was used, oxygen commonly used as an inhibitor of dissociation of SiO_2 from the ampoule during growth was proposed as a principal compensating impurity. After making the preparation of semi-insulating GaAs more reproducible by intentionally adding Cr, a deep acceptor, there has been considerable loss of interest in the electrical compensation mechanism. In this topic the paper of ZUCCA [5] has changed the situation. He believes it is an

* Presented at the Workshop Seminar on the Methods and Apparatus for the Investigation of the Physical Parameters of A^{III}—B^{V} Compounds, organised by the Research Institute for Technical Physics of the Hungarian Academy of Sciences, Budapest, 13—18 November 1978.

oversimplification to explain the high resistivity of the material by compensation of residual shallow donors by the deep Cr acceptors.

Regardless of whether the required doped regions are produced by epitaxial growth or by ion implantation the characteristics of the SI substrate material are found to strongly influence device performance.

A number of substrate problems have been identified, as outlined in the following [6]:

Imbalanced stoichiometry
— vacancy generation
Rapidly diffusing contaminant atoms
— O, C, Si, Cu, Mn
Crystalline defects
— dislocations, precipitates, lattice strain
Carrier traps, shallow and deep
$n - p$
Type conversion

i) *Imbalanced stoichiometry*

A major problem which GaAs has in common with all other binary semiconductors is that of doping effects caused by imbalanced stoichiometry. Even if the substrate material is cut from an ingot with perfect stoichiometry, unavoidable changes in stoichiometry occur during the device fabrication process. It is well known that heating GaAs in vacuum at temperatures greater than 450 °C produces relatively deep level acceptor states. For example the data of HARRIS [7] show the decrease in electron concentration at the surface of Sn doped, n-type epitaxial layers after annealing in a vacuum of 1×10^{-8} torr. The surface of the more lightly doped sample had converted to p-type after annealing. (The considerable change in concentration was observed in a depth of 3 μm from the surfaces.)

It has been clearly established that the cause of the acceptor states is vacancies or vacancy complexes generated during annealing. It apperas that a general agreement has developed in recent years that Ga vacancies are involved, but some uncertainty remains.

An alternative corrective measure which can be used rather than the SiO_2 coating to prevent vacancy generation in doped layers produced by ion implantation is the technique of dual implantation. HECKINGBOTTOM [8] has shown theoretically that the implantation of an equal dose of Ga along with a desired dose of Te should result in a higher electron concentration than the implantation of Te alone.

ii) *Contaminant atoms*

Another problem of GaAs SI substrates that can result in carrier traps and $n - p$ type conversion is that of contaminant atoms. These can be incorporated into the substrate material when the ingot is formed or they can be introduced by diffusion during high temperature equilibration prior to expitaxial layer growth. Si and Cu are common contaminants when the growing takes place in quarz boats. Use of graphite boats reduces Si and Cu contamination but then C and absorbed O_2 from the boat can contaminate the GaAs.

The trapping levels created by contaminant atoms have deleterious effects on devices fabricated in the substrates by ion implantation, or on the substrates by epitaxial growth. (This is well understandable in the former case, in the latter case the impurities are introduced into the epitaxial layer by outdiffusion from the substrate.) For example hysteresis-like loops are frequently observed on GaAs voltage-current characteristics when displayed on a curve-tracer with a low frequency sweep [6, 9] and generally are accompanied by degraded microwave — frequency performance.

Similar deep-level traps caused by oxygen contamination have been found to produce frequency dispersion in the gate characteristics of GaAs MISFETs [10], while Ishi [11] reports that O traps are responsible for "dark spot" defects in injection lasers.

iii) *Non-uniformity of compensating dopants*

Probably the most important characteristic of SI substrates in which devices are fabricated by direct ion-implantation doping is the uniformity of the intentionally added compensating dopant, usually Cr but sometimes O. A wide variation in doping efficiency (=carrier concentration/implanted ion dose) and carrier mobility has been found in S implanted n-layers formed in Cr doped wafers from different sources [12] which probably is due to the non-uniformity of chromium concentration. The variations in doping efficiency and mobility are related to varying concentrations of compensating centres in different wafers.

Measurements made on a large number of SI substrates show that the mobility linearly increases (at least in a rather narrow interval: 2200—3600 $cm^2/vsec$) with increasing carrier concentration rather than decreasing. This fact indicates that there are more compensating centres in the samples with low mobility.

The most effective corrective measure for overcoming the problem of non-uniform compensating dopant concentration is to epitaxially grow a relatively thick buffer layer of high resistivity GaAs on the substrate [13, 14, 15].

2. Theoretical model for electrical compensation

The resistivity ϱ of the material is governed by the well-known general equations [16]:

$$\varrho = (q\mu_e n + q\mu_k p)^{-1},$$

where:

$$n = N_C \exp\{-(E_C - E_F)/kT\},$$

$$p = N_V \exp\{-(E_F - E_V)/kT\}.$$

The Fermi level is determined by the neutrality condition:

$$n + N_a^- = p + N_d^+,$$

where N_a^- and N_d^+ are the electrically charged acceptor and donor concentrations, respectively. Since the free electron and hole concentrations in semi-insulating GaAs can be neglected with respect to the donor and acceptor concentrations, to calculate the Fermi-energy one can use the more simple equation

$$N_a^- = N_d^+$$

making use of which gives for the resistivity:

$$\varrho^{-1} = \frac{q\mu_e N_c}{G} e^{-\frac{E_c - E_0}{kT}} + \frac{q\mu_h N_v}{G} e^{-\frac{E_0 - E_v}{kT}},$$

where:

$$E_0 = \frac{1}{2}(E_d + E_a),$$

and

$$G = \frac{1}{2g_a}\left\{\left(\frac{N_a}{N_d} - 1\right) e^{\frac{E_d - E_a}{kT}} + \left[\left(1 - \frac{N_a}{N_d}\right)^2 e^{\frac{E_d - E_a}{kT}} + 4\frac{N_a}{N_d} g_d g_a\right]\right\}.$$

The resistivity of a semi-insulating GaAs as a function of donor and acceptor concentration, energy levels, degeneracy factors and the temperature can be determined making use of these relations.Note that the ratio of acceptor and donor concentrations enter into the expression only.

Two models were investigated in the quoted paper of ZUCCA in detail: i) one deep (acceptor) level; ii) one deep acceptor and one deep donor level.

Deep-acceptor model

In this model, residual shallow impurities, which are mostly Si donors, are compensated by Cr acting as a deep acceptor. The acceptor density N_a must always be larger than the residual donor density N_d, otherwise the Fermi level would lie close to the donor level and be near the conduction band.

Cr-doped semi-insulating GaAs can display either *n*- or *p*-type conduction at room temperature [17, 18]. It is difficult to account for such dual behaviour with the deep-acceptor model. The only variable parameter is the compensation ratio N_a/N_d the variation of which, in principle, can change the conductivity type. In reality, however, the range over which N_a/N_d may vary is narrow and is severely limited by the low solubility of Cr in GaAs.

After some simplification assuming all the donors to be ionized ($N_d^+ \approx N_d$) (because the Fermi level is located many kT's below the shallow donor level) one can get a simple expression for the resistivity ϱ:

$$\varrho = \frac{N_a/N_d - 1}{q\mu_e N_c g_a} e^{\frac{E_c - E_a}{kT}}.$$

Deep-donor-deep-acceptor model

In this model, there are both deep Cr acceptors and deep donors associated with oxygen impurities. The acceptor level is deep, allowing the density of deep donors N_d to be larger or smaller than the density of deep acceptors N_a. In this case the Fermi level may move from above E_d to below E_a. The range over which the Fermi level may vary as a function of realistic impurity concentrations is broader than in the former model, making this model more suited for explaining the existence of either *n*- or *p*-type Cr doped semi-insulating material.

In the case when all of the donor and acceptor levels are ionised:

$$\varrho = \frac{N_a/N_a - 1}{q\mu_e N_c g_a} e^{\frac{E_c - E_a}{kT}}, \quad (N_a \gg N_d)$$

$$\varrho = \frac{N_d/N_a - 1}{q\mu_p N_c} g_d e^{\frac{E_c - E_d}{kT}}, \quad (N_d \gg N_a).$$

Because the comparison of experiments made on samples with medium and high Cr concentrations with the above discussed model results in a deep acceptor level situated between 0.64 and 0.72 eV under the conduction band edge, a "three-level-model" has been proposed in the cited paper: one shallow donor, one deep Cr acceptor and a deep donor level which can be associated with the O impurity.

3. Determination of the compensation ratio

Luminescent measurements
Hall measurements
Electron beam microprobe (EMB)

Electron microprobe Auger spectrometry (EMAS)
Scanning electron microscope (SEM)
Secondary ion mass spectroscopy (SIMS)
Spark source mass spectroscopy (SSMS)
Photoconductivity
Transmission X-ray topography
Etching/microscopy
Measurements of device properties

The basic analysis techniques used to characterize traps produced by contaminant atoms are measurements of *photoluminescence spectra*, and Hall measurements of carrier concentration as a function of temperature. An interesting example of application of these techniques to identify an unknown contaminant atom is found in the work of ZUCCA [5], and HALLAIS et al [19]. In this case both works led to the same conclusion — that Mn contamination was responsible for highly conductive *p*-type interfacial layers found in *n*-type epitaxial layers grown on SI GaAs substrates. In the photoluminescent spectra one significant emission line (1.491 eV) was identified with shallow acceptors like Be, Mg, C, Zn and another (1.409 eV) along with its long wavelength phonon replicas was identified with Mn. The photoluminescence data alone do not clearly identify which acceptor is responsible for the observed *p*-type thermal conversion. However, measurements of resistivity and Hall constant as a function of temperature then were used to establish that the acceptor level responsible lies 0.098 eV above the valence band edge. Transitions between the conduction band and this energy level correspond to emission at the 1.409 eV peak. Hence Mn is identified as the contaminant involved.

The electron microprobe Auger spectrometer (EMAS) [20], with a beam diameter 0.3 μm, can be used to analyze impurity concentration profiles in bevelled samples (3°) with a resolution of 150 Å in depth.

The electron beam microprobe (EBM) and *secondary ion mass spectrometer* (SIMS) can also be used to measure impurity concentration profiles, but with less depth resolution because of their larger beam size. Measuring the uniformity of the electrical properties of ion implanted doped layers in Si substrate is an effective way of analyzing the uniformity of Cr (or O) compensating centres. However, it is not very convenient and consumes too much material. A more convenient tool is the SIMS in which an ion beam (usually argon) is focussed onto wafer while a mass spectrograph is used to identify the sputtered secondary ions released from the surface. KIM et al [21] have found that in general Cr content varied with depth as well as over the wafer surface. Variations in Cr concentration in the substrate are obviously extremely damaging to devices fabricated in the substrate by ion implantation. However, devices fabricated on top of such substrates by epitaxial layer growth are not

immune to these difficulties, because Cr (or O) can diffuse into the epi layer from the substrate [13]. Strains, dislocations, and slips generated in the interfacial region can be observed and characterized by means of either *photochemical etching* [22], *optical microscopy*, or *transmission* X-ray topography [23].

One of the most important techniques, the *analysis of photoluminescence spectra* shall be discussed in more detail. A new method has been developed to determine the ratio of compensation in *n*-GaAs by TAKESHI [24] et al. Using the net carrier concentration data at room temperature there is a possibility to determine the compensation ratio by the analysis of photoluminescence spectrum. It was shown by their measurements made on LPE GaAs with carrier concentration between 10^{13} cm^{-3} and 5×10^{15} cm^{-3} that this method is much more sensitive than the transport measurements based on mobility analysis.

The lower mobility in highly compensated GaAs samples can be explained by a scattering mechanism other than the ionised impurity scattering and this causes an overestimation in determining the compensation ratio. On the other hand: the pair formation of ionised scattering centres causes an underestimation in the compensation ratio.

The usual drawback of galvanomagnetic measurement techniques: the effect of inhomogeneous dopant distribution and of the contact geometry further decreases the reliability of these measurements.

Although the Van der Pauw measurement carried out over a broad temperature interval is suitable to determine the compensation ratio, the need for good ohmic contacts even at very low temperatures and the time consuming nature is the considerable drawback of this method.

The method described in the paper of TAKESHI is principally different from previous methods and is suitable to determine an extremely high compensation ratio ($N_A/N_D \geqslant 0.99$).

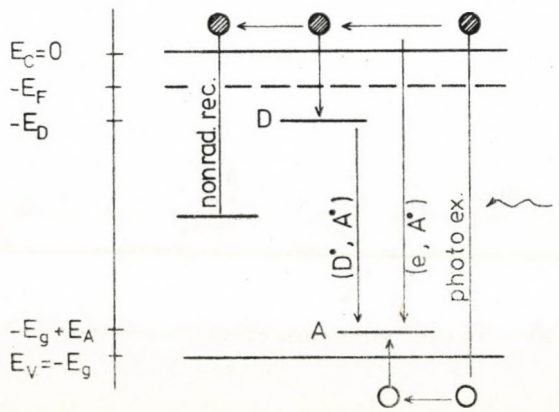

Fig. 1

The shape of the spectrum line and the location of the peak of a radiation recombination of a neutral donor depend on the majority carrier concentration in the semiconductor.

Since the photon energy belonging to this neutral donor-acceptor transition contains the Coulomb interactions of these energy states the shape of the spectrum line gives a direct information on the Poisson distribution of the nearest neighbours.

The recombination transitions together with the excited and nonradiative recombination transitions playing a role in the photoluminescence spectra are shown in Fig. 1 [24].

The transition $[D^\circ, A^\circ]$ is the neutral donor—neutral acceptor radiative recombination, the $[e, A^\circ]$ transition is the radiative recombination of electrons captured from conductive band by neutral acceptor level.

To determine the compensation ratio by the shape of a spectrum line the difference of the density of donor and acceptor states $N_d - N_a$ has to be determined in an independent way. (This can be obtained from a Van der Pauw or a Schottky capacitance measurement made at room temperature.) In this way the three unknown parameters: the donor concentration N_d, the acceptor concentration N_a, and the nonradiative recombination rate W_{NR} can be determined by the measured values of the location of the peak of $[D^\circ, A^\circ]$ spectrum line, by the intensity ratio of this transition and the $[e, A^\circ]$ transition and by the room temperature carrier concentration ($n = N_d - N_a$). (In practice the set of parameters N_D, N_A, W_{NR} has to be chosen to get the best fit to the spectrum lines of $[D^\circ, A^\circ]$ and $[e, A^\circ]$ transitions — and this procedure gives the check of the selfconsistence of the model.) Since the spectrum line shape is determined by the carrier distribution which is determined by the Fermi level, the fit gives some combination of values N_d and N_a. Using the value $n = N_d - N_a$, measured independently, N_d and N_a can be calculated separately. To calculate the carrier concentration n, the usual equilibrium statistics is used because of the low excitation level. A further simplification arises from the fact that the bonding energy of shallow donor centres in GaAs is independent of the nature of doping material (5.8 meV).

Unfortunately, the situation is quite different in the case of acceptor bonding energy. The uncertainty of this value is one of the limiting factors of reliability of the proposed method. (The data used in the paper are: $E_{AC} = 26.2 \pm 0.1$ meV, $E = 34.3 \pm 0.1$ meV.)

The model used for the shape-analysis of the $[D^\circ, A^\circ]$ and $[e, A^\circ]$ transitions is the following. The acceptor states are almost fully ionised. The free holes produced by low excitation are captured partially by ionised acceptor states establishing neutral acceptor levels which are unstable because of the following recombination processes:

i) radiative recombination between states D° and A° close to each other;

ii) radiative recombination between the conductive band and neutral acceptor levels;

iii) nonradiative transitions.

The spectral recombination rate by the theory is the following: For the neutral donor — neutral acceptor transitions:

$$I_{(D^\circ,A^\circ)}(E)\,dE = P[R(E)]\,\frac{dR}{dE}\,W_{(D^\circ,A^\circ)}[R(E)]\,P_A^\circ[R(E)]\,N_A dE,$$

for the conductive band — neutral acceptor level transitions:

$$I_{(e,A^\circ)}(E)\,dE = c(E - E_g + E_A)^{1/2}\,e^{-\frac{E-Eg+E_A}{kT}}\,n_A^\circ dE.$$

The $P(R)$ denotes the transition probability between the nearest neighbours distributed randomly in the crystal for which, in the case of not too high compensation, hold:

$$P(R)\,dR = 4\pi R^2\,e^{-\frac{4}{3}\pi R^3 N}\,DdR.$$

In the case of highly compensated material the interaction between the minority doping atoms (acceptors) has to be taken into account, as well. (This can be the object of the future investigation.)

Table I shows a considerable misfit between the compensation ratio determined by optical and electrical methods.

This large anomaly can be reduced partly taking into account the strong change of compensation ratio along the depth in the epitaxial layer from the surface. (The step-by-step mobility measurement — using the usual etching technique — gave a high negative gradient.) Since the optical method is sensitive for the surface only while the electrical measurement gives an average

Table I

Compensation ratio by optical and electrical methods

n(cm^{-3}) 300 K	Hall mobility (cm^2/Vs)		Comp. ratio N_A/N_D			Acceptor conc. N_A(cm^{-3})		
			Opt.	El. mob. anal.		Opt.	Electr. mobility an.	
	300 K	77 K		300 K	77 K		300 K	77 K
9.1×10^{12}	8740	174000	0.25	0.9	0.8	3×10^{12}	—	—
5.1×10^{13}	8150	115200	0.12	0.9	0.8	7×10^{12}	—	—
1.0×10^{15}	7050	35300	0.005	0.86	0.8	5×10^{12}	6.5×10^{15}	4×10^{15}
2.3×10^{15}	6677	31700	0.01	0.77	0.60	2.3×10^{13}	7.7×10^{15}	3.5×10^{15}
4.4×10^{15}	6750	33100	0.005	0.63	0.30	2.2×10^{13}	7.5×10^{15}	1.9×10^{15}

value over the entire layer, the optical result must be under the electrical one in the case of a negative mobility gradient. Using the *layer removal techniques* and the *optical compensation ratio determination* the real *concentration profile* was measured and the above argument was established by the authors.

The *photoelectric methods* can be successfully used in the determination of the compensation ratio and energy levels of GaAs:Cr [25].

As is well known the chromium atoms are located in the place of Ga in GaAs. The electron configuration of ions Cr^{2+} in SInGaAs is $3d^4$. In the SIpGaAs there are neutral Cr^{3+} acceptors, together with Cr^{2+} ions, with electron configuration $3d^3$. Heat conductivity measurements and electron-microscope investigations show the presence of microprecipitates with the average diameter of 20 Å if the Cr concentration exceeds the value of 10^{18} cm^{-3}.

It was shown by photoelectric measurements that the energy level of chromium acceptor is 0.8 eV below the conduction band independently of the temperature [26], while by other authors this value corresponds to the 0K with the temperature coefficient of -8×10^{-4} eV/K.

The complex nature of the doping centres associated with chromium atoms has been disclosed in the course of the systematic investigation of nGaAs:Cr by *photoluminescence*, *photoconductive* [27, 28], *photomagnetoresistance* [29] and *photocapacitance* [30] methods. In the steady-state case the following centres may exist:

i) compensated Cr acceptors with 0.6 eV under the conduction band with the electron capture cross section of 10^{-18} cm^2.

ii) Cr acceptor — ionised donor pair with 0.8 eV under the conduction band and with electron capture cross section of 10^{-17} cm^2.

The density of these centres can be modified by electric field and/or illumination — affecting the recombination cross section and, in this way, the photoluminescence and photoconductivity.

Using the TSC (thermostimulated current) method, measuring the *photoconductivity vs wavelength*, using the *photo-Hall effect*, measuring the *photoconductivity* as a function of *temperature* and/or *intensity* very useful results can be derived regarding the nature of the Cr^{3+} neutral acceptor states with $3d^3$ electron structure.

The experiments were carried out on Czochralski monocrystals. The doping concentration was determined by a "JEOL JXA-50 A" scanning microprobe electronmicroscope. The photogalvanomagnetic measurements were carried out in the temperature interval of 90—300 K, at the photon energies of 0.5—2.5 eV with intensity varied through 5 orders of magnitude. The conclusions based on the measurements are:

i) The TSC and the photogalvanomagnetic measurements have made possible to determine the nature of traps in Si—pGaAs: Cr. There are two types of traps:

a) hole trap with 0.15 eV above the valence band (10^{15} cm^{-3}). (Probably connected with $V_{As}^{+}Cu_{Ga}$ pairs.)

b) deep hole trap with 0.23 eV above the valence band (5×10^{16} cm^{-3}). (Probably connected with "Cu-donor" complexes.)

ii) The extrinsic photoconductivity can be explained by the electrons excited by light from valence band to neutral Cr acceptors with $3d^3$ electron configuration. (These acceptor levels are located at 0.77 eV above the valence band independently of the temperature.)

iii) The photoionisation cross section of Cr acceptor is 3×10^{-17} cm^2, which decreases to 10^{-20} cm^2 after an electron capture.

iv) The potential of neutral Cr^{3+} acceptor is delta-function like with a small Coulomb field. The Bohr radius of ground state is 4 atomic units.

The above list shows that combining different measurement methods one can get a deep insight into the nature of electrically active centres in semi-insulating GaAs. Not only the density and compensation ratio, the electron capture cross section and even the potential field of an individual center can be determined, as well.

REFERENCES

1. C. Hilsum, Progress in Semiconductors, edited by A. F. Gibson and R. E. Burgess, Temple Press, 1965, Vol. 9., p. 135.
2. C. H. Gooch, C. Hilsum and B. R. Holeman, J. Appl. Phys., **32**, 2069, 1961.
3. R. W. Haisty, E. W. Mehal and R. Stratton, J. Phys. Chem. Solids, **23**, 829, 1962.
4. G. R. Cronin and R. W. Haisty, J. Electrochem. Soc., **111**, 874, 1964.
5. R. Zucca, Proc. of North American Conf. on GaAs Related Compounds, St. Louis, Mo. September 1976.
6. R. G. Hunsperger and N. Hirsch, Solid-State Electronics, **18**, 349, 1975.
7. J. S. Harris, Y. Nannichi and G. L. Pearson, J. Appl. Phys., **40**, 4575, 1969.
8. R. Heckingbottom and A. Ambridget Radiation Effects, **17**, 31, 1973.
9. S. Asai, Ishiokas, H. Kurono, S. Takahashi and H. Kodera, Proc. of the 4th Conference on Solid State Devices, Tokyo, 1972. Supplement of the J. Japan Society of Applied Physics, **42**, 71, 1973.
10. T. Milyazaki, N. Nakamura, A. Doi and T. Tokuyana, Proc. 2nd Int. Conf. on Solid Surfaces, 1974, Japanese J. Applied Physics, Supplement **2**, 441.
11. M. Ishi, Applied Physics Letters, **29**, 375, 1976.
12. R. G. Hunsperger, Le Vide, **185**, 175, 1976.
13. M. G. Alderstein, Electronics Letters, **12**, 297, 1976.
14. N. Yokoyama, A. Shibutomi, S. Ohkawa, M. Fokuta and H. Ishikawa, Proc. of North American Conf. on GaAs and Related Compounds, St. Louis, Mo., September 1976.
15. I. Crossley, I. Goodrige, M. Cardwell and R. Butlin, Proc. of North. American Conf. on GaAs and Related Compounds, St. Louis, Mo., September 1976.
16. R. Zucca, J. Appl. Phys., **48**, 1987, 1977.
17. D. C. Look, J. Phys. Chem. Solids, **36**, 1311, 1975.
18. A. T. Philadelphus and P. C. Euthymiov, J. Appl. Phys. **41**, 3182, 1970.
19. J. Hallais, A. Mircea-Roussel, J. P. Farges and G. Poiblavd, Proc. North American Conf. on GaAs and Related Compounds, St. Louis Mo., September 1976.
20. T. Ishida, M. Ichiyama, Z. Oda and H. Hashimoto, J. Vacuum Science and Technology, **13**, 711, 1976.
21. H. B. Kim, D. L. Barett, G. G. Sweeney and T. M. S. Heng, Proc. North American Conf. on GaAs and Related Compounds, St. Louis, Mo., September 1976.
22. T. Saitoh, S. Matsubara and S. Minagawa, J. Electrochem. Society, **122**, 670, 1975.

23. H. KASANO, J. Appl. Physics, **47,** 2882, 1976.
24. K. TAKESHI and E. WAGNER, J. Appl. Phys., **48,** 1928, 1977.
25. W. PLESIEWICZ, Solid State Electron, **33,** 1079, 1977.
26. W. I. TURNER and G. D. PETIT, Bull Am. Phys. Soc., **9,** 269, 1964.
27. N. V. VOROBEVA, I. V. VOROBEV and O. V. TRETAK, Phys. Status Solidi (a), **17,** 155, 1973.
28. N. V. VOROBEVA, I. V. VOROBEV, I. I. KARKHANIN and N. G. FOMIN, Fiz. Tekhn. Poluprov., **9,** 1053, 1075.
29. A. G. ILASHENKO and I. V. VOROBEV, Phys. Status Solidi (a) **16,** K1, 1973.
30. A. A. GUTKIN, D. N. NASLEDOV and T. A. SHAPOSHNIKOVA, Fiz. Tekhn. Poluprov, **7,** 1299, 1973.

Acta Physica Academiae Scientiarum Hungaricae, Tomus 48 (2—3), pp. 131—146 (1980)

ELECTRICAL MODELLING OF OHMIC CONTACTS FORMATION ON METAL-n-GaAs SYSTEMS*

By

I. MOJZES

RESEARCH INSTITUTE FOR TECHNICAL PHYSICS OF THE HUNGARIAN ACADEMY OF SCIENCES
H-1325 BUDAPEST, ÚJPEST, 1. P.O.B. 76, HUNGARY

(Received 29. XI. 1979)

The contact resistance and quality can be determined by various methods. A common disadvantage of these methods is to investigate the contact after its formation occasionally by means of a special measuring sample. In the present work a new method for the in situ investigation of the metal—semiconductor contact is proposed. This method was used for the control of the technology of the metal—semiconductor ohmic contacts for high power Gunn diodes. A numerical analysis for the GaAs-AuGe$_{eut}$ system was made based on the electrical modelling of the contact formation.

1. Introduction

The investigation of metal—semiconductor contacts is a very important task from both the practical and theoretical point of view. The modern, often compound-semiconductor based, semiconductor devices operating with high current densities raise new demands for both the properties of contact and contacting technology.

One important feature of contacts is their resistivity, and for its measurement several methods have been designed to match the given basic material, layer structure (bulk crystal or a multi-layer epitaxial structure on conducting or semi-insulating substrate) and measurement accuracy.

Contact assessing methods usable in technological research should comply with the following requirements:

1. It is to be carried out on the device or specimen to be measured, i.e. no separate test piece should be needed.
2. Its realization should be simple and rapid.
3. The accuracy of measurement should be high.
4. Measurement data should permit to draw conclusions on the effect of factors influencing contact properties.

The determination of contact resistance consists, in fact, in separating the resistance of the bulk (which may be of homogeneous or layered structure) and contact resistance from the total resistance measured.

* Presented at the Workshop Seminar on the Methods and Apparatus for the Investigation of the Physical Parameters of A^{III}—B^{V} Compounds, organised by the Research Institute for Technical Physics of the Hungarian Academy of Sciences, Budapest, 13—18 November 1978.

The contact resistance can be determined by measuring the resistance between contacts of various geometrical shapes prepared on the bulk material [1, 2], or by measuring the potential distribution [3]. However, these methods are inaccurate, the accuracy is spoiled by inhomogeneities of contact and bulk [4]. The contact resistance can be determined by comparing the total resistance measured with contacts of different surfaces [5]; measuring the capacity and loss angle of the specimen [6]; comparing the resulting resistance of specimens of different thicknesses [7], and measuring the split temperature [8]. The specific contact resistance can also be determined by measuring the geometrical magnetoresistance [9, 10], the contact quality factor [11], or by a special method using four electrodes [12], by means of an angle-dependent geometrical magnetoresistance [13], and by measuring the pulse time-constant of the specimen [14].

These methods demand data either from independent measurements on the specimen [6, 8, 11, 14], or from another specimen [9, 10], or a measuring sample of special geometry [1, 2, 3, 5, 7, 12], or require knowledge of band structural properties [13]. The conductivities are generally obtained with a given specimen, but by an independent measurement, while data resulting from an independent specimen are generally mobilities measured on an accompanying slice grown on semi-insulating substrate. That and the value measured on a conducting substrate may show significant deviations depending on device technology [11, 15] or, alternatively, this deviation may be insignificant [16]. The method which can be used most suitably with a ready-made GaAs device or structure is the one of angle-dependent geometrical magnetoresistance [13, 17].

A common disadvantage of the above mentioned methods [1, 2, 3, 5, . . ., 15], is the need to investigate the contact after its formation, eventually by means of a special measuring sample. However, the control of the technology is more easily realized by checking at least one parameter of the contact during its formation, so information may be obtained from the contact during its formation. For that purpose we may use the record of a low (0.5 . . . 1 mA) measuring current applied to the specimen and of the potential drop effected by it [18] during the annealing necessary for the formation of an ohmic contact. This method has been used for controlling the technology for the purpose of producing contacts of high power Gunn diodes [19].

2. Experimental

The measuring setup is shown in Fig. 1. A constant current flows through the specimen provided with contacts prepared by evaporation. According to our experience the specimen resistance varies in the range of several orders of magnitude, so the voltage across it is amplified by a logarithmic amplifier.

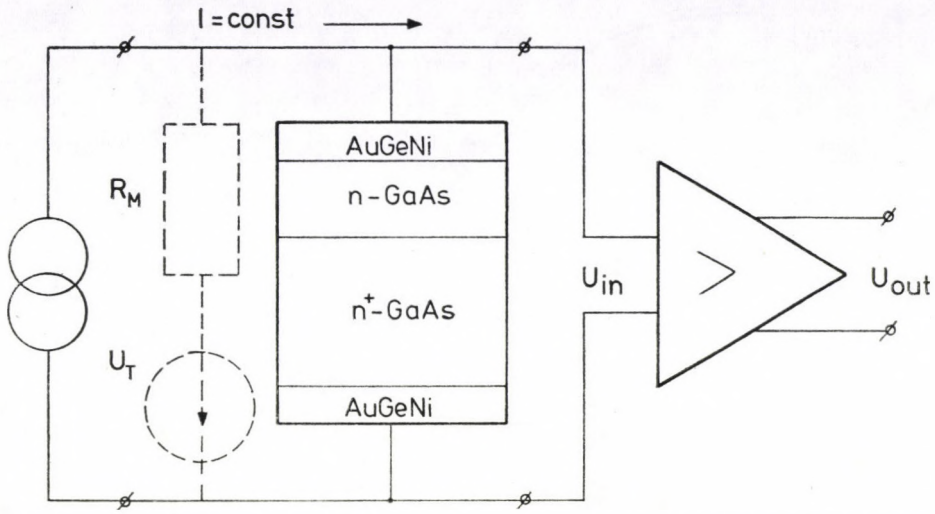

Fig. 1. Schematic diagram of the in situ resistance measurement carried out during annealing. The equivalent circuit is shown with dotted lines

The above measurement has been used in the preparation of contacts of Gunn diodes. After having inserted the diode-structure in the case, a current has been applied to the specimen.

The voltage change caused by a current of 1 mA as a function of temperature is shown in Fig. 2 for a diode produced by a technology optimized in a way described in [17].

The initial resistance i.e. the resistance of two metal—semiconductor transitions connected in series, as measured at room temperature, is high. In the cooling region the resistance of the specimen decreases with temperature. This type of curve is called Type No. 1. If the chosen annealing temperature is higher, the resistance of the strucure formed has generally not decreased with decreasing temperature on the descending branch of the annealing line. That type of curve is called Type No. 2.

A distribution of Gunn diodes between the two types mentioned above, depending on the maximum annealing temperature, is shown in Fig. 3. The maximum value of microwave output power is also shown in the Figure.

Based on measurements performed on several thousand specimens the following conclusions can be drawn:

1) If the diode resistance increases during cooling (curve Type No. 2), then no microwave power can be measured on them, since they generally burn out at low voltages.

2) Such specimens mainly occur among diodes annealed at higher temperature.

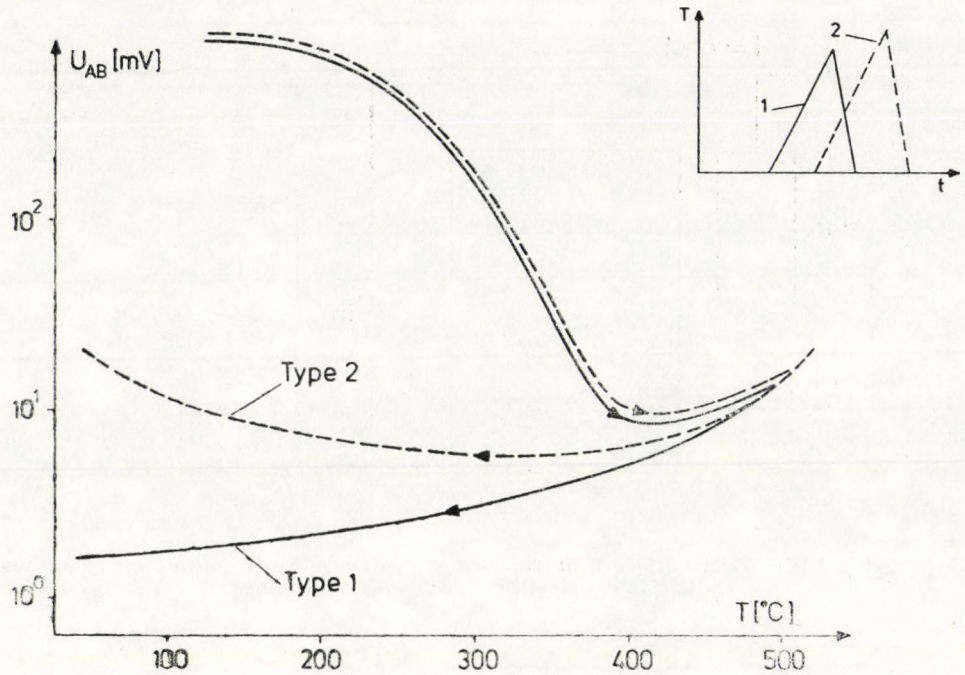

Fig. 2. Change of the voltage across the specimen during annealing: ——— diode produced at optimized temperature; - - - - diode produced at a temperature higher than optimized

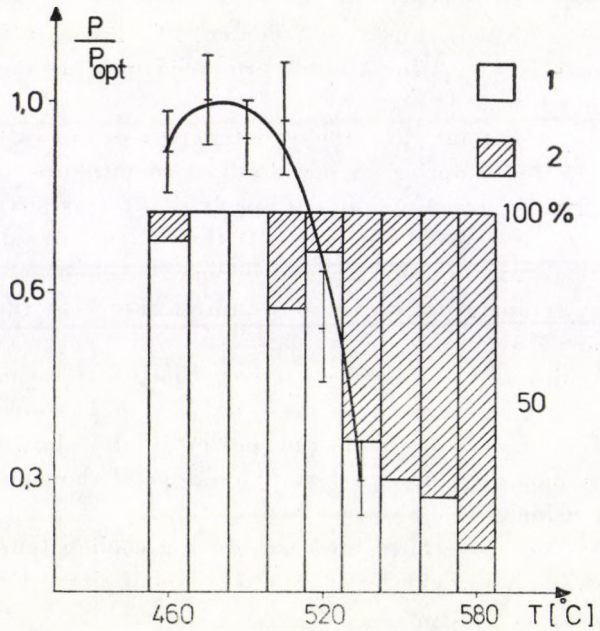

Fig. 3. Distribution of diodes between the two types previously mentioned and the maximum microwave power in function of contact annealing temperature

3) If the diode resistance decreases with decreasing temperature, such devices function as diodes, and microwave power can be measured. The output power of diodes shows an optimum depending on annealing temperature.

3. Results and discussion

3.1. *Modelling of the temperature-dependence of specimen resistance during annealing*

To provide a basis for a better understanding of our experimental results and to describe the contact formation an equivalent diagram is presented as shown in Fig. 4.

The voltage drop on the specimen caused by current $I = \text{const.}$ is the following:

$$IR_{k1} + IR_a + IR_{k2}. \tag{1}$$

The resulting voltage drop on the specimen:

$$U_{AB} = IR_{k1} + IR_a + IR_{k2} + U_T. \tag{2}$$

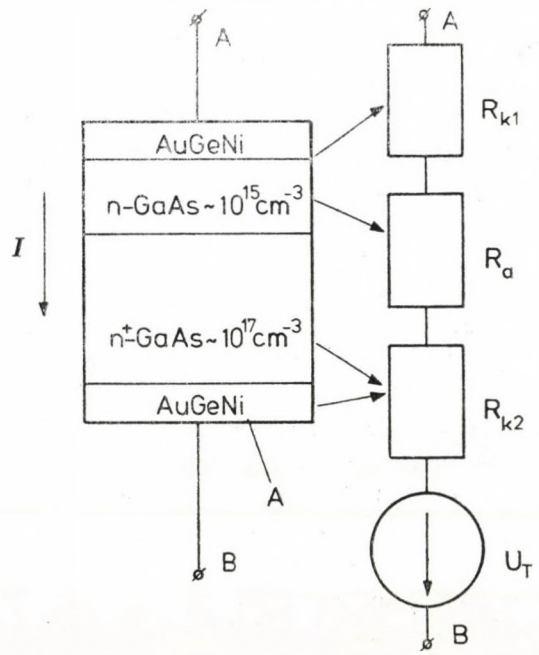

Fig. 4. Equivalent diagram of the Gunn structure for modelling the temperature dependence of the voltage across the sample

In the above formula, U_T is the resultant thermovoltage in the specimen (mainly ocurring at the $n - n^+$ junction), as well as between the specimen and case, and also between the upper contacts. Of course, it is inconvenient to calculate the thermovoltage in the case of a system containing so many junctions and materials, so it has been determined experimentally. Consequently, the voltage on the specimen is always the sum of the thermovoltage and the voltage drop along the specimen resistance. The direction of thermovoltage is shown in Fig. 4, and the temperature dependence of data determined by experiments can be approximated by the following formula:

$$U_T = 14.28 \times 10^{-6}\, T^2 - 142.85 \times 10^{-3}\ (\text{mV}) \qquad (3)$$

where T is the specimen temperature in °C.

Naturally, new measurements have to be carried out for other material systems and heating-up conditions. The specimen resistance, i.e. the resultant of R_{k1}, R_a and R_{k2} can be approximated by the following formula:

1) Prior to the thermal pulse a Schottky junction is created by the materials forming an ohmic contact on both sides of the specimen. The resistance of the contact on the substrate is lower and more ohmic, because the resistivity of the contact prepared to match the layer containing impurities corresponding to the carrier concentration in the substrate layer is by at least two orders of magnitude lower than the resistivity of the contact prepared to match the active layer.

2) After switching on the thermal pulse the ohmic contact begins to be formed. The resistance of the Schottky junction rapidly decreases with increasing temperature. The thermovoltage starts to increase. At the peak value of the thermal pulse the voltage on the specimen — with the chosen diode construction and measuring current — is determined by the thermovoltage.

3) During the course of the thermal pulse the molten layer recrystallizes forming a highly doped contact layer. In the upper descending part of the thermal pulse the resultant voltage is made up of the thermovoltage and the voltage drop on the active layer resistance. In the case of curve Type No. 1 introduced in Paragraph 2 an ohmic contact is formed on the specimen. That resistance is independent of temperature [20], and if the specimen is of low resistivity, then the active layer resistance will dominate in the total resistance of the specimen. (The substrate resistance is essentially lower and may be incorporated in resistance R_{k2}). When during the cooling period the resultant resistance is increasing, then the contact formed will be of poor quality. If the recrystallization fails, then a damaged layer will be formed. In this case the contact resistance is approximated by a relation valid for contacts which have been prepared on structures with high resistivity intermediate layer.

4) During the measurement period the current passes through several mechanical contact points. These are the following: between the lower part

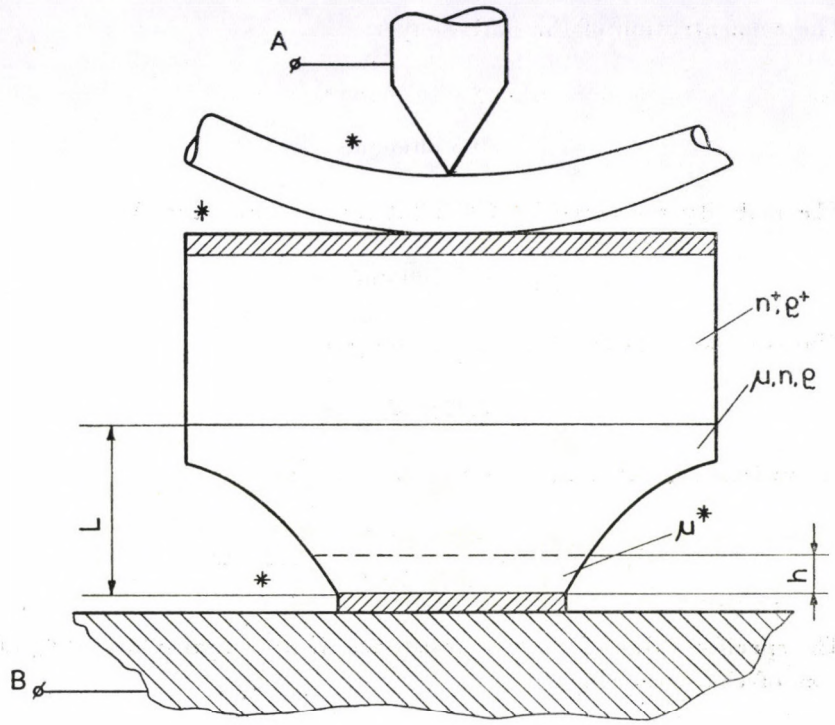

Fig. 5. High power Gunn diode

of the chip and the case; between the upper part of the chip and gold filament; between gold filament and tungsten needle provided with a wedge shaped top (see Fig. 5).

Because of the low measuring current ($I = 1$ mA) and the value of thermovoltage being a few millivolt only, particularly in the region of higher temperatures, where the contact is in molten state and thermal expansion may also cause displacements, small inconsistencies may occur in the shape of the curve. However, that will not occur in the region most interesting for us, i.e. at the end of the descending branch of the curve, since the chip has been soldered up, and the gold filament has also been soldered up to the upper contact.

A setup and symbols are shown in Fig. 5 to model the temperature dependence of the resistance of high power diodes.

The modelling is discussed in two parts: the ascending branch and the descending branch of thermal pulse used for annealing.

The modelling is demonstrated in the example of a GaAs Gunn diode, hence also the numerical data relate to a high power X-band diode.

In the calculations an abrupt $n - n^+$ junction, a homogeneous dopant distribution, uniform contact surface and an active layer of cylindrical form have been assumed.

The concentration of the active layer:

$$n = 2 \times 10^{15} \text{ cm}^{-3},$$

$$\varrho = 0.5 \text{ ohmcm}.$$

The mobility measured by GMR (at room temperature:)

$$\mu_{300} = 7\,100 \text{ cm}^2/\text{Vs}.$$

The surface of active layer at Ø 300 μm:

$$A = 7.07 \times 10^{-4} \text{ cm}^2.$$

Its resistance, for a thickness of $L = 10$ μm

$$R_a = \varrho \frac{L}{A} = \frac{0.5 \times 10^{-3}}{7.07 \times 10^{-4}} = 0.71 \text{ ohm}.$$

The specific value of contact resistance, if its magnitude is 10% of the resistance of the active layer,

$$R_{k1} = 5.0 \times 10^{-5} \text{ ohmcm}^2.$$

(The value practically obtainable is 1—6%.)

The temperature dependence of the high purity active layer resistance has been discussed in several papers [21,22, 23, 24].

A distinct difference appears in the temperature dependence of Hall constant in epitaxial and bulk crystals, respectively. Generally, more deep levels are to be found in bulk crystals. For example, AKITA [22] detected in oxygen-doped bulk crystals two deep levels and a shallow donor level, as well as a shallow acceptor level. In an epitaxial layer deep levels have been found mainly near to the $n - n^+$ junctions. These levels are distributed homogeneously [23]. A different behaviour is shown by slices grown by vapour and liquid phase techniques.

The measurement at high temperature is made difficult by the self-conduction of the substrate, contact degradation and As-evaporation.

Regarding the conduction mechanism, RUD pointed out that below 700 °C the mechanism is of extrinsic conduction, while above this temperature an intrinsic conduction mechanism appears [24].

The numerical evaluation of data published in the papers mentioned above has shown that the relations cannot be generalized in higher temperature ranges and are specific of a given crystal. Therefore a formula given by

BRAVMAN [25] has been used to evaluate the resistance of the active layer. We checked this formula experimentally also in the low temperature range and found that it describes with percentage accuracy the temperature dependence of low-field resistance of the slices investigated.

The application limit of the relation is set by BRAVMAN to 300—600 K, because in this range the electron concentration does not depend on temperature in epitaxial *n*-GaAs containing shallow donor levels. This temperature range is most important partly because in the given configuration at higher temperatures the thermovoltage is higher than the voltage drop on the specimen, caused by the measuring current, on the other hand the contact being yet in a molten state. (On the ascending branch of thermal pulse the resistance of the metal—semiconductor junction dominates.)

The resistance of the active layer is determined by the temperature dependence of mobility, which could be approximated by the following formula [25]:

$$\mu(T) = \mu_0 \cdot \frac{225}{T - 73} . \tag{4}$$

Modelling the contact formation in the function of temperature and other parameters has been carried out on computer. The experimental results have been proved suitable for modelling by the aid of the program.

3.2. *Modelling the temperature dependence in the ascending branch of thermal pulse*

The AuGe eutectic evaporated on a cleaned GaAs surface at a temperature of 200 °C creates a metal — semiconductor junction. The quality of this junction is decreased by the effect of temperature.

In the case investigated in this work, the objective was to eliminate the metal—semiconductor junction, consequently for modelling the ohmic contact formation in this region only an approximative description will be used.

Modelling has been carried out under the following conditions:

1) The surface of the specimen is homogeneous.

2) The idealization factor $b = 1$. i.e. the junction is ideal. A real specimen always allows a lower value of open-direction current. The current flowing through a metal — semiconductor junction under the effect of bias voltage V is the following [26]:

$$I = AA^* T^2 \exp\left(\frac{-q\varphi_B}{kT}\right)\left[\exp\left(\frac{qV}{kT}\right) - 1\right]. \tag{5}$$

The voltage across the metal—semiconductor junction in the case of low-signal current-generator drive:

$$V = \frac{bkT}{q}\left\{\ln\left[I + AA^* T^2 \exp\left(-\frac{q\varphi_B}{kT}\right)\right] - \right.$$
$$\left. - \ln\left[AA^* T^2 \exp\left(-\frac{q\varphi_B}{kT}\right)\right]\right\}. \qquad (6)$$

The temperature dependence of the voltage on the specimen for various φ_B values is shown in Fig. 6.

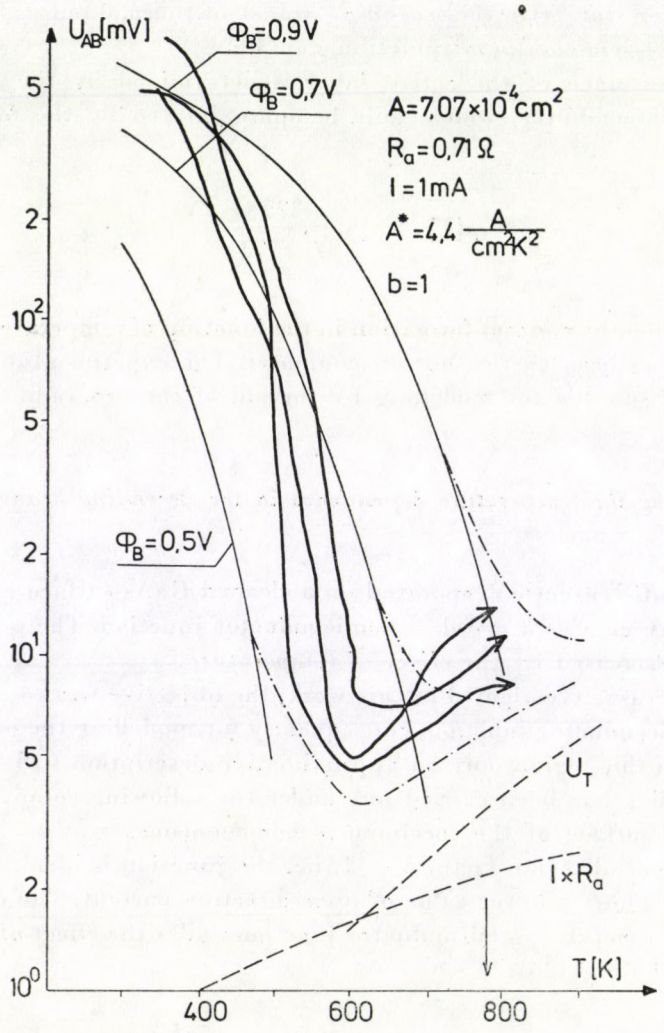

Fig. 6. The voltage on the sample investigated on the ascending branch of the thermal pulse. —·—·— theory; ——— experiment

The voltage on the sample in this region is composed of the voltage drop on the metal-semiconductor transition and the thermovoltage at higher temperatures. With the sample construction chosen the voltage drop on the active layer is negligibly small.

A great majority of measurements carried out have shown a tendency of fitting to the course of the $\varphi_B = 0.90$ V curve in the low temperature range and to the course of the $\varphi_B = 0.50$ V curve in the high temperature range, but regarding absolute values they often exhibited a higher resistance. This implies that in the low temperature range the gold dominates which is in a good agreement with results obtained by the investigation of the Au—GaAs junction for which a value of $\varphi_B = 0.90$ V was obtained by SINHA [27]. At high temperatures the value of $\varphi_B = 0.50$ V is in good agreement with the value obtained by PRUNIAUX for the AuGe—GaAs systems [28].

In the modelling, for the idealization factor of the metal—semiconductor junction the value of $b = 1.0$ has been chosen. Actually this value ranges from 1.1 to 1.2, and this results in a further voltage increase on the sample, if the drive is of the current-generator type (see formula (6)).

3.3. *Modelling the temperature dependence during the cooling period*

The molten contact system — if alloy formation is supposed — enters into interaction with GaAs, and contact formation will start. In the descending branch of the thermal pulse the melt recrystallizes and a highly doped layer is formed.

Let us examine first the case, when a resistance curve of Type No. 1 is formed (see Fig. 2). The voltage on the sample, if $R_{k1} \gg R_{k2}$, will be

$$U_{AB} = U_{in} = I\,(R_a + R_{k1}) + U_T = f(T). \tag{7}$$

R_{k1} practically does not depend upon temperature (20), the resistance of the active layer is described by relation (4).

The calculated value of temperature dependence of a high power diode of Ø 300 μm is shown in Fig. 7. We should note two cases in the diagram; first when the contact resistance is equal to the resistance of the active layer, and the second when it is 10% of the latter.

The optimum annealing temperature that has been experimentally determined for a given thermal pulse is also indicated in Fig. 7.

It is to be seen that the voltage on the sample in the lower temperature ranges follows with close approximation the voltage drop caused by the measuring current, i.e. here the function is proportional to the temperature dependence of the resistance.

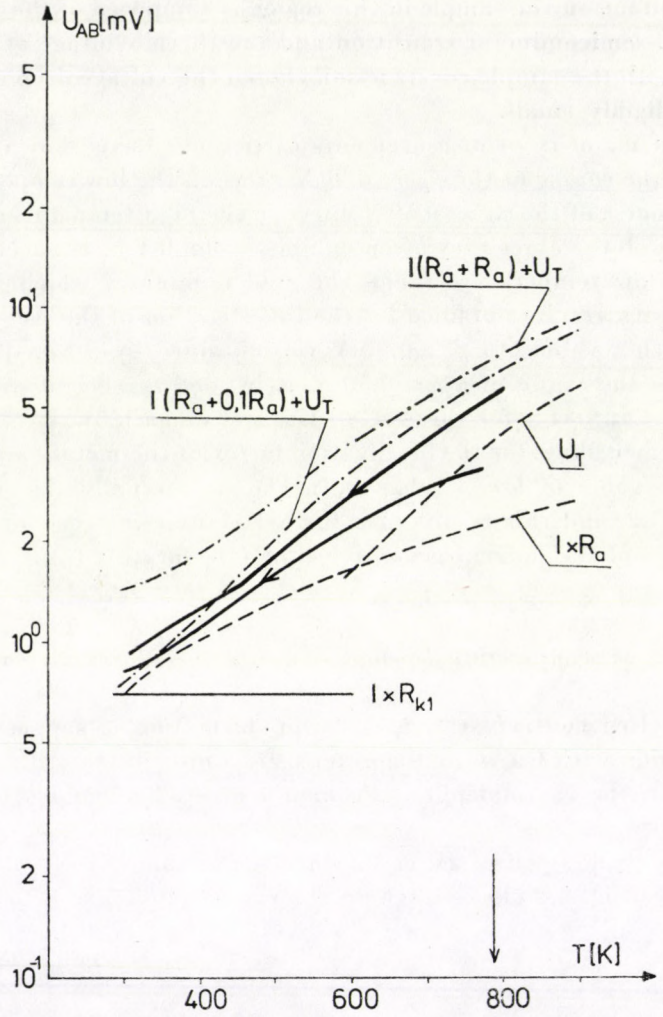

Fig. 7. Temperature dependence of the voltage on the sample during the cooling period: → optimum annealing temperature; —·—·— theory; ——— experiment

Such a course could be noted in the case of diodes produced at optimum annealing temperature on the voltage-temperature diagram. The contact formed is ohmic and during the annealing process the diodes which have exhibited the largest resistance changes have proved to have the lowest contact resistivities.

Let us investigate the case, when a diode Type No.2 is formed, i.e. whose resistance increases in the cooling period, and the annealing temperature is higher than optimum. It is known that contacting such systems with different physical properties (lattice structure, type of conduction, thermal expan-

sion coefficient, etc.) at and along the interfaces certain inhomogeneities occur. In contact formation the metal layer applied incorporates into the semiconductor modifying its conduction mechanism. In the modelling of the curve Type No. 2 the starting point was that the layer under the metal contact had been degraded. Reference to this point may be found in literature [29, 30].

This layer has been assumed to be of high resistivity and the course of the resistance curve has been modelled by the aid of relation deduced for the contact resistance of high resistivity layers (From Eq. 83. on p. 413 in[26]).

The contact resistance in the case of a high resistivity intermediate layer is:

$$R_k = \frac{h}{q\mu_a n} \frac{kT}{qV_k} \exp\left(\frac{qV_k}{kT}\right). \tag{8}$$

The same expression was used by BARÜBIN et al for the characterisation of the temperature variation of the InGeAg contact after its formation [30].

The value of the above relation depending upon V_k may result in a decreasing or increasing value as function of temperature.

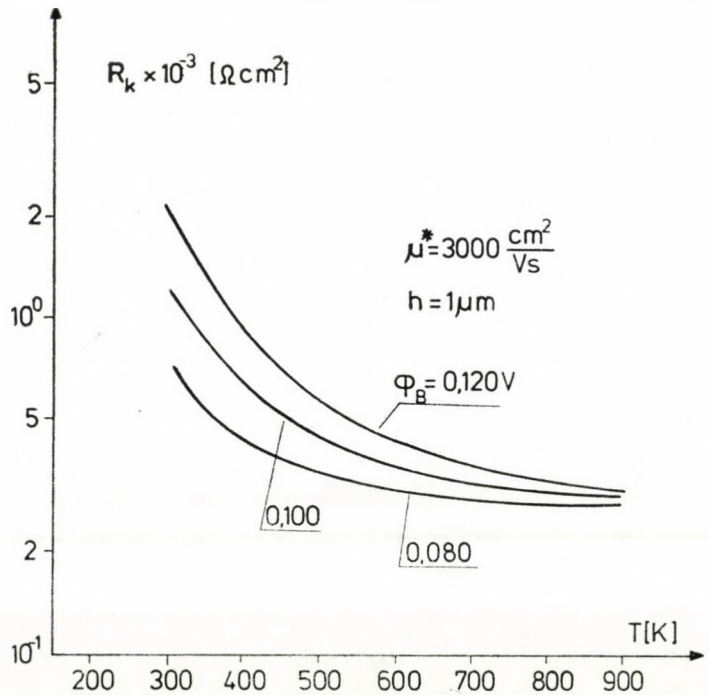

Fig. 8. Resistance of a high resistivity semiconductor—metal contact as function of temperature

Expressing V_k from (8):

$$\ln\left(\frac{q^2 \mu_a n R_k}{hkT}\right) = \frac{qV_k}{kT} - \ln V_k. \tag{9}$$

The transcendent equation (9) has been solved numerically. Thus, it has been made possible to approximate the values of V_k. For the condition and numerical data given in Paragraph 3.2. this value has been found to lie in the range of

$$V_k = 80 \ldots 120\,\text{mV}.$$

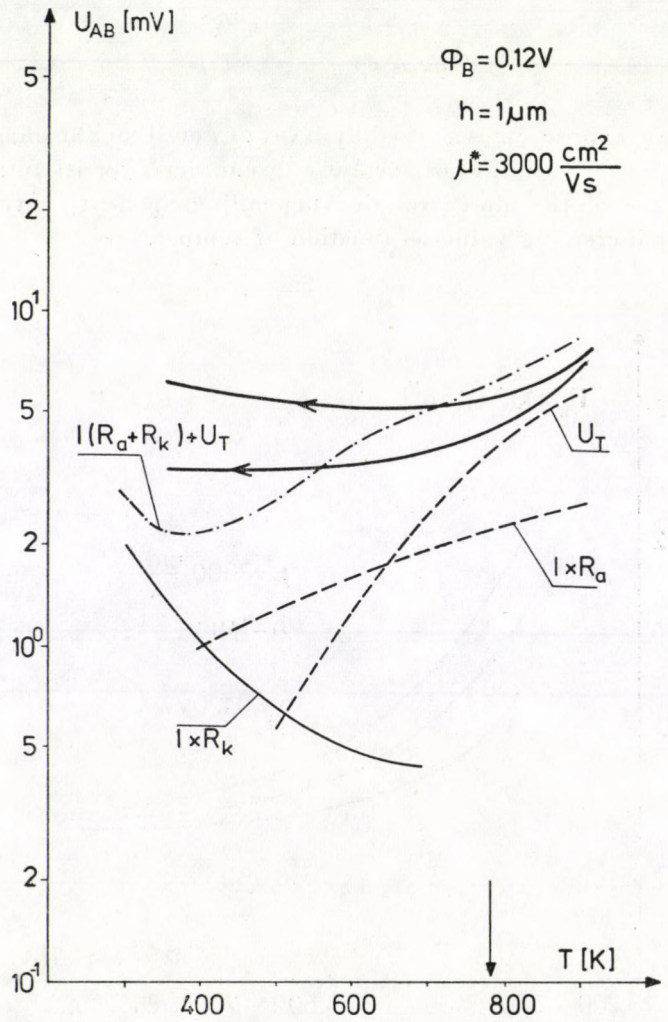

Fig. 9. Resultant voltage on the sample occurring when a high resistivity layer is formed. —·— theory; —— experiment

The temperature dependence of the resistance of a semiconductor—metal contact in the case of high resistivity intermediate layer is shown in Fig. 8.

It may be observed that within the temperature range investigated this resistance decreases with increasing temperatures. A case is illustrated in Fig. 9, when a 1 μm thick high resistivity layer was formed. In this layer the mobility is decreased to half of its usual value. The resultant resistance — as is to be seen in Fig. 9 — is determined by the resistance of the high resistivity intermediate layer.

When a higher annealing temperature was chosen, diodes of curve Type No. 2 were obtained in a distribution shown in Fig. 3. It is important to emphasize distribution, because the optimum temperature range of annealing is relatively narrow, which also means that a great deal depends on heat transfer and surface quality. One of the major advantages of the method proposed in this work lies just in eliminating this uncertainity, for implications can be made from the shape of curves to the quality of the contact formed. If the annealing proves insufficient under the effect of the first pulse, it may be continued by applying repeated pulses. It may be decided by the aid of the record, whether the annealing process has succeeded in setting right the contact. Diodes annealed at temperatures below optimum show also characteristics of Type No. 2. With such diodes no ohmic contact has been formed, their resultant resistance follows that of the metal — semiconductor junction.

In summarising the results, the proposed method has proved well usable to investigate the formation and quality of ohmic contacts.

REFERENCES

1. F. Nibler, J. Appl. Phys., **34**, 1572, 1963.
2. K. L. Klohn and L. Wandinger, J. El. Chem. Soc., **116**, 507, 1969.
3. W. Shockley, Final Techn. Rep. N° AL-TRD-64 207.
4. Yu. F. Sokolov and B. B. Elenkrig, FTP, **7**, 627, 1973.
5. R. Cox and H. Strack, Solid-State Electronics, **10**, 1213, 1967.
6. G. A. Armantrout and J. C. Looney, Solid-State Electronics, **11**, 29, 1968.
7. Yu. A. Goldberg and V. B. Tsarenkov, FTP, **3**, 1718, 1969.
8. W. Tantraporn, J. Appl. Phys., **41**, 4669, 1970.
9. T. R. Jervis and E. F. Johnson, Solid-State Electronics, **13**, 181, 1970.
10. P. Blood, Acta Electronica, **15**, 33, 1972.
11. W. S. C. Gurney, El. Lett., 711, 1971.
12. J. P. Nougier and M. Rolland, Solid-State Electronics, **16**, 1399, 1973.
13. L. Gútai and L. Mojzes, Appl. Phys. Lett., **26**, 325, 1975.
14. S. Dhar and B. R. Nag, J. El. Chem. Soc., **125**, 508, 1978.
15. M. Kotani, IEEE Trans. ED—**23**, 567, 1976.
16. B. Pődör, I. Mojzes and B. Szentpáli, Acta Phys. Hung., **44**, 79, 1978.
17. I. Mojzes, Á. Barna and B. P. Barna, Proc. of MICROCOLL' 78, Budapest, Aug. 1978, II, V-2/10. 1.
18. I. Mojzes, phys. stat. sol., (a), **47**, K183, 1978.
19. Hung. Pat. No. 173621.
19. Hung. Pat. No. 173621.
20. B. V. Morozov, E. M. Skok, A. A. Velichko, E. V. Ivanov, L. Gútai and I. Mojzes, Thin Solid Films, **36**, 419, 1976.

21. F. E. ROBERTS, Phys. Lett., **17**, 21, 1965.
22. K. AKITA, H. IIDA and O. RYUSAN, Jap. J. Appl. Phys., **10**, 392, 19.
23. V. I. KHOKLOV, YU. G. SIDOROV and S. A. DVORETSKIJ, phys. stat. sol. (a), **25**, 311, 1974.
24. YU. V. RUD and K. V. SANIN, Neorg. Mat. **11**, 1876, 1975.
25. J. S. BRAVMAN and L. F. EASTMAN, IEEE Trans., ED— **17**, 744, 1970.
26. S. M. SZE, Physics of Semiconductor Devices, John Wiley and Sons, New York, 1969.
27. A. K. SINHA and J. M. POATE, Appl. Phys. Lett., **23**, 666, 1973.
28. B. R. PRUNIAUX, J. Appl. Phys., **42**, 3575, 1971.
29. J. GYULAI, J. W. MAYER, V. RODRIGEZ, A. Y. G. YU and H. J. GOPEN, J. Appl. Phys., **42**, 3578, 1971.
30. A. A. BARÜBIN, A. A. ZAHAROV, L. B. LJUHINA and V. M. PRIGOROVSZKIJ, Proc. of Sym. on Generation of Microwaves, Novosibirsk, USSR, 457, 1974 (in Russian).

Notation

A	area of diode, cm^2	R_a	active layer resistivity, ohm
A^*	effective Richardson's constant, $A/cm^2/K$	R_k	specific contact resistivity, $ohmcm^2$
b	ideality factor of diode	T	absolute temperature, K
h	thickness, cm	U_T	thermovoltage, mV
I	current, A	V	applied voltage, V
k	Boltzmann's constant, $1{,}38 \cdot 10^{-23}$ J/K	μ	mobility, $cm^2/V/s$
L	active layer thickness, μm	μ^*	mobility in high resistivity layer
n	carrier concentration, cm^{-3}	ϱ	specific resistivity, ohmcm
q	electronic charge, $1{,}602 \cdot 10^{-19}$ C	φ_B	barrier height, eV

Acta Physica Academiae Scientiarum Hungaricae, Tomus 48 (2—3), pp. 147—152 (1980)

ON THE SELF-COMPENSATION OF DONORS IN LIQUID PHASE EPITAXIAL GaAs*

By

B. PŐDÖR

RESEARCH INSTITUTE FOR TECHNICAL PHYSICS OF THE HUNGARIAN ACADEMY OF SCIENCES**
H-1325 BUDAPEST, ÚJPEST 1, P.O.B. 76, HUNGARY

(Received 29. XI. 1979)

Self-compensation of donors and acceptors due to Si incorporation in liquid phase epitaxial GaAs layers was studied with the help of electrical measurements. The compensation degree, i.e. the ratio of acceptors (Si atoms on As sites) to the donors (Si atoms on Ga sites) deduced from the electrical data agree well with the results of theoretical estimations, above a certain Si concentration. Below this the compensation degree is increased due to the formation of vacancies behaving as acceptors.

1. Introduction

It is widely believed that GaAs epitaxial layers as well as bulk single crystals are more or less compensated, independently of the method of crystal growth. This means that the concentration of electrically active impurities or defects is always greater than the concentration of free current carriers. The occurrence of compensation is usually inferred from the values of the electron mobility measured at a given electron concentration. It turned out that the electron mobilities, usually measured at the temperature of liquid nitrogen, are always less than the theoretical values calculated under the assumption that the concentration of ionized impurities equals the concentration of free current carriers (see [1—5] and other papers referred to in these works.)

Several different possible mechanisms are proposed in the literature to explain the compensation of electrically active impurities in GaAs.

One of these mechanisms is based on the amphoteric behaviour of elements of the IV group of the periodic table, chiefly of Si, and also of Ge and Sn as impurities in GaAs. These impurities can be incorporated into both sublattices of the binary compound, depending on the conditions of crystal growth, thus causing compensation. It is known that Si is the dominant resi-

* Presented at the Workshop Seminar on the Methods and Apparatus for the Investigation of the Physical Parameters of A^{III}—B^{V} Compounds, organised by the Research Institute for Technical Physics of the Hungarian Academy of Sciences, Budapest, 13—18 November 1978.

** Present address: Research Laboratory for Inorganic Chemistry of the Hungarian Academy of Sciences .H-1052 Budapest, P.O. Box 132

dual impurity in non-doped bulk GaAs crystals. It is also established that Si is one of the dominant residual donors in high purity intentionally non-doped epitaxial layers of GaAs [6, 7]. Further on Si is the chief compensating acceptor in liquid phase epitaxial layers [8, 9].

The role of Si in causing compensation of vapour phase epitaxial GaAs layers is also discussed in the literature. DILORENZO [10] explained the observed compensation of layers grown using the $AsCl_3/Ga/H_2$ method by the behaviour of residual Si impurities. On the other hand ASHEN et al. [8, 9] have shown that the dominant residual acceptor impurity in vapour phase epitaxial GaAs is Zn.

Another mechanism of compensation was proposed by WOLFE and STILLMAN [3] based mainly on experimental findings on vapour phase epitaxial GaAs. It was proposed that the substitutional donors of group IV and VI (IV_{Ga}^{+} and VI_{As}^{+}), respectively, are compensated by acceptor-like complexes of the type $(IV_{Ga}V_{Ga})^{-}$ and $(VI_{As}V_{As})^{-}$, respectively. The possibility of the occurrence of acceptor complexes of $Si_{Ga}\,V_{Ga}$ was already postulated in [11, 12] from photoluminescence results. Later photoluminescence measurements have been interpreted in general with the help of such acceptor complexes consisting of donor atoms and gallium or arsenic vacancies, respectively [13].

In this respect it is to be noted that recently POTH et al [2] could not reconcile their extensive experimental data obtained on vapour phase epitaxial layers either with the compensation model based on the amphoteric behaviour of group IV impurities or with the model proposed by WOLFE and STILLMAN [3].

Naturally, several more complex models of self-compensation can be constructed. Examples of such models are the one of KENDALL [14] invoking divacancy-gallium lattice atom reactions, or the other one by KASANO [15] invoking diatomic complexes.

In this paper results of the analysis of electrical properties and compensation of liquid phase epitaxial GaAs layers grown in our laboratory are described. On the basis of evidence presented below it is thought that the behaviour of self-compensation is governed by the incorporation of Si impurities and can be explained by invoking the amphoteric behaviour of Si.

2. Experimental results

The behaviour of compensation degree ($K = N_A/N_D$) and the dependence of total concentration of ionized impurities ($N_I = N_D + N_A$) on the electron concentration n_0 was studied on intentionally non-doped liquid phase epitaxial GaAs layers grown under approximately identical conditions. Details of the experimental procedures and some results were reported in [1, 16]. Only a brief review will be made here.

Liquid phase epitaxial layers were grown from nominally 6N purity Ga melts onto (100) oriented Cr-doped semi-insulating substrates in purified H_2 atmosphere. The Ga melt was saturated with pure boat or Czochralski grown single crystalline GaAs. The starting temperature of the epitaxial growth was 800 °C. Before growth the saturated melt was preheated to 850 °C for 8—12 hours. The cooling rate at growth was 0.25—0.5 °C/min. The grown epitaxial layers had a thickness of 10 to 30 μm. The epitaxial layers were not intentionally doped.

The compensation degree and the total concentration of ionized impurities were determined from the analysis of electron mobilities measured at temperatures of 77 and 300 K taking into account lattice scattering, ionized impurity scattering and scattering on space charge regions as discussed in our earlier work [1]. Very similar results were obtained also by using the semi-empirical method of analysis due to WOLFE et al [17] (cf. also [3]).

The dependence of acceptor concentration on donor concentration in non-doped liquid phase epitaxial layers is presented in Fig. 1. The following points should be mentioned. The compensation degree, above about $N_D =$

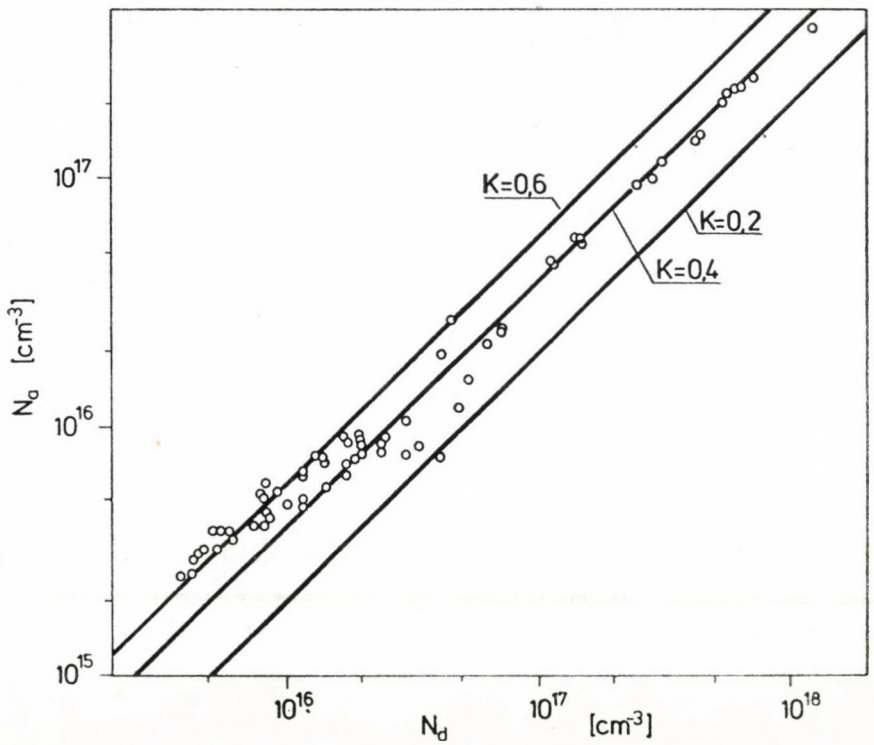

Fig. 1. Acceptor concentration vs donor concentration in LPE GaAs layers. Lines corresponding to compensation degrees of 0.2, 0.4 and 0.6, respectively, are also shown

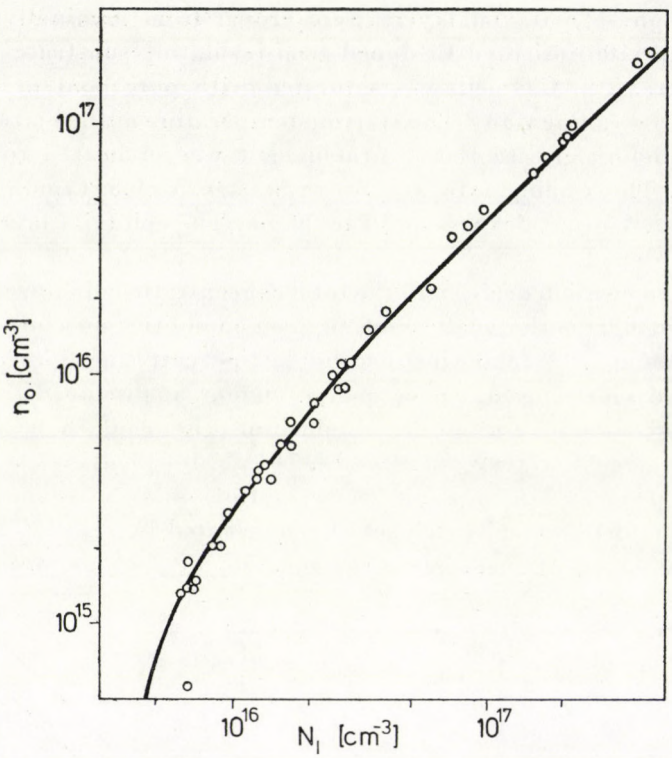

Fig. 2. Electron concentration measured at 77 K vs total ionized impurity concentration in LPE layers. Calculated curve for $K_i = 0.40$ and $[V] = 1.0 \times 10^{15}$ cm^{-3} is also shown

$= 3 \times 10^{16}$ cm^{-3} is practically constant, having a value of about 0.4. Below this concentration value the dependence of acceptor concentration on donor concentration deviates from the linear relationship. These deviations become more distinct if the carrier concentration (measured at liquid nitrogen temperature), $n_0 = N_D - N_A$, is plotted against the total impurity concentration, $N_I = N_D + N_A$, as done in Fig. 2.

3. Discussion

We will try to show that the above results (cf. Fig. 2) can be interpreted on the basis of the model concerning the behaviour of amphoteric impurities (in our case of Si) in semiconductors due to LONGINI and GREENE [18] and RYTOVA and FISTUL [19]. According to this theory the relationship between n_0 and N_I can be written as

$$N_I = [D] + [A] + [V] = (n_0 + [V]) \frac{1 + (n/n_i)^2 K_i}{1 - (n/n_i)^2 K_i} + [V], \qquad (1)$$

where $[D]$ and $[A]$ are the concentrations of donors and acceptors due to the incorporation of amphoteric impurities into the gallium and arsenic sublattices, n_i and n are the intrinsic and total concentrations of electrons at the temperature of growth, $[V]$ is the vacancy acceptor concentration, and $K_i = f(T)P_{As_4}^{-1/2}$ is the coefficient of self-compensation of the amphoteric impurity (in our case of Si) in the intrinsic material.

The compensation degree K_a due only to the incorporation of amphoteric impurities is given as

$$K_a = [A]/[D] = K_i(n/n_i)^2. \tag{2}$$

In the present case of epitaxial growth temperature of 1073 K the intrinsic carrier concentration is estimated as $n_i \cong (2-3)\times 10^{17}$ cm^{-3}, then for electron concentrations below about $(3-5)\times 10^{16}$ cm^{-3}, we can put approximately $n \cong n_i + n_0 \cong n_i$ and $K_a \cong K_i$. Then, accordingly

$$N_I \cong (n_0 + [V])\frac{1 + K_i}{1 - K_i} + [V]. \tag{3}$$

Eq. (3) was fitted to the experimental data presented in Fig. 2. The resulting theoretical curve is also shown in Fig. 2. We got $K_i = 0.40 \pm 0.03$ and $[V] = (1.0 \pm 0.2)\times 10^{15}$ cm^{-3}.

These results are analogous to those of IKOMA and NAKAGAWA [20] obtained for vapour phase epitaxial growth in the $Ga(AsCl_3)H_2$ system at growth temperatures from 700 to 810 °C.

Concerning the role of vacancies causing an increased level of compensation at low Si concentrations it is to be noted that IKOMA and NAKAGAWA [20] have observed in vapour phase epitaxy that the concentration of vacancy-acceptors decreased with increasing arsenic pressure, P_{As_4}, and have supposed that arsenic vacancies play a dominant role as compensating acceptors over gallium vacancies. In the literature there is some evidence that the arsenic vacancies behave as acceptors [3, 21]. Our findings do not contradict this proposition.

4. Acknowledgements

Grateful acknowledgements are due to Dr. I. BERTÓTI for the growth of epitaxial layers and Mrs. Zs. PÜSPÖKI for her help in the electrical measurements.

REFERENCES

1. B. PŐDÖR, N. NÁDOR and I. BERTÓTI, phys. stat. sol. (a), **29**, 173, 1975.
2. H. POTH, H. BRUCH, M. HEYEN and P. BALK, J. Appl. Phys., **49**, 285, 1978.
3. C. M. WOLFE and G. E. STILLMAN, Appl. Phys. Lett., **27**, 564, 1975.
4. D. L. RODE and S. KNIGHT, Phys. Rev., **B3**, 2534, 1971.
5. D. L. RODE, in Semiconductors and Semimetals, Ed. R. K. Willardson and A. C. Beer, Academic Press, New York, 1975, Vol. 10, p. 1.

6. G. E. Stillman, D. M. Larsen, C. M. Wolfe and R. C. Brandt, Solid State Comm., **9**, 2245, 1971.
7. R. A. Cooke, R. A. Hoult, R. F. Kirkman and R. A. Stradling, J. Phys. D, **11**, 945, 1978.
8. D. J. Ashen, P. J. Dean, D. T. J. Hurle, J. B. Mullin and A. M. White, Proc. 4th Symposium on Gallium Arsenide and Related Compounds, Deauville, 1974, Inst. Phys. Conf. Ser. **24**, 229, 1975.
9. D. J. Ashen, P. J. Dean, D. T. J. Hurle, J. B. Mullin, A. M. White and P. D. Green, J. Phys. Chem. Sol., **36**, 1041, 1975.
10. J. V. DiLorenzo, J. Crystal Growth, **17**, 189, 1972.
11. E. M. Williams, Phys. Rev., **168**, 922, 1968.
12. C. J. Hwang, J. Appl. Phys., **40**, 4200, 1969.
13. E. W. Williams and H. B. Bebb, in Semiconductors and Semimetals, Ed. R. K. Willardson and A. C. Beer, Academic Press, New York, 1972, Vol. 8, p. 231.
14. D. L. Kendall, in Semiconductors and Semimetals, Ed. R. K. Willardson and A. C. Beer, Academic Press, New York, 1968. Vol. 4, p. 163.
15. H. Kasano, J. Appl. Phys., **49**, 4021, 1978.
16. B. Pődör, I. Mojzes and B. Szentpáli, Acta Phys. Hung., **44**, 79, 1978.
17. C. M. Wolfe, G. E. Stillman and J. O. Dimmock, J. Appl. Phys., **41**, 504, 1970.
18. R. L. Longini and R. F. Greene, Phys. Rev., **102**, 992, 1956.
19. Н. С. Рытова, В. И. Фистуль, ФТП, **4**, 1109, 1970.
20. H. Ikoma and M. Nakagawa, Jap. J. Appl. Phys., **11**, 338, 1972.
21. E. Munoz, W. L. Snyder and J. L. Moll, Appl. Phys. Lett., **6**, 262, 1970.

Acta Physica Academiae Scientiarum Hungaricae, Tomus 48 (2—3), pp. 153—160 (1980)

INVESTIGATION OF OXIDIZED $A^{III}B^{V}$ SURFACES BY PHOTORESPONSE*

By

M. SOMOGYI

RESEARCH INSTITUTE FOR TECHNICAL PHYSICS OF THE HUNGARIAN ACADEMY OF SCIENCES
H-1325, BUDAPEST, ÚJPEST 1., P.O.B. 76, HUNGARY

(Received 29. XI. 1979)

The wavelength dependence of photoresponse was studied, observed in the sub band gap energy region of Au-GaP Schottky barriers. Anomalously high response was measured in this energy region if the metal layer was prepared immediately after chemical cleaning, just after etching. The high response diminished pronouncedly when electrodes were made onto surfaces oxidized during storage in air. The presence of a transparent layer on the surface could be established by electron diffraction and ellipsometry as well. The layer structure depended on surface treatment. It was concluded that the high response is located in the interface region, and is characteristic of the slightly oxidized surface.

General remarks on photoresponse

An illuminated semiconductor sample, supplied with electrical contacts produces electrical response without external bias, if the following criteria are fulfilled: i) the sample must contain built-in fields; ii) the light must reach the region of built-in fields; iii) within this region carriers can be excited optically into the valence and/or conduction band, respectively. The phenomenon is called photoresponse and finds its important application in the form of solar cells.

Most simple examples are any kind of junctions and barriers. In this paper the main attention is paid to the problems of photoresponse observed on Schottky barriers. As shown in Fig. 1 the short circuit current vs light energy measured from the band gap energy downwards can be used for barrier height and band gap determination as well [2, 3] by calculating the Fowler plot. At energies smaller than the barrier height the carriers are electrons excited from the electrode metal. Reaching the energy of the band gap the amount of excited carriers, i.e. holes and electrons, increases abruptly, as demonstrated by Fig. 1. By taking the square root of the response per incident photon, the Fowler plot is obtained. (The Fowler plot is applicable to the simple case of metal-semiconductor interface as represented by Fig. 1/b [3]. Naturally,

* Presented at the Workshop Seminar on the Methods and Apparatus for the Investigation of the Physical Parameters of A^{III}—B^{V} Compounds, organised by the Research Institute for Technical Physics of the Hungarian Academy of Sciences, Budapest, 13—18 November 1978.

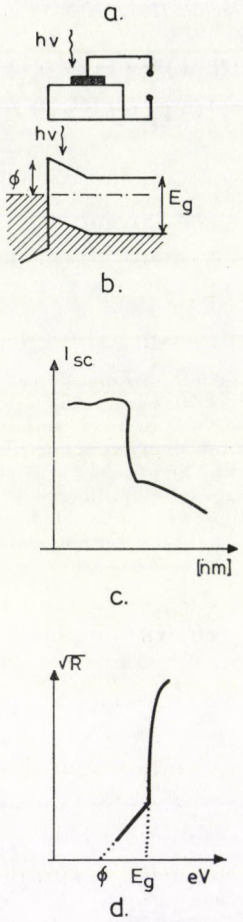

Fig. 1. a) Geometry of sample; b) Barrier-region; c) Short circuit current vs wavelength in nm; d) Fowler plot: square root of photocurrent per incident photon as a function of photon energy

p — n junctions give also a photoresponse but the shape of the curve corresponding to Fig. 1/c depends on numerous parameters. In simple cases usually maximal response is obtained at the energy of the band gap.)

Particularly high response is observed when the metal electrode is semitransparent, however, even in case of nontransparent electrodes sufficient light will reach the depletion layer by internal reflection, provided the light spot is larger than the electrode. Thus the curve preserves its shape characteristic of Schottky barriers and can be used for barrier height and band gap determination.

Photoresponse of III—V systems

As photoresponse gives direct information on the depletion layer, it is successfully used for the band gap determination of ternary III—V compounds [4, 5, 6]. The method can be developed further by preparing a series of barriers onto an angle-lapped section of the sample. In this way the change of band gap through the graded region can be determined. Of course a calibration curve must be prepared by another independent method if absolute values are necessary. Furthermore, when the system of built-in fields is adjusted properly, conclusions may be drawn [7, 8] concerning dopants.

It was observed that the photoresponse of Schottky barriers prepared onto GaP is very sensitive to surface treatments [9], consequently it may contain information about the real nature of GaP-metal interface or GaP surface. The shape of the Fowler plot, or short circuit current vs wavelength curve deviated from that shown in Fig. 1/c and Fig. 1/d, and the deviation could be correlated with surface treatments. Similar observations were made on $GaAs_{1-x}P_x$ where $x > 0.7$, but systematic studies were carried out only on GaP. However, certain Fowler plots and photoresponse curves of Si, GaAs and CdS published in the literature [10, 11, 12] deviate also to some extent from the ideal shape indicating a similar but less pronounced sensitivity.

In the present case photoresponse is used as a tool of surface and interface investigations. That means, the idealistic representation of Fig. 1/b is rejected, and a thin interface region is postulated between the metal and bulk material. It is supposed that this region has structure and composition different from the bulk and being within the depletion region optical excitation can produce carriers from the interface. The surface region is regarded as the end product of the usual surface cleaning procedures, and its properties may influence electrical characteristics too.

Experimental part

The mechanically polished GaP slices were chemically etched. Several etchants were used, but the results in this paper refer to the etchant 1 vol cc HN_3O + 3 vol cc HCl known as aqua regia. Technical details and problems of GaP etching are given elsewhere [13].

Schottky barriers were prepared onto the (100) oriented slices by evaporation of gold. The slices were cut from Czochralski grown ingot and Te doped to a carrier concentration of $1-4 \cdot 10^{17}$ cm^3. Evaporation was carried out under the usual conditions at a pressure of $1 \cdot 3 \cdot 10^{-3}-2 \cdot 6 \cdot 10^{-4}$ P when oil diffusion pump was used without liquid nitrogen trap and substrate heating. The gold electrodes were either nontransparent or had a thickness between 50—80 nm. As it will be seen later the thickness of electro de metal may be of

importance in certain cases. The photoresponse was measured with the aid of a Zeiss monochromator of type SPM—1, and a Keithley 610 C electrometer. On samples prepared in parallel experiments the formation of surface layer after etching was observed when the sample was kept in air at room temperature. The growth of layer thickness could be followed and determined by ellipsometry from about the 5^{th}—10^{th} minute.

The instrument used was a Gaertner ellipsometer of type L-119. Similarly, from the first few minutes electron diffraction investigations were made on separate samples to collect information about the surface structure. Composition was also measured by Rutherford backscattering. The results of the detailed investigations are presented elsewhere [14].

Results

If the metal electrode was prepared immediately after aqua regia etching on the resulting Schottky barrier anomalously high photoresponse could be measured in the sub band gap region as shown in Fig. 2 (curve 1). (Qualitatively the same effect could be observed by using any other strongly oxidant etchant.(This observation was the starting point of the work. In the first series of experiments semitransparent gold electrodes were prepared, and the samples gave very high response but only just after evaporation. Because the response slowly diminished with time, nontransparent electrodes were prepared. In the latter case the response was not so high in the entire wavelength region but stability increased with time. When the sample was illuminated from the reverse side, the $\sim 500\ \mu$ thick crystal acted as an optical filter. Fowler plots obtained by both illuminations of the same electrode without correction or normalization are shown in Fig. 2. In case of back side illumination the response was somewhat higher as more light reached the interface, but the character of the curves was similar.

The electron diffraction patterns showed that using cold aqua regia the structure of the surface layer was amorphous after etching and the half-width of the rings of the pattern diminished very slowly. The thickness of the layer in the first minutes was found to be 2.0—3.0 nm and increased logarithmically with time until 4.0 nm was reached. Above this thickness value the scatter of data increased abruptly so that the readings could not be evaluated. This indicates an uneven, inhomogeneous layer. According to the preliminary Rutherford backscattering determinations [14], which were supported also by further work, the etched surface is covered by a layer of suboxide of the disordered substrate atoms. Preparing another Schottky barrier onto a surface kept for longer time (133 days) in air the curve No. 2 of Fig. 3 was obtained. As seen

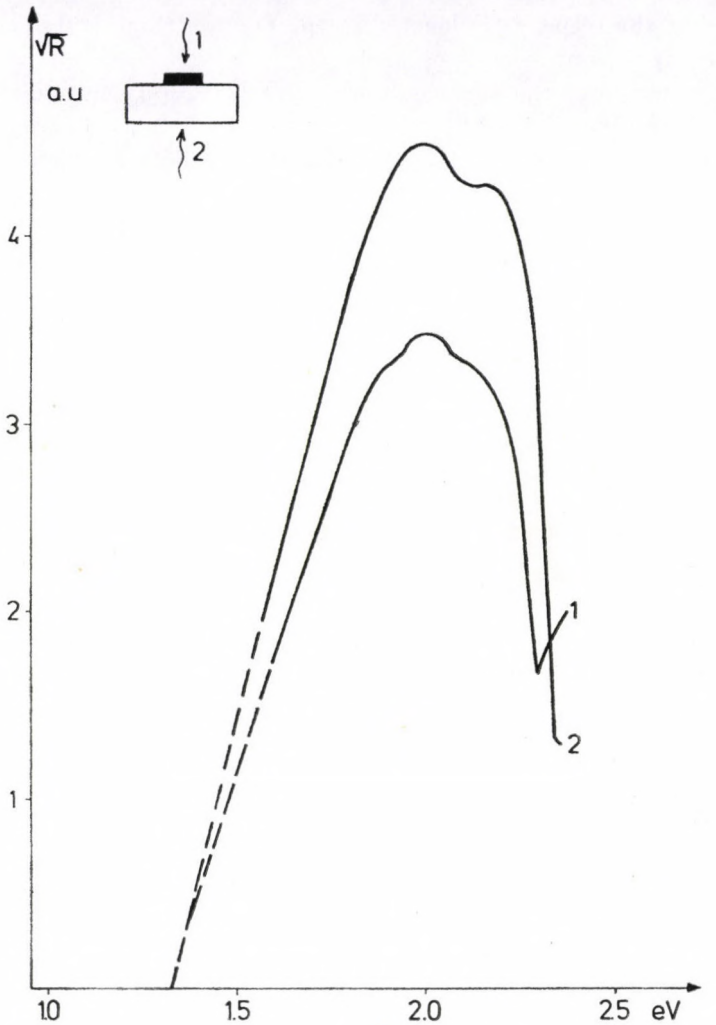

Fig. 2. Fowler plot of GaP-Au system. Etchant: cold aqua regia. 1) Illumination from the front side; 2) Illumination from the reverse side

in the Figure the sub band gap response disappeared almost completely, while the electrical characteristics were also inferior to that of the freshly made diode.

Using aqua regia at boiling point the initial layer thickness is between 1.0—2.0 nm and increases also logarithmically in time. The electron diffraction pattern shows a definite microcrystalline structure which turns in the next days into an amorphous one. Schottky barriers were made first on hot etched surface immediately after etching, on the next and on the third day repeatedly. The Fowler plots shown in Fig. 4 demonstrate again that the high sub band gap response is characteristic of the freshly etched surface. At the same time

it proves that the response is located in the few nm thick interface region of suboxide composition.

The structure of the surface layer in fresh state as an additional parameter can be easily explained by the chemistry of the Ga ion in aqueous media. At low temperature gel-like amorphous $Ga(OH)_3$ is formed which looses water and turns into microcrystalline at elevated temperature [15]. Similar processes are very probable on the GaP surface, consequently the cold etched amorphous surface may contain more water, while the hot etched crystalline surface may be more compact. In both cases a slow oxidation process can be supposed, the initial stage being the freshly etched surface with the lowest amount of oxygen. The presence of oxygen cannot be excluded as the existence of a transparent

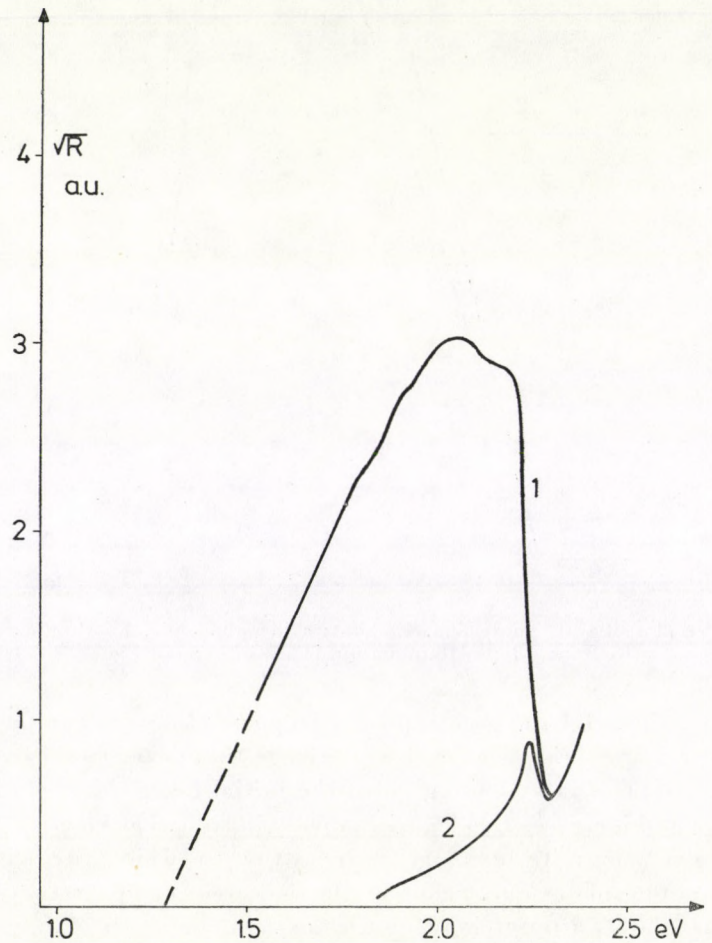

Fig. 3. Fowler plot of GaP-Au system. Etchant: cold aqua regia. Front illumination. 1) electrode evaporated ~200 min after etching; 2) 133 days after etching

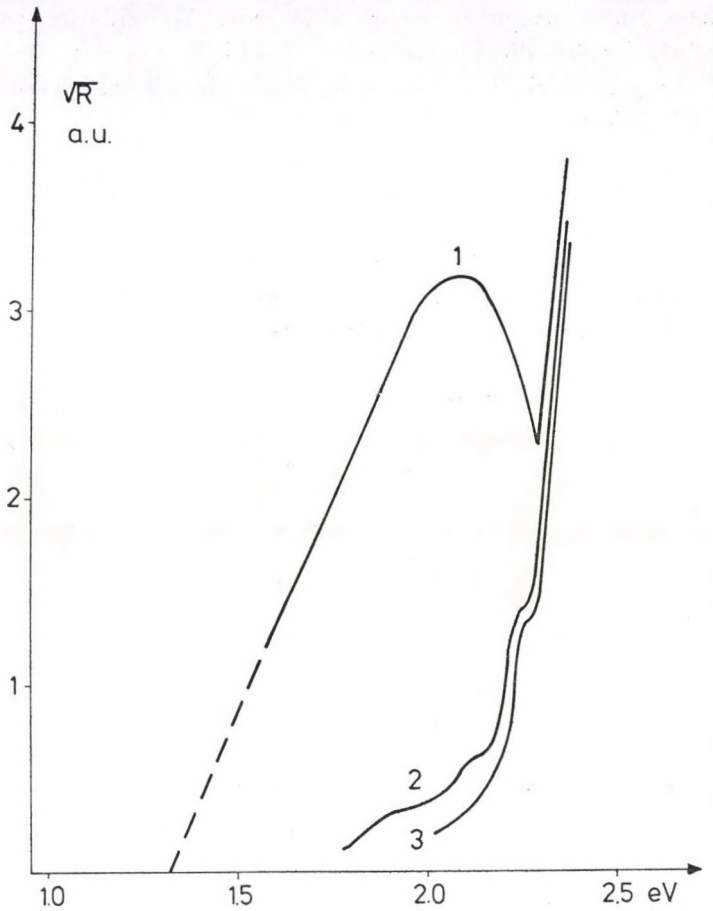

Fig. 4. Fowler plot of GaP-Au system. Etchant: boiling aqua regia. Front illumination. 1) electrode evaporated 200 min after etching; 2) 1500 min after etching; 3) 4300 min after etching

layer can be stated by ellipsometric readings taken just after etching. The high sub band gap response is connected with the freshly etched surface where disordered substrate atoms and oxygen atoms form an interface region. When in contact with the metal electrode the optical excitation of carriers is possibe from that region and states of unknown nature are assumed to be present there.

Accepting that the sub band gap region of the Fowler plot consists of two parts, one attributed to the metal electrodes and the other due to the interface region, a closer inspection of their shape may be of interest. Extremely broad curve is obtained in case of cold etched samples, the response being very pronounced from about 1.8 eV to 2.2 eV. At hot etched surfaces the region

between 2.0—2.2 eV seems to be more intense. As oxidation proceeds the response of this region disappears rather quickly and a peak about 2.24 eV beings to emerge, which becomes well discernible in the case of an old "weathered" surface.

Conclusions

The photoresponse of Schottky barrier is a useful method for the investigation the surface properties of III—V systems. Whereas in ternary systems it serves for band-gap determination, in the case of GaP, it appears to be sensitive to surface properties. High sub band gap response is observed whenever an oxidant is used for surface cleaning; however, this response disappears as the oxidation of the surface proceeds. It can be concluded that it is located in the surface region, i.e. interface region, and it is characteristic only of the slightly oxidized surface in contact with the metal electrode. As the response shows signs of structure the existence of optically excitable states can be postulated within the slightly oxidized interface.

REFERENCES

1. J. TAUC, Photo and Thermoelectric Effects in Semiconductors, Pergamon, Oxford, 1962.
2. A. L. HUGHES and L. A. DUBRIDGE Photoelectric Phenomena, McGraw-Hill, New York, 1932.
3. W. G. SPITZER and C. A. MEAD, Phys. Rev., **133**, 872, 1964.
4. M. SOMOGYI and A. BARNA, Krist. und Techn., **9**, K83, 1974.
5. K. GRAFF and H. PIEPER, Solid State El., **15**, 831, 1972.
6. Y. NANNICHI, K. NISHIDA and K. MIZUSAVA, Japan J. Appl. Phys., **9**, 332, 1970.
7. R. ZUCCA and E. I. WOOD, J. Appl. Phys., **46**, 1396, 1975.
8. H. GOLLNAST, G. RICHTER and H. HERMAN, phys. stat. sol. (a), **38**, K89, 1976.
9. M. SOMOGYI, Acta Phys. Hung., **44**, 49, 1978.
10. P. A. TOVE and M. P. ALI, Solid State El., **21**, 919, 1978.
11. A. AMINTH and P. MARK, J. Vac. Sci. Technol., **15**, 1344, 1978.
12. B. LEPLEY, S. RAVELET and P. RENARD, phys. stat. sol. (a), K191, 1974.
13. M. SOMOGYI and V. SCHILLER, Krist. und Techn., **13**, 293, 1978.
14. M. SOMOGYI, M. FARKAS-JAHNKE, G. MEZEY and J. GYULAI, Thin. Solid Films, **60**, 377, 1979.
15. I. A. SHEKA, I. S. CHAUS and T. T. MITYUREVA, The Chemistry of Gallium, Elsevier, Amsterdam, 1966.

Acta Physica Academiae Scientiarum Hungaricae, Tomus 48 (2—3), pp. 161—167 (1980)

A NEW DLTS METHOD*

By

B. SZENTPÁLI

RESEARCH INSTITUTE FOR TECHNICAL PHYSICS OF THE HUNGARIAN ACADEMY OF SCIENCES
H-1325, BUDAPEST, ÚJPEST 1. P.O.B. 76, HUNGARY

(Received 29. XI. 1979)

A method and an apparatus used for measuring of the deep level content of semiconducting crystals are described. The investigation is based on the observation of capacitance (voltage) relaxation of diodes. The evaluation of the relaxation curve is the same as proposed first by LANG [1], the so-called DLTS (deep level transient spectroscopy) method. The difference between the apparatus presented here and LANG's original is the using of a commercial capacitance meter and the possibility of the measurement of voltage relaxation at fixed capacitance value. Deep centres in GaAs or GaP layers having ionization energies between 0,2 . . . 1 eV can be detected if their concentration is not less then $3 \cdot 10^{-3}$ part of the shallow donor (acceptor) concentration.

I. Introduction

Impurities, lattice defects, or their complex formation in semiconductors are associated with electronic states in the forbidden gap. Fig. 1 shows the characteristic energy levels of electrons in an n-type semiconductor. The level E_D is energetically close to the conduction band, i.e. $E_C - E_D \lesssim kT$. It behaves as a shallow donor centre (e.g. Te in GaAs). In the device fabricating technology the concentration of this level is the result of intentional doping. The other level E_T has an activation energy much higher than the thermal energy, it is called deep level. In general the presence of deep levels damages the quality of crystals resulting in a lower mobility higher noise or even some instabilities. It should be noted that sometimes also the deep levels are intentionally doped into the semiconductor, e.g. Au in Si for fast switching $p - n$ junctions.

In the following Sections the theoretical principles of the measurement will be shortly reviewed and the experimental set-up described.

II. Theory

The ionization rate of the deep levels is determined by the dynamic equilibrium of captures and emissions of electrons. In general, there are four possible processes: the capture of electrons from conduction band, the emission

* Presented at the Workshop Seminar on the Methods and Apparatus for the Investigation of the Physical Parameters of A^{III}—B^{V} Compounds, organised by the Research Institute for Technical Physics of the Hungarian Academy of Sciences, Budapest, 13—18 November 1978.

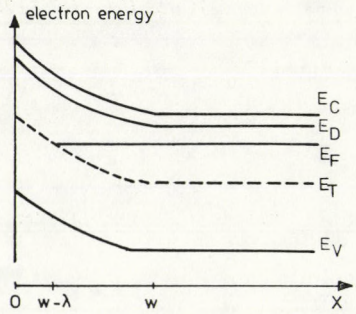
electron energy
E_C
E_D
E_F
E_T
E_V
0 w-λ w X

1

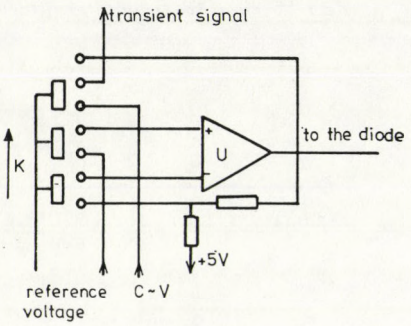
transient signal
to the diode
K
U
+5V
reference voltage
C~V

4

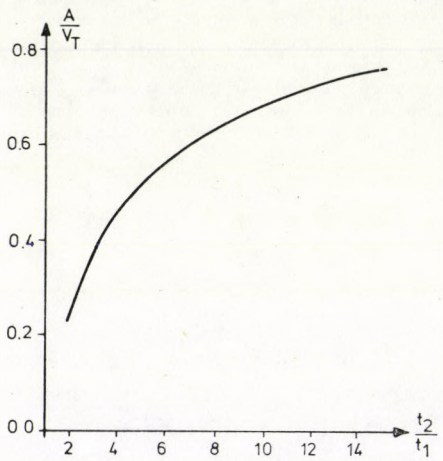
A/V_T
0.8
0.6
0.4
0.2
0 0
2 4 6 8 10 12 14
t2/t1

2

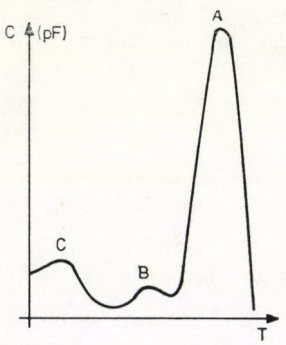
C (pF)
A
C
B
T

5

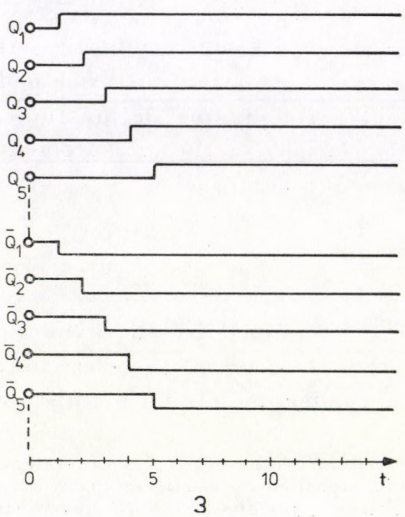
Q_1
Q_2
Q_3
Q_4
Q_5
$\bar{Q}_1$
$\bar{Q}_2$
$\bar{Q}_3$
$\bar{Q}_4$
$\bar{Q}_5$
0 5 10 t

3

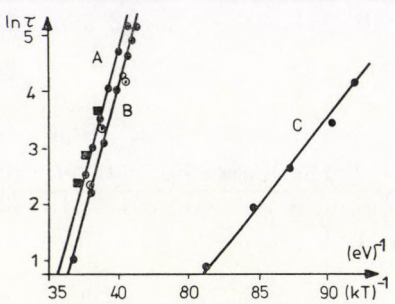
ln τ
5
4
3
2
1
A
B
C
35 40 80 85 90
(eV)⁻¹
(kT)⁻¹

6

of electrons into the valence band, that is the capture of holes, the emission of electrons into the conduction band and the emission of holes, that is the capture of electrons from the valence band. The general theory of deep level statistics has been worked out by SHOCKLEY and READ [2]. Here only the special case is treated, when the deep centre in the bulk of the n-type material is practically completely filled by electrons, that is the probability of electron capture from the conduction band is much larger than the emission of electrons.

However, in the depletion layer of a Schottky barrier or a $p - n$ diode fabricated on the surface of the crystal the probability of electron capture decreases to a very small value due to the lack of conduction electrons, and so the major process is the thermal emission of electrons from previously filled centres. This effect can be utilized for detecting and measuring of the parameters of deep levels. The first work in this field was made by SAH and REDDI [3]. They used the frequency dependence of the diode capacitance at low frequencies, where the charging and discharging of the deep level can follow the measuring frequency. Comparing the capacitance value obtained by low and high frequency signals, where only the free carriers follow the measuring voltage, they calculated the emission rate and also the concentration of the deep level. On the basis of their model SENECHAL and BASINSKI suggested another method [4, 5]. They utilized the transient behaviour of the diode capacitance after switching on the reverse bias. An improved version of this method is the observation of the relaxation of the reverse voltage while the capacitance is kept at a given constant value [6, 7].

The reason for this relaxation can be understood by looking at Fig. 1. The deep levels are occupied by electrons in the region $x > W - \lambda$. In the region $0 \leq x \leq w - \lambda$ thermal emission of the captured electrons takes place after having applied the reverse voltage. The distribution of the charge density

Fig. 1. The energy levels in the space charge region of an n-type semiconductor E_C, E_V, E_F, E_D and E_T represent the energy positions of the conducting band edge, the valence band edge, the Fermi level, the donor level and the deep centrum, respectively.

Fig. 2. Amplitude and the DLTS signal as function of t_2/t_1

Fig. 3. Working principle of the control unit. The figure shows the the dependence of output signals at the points Q_i and $\bar{Q}_i$ of the shift register. The inputs of the AND gate switching a control unit between the 2. and 5. period are connected to Q_2 and $\bar{Q}_5$

Fig. 4. Diode biasing unit. The reference voltage switched by the control unit and the voltage proportional to the capacitance are connected to the marked points to the microswitch K. In the lower position of the switch K capacitance relaxation is measured. The amplifier U has a fixed gain of 20. The shift of the voltage level to +5 V ensures the possibility of forward biasing the diode, thus the reference voltages can be varied between 0 V and —7 V according to the output of the capacitance meter. The moving of the switch K to the upper position, as shown by the arrow, makes the measurement of voltage relaxations possible. In this case the amplifier U has open circuit gain and compares the output of the capacitance meter to the reference voltage. The negative feedback is ensured by the capacitance-voltage characteristic of the diode under test

Fig. 5. A measured DLTS spectrum

Fig. 6. Temperature dependence of the peaks of the DLTS spectrum shown in Fig. 5

is described by the step-like function approximation valid for $kT \ll E_F - E_T$. The quasi Fermi level of electrons is constant at least up to the point $w - \lambda$ in the case of not too high biases [8]. If a forward voltage has been applied on the diode for a sufficiently long time before putting on the reverse bias practically all of the deep levels have been occupied and the charge density can be described by the equation

$$qn_T(t) = qN_T\{1 - \exp(-t/\tau)\}, \tag{1}$$

where N_T is the concentration of the deep level, τ the characteristic relaxation time. The reverse voltage has been switched on at $t = 0$. Taking into account the above mentioned assumptions on the electron capture and emission processes, the characteristic relaxation time constant

$$\tau^{-1} = N_C\sigma_n v \exp\{(E_T - E_C)/kT\}, \tag{2}$$

where N_C, σ_n, and v are the effective densities of states in the conduction band, the electron capture cross-section and the velocity of electrons, respectively.

The integration of the Poisson equation leads to the following result

$$V = \frac{q}{\varepsilon}\int_0^w xN_D\,dx + \frac{q}{\varepsilon}\int_0^{w-\lambda} xN_T\{1 - \exp(-t/\tau)\}dx =$$

$$= V_0 + V_T\{1 - \exp(-t/\tau)\}, \tag{3}$$

i.e. the reverse biased voltage of the diode has an exponential character with the time constant τ, while the width of the space charge region w is kept constant. The earlier works mentioned above measured the transient of capacitance, at fixed reverse voltage. It can be shown [9] that this transient is also nearly exponential with the same time constant if the condition $N_T/N_D \ll 1$ is fulfilled. The advantages of the measurement of capacitance relaxations are the simpler electronic apparatus and so the ability of measuring faster relaxations. However, in cases when the concentration of deep levels is not very small compared to the concentration of shallow donors rather high distortions can occur on the transient signal.

The ionization energy and capture cross-section of the deep level is determined on the basis of Eq. (2) by measuring the temperature dependence of τ. τ can be measured by fitting the experimental curve corresponding to one given temperature to the exponential function, or in the way suggested by LANG [1]. In the latter case the function

$$\varphi(t_1; t_2) = V(t_1) - V(t_2) \tag{4}$$

is measured for different temperatures. At the temperature T corresponding to the maximum of the function the relaxation time τ is

$$\tau = \frac{t_1 - t_2}{\ln (t_1/t_2)} . \tag{5}$$

The concentration of deep levels can be calculated from the amplitude of the relaxation (9) according to the formula

$$\frac{V_T}{V_0} = -\frac{N_T}{N_D}\left[1 - \frac{\lambda}{w}\right]^2 . \tag{6}$$

In the case of capacitance relaxations the function

$$\varphi(t_1; t_2) = C(t_1) - C(t_2) \tag{7}$$

is measured, the relaxation time is expressed by (5) and the concentration

$$\frac{C_T}{C_0} = \frac{N_T}{2N_D}\left[1 - \frac{\lambda}{w}\right]^2 . \tag{8}$$

The comparison of (6) and (7) shows that the sensitivity of the capacitance relaxation is smaller by a factor of two. The decrease of sensitivity arises from the fact that in the case of capacitance relaxation the increase in the space charge due to the thermal ionization of deep levels is compensated by the decrease of space charge in the neighbourhood of w, which part has the maximum weight factor in Eq. (3).

It should be noted that the amplitude of peaks in LANG's method do not give the V_T or C_T values directly, but the equation

$$\frac{A}{V_T} = \frac{V(t_2) - V(t_1)}{V_T} = \exp(-t_1/\tau) - \exp(-t_2/\tau) \tag{9}$$

is valid and a similar expression holds for the capacitance relaxation. Fig. 2 shows the amplitude of the DLTS peak as the function of t_2/t_1.

Even the profile of the deep level concentration can be obtained by measuring the bias dependence of the peaks. The distance λ can be calculated from the N_D and E_T values.

III. The instrument

The instrument consist of the following three parts:

— capacitance meter (Boonton model 75D) ha vinga resolution of 10^{-3} pF

— cryostat and temperature regulator which works in the temperature region between 77 K and 450 K with a stability of 0.1 K;

— central control unit which supplies periodically the forward and reverse bias to the diode, signals to the temperature regulator after the measuring periods and controls the work of the sample and hold circuits for measuring the voltage differences during the transient process.

The functioning of the central control unit is based on a shift register having a 15 bits capacity, its input is fed by a precision pulse generator. Fig. 3 shows the working principle of the circuit. The biasing and measuring units are switched by the outputs of AND gates. The sequence of the biasing and measuring time intervals can be changed by altering of the flexible connections between the Q and $\bar{Q}$ points of the shift register and the inputs of the AND gates.

The instrument contains three independent reference voltage sources, each of which can be controlled by a calibrated potentiometer. The biasing circuit converts the signal of the reference sources to diode bias. *The biasing circuits* can be switched into two positions. One of them supplies the constant voltage on the diode, the other ensures the constant capacitance i.e. voltage relaxation can be measured. Fig. 4 shows the biasing circuit.

The DLTS signals are formed by three sample and hold circuits. Two of them measure the relaxation signal at moments controlled by the AND gates, the third holds the previous voltage difference value during the measuring period and at the end it takes a sample of the new voltage difference. For decreasing the noise integrating RC circuits having variable time constants are applied at the inputs of the sample and hold circuits.

After several (1 . . . 8) measuring periods the temperature regulator gets a pulse from the central control unit and stabilizes a new temperature value differing by about 1K from the former one and the central control unit is stopped for 15. . .50 s, while the new temperature value is stabilized.

Fig. 5 shows a measured DLTS spectrum obtained on an n-type GaAs epitaxial layer grown by vapour phase epitaxial technics for Gunn device purposes. The temperature dependence of values was also investigated by altering the frequency of the pulse generator. The result is illustrated in Fig. 6. The deep level parameters evaluated from the temperature dependence of (E_T) and from the amplitude of the peaks (N_T/N_D) are listed in Table I. On the basis of the spectrum the resolution of the instrument can be estimated as $N_T/N_D \approx 3 \cdot 10^{-3}$. The left part of the spectrum (not visible in the Figure) is flat, i.e. there is no considerable amount of deep levels having ionization

Table I

Crystal N° 1-43-965-3	$N_D = 1.9 \cdot 10^{15}$ cm^{-3}		
Deep level	A	B	C
Ionization energy	0.83 eV	0.68 eV	0.48 eV
N_D/N_T	0.13	0.005	0.009

energies higher than the approximated 0.2 eV in the crystal. The chemical identification of deep centres is problematic; all of them are often attributed to O impurities [10].

REFERENCES

1. D. V. Lang, J.A.P. **45**, 3023, 1974.
2. W. Shockley and W. T. Read, Phys. Rev., **87**, 835, 1952.
3. C. T. Sah and V. G. R. Reddi, IEEE Trans. on El. Dev. ED-11, 345, 1964.
4. R. R. Senechal and J. Basinski, J.A.P., **39**, 3725, 1968.
5. R. R. Senechal and J. Basinski, J.A.P., **39**, 4581, 1968.
6. G. Goto, S. Yanagisawa, O. Wada and H. Takanashi, Appl. Phys. Lett., **23**, 150, 1973.
7. J. A. Pals, Solid-State Electronics, **17**, 1139, 1974.
8. E. H. Rhoderick, J. of Phys. D. Appl. Phys., **5**, 1920, 1972.
9. B. Szentpáli, Thesis, Budapest, 1979.
10. Lars-Ake Lebedo, Thesis, Lund, 1974.

Acta Physica Academiae Scientiarum Hungaricae, Tomus 48 (2—3), pp. 169—185 (1980)

EXACT SOLUTION OF A QUASI-ONE-DIMENSIONAL MODEL WITH LONG RANGE INTERACTION (COUPLED TOMONAGA CHAINS)

By

NGUYEN MINH KHUE and J. SÓLYOM

CENTRAL RESEARCH INSTITUTE FOR PHYSICS, BUDAPEST, HUNGARY

(Received 14. XII. 1979)

The novel method proposed by one of the authors to calculate exactly the response functions of the one-dimensional Tomonaga model is described in more detail. The method is generalized for the case of a system of coupled chains where both the intrachain and interchain interactions have forward scattering components only. The model does not show real phase transition at any finite temperature indicating that the interchain backward scattering or hopping is needed to have an ordering of the chains at finite temperature.

1. Introduction

Recently quasi-one-dimensional (quasi-1-d) conductors attracted a great deal of interest because of their unusual properties. For a review of works done in the past few years see [1]—[3]. These systems are built usually of large, flat molecules which are relatively closely stacked in one direction to form chains, the adjacent chains being at a relatively larger distance. Thus the motion of electrons is confined predominantly to motion along the chains with rare hoppings between them.

Various theoretical models have been worked out to study the properties of these systems. One of these models is the Fermi gas model which has been investigated in the strictly 1-d case in great detail. A review of the properties of this model can be found in [4]. Since a 1-d system may have specific properties or behaviour (such as absence of phase transition at finite temperature) which are characteristic for 1-d systems but are not necessarily true in higher dimensions, any realistic model of quasi-1-d conductors should contain some kind of interaction between the chains. Generalizations of the 1-d Fermi gas model in this direction have indeed been attempted [5]—[9]. The Fermi gas model is a model with infrared singularities difficult to treat in a satisfactory manner at low temperatures and low energies even in its strictly 1-d version already. The treatment becomes increasingly more complicated when interchain interactions are taken into account. Therefore any simplified model which can be solved exactly is of great value in finding out what the effect of the interaction terms is.

The 1-d TOMONAGA model [10] is a well known exactly soluble model of a 1-d interacting electron system. The two important features which make it soluble are the linear dispersion relation and the neglect of backward scattering. In the present paper we will consider a generalization of the model to a set of coupled chains but keeping these two features intact, i.e. a one-dimensional linear dispersion relation is taken for every chain which means that no hopping between the chains is allowed and only forward scattering processes are taken into account for both the intrachain and interchain scatterings.

There are various ways to solve the 1-d TOMONAGA model. The excitations of the model have been shown to be the boson-like charge- and spin-density excitations [11]. Therefore the calculation of the one-particle Green's function and the response functions or two-particle correlation functions in which the fermion operators cannot be easily expressed in terms of the charge- or spin-density operators was a formidable task [12]. It was shown, however, by LUTHER and PESCHEL [13] and by MATTIS [14] that an exact operator identity can be found which allows to represent the fermion operators in terms of the boson-like density operators. Since the TOMONAGA Hamiltonian can be transformed to a diagonal form of the boson operators, the Greens' function and response functions can be calculated by calculating harmonic averages. The operator identity involves, however, a delicate limiting procedure, which is not always easy to perform and therefore other methods are also of interest. FOGEDBY [15] used functional integrals to solve the 1-d TOMONAGA model. Another very elegant method was used by DZYALOSHINSKY and LARKIN [16] to calculate the Green's function. They could derive a Ward identity between the Green's function and the vertex appearing in the Dyson equation. Making use of this relation, the Dyson equation could be solved exactly. This method has been generalized by one of the authors [17] to calculate the response functions. In this paper we will make a further generalization to study the behaviour of the quasi-1-d system of TOMONAGA chains.

First in Section 2 the method of DZYALOSHINSKY and LARKIN [16] is briefly presented since it is the basis of all further considerations. Then the generalization of the method to calculate response functions is described in Section 3. Section 4 contains the results obtained for the quasi-1-d system of TOMONAGA chains. Finally the results are discussed in Section 5.

2. The Dzyaloshinsky—Larkin method of summing diagrams in the Tomonaga model

The TOMONAGA model was defined originally as a 1-d model of interacting electrons

$$H = \sum_{k,\alpha} \frac{k^2}{2m} c^+_{k\alpha} c_{k\alpha} + \frac{1}{2L} \sum_{\substack{k,k',p \\ \alpha,\beta}} \lambda(p)\, c^+_{k+p\alpha}\, c^+_{k'-p\beta}\, c_{k'\beta}\, c_{k\alpha}, \qquad (1)$$

where L is the length of the system and the interaction potential is supposed to be of long range and therefore the Fourier components $\lambda(p)$ are non-zero for small momenta only. If the cutoff on the momentum transfer Λ is much smaller than the Fermi momentum k_F, one can distinguish between particles near the Fermi point $+k_F$ and particles near the other Fermi point $-k_F$, since in the absence of large momentum transfer interaction (backward scattering) the electrons stay always in the neighbourhood of the same Fermi point after any interaction process. In order to make this distinction more explicit, we will denote the creation (annihilation) operators of electrons near the right and left Fermi points by a_k^+ (a_k) and $b_k^+(b_k)$, respectively.

The kinetic energy term can be approximated by a linear relationship near the Fermi points and the free part of the Hamiltonian can be written as

$$H_0 = \sum_{k,\alpha} v_F(k - k_F)\, a_{k\alpha}^+ a_{k\alpha} + \sum_{k,\alpha} v_F(-k - k_F)\, b_{k,\alpha}^+ b_{k,\alpha}. \tag{2}$$

The interaction part of the Hamiltonian can be generalized by allowing for different coupling strengths for the cases when the scattered electrons are from the same or different branches of the spectrum and for parallel or antiparallel orientation of the scattered electrons. In the most general case the Hamiltonian reads:

$$\begin{aligned} H_{int} = \frac{1}{2L} \sum_{\substack{k,k',p \\ \alpha,\beta}} (\lambda_{1\parallel}\, \delta_{\alpha\beta} + \lambda_{1\perp}\, \delta_{\alpha,-\beta})\, (a_{k+p\alpha}^+ a_{k'-p\beta}^+ a_{k'\beta} a_{k\alpha} + \\ + b_{k+p\alpha}^+ b_{k'-p\beta}^+ b_{k'\beta} b_{k\alpha}) + \\ + \frac{1}{L} \sum_{\substack{k,k',p \\ \alpha,\beta}} (\lambda_{2\parallel}\, \delta_{\alpha\beta} + \lambda_{2\perp}\, \delta_{\alpha,-\beta})\, a_{k+p\alpha}^+ b_{k'-p\beta}^+ b_{k'\beta} a_{k\alpha}. \end{aligned} \tag{3}$$

To make contact with other works on the Fermi gas model [4] where backward scattering is also included, the present choice of couplings corresponds in the language of. 'g'-ology to $\lambda_1 = g_4$ and $\lambda_2 = g_2$. The scattering processes can be represented diagrammatically as

where the solid and dashed lines correspond to electrons on the right or left branch of the spectrum.

DZYALOSHINSKY and LARKIN [16] recognized that the two particular features of the TOMONAGA model, namely the linearized dispersion relation

and the neglect of backward scattering terms lead to an enormous simplification in the contribution of diagrams. They have found that all diagrams which contain electron bubbles with more than two interaction legs are mutually cancelled and only simple bubbles with two interaction legs and series of simple bubbles remain.

Effective interactions can be introduced by summing these series of bubbles, in the same way as the screened interaction is introduced in a RPA calculation, but here working with these interactions will lead to an exact procedure. The diagrammatic equations for the effective interactions denoted by $D_{1\|}$, $D_{1\perp}$, $D_{2\|}$ and $D_{2\perp}$ are as follows:

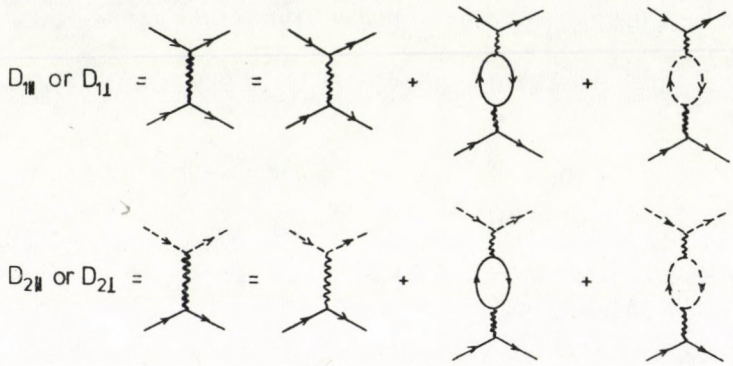

The diagrammatic equations are the same for parallel and antiparallel spin orientations. It is worth mentioning that though the bare λ_1 coupling is the same for electrons on the right or left branches, the effective couplings will be different.

The analytic form of these equations is

$$\begin{aligned}
D_{1\|} &= \lambda_{1\|} + \lambda_{1\|}\Pi_+ D_{1\|} + \lambda_{1\perp}\Pi_+ D_{1\perp} + \lambda_{2\|}\Pi_- D_{2\|} + \lambda_{2\perp}\Pi_- D_{2\perp},\\
D_{1\perp} &= \lambda_{1\perp} + \lambda_{1\|}\Pi_+ D_{1\perp} + \lambda_{1\perp}\Pi_+ D_{1\|} + \lambda_{2\|}\Pi_- D_{2\perp} + \lambda_{2\perp}\Pi_- D_{2\|},\\
D_{2\|} &= \lambda_{2\|} + \lambda_{2\|}\Pi_+ D_{1\|} + \lambda_{2\perp}\Pi_+ D_{1\perp} + \lambda_{1\|}\Pi_- D_{2\|} + \lambda_{1\perp}\Pi_- D_{2\perp},\\
D_{2\perp} &= \lambda_{2\perp} + \lambda_{2\|}\Pi_+ D_{1\perp} + \lambda_{2\perp}\Pi_+ D_{1\|} + \lambda_{1\|}\Pi_- D_{2\perp} + \lambda_{1\perp}\Pi_- D_{2\|},
\end{aligned} \tag{4}$$

where Π_+ and Π_- are the polarization bubbles for electrons on the right and left branches, for one spin orientation. These equations can be solved using the expressions

$$\Pi_+(k,\omega) = \frac{k}{2\pi(\omega - v_F k)}, \quad \Pi_-(k,\omega) = -\frac{k}{2\pi(\omega + v_F k)} \tag{5}$$

giving e.g. for $D_{1\parallel}$ which couples two electrons on the right branch

$$D_{1\parallel}(k,\omega) = (\omega - v_F k)\left[\frac{A+B}{\omega - u_\sigma k + i\delta \operatorname{sign} k} + \frac{A-B}{\omega + u_\sigma k - i\delta \operatorname{sign} k} + \right.$$
$$\left. + \frac{C+D}{\omega - u_\varrho k + i\delta \operatorname{sign} k} + \frac{C-D}{\omega + u_\varrho k - i\delta \operatorname{sign} k}\right], \tag{6}$$

where

$$u_\sigma^2 = \left[v_F + \frac{1}{2\pi}(\lambda_{1\parallel} - \lambda_{1\perp})\right]^2 - \left[\frac{1}{2\pi}(\lambda_{2\parallel} - \lambda_{2\perp})\right]^2$$
$$u_\varrho^2 = \left[v_F + \frac{1}{2\pi}(\lambda_{1\parallel} + \lambda_{1\perp})\right]^2 - \left[\frac{1}{2\pi}(\lambda_{2\parallel} + \lambda_{2\perp})\right]^2,$$
$$A = \frac{1}{4}(\lambda_{1\parallel} - \lambda_{1\perp}),\ B = \frac{\pi}{2u_\sigma}\left\{u_\sigma^2 - v_F\left[v_F + \frac{1}{2\pi}(\lambda_{1\parallel} - \lambda_{1\perp})\right]\right\}, \tag{7}$$
$$C = \frac{1}{4}(\lambda_{1\parallel} + \lambda_{1\perp}),\ D = \frac{\pi}{2u_\varrho}\left\{u_\varrho^2 - v_F\left[v_F + \frac{1}{2\pi}(\lambda_{1\parallel} + \lambda_{1\perp})\right]\right\}$$

and for $D_{2\parallel}$

$$D_{2\parallel}(k,\omega) = \frac{1}{2}\frac{\omega^2 - v_F^2 k^2}{\omega^2 - u_\sigma^2 k^2 + i\delta}(\lambda_{2\parallel} - \lambda_{2\perp}) +$$
$$+ \frac{1}{2}\frac{\omega^2 - v_F^2 k^2}{\omega^2 - u_\varrho^2 k^2 + i\delta}(\lambda_{2\parallel} + \lambda_{2\perp}). \tag{8}$$

Once the effective interactions are used, the Dyson equation can be written diagrammatically as

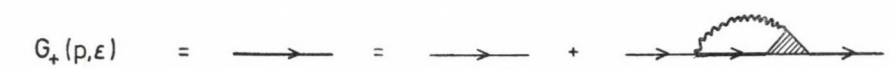

in which the three-leg vertex has two solid line legs coupled by effective interactions in all possible ways.

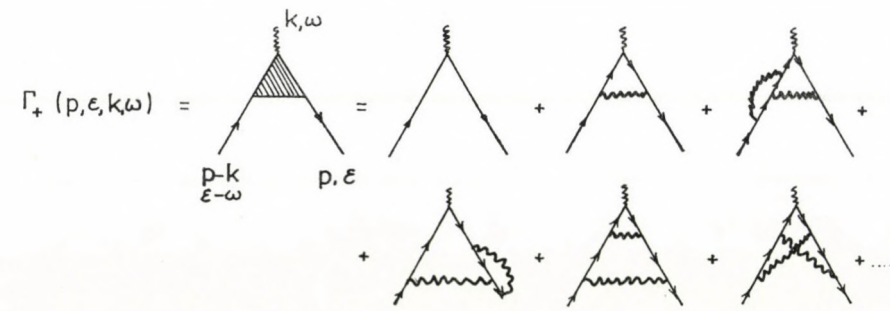

A further consequence of the particular features of the TOMONAGA model is that, as shown by DZYALOSHINSKY and LARKIN [16], a Ward identity can be found for general energy and momentum variables by use of which the vertex Γ_+ can be expressed in terms of the Green's function

$$\Gamma_+(p, \varepsilon, k, \omega) = \frac{1}{\omega - v_F k} [G_+^{-1}(p, \varepsilon) - G_+^{-1}(p - k, \varepsilon - \omega)] \tag{9}$$

and an analogous relation

$$\Gamma_-(p, \varepsilon, k, \omega) = \frac{1}{\omega + v_F k} [G_-^{-1}(p, \varepsilon) - G_-^{-1}(p - k, \varepsilon - \omega)] \tag{10}$$

holds for the vertex in which the electrons on the external legs belong to the left branch of the spectrum.

By making use of the Ward identity the Dyson equation for the Green's function can be written in a closed integral equation form

$$[\varepsilon - v_F(p - k_F)]\, G_+(p, \varepsilon) = 1 + \frac{i}{4\pi} \int dk\, d\omega\, \frac{D_{1|1|}(k, \omega)}{\omega - v_F k} G_+(p - k, \varepsilon - \omega), \tag{11}$$

where the term leading to Fermi energy renormalization has been neglected. In real space and time representation we get

$$\left(\frac{\partial}{\partial t} + v_F \frac{\partial}{\partial x}\right) G_+(x, t) = K_{1|1|}(x, t)\, G_+(x, t) \tag{12}$$

with

$$K_{1|1|}(x, t) = \frac{1}{4\pi^2} \int dk\, d\omega\, \frac{D_{1|1|}(k, \omega)}{\omega - v_F k} e^{-i(\omega t - kx)}. \tag{13}$$

This equation can be solved in the form

$$G_+(x, t) = G_+^{(0)}(r) \exp\left\{\frac{1}{2v_F} \int_r^s K_{1|1|}(r, s')\, ds'\right\} f_+(r), \tag{14}$$

where the new variables $r = x - v_F t$ and $s = x + v_F t$ were introduced.

$$G_+^{(0)}(x, t) = \frac{1}{2\pi} \frac{1}{x - v_F t + i\delta(t)} \tag{15}$$

with $\delta(t) = \delta$ sign t and $f_+(r)$ has to be chosen in a way to ensure the correct analytic properties. Performing the integrations in Eqs. (13) and (14) with

the cut-off factor $\exp(-|k|/\Lambda)$ for the momentum transfer, the final result is

$$G_+(x,t) = \frac{1}{2\pi}\,\frac{1}{x - v_F t + i\delta(t)}\,\frac{x - v_F t + i/\Lambda(t)}{[x - u_\sigma t + i/\Lambda(t)]^{1/2}\,[x - u_\varrho t + i/\Lambda(t)]^{1/2}} \times$$
$$\times [\Lambda^2(x - u_\sigma t + i/\Lambda(t))\,(x + u_\sigma t - i/\Lambda(t))]^{-\alpha_\sigma} \qquad (16)$$
$$\times [\Lambda^2(x - u_\varrho t + i/\Lambda(t))\,(x + u_\varrho t - i/\Lambda(t))]^{-\alpha_\varrho}$$

with

$$\alpha_\sigma = \frac{1}{4u_\sigma}\left[v_F + \frac{1}{2\pi}(\lambda_{1\parallel} - \lambda_{1\perp}) - u_\sigma\right],$$
$$\alpha_\varrho = \frac{1}{4u_\varrho}\left[v_F + \frac{1}{2\pi}(\lambda_{1\parallel} + \lambda_{1\perp}) - u_\varrho\right] \qquad (17)$$

and $\Lambda(t) = \Lambda \operatorname{sign} t$. The velocities u_σ and u_ϱ are given in Eq. (7).

The Green's function of the electrons on the left branch can be calculated similarly leading to the result:

$$G_-(x,t) = G_+(x,-t). \qquad (18)$$

3. Generalized Ward identities and response functions of the 1-d model

One of the best ways to get information about the possibility of phase transition to an ordered state is to calculate the response of the system to various external perturbations. A singularity in the response function is an indication that a spontaneous ordering can take place. We will consider the density and pairing responses since they contain logarithmically singular terms in every order of perturbation theory and therefore there is a high chance for them to be singular when an exact summation of all contributions is performed.

These functions can be defined as

$$R(k,\omega) = -i\int dt\, e^{i\omega t}\langle T\{O(k,t)\,O^+(k,0)\}\rangle, \qquad (19)$$

where

(i)
$$O(k,t) = \frac{1}{L^{1/2}}\sum_p b^+_{p\uparrow}(t)\,a_{p+k\uparrow}(t) \qquad (20)$$

for the charge-density response function $N(k,\omega)$ with large momentum $(k \sim 2k_F)$,

(ii)
$$O(k,t) = \frac{1}{L^{1/2}}\sum_p b^+_{p\uparrow}(t)\,a_{p+k\downarrow}(t) \qquad (21)$$

for the spin-density response function $\chi\ (k, \omega)$ with large momentum ($k \sim 2k_F$).

(iii) $$O(k, t) = \frac{1}{L^{1/2}} \sum_p b_{p\uparrow}(t)\ a_{-p+k\downarrow}(t) \tag{22}$$

for the singlet-superconductor response $\Delta_s(k, \omega)$ with small momentum k, and

(iv) $$O(k, t) = \frac{1}{L^{1/2}} \sum_p b_{p\uparrow}(t)\ a_{-p+k\uparrow}(t) \tag{23}$$

for the triplet-superconductor response $\Delta_t(k, \omega)$.

The diagrams representing these response functions have one solid and one dashed line running from one external vertex to the other and these lines are dressed and connected by effective interactions in all possible ways. The charge-density response function can be represented as

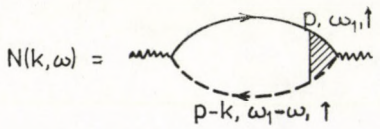

where the two lines are renormalized lines and the vertex

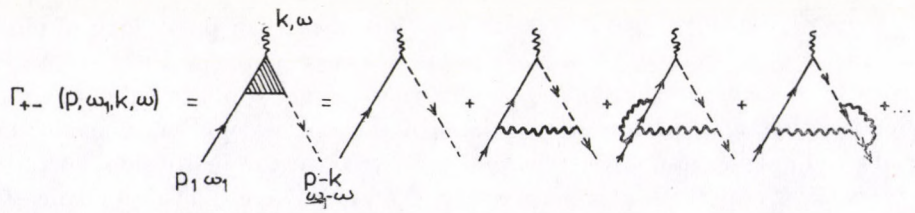

is analogous to the vertices Γ_+ and Γ_-, but here the two legs belong to different branches.

Unfortunately, there is no Ward identity which could relate this vertex to the Green's functions. There is, however, an alternative way to write the response functions. All the diagrams can be classified into three classes. Either there is no interaction line coupling to the solid line, or if there is one, the first of them can couple back to the solid line in which case this is an effective $D_{1\|}$ interaction or it couples to the dashed line in which case it is an effective $D_{2\|}$ interaction. Accordingly

where two new vertices have been introduced:

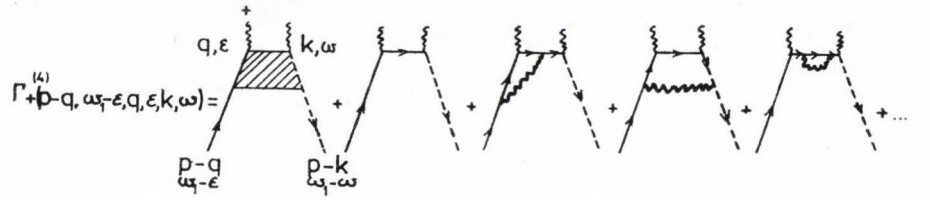

in which the small momentum transfer interaction couples to the solid line, and

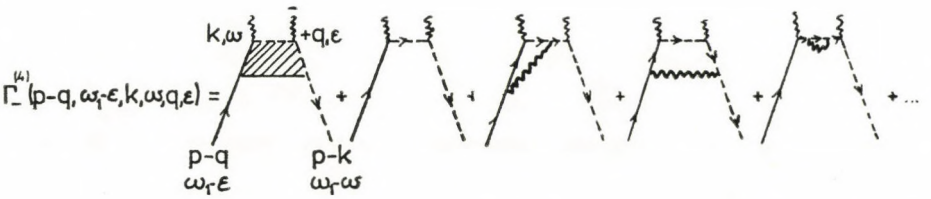

in which the small momentum transfer interaction couples to the dashed line. The two legs and the intermediate line are connected by effective couplings in all possible ways and self energy corrections on the intermediate line should also be considered. The diagrammatic representation of the spin-density response is similar, but instead of $D_{2\|}$ the effective interaction $D_{2\perp}$ should appear. In the pairing responses the vertices have two incoming lines, otherwise the representations are similar.

As was pointed out by SÓLYOM [17], the particular features of the TOMONAGA model allow to derive generalized Ward identities relating the four-leg vertices $\Gamma_{+}^{(4)}$ and $\Gamma_{-}^{(4)}$ to three-leg vertices Γ_{+-} with large momentum transfer. These relations are the consequence of the conservation law for particles in each branch and for each spin orientation and are straightforward generalizations of the Ward identities given in Eqs. (9) and (10). They can be written analytically as

$$\Gamma_{+}^{(4)}(p-q,\omega_1-\varepsilon,q,\varepsilon,k,\omega)=\frac{1}{\varepsilon-v_Fq}\left[\Gamma_{+-}(p-q,\omega_1-\varepsilon,k-q,\omega-\varepsilon)-\right.$$

$$\left.-G_{+}^{-1}(p-q,\omega_1-\varepsilon)\,G_{+}(p,\omega_1)\,\Gamma_{+-}(p,\omega_1,k,\omega)\right] \tag{24}$$

and

$$\Gamma_{-}^{(4)}(p-q,\omega_1-\varepsilon,k,\omega,q,\varepsilon)=\frac{-1}{\varepsilon+v_Fq}\left[\Gamma_{+-}(p-q,\omega_1-\varepsilon,k-q,\omega-\varepsilon)-\right.$$

$$\left.-G_{-}^{-1}(p-k,\omega_1-\varepsilon)G_{-}(p-k-q,\omega_1-\varepsilon-\omega)\Gamma_{+-}(p-q,\omega_1-\varepsilon,k,\omega)\right] \tag{25}$$

or diagrammatically as

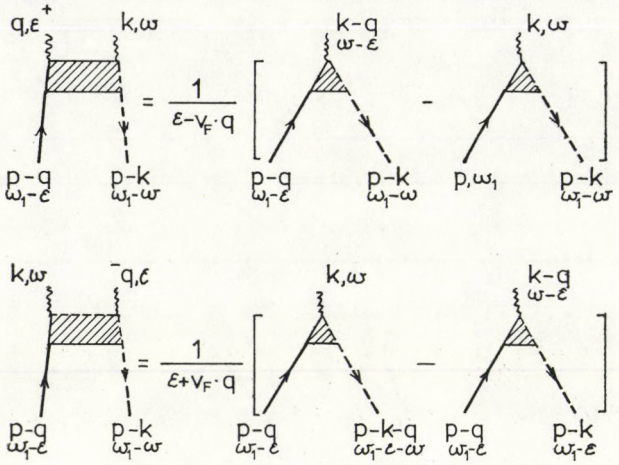

where the external renormalized Green's function legs should also be taken into account.

The analytic expressions for the charge-density response function $N(k, \omega)$, when the two representations are used, are

$$N(k, \omega) = -i \int \frac{dp}{2\pi} \frac{d\omega_1}{2\pi} G_+(p, \omega_1)\, \Gamma_{+-}(p, \omega_1, k, \omega)\, G_-(p - k, \omega_1 - \omega) \quad (26)$$

and

$$\begin{aligned} N(k, \omega) = -i \int \frac{dp}{2\pi} \frac{d\omega_1}{2\pi} G_+^{(0)}(p, \omega_1)\, G_-(p - k, \omega_1 - \omega) + \\ + \int \frac{dp}{2\pi} \frac{d\omega_1}{2\pi} G_+^{(0)}(p, \omega_1) \int \frac{dq}{2\pi} \frac{d\varepsilon}{2\pi} \frac{D_{111}(q, \varepsilon)}{\varepsilon - v_F q} \times \\ \times G_+(p - q, \omega_1 - \varepsilon)\, \Gamma_+^{(4)}(p - q, \omega_1 - \varepsilon, q, \varepsilon, k, \omega) \times \\ \times G_-(p - k, \omega_1 - \omega) + \int \frac{dp}{2\pi} \cdot \frac{d\omega_1}{2\pi} G_+^{(0)}(p, \omega_1) \times \\ \times \int \frac{dq}{2\pi} \frac{d\varepsilon}{2\pi} \frac{D_{211}(q, \varepsilon)}{\varepsilon - v_F q} G_+(p - q, \omega_1 - \varepsilon) \times \\ \times \Gamma_-^{(4)}(p - q, \omega_1 - \varepsilon, k, \omega, q, \varepsilon)\, G_-(p - k, \omega_1 - \omega). \end{aligned} \quad (27)$$

Introducing the quantity

$$N(p, \omega_1, k, \omega) = G_+(p, \omega)\, \Gamma_{+-}(p, \omega_1, k, \omega)\, G_-(p - k, \omega_1 - \omega) \quad (28)$$

from which $N(k, \omega)$ is obtained by simple integration, making use of the generalized Ward identities in Eq. (27) and comparing Eqs. (26) and (27) gives

$$N(p, \omega_1, k, \omega)\, G_+^{(0)-1}(p, \omega_1) = G_-(p - k, \omega_1 - \omega) +$$
$$+ i\int \frac{dq}{2\pi}\frac{d\varepsilon}{2\pi}\frac{D_{1\|1}(q, \varepsilon)}{\varepsilon - v_F q}\,[N(p - q, \omega_1 - \varepsilon, k - q, \omega - \varepsilon) -$$
$$- N(p, \omega_1, k, \omega)] + i\int \frac{dq}{2\pi}\frac{d\varepsilon}{2\pi}\frac{D_{2\|1}(q, \varepsilon)}{\varepsilon - v_F q}\,[N(p - q, \omega_1 - \varepsilon, k, \omega) -$$
$$- N(p - q, \omega_1 - \varepsilon, k - q, \omega - \varepsilon)]. \tag{29}$$

This equation can be solved by writing it in Fourier transformed form with

$$N(p, \omega_1, k, \omega) = \int dx_1\, dt_1\, dx\, dt\, N(x_1, t_1, x, t)\, e^{i(\omega_1 t_1 - p x_1)}\, e^{i(\omega t - k x)} \tag{30}$$

since then

$$i\left(\frac{\partial}{\partial t_1} + v_F\frac{\partial}{\partial x_1}\right) N(x_1, t_1, x, t) = \delta(x + x_1)\,\delta(t + t_1)\,G_-(-x, -t) +$$
$$+ i\,K_{1\|1}(x + x_1, t + t_1)\,N(x_1, t_1, x, t) - \tag{31}$$
$$- i[K_{2\|1}(x + x_1, t + t_1) - K_{2\|1}(x_1, t_1)]\,N(x_1, t_1, x, t),$$

where the term leading to a Fermi energy renormalization has again been neglected and

$$K_{2\|1}(x, t) = \int \frac{dq}{2\pi}\frac{d\varepsilon}{2\pi}\frac{D_{2\|1}(q, \varepsilon)}{\varepsilon - v_F q}\, e^{-i(\varepsilon t - q x)}\,. \tag{32}$$

The solution can be looked for in the form

$$N_1(x_1, t_1, x, t) = N_1(x + x_1, t + t_1)\,N_2(x_1, t_1) N_3(x, t). \tag{33}$$

Eq. (31) can be separated into two equations for N_1 and N_2, and furthermore $N_3(x, t) = G_-(-x, -t) N_2^{-1}(-x, -t)$. These equations are solved in the same way as Eq. (12). Putting everything together, taking into account that $N(k, \omega)$ is obtained from $N(p, \omega_1, k, \omega)$ by a simple integration, which means that the Fourier transform $N(k, t)$ of $N(k, \omega)$ is obtained by putting $x_1 = t_1 = 0$ in $N(x_1, t_1, x, t)$, we finally get

$$N(x, t) = -i\,G_+(x, t)\,G_-(-x, -t)\,[\Lambda^2(x - u_\sigma t + i/\Lambda(t))\,(x + u_\sigma t - i/\Lambda(t))]^{\beta\sigma}\times$$
$$\times[\Lambda^2(x - u_\varrho t + i/\Lambda(t))\,(x + u_\varrho t - i/\Lambda(t))]^{\beta\varrho} \tag{34}$$

with

$$\beta_\sigma = \frac{1}{4\pi u_\sigma}(\lambda_{2\parallel} - \lambda_{2\perp}),$$

$$\beta_\varrho = \frac{1}{4\pi u_\varrho}(\lambda_{2\parallel} + \lambda_{2\perp}). \tag{35}$$

Since the spin-density response function contains $D_{2\perp}$ instead of $D_{2\parallel}$, a similar expression is obtained for $\chi(x, t)$ with $-\beta_\sigma$ instead of β_σ in the exponent.

The calculation of the pairing responses can be done in a similar way. The generalized Ward identities are also similar with one overall sign difference in the case when the small momentum transfer interaction leg couples to the dashed line due to the opposite orientation of this line. The result for the singlet-superconductor response is

$$\Delta_s(x, t) = iG_+(x, t)\, G_-(x, t)\, [\Lambda^2(x - u_\sigma t + i/\Lambda(t))\,(x + u_\sigma t - i/\Lambda(t))]^{\beta_\sigma} \times$$
$$\times [\Lambda^2(x - u_\varrho t + i/\Lambda(t))\,(x + u_\varrho t - i/\Lambda(t))]^{-\beta_\varrho}. \tag{36}$$

The triplet-superconductor response has $-\beta_\sigma$ in the exponent instead of β_σ.

Writing in the expressions for the Green's functions from Eqs. (16) and (18) we finally get

$$R(x, t) = \mp i \frac{x - v_F t + i/\Lambda(t)}{x - v_F t + i\delta(t)} \cdot \frac{x + v_F t - i/\Lambda(t)}{x + v_F t - i/\delta(t)} \Lambda^{\nu} \times$$
$$\times [(x - u_\sigma t + i/\Lambda(t))\,(x + u_\sigma t - i/\Lambda(t))]^{\mu_\sigma} \times \tag{37}$$
$$\times [(x - u_\varrho t + i/\Lambda(t))\,(x + u_\varrho t - i/\Lambda(t))]^{\mu_\varrho},$$

where

(i)
$$\mu_\sigma = \frac{1}{2}\gamma_\sigma, \quad \mu_\varrho = \frac{1}{2}\gamma_\varrho, \tag{38}$$

with

$$\gamma_\sigma = \left[\frac{v_F + \frac{1}{2\pi}(\lambda_{1\parallel} - \lambda_{1\perp}) - \frac{1}{2\pi}(\lambda_{2\parallel} - \lambda_{2\perp})}{v_F + \frac{1}{2\pi}(\lambda_{1\parallel} - \lambda_{1\perp}) + \frac{1}{2\pi}(\lambda_{2\parallel} - \lambda_{2\perp})}\right]^{1/2},$$

$$\gamma_\varrho = \left[\frac{v_F + \frac{1}{2\pi}(\lambda_{1\parallel} + \lambda_{1\perp}) - \frac{1}{2\pi}(\lambda_{2\parallel} + \lambda_{2\perp})}{v_F + \frac{1}{2\pi}(\lambda_{1\parallel} + \lambda_{1\perp}) + \frac{1}{2\pi}(\lambda_{2\parallel} + \lambda_{2\perp})}\right]^{1/2} \tag{39}$$

for the charge-density response function,

(ii) $$\mu_\sigma = \frac{1}{2\gamma_\sigma}, \quad \mu_\varrho = \frac{1}{2}\gamma_\varrho \tag{40}$$

for the spin-density response function,

(iii) $$\mu_\sigma = \frac{1}{2}\gamma_\sigma, \quad \mu_\varrho = \frac{1}{2\gamma_\varrho} \tag{41}$$

for the singlet-superconductor response, and

(iv) $$\mu_\sigma = \frac{1}{2\gamma_\sigma}, \quad \mu_\varrho = \frac{1}{2\gamma_\varrho} \tag{42}$$

for the triplet-superconductor response.

In the case of spin-independent interaction these results agree will those obtained by FOGEDBY [15].

4. System of coupled Tomonaga chains

It was shown in the previous Sections how the strictly 1-d TOMONAGA model can be solved exactly by summing all diagrams by the use of Ward identities. Now this method will be extended to study the properties of a quasi-1-d system, in which 3-d couplings are taken into account.

The model is defined as follows: a set of 1-d TOMONAGA chains with linear dispersion relation and intrachain forward scattering is coupled together by interchain coupling which has forward scattering components only. Assigning a chain index i to the electrons on the chain at position R_i, the Hamiltonian of the system can be written as

$$H = H_0 + H_{int} \tag{43}$$

with

$$H_0 = \sum_{i,k,\alpha} v_F(k - k_F)\, a^+_{ik\alpha}\, a_{ik\alpha} + \sum_{i,k,\alpha} v_F(-k - k_F)\, b^+_{ik\alpha}\, b_{ik\alpha} \tag{44}$$

and

$$\begin{aligned} H_{int} = \frac{1}{2L} \sum_{\substack{i,j \\ k,k',p \\ \alpha,\beta}} (\lambda_{1\|ij}\, \delta_{\alpha\beta} + \lambda_{1\perp ij}\, \delta_{\alpha,-\beta})\, (a^+_{ik+p\alpha}\, a^+_{jk'-p\beta}\, a_{jk'\beta}\, a_{ik\alpha} + \\ + b^+_{ik+p\alpha}\, b^+_{jk'-p\beta}\, b_{jk'\beta}\, b_{ik\alpha}) \\ + \frac{1}{L} \sum_{\substack{i,j \\ k,k',p \\ \alpha,\beta}} (\lambda_{2\|ij}\, \delta_{\alpha\beta} + \lambda_{2\perp ij}\, \delta_{\alpha,-\beta})\, a^+_{ik+p\alpha}\, b^+_{jk'-p\beta}\, b_{jk'\beta}\, a_{ik\alpha}, \end{aligned} \tag{45}$$

where λ_{1ij}, and λ_{2ij} are the coupling constants between electrons on i^{th} and j^{th} chains. For simplicity equivalent chains are considered, i.e. v_F and k_F are taken to be the same for all chains.

The method of solution is a straightforward generalization of the method used in the strictly 1-d case. Since the quasi-1-d model has the two main characteristic features of the 1-d TOMONAGA model, namely the linearity of the dispersion relation and the absence of large momentum transfer (backward scattering) terms, diagrams with simple bubbles and series of bubbles will only contribute, the effect of more complicated diagrams being cancelled by each other. As a consequence, effective interactions can again be introduced, satisfying the same diagrammatic equations as in the 1-d case, but the electron-hole pair in the intermediate state can be on any chain. The analytic equations for the effective interactions are

$$\begin{aligned}
D_{1\|\|ij} &= \lambda_{1\|\|ij} + \sum_l [\lambda_{1\|\|il}\Pi_+ D_{1\|\|lj} + \lambda_{1\perp il}\Pi_+ D_{1\perp lj} + \lambda_{2\|\|il}\Pi_- D_{2\|\|lj} + \lambda_{2\perp il}\Pi_- D_{2\perp lj}],\\
D_{1\perp ij} &= \lambda_{1\perp ij} + \sum_l [\lambda_{1\|\|il}\Pi_+ D_{1\perp lj} + \lambda_{1\perp il}\Pi_+ D_{1\|\|lj} + \lambda_{2\|\|il}\Pi_- D_{2\perp lj} + \lambda_{2\perp il}\Pi_- D_{2\|\|lj}],\\
D_{2\|\|ij} &= \lambda_{2\|\|ij} + \sum_l [\lambda_{2\|\|il}\Pi_+ D_{1\|\|lj} + \lambda_{2\perp il}\Pi_+ D_{1\perp lj} + \lambda_{1\|\|il}\Pi_- D_{2\|\|lj} + \lambda_{1\perp il}\Pi_- D_{2\perp lj}],\\
D_{2\perp ij} &= \lambda_{2\perp ij} + \sum_l [\lambda_{2\|\|il}\Pi_+ D_{1\perp lj} + \lambda_{2\perp il}\Pi_+ D_{1\|\|lj} + \lambda_{1\|\|il}\Pi_- D_{2\perp lj} + \lambda_{1\perp il}\Pi_- D_{2\|\|lj}].
\end{aligned} \tag{46}$$

These effective interactions are of course functions of the momentum component $k_\|$ which is parallel to the chain direction, and the energy variable ω through the dependence of Π on these variables. Performing a Fourier transformation in the perpendicular direction with

$$D_{\mu ij}(k_\|,\omega) = \frac{1}{N}\sum_{k\perp} D_\mu(k_\|, k_\perp, \omega)\, e^{ik_\perp(R_i - R_j)}, \quad \mu = 1\|, 1\perp, 2\|, 2\perp \tag{47}$$

we have

$$\begin{aligned}
D_{1\|}(k_\perp) = \lambda_{1\|}(k_\perp) + \lambda_{1\|}(k_\perp)\,\Pi_+ D_{1\|}(k_\perp) + \lambda_{1\perp}(k_\perp)\,\Pi_+ D_{1\perp}(k_\perp) +\\
+ \lambda_{2\|}(k_\perp)\,\Pi_- D_{2\|}(k_\perp) + \lambda_{2\perp}(k_\perp)\,\Pi_- D_{2\perp}(k_\perp)
\end{aligned} \tag{48}$$

and three similar equations with

$$\lambda_\mu(k_\perp) = \sum_i \lambda_{\mu ij}\, e^{-ik_\perp(R_i - R_j)}, \quad \mu = 1\|, 1\perp, 2\|, 2\perp. \tag{49}$$

The $k_\perp$-dependent effective interactions obey exactly the same equations as the effective interactions in the 1-d case, except that everywhere λ should

be replaced by $\lambda(k_\perp)$. Keeping this in mind, the solution of these equations is obtained from Eqs. (6)—(8) if the dependence on $k_\perp$ is taken into account. The velocities u_σ and u_ϱ will also depend on $k_\perp$, e.g.

$$u_\sigma(k_\perp) = \left\{\left[v_F + \frac{1}{2\pi}(\lambda_{1\|}(k_\perp) - \lambda_{1\perp}(k_\perp))\right]^2 - \left[\frac{1}{2\pi}(\lambda_{2\|}(k_\perp) - \lambda_{2\perp}(k_\perp))\right]^2\right\}^{1/2}. \tag{50}$$

A very important consequence of the neglect of hopping and backward scattering is that perturbations created on any chain can propagate along that chain only. The neighbouring chains can influence this propagation, but there is no response on other chains. The Green's function

$$G_{+ij}(p, \varepsilon) = -i \int dt\, e^{i\varepsilon t} \langle T\{a_{ip}(t)\, a_{jp}^+(0)\}\rangle \tag{51}$$

will be diagonal in the chain index, $G_{+ij} = G_{+il} \cdot \delta_{ij}$, and similarly all the response functions

$$R_{ij}(k, \omega) = -i \int dt\, e^{i\omega t} \langle T\{O_i(k, t)\, O_j^+(k, 0)\}\rangle \tag{52}$$

with e.g.

$$O_i(k, t) = \frac{1}{L^{1/2}} \sum_p b_{ip\uparrow}^+(t)\, a_{ip+k\uparrow}(t) \tag{53}$$

for the charge-density response function, will be diagonal in the chain index.

This is easily seen since in the density responses a large ($\sim 2\, k_F$) momentum is given to the electrons on one chain and this momentum cannot be transferred to other chains if only small momentum transfer processes are allowed. In the superconducting responses the Cooper pair added to a chain cannot propagate to other chains if hopping is not allowed.

Due to this property, the vertices appearing in the Dyson equation for the Green's function and in the two alternative representations of the response functions have identical chain index on the two electron legs. The Ward identities used in the 1-d case will be valid here as well, because the problem is reduced to a one chain problem with effective interactions

$$D_{\mu il}(k_\|, \omega) = \frac{1}{N} \sum_{k_\perp} D_\mu(k_\|, k_\perp, \omega), \quad \mu = 1\|, 1\perp, 2\|, 2\perp. \tag{54}$$

Using these expressions for the effective intrachain interactions, the Dyson equation (11), Eq. (29) for the charge-density response and the analogous equations for the other response functions can be solved by taking over the results of the 1-d case to get

$$G_{+ij}(x, t) = \delta_{ij} \prod_{k_\perp} [G_+(x, t, k_\perp)]^{1/N} \tag{55}$$

and

$$R_{ij}(x, t) = \delta_{ij} \prod_{k_\perp} [R(x, t, k_\perp)]^{1/N} , \tag{56}$$

where N is the number of chains, $G_+(x, t, k_\perp)$ and $R(x, t, k_\perp)$ have the same form as the corresponding expressions for a single chain with $\lambda_\mu(k_\perp)$ instead of λ_μ. E.g.

$$\begin{aligned} R(x, t, k_\perp) = \mp i \frac{x - v_F t + i/\Lambda(t)}{x - v_F t + i\delta(t)} \frac{x + v_F t - i/\Lambda(t)}{x + v_F t - i\delta(t)} \Lambda^\nu \times \\ \times [(x - u_\sigma(k_\perp)t + i/\Lambda(t))\,(x + u_\sigma(k_\perp)\,t - i/\Lambda(t)]^{\mu_\sigma(k_\perp)} \\ \times [(x - u_\varrho(k_\perp)\,t + i/\Lambda(t))\,(x + u_\varrho(k_\perp)\,t - i/\Lambda(t))]^{\mu_\varrho(k_\perp)}, \end{aligned} \tag{57}$$

where for the charge-density response $\mu_\sigma(k_\perp) = \frac{1}{2}\gamma_\sigma(k_\perp)$ and $\mu_\varrho(k_\perp) = \frac{1}{2}\gamma_\varrho(k_\perp)$ with

$$\begin{aligned} \gamma_\sigma(k_\perp) &= \left\{ \frac{v_F + \frac{1}{2\pi}[\lambda_{1\parallel}(k_\perp) - \lambda_{1\perp}(k_\perp)] - \frac{1}{2\pi}[\lambda_{2\parallel}(k_\perp) - \lambda_{2\perp}(k_\perp)]}{v_F + \frac{1}{2\pi}[\lambda_{1\parallel}(k_\perp) - \lambda_{1\perp})k)] + \frac{1}{2\pi}[\lambda_{2\parallel}(k_\perp) - \lambda_{2\perp}(k_\perp)]} \right\}^{1/2}, \\ \gamma_\varrho(k_\perp) &= \left\{ \frac{v_F + \frac{1}{2\pi}[\lambda_{1\parallel}(k_\perp) + \lambda_{1\perp}(k_\perp^-)] - \frac{1}{2\pi}[\lambda_{2\parallel}(k_\perp) + \lambda_{2\perp}(k_\perp]}{v_F + \frac{1}{2\pi}[\lambda_{1\parallel}(k_\perp) + \lambda_{1\perp}(k_\perp)] + \frac{1}{2\pi}[\lambda_{2\parallel}(k_\perp) + \lambda_{2\perp}(k_\perp)]} \right\}^{1/2} \end{aligned} \tag{58}$$

and the exponents of the other response functions are obtained by the rules given in Eqs. (40)—(42).

In the limit of weak nearest neighbour interchain interaction this result agrees with that obtained by KLEMM and GUTFREUND [7].

5. Discussion

We have given an exact solution of a quasi-1-d model of interacting electrons. Although the model contains explicitly a 3-d interchain coupling, due to the particular choice of this coupling (only forward scattering terms were considered), this model turns out to be equivalent to a set of effectively decoupled chains. The perturbations can propagate along the chains only, no response is obtained on other chains. Earlier approximate treatments of the backward scattering model [6]—[8] have indicated already that backward scattering terms or interchain hopping are important to have a phase transition in quasi-1-d system. Our exact calculation proves that without these terms no ordering is possible at any finite temperature, since the ordered phase would have a non-decaying response function.

REFERENCES

1. "Chemistry and Physics of One-Dimensional Metals", Proceedings of NATO Advanced Study Institute, Bolzano, Italy, 1976, edited by H. J. Keller, Plenum Press, New York, 1977.
2. "Organic Conductors and Semiconductors", Lecture Notes in Physics, Vol. 65, edited by L. Pál, G. Grüner, A. Jánossy and J. Sólyom, Springer Verlag, Berlin, 1977.
3. "Quasi-One-Dimensional Conductors", Lecture Notes in Physics, Vols. 95—96, edited by S. Barisic, A. Bjelis, J. R. Cooper and B. Leontic, Springer Verlag , Berlin, 1979.
4. J. Sólyom, Advances in Physics, **28**, 201, 1979.
5. L. P. Gorkov and I. E. Dzyaloshinsky, Zh. Eksp. i Teor. Fiz., **67**, 397, 1974.
6. L. Mihály and J. Sólyom, J. Low Temp. Phys., **24**, 579, 1976.
7. R. A. Klemm and H. Gutfreund, Phys. Rev. B, **14**, 1086, 1976.
8. P. A. Lee, T. M. Rice and R. A. Klemm, Phys. Rev., B **15**, 2984, 1977.
9. N. Menyhárd, in Lecture Notes in Physics, Vol. 65, edited by L. Pál, G. Grüner, A. Jánossy and J. Sólyom, Springer Verlag, Berlin, p. 165, 1977.
10. S. Tomonaga, Prog. Theor. Phys., **5**, 349, 1950.
11. D. C. Mattis and E. H. Lieb, J. Math. Phys., **6**, 304, 1965.
12. A. Theumann, J. Math. Phys., **8**, 2460, 1967.
13. A. Luther and I. Peschel, Phys. Rev., B **9**, 2911, 1974.
14. D. C. Mattis, J. Math. Phys., **15**, 609, 1974.
15. H. C. Fogedby, J. Phys. C, **9**, 3757, 1976.
16. I. E. Dzyaloshinsky and A. I. Larkin, Zh. Eksp. i Teor. Fiz., **65**, 411, 1973.
17. J. Sólyom, in Lecture Notes in Physics, Vol. 96, p. 100, Springer Verlag, Berlin, 1979.

Acta Physica Academiae Scientiarum Hungaricae, Tomus 48 (2—3), pp. 187—195 (1980)

TWO KERR-NUT TYPE SOLUTIONS OF EINSTEIN'S EQUATIONS

By

I. C. PATEL, R. P. AKABARI and L. K. PATEL

DEPARTMENT OF MATHEMATICS, GUJARAT UNIVERSITY, AHMEDABAD 380 009, INDIA

(Received 15. XII. 1979)

Two exact solutions of Einstein's field equations are obtained. One of them describes the Kerr-NUT metric in the background of Einstein's Universe. The metric of this solution is such that in the vicinity of the source it reduces to the Kerr-NUT metric and in the absence of the source it reduces to the metric of Einstein's Universe. The other solution describes the Kerr-NUT metric with a non-zero cosmological constant. The details regarding the two solutions are also discussed.

1. Introduction

The study of gravitational fields due to rotating bodies plays a significant role in relativistic astrophysics. Therefore many researchers have taken keen interest in studying the gravitational fields of rotating bodies. Two rigorous solutions of Einstein's vacuum field equations are well-known in the literature. They are the KERR solution [1] and the NUT solutions [2]. Both solutions admit a shear-free congruence of null geodesics with non-zero expansion and twist. The combined Kerr-NUT metric can be expressed as (DEMIANSKI [3])

$$ds^2 = 2[du + (a\sin^2\alpha - 2l\cos\alpha)d\beta][dr - a\sin^2\alpha d\beta]$$

$$+\left(1 - \frac{2mr + 2lF}{r^2 + F^2}\right)[du + (a\sin^2\alpha - 2l\cos\alpha)\,d\beta]^2$$

$$-(r^2 + F^2)(d\alpha^2 + \sin^2\alpha d\beta^2), \tag{1}$$

where $F = a\cos\alpha + l$. The constants m, a, l represent respectively the mass, angular momentum per unit mass and magnetic monopole-type mass. The choice $l = 0$ gives us the Kerr metric and the choice $a = 0$ gives us the NUT metric.

VAIDYA [4] has found out what the Kerr metric looks like in the background of a homogeneous model of the Universe. He has expressed the metric of the Einstein's Universe in the rotating spheroidal polar coordinates.

It is given by

$$ds^2 = 2(du + a\sin^2\alpha d\beta)(dr - a\sin^2\alpha d\beta] - M^2\left[\left(1 - \frac{a^2}{R^2}\sin^2\alpha\right)^{-1} d\alpha^2 + \sin^2\alpha d\beta^2\right] + (du + a\sin^2\alpha d\beta)^2, \tag{2}$$

with $M^2 = (R^2 - a^2)\sin^2\left(\frac{r}{R}\right) + a^2\cos^2\alpha$. Here R and a are constants.

PATEL and AKABARI [5] have discussed the NUT metric in the background of Einstein's Universe.

Many investigators have discussed Kerr metric with a non-zero cosmological constant (see [6], [7], [8]).

The object of the present investigation is to obtain (i) Kerr-NUT metric in the background of Einstein's Universe and (ii) Kerr-NUT metric with a non-zero cosmological constant. For this purpose we consider the metric in the form

$$ds^2 = (1/F^2)\,[2(du + g\sin\alpha d\beta)\,(dr + h\sin\alpha d\beta) - 2L(du + g\sin\alpha d\beta)^2 - M^2(d\alpha^2 + \sin^2\alpha d\beta^2)] \tag{3}$$

with $g = g(\alpha)$, $h = h(\alpha)$, $M = M(\alpha, r)$, $L = L(\alpha, r)$ and $F = F(\alpha, r)$.

2. Equations of structure

Introducing the basic 1-forms

$$\theta^{(1)} = \frac{1}{F}(du + g\sin\alpha d\beta), \quad \theta^{(2)} = (M/F)\,d\alpha,$$

$$\theta^{(3)} = (M/F)\sin\alpha d\beta, \quad \theta^{(4)} = \frac{1}{F}(dr + h\sin\alpha d\beta) - L\theta^{(1)} \tag{4}$$

we can write the metric (3) as

$$ds^2 = 2\theta^{(1)}\theta^{(4)} - (\theta^{(2)})^2 - (\theta^{(3)})^2 = g_{(ab)}\,\theta^{(a)}\,\theta^{(b)}. \tag{5}$$

Here and in what follows a bracketed index implies the corresponding tetrad component. It is now easy to compute the exterior derivative $d\theta^{(a)}$ from (4). The substitution of $d\theta^{(a)}$ in the Cartan's first structure equation $d\theta^{(a)} = -\omega^{(a)}_{(b)} \wedge \theta^{(b)}$ yields the connection 1-forms $\omega^{(a)}_{(b)}$. Using these $\omega^{(a)}_{(b)}$ in the

Cartan's second structure equation $\Omega^{(a)}_{(b)} = d\omega^{(a)}_{(b)} + \omega^{(a)}_{(c)} \wedge \omega^{(c)}_{(b)}$ we can obtain the connection 2-forms $\Omega^{(a)}_{(b)}$. The computations of $\omega^{(a)}_{(b)}$ and $\Omega^{(a)}_{(b)}$ are lengthy but straightforward and so are not given here. The relation between $\Omega^{(a)}_{(b)}$ and the curvature tensor is given by

$$\Omega^{(a)}_{(b)} = \frac{1}{2} R^{(a)}_{(bcd)} \cdot \theta^{(c)} \wedge \theta^{(d)}. \tag{6}$$

Using (6) and the expressions of $\Omega^{(a)}_{(b)}$ one can obtain the tetrad components $R_{(ab)} = R^{(c)}_{(abc)}$ of Ricci tensor. The explicit expressions for $R_{(ab)}$ are

$$R_{(23)} = (2h^2F/M^2)\,[F_{rz} - F_zMr/M + F_rH/h^2 - F_rN/h^2M],$$

$$R_{(24)} = -(hF/M)\left[2F_{rz} - 2F_zMr/M - F\left(\frac{Mr}{M}\right)_z + F^3\frac{fG}{M^2F^2}\right)_r\Bigg],$$

$$R_{(34)} = (hF/M)\left[2F_{rr} - 2F_r(Mr/M) - F^3\left(\frac{G}{M^2F^2}\right)_z - F(Mr/M)_r\right],$$

$$R_{(44)} = 2F[FM_{rr}/M - G^2F/M^4 - F_{rr}],$$

$$R_{(12)} = (F^4h/M)\,[(L_z/F^2)_r + \{(2LG - H)/M^2F^2\}_r] + LR_{(24)}$$

$$R_{(13)} = (F^4h/M)\,[-(L_r/F^2)_r + \{(2LG - H)/M^2F^2\}_z] + LR_{(34)},$$

$$R_{(11)} = L^2R_{(44)} + (hF/M)^2\,[L_{zz} + L_{rr} - 2(L_zF_z + L_rF_r)/F] +$$
$$+ 2H(F/M)^2\,[L_z - (H - 2LG)/M^2],$$

$$R_{(14)} = F^2[L_{rr} + (2/M)\,\{(LM_r)_r - (G/M)\,(H - LG)/M^2\}] -$$
$$- 3(h/M)^2\,(F_r^2 + F_z^2) + 2HFF_z/M^2 + F(h/M)^2\,(F_{rr} + F_{zz})$$
$$- 4FL_rF_r + 2LF(-2F_{rr} + 3F_r^2/F - 2F_rM_r/M),$$

$$R_{(22)} = (F^2/M^2)\left[hg\left(\frac{h}{g}\cdot\frac{Mz}{M}\right)_z + \frac{2Gh}{g}\left(\frac{Mz}{M}\right)\right.$$
$$- 1 + 4LG^2/M^2 - 4GH/M^2 - \{L(M^2)_r\}_r$$
$$\left. + h^2(M_r/M)_r\right] + F(h/M)^2\,(F_{rr} + 3F_{zz})$$
$$- 2LF(F_{rr} + 4F_rM_r/M - 3F_r^2/F) - 2FF_rL_r - (h/M)^2(F_r^2 + F_z^2)$$
$$- 2h^2F_r(FM_r/M - F_r)/M^2 + (3hFF_z/M^2)\left[h_z - hM_z/M - \frac{N}{M}\right],$$

$$R_{(33)} = R_{(22)} - (2hF/M)\,[(hF_z/M)_z + F_rhM_r/M^2$$
$$- (hF_r/M)_r - (NF_z/M^2)],$$

where

$$2G = g_\alpha + g \cot \alpha, \quad 2H = h_\alpha + h \cot \alpha \tag{7}$$

$$N = M_\alpha + M \cot \alpha \tag{8}$$

and the variable α is replaced by the variable z defined by

$$h d\alpha = dz. \tag{9}$$

Here and in what follows the suffix indicates the derivatives e.g.

$$h_z = \partial h/\partial z, \quad L_{rr} = \partial^2 L/\partial r^2 \text{ etc.}$$

3. The case F = 1

We shall now try to show that the metric (3) with $F = 1$ is compatible with the perfect fluid distribution. The field equation for the perfect fluid distribution can be expressed in the tetrad form as

$$R_{(ab)} = \lambda g_{(ab)} - 8\pi \left[(p + \varrho)\, v_{(a)}\, v_{(b)} - \frac{1}{2}(\varrho - p)\, g_{(ab)} \right]. \tag{10}$$

Here p, ϱ,$v_{(a)}$ and λ are respectively the pressure, the density, the tetrad components of the flow vector satisfying $v_{(a)}v^{(a)} = 1$ and the cosmological constant. We choose the tetrad component $v_{(a)}$ as

$$v_{(a)} = \left(\frac{1}{2n},\ 0,\ 0,\ n \right), \tag{11}$$

where n is a parameter to be determined from the field equations.

Putting $F = 1$ in (7) it is easy to see that

$$R_{(23)} = 0 \text{ and } R_{(22)} = R_{(23)}\,. \tag{12}$$

The results (5), (10) and (11) imply the following relations

$$8\pi p = \lambda - R_{(14)}, \tag{13}$$

$$8\pi \varrho = -\lambda - R_{(22)} - [R_{(11)}\, R_{(44)}]^{1/2}, \tag{14}$$

$$R_{(44)} = 4n^4 R_{(11)}\,, \tag{15}$$

$$R_{(14)} + R_{(22)} = [R_{(11)}\ R_{(44)}]^{1/2}, \tag{16}$$

$$R_{(24)} = 0,\ R_{(34)} = 0, \tag{17}$$

$$R_{(12)} = 0,\ R_{(13)} = 0. \tag{18}$$

Using (7) and (17) and the result $F = 1$ we obtain

$$M^2 = Q^2(CX^2 + Y^2), \; G^2 = Q^2 Y Y_z, \tag{19}$$

where Q is an arbitrary function of z and the functions $X = X(r)$ and $Y = Y(z)$ satisfy the relations

$$X_{rr} = -X/R^2, \; X_r^2 = 1 - X^2/R^2, \; Y_{zz} = Y/R^2, \; Y_z^2 = C + Y^2/R^2. \tag{20}$$

Here C and R are constants.

From (7), (18), (19) and (20) we obtain

$$2L = -1 + 2(mXX_r + YY_z)/(CX^2 + Y^2) \tag{21}$$

and

$$\frac{H}{F^2} = l(2Y^2/R^2 + C) - YY_z, \tag{22}$$

where m and l are constants. The use of (7), (19), (20), (21) and (22) in the equations (15) and (16) yields the results

$$2n^2 = -L^{-1} \tag{23}$$

and

$$(h^2/Q^2)(Q_z/Q)_z + (2H/Q^2)(Q_z/Q) - 1/Q^2 + C - 4lYY_z/R^2 + 2Y^2/R^2 = 0. \tag{24}$$

The results (19), (20), (21), (22) and (24) determine the functions M, g, h and L completely. The result (23) gives us the value of n where we have assumed that L is negative. The pressure and density can be obtained from (13) and (14). The expressions for p and ϱ are

$$8\pi p = \lambda + 2L/R^2, \quad 8\pi\varrho = -\lambda - 3L/R^2, \tag{25}$$

where $2L$ is given by (21). Thus we have seen that the metric (3) with $F = 1$ is compatible with perfect fluid distribution.

4. An Einstein—Kerr-NUT metric

The principal goal of this Section is to give the physical interpretation of the solution obtained in the previous Section. For this purpose we shall use the variable ψ instead of z defined by the equation

$$(Y^2 + l^2 - a^2\cos^2\psi)^2 = 4l^2Y^2(1 - a^2/R^2 + Q^2/R^2), \tag{26}$$

where Y is given as a function of z by (20) and a is a constant. We also take

$$X(r) = R \sin (r/R). \tag{27}$$

Therefore (20) gives us $C = 1 - a^2/R^2$. Using (26) and (27) it can be easily seen that the differential equations (22) and (24) admit simple solutions.

$$h \sin \alpha = -a \sin^2 \psi, \; Q \sin \alpha = \sin \psi. \tag{28}$$

Using (26) and (27) in the equation $G = Q^2 Y Y_z$ we obtain

$$ag \sin \alpha = l^2 + a^2 - Y^2, \tag{29}$$

where Y is given as a function of ψ by (26). The metric of our solution can be expressed in the final form as

$$\begin{aligned} ds^2 = {} & 2[du + (1/a)\,(l^2 + a^2 - Y^2) d\beta]\,[dr - a \sin^2 \psi d\beta] \\ & - M^2 \left[\frac{d\psi^2}{N^{*2}} + \sin^2 \psi \, d\beta^2 \right] + [1 - 2m\mu - 2l\gamma] \times \\ & \times [du + (1/a)\,(l^2 + a^2 - Y^2)\, d\beta]^2, \end{aligned} \tag{30}$$

where

$$\mu = R \sin (r/R) \cos (r/R)/M^2, \; \gamma = Y Y_z/M^2,$$

$$N^* = (a \cos \psi)^{-1} [2lY^2/R^2 + l(1 - a^2/R^2) - Y Y_z]$$

and

$$M^2 = (R^2 - a^2) \sin^2 (r/R) + Y^2. \tag{31}$$

Here Y is expressed as a function of ψ by (26).

When $R \to \infty$, we have $X \to r$, $Y \to z$. In this case it can be easily seen that the metric (30) goes over to Kerr-NUT metric (1) with slight change of notations. In this case $p + \varrho = 0$. Hence $p = 0$, $\varrho = 0$ and consequently $\lambda = 0$.

If we put $m = l = 0$, then it is painless to verify that the metric (30) reduces to the metric (2) of the Einstein's Universe. Thus the metric (30) reduces to the Kerr-NUT metric in the vicinity of the source and it reduces to the metric of the Einstein's Universe in the absence of the source. We designate the metric (30) as an Einstein—Kerr-NUT metric.

If we set $l = 0$ in (30), we obtain the metric

$$\begin{aligned} ds^2 = {} & 2(du + a \sin^2 \psi d\beta)(dr - a \sin^2 \psi d\beta) \\ & - M^2 \left[\left(1 - \frac{a^2}{R^2} \sin^2 \psi \right)^{-1} d\psi^2 + \sin^2 \psi \, d\beta^2 \right] \\ & + (1 - 2m\mu)\,(du + a \sin^2 \psi d\beta)^2 \end{aligned} \tag{32}$$

where

$$M^2 = (R^2 - a^2)\sin^2(r/R) + a^2\cos^2\psi$$

and

$$\mu = R\sin(r/R)\cos(r/R)/M^2. \tag{33}$$

The metric (32) is the Kerr metric in the background of Einstein's Universe discussed by VAIDYA [4].

In the above analysis we cannot take $a = 0$ because $a = 0$ implies $h = 0$ which is contrary to our assumption. Therefore one should not expect to recover the results of PATEL and AKABARI [5] from the above results.

5. Kerr-NUT metric with a λ-term

In this Section we shall obtain a solution of the field equations

$$R_{(ab)} = \lambda g_{(ab)} \tag{34}$$

in terms of the metric (3).

The results (5) and (34) imply the following relations

$$R_{(23)} = 0,\ R_{(22)} = R_{(33)}, \tag{35}$$

$$R_{(34)} = 0,\ R_{(24)} = 0, \tag{36}$$

$$R_{(12)} = 0,\ R_{(13)} = 0, \tag{37}$$

$$R_{(11)} = 0,\ R_{(44)} = 0, \tag{38}$$

$$R_{(14)} = \lambda,\ R_{(22)} = -\lambda, \tag{39}$$

where $R_{(ab)}$ are given by (7).

The Eqs. (35) simplify to the equations

$$\mu(F_r^2 + F_z^2) = p(F), \tag{40}$$

$$\mu(F_{rr} + F_{zz}) = \frac{dp}{dF}, \tag{41}$$

where p is an arbitrary function of F and μ is defined by

$$\mu = h/M^2\sin\alpha. \tag{42}$$

The Eq. (36) reduces to

$$\{(G/M^2 - q_r)/F^2\}_r - (p_r/2pF^2)_z = 0 \tag{43}$$

and

$$\{(G/M^2 - q_r)/F^2\}_z + (p_r/2pF)_r = 0 \tag{44}$$

where $\tan q = F_r/F_z$.

From the above two equations it is clear that $(p_r/2pF^2)$ satisfies Laplace's equation in r and z. This fact leads us to $p = 1$ or $p = F^3$. In the present paper we take $p = 1$. In this particular case the differential equations (40), (41), (43) and (44) admit the following solutions:

$$\mu = (cx^2 + dy^2)^{-1},\ g \sin \alpha = K + dy^2,\ F = AX_rY_z, \tag{45}$$

where c, d, K and A are constants and the functions $X = X(r)$ and $Y = Y(z)$ satisfy the relations

$$X_{rr} = -X/R^2;\ X_r^2 = d - X^2/R^2;\ Y_{zz} = Y/R^2;\ Y_z^2 = c + Y^2/R^2. \tag{46}$$

Here R is a constant.

Using the result (45) and (46) the two equations (37) can be easily solved for the functions L and h. The solutions are given by

$$2L = -1 + 2(mXX_r^3 + lYY_z^3)/(cx^2 + dy^2), \tag{47}$$

$$h \sin \alpha = -\bar{K} - dy^2 + 2lYY_z^3, \tag{48}$$

where m, l and $\bar{K}$ are constants.

With the aid of the results (45), (46), (47) and (48) we have verified that the two equations (38) are identically satisfied. Let us now consider the equation $R_{(14)} = \lambda$. Using the relevant results, this equation gives us the value of the cosmological constant λ. This value is given by

$$\lambda = -3(A^2/R^2)\,(cd - \bar{K}/R^2). \tag{49}$$

Using the results (45), (46), (47), (48) and (49) we have verified by a lengthy computation that the equation $R_{(22)} = -\lambda$ is identically satisfied. This completes the task of solving the field equations $R_{ik} = \lambda g_{ik}$ for the metric (3). Let us now try to give the physical interpretation to our solution. When $R \to \infty$ we have $F = A$, $X = r$, $y = z$ and $c = d = 1$. In this case it is clear from (49) that λ becomes zero. Choosing the constants K, A and $\bar{K}$ as

$$A = 1,\ K = -(r^2 + l^2),\ \bar{K} = l^2 - a^2 \tag{50}$$

and using the variable ψ instead of z defined by

$$z = a \cos \psi + l \tag{51}$$

the final form of metric becomes

$$ds = 2[du + a(2l \sin\psi - a \sin^2\psi)d\beta]\,[dr + a^2 \sin^2\psi d\beta]$$
$$- (r^2 + z^2)(d\psi^2 + a^2 \sin^2\psi d\beta^2)$$
$$+ \left(1 - \frac{2mr + 2lz}{r^2 + z^2}\right)[du + a(2l \cos\psi - a \sin^2\psi)\, d\beta], \qquad (52)$$

where z is given by (51). Here a and l are constants.

It can be easily seen that the metric (52) with the coordinates transformation $-ad\beta = d\bar{\beta}$ is equivalent to the Kerr-NUT metric (1). Hence our solution describes the Kerr-NUT metric with a non-zero cosmological constant. The Kerr-NUT metric with a λ-term can be expressed in the form

$$ds^2 = (AX_rY_z)^{-2}\,[2(du + g \sin\alpha d\beta)\,(dr + h \sin\alpha d\beta)$$
$$- (cX^2 + dY^2)\{(dz^2/h \sin\alpha) + h \sin\alpha d\beta^2\}$$
$$+ \{1 - (2mXX_r^3 + 2lYY_z^3)/(X^2 + dY^2)\}(du + g \sin\alpha d\beta)^2], \qquad (53)$$

where $g \sin\alpha$, X and Y and $h \sin\alpha$ are given by (45), (46) and (48), respectively.

We have also verified that when $l = 0$ the metric (53) reduces to the Kerr metric with a non-zero cosmological constant given by DEMIANSKI [6].

The other mathematical details regarding the metric (3) and the charged versions of the solutions obtained in this paper are at present under investigation and will be discussed elsewhere.

Acknowledgement

One of us (I. C. P.) is thankful to the University Grants Commission for the award of a teacher fellowship.

REFERENCES

1. R. P. KERR, Phys. Rev. Lett., **11**, 237, 1963.
2. E. NEWMAN, L. TAMBURINO and T. UNTI, J. Math. Phys., **4**, 915, 1963.
3. M. DEMIANSKI, Phys. Lett., **42A**, 157, 1972.
4. P. C. VAIDYA, Pramana, **8**, 512, 1977.
5. L. K. PATEL and R. P. AKABARI, Acta. Phys. Hung., **44**, 181, 1978.
6. M. DEMIANSKI, Acta Astronomica, **23**, 221, 1973.
7. B. CARTER, Phys. Lett., **A26**, 399, 1968.
8. V. P. FROLOV, Teor. Mat. Fiz., **21**, 213, 1974 (in Russian).

Acta Physica Academiae Scientiarum Hungaricae, Tomus 48 (2—3), pp. 197—201 (1980)

DISSOCIATION ENERGY OF Si_2 MOLECULE*

By

T. V. RAMAKRISHNA RAO and R. RAMAKRISHNA REDDY

DEPARTMENT OF PHYSICS, S. V. UNIVERSITY POST-GRADUATE CENTRE
ANANTAPUR 515 003, A.P. INDIA

(Received in revised form 20. XII. 1979)

The true potential energy curves have been constructed for the different electronic states of the Si_2 molecule by the methods of LAKSHMAN and RAO as well as MORSE. The dissociation energy for the ground state of the Si_2 molecules has been estimated to be 3.28 eV by the method of curve fitting using the three parameter LIPPINCOTT potential function. The estimated D_e is in good agreement with the mass spectrometric value 3.25 $\pm$ 0.22 eV as well as GAYDON's value 3.35 $\pm$ 0.2 eV.

Introduction

The spectrum of the Si_2 molecule is of interest for a variety of reasons. One would expect the Si_2 and C_2 molecules to be related and the similarities and differences in their spectra are of interest from the point of view of the theory of electronic structure of diatomic molecules. DOUGLAS [1] first found two band systems of the Si_2 molecule and designated them as $^3\pi—^3\pi$ and $^3\Sigma—^3\Sigma$. VERMA and WARSOP [2] investigated three band systems of Si_2 in absorption using flash photolysis technique. Two of the band systems at 320 and 210 nm are new, whereas the third is an extension of the $^3\Sigma—^3\Sigma$ system observed by DOUGLAS in emission. VERMA and WARSOP [2] have pointed out that it is not definite whether the ground state of Si_2 is the $^3\Sigma_g^-$ state or not because of the low-lying triplet states. Some of the bands of C_2 are not yet known and also Si_2 has close resemblance with the C_2 molecule. The theoretical knowledge of the Si_2 may be useful to understand the spectrum of the C_2 molecule. Keeping this aim in mind, the authors took up the estimation of the dissociation energy of the Si_2 molecule. A knowledge of the exact value of the dissociation energy of diatomic molecules is of fundamental importance for thermochemistry and it is often of interest in astrophysics. The dissociation energy of Si_2 has been estimated by various methods, but the values reported show a lack of agreement with one another. VERMA and WARSOP [2] have reported the value of D_e to be 3.0 $\pm$ 0.2 eV. Mass spectroscopic studies have yielded 3.25 $\pm$ 0.22 eV. GAYDON [3] has recommended the

* Paper presented at the National Conference on Molecular Spectroscopy, held at Annamalai University, 16—18th August 1979, India.

value 3.35 $\pm$ 0.2 eV. The investigation deals with the estimation of dissociation energy of Si_2 molecule by fitting the LIPPINCOTT function with the true potential energy curve using the molecular constants reported by VERMA and WARSOP [2].

The method of curve fitting

The turning points for different electronic states of the Si_2 molecule are calculated using the method of LAKSHMAN and RAO [4]. The present method [4] was successfully verified in a number of cases [4, 5, 6, 7, 8]. CHAKRABORTY and PAN [9] suggested that this method is considered as reliable and accurate with less mathematical computations. The turning points as obtained by LAKSHMAN and RAO's [4] method for different electronic states of Si_2 are given in Table I along with those obtained by the MORSE [10] method for comparison purpose.

The true potential energy curves (RKRV) have been used to estimate the dissociation energies of diatomic molecules in a number of cases by fitting

Table I

The true potential energy curves for different electronic states of Si_2 molecule

v	$U + T_e$ (cm^{-1})	r_{min}(nm)		r_{max}(nm)	
		Present method	MORSE	Present method	MORSE
	$T_e = 0$		$X^3\Sigma_g^-$ state		
0	254.98	0.2179	0.2180	0.2317	0.2317
1	761.92	0.2135	0.2135	0.2374	0.2374
2	1264.83	0.2106	0.2106	0.2416	0.2416
3	1763.68	0.2083	0.2083	0.2451	0.2451
4	2258.50	0.2064	0.2064	0.2482	0.2483
5	2749.28	0.2048	0.2048	0.2512	0.2512
6	3236.02	0.2033	0.2033	0.2539	0.2539
	$T_e = 24582.64$		$H^3\Sigma_u^-$ state		
0	24717.80	0.2574	0.2574	0.2763	0.2763
1	24985.14	0.2514	0.2515	0.2843	0.2845
	$T_e = 30768.77$		$K\,^3\Sigma_u^-$ state		
0	30998.58	0.2283	0.2282	0.2428	0.2427
1	31449.28	0.2242	0.2240	0.2496	0.2494
2	31888.08	0.2217	0.2213	0.2449	0.2545
	$T_e = 46762.21$		$N\,^3\Sigma_u^-$ state		
0	46986.93	0.2276	0.2276	0.2423	0.2423
1	47426.63	0.2232	0.2234	0.2489	0.2491
2	47853.33	0.2204	0.2207	0.2541	0.2544

a potential function with the RKRV curves. In the present investigation it was found that the LIPPINCOTT potential function [11] gives the best fit with an average percentage deviation less than 0.05 in the value of $\frac{V - V_{RKRV}}{D_e}$ for the ground state of Si_2 molecule.

The LIPPINCOTT function as modified by STEELE [11] is

$$U(r) = D_e\left[1 - \exp\left\{\frac{-n(r - r_e)^2}{2r}\right\}\right]X$$

$$\left[1 - a\left(\frac{b^2 n}{2r}\right)^{1/2}(r - r_e)\exp\left\{-\left(\frac{b^2 n}{2r_e}\right)^{1/2}(r - r_e)\right\}\right],$$

in which

$$a = \frac{F}{1 + \frac{5}{4}F}, \quad n = \frac{2F^2}{r_e(ab)^2}, \text{ where } b = 1.065 \text{ and } F = \frac{\alpha_e \omega_e}{6B_e^2}$$

The RKRV turning points are used in the above expression and for a particular value of D_e, the energy values $U(r)$ are compared with U. This is repeated for different values of D_e in steps of 0.06 eV and the value for which

Table II

Comparison of the observed and calculated energy values

r (nm)	U (cm^{-1})	$D_e = 3.22$ eV	$D_e = 3.28$ eV	$D_e = 3.34$ eV
0.2317	254.9	244.9	249.6	254.3
0.2374	761.9	740.6	754.9	769.1
0.2415	1264.8	1226.8	1250.4	1273.9
0.2451	1763.6	1727.0	1760.3	1793.5
0.2483	2258.5	2220.6	2263.3	2306.0
0.2512	2749.2	2701.8	2753.8	2805.7
0.2539	3236.0	3174.7	3235.8	3296.8
0.2179	254.9	260.5	265.5	270.6
0.2135	761.9	757.5	772.1	786.7
0.2106	1264.8	1256.7	1280.9	1305.1
0.2083	1763.6	1758.2	1792.0	1825.8
0.2064	2258.5	2247.8	2291.1	2334.3
0.2048	2749.2	2720.4	2772.7	2825.1
0.2033	3236.0	3211.6	3273.4	3335.1
Average deviation %		0.089	0.053	0.167

the best fitting of the energy values is achieved is taken to be accurate dissociation energy of the molecule. Such a procedure has been employed for the ground states of TiO [12], SO, SeO and TeO [13], BiO and BiS [14] and P_2^+ [15] molecules. The results of these calculations in the case of the ground state of Si_2 which are necessary for comparison are given in Table II.

Results and discussion

The RKRV turning points agree well with those of MORSE [10] for the ground state, as the deviation between the experimental value of α_e (0.0013 cm^{-1}) and that calculated from the Pekeris relation α_e (0.001279 cm^{-1}) is negligible. The results of Table II show that the best fitting of the energy values is achieved for $D_e = 3.28 \pm 0.18$ eV, since the average percentage deviation in this case is minimum. This value is significant because it has been estimated by using the true potential energy curves based on experimental data. This is in very good agreement with the mass spectroscopic value 3.25 ± 0.22 eV and also with GAYDON's [3] recommended value 3.35 ± 0.2 eV. The above results support the view that the electronic state $^3\Sigma_g^-$ is the ground state of the Si_2 molecule. As has been pointed out by VERMA and WARSOP [2], there is not sufficient evidence to assign the $N^3\Sigma_g^-$ state to any electronic configuration. The D_e value for this state is not determined in the present study.

Using the same LIPPINCOTT function [11] the estimated dissociation energies for H and K states are 9,100 and 5,200 cm^{-1}, respectively. With these values the dissociation products in the upper and lower states are determined as follows

$$D_e'(H^3\Sigma_u^-) + T_e = D_e'(X^3\Sigma_g^-) + E_A.$$

Therefore $E_A = 7{,}183$ cm^{-1} which is in good agreement with the value of 6,300 cm^{-1}, the atomic excitation of $^1D_2$ for Si atom. The Birge—Sponer extrapolation gives the dissociation limits of 33,700 and 39,500 cm^{-1} for H and K states, respectively.

Thus $D_e'(H^3\Sigma_u^-) = 33{,}700 - 24{,}583 = 9{,}117$ cm^{-1}, which is in good agreement with the curve fitting value of 9,100 cm^{-1}.

Similarly, $D_e'(K^3\Sigma_u^-) = 39{,}500 - 30{,}768 = 8{,}732$ cm^{-1}, which is comparable with the value of 5,200 cm^{-1} obtained by curve fitting method. STEELE et al [16] concluded, based on a large number of computations on different molecules, that no single potential function is suitable to represent adequately all the states of the same molecule. The authors are of the opinion that the conclusion drawn by STEELE et al is quite applicable to the K state of Si_2 molecule. The atomic excitation corresponding to the K state is obtained as

$$8{,}732 + 30{,}768 - 26{,}500 = 13{,}000 \text{ cm}^{-1}.$$

This value is in close agreement with the atomic excitation of $^1S_0$ for Si atom. Thus the molecule gets dissociate in the upper and lower states as

$$\mathrm{Si}(^3P) + \mathrm{Si}(^3P) \text{ in the } X^3\Sigma_g^- \text{ state,}$$

$$\mathrm{Si}(^3P) + \mathrm{Si}(^1D_2) \text{ in the } H^3\Sigma_u^- \text{ state,}$$

$$\mathrm{Si}(^3P) + \mathrm{Si}(^1S_0) \text{ in the } K^3\Sigma_u^- \text{ state.}$$

Acknowledgement

The authors wish to express their thanks to Prof. S. V. J. LAKSHMAN and Prof. S. V. SUBRAHMANYAM for their interest in the present work.

REFERENCES

1. A. E. DOUGLAS, Can. J. Phys. **33**, 810, 1955.
2. R. D. VERMA and P. A. WARSOP, Can. J. Phys., **41**, 152, 1963.
3. A. G. GAYDON, Dissociation Energies, Chapman and Hall Ltd. London, 1968.
4. S. V. J. LAKSHMAN and T. V. RAMAKRISHNA RAO, J. Phys. B**4**, 269, 1971.
5. T. V. RAMAKRISHNA RAO and S. V. J. LAKSHMAN, Physica, **56**, 322, 1971.
6. T. V. RAMAKRISHNA RAO and S. V. J. LAKSHMAN, J. Quant. Spectro. Radiat. Transfer, **12**, 1063, 1972.
7. T. V. RAMAKRISHNA RAO and R. RAMAKRISHNA REDDY, Physica C, **95**, 412, 1978.
8. T. V. RAMAKRISHNA RAO and R. RAMAKRISHNA REDDY, Curr. Sci, **48**, 95, 1979.
9. B. CHAKRABORTY and Y. K. PAN, Applied. Spectro. Rev. **7**, 283, 1973.
10. P. M. MORSE, Phys. Rev., **34**, 57, 1929.
11. D. STEELE, Spectrochim. Acta, **19**, 411, 1963.
12. S. V. J. LAKSHMAN, T. V. RAMAKRISHNA RAO and G. T. NAIDU, Curr. Sci., **47**, 7, 1978.
13. S. V. J. LAKSHMAN, T. V. RAMAKRISHNA RAO and G. T. NAIDU, Ind. J. Pure and Appl. Physics, **15**, 834, 1977.
14. B. P. ASTHANA, V. S. KUSHAWAHA and K. P. R. NAIR, Acta Physica Polonica A, **42**, 739, 1972.
15. T. V. RAMAKRISHNA RAO and R. RAMAKRISHNA REDDY, Proc. Indian Acad. Sci A, **88**, 257, 1979.
16. D. STEELE, E. R. LIPPINCOTT and J. T. VANDERSLICE, Rev. Mod. Phys., **34**, 239, 1962.

Acta Physica Academiae Scientiarum Hungaricae, Tomus 48 (2—3), pp. 203—212 (1980)

LEVEL STRUCTURE OF ^{175}Lu

By

H. A. Ismail,* H. Hanafi,** A. El-Naem, W. Arafa and H. Abou-Leila

NUCLEAR PHYSICS LABORATORY, FACULTY OF GIRLS, AIN SHAMS UNIVERSITY, CAIRO, EGYPT

(Received in revised form 20. XII. 1979)

Eleven gamma-ray transitions have been identified in ^{175}Lu, by performing singles, prompt γ—γ coincidence and delayed γ—γ coincidence measurements using Ge(Li), hyper pure Ge and NaI (Tl) detectors. Two of these transitions (18 and 28.5 keV) have been observed for the first time and are of value in supporting a recently reported energy level at 371 keV.

Energy levels of rotational bands, $1^-/2$ [541]; $5^+/2$ [402] and $7^+/2$ [404] have been fitted using the angular momentum expansion. The required parameters are given. The previously doubted spins $15^-/2$ (1137 keV) and the $21^-/2$ (1078 keV) in the band $1^-/2$ [541] have been theoretically confirmed while an experimental energy state at 845 keV of doubted spin $13^+/2$ could be reasonably fitted to the $5^+/2$ [402] rotational band.

Introduction

Several discrepancies concerning the gamma-transitions and/or level structure of ^{175}Lu have been reported [1—7].

It should be noted that the most recent gamma spectrum analysis, published so far, is due to Johansen et al [6] suggesting an energy level at 358 keV based on a transition of energy 156.7 keV. Using nuclear reactions, Winter et al [7] ruled out this state and proposed a new level at 371 keV on account of observing a new gamma transition of energy 144 keV feeding this state.

So it seems necessary to reinvestigate the level structure of ^{175}Lu in a trial to solve the above mentioned discrepancy as well as to check the validity of the doubted spins of some of the high energy levels observed in nuclear reactions.

Experimental procedure

The ^{175}Hf ($T_{1/2} = 70$ d) has been prepared by thermal neutron capture in natural Hf {0.163% ^{174}Hf ($\sigma_c = 400$ barn), 35.22% ^{180}Hf ($\sigma_c = 10$ barn) in addition to 5.2% ^{176}Hf, 18.56% ^{177}Hf, 27.1% ^{178}Hf and 13.75% ^{179}Hf} in the ARE recator at Inchas, Cairo, Egypt. Needless to say that ^{177}Hf, ^{178}Hf, ^{179}Hf and ^{180}Hf nuclides have stable nuclei, besides the isomeric states which, if such exist, are of very short half life.

* Physics Department, Faculty of Education, Ain Shams University.
** Physics Department, Faculty of Science, Ain Shams University.

The gamma transitions associated with the decay of ^{175}Hf into ^{175}Lu have been investigated using 76.1 cc Ge(Li) detector, ORTEC, provided with an ORTEC 120-B preamplifier, spectroscopy amplifier in conjunction with a 4096 channels pulse-height analyzer, ORTEC 6240 B. The gamma transitions of low energy (<140 keV) have been studied using a hyper pure Ge detector (ORTEC 1000 series Hyper Pure Ge LEPS, planer type, 10 mm active diameter and 7 mm active depth) in conjunction with an ORTEC 117 B, preamplifier, spectroscopy amplifier and 4096 channels pulse height analyzer. Relative gamma-ray intensities have been estimated using the efficiency versus energy curves [8, 9] — for the Ge(Li) and hyper pure Ge detectors based upon experimentally measured relative photopeak efficiencies for different sources.

The gamma-gamma coincidence measurements have been carried out using a fast-low coincidence system. In this study, two gamma-gamma coincidence spectrometers have been used, i.e. a pure Ge—NaI(Tl) and a Ge(Li)—NaI(Tl) coincidence spectrometer.

Using the pure Ge—NaI(Tl) coincidence spectrometer, a run was performed through allowing the NaI(Tl) to select the 343.3 keV gamma transition for gating purposes. Moreover, a delayed coincidence run has been also carried out, where the NaI(Tl) detector was used to select the 353.6 keV gamma-transition as a gating transition (the 353.6 keV energy level has a lifetime of 1.49 μsec).

Applying the Ge(Li)—Na(Tl) coincidence spectrometer two prompt coincidence runs have been performed, where the NaI(Tl) detector was used to select the 113 and then the 229 keV gamma transitions for gating purposes. Delayed coincidence run was also carried out where the 353.6 keV gamma transition (selected by the NaI (Tl) detector) was used as a gate.

In this work successive singles and coincidence spectra have been investigated during a period of about 12 months, to differentiate between gamma transitions due to ^{175}Hf $\rightarrow$ ^{175}Lu ($T_{1/2}$ = 70 days) and those due to ^{181}Hf $\rightarrow$ ^{181}Ta ($T_{1/2}$ = 42 days).

Results and discussion

A — *Gamma-ray singles spectra*

Fig. 1 illustrates the gamma singles spectrum obtained using the Ge(Li) spectrometer. From this Figure, it is obvious that eight transitions have been identified as belonging to ^{175}Hf $\rightarrow$ ^{175}Lu decay. These are 89.4, 113.8, (161), 229.6, 318, 343.3, 353.6 and 432.8 keV gamma transitions.

Fig. 2 presents the gamma singles spectrum obtained using the hyper pure Ge spectrometer. From this Figure it is obvious that a new gamma transition

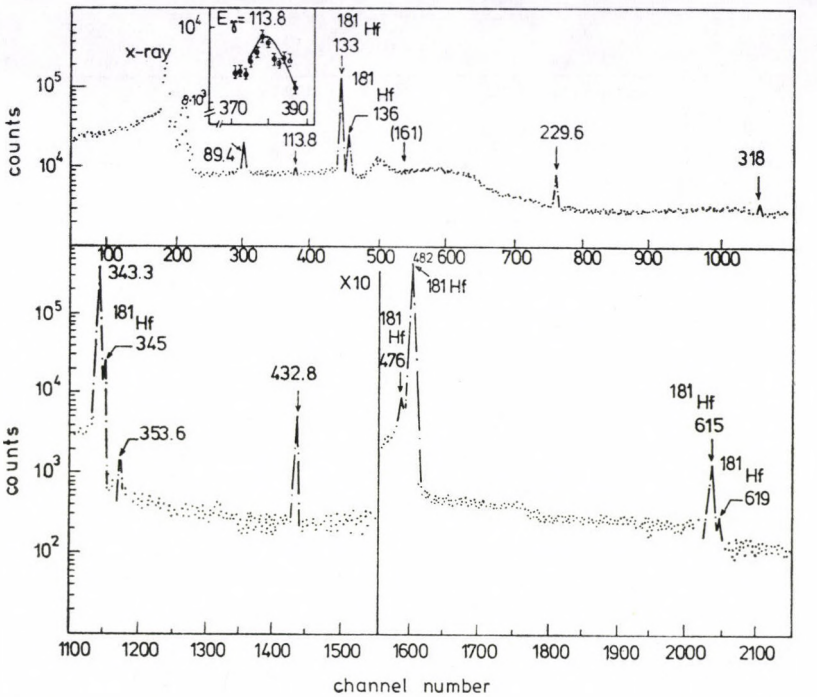

Fig. 1. Gamma-ray singles spectrum (^{175}Hf → ^{175}Lu) obtained using Ge(Li) spectrometer

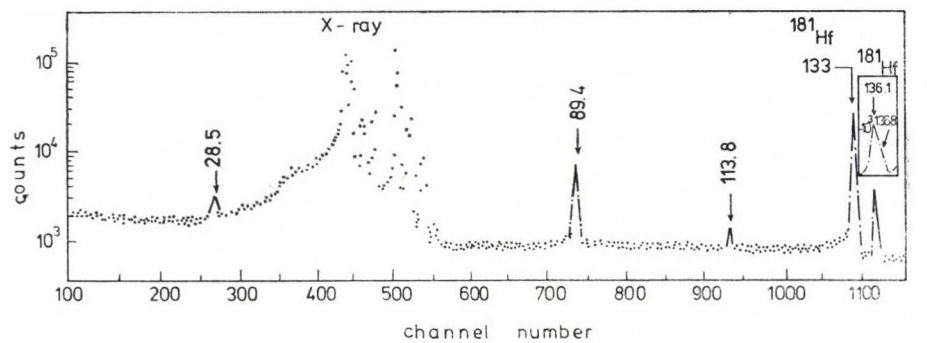

Fig. 2. Gamma-ray singles spectrum (^{175}Hf → ^{175}Lu) obtained using hyper pure Ge spectrometer

of 28.5 keV energy together with 89.4 and 113.8 keV have been identified as belonging to ^{175}Hf → ^{175}Lu decay.

Table I includes the gamma transitions (in ^{175}Lu) mentioned above and their estimated relative intensities together with the most recent previous work for the sake of comparison.

Table I

Gamma transitions in ^{175}Lu

Present work		JOHANSEN et al. [6]	
E_γ (keV)	I	E_γ (keV)	I
18[a]	—	—	
28.5	2.13 ± 0.28	—	
89.4	25.40 ± 1.17	89.4	26.136 ± 3.4
113.8	3.60 ± 0.24	113.8	6.636 ± 0.45
144[b]	—	—	
		156.7	c. n. s.
161	0.8 ± 0.12	161.3	0.273 ± 0.1
229.6	9.68 ± 0.22	229.6	8.863 ± 1.82
318.0	1.98 ± 0.07	319	2.04 ± 0.45
343.3	1000	343.4	1000
353.6	2.42 ± 0.08	353.6	2.72 ± 0.45
432.8	16.12 ± 0.49	432.8	17.04 ± 2.26

[a] Identified from the $\gamma-\gamma$ coincidence studies (Table II).
[b] Identified from the $\gamma-\gamma$ coincidence studies (Tables II, III).

Table II

Results of gamma—gamma coincidence studies using pure Ge—NaI(Tl) spectrometer

E_γ in gate	Observed γ-transitions in coincidence with E_γ in gate	Remarks
353 keV delayed coincidence	18, 144 and 161 keV	18 and 144 keV transitions are identified for the first time
343 keV prompt-coincidence	28.5 and 89 keV (133 and 136)	The 133 and 136 keV peaks in Fig. 4 are due to chance coincidence

Table III

Results of gamma—gamma coincidence studies using Ga(Li)—NaI(Tl) spectrometer

E_γ in gate	Observed γ-transitions in coincidence with E_γ in gate
229 keV	89 and 113 keV
113 keV	89, 229 and 318 keV
353 keV delayed coincidence	144 and 161 keV (353)

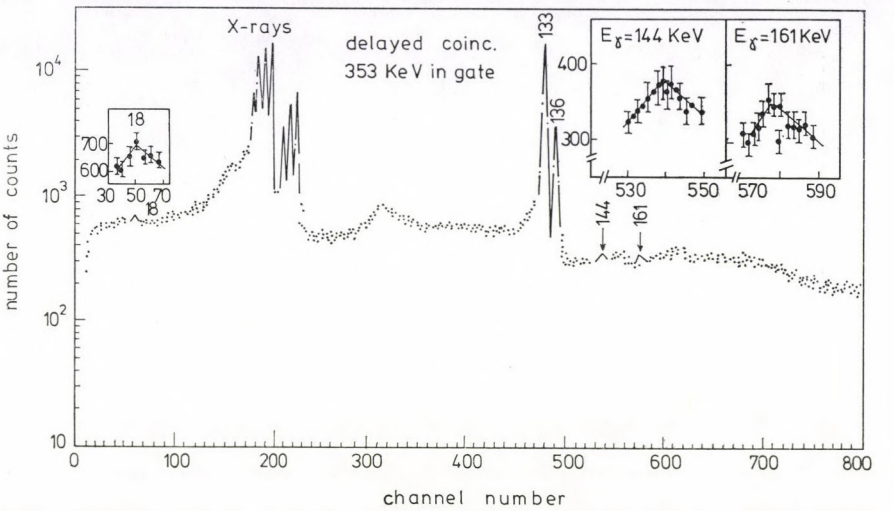

Fig. 3. γ—γ coincidence spectrum obtained using pure Ge-NaI(Tl) spectrometer (E_γ in gate = 353 keV)

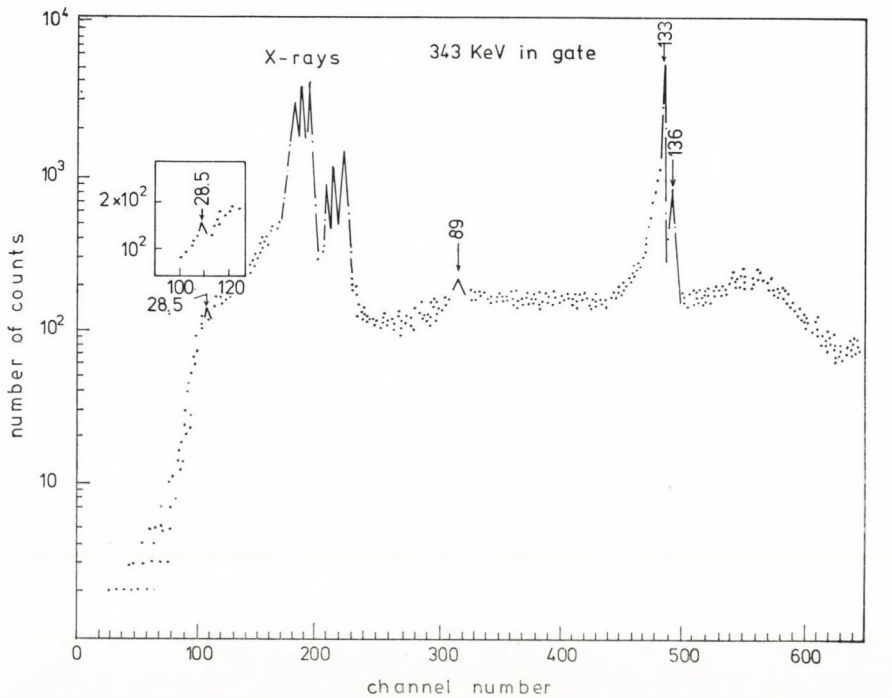

Fig. 4. γ—γ coincidence spectrum obtained using pure Ge-NaI(Tl) spectrometer (E_γ in gate = 343 keV)

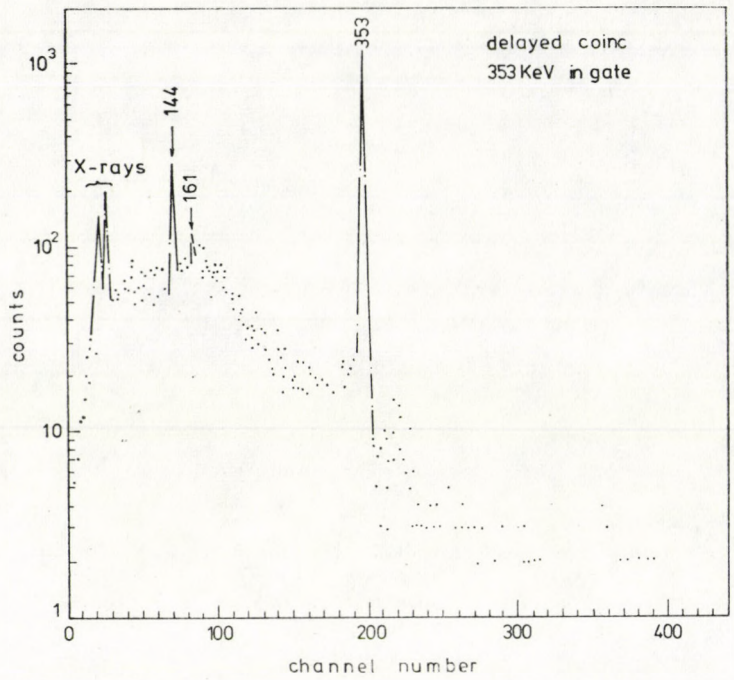

Fig. 5. γ—γ coincidence spectrum obtained using Ga(Li)-NaI(Tl) spectrometer (E_γ in gate = 353 keV)

B — *Gamma-gamma coincidence spectra*

i) When the Na(Tl) detector in the pure Ge—NaI(Tl) coincidence spectrometer was used to select the 353 keV gating gamma-transition (delayed coincidence), three gamma transitions were observed to be in coincidence with E_γ = 353.6 keV. These transitions are 18 keV, 144 keV and possibly 161 keV [Table II and Fig. 3].

The 18 keV transition could be identified from three different experimental runs, besides the observation of 144 keV transition when E_γ in gate = = 353 keV could not be explained unless such a transition (18 keV) exists.

ii) When the NaI(Tl) detector in the above mentioned spectrometer was used to select the 343 keV gating gamma transition (prompt coincidence), two gamma transitions (28.5 and 79.4 keV) were found to be in coincidence with E_γ = 343 keV. This is listed in Table II and illustrated in Fig. 4.

iii) Table III presents the γ—γ coincidence studies using the Ge(Li)—NaI(Tl) coincidence spectrometer. It is obvious that the 161 keV transition has been clearly observed in the coincidence spectrum when E_γ (in gate) = 353 keV as shown in Fig. 5.

The gamma transitions identified in the present singles spectra and/or $\gamma-\gamma$ coincidence studies are fitted in a suggested level structure of ^{175}Lu illustrated in Fig. 6.

It should be pointed out that the 514.9 keV energy level suggested by JOHANSEN et al [6] from gamma spectroscopy and observed later by WINTER et al [7] from nuclear reaction has been supported on basis of 161/353 keV cascade (Figs. 3, 5).

Moreover, the present work has confirmed an energy level at 371 suggested by WINTER et al [7] as the head of a rotational band $1^-/2$ [541]. This confirmation is due to observing two new gamma transitions of energy 18 and 28.5 keV which can depopulate this state beside the 144 keV transition feeding it. A further support lies in detecting 144/18/353 keV cascade (Fig. 3).

It should be also pointed out that this 371 keV state has not been measured by K-conversion technique owing to the fact that the B. E. of the K-shell

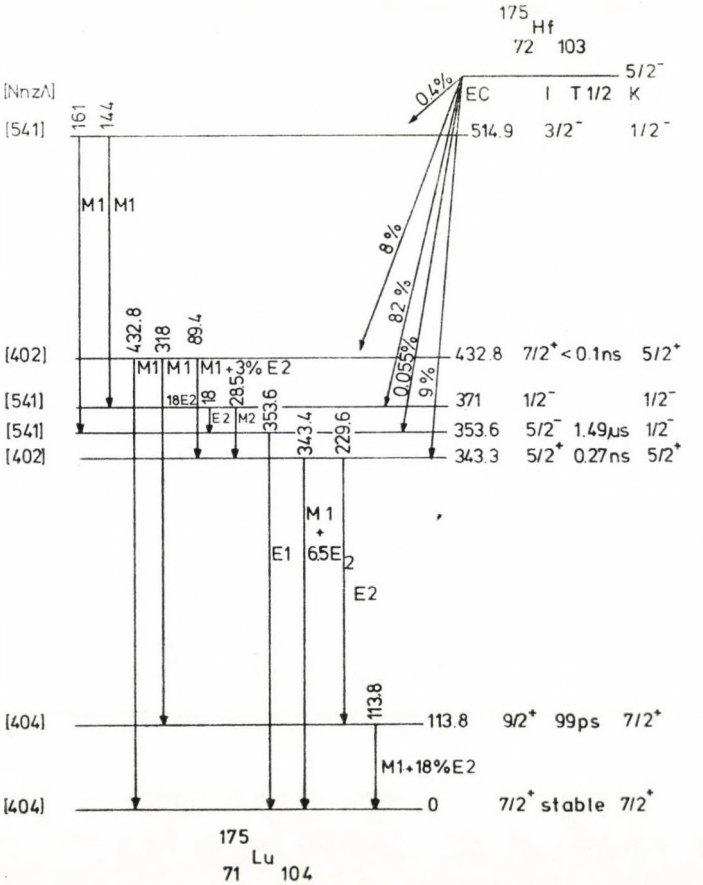

Fig. 6. Suggested level structure of ^{175}Lu

electron is ~63 keV which is greater than either 28.5 and 18 keV depopulated from it. On the other hand, the B. E. of the L-shell electron is ~10 keV that is the L-conversion electron energy is too small to be detected by electron spectroscopy techniques unless acceleration methods are used.

However, the percentage of the electron capture decay feeding that state could be estimated from the present relative intensities of the gamma transitions concerning that state and using their known internal conversion coefficient (LADERER et al [10]) . This gives a value of about 82%. Such a high value affects the previously published data concerning the feeding of possible other states 343.3, 353.7, 432.8 and 514.9 keV which are found to have electron capture decay percentages 9, 0.055.8 and 0.4, respectively.

C — *Analysis of rotational bands*

Since the ^{175}Lu nucleus is a strongly deformed nucleus, the members of different rotational bands can be calculated using the following angular momentum expansion [11]

$$E = E_0 + AI(I+1) + BI^2(I+1)^2 + CI^3(I+1)^3 + \ldots + \\ + (-1)^{I+k}(I+k)!/(k-k)![A_{2k} + B_{2k}I(I+1) + \ldots]. \qquad (1)$$

The energy parameter E_0, together with A, B, C, A_{2k} and B_{2k} are fitting parameters which must be deduced using a least square fit to satisfy the established experimental energy levels.

The present experimental results could be classified according to the head bands as follows:

1. The ground state band $7^+/2$ [404] where only the first member $9^+/2$ (113.8 keV) has been observed in this work.

Other members of this band have been observed using Coulomb excitation (d, t) and $(p, 2n\gamma)$ reactions as follows [12]: $11^+/2$ (251.46 keV), $13^+/2$ (412.25 keV), $15^+/2$ (595.712 keV), $17^+/2$ (799.3 keV) and $19^+/2$ (1024.7 keV). Using Eq. (1), the required fitting parameters are: $E_0 = -201.339$ keV, $A = 12.87$ keV; $B = -5.9256$ eV, $C = -0.3389$ meV, and $A_{2k} = -0.23207$ meV and $B_{2k} = 1.46629\ \mu$eV.

The difference between theoretical and experimental results over the whole range of energy and spin lies between 0.0 keV and 0.053 keV (Fig. 7). The relation between $\dfrac{E_I - E_{I-1}}{21}$ versus $(21)^2$ is illustrated in Fig. 8. No oscillation is obtained which is due to the small value of A_{2k} which is responsible for the strength of Coriolis coupling.

2. The head of band $5^+/2$ [402] at energy 343.3 keV, and its first member $7^+/2$ (432.8 keV) have been identified in the present experimental work. Other

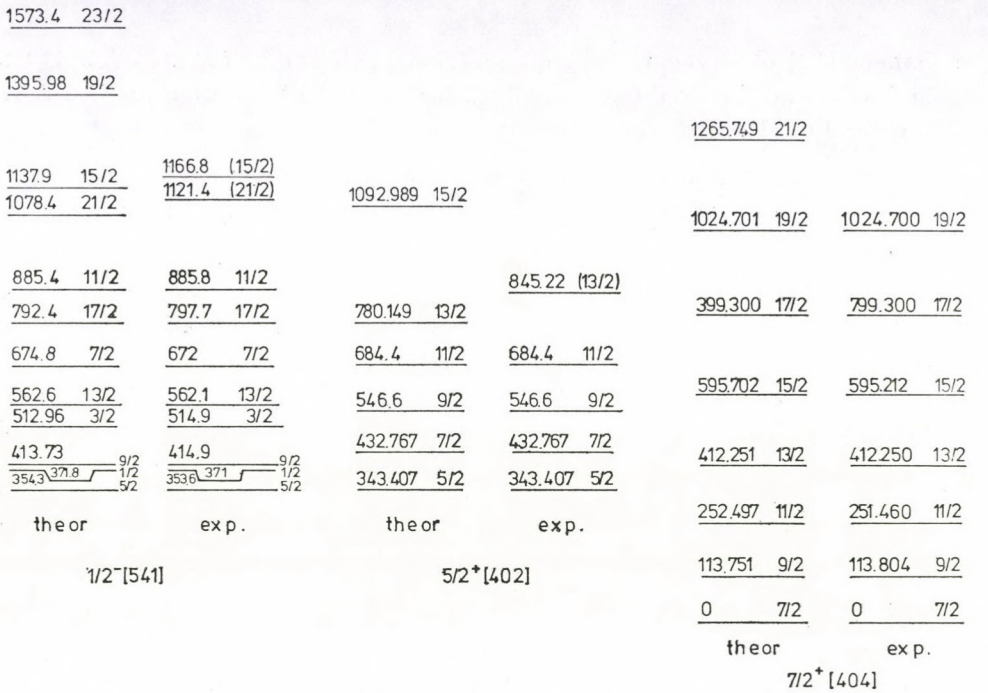

Fig 7. **Experimental and theoretical levels (calculated using Eq. (1)) using in ^{175}Lu**

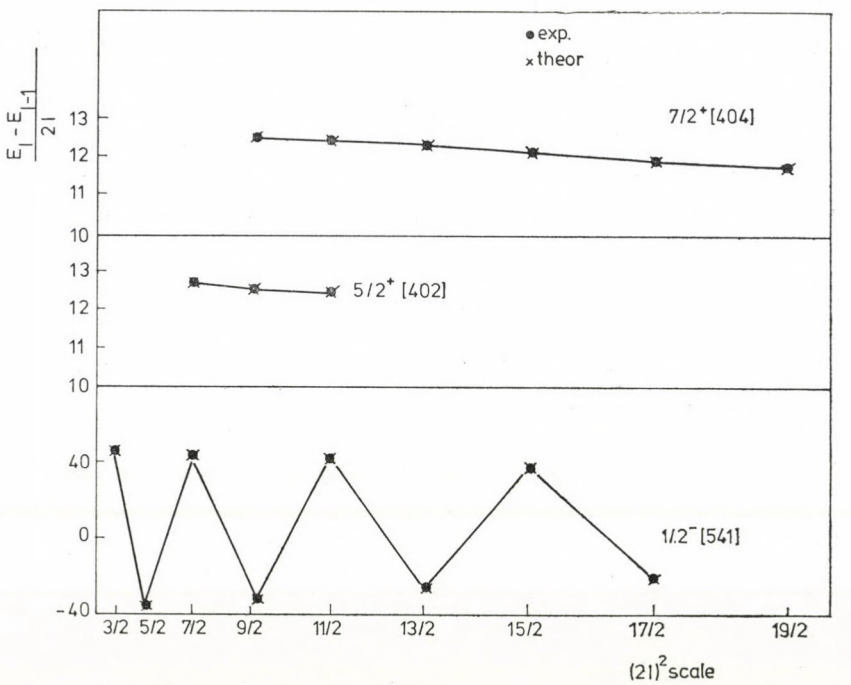

Fig. 8. **Coupling effects in rotational bands in ^{175}Lu**

members [12] observed in $(p, 2n\gamma)$ reaction having $9^+/2$ (546.6 keV), $11^+/2$ (684.4 keV) and the doubted spin $13^+/2$ (845.22 keV) have been predicted by fitting in Eq. (1), with the following parameters:

$$E_0 = 227.423 \text{ keV}; A = 13.36 \text{ keV}, B = -13.9755 \text{ eV}$$
$$C = -0.2302 \text{ eV}, A_{2k} = -2.9586 \text{ eV and } B_{2k} = 0.11373 \text{ eV}.$$

The calculated results are in excellent agreement with experimental ones (Fig. 7) for all levels except the spin $13^+/2$ state which is theoretically found at 780.149 keV. This may not correspond to the above mentioned experimental state at 845 keV having a doubted spin $13^+/2$.

3. The $1^-/2$ [541] rotational band – in the present work – has three energy levels $1^-/2$ (371.0 keV), $3^-/2$ (514.9 keV) and $5^-/2$ (353.63 keV). Two doubted spin states $15^-/2$ (1166.8 keV) and $21^-/2$ (1121.4 keV) together with the definite spin states $7^-/2$ (672.3 keV), $9^-/2$ (414.9 keV), $11^-/2$ (885.8 keV), $13^-/2$ (562.1 keV) and $17^-/2$ (797.7 keV) have been observed using $(p, 2n\gamma)$ and (^{3}He, d) reactions [12]. For this rotational band the required fitting parameters have been found to be:

$$E_0 = 406.602 \text{ keV}; A = 7.15 \text{ keV}; B = 20.1875 \text{ eV}$$
$$C = -0.15558 \text{ eV}; A_{2k} = 40.283 \text{ keV}; \text{ and } B_{2k} = -0.1738 \text{ keV}.$$

The large value of A_{2k} is considered to be normal for $k = 1/2$ band, due to the Coriolis coupling effect. This can lead to a high decoupling parameter $a = \frac{A_{2k}}{A} = 5.6$ which is responsible for large oscillations as illustrated in Fig. 8. The calculated values for the doubted spin states are $15^-/2$ (1137.935 keV) and $21^-/2$ (1078.448 keV), Fig. 7 differing by 28 and 43 keV, respectively, which could be allowed in this case. For other states in this band the errors in the calculations differ between 0.048 keV and 1.536 keV which is very small.

REFERENCES

1. F. T. Avignone III and J. H. Trueblood, Nucl. Phys., **A167**, 29, 1971.
2. J. P. Miz, M. E. Bunker and J. W. Starrar, Phys. Rev., **100**, 90, 1955.
3. E. N. Hatch, F. Boehm, P. Marmier and J. Dumond, Phys. Rev., **104**, No. 3, 745, 1956.
4. E. D. Klema, Phys. Rev., **109**, 1952, 1958.
5. L. Funke, H. Graber, K. Kaum, H. Sodan and L. Werner, Nucl. Phys., **70**, 347, 1965.
6. K. H. Johansen, B. Bengtson and P. Hasen, Nucl. Phys., **A133**, 213, 1969.
7. G. Winter, W. Andery, L. Funke, P. Manfrass and H. Sodan, Nucl. Phys., **A223**, 320, 1974.
8. H. El-Saman, M. Sc. Thesis, Phys. Dept., Faculty of Girls, Ain Shams University, Egypt, 1978.
9. W. Arafa, M. Sc. Thesis, Phys. Dept., Faculty of Girls, Ain Shams University, Egypt, 1979.
10. G. M. Laderer, J. M. Hollander and I. Perlman, Table of Isotopes, Lawrence Radiation Laboratory, University of California, Berkeley, 1967.
11. A. Bohr and B. R. Mattelson, Nuclear Structure II, 1975. W. A. Benjamin, Inc.
12. Nuclear Data Sheets for A = 175, 18, 331–355, 1976.

Acta Physica Academiae Scientiarum Hungaricae, Tomus 48 (2—3), pp. 213—224 (1980)

ON SPONTANEOUS SYMMETRY BREAKDOWN AND THE HIGGS MECHANISM

By

C. v. WESTENHOLZ

DEPARTMENT OF MATHEMATICS, THE UNIVERSITY OF ZAMBIA, LUSAKA, ZAMBIA

(Received 20. XII. 1979)

A geometric description of Higgs fields as cross sections of some fibre bundle is given. Within such a framework of fibre bundles the Higgs mechanism is characterized in terms of a reduction of a principal bundle, which stands for a certain gauge structure to a subbundle. This subbundle is defined in terms of a given Higgs field.

The 't Hooft—Polyakov model is described within the aforementioned framework. A homology classification of Higgs fields and monopoles is given. It is shown that the magnetic charge originates from the topological structure of Higgs fields.

I. Introduction

Most of the symmetries observed in nature are not exact. For instance SU(3)-symmetry is broken, as indicated by the proton-lambda mass difference. This type of symmetry breaking may be described by adding non-invariant terms to a given Lagrangian which is invariant under a certain symmetry group. Alternately, a symmetry can also be broken in terms of a "spontaneous symmetry breaking" mechanism. The defining Lagrangian is still exactly symmetric under the given symmetry G. For dynamical reasons, however, there is a ground state, the vacuum state Φ_0 (i.e. the state with no particles), in the theory which is not invariant under G. Spontaneous breakdown of a symmetry is then an effect which is due to non-invariance of Φ_0 under G. Thus, in a theory with spontaneously broken symmetry the symmetry properties of the vacuum are as significant as those of the defining Lagrangian.

Spontaneous breaking of some global symmetry introduces massless particles, the Goldstone bosons. On the other hand, gauge fields arising from Yang—Mills theories describe massless particles as well. Such features, however, are devoid of any physical interest. It is the Higgs mechanism, in circumventing these features, which allows for a construction of realistic physical models: In a theory with spontaneously broken gauge symmetry, previously massless gauge vector bosons acquire a mass. The massless would-be Goldstone bosons decouple and disappear.

This paper, in the subsequent Part II, provides a geometric description of Higgs fields. In Part III a differential geometric characterization of the phenomenon of spontaneous symmetry breaking is given. This type of sym-

metry breaking amounts to what is termed a reduction of some principal fibre bundle (the given gauge structure) over space-time M^4, with structure group the gauge group G, to a principal bundle over M^4 with structure group a certain isotropy subgroup H of G. In particular, the study of the 't Hooft—Polyakov model with monopole solutions exhibits that spontaneous symmetry breakdown of the gauge symmetry $G = \mathrm{SO}(3)$ reduces a certain trivial principal bundle, whose structure group is SO(3), to a nontrivial U(1)-bundle. In Part IV, finally, a homology classification of Higgs fields and monopoles is given.

II. Geometric description of Higgs fields

Let a gauge structure be given by a principal fibre bundle $P = P(M^4, G)$ over space-time M^4 with structure group G [1], [2], [3]. Let ω be the connection 1-form of a connection in P and let $s: \mathrm{U} \subset M^4 \to P$ be a local cross-section on an open subset U of the base manifold M^4. Then, with respect to a frame (e_α):

$$A = s^*\omega = \Sigma\, A^\alpha_\mu dx^\mu e_\alpha \tag{1}$$

and

$$F = s^*\Omega = \Sigma\, F^\alpha_{\mu\nu}\, dx^\mu\, dx^\nu\, e_\alpha\,, \tag{2}$$

where

$$F^\alpha_{\mu\nu} = \partial_\nu A^\alpha_\mu - \partial_\mu A^\alpha_\nu + c^\alpha_{\varrho\sigma} A^\varrho_\mu A^\sigma_\nu \tag{3}$$

stand for the Yang—Mills potential and the Yang—Mills field, respectively. (Ω is the curvature form of the connection ω, $s^*\omega$ and $s^*\Omega$ are the pullbacks by s).

Let now $E(M^4, V, G, P)$ be the fibre bundle over M^4, with standard fibre V (a vector space) and structure group G, which is associated with the principal fibre bundle P. A Higgs field is then described by a cross-section of $E(M^4, V, G, P)$,

$$\varphi : P \to V \tag{4}$$

or

$$\Phi = s^*\varphi = \varphi \circ s : U \subset M^4 \to V \tag{5}$$

which is the pull-back of φ by a section s.

The covariant exterior derivative of the Higgs field (4) or (5), respectively, is, with respect to a frame (e_α):

$$\nabla\Phi = \nabla_\mu \Phi^\alpha dx^\mu e_\alpha = s^*\nabla\varphi; \tag{6}$$

$$\nabla_\mu \Phi^\alpha = \frac{\partial \Phi^\alpha}{\partial x^\mu} + c^\alpha_{\varrho\sigma} A^\varrho_\mu \Phi^\sigma \tag{7}$$

whenever V is taken to be $\mathfrak{g}(G)$, the Lie-algebra of G. The quantities $(c^\alpha_{\varrho\sigma})$ are the structure constants of G.

III. Spontaneous symmetry breaking

Let (M^4, g) be an oriented space-time with metric g and $\eta := dx^0 \wedge \wedge dx^1 \wedge dx^2 \wedge dx^3$ the canonical volume 4-form on M^4.

A Lagrangian field theoretical model which is susceptible to account for spontaneous symmetry breaking of some gauge symmetry can be given in terms of a Lagrangian differential 4-form which describes the interaction between a gauge field $A = s^*\omega$ (Eq. (1)) and a Higgs field φ (Eq. (4)). Let now $||\varphi|| = g_{\alpha\beta}\varphi^\alpha\varphi^\beta$ be an ad-invariant metric on $\mathfrak{g}(G)$ [1], [2], [3]. Self-interaction of the Higgs field φ is then described by the potential 4-form $U(||\varphi||)\eta$. Thus we have for the Lagrangian model 4-form:

$$\lambda := L\eta := -\frac{1}{4} F \wedge {}^*F = \bar{g}_{\alpha\beta}\, {}^*\nabla\varphi^\alpha \wedge \nabla\varphi^\beta + U(||\varphi||)\,\eta \tag{8}$$

The kinetic energy term is, on account of Eq. (2), given by

$$F \wedge {}^*F = F^\alpha_{\mu\nu}\, F^{\alpha\mu\nu}\,\eta, \tag{9}$$

where the dual 2-form ${}^*F$ has as coefficients the components of the dual field strength tensor (* stands for the Hodge star operator [1], [2], [3]).

Spontaneous symmetry breaking can now be described in terms of the following set up: The Higgs field (4) whose self-interaction is the potential 4-form $U(||\varphi||)\eta$ breaks a gauge symmetry G spontaneously:

(i) The gauge group G (structure group G of a principal fibre bundle $P(M^4, G)$) is reducible to a certain isotropy subgroup H of G, iff $E(M^4) = = E(M^4, G/H, G, P)$, the bundle associated with P, with standard fibre $G/H \subset V$, admits a cross section $\emptyset$: $U \subset M^4 \to E$. Then $P(M^4, G)$ is reducible to a subbundle $P'(M^4, H)$.

(ii) The reduced subbundle $P'(M^4, H)$ with base manifold the space-time manifold M^4 and structure group H is defined by a Higgs field (4).

(iii) Let $J^1(E(M^4)$ be the manifold of first order jets of cross sections (for a description of this manifold refer to [4]). A Lagrangian is then a real-valued function

$$L: J^1(E(M^4)) \to R \text{ on } J^1(E(M^4)) \tag{10}$$

[4], [5]. In terms of a suitable parametrization of $J^1(E(M^4))$ (cf. subsequent remark) the Lagrangian corresponding to Eq. (8) can be shown to satisfy (10). A Lagrange 4-form on $J^1(E(M^4))$ which is the pull-back of (8) by the map π^1 is obtained in terms of the diagram

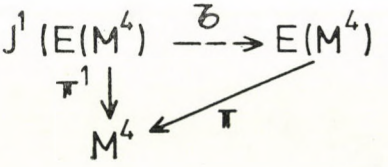

(11)

(π and π^1 are projective mappings) as follows:

$$\bar{\lambda} = L\pi^{1*}\eta. \tag{12}$$

A symmetry corresponding to a gauge transformation which preserves the Lagrangian (12) is then characterized by the condition

$$\Psi_g^*\bar{\lambda} = \bar{\lambda}, \tag{13}$$

where $\psi: G \to \mathrm{Diff}\,(J^1(E))$; $(g, p) \to \psi_g(p)$; $g \in G$, $p \in J^1$ is a differentiable action of the gauge group G on $J^1(E)$ [3].

Remark. A parametrization of $J^1(E)$ may be a specified by $(x, \Phi^\alpha, \partial_\mu \Phi^\alpha)$, where $x \to \emptyset(x) = (\emptyset^\alpha(x))$ is a vector-valued map, i.e. a cross section of E. Let a linear bundle isomorphism

$$A: J^1(E) \to J^1(E) \tag{14}$$

such that

$$A^*(\Phi^\alpha) = \Sigma\, A_{\alpha\beta}\, \Phi^\beta \qquad \text{with} \quad A_{\alpha\beta} = \delta_{\alpha\beta} \tag{15}$$

$$A^*(\partial_\mu \Phi^\alpha) = \Sigma\, A_{\alpha\mu\beta}\, \Phi^\beta + \partial_\mu \Phi^{\alpha(+)} \qquad A_{\alpha\mu\beta} = -A_\mu\, \delta_{\alpha\beta}.$$

Then, given a Lagrangian (10) on $J^1(E)$ one obtains a transformed Lagrangian by the law $A^*(L)(j) = L(A(j))$ whenever $j_1(\Phi) \in J^1(E)$ is a 1-jet, i.e. $x \to j_1(\Phi)(x)$ is a cross section of $J^1(E)$ [4], [5]. The transformed Lagrangian satisfies the Euler—Lagrange equations for the principle of minimal electromagnetic interaction as shown in [5].

III. 1. *Characterization of the reduced subbundle $P'(M^4, H)$*

Let Φ_0 be a constant solution, i.e. a vacuum state, of some equation of motion, i.e. a field configuration which minimizes the energy $U(\Phi)$. All other configurations with the same energy are obtained from Φ_0 by the action of the group $G^{(++)}$

$$M_0 = D(G)\,\Phi_0 = \{D(g)\,\Phi_0 / g \in G\} = G/H, \tag{16}$$

where

$$H := G_{\Phi_0} = \{g \in G / D(g)\,\Phi_0 = \Phi_0\}. \tag{17}$$

The homogeneous space M_0 is referred to as vacuum manifold, i.e. G acts transitively on M_0. H is the isotropy subgroup of G at Φ_0. The statement of spontaneous symmetry breakdown means that M_0 contains more than one point.

(+) A^* denotes the dual map induced by the map A.
(++) $D(G)$ is a representation of G.

A Higgs field (4) with range M_0 or its pull-back to the base manifold, i.e.

$$\varphi : P \to G/H \tag{4'}$$

or

$$\Phi := \varphi \circ s : U \subset M^4 \to G/H \tag{5'}$$

then characterizes a reduced subbundle

$$P' = \{p \in P \mid \varphi(p) = \Phi_0\} \tag{18}$$

of $P(M^4, G)$. Conversely: A reduced subbundle P' of a bundle P which represents a gauge structure, i.e a reduction of the structural group G of P to H determines a Higgs field φ. Then the connection defined by a connection 1-form in P is reducible to a connection in the subbundle P' iff the restriction of the connection 1-form ω to P' is $\mathfrak{g}(H)$-valued, which is the case iff

$$\nabla\Phi = 0 \quad \text{or} \quad \nabla_\mu \Phi = 0 \tag{19}$$

[6], [7], which means that the cross section $\emptyset$ is parallel to the given connection in $P(M^4, H)$. The relation (19) expresses the physical condition for a Higgs vacuum, following which solutions with vanishing covariant derivative are identified with a vacuum state.

III.2. *Monopole-model of 't Hooft—Polyakov*

This model constitutes the simplest non-abelian generalization of models which admit vortex solutions [8].

Let the Lagrangian 4-form be specified as follows:

$$\lambda = L\eta = -1/4\, F \wedge {}^*F + 1/2 {}^*\nabla\varphi^\alpha \wedge \nabla\varphi^\alpha + \left[\frac{1}{2}(\varphi^\alpha\varphi^\alpha) - \frac{\varkappa}{4}(\varphi^\alpha\varphi^\alpha)^2\right]\eta \tag{8'}$$

with gauge-covariant field strength

$$F^\alpha_{\mu\nu} = \partial_\mu A^\alpha_\nu - \partial_\nu A^\alpha_\mu + e\varepsilon^\alpha_{\varrho\sigma} A^\varrho_\mu A^\sigma_\nu \tag{3'}$$

and

$$\nabla_\mu \varphi^\alpha = \partial_\mu \varphi^\alpha + e\varepsilon^\alpha_{\varrho\sigma} A^\varrho_\mu \varphi^\sigma . \tag{7'}$$

Here the SO(3)-gauge Yang—Mills field A^α_μ interacts with a Higgs isotriplet $\Phi = (\varphi^\alpha)$.

Let now $t \in \mathbb{R}$ be fixed and $r > 0$. Then the base manifold M^4 may be identified with S^2 and the corresponding gauge structure

$$P(S^2, SO(3)) = S^2 \times SO(3) \tag{20}$$

is a trivial SO(3)-principal fibre bundle over S^2 [1], [2], [3].

Necessary boundary conditions at infinity for monopole solutions with finite energy are

$$F_{\mu\nu} \to 0, \tag{21a}$$

$$\nabla_\mu \Phi \to 0, \tag{21b}$$

and

$$\Phi\Phi \to 1. \tag{21c}$$

On account of condition (21c) introduce the map

$$\hat{\Phi} : S^2(r) \to S^2_\Phi = \{\Phi / \Phi\Phi = 1\} \; (r \to \infty \text{ fixed}) \tag{22}$$

defined by $(\hat{\Phi}^1(\theta, \varphi), \; \hat{\Phi}^2(\theta, \varphi) = (\theta, n\varphi)$.

$S^2(r)$ is a sphere at infinity. The unit sphere S^2_Φ is determined by the Higgs triplets

$$\Phi = \begin{pmatrix} \Phi^1 \\ \Phi^2 \\ \Phi^3 \end{pmatrix} = \begin{pmatrix} \Phi(r) \sin\theta \cos(n\varphi) \\ \Phi(r) \sin\theta \sin(n\varphi) \\ \Phi(r) \cos\theta \end{pmatrix} . \tag{23}$$

Note that the map $\hat{\Phi}$ is viewed as normalized Higgs field, which, on the space-time manifold, is

$$\hat{\Phi}(x) = \frac{\Phi(x)}{||\Phi(x)||} , \quad x = (x^0, x^1, x^2, x^3) \in M^4. \tag{24}$$

Formulae (22)—(24) will be used in the construction of monopoles in the subsequent Section IV.

Spontaneous symmetry breaking $G \to H$ can now be described as follows: Let $G = SO(3)$. The isotropy subgroup of G at $\emptyset_0^\alpha = (0, 0, \emptyset_0)$, $\emptyset_0 = \sqrt{-\varkappa^2} (\varkappa^2 < 0)$ is $H = SO(2)$. In fact:

$$D(g) \, \Phi_0^\alpha = \Phi_0^\alpha \Leftrightarrow D(g) = \begin{pmatrix} & & 0 \\ & A & 0 \\ 0 & 0 & 1 \end{pmatrix} ; \quad A \in SO(2) ,$$

where the natural C^∞ action

$$SO(3) \times S^2_\Phi \to S^2_\Phi ; \; (g, \Phi) \to D(g) \, \Phi ; \; ||D(g) \, \Phi|| = ||\Phi||$$

is transitive. Thus, the vacuum manifold (16) is given to be the homogeneous space of $G = SO(3)$,i.e.

$$M_0 = S^2_\Phi = SO(3)/SO(2) \tag{16'}$$

[1], [2], [3].

The spontaneous symmetry breakdown mechanism as characterized by (16′) is more rigorously characterized in the use of the reduced bundle (18) as follows:

Proposition 1. Let a gauge structure be given by a SO(3)-principal bundle $P(S^2, SO(3))$ (cf. (20)). Spontaneous symmetry breaking then corresponds to a reduction of the structure group $G = SO(3)$ of $P(S^2, SO(3))$ to $H = SO(2)$, the structure group of the reduced subbundle (cf. (18))

$$P'(S^2, H) = \{(\Phi, g) \in P = S^2_\Phi \times SO(3)/\varphi(\Phi, g) = \Phi_0 \in M_0\}, \tag{18'}$$

where (4″) $\widetilde{\varphi}$: $P \to S^2_\Phi \subset |R^3$; $\varphi(\Phi, g) = g^{-1}\Phi$, $\Phi \in S^2$, $g \in SO(3)$ stands for the Higgs field (4′).

Proof. The proof is based on the following

Lemma 2 [1]. The structure group G of $P(M, G)$ is reducible to a closed subgroup H iff the associated fibre bundle $E(M, G/H, G, P)$ admits a cross section $\emptyset$: $M \to E$.

Then, on account of (4′), (4″) and (5′) $\emptyset = s^*\varphi$: $M^4 \to S^2_\Phi$, thus achieving the proof.

Remark. There are 2 equivalence classes of principal bundles $P(S^2, SO(3))$, hence the statement of proposition 1.

Denote by $M = M^4$ or $M = S^2$, following if $t \in |R$ is fixed and $r > 0$. The following Proposition then holds:

Proposition 3. Let $P(M, SO(3))$ and $E(M, S^2, SO(3), P)$ be a SO(3)-principal bundle and its associated fibre bundle, respectively. Let Φ: $M^4 \to$ $\to SO(3)/SO(2) = S^2$ be a cross section of E. Then a connection in P with connection 1-form ω is determined by $\pi^*(A) = \omega^{(+)}$ where

$$A = A_\mu dx^\mu = \Phi \wedge \frac{\partial \Phi}{\partial x^\mu} dx^\mu + \Phi\alpha; \quad \alpha = a_\mu \, dx^\mu. \tag{25}$$

The curvature form of this connection is $\Omega = \pi^* F$, where

$$F = (\partial_\mu \Phi \wedge \partial_\nu \Phi) \, dx^\mu \, dx^\nu + \Phi(\partial_\mu a_\nu - \partial_\nu a_\mu) \, dx^\mu dx^\nu . \tag{26}$$

Proof. Assuming the relations (21) through (24) to hold, one calculates that the field tensor 2-form F in the Higgs vacuum is given by (26).

(+) π:$P \to M$ is a projective map (i.e. a surjective map), π^* the dual map induced by π.

Corollary 4. Let A be given by Eq. (25). Then the corresponding connection $\omega = \pi^*(A)$ in $P(M, \mathrm{SO}(3))$ is reducible to a connection $\omega' = \pi'^*(A')$ in $P(M, \mathrm{SO}(2))$ such that

$$F' = dA' = \Phi \wedge F = \Phi(\partial_\mu \Phi \wedge \partial_\nu \Phi)\, dx^\mu dx^\nu + (\partial_\mu a_\nu - \partial_\nu a_\mu)\, dx^\mu dx^\nu \quad (27)$$

induces the curvature of this connection, i.e. $\Omega = \pi^* F$.

Proof. The conditions (21b), (21c) and Eq. (19) Section III.1 express that the cross section under consideration, $\emptyset$, is parallel to the given connection. The proof is then obtained in the use of the following

Lemma 5 [1], [3]. Let $P(M, G)$ be a principal bundle whose associated fibre bundle is $E(M, G/H, G, P)$ with standard fibre G/H. The map $\emptyset\colon U \subset M \to E$ is a cross section of E iff $f\colon P'(M, H) \to P(M, G)$ is a reduction of the structure group G. If, moreover, $\emptyset$ is parallel to a connection ω in P, then this connection in $P(M, G)$ is reducible to a connection in $P(M, H)$.

IV. Monopole solutions in terms of topology

IV. 1. *The 't Hooft—Polyakov monopole condition*

Let a monopole field $B = g\Phi/||\Phi||^3$, associated with a Higgs triplet $\Phi = (\Phi^i)$ be given by the closed 2-form

$$F = \frac{g}{||\Phi||^3}(\Phi^1 d\Phi^2 \wedge d\Phi^3 + \Phi^2 d\Phi^3 \wedge d\Phi^1 + \Phi^3 d\Phi^1 \wedge d\Phi^2) =$$

$$= \frac{g}{2||\Phi||^3}(\varepsilon_{ijk}\, \Phi^i\, d\Phi^j \wedge d\Phi^k); \quad dF = 0, \quad (28)$$

where g is the magnetic pole strength of a magnetic pole. Then there is a monopole condition associated with the magnetic flux of (28) through S^2 (more generally through a closed compact surface), given by Eq. (29) of the subsequent proposition 6 which enjoys the following properties: There is an integral cohomology class determined by a Maxwell—Higgs field F which yields the monopole condition $g = n/2e$, $n \in Z$, where (i) The internal structure of the ('t Hooft—Polyakov) monopole derives from a SO(3) gauge structure (without external sources). (ii) The class of 't Hooft—Polyakov monopoles refers to a classical framework. The constant e is a coupling constant, not an electric charge. It is related to the charge q of charged vector bosons by $q = \pm e\hbar$. (iii) Outside the regions of the monopoles, the SO(3) gauge theory is locally indistinguishable from the electromagnetic theory.

Proposition 6. Let $P(M, \mathrm{SO}(2))$ and let the curvature 2-form of a connection in $P(M, \mathrm{SO}(2))$ be determined by

$$F' = \frac{g'}{||\Phi||^3}\varepsilon_{ijk}\Phi^i\frac{\partial\Phi^j}{\partial x^\mu}\frac{\partial\Phi^k}{\partial x^\nu}dx^\mu \wedge dx^\nu - (\partial_\mu a_\nu - \partial_\nu a_\mu)dx^\mu dx^\nu g' := \frac{g}{2}, \qquad (27')$$

where Φ is given by Eq. (23) and F' is the Maxwell—Higgs field (27). The cohomology class of F, $[F]$, where F is given by (28), is integral, i.e. $e/2\pi\int F = n \in Z$ iff $g = n/2e$ (i.e. g is an integral multiple of $1/2e$). The magnetic flux derived from (27′) through S^2 which satisfies this monopole condition, is given by

$$4\pi g = \frac{1}{2e||\Phi||^3}\int_{S^2}\varepsilon_{ijk}\Phi^i\frac{\partial\Phi^j}{\partial x^l}\frac{\partial\Phi^k}{\partial x^m}dx^l\,dx^m. \qquad (29)$$

Proof. Let $\zeta = P(M, \mathrm{SO}(2))$ (t fixed, $r > 0$). The Riemannian connection on M is given by the matrix $\begin{pmatrix} 0 & \omega \\ -\omega & 0 \end{pmatrix}$ such that there exists a unique 2-form Ω on M satisfying $d\omega = \pi^*(\Omega)$ [1]. Setting $\mathrm{SO}(2) \cong U(1)$, P is a $U(1)$-bundle, whose characteristic or first Chern class $c(\zeta)$ is represented by $\Omega/2\pi$. For compact M (which is the case, since $M = S^2$):

$$c(\zeta) = \int_M \Omega = 2\pi\chi(M) \qquad (30)$$

i.e.

$$c(\zeta) = \int_{S^2}\Omega = 4\pi, \quad F = g\Omega, \qquad (30')$$

where $\chi(M)$ is the Euler characteristic of M [1], [2], [3], and where $\chi(S^2) = 2$ and $\Omega = 1/||\Phi||^3\,(\Phi^1 d\Phi^2 \wedge d\Phi^3 + \Phi^2 d\Phi^3 \wedge d\Phi^1 + \Phi^3 d\Phi^1 \wedge d\Phi^2)$ such that, by (28) $F = g\Omega$. Then

$$\int\frac{e}{2\pi}F = n \Rightarrow \frac{ge}{2\pi}\int\Omega = n(\text{by } (30')) \Leftrightarrow g = \frac{n}{2e}.$$

Moreover, using Eq. (27′) and owing to the fact that the contribution of a^μ vanishes by Stokes theorem one obtains Eq. (29).

IV.2. *Homology classification of Higgs fields and monopoles*

Eq. (29) can be recasted, on account of the monopole condition $g = n/2e$ as

$$n = \frac{1}{4\pi||\Phi||^3}\int_{S^2}\varepsilon_{ijk}\Phi^i\frac{\partial\Phi^j}{\partial x^m}\frac{\partial\Phi^k}{\partial x^l}dx^m\,dx^l. \qquad (29')$$

Geometrical interpretation of n: Let the diagram $\Phi: S^2(r) \to S^2_\Phi$ (cf. Eq. (22′) Section III.2) where

$$\hat{\Phi}^\alpha = n^\alpha = (\sin\theta\cos(n\varphi), \sin\theta\sin(n\varphi), \cos\theta);\ ||\Phi|| = \sqrt{\Phi^2(r)} \qquad (22')$$

is the normalized Higgs field (23). The integer n in (22′) is identified as the mapping degree (or Brouwer degree [10]) of the map Φ (cf. subsequent proposition 7) and corresponds to the number of times $\Phi(x)$ covers the vacuum manifold $M_0 = S^2$ as x covers once $S^2(r)$. The integer n labels the homotopy classes (equivalence classes under homotopy) of the mappings Φ: $S^2 \to M_0$. Mappings belonging to the same class (n) are continuously deformable into another. Corresponding solutions are then gauge equivalent with the same magnetic charge. This magnetic charge which is topologically conserved and quantized in units of $1/2e$ is related to a new type of conservation law, i.e. a topological one. The corresponding charges are referred to as topological charges. A homology classification of topological charges refers to the Brouwer degree of mappings [2], [3], [8], [9], [10] in the following sense: Consider the diagram (31), where Φ^* is induced by (22):

$$\begin{array}{ccc} H^2(S^2(r)) & \xleftarrow{\Phi^*} & H^2(S^2_\Phi) \\ I_1 \downarrow & & \downarrow I_2 \\ R & \xleftarrow{f^*} & R \end{array} \qquad (31)$$

$H^2(S^2)$ stands for the second de Rham cohomology group of S^2. $I_1 := \int_{S^2(r)}$: $H^2(S^2(r)) \to R$ and $I_2 = \int_{S^2_\Phi}$: $H^2(S^2) \to R$ are canonical linear isomorphisms which determine a unique linear map $f^* \in L(|R, |R)$: $t \to kt, k \in |R$, such that the diagramme (31) commutes. Then, by definition

$$\deg(\hat{\Phi}) = f^*_{\hat{\Phi}}(1) \qquad (32)$$

is termed the Brouwer degree of $\hat{\Phi}$. Since $I_1 \circ \hat{\Phi}^* = f^* \circ I_2$ and since $\Omega \in [\Omega] \in H^2(S^2(r))$ one infers from (31)

$$\int_{S^2(r)} \hat{\Phi}^* \Omega = k \int_{S^2\Phi} \Omega\,. \qquad (33)$$

Let $x = (\theta, \varphi) \in S^2(r)$ be a regular point of $\hat{\Phi}$, so that $d\hat{\Phi}(x)$: $T_x(S^2(r)) \to$ $\to T_{\hat{\Phi}}(S^2)$ is a linear isomorphism between oriented vector spaces. Then $\hat{\Phi}$ determines a n integer-valued function $M \to \{1, -1\}$; $x \to \operatorname{sgn}(\det(d\hat{\Phi}(x))) =$ $= \operatorname{sgn} J_x(\hat{\Phi})$ (= signature of the Jacobian of Φ) where

$$\operatorname{sgn}(J_x(\hat{\Phi})) = \begin{cases} +1 & \text{if } d\Phi_x \text{ preserves the orientations} \\ -1 & \text{if } d\Phi_x \text{ reverses the orientations} \end{cases}$$

with $J_x(\hat{\Phi}) = \det(d\hat{\Phi}(x)) = \det(\partial\hat{\Phi}^j(x)/\partial x^i)$. So

$$\int_{S^2(r)} \hat{\Phi}^* \Omega = \sum_{x \in \hat{\Phi}^{-1}(y)} \operatorname{sgn}(J_x(\hat{\Phi})) \cdot \int_{S^2\Phi} \Omega = k \int_{S^2\Phi} \Omega.$$

Hence

$$\deg(\hat{\Phi}) = k = \sum_{x \in \hat{\Phi}^{-1}(y)} \operatorname{sgn}(J_x(\hat{\Phi}) \in Z;\ \hat{\Phi}^{-1}(y) = \{x_1, \ldots, x_r\} \tag{34}$$

is an integer [10]. On account of the Higgs field (23), i.e. the definition $(\Phi^1(\theta, \varphi)$, $\Phi^2(\theta, \varphi) = (\theta, n\varphi)$ (Eq. (22)) the integer (34) equals n. In fact

$$\left(\frac{\partial\hat{\Phi}^j}{\partial x^i}(x)\right) = \begin{pmatrix} \dfrac{\partial\hat{\Phi}^1(x)}{\partial x^1} & \dfrac{\partial\hat{\Phi}^1}{\partial x^2}(x) \\ \dfrac{\partial\hat{\Phi}^2(x)}{\partial x^1} & \dfrac{\partial\hat{\Phi}^2}{\partial x^2}(x) \end{pmatrix} = \begin{pmatrix} \dfrac{\partial\hat{\Phi}^1}{\partial\theta}(x) & \dfrac{\partial\hat{\Phi}^1}{\partial\varphi}(x) \\ \dfrac{\partial\hat{\Phi}^2}{\partial\theta}(x) & \dfrac{\partial\hat{\Phi}^2}{\partial\varphi}(x) \end{pmatrix} = \begin{pmatrix} 1 & 0 \\ 0 & n \end{pmatrix}.$$

Hence, by relation (34) one obtains

$$\deg(\Phi) = \sum_i \operatorname{sgn} J_{xi} = \sum_i \operatorname{sgn} \det \begin{pmatrix} 1 & 0 \\ 0 & n \end{pmatrix} = \sum_i (+1) = n. \tag{35}$$

Proposition 7. There is a topological 2-field (Ω, c) and a nondegenerate bilinear map β, satisfying

$$\beta\colon (\Omega', c) \to n = \deg(\hat{\Phi}) = 1/4\pi \int_{S^2(r)} \hat{\Phi}^* \Omega. \tag{36}$$

This is the conserved quantum number (29′), where $\Omega' = \hat{\Phi}^* \Omega$; $c \subseteq S^2(r)$ and $\hat{\Phi}^*$ is the map induced by (22). Ω is given by $\Omega = 1/||\Phi||^3 (\Phi^1 d\Phi^2 \wedge d\Phi^3 + \Phi^2 d\Phi^3 \wedge \wedge d\Phi^1 + \Phi^3 d\Phi^1 \wedge d\Phi^2$.

V. Conclusion

A geometric description of the mechanism of spontaneous symmetry breaking depends on a degenerate vacuum and thus on a certain vacuum manifold M_0, which, in the case of 't Hooft—Polyakov model is S^2. Topological quantum numbers or charges which depend on the topological properties of solutions to field equations arise in connection with the Higgs mechanism. As exhibited by the proposition 7, topological charges display, besides certain homotopic properties, additional homological features. In the case of the

't Hooft—Polyakov model, the homological property (36) is equivalent to the homotopic property of the second homotopy group of $M_0 = S^2$, i.e.

$$\Pi_2(SO(3)/SO(2)) = \Pi_2(S^2) = Z \ . \tag{36'}$$

This means that there are soliton solutions which are labelled by a topological charge n and which are linked to magnetic charge quantization. Whence the necessity to investigate the class of topological currents transporting conserved quantities, which unlike Noether currents or charges, are not associated with any symmetry of a Lagrangian, but nevertheless relate to a common mathematical structure which is de Rham cohomology. This has been investigated in [4]. As was investigated there, topological current fields differ from Noether current fields in that they exhibit homotopic properties.

VI. Acknowledgements

Sections III and IV constitute an extended version presented at the summerschool on "Differential geometric methods in mathematical physics" July-August 1979, Technical University of Clausthal, West-Germany. The author wishes to thank Professor H. D. DOEBNER for the invitation to this summerschool. Discussions with Professor A. CRUMEYROLLE and Professor BANCEL (Université Paul Sabatier, Toulouse) are also acknowledged. Valuable criticism and comments from Professor J. VOISON (Université de Namur), Professors D. SPEISER and ANTOINE (Université Catholique de Louvain) and Professor BECKER (Université de Liège) are also acknowledged. Finally, useful constructive comments from the Referee have been taken into account for the revised version of this paper.

REFERENCES

1. S. KOBAYASHI and K. NOMIZU, Foundations of Differential Geometry, Interscience Publishers, New York, 1963.
2. S. STERNBERG, Lectures on Differential Geometry, Prentice Hall, Inc. Englewood Cliffs, N. J. USA, 1972.
3. C. v. WESTENHOLZ, Differential Forms in Mathematical Physics, North Holland Publishing Comp., Amsterdam, 1978.
4. C. v. WESTENHOLZ, Ann. Inst. H. Poincaré, **33**, 353, 1979.
5. R. HERMANN, Vector Bundles in Mathematical Physics, Benjamin, New York, 1970.
6. A. TRAUTMAN, Symposia mathematica, **12**, 140, 1973.
7. M. HONDA, Fiber Bundle Structure of Gauge Fields and Reduction by the Higgs Mechanism, Preprint TU/79/195 Tohoku University, Sendai 980, Japan.
8. C. v. WESTENHOLZ, Ann. Inst. H. Poincaré, **29**, 285, 1978.
9. J. ARAFUNE, P. G. O. FREUND and H. GOEBEL, Journ. of Math. Phys., **16**, 433, 1975.
10. N. MILNOR, Topology from the Differentiable Viewpoint, The University Press of Virginia, Charlottesville, 1965.
11. W. GREUD and H. PETRY, Journ. of Math. Phys., **16**, 1347, 1975.

Acta Physica Academiae Scientiarum Hungaricae, Tomus 48 (2—3), pp. 225—234 (1980)

DEPENDENCE ON THE GEOMETRY AND ON THE BASIS SET OF LOCALIZED ORBITAL ENERGY AND MOMENT CONTRIBUTIONS

III. ELECTRIC MOMENTS

By

E. KAPUY, C. KOZMUTZA and ZS. OZORÓCZY

QUANTUM THEORY GROUP, PHYSICAL INSTITUTE, TECHNICAL UNIVERSITY, BUDAPEST, HUNGARY

(Received 3. I. 1980)

Several regularities have been found for the localized orbital energy contributions in a study by using various basis sets and molecular geometries. The localized charge densities have been further analyzed in terms of its first and second order electric moments. The results obtained for these localized moments of the systems investigated (HF, H_2O and NH_3, respectively) affirm that there are systematic changes in the localized charge distributions as going from the experimental to the theoretically determined equilibrium geometries.

1. Introduction

In a series of papers we investigate the localized orbital contributions determined for the HF, H_2O and NH_3 molecules, respectively. The investigations were done using various basis sets and the calculations carried out at the experimental and the theoretical equilibrium geometries. In the first [1] and the second [2] part some energy quantities were discussed and it was shown that they suitably characterize the different types of localized charge densities (cores, bonds and lone pairs). It is interesting to investigate, in addition, whether the electric moments determined for localized orbitals (the so-called localized moments) also show similar regularities at different molecular geometries. A detailed analysis on the basis set dependence of H_2O localized charge distributions [3] resulted in that the changes in the self, the Coulomb and the exchange interaction energy contributions can be related to the changes in the localized moments. It is worthwhile to study whether this conclusion holds even for other molecules. As the importance of inclusion of polarization functions is well known, we also carried out the calculations by the use of *d*-type functions on the heavy (F, O and N) atoms.

Experimental and calculated equilibrium geometries were taken as given in Part I [1]. The HF—SCF calculations were performed on a CDC 3300 computer (Hungarian Academy of Sciences, Budapest). The basis sets used were the following: the (*sp*/*s*) type one as that introduced in [4], this is the so-called basis 6-31G, while the *d*-type functions were taken into consideration by using basis 6-31G/d [5].

2. Total molecular electric moments

As there are many confusions in the literature (we only refer to [6]), first we give the definition of some lower order moments.

The charge distributions of quantum mechanical systems can be expanded in terms of their multipole electric moments. The so-called zeroth order moment is the total charge Z

$$Z = \sum_i e_i. \tag{1}$$

The first order electric moment is the dipole moment μ

$$\mu = \sum_i e_i r_i. \tag{2}$$

The electric moments are not invariant under a shift of the origin of the coordinate system. It has been pointed out [7], however, that the first non-vanishing moment is usually independent of the choice of the coordinates. The origin of coordinate system is often chosen as the centre of gravity or the centre of the charge distribution.

In case of molecules the first order electric moments in atomic units can be expressed in the following way:

$$\mu_u^e = -\sum_{i=1}^{N} \langle \Phi | r_{ui} | \Phi \rangle, \quad u = x, y, z, \tag{3}$$

where Φ denotes the solution (eigenfunction) of the Schrödinger equation for the system, N is the number of electrons. The contribution of the nuclei:

$$\mu_u^n = \sum_{a=1}^{n} Z_a \, \delta(r_u - r_{ua}) \, r_u \qquad u = x, y, z \tag{4}$$

is determined by the position (r_a) and the charge (Z_a) of nuclei. The total dipole moment of a molecular system is obtained by the sum of (3) and (4) in all of three coordinate directions:

$$\mu = \mu^e + \mu^n. \tag{5}$$

In order to describe molecular wavefunctions, one commonly uses the independent particle model [8]. In the framework of the one-determinantal approximation the first order properties, as, e.g. the electric moments can be written

as the sum of contributions from the individual orbitals. The first order moments, according to (3), will then have the following form:

$$\mu_u^e = \sum_{k=1}^{N} \mu_u^e(k) = -\sum_{k=1}^{N} \langle \varphi_k | r_u | \varphi_k \rangle = -\sum_{k=1}^{N} r_u(k), \quad u = x, y, z \tag{6}$$

where φ_k denotes the k-th one-particle function (orbital). If the orbitals are subjected to a unitary transformation (symmetry transformation, localization):

$$\bar{\varphi}_j = \sum_{k=1}^{N} U_{jk} \varphi_k \text{ for all } j, \quad j = 1, N \tag{7}$$

the individual components $r_u(k)$ change but their sum μ^e is invariant. The first order moments are often called the centroids of charge. More precisely we call centroid length for $\bar{\varphi}_k$ the scalar quantity $|r(k)|$ and by the name centroid we mean the endpoint of the vector $r(k)$.

In contrast to the case of zeroth and first order electric moments there are several different definitions for the second order ones. In order to be consistent with (1) and (2), the quadrupole moment can be defined in a similar way:

$$\mathbf{Q} = \sum_i e_i r_i \circ r_i, \tag{8}$$

where $\mathbf{Q}$ is the quadrupole tensor with nine components [6, 7]. It is more convenient, however, to use a definition of a traceless tensor $\mathbf{\Theta}$,

$$\mathbf{\Theta} = \sum_i e_i (3 r_i \circ r_i - r_i^2) \tag{9}$$

and so the sum of the diagonal elements of $\mathbf{\Theta}$ is zero:

$$\Theta_{xx} + \Theta_{yy} + \Theta_{zz} = 0. \tag{10}$$

For a cylindrically symmetric charge distribution:

$$-2\Theta_{xx} = -2\Theta_{yy} = \Theta_{zz}. \tag{11}$$

The one scalar quantity Θ_{zz} ($\equiv \Theta$) is simply referred to as the quadrupole moment. $\mathbf{Q}$ and $\mathbf{\Theta}$ are both symmetric. The components of the tensor $\mathbf{Q}$ can be related to those of $\mathbf{\Theta}$:

$$\Theta_{uv} = \frac{1}{2}\left(3Q_{uv} - \delta_{uv} \sum_w Q_{ww}\right), \quad u \neq v,$$

$$\Theta_{uu} = \frac{1}{2}(2Q_{uu} - Q_{vv} - Q_{ww}), \quad u, v, w = x, y, z. \tag{12}$$

In case of molecular systems one should determine the quadrupole moment components for the electrons as well as for the nuclei. The second order moment components of electrons can be defined in atomic units as follows:

$$Q^{e}_{uv} = -\sum_{i=1}^{N} \langle \Phi | r_{ui}\, r_{vi} | \Phi \rangle, \quad u, v = x, y, z. \tag{13}$$

The meaning of r_{ui}, r_{vi} and Φ are the same as in Eq. (3). The quadrupole moment components of nuclei can be written as

$$Q^{n}_{uv} = -\sum_{a=1}^{N} Z_a\, \delta(r_u - r_{ua})\, \delta(r_v - r_{va})\, r_u r_v, \quad u, v = x, y, z. \tag{14}$$

The sum of (13) and (14) yields the components of the total quadrupole moment of the system. In actual calculations it is convenient to use a coordinate system fixed with respect to the centre of charge distribution.

For canonical molecular orbitals this does not seem to be helpful, in case of localized charge densities, on the other hand, the centroid of the individual orbitals can be taken as the centre of the quadrupole tensor. The shifting causes a change in the values of components, so, e.g. for a given localized orbital $\bar{\varphi}_k$ the components $\bar{Q}_{uv}(k)$ could be determined in the following way:

$$\bar{Q}_{uv}(k) = \langle \bar{\varphi}_k \mid [u - r_u(k)]\, [v - r_v(k)] \mid \bar{\varphi}_k \rangle, \quad u, v = x, y, z$$

where the index e is omitted for clarity, $r_u(k)$ and $r_v(k)$ are the components of centroid vector of orbital $\bar{\varphi}_k$. These shifted components define a quadrupole moment tensor **Q** for the individual localized orbital from $\{\bar{\varphi}_k\}_{k=1}^{N/2}$.

Before analyzing the localized orbital electric moments, the total molecular moments are discussed for the compounds HF, H_2O and NH_3, respectively.

The total dipole moments obtained are given in Table I. The corresponding experimental values (taken from [9]) are the following (in atomic units):

HF: 0.715

H_2O: 0.706

NH_3: 0.578

As to the values obtained by using basis 6-31G, the total dipole moments are quite wrong, as expected because of the not too large (*sp*/*s*) basis set. The dipole moments calculated by basis set 6-31G/d, especially those obtained at the calculated equilibrium geometries are not too far from the near HF limiting values.

Table I

Non-vanishing total dipole and quadrupole moments (in atomic units, for definitions see text)

		Total dipole moment	
		Basis 6-31G	Basis 6-31G/d
HF	Exp.	0.903	0.784
	Calc.	0.905	0.778
H_2O	Exp.	1.046	0.876
	Calc.	0.996	0.866
NH_3	Exp.	0.928	0.772
	Calc.	0.567	0.761

Total quadrupole moment components			
		Θ_{xx}	
		Basis 6-31G	Basis 6-31G/d
HF	Exp.	—0.866	—0.899
	Calc.	—0.873	—0.886
H_2O	Exp.	1.632	1.681
	Calc.	1.952	1.704
NH_3	Exp.	0.899	0.898
	Calc.	1.299	0.910

		Θ_{yy}	
		Basis 6-31G s	Basis 6-31G/d
HF	Exp.	—0.866	—0.899
	Calc.	—0.873	—0.886
H_2O	Exp.	—1.765	—1.845
	Calc.	—1.785	—1.821
NH_3	Exp.	0.899	0.898
	Calc.	1.299	0.910

		Θ_{zz}	
		Basis 6-31G	Basis 6-31G/d
HF	Exp.	1.733	1.798
	Calc.	1.746	1.772
H_2O	Exp.	0.133	0.164
	Calc.	0.167	0.117
NH_3	Exp.	—1.799	—1.795
	Calc.	—2.599	—1.821

Table II

First order electric moments obtained for localized orbitals (in atomic units)

		Bonds	
		Basis 6-31G	Basis 6-31G/d
HF	Exp.	0.8431	0.8527
	Calc.	0.8447	0.8492
H_2O	Exp.	0.9815	0.9892
	Calc.	0.9705	0.9815
NH_3	Exp.	1.1491	1.1615
	Calc.	1.1146	1.1539
CH_4	Exp.	1.3830	1.4021
	Calc.	1.3721	1.3949

		Lone pairs	
		Basis 6-31G	Basis 6-31G/d
HF	Exp.	0.5215	0.5120
	Calc.	0.5215	0.5118
H_2O	Exp.	0.6064	0.5870
	Calc.	0.6035	0.5859
NH_3	Exp.	0.7194	0.6859
	Calc.	0.6380	0.6838

Similar conclusions hold for the quadrupole moments (see Table I). The corresponding values obtained from the experiment (as summarized in [9]) in atomic units are as follows:

$$\text{HF}\quad \Theta_{zz}: \quad -$$

$$\text{H}_2\text{O}\quad \Theta_{xx}: \quad -1.859$$

$$\Theta_{yy}: \quad 1.956$$

$$\Theta_{zz}: \quad -0.097$$

$$\text{NH}_3\quad \Theta_{zz}: \quad -1.725$$

It should be mentioned, however, that the calculated quadrupole moments even by using a basis with polarization functions are usually rather far from the corresponding experimental values. In this connection, see, e.g. [10].

3. First order localized moments

The first order electric moments obtained for the bonds of HF, H_2O and NH_3, respectively, are given in Table II. It is remarkable that, where the nuclear potentials are larger (i.e. at short bond lengths), the centroid lengths of bond orbitals are always shorter. This result can well be seen especially in the case of molecule HF: the theoretically obtained interatomic distance is shorter than the experimental one, if one uses (*sp*/*s*) basis set (see Part I of this series). As a consequence, the centroid lengths of bond orbitals are also shorter at the calculated than at the experimental equilibrium geometry. The case is the opposite, however, by using basis sets with *d*-type polarization functions. These results can be seen from Table II.

It generally holds that the smallest difference between the first order localized moments determined by basis sets including polarization functions at the experimental and the calculated equilibrium geometries can be fonud for symmetric molecules. We have also obtained similar results: the smallest deviation was obtained for CH_4 (see Table II).

Table II

Dispersions in major axis directions
(in atomic units, for definitions see text)

		Bonds	
		Basis 6-31G	Basis 6-31G/d
HF	Exp.	0.8686	0.8478
	Calc.	0.8714	0.8428
H_2O	Exp.	0.9437	0.9227
	Calc.	0.9330	0.9141
NH_3	Exp.	1.0182	0.9993
	Calc.	0.9861	0.9922
CH_4	Exp.	1.0954	1.0687
	Calc.	1.0874	1.0640

		Lone pairs	
		Basis 6-31G	Basis 6-31G/d
HF	Exp.	0.7256	0.7299
	Calc.	0.7255	0.7301
H_2O	Exp.	0.8547	0.8624
	Calc.	0.8611	0.8614
NH_3	Exp.	1.0121	1.0204
	Calc.	1.1077	1.0246

The first order electric moments obtained for the lone pair orbitals are also given in Table II. It is interesting that the values calculated at the experimental and the theoretical equilibrium geometries are always very close to each other (except the case of NH_3, by using basis 6-31G, but its calculated equilibrium geometry is very far from the experimental one). This result suggests that the displacement of the centre of the lone pair charge densities from the central atom does not depend much on the molecular geometry.

4. Second order localized moments

The dispersions in the three directions of diagonalized ellipsoid (see Section 2) have also been determined for the compounds studied. It is already kown from earlier studies [11] that the dispersion in the main axis direction is about 20—30% larger than that in the two minor axis directions. As to the values obtained for the bond orbitals, the dispersions in major axis direction (see Table III) do also show systematic changes with the change in the molecular

Table IV

Dispersions in minor axis directions
(in atomic units, for definitions see text)

		Bonds	
		Basis 6-31G	Basis 6-31G/d
HF	Exp.	0.5920	0.5919
	Calc.	0.5931	0.5899
H_2O	Exp.	0.6612	0.6594
	Calc.	0.6591	0.6561
NH_3	Exp.	0.7386	0.7366
	Calc.	0.7395	0.7338
CH_4	Exp.	0.8262	0.8224
	Calc.	0.8223	0.8200

		Lone pairs	
		Basis 6-31G	Basis 6-31G/d
HF	Exp.	0.5823	0.5831
	Calc.	0.5824	0.5929
H_2O	Exp.	0.6816	0.6864
	Calc.	0.6806	0.6859
NH_3	Exp.	0.8032	0.8094
	Calc.	0.8008	0.8089

Table V

Ratios of dispersions in two minor axis directions

		Bonds	
		Basis 6-31G	Basis 6-31G/d
HF	Exp.	1.0000	1.0000
	Calc.	1.0000	1.0000
H_2O	Exp.	1.0030	1.0034
	Calc.	1.0010	1.0033
NH_3	Exp.	1.0012	1.0015
	Calc.	1.0045	1.0016
CH_4	Exp.	1.0000	1.0000
	Calc.	1.0000	1.0000

		Lone pairs	
		Basis 6-31G	Basis 6-31G/d
HF	Exp.	1.0014	1.0020
	Calc.	1.0015	1.0022
H_2O	Exp.	1.0010	1.0022
	Calc.	1.0010	1.0017
NH_3	Exp.	1.0000	1.0000
	Calc.	1.0000	1.0000

geometry. It means that the decrease of the values of dispersions parallels the increase of nuclear potentials: their sensitivity to the geometry changes is, however, larger than that of the centroid lengths. The major axis dispersions obtained for the lone pair orbital densities do show a bit larger difference between the experimental and the calculated equilibrium geometries than the first order moments. The discrepancies of the values obtained, however, by basis set 6-31G/d, e.g. are still less than 0.5% for any of the HF, H_2O and NH_3 molecules. These results affirm that the lone pair densities are no too much affected by the changes in the molecular geometry.

As the values of the two minor axes dispersions are rather close to each other, only those obtained in the y direction are given in Table IV. It is interesting that the dispersions calculated at the experimental and theoretical equilibrium geometries for the bond orbitals do not differ much from each other: their deviations amount to less than 0.5%. This result suggests that one could draw a similar conclusion to that found for the lone pair centroid lengths and dispersions in the major axis direction. This means that while the displacements of the centres of bond orbital densities depend much on the molecular

geometry, the "extent" of the densities does not depend strongly on the bond angles and distances. The minor axis dispersions for the lone pair orbital distributions depend still much less on the actual molecular geometry, as expected (see Table IV). Their deviations from each other obtained for the molecules studied are less than 0.1% by the use of basis of 6-31G/d type.

In order to have an estimate for the differences between the two minor axis dispersions, their ratios are given in Table V. Apart from the symmetric cases (HF bond, NH_3 lone and CH_4 bond orbitals) the differences for other localized orbitals are even smaller. It is interesting that the ratios obtained at the calculated equilibrium geometry are smaller than at the experimental one by using basis 6-31G/d for the localized orbital densities of H_2O molecule. This result would suggest a "more symmetric form" of charge distributions at the theoretically obtained equilibrium of H_2O.

5. Conclusion

Some regularities have been found as investigating the total and the localized electric moments at different molecular geometries for three ten-electron compounds. The calculated molecular dipole and quadrupole moments are in agreement with the results obtained from other studies. The investigation was carried out using basis sets of (*sp*/*s*) and (*spd*/*s*) types. It generally holds that the first order localized moments (more precisely the lengths of centroids) are parallel changing with the nuclear potential changes for bond orbitals. The lone pair charge distributions are not much dependent on the actual values of bond lengths and angles in the vicinity of the equilibrium geometries.

REFERENCES

1. E. KAPUY, C. KOZMUTZA, Zs. OZORÓCZY and J. PIPEK, Acta Phys. Hung., **46**, 333, 1979.
2. E. KAPUY, C. KOZMUTZA and Zs. OZORÓCZY, Acta Phys. Hung., **47**, 303, 1979.
3. E. KAPUY, C. KOZMUTZA, R. DAUDEL and M. E. STEPHENS, Theoret. Chim. Acta (Berl.), **50**, 31, 1978.
4. W. J. HEHRE, R. DIETCHIEFELD and J. A. POPLE, J. Chem. Phys., **56**, 2257, 1972.
5. P. C. HARIHARAN and J. A. POPLE, Theoret. Chim. Acta (Berl.), **28**, 213, 1973.
6. A. D. BUCKINGAM, Electric Moments of Molecules, in Physical Chemistry, Vol. IV., p. 349, Eds. Hy Erying, D. Henderson, and W. Jost, Academic Press, New York, 1970.
7. J. O. HIRSCHFELDER, C. F. CURTISS and R. B. BIRD, Molecular Theory of Gases and Liquids, J. Wiley and Sons, New York, 1954.
8. E. KAPUY and F. TÖRÖK, Quantum Theory of Atoms and Molecules (in Hungarian), Akadémiai Kiadó, Budapest, 1975.
9. C. KOZMUTZA, Characterization of Molecules by Using Localized Orbitals (in Hungarian), Thesis, Budapest, 1976.
10. T. H. DUNNING, J. Chem. Phys. **55**, 716, 3958, 1971.
11. E. KAPUY, C. KOZMUTZA and M. E. STEPHENS, Theoret. Chim. Acta (Berl.), **43**, 175, 1976.

Acta Physica Academiae Scientiarum Hungaricae, Tomus 48 (2—3), pp. 235—241 (1980)

DEPENDENCE ON THE GEOMETRY AND ON THE BASIS SET OF LOCALIZED ORBITAL ENERGY AND MOMENT CONTRIBUTIONS

IV. MOMENT CHARACTERISTICS

By

E. KAPUY, C. KOZMUTZA and ZS. OZORÓCZY

QUANTUM THEORY GROUP, PHYSICAL INSTITUTE, TECHNICAL UNIVERSITY, BUDAPEST, HUNGARY

(Received 3. I. 1980)

In a series of papers the localized orbital energies and the first and second order electric moments have been investigated. In the present paper several moment characteristics obtained for the HF, H_2O and NH_3 molecules, respectively, are discussed. The calculations were carried out at the experimental and at the theoretical equilibrium geometries of the compounds. The results have shown that some moment characteristics are especially useful in pointing out the main differences in the behaviours of bond and lone pair charge densities.

1. Introduction

Several regularities have been pointed out when investigating the localized orbital energy contributions of some small neutral compounds (Papers I and II of this series [1]). The geometries were fixed first at the experimental then at the theoretically obtained equilibria. The properties of the localized molecular orbitals were studied by using various basis sets: the calculations have been done by the use of the so-called 6-31G [2] and 6-31G/d basis sets [3] in each case. This geometry and basis set dependence analysis of localized orbitals has been extended to the investigation of the electric moments as well. Namely, the total molecular dipole and quadrupole moments and their decompositions into the localized orbital contributions (localized moments) have been investigated for the HF, H_2O and NH_3 molecules, respectively. The results have been published in Paper III of this series [4]. The results obtained affirmed that systematic differences can be found between the localized charge distributions if one compares the values obtained at the experimental and at the calculated equilibrium geometries.

It has already been pointed out that there are close relationships between the energy and the moment contributions of localized orbitals (see, e.g. [5—6]). The moment characteristics defined in [5] seemed to be useful for a description of localized charge densities of some small molecules, and even their transferability property has been shown recently [7]. No systematic work has yet been done, however, to investigate whether the geometry data chosen influence the overall regularities and/or the basis sets used cause differences in

the values. This study would help to point out the usefulness of the moment characteristics in analysing any localized charge densities.

All details concerning the actual calculations can be found in Parts I—III of this series. The molecules investigated were the following: HF, H_2O and NH_3, respectively, and their bond and lone pair localized orbitals were characterized by several measures. Two well-defined characteristics: the orbital asymmetry and the effective solid angle will be analyzed in this paper in detail. Some further properties connected with localized orbital moments will also be investigated.

2. Orbital asymmetries

The quantity named orbital asymmetry measures the asymmetry of the given localized charge density with respect to the nucleus of the central atom. The definition expressed by using the electric moments of localized charge distributions is given in [5]. The values obtained for bond pair orbitals are given in the first part of Table I. The results show that the inclusion of polarization functions causes a systematic increase of about 3—4% in the orbital asymmet-

Table I

Orbital asymmetries obtained for localized orbitals

		Bonds	
		Basis 6-31G	Basis 6-31G/d
HF	Exp.	0.971	1.006
	Calc.	0.969	1.008
H_2O	Exp.	1.040	1.072
	Calc.	1.040	1.074
NH_3	Exp.	1.129	1.162
	Calc.	1.130	1.163
CH_4	Exp.	1.263	1.312
	Calc.	1.262	1.311
		Lone pairs	
		Basis 6-31G	Basis 6-31G/d
HF	Exp.	0.717	0.701
	Calc.	0.719	0.710
H_2O	Exp.	0.709	0.681
	Calc.	0.701	0.678
NH_3	Exp.	0.711	0.672
	Calc.	0.576	0.667

ries of bond orbitals. It generally holds, however, that there are only very small (less than 0.2%) differences between the values obtained at the experimental and the calculated equilibrium geometry. These results suggest that these quantities do not depend much on the bond lengths and/or bond angle changes in the molecule. The opposite case has been found for the lone pair orbital asymmetries: the values increase with enlarging basis sets, and the quantities depend more on the actual geometry. The results obtained at the experimentally and the theoretically obtained equilibria differ by about 0.5—1.0%.

3. Effective solid angles

These quantities are — approximately — the measures of the space requirement of the localized orbitals (the definition is given precisely in [5]). The values calculated for the studied systems by using the basis sets 6-31G and 6-31G/d, respectively, are given in the first part of Table II. As to the results obtained for FH, OH, NH and CH bond orbitals, they become smaller (by

Table II

Effective solid angles obtained for localized orbitals (in steradian)

		Bonds	
		Basis 6-31G	Basis 6-31G/d
HF	Exp.	1.141	1.122
	Calc.	1.141	1.123
H_2O	Exp.	1.070	1.052
	Calc.	1.085	1.057
NH_3	Exp.	0.997	0.976
	Calc.	1.044	0.980
CH_4	Exp.	0.889	0.863
	Calc.	0.894	0.867

		Lone pairs	
		Basis 6-31G	Basis 6-31G/d
HF	Exp.	2.090	2.135
	Calc.	2.090	2.136
H_2O	Exp.	2.106	2.197
	Calc.	2.113	2.200
NH_3	Exp.	2.091	2.221
	Calc.	2.368	2.227

about 2—3%) if a set of polarization *d* functions is included in the calculation. The differences between the effective solid angles determined at the experimental and the theoretical equilibrium geometries are a bit larger than those resulting for the orbital asymmetries but still less than 0.5% for any bond orbital investigated.

The effective solid angles of lone pair charge distributions (second part of Table II) are nearly twice as large as those of bond pair orbitals. This result has already been shown in a previous study [5]. As to the basis set dependence of these angles, they are larger by using basis set 6-31G/d than 6-31G. The deviations between the values calculated at the experimentally and theoretically obtained equilibrium geometries are small, less than 0.3%. The effective solid angles increase with decreasing nuclear charge of the central atom by using a basis set of (*spd*/*s*) type. This is interesting, because a decrease was found by the use of (*sp*/*s*) type basis set [5].

4. Dispersion ratios

As has already been pointed out in Paper III of this series, the minor axes of the diagonalized second moment tensor do not deviate from each other by more than 0.4% (values obtained by using a basis set of 6-31G/d type). The deformations of the localized charge densities from the spherical distribution, can be measured by the dispersion ratios (for definition see [5]). Because of the above arguments, the dispersion ratios were calculated as taking the ratios of the major axis dispersion and that of the average values of the two minor axes. The values obtained by basis sets of (*sp*/*s*) and (*spd*/*s*) types are given in Table III. As to the results for bond orbitals, the dispersion ratios become larger by the introduction of polarization functions. There are not too many differences, however, between the values obtained at the experimental and the calculated equilibrium geometries. This result suggests that the "form" of the second moment tensor of the bond orbitals does not depend much on the changes of the geometrical arrangement of the molecule. Similar results were found for the lone pair orbitals, the deviations of the values obtained at the experimentally and the theoretically obtained equilibrium geometries are rather small, less than 0.5%, as calculated by basis 6-31G/d.

It is interesting that the dispersion ratios of bond and lone pair orbitals do deviate from each other differently: their deviation depends strongly on the molecular system. Namely, the dispersion ratios of bond pair localized orbitals of HF are larger than those of lone pair ones by about 18%, while the deviation for the NH_3 molecule is less than 10%. This result suggests that the "weight" of bond localized charge densities is larger if the number of bonds is smaller in the molecular system studied.

Table III

Major/minor axis dispersion ratios obtained for localized orbitals

		Bonds	
		Basis 6-31G	Basis 6-31G/d
HF	Ekp.	1.467	1.432
	Calc.	1.469	1.429
H_2O	Exp.	1.427	1.399
	Calc.	1.416	1.393
NH_3	Exp.	1.379	1.357
	Calc.	1.334	1.352
CH_4	Exp.	1.326	1.300
	Calc.	1.323	1.305

		Lone pairs	
		Basis 6-31G	Basis 6-31G/d
HF	Exp.	1.246	1.252
	Calc.	1.246	1.253
H_2O	Exp.	1.254	1.256
	Calc.	1.265	1.256
NH_3	Exp.	1.260	1.261
	Calc.	1.383	1.267

5. Dispersion products

There is still a very important question to analyse, and this is the "size" of the localized charge densities. The measure of the size or the extent for a localized charge distribution can be defined in various ways (see, e.g. [8]). One of these is the so-called dispersion product, as defined in [5], the product of dispersions in the three (shifted) coordinate directions. This quantity is interesting to investigate as there are some expectations concerning the relative magnitude of bond and lone pair orbitals. First it was believed that the "size" of the lone pair orbitals ought to be always larger than the bond pair ones [8]. Furthermore, as investigating these measures using different basis sets for some small molecules it was pointed out that there is an "inflexion point" in the trend of the sizes of bond and lone pair orbitals. More precisely, it was shown that there are some systems for which the lone pair orbital sizes are always larger (e.g. NH_3,) but for others, however, the bond pair ones have larger sizes. In order to investigate the "sizes" of localized charge densities

Table IV

Dispersion products obtained for localized orbitals (in (a.u.)^3)

		Bonds	
		Basis 6-31G	Basis 6-31G/d
HF	Exp.	0.304	0.297
	Calc.	0.307	0.293
H_2O	Exp.	0.401	0.400
	Calc.	0.405	0.392
NH_3	Exp.	0.555	0.541
	Calc.	0.537	0.533
CH_4	Exp.	0.748	0.723
	Calc.	0.735	0.717

		Lone pairs	
		Basis 6-31G	Basis 6-31G/d
HF	Exp.	0.246	0.248
	Calc.	0.246	0.248
H_2O	Exp.	0.397	0.405
	Calc.	0.398	0.406
NH_3	Exp.	0.653	0.688
	Calc.	0.710	0.670

we use the products of dispersions, calculated by basis sets of 6-31G and 6-31G/d. The calculations were carried out at the experimentally and at the theoretically obtained equilibrium geometries of the studied systems. The results are given in Table IV.

First it is interesting to mention that the bond pairs dispersion products are slightly larger using a basis of set (*sp*/*s*) type than by the use of (*spd*/*s*) type. The opposite result was found for lone pair orbital "sizes". Secondly, the dispersion products do not differ much from each other whether determined at the experimentally or at the calculated equilibrium geometries. This is especially valid for lone pair orbitals. It is also worthwhile to mention, however, that there are no systematic differences between the bond and lone pair orbital dispersion products. Namely, the bond pair "sizes" are larger than the lone pair ones by using 6-31G for HF and H_2O, respectively, but not for NH_3. The dispersion products of bond pair orbitals are larger than those obtained for the lone pair orbitals for the HF molecule but not for H_2O and NH_3, respectively, if a basis set of (*spd*/*s*) type was used in the calculations.

These results affirm that there is no reason to expect that the lone pair orbitals were systematically larger than the bond pair orbitals. The results, on the other hand, do not suggest that the dispersion products cannot be used as suitable quantities for characterizing localized charge densities. It should be taken into consideration, however, that the dispersion products (as second order moment derivatives) are sensitive to the basis set chosen.

It is difficult to predict, what the relative magnitudes of these quantities for different types of localized orbitals look like near the Hartree—Fock limit. It is possible to assume that they tend to be equal at the HF limit for bond and lone pair charge distribution of certain systems and/or they may also depend on the molecular system investigated.

6. Conclusion

Several moment characteristics have been discussed for three small molecules by using different basis sets. The results affirm that these quantities characterize suitably the different types of localized charge densities. The investigation of moment characteristics has shown that the bond and lone pair charge distributions have different behaviours as compared to the geometry variations. It has already been shown [9], however, that even the systematic enlargement of the basis set does not provide the experimental geometry, only the Hartree—Fock limit can be reached. Therefore if we want to know what the localized orbitals look like in (or near) the experimental geometry the extrapolation must be done very carefully. Further studies are planned in this direction. The behaviour of wavefunction near the experimental geometry should be investigated by taking into consideration the deviation from the virial theorem [10].

REFERENCES

1. E. Kapuy, C. Kozmutza, Zs. Ozoróczy and J. Pipek, Acta Phys. Hung., **46**, 333, 1979. E. Kapuy, C. Kozmutza and Zs. Ozoróczy, Acta Phys. Hung. **47**, 303, 1979..
2. H. J. Hehre, R. Dietchfield and J. A. Pople, J. Chem. Phys. **56**, 2257, 1972.
3. P. C. Hariharan and J. A. Pople, Theoret. Chim. Acta (Berl.), **28**, 213, 1973.
4. E. Kapuy, C. Kozmutza and Zs. Ozoróczy, Acta Phys. Hung. **48**, 225, 1980.
5. E. Kapuy, C. Kozmutza and M. E. Stephens, Theoret. Chim. Acta (Berl.), **43**, 175, 1976.
6. E. Kapuy, C. Kozmutza, R. Daudel and M. E. Stephens, Theoret. Chim. Acta (Berl.), **50**, 31, 1978.
6. E. Kapuy, C. Kozmutza, R. Daudel and M. E. Stephens, Theoret. Chim. Acta (Berl.), **53**, 147, 1979.
8. R. Daudel, E. Kapuy, C. Kozmutza, J. D. Goddard and I. G. Csizmadia, Chem. Phys. Letters, **44**, 197, 1976.
9. S. Bell, J. Chem. Phys., **68**, 3014, 1978.
10. E. Kapuy and F. Török, Quantum Theory of Atoms and Molecules (in Hungarian). Akadémiai Kiadó, Budapest, 1975.

Acta Physica Academiae Scientiarum Hungaricae, Tomus 48 (2—3), pp. 243—250 (1980)

ON X-RAY LUMINOSITY BY MATTER ACCRETION ON A NEUTRON STAR

By

L. BARONI

ISTITUTO DI FISICA, UNIVERSITA DI BOLOGNA, BOLOGNA, ITALY

P. L. FORTINI

ISTITUTO DI ASTRONOMIA, BOLOGNA, ITALY

C. GUALDI and G. CALLEGARI

ISTITUTO DI FISICA, UNIVERSITA DI FERRARA, FERRARA, ITALY

(Received 11. I. 1980)

When the accretion rate on a non magnetic neutron star is determined by stellar wind and not by overflowing the Roche lobe, it is shown that X-ray luminosity cannot exceed 10^{36}—10^{37} erg/sec. This very low limit is essentially set by radiation pressure which causes an effective braking on the falling matter.

1. Introduction

In a preceding paper [1] we have examined the phenomenon of accretion on single stars. Those results can also be applied to the accretion onto a neutron star in a binary system with a non collapsed companion. The various possibilities that such a system can emit X-radiation have been extensively studied by VAN DEN HEUVEL [2]. It turns out that the process can develop in two different ways:

1) The companion emits a strong stellar wind which is captured by the neutron star.

2) The companion, after filling its own Roche lobe, can transfer matter on the neutron star through the inner Lagrangian point.

In both cases radiation pressure plays a very important role in determining the X-ray luminosity of the source. So far the effects of radiation pressure have been taken into account for supercritical accretion by [3], [4], [5], [6]. These authors consider an arbitrary accretion rate which is therefore not linked to the accretion radius of the neutron star (which is supposed without a magnetic field). Such a situation can occur when mass is transferred by overflowing the Roche lobe: all the matter which crosses the inner Lagrangian point must necessarily fall on the neutron star. As a result all the matter inside

the Roche lobe of the neutron star, being optically thick, acts as a source of X radiation. The luminosity can consequently be greater than the Eddington limit (see below formula (1′)).

In the case of a stellar wind, an arbitrary rate cannot be considered any longer. In fact, beside the physical condition of the wind, one must take into account also the accretion radius and the radiation pressure. It can be no longer admitted that the gas is optically thick because of the matter density being many orders of magnitude less than in the preceding case: as matter is practically thin all radiation comes almost entirely from a very thin layer around the star surface. In this paper we shall consider this latter case and show that the braking of the falling matter caused by radiation pressure has two major effects:

1) The kinetic energy with which matter hits the star surface is less than in the case in which radiation pressure is neglected.

2) The accretion radius is diminished and the neutron star can capture a lesser part of the stellar wind.

As we shall see the overall effect of radiation pressure on accretion onto non magnetic stars of about 1 $M_\odot$ is to cause an X-ray luminosity as low as $10^{36}-10^{37}$ erg/sec.

2. The effect of radiation pressure

Let us consider a close binary system formed by a normal O—F star with mass $M \gg 1M$ and a strong stellar wind and a neutron star. The accretion is of the stellar wind type with 0.1% of the matter captured by the gravitational field of the neutron star. If the radiation pressure is sufficiently strong, matter cannot fall any longer onto the collapsed object (EDDINGTON [8]).

As far as we know it has not yet been analyzed whether this limit is effectively reached or the way and the time in which the limit is eventually attained. It is said for instance (DAVIDSON and OSTRIKER, [7]) that matter which can be accreted is that contained in a cylinder with radius

$$R_{\mathrm{acc}} = 2Gm_{\mathrm{x}}/v_{\mathrm{rel}}^2,$$

where m_x is the mass of the neutron star, v_{rel} is the stellar wind velocity relative to the neutron star, and G is the Newtonian gravitational constant. The rate of accretion is accordingly:

$$dM/dt = \pi\xi R_{\mathrm{acc}}^2 \, v_{\mathrm{rel}} \, \varrho,$$

where ϱ is the mass density of the stellar wind and ξ is a factor less than unity which takes into account radiation pressure

$$\xi \simeq [1 - 10^{-46}(L_{\mathrm{x}}/L_\odot)\,(M_\odot/m_{\mathrm{x}})]^2.$$

From this it is clear that for $m_x = 1M_\odot$, when $L_x \sim 10^{38}$ erg/sec, accretion is no longer possible.

In a strongly ionized low density plasma as the stellar wind is, the main source of opacity is Compton scattering. The force caused by radiation pressure on a free electron is:

$$Fe = \Sigma q/c,$$

where q is the flux of radiation, $\Sigma = 6.7 \times 10^{-25}$ cm^2 is the Thomson cross section, c is the speed of light. If there is equilibrium the force due to radiation pressure equals the gravitational force acting on a proton

$$Gm_x m_p/r^2 = \Sigma q/c.$$

The flux of radiation is given by

$$q = L/4\pi r^2,$$

where L is the luminosity.

So we get at equilibrium:

$$G\, m_x\, m_p/r^2 = \Sigma L/4\pi r^2 c. \tag{1}$$

From (1) one gets the "EDDINGTON luminosity"

$$L_E = 1.3\ 10^{38}\ (m_x/M_\odot)\ \text{erg/sec}. \tag{1'}$$

The net force which acts on the electron-proton system at a distance r from the star is:

$$(G\, m_x\, m_p/r^2) - (L\Sigma/4\pi r^2 c), \tag{2}$$

where m_x is the mass of the neutron star.

This is an inverse square law force which comes from the potential:

$$(Gm_x/r) - (L\Sigma/4\pi r c m_p). \tag{3}$$

We get an estimate of the accretion radius, in the case of symmetrical accretion (DAVIDSON and OSTRIKER, [7]), equating kinetic to potential energy

$$R_{\text{acc}} = (2Gm_x/v_\infty^2) - (L\Sigma/2\pi m_p\, v_\infty^2\, c), \tag{4}$$

where v_∞ is the stellar wind velocity on the orbit of the neutron star.

The rate of accreted matter is therefore

$$dM/dt = \pi v_\infty n_\infty m_p R_{\text{acc}}^2 = 4\pi n_\infty m_p/v_\infty^3 (Gm_x - L\Sigma/4\pi\ c\ m_p)^2, \tag{5}$$

where n_∞ is the number density of the stellar wind on the orbit of the neutron star.

On evaluating the internal energy of the neutron star one must recall that the interacting neutrons are only those of the tail in the Fermi distribution which have a number density given by

$$n_{\text{int}} \simeq nkT/E_F, \tag{6}$$

where n is the neutron number density, k is the Boltzmann constant and T is the temperature in °K.

From (6) we get:

$$d/dt(3Vnk^2T/E_F) = (3Vnk^2T/E_F)\,(dT/dt). \tag{7}$$

The total black-body radiation is given by:

$$\sigma T^4 4\pi R^2, \tag{8}$$

where σ is the Stefan—Boltzmann constant, R is the radius of the neutron star.

The energy withdrawn from infalling matter is

$$\Phi dM/dt\,, \tag{9}$$

where Φ is the gravitational potential at the surface of the neutron star:

$$\Phi = (Gm_x/R) - (L\Sigma/4\pi Rcm_p). \tag{10}$$

From (5), (9) and (10) one gets:

$$\Phi dM/dt = (4\pi\, n_\infty\, m_p/v_\infty^3 R)\,(Gm_x - L\Sigma/4\pi cm_p)^3. \tag{11}$$

From (7), (8) and (11) we get:

$$(3nVk^2T/E_F)\,(dT/dt) = -\sigma T^4\, 4\pi\, R^2 + (4\pi n_\infty m_p/v_\infty^3 R)\,(Gm_x - \sigma T^4 \Sigma R^2/cm_p)^3, \tag{12}$$

i.e.

$$TdT/dt = -\alpha T^{12} + \beta T^8 - \gamma T^4 + \delta, \tag{13}$$

where

$$\alpha = 4\pi n_\infty \sigma^3 \Sigma^3 R^5 E_F/3nVk^2 v_\infty^3 c^3 m_p, \tag{13a}$$

$$\beta = 4\pi n_\infty G m_x \sigma^2 \Sigma^2 R^2 E_F/nVk^2 v_\infty^3 c^2 m_p, \tag{13b}$$

$$\gamma = (4\pi R^2 \sigma E_F/3nVk^2)\,(1 + 3n_\infty G^2 m_x^2 \Sigma/v_\infty^3 cR), \tag{13c}$$

$$\delta = 4\pi n_\infty m_p G^3 m_x^3 E_F/3nVk^2 v_\infty^3 R. \tag{13d}$$

From (1) the EDDINGTON luminosity can be written as:

$$L_E = Gm_x\, m_p 4\pi c/\Sigma, \tag{14}$$

but

$$L_E = 4\pi\, R^2\, \sigma T_E^4, \tag{15}$$

where T_E is the "EDDINGTON temperature".

On substitution of (15) in (14) one gets

$$T_E^4 = Gm_x\, m_p\, c/\Sigma\sigma R^2. \tag{16}$$

Introducing the dimensionless variable y defined by

$$T = yT_E$$

one gets:

$$-ydy/dt = \alpha T_E^{10}[y^{12} - (\beta/\alpha T_E^4)\, y^8 + (\gamma/\alpha T_E^8)\, y^4 - \delta/\alpha T_E^{12}]. \tag{17}$$

From formulae (13) one easily sees that

$$\beta/\alpha T_E^4 = 3, \tag{17a}$$

$$\gamma/\alpha T_E^8 = (v_\infty^3 Rc/n_\infty \Sigma G^2\, m_x^2) + 3 = \tau + 3, \tag{17b}$$

where

$$\tau = v_\infty^3\, Rc/n_\infty \Sigma G^2\, m_x^2,$$

$$\delta/\alpha T_E^{12} = 1. \tag{17c}$$

In this way our equation takes up the simple form

$$-ydy/dt = \alpha T_E^{11}(y^{12} - 3y^8 + (\tau + 3)\, y^4 - 1). \tag{18}$$

By elementary integration one gets:

$$t = (1/\alpha T_E^{10})\left\{[A \ln\left|(y^2 + y_1^2)/(y^2 - y_1^2)\right| + \frac{C}{2}\ln\left|(y^4 - ay^2 + b)/\right.\right.$$

$$\left./(y^4 + ay^2 + b)\right| - [(2D - Ca)/\sqrt{4b - a^2}]$$

$$\left.(\text{arc tg}\,[(2y^2 - a)/\sqrt{4b - a^2}] + \text{arc tg}\,[(2y^2 + a)/\sqrt{4b - a^2}])]\right\}, \tag{19}$$

where y_1 is the real solution of the equation

$$y^{12} - 3y^8 + (\tau + 3)\, y^4 - 1 \tag{19a}$$

and

$$A = -B = 1/2y_1^2(3y_1^8 - 6y_1^4 + \tau + 3), \tag{19b}$$

$$E = -C = (2y_1^4 - 3 - b)/2ab(2y_1^8 - 3y_1^4 + b^2), \tag{19c}$$

$$F = D = (-2y_1^4 + 3)/2b(2y_1^8 - 3y_1^4 + b^2), \tag{19d}$$

$$a = \sqrt{-y_1^4 + 3 + 2\sqrt{y_1^8 + 3 - 3y^4 + \tau}} \tag{19e}$$

$$b = \sqrt{y_1^8 + 3 - 3y_1^4 + \tau}\ . \tag{19f}$$

An approximate formula derived by (19) with a development in power series is

$$t = (1/\alpha T_E^{10})\,(y^2 A/y_1^2 - 2D/b)\,y^2. \tag{20}$$

We have plotted formula (19) for various values of the stellar wind parameters and the results are reported in Figs. 1,2, 3.

We therefore arrive at the following results:

1) The limit is always less than the "EDDINGTON limit" by one or two orders of magnitude.

2) The time required to attain such limit ($\simeq 10^7$ sec) is small compared with the mean life of the system ($\simeq 10^4$ years).

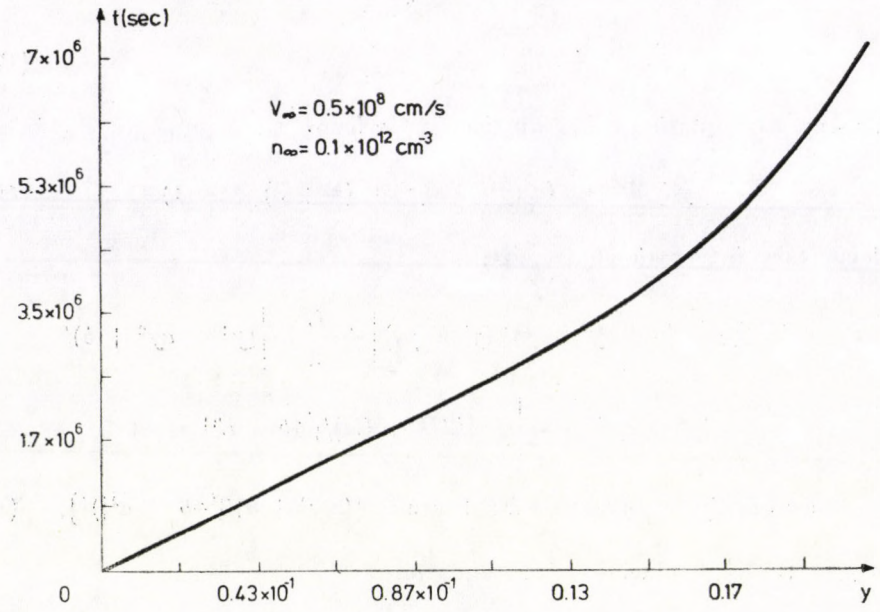

Fig. 1

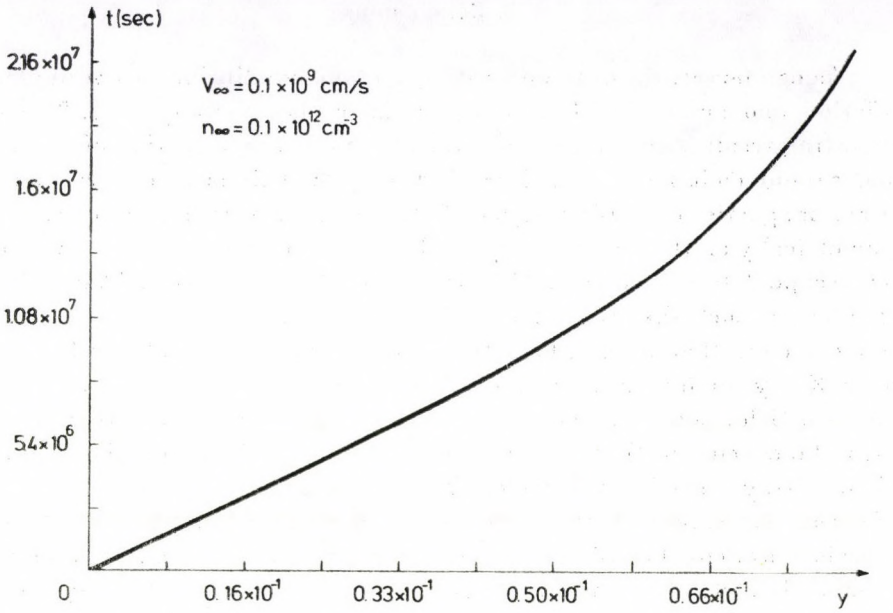
t(sec)
2.16×10^7
1.6×10^7
1.08×10^7
5.4×10^6
V∞ = 0.1 ×10^9 cm/s
n∞ = 0.1 × 10^12 cm^-3
0
0.16×10^-1
0.33×10^-1
0.50×10^-1
0.66×10^-1
y

Fig. 2

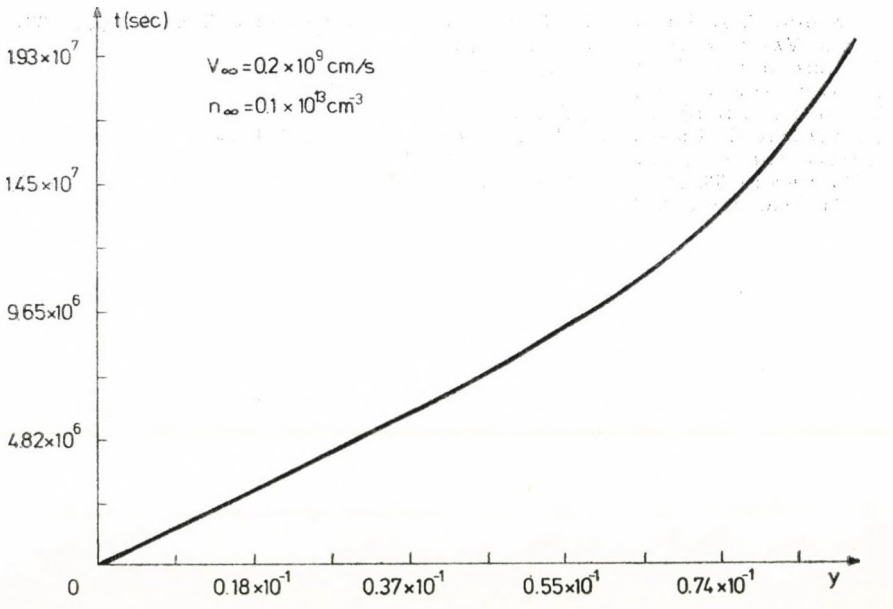
t(sec)
1.93×10^7
1.45×10^7
9.65×10^6
4.82×10^6
V∞ = 0.2 ×10^9 cm/s
n∞ = 0.1 × 10^13 cm^-3
0
0.18×10^-1
0.37×10^-1
0.55×10^-1
0.74×10^-1
y

Fig. 3

3. Conclusions

As can be seen from the preceding Section, equilibrium between emitted radiation and amount of falling matter is reached very quickly. The most interesting result is that a neutron star of 1 $M_\odot$ in any situation of the stellar wind cannot emit more than $10^{36}-10^{37}$ erg/sec. This is of course true only for non magnetic stars. If a magnetic field is present, then matter does not fall symmetrically on the star but only on the magnetic poles: radiation can therefore escape laterally without hindering the falling matter. This different behaviour is such that for a magnetic star our limit is no longer true. It is therefore clear that, even when stellar wind conditions would be favourable for an X-ray luminosity greater than 10^{37} erg/sec, if the neutron star has no magnetic field, such greater an emission cannot occur. From that one also draws the conclusion that at the same flux level on the earth, the number of pulsed X-ray binaries for which X-ray luminosity can be as great as 10^{38} erg/sec is greater than the number of non pulsed binaries for which the luminosity is less or equal to 10^{37} erg/sec. This is strongly supported by experimental evidence. In fact, of the ten or so X-binaries so far studied it is only one, viz. AM-Herculis that is not pulsating and has a luminosity of $\sim 10^{36}$ erg/sec as predicted by the present theory.

REFERENCES

1. L. Baroni, P. L. Fortini, C. Gualdi and G. Callegari, Acta Phys. Hung., **46**, 277, 1979.
2. E. P. J. Van den Heuvel, Ap. J., **198**, L109, 1975.
3. M. I. Shakura, Soviet Astr. AJ., **18**, 259, 1974.
4. J. P. Cassinelli and J. J. Castor, Ap. J. **179**, 189, 1973.
5. T. Okuda and S. Sakashita, Ap. Space Sci., **52**, 35, 1977.
6. L. Maraschi, C. Reina and A. Treves, Astr. Ap., **35**, 389, 1974
7. K. Davidson and J. Ostriker, Ap. J., **179**, 585, 1973.
8. A. Eddington, The Internal Constitution of the Stars, 1926. (reprinted Dover Publishing Co. New York, 1959).

Acta Physica Academiae Scientiarum Hungaricae, Tomus 48 (2—3), pp. 251—267 (1980)

EFFECT OF HALL CURRENT AND FINITE LARMOR RADIUS ON THE STABILITY OF A PLASMA

By

P. D. ARIEL*

DEPARTMENT OF MATHEMATICS, UNIVERSITY OF CALGARY, CALGARY, CANADA

(Received 15. I. 1980)

The simultaneous effects of finite Larmor radius and Hall current are investigated on the stability of a plasma having a one-dimensional density gradient along the direction of the static uniform magnetic field. The solution is shown to be characterized by a variational principle. Based on the existence of the variational principle, dispersion relation has been obtained for a continuously stratified plasma layer of finite depth. It has been found that the Larmor radius, though ineffective in changing the stability criterion in the absence of Hall currents stabilizes the configuration for disturbances corresponding to large wave numbers when the effects of Hall currents are also taken into consideration.

1. Introduction

The effects of finite Larmor radius (F.L.R.) which manifest in "weakly" unstable systems such as mirror machines, slowly rotating plasmas, large aspect torii etc. have been investigated on plasma instabilities by ROSENBLUTH et al [13] by considering the self-consistent solution of Maxwell's equations and the collisionless Boltzmann equations. ROBERTS and TAYLOR [12] provided an alternative approach for the study of macroscopic motion of a plasma by demonstrating that the finite Larmor radius effects can be incorporated in the form of "magnetic viscosity" by suitably modifying the pressure tensor term. JUKES [10] subsequently studied the resistive instability of a plasma supported by a planar sheared magnetic field taking into consideration the finiteness o the ion Larmor radius.

The stabilizing influence of F.L.R. on the Rayleigh—Taylor instability of two superposed fluids has been shown by SINGH and HANS [14] for horizontal orientation of the magnetic field. CHANDRASEKHAR [6] among others has pointed out that the case of exponentially varying density in the vertical direction is equally interesting and important. For this density distribution also, ARIEL and BHATIA [4, 5] have demonstrated that the F.L.R. effects stabilize the potentially unstable plasmas. However, in the case of vertical direction of magnetic field, ARIEL [3] has pointed out that the F.L.R. effects

* On leave of absence from Malaviya Regional Engineering College, Jaipur, India.

do not affect the stability criterion, for contrary to the case of horizontal magnetic field, the ion Larmor radius motion, in the present situation, is in horizontal plane and, therefore, does not displace particles of different densities.

In a low density, high temperature plasma such as interstellar matter (HI region) the finite ion Larmor frequency, appearing in the form of Hall-current term in the generalized Ohm's law, cannot be ignored (COWLING [7]). HOSKING [9] has shown that new unstable modes make appearance for infinitely conducting plasma supported on vacuum by the magnetic pressure due to a jump in the field strength at the interface. ARIEL [1, 2] has also demonstrated that for a new wave-length range, a plasma having exponentially increasing density in the upward direction is rendered unstable on account of inclusion of Hall currents.

The joint effects of F.L.R. and Hall currents on the Rayleigh—Taylor instability were first investigated by NAYYAR and TREHAN [11] who considered the stability of a plasma supported on the vacuum by a static magnetic field. In the present paper it is our aim to consider the joint effects of F.L.R. and Hall currents on the stability of a continuously stratified plasma of finite depth. The linearized perturbation equations are shown to be characterized by a variational principle. Use is made of same to obtain an approximate dispersion relation from which the stability criteria have been derived.

2. Perturbation equations

We consider a plasma configuration stratified in the vertical direction. The plasma is assumed to be incompressible and infinitely conducting. A uniform magnetic field is pervading the configuration. The linearized perturbation equations appropriate to the problem are

Momentum:

$$\varrho \frac{\partial \mathbf{u}}{\partial t} = -\nabla \cdot \ddot{\Pi} + \frac{1}{4\pi}(\nabla \times \mathbf{h}) \times \mathbf{H} + \mathbf{g}\delta\varrho. \tag{1}$$

Incompressibility:

$$\frac{\partial}{\partial t}\delta\varrho + \mathbf{u} \cdot \nabla\varrho = 0. \tag{2}$$

Continuity:

$$\nabla \cdot \mathbf{u} = 0. \tag{3}$$

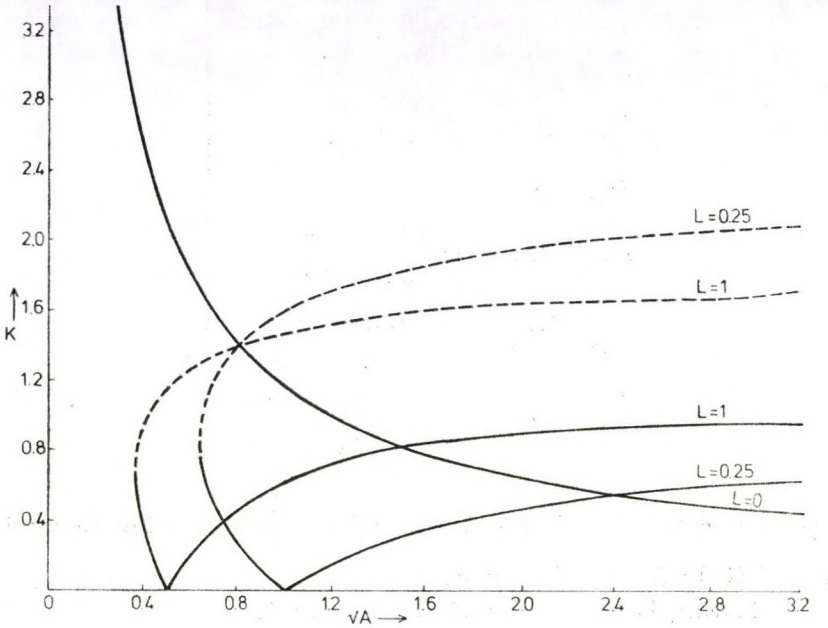

Fig. 1. Variations of k_1 and k_2 with $A^{1/2}$ for $B = 0.5$ and for various values of L. ——— correspond to k_1 and - - - - correspond to k_2.

Maxwell's equations:

$$\nabla \times \mathbf{h} = \frac{4\pi}{c}\mathbf{J}, \quad \nabla \times \mathbf{E} = -\frac{1}{c}\frac{\partial \mathbf{h}}{\partial t}, \quad \nabla \cdot \mathbf{h} = 0. \tag{4}$$

Generalized Ohm's law:

$$\mathbf{E} + \frac{1}{c}\mathbf{u} \times \mathbf{H} - \frac{1}{Nec}\mathbf{J} \times \mathbf{H} = 0, \tag{5}$$

where ϱ is the density at a point, the vectors $\mathbf{H}$ and $\mathbf{g}$ are the magnetic field and acceleration due to gravity, both directed along the vertical direction. $\delta\varrho$ and $\mathbf{h}(=h_x, h_y, h_z)$ are the perturbations in density and magnetic field consequent to a small disturbance which produces a velocity field $\mathbf{u}(= u, v, w)$. $\mathbf{E}$ is the perturbed electric field and $\mathbf{J}$ is the current density arising due to the disturbance. N, e and c denote respectively the number density of particles, electric charge per particle and the velocity of light. Following NAYYAR and TREHAN [11] the electron pressure term has been neglected in the generalized Ohm's law (5) as its magnitude is very small compared to other terms in the equation. Finally, $\delta\overleftrightarrow{\Pi}$ is the perturbation in the stress tensor $\overleftrightarrow{\Pi}$ which, after taking into consideration the effects of F.L.R., has the following components (ROBERTS and TAYLOR [12])

$$\left.\begin{aligned}
\Pi_{xx} &= p - \varrho\nu\left(\frac{\partial v}{\partial x} + \frac{\partial u}{\partial y}\right)\\
\Pi_{yy} &= p + \varrho\nu\left(\frac{\partial v}{\partial x} + \frac{\partial u}{\partial y}\right)\\
\Pi_{zz} &= p\\
\Pi_{xy} &= \Pi_{yx} = \varrho\nu\left(\frac{\partial u}{\partial x} - \frac{\partial v}{\partial y}\right)\\
\Pi_{yz} &= \Pi_{zy} = 2\varrho\nu\left(\frac{\partial w}{\partial x} + \frac{\partial u}{\partial z}\right)\\
\Pi_{zx} &= \Pi_{xz} = -2\varrho\nu\left(\frac{\partial v}{\partial z} + \frac{\partial w}{\partial y}\right)
\end{aligned}\right\}. \tag{6}$$

Here p is the scalar part of the pressure and $\nu = \frac{1}{4}a^2\Omega$, a being the ion Larmor radius and Ω the ion gyrofrequency.

Eliminating **E** and **J** from Eqs. (4) and (5), we have

$$\frac{\partial \mathbf{h}}{\partial t} = \mathbf{H}\cdot\nabla\mathbf{u} - \frac{c}{4\pi Ne}\nabla\times[(\nabla\times\mathbf{h})\times\mathbf{H}]. \tag{7}$$

Analysing in terms of normal modes, we seek solutions in which **r** and t dependence is given by

$$\exp(i\mathbf{k}\cdot\mathbf{r} + nt),$$

where $k(= k_x, k_y, 0)$ is the wave vector and n is the growth rate of disturbance.

The z-components of curl and curl curl of Eq. (1) and the z-components of Eq. (7) and its curl, on making use of Eqs. (2), (3), (4) and (6) are

$$n^2[k^2\varrho w - D(\varrho Dw)] + n\nu k^2 D(\varrho\zeta) - 2\nu n(D^2 + k^2)\,(\varrho D\zeta) + \\ + \frac{Hn}{4\pi}(D^2 - k^2)\,Dh_z - gk^2(D\varrho)\,w = 0, \tag{8}$$

$$n\varrho\zeta = -\varrho\nu k^2 Dw + 2\nu D[\varrho(D^2 + k^2)\,w] + \frac{H}{4\pi}D\xi, \tag{9}$$

$$n\xi - \frac{cH}{4\pi Ne}(D^2 - k^2)\,Dh_z = HD\zeta, \tag{10}$$

$$nh_z + \frac{cH}{4\pi Ne}D\xi = HDw, \tag{11}$$

where ζ and ξ are the vertical components of the vectors curl **u** and curl **h** given by

$$\zeta = ik_x v - ik_y u, \tag{12}$$

$$\xi = ik_x h_y - ik_y h_x,$$

and D stands for d/dz.

3. Boundary conditions

The boundary conditions in the type of problem under study are not simple and quite often assumptions are made to make the analysis tractable.

If the plasma is confined between two rigid planes, naturally, there cannot be any vertical component of velocity there, thus

$$w = 0 \text{ at a rigid boundary.} \tag{13a}$$

In addition, if the rigid planes are ideally conducting, no disturbance within the plasma can alter **E** and **H** outside. Since surface charges and surface currents can allow discontinuities in E_z, h_x and h_y only, we require

$$h_z = 0 \text{ and } E_x = E_y = 0$$

on a plane boundary adjoining a perfect conductor.

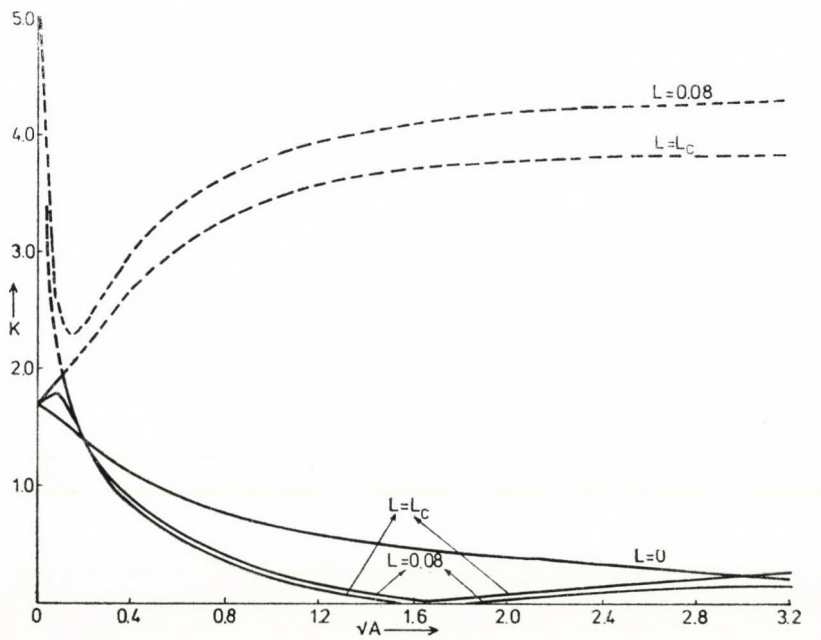

Fig. 2a. Variations of k_1 and k_2 with $A^{1/2}$ for $B = 1.35$ and for various values of L. ——— correspond to k_1 and - - - - correspond to k_2.

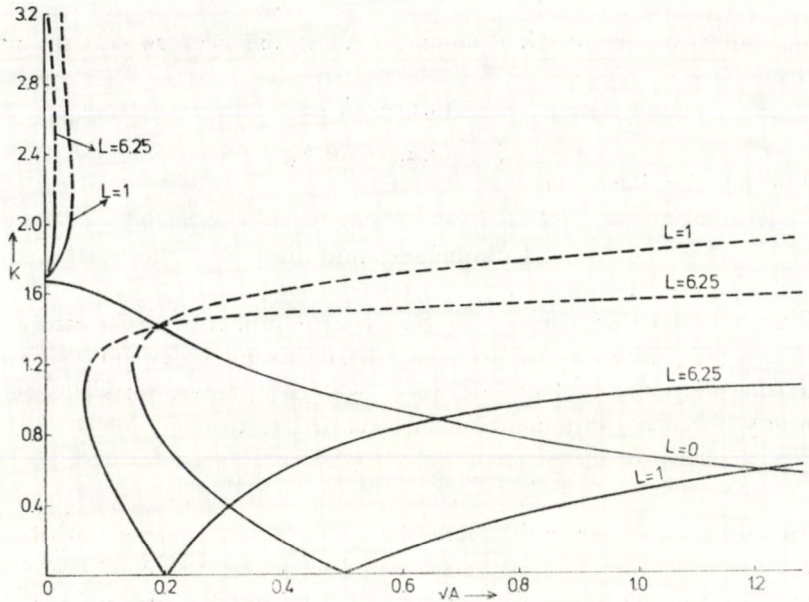

Fig. 2b. Variations of k_1 and k_2 with $A^{1/2}$ for $B = 1.35$ and for various values of L. ——— correspond to k_1 and - - - - correspond to k_2.

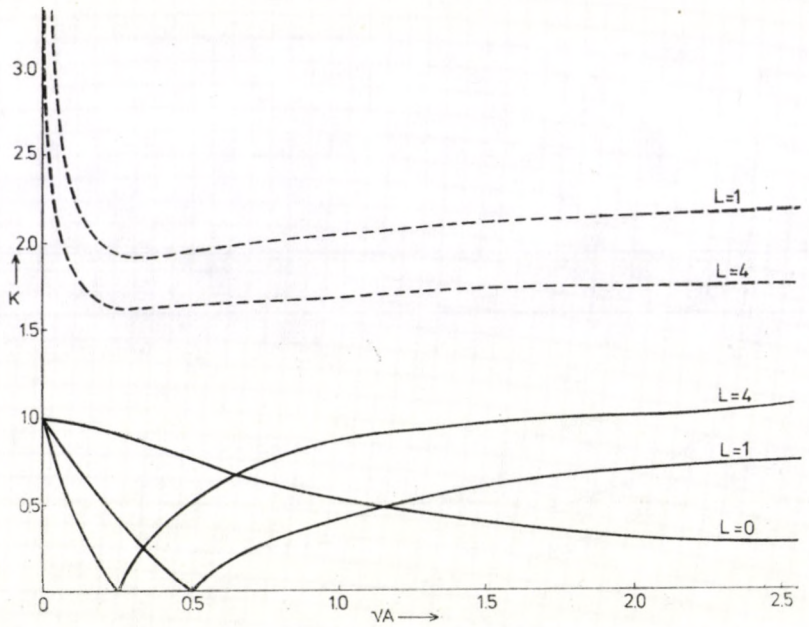

Fig. 3. Variations of k_1 and k_2 with $A^{1/2}$ for $B = 2.0$ and for various values of L. ——— correspond to k_1 and - - - correspond to k_2.

Substituting for E_x and E_y from Eq. (5), we get the following conditions

$$\frac{cH}{4\pi Ne}(D^2 - k^2)\, h_z + H\zeta = 0, \quad \frac{cH}{4\pi Ne} D\xi - HDw = 0.$$

Following HIDE [8], we place suitable restrictions on w, h_z, ζ and ξ as under

$$Dw = 0, \quad h_z = 0, \quad D^2 h_z = 0, \quad \zeta = 0 \text{ and } D\xi = 0 \tag{14}$$

on a surface bounded by an ideal conductor.

Some of the above conditions are redundant, however, they can be useful for deriving the existence of the variational principle.

On the other hand if the boundaries are free to move, we shall still forbid vertical motion at the boundaries (HIDE, [8]) and therefore take

$$w = 0 \text{ at the free boundaries.} \tag{13b}$$

Further at free boundaries there cannot be tangential stresses. Thus $-\Pi_{xz} + Hh_x/4\pi$ and $-\Pi_{yz} + Hh_y/4\pi$ must vanish at the free surfaces, thereby leading to

$$2\varrho\nu D\zeta - \frac{H}{4\pi} Dh_z = 0, \; 2\varrho\nu(D^2 + k^2)\, w + \frac{H}{4\pi}\xi = 0$$

at a free surface.

Again we find it convenient to assume

$$D^2 w = 0, \; Dh_z = 0, \; D\zeta = 0 \text{ and } \xi = 0 \tag{15}$$

at a free surface.

4. A variational principle

The non-trivial solution of Eqs. (8)—(11) under boundary conditions (13)—(15) leads to the dispersion relation. However, the task of finding this exact solution is rather too involved to be of any practical use. Hence we shall strive to find an approximate but highly simplified solution of these equations. We shall first establish that the solution is characterized by a variational principle which in turn will pave the way for the determination of an approximate solution. In the following, we shall drop the suffix z from h_z.

Multiplying the ith component of Eq. (8) by w_j and integrating across the vertical extent of the configuration (denoted by L), we obtain

$$n_i^2 \int_L \varrho(k^2 w_i w_j + Dw_i Dw_j)\, dz + n_i \int_L D(vk^2 \varrho\zeta_i)\, w_j\, dz -$$

$$- n_i \int_L 2[(D^2 + k^2)\,(\varrho D\zeta_i)]\, w_j\, dz +$$

$$+ \frac{Hn_i}{4\pi} \int_L (D^2 - k^2)\, Dh_i\, w_j\, dz - gk^2 \int_L D\varrho\, w_i\, w_j\, dz = 0, \qquad (16)$$

where the first term has been integrated by parts, the integrated part of it vanishing on account of boundary conditions (13). Throughout the subsequent integrations we shall find that the integrated parts vanish because either one of the conditions (14) or (15) is satisfied.

Integration by parts of the magnetic term in Eq. (16) gives

$$I = \frac{Hn_i}{4\pi} \int_L (D^2 - k^2)\, Dh_i\, w_j\, dz = - \frac{Hn_i}{4\pi} \int_L (D^2 - k^2)\, h_i\, Dw_j\, dz. \qquad (17)$$

Substituting for Dw_j from Eq. (11) in Eq. (17), we obtain

$$I = \frac{n_i n_j}{4\pi} \int_L (Dh_i\, Dh_j + k^2 h_i h_j)\, dz - \frac{n_i}{4\pi} \int_L (D^2 - k^2)\, h_i \frac{cH}{4\pi Ne} D\xi_j\, dz.$$

Now

$$- \frac{n_i}{4\pi} \int_L (D^2 - k^2)\, h_i \frac{cH}{4\pi Ne} D\xi_j\, dz = \frac{n_i}{4\pi} \int_L (D^2 - k^2)\, Dh_i \frac{cH}{4\pi Ne} \xi_j dz$$

which, on making use of Eq. (10), becomes

$$\frac{n_i}{4\pi} \int_L (n_i \xi_i - HD\zeta_i)\, \xi_j dz = \frac{n_i}{4\pi} \int_L (n_i \xi_i \xi_j + H\zeta_i D_j \xi)\, dz$$

and upon substituting the value of $D\xi_j$ from Eq. (9) is equal to

$$n_i \int_L \left(\frac{n_i}{4\pi} \xi_i \xi_j + n_j \varrho \zeta_i \zeta_j \right) dz - n_i \int_L D(vk^2 \varrho\zeta_i)\, w_j\, dz +$$

$$+ n_i \int_L 2v[(D^2 + k^2)\,(\varrho D\zeta_i)]\, w_j\, dz.$$

Thus, the Eq. (16) can be finally written as

$$n_i^2\left\{\int_L \varrho(Dw_i\, Dw_j + k^2 w_i w_j)\, dz + \frac{1}{4\pi}\int_L \xi_i\, \xi_j\, dz\right\} -$$

$$- gk^2\int_L D\varrho\, w_i\, w_j\, dz +$$

$$+ n_i n_j\left\{\frac{1}{4\pi}\int_L (Dh_i\, Dh_j + k^2 h_i h_j)\, dz + \int_L \varrho\zeta_i\zeta_j\, dz\right\} = 0. \tag{18}$$

We consider two solutions characterized by n and its complex conjugate n^*. Expecting the corresponding solutions also to be the complex conjugate of each other (i.e. if $w_i = w$, $w_j = w^*$ etc.), we can rewrite Eq. (18) as

$$n^2\left\{\int_L \varrho(|Dw|^2 + k^2|w|^2)\, dz + \frac{1}{4\pi}\int_L |\xi|^2\, dz\right\} =$$

$$= gk^2\int_L D\varrho|w|^2\, dz - |n|^2\left\{\frac{1}{4\pi}\int_L (|Dh|^2 + k^2|h|^2)\, dz + \int_L \varrho\,|\zeta|^2\, dz\right\}, \tag{19}$$

implying that n^2 is purely real. Thus the configuration will be stable or unstable according as $n^2 \lesseqgtr 0$.

Setting $i = j$ in Eq. (18), we find that

$$n^2(I_1 + I_3 + I_4 + I_5) - gk^2 I_2 = 0, \tag{20}$$

where

$$I_1 = \int_L \varrho[(Dw)^2 + k^2 w^2]\, dz, \tag{21}$$

$$I_2 = \int D\varrho\, w^2 dz, \tag{22}$$

$$I_3 = \frac{1}{4\pi}\int_L [(Dh)^2 + k^2 h^2]\, dz, \tag{23}$$

$$I_4 = \frac{1}{4\pi}\int_L \xi^2\, dz, \tag{24}$$

and

$$I_5 = \int_L \varrho\zeta^2\, dz. \tag{25}$$

Consider the change δn^2 in n^2 (determined from Eq. (20)), consequent upon first order arbitrary variations δw, δh, $\delta\zeta$ and $\delta\xi$ in w, h, ζ and ξ, respectively, that satisfy the boundary conditions of the problem.

We have to the first order

$$-\delta n^2(I_1 + I_3 + I_4 + I_5) = n^2(\delta I_1 + \delta I_3 + \delta I_4 + \delta I_5) - gk^2\delta I_2, \quad (26)$$

where

$$\frac{1}{2}\delta I_1 = \int_L [\varrho k^2 w - D(\varrho Dw)]\,\delta w\,dz, \quad (27)$$

$$\frac{1}{2}\delta I_2 = \int_L D\varrho\, w\delta w\,dz, \quad (28)$$

$$\frac{1}{2}\delta I_3 = -\frac{1}{4\pi}\int_L (D^2 - k^2)\,h\,\delta h\,dz, \quad (29)$$

$$\frac{1}{2}\delta I_4 = \frac{1}{4\pi}\int_L \xi\,\delta\xi\,dz, \quad (30)$$

$$\frac{1}{2}\delta I_5 = \int_L \varrho\zeta\,\delta\zeta\,dz. \quad (31)$$

The expressions of δI_1 and δI_3 given by Eq. (27) and (29) have been obtained by integration by parts, the integrated parts again vanishing in view of the assumption that δw and δh satisfy the boundary conditions (13) and (14), respectively.

Further δw, δh, $\delta\xi$ and $\delta\zeta$ are not completely arbitrary. In fact, they are connected by the relations

$$\frac{1}{2}\delta n^2\varrho\zeta + n^2\varrho\,\delta\zeta = -n\varrho\nu k^2 D\delta w + 2n\nu D[\varrho(D^2 + k^2)\,\delta w] + \frac{Hn}{4\pi}D\,\delta\xi, \quad (32)$$

$$\frac{1}{2}\delta n^2\xi + n^2\,\delta\zeta - \frac{cHn}{4\pi Ne}(D^2 - k^2)\,D\delta h = Hn\,D\delta\zeta, \quad (33)$$

and

$$\frac{1}{2}\delta n^2 h + n^2\delta h + \frac{cHn}{4\pi Ne}D\delta\xi = Hn\,D\delta w. \quad (34)$$

Substituting the values of δI's from Eqs. (27)—(31) in Eq. (26) we obtain after making use of Eqs. (9)—(11) and (32)—(34) and performing a series of integrations by parts

$$-\delta n^2(I_1 + I_4) = 2\int_L \Big\{n^2[k^2\varrho w - D(\varrho Dw)] + n\nu k^2 D(\varrho\zeta) -$$

$$- 2\nu n(D^2 + k^2)(\varrho D\zeta) + \frac{Hn}{4\pi}(D^2 - k^2)\,Dh - gk^2(D\varrho)\,w\Big\}\,\delta w\,dz. \quad (35)$$

We observe that the quantity occurring as the factor of δw in equation (35) vanishes if Eq. (8) is satisfied. Thus a necessary and sufficient condition that δn^2 be zero to the first order for arbitrary variations δw, δh etc. connected by relations (9)—(11) and compatible with the boundary conditions, is that w, h etc. satisfy the characteristic value problem. Hence for the problem under consideration, namely for any ϱ and **H** directed parallel to the direction of gravity, a variational procedure for obtaining an approximate solution exists even when the effects of F.L.R. and Hall currents are taken into consideration.

5. A continuously stratified plasma of finite depth

In this Section we shall make use of the variational principle to obtain an approximate solution for the case of a continuously stratified plasma confined between two free boundaries $z = 0$ and $z = d$ in which the undisturbed density distribution is given by

$$\varrho = \varrho_0 \exp \beta z, \tag{36}$$

where ϱ_0 and β are constants. It may be recalled here that free boundaries are perhaps more relevant for the problem under consideration. (See e.g. SPIEGEL, [15]).

Further, for the sake of mathematical simplicity in the ensuing analysis we shall assume

$$|\beta d| \ll 1 \tag{37}$$

which merely implies that the density difference between two points of different layers is a good deal less than the average density of the configuration.

Consistent with the boundary conditions (13)—(15), we choose the following trial functions for w etc.

$$w(z) = W \sin lz, \quad \zeta(z) = Z \cos lz,$$

$$h(z) = K \cos lz, \quad \xi(z) = X \sin lz, \tag{38}$$

where W, Z, K and X are constants.

To ensure that the boundary conditions at the upper boundary $z = d$ are also satisfied, we require

$$l = \frac{\pi s}{d} \tag{39}$$

s being any integer.

Substituting for $w(z)$, $\zeta(z)$, $h(z)$ and $\xi(z)$ in Eqs. (9)—(11) and consistently making use of Eq. (37), we obtain

$$\begin{aligned} nZ - vl(k^2 - 2l^2)\, W &= \frac{Hl}{4\pi\varrho_0} X, \\ nX - \frac{cHl}{4\pi Ne}(l^2 + k^2)\, K &= -HlZ, \\ nK + \frac{cHl}{4\pi Ne} X &= HlW. \end{aligned} \tag{40}$$

Evaluating the integrals contained in Eq. (20) after substituting the assumed values of w etc. and eliminating the constants W, Z, K and X with the help of Eq. (40), we obtain the following dispersion relation

$$\begin{aligned} &n^4 + n^2\left[2l^2V^2 + \frac{v^2(k^2 - 2l^2)^2 - g\beta k^2}{l^2 + k^2} + \left(\frac{cHl}{4\pi Ne}\right)^2 (l^2 + k^2)\right] + \\ &+ \left[l^2V^2 + vl(k^2 - 2l^2)\frac{cHl}{4\pi Ne}\right]^2 - \frac{g\beta k^2}{l^2 + k^2} l^2V^2 - \left(\frac{cHl}{4\pi Ne}\right)^2 g\beta k^2 = 0, \end{aligned} \tag{41}$$

where $V = (H^2/4\pi\varrho_0)^{1/2}$ is the Alfvén velocity in the medium.

We shall find it convenient to treat Eq. (41) in the non-dimensional form. Measuring n and k in terms of $(\pi sV/d)$ $\sec^{-1}$ and $(\pi s/d)$ cm^{-1}, the Eq. (41) takes the form

$$\begin{aligned} &n^4 + n^2\left[2 + \frac{L(k^2 - 2)^2 - Bk^2}{1 + k^2} + A(1 + k)^2\right] + \\ &+ [1 + \sqrt{LA}\,(k^2 - 2)]^2 - \frac{Bk^2}{1 + k^2} - ABk^2 = 0, \end{aligned} \tag{42}$$

where

$$L = \frac{v^2\pi^2 s^2}{V^2 d^2}, \tag{43}$$

$$A = \left(\frac{cH}{4\pi Ne}\right)^2 \frac{\pi^2 s^2}{V^2 d^2} \tag{44}$$

and

$$B = \frac{g\beta d^2}{\pi^2 s^2 V^2} \tag{45}$$

are the suitable dimensionless parameters of magnetic viscosity, Hall currents and buoyancy forces in terms of magnetic field. The two parameters A and B were first introduced by ARIEL [1] and HIDE [8], respectively.

6. Discussion

Stable stratification: It can be seen from Eq. (42) that if B is negative i.e. if the stratification is potentially stable, it remains so, whether or not we take into account the effects of F.L.R. and Hall currents, separately or jointly, for the two values of n^2 given by Eq. (42) are negative.

Unstable stratification: Before discussing the general case in detail, in which the joint effects of F.L.R. and Hall currents are considered, we shall briefly study the special cases in which each effect is considered separately.

6.1. *Special case* a) $A = 0$

When Hall effect is ignored, Eq. (42) reduces to the following dispersion relation obtained by ARIEL [3] for non-rotating configuration:

$$n^4 + n^2\left[2 + \frac{L(k^2-2)^2 - Bk^2}{1+k^2}\right] + 1 - \frac{Bk^2}{1+k^2} = 0. \tag{46}$$

For the stability of the system, we require the absolute term of Eq. (46) to be positive. This occurs if k, the wave number of disturbance, is less than a critical value k_* given by

$$k_* = (B-1)^{-\frac{1}{2}}. \tag{47}$$

Instability takes place for $k > k_*$.

Clearly k_* is independent of L, the measure of F.L.R. effects and is precisely the same as derived by HIDE [8] for the classical problem of Rayleigh-Taylor instability in hydromagnetics. Hence the stability criterion in the absence of Hall currents does not depend on the finiteness of the Larmor radius of the ions.

6.2. *Special case* b) $L = 0$

When the F.L.R. effects are not taken into consideration, Eq. (42) takes the following form

$$n^4 + n^2\left[2 - \frac{Bk^2}{1+k^2} + A(1+k^2)\right] + 1 - \frac{Bk^2}{1+k^2} - ABk^2 = 0. \tag{48}$$

Eq. (48) is identical with the corresponding dispersion relation obtained by ARIEL [2] who has shown that the system is rendered unstable for $k > k^*$, where

$$k^* = 2^{\frac{1}{2}}\{[(B-1+AB)^2 + 4AB]^{\frac{1}{2}} + B - 1 + AB\}^{-\frac{1}{2}}. \tag{49}$$

It can be easily verified that k_* is greater than k^*. Thus the wave-number band $k^* < k < k_*$ which was otherwise stable is destabilized when the effects of Hall currents are included.

6.3. *General case.* $A \neq 0, L \neq 0$

We now take into account the joint effects of F.L.R. and Hall currents. The necessary and sufficient condition for the stability of the system is that the absolute term of Eq. (42) be positive i.e.

$$f(K) \equiv a_0 K^3 + a_1 K^2 + a_2 K + a_3 > 0, \tag{50}$$

where

$$\left.\begin{aligned} K &= k^2 \\ a_0 &= LA \\ a_1 &= 2(LA)^{\frac{1}{2}} - 3LA - AB \\ a_2 &= 1 - 2(LA)^{\frac{1}{2}} - B - AB \\ a_3 &= [1 - 2(LA)^{\frac{1}{2}}]^2. \end{aligned}\right\} . \tag{51}$$

Eq. $f(K) = 0$ possesses at least one real negative root say $-K_3$ $(K_3 > 0)$, therefore one can write

$$f(K) = (a_0 K^2 + b_1 K + b_2)(K + K_3), \tag{52}$$

where b_1 and b_2 are appropriate functions of L, A and B.

Since the linear factor of $f(K)$ is positive definite, the sign of $f(K)$ depends on that of the quadratic factor. This factor will also be positive for all values of K if the roots of the corresponding quadratic equation, or equivalently, two of the roots of the cubic $f(K) = 0$ are complex conjugate. Now the cubic $f(K) = 0$ has all real and unequal roots or a pair of complex conjugate roots according as

$$F(A, L, B) = \frac{4}{27}\left(\frac{1}{3}a_1^2 - a_0 a_2\right)^3 - \left(a_0^2 a_3 - \frac{1}{3}a_0 a_1 a_2 + \frac{2}{27}a_1^3\right)^2 \gtrless 0. \tag{53}$$

It can be seen that the equation $F(A, L, B) = 0$ has at the most two positive roots of A say A_1 and $A_2 (A_1 < A_2)$. For $A = A_1$ and $A = A_2$, equation $f(K) = 0$ gives a pair of equal roots. It can be further verified that $F(A, L, B) < 0$ for $A_1 < A < A_2$ implying that in this range of A, $f(K)$ is positive for all values of K. Hence the stratification remains stable for $A_1 < A < A_2$ for any disturbance, provided that the values of A_1 and A_2 are real and positive.

When A lies outside the range (A_1, A_2), $F(A, L, B)$ is positive, and therefore in this case the quadratic factor can be further split into two linear factors. Thus we can write

$$f(K) = a_0(K - K_1)(K - K_2)(K + K_3). \tag{54}$$

The two quantities K_1 and K_2 will obviously have the same sign, since a_0 and a_3 also have the same sign. In case K_1 and K_2 are positive, we have

$$f(k^2) = a_0(k^2 - k_1^2)(k^2 - k_2^2)(k^2 + k_3^2), \tag{55}$$

where $K_i = k_i^2 (i = 1, 2, 3)$.

From Eq. (55) we note that if k lies between k_1 and k_2 the sign of $f(k^2)$ is negative and therefore the stratification is rendered unstable for the wave-number band $k_1 < k < k_2$. However, either if $k < k_1$ or $k > k_2$, the sign of $f(k^2)$ is positive, thereby implying the stability of the stratification. We thus observe that when the effects of F.L.R. and Hall currents are considered simultaneously, there are two possible wave number ranges, $k < k_1$ (short wave-number range) and $k > k_2$ (large wave-number range) for which the stratification is stabilized. In contrast, when the effects of F.L.R. and Hall currents are considered separately, there is only one possible stabilized wave-number range $k < k_*$ or k^* (short wave-number range). Hence we conclude that the joint effects of F.L.R. and Hall currents stabilize the disturbances corresponding to the large wave numbers.

In diagrams 1, 2 and 3, the real positive roots of $f(k^2) = 0$ are plotted against $A^{\frac{1}{2}}$. The stability regions are confined between the curves $k = k_1$ and $k = k_2$. We must distinguish between the following ranges of the values of B. (i) $B < 1$ (ii) $1 < B < 3/2$ (iii) $B > 3/2$. We shall now treat each of these cases in detail.

(i) $B < 1$. In the absence of Hall currents ($A = 0$), the configuration represented by $B < 1$ is completely stabilized for any disturbance, because the effects of magnetic field are sufficient to overcome those of gravity. However, the presence of Hall currents tends to loosen the stabilizing influence of the magnetic field. In fact, when the F.L.R. effects are ignored, there is always a wave-number range $k < k^*$ for which the system is rendered unstable, no matter what amount of Hall current is present. When the F.L.R. effects are also included, the wave-number range for which the configuration is stabilized depends, in general, on the value of A.

For $A < A_1$ it can be shown that the two quantities K_1 and K_2 in (54) are both negative, therefore $f(k^2)$ is positive for all values of k. Thus, for a small amount of Hall current ($A < A_1$) the stratification which was unstable for some disturbances in the absence of magnetic viscosity is completely stabilized.

For a moderate value of Hall current ($A_1 < A < A_2$) similar conclusions hold, as has already been pointed out earlier. However, for a large value of $A(A > A_2)$ both K_1 and K_2 are positive, therefore in this case there will be two regions of stability $k < k_1$ and $k > k_2$. We note that, whereas the former region is only modified due to the interaction of F.L.R. effects and Hall currents, the latter region comes into existence because of the same. As a matter of fact, no amount of Hall current can destabilize the large wave-number band

$$k > \left\{\frac{B + 4L + (B^2 + 8BL)^{\frac{1}{2}}}{2L}\right\}^{\frac{1}{2}}. \tag{56}$$

(ii) $1 < B < 3/2$. For $B > 1$, the system is not stabilized for all disturbances in the absence of Hall currents — the wave-number range $k < k_*$ being unstable. This range is further spread on inclusion of Hall effects when $L = 0$. Inclusion of F.L.R. effects sets up two stability regions corresponding to the short and long wave numbers. The nature of these regions will depend on the values of L separated by a critical value L_c given by

$$L_c = \frac{(B-1)^2}{4(3-2B)}. \tag{57}$$

If $L < L_c$, there are no real positive values of A given by the equation $F(A, L, B) = 0$, however, the values of K_1 and K_2 in (54) are both positive for all values of A. Thus, in this case one can conclude that for any amount of Hall current, there are always two stability regions $k < k_1$ and $k > k_2$. It can be further noted that the wave-number band

$$k_a < k < k_b, \tag{58}$$

where

$$k_{a,b} = \left\{\frac{4L + B - 1 \mp [(B-1)^2 - 4L(3-2B)]^{\frac{1}{2}}}{2L}\right\}^{\frac{1}{2}} \tag{59}$$

remains unstable for any value of A. Any other disturbance can be stabilized if the right amount of Hall current is present.

If $L > L_c$, the Eq. $F(A, L, B) = 0$ admits two positive roots of A, A_1 and A_2. Unlike the case $B < 1$, for $A < A_1$ the two quantities K_1 and K_2 in (54) will be now positive. Thus except for moderate values of $A(A_1 < A < A_2)$ there will be always two stability regions. It is interesting to note that for moderate values of A and large values of $L(L > L_c)$ the system can be thoroughly stabilized even when $B > 1$.

(iii) $B > 3/2$. In this case there is no distinction in the nature of stability regions for any value of L, because for no value of L, $F(A, L, B) = 0$ admits real positive values of A. The quantities K_1 and K_2 again remain positive. Thus for this case too, two stability regions exist. For no values of A and L, can it be noted that the region is thoroughly stabilized. Further the wave-number band defined by relation (58) remains unstable for any value of A.

Acknowledgement

Financial assistance of the National Research Council of Canada is gratefully acknowledged.

REFERENCES

1. P. D. ARIEL, J. Plasma Phys., **4**, 523, 1970.
2. P. D. ARIEL, Aust. J. Phys., **23**, 595, 1970.
3. P. D. ARIEL, Nuovo Cimento, **6B**, 124, 1971.
4. P. D. ARIEL and P. K. BHATIA, Can. J. Phys., **47**, 2235, 1969.
5. P. D. ARIEL and P. K. BHATIA, Nucl. Fusion, **10**, 141, 1970.
6. S. CHANDRASEKHAR, Hydrodynamic and Hydromagnetic Stability p. 456, Clarendon Press, 1961.
7. T. G. COWLING, Magnetohydrodynamics, Interscience Tracts on Physics and Astronomy, Interscience Publishers, New York, 1957.
8. R. HIDE, Proc. Roy. Soc. (London), **A 233**, 376, 1955.
9. R. J. HOSKING, Phys. Rev. Letters, **15**, 244, 1965.
10. J. D. JUKES, Phys. Fluids, **7**, 52, 1966.
11. N. K. NAYYAR and S. K. TREHAN, J. Plasma Phys., **4**, 563.
12. K. V. ROBERTS and J. B. TAYLOR, Phys. Rev. Letters, **8**, 197, 1962.
13. M. N. ROSENBLUTH, N. A. KRALL and N. ROSTOKER, Nucl. Fusion Suppl. Pt. **1**, 143, 1962.
14. S. SINGH and H. K. HANS, Nucl. Fusion, **6**, 6, 1966.
15. E. A. SPIEGEL, Astrophys. J., **141**, 1068, 1965.

Acta Physica Academiae Scientiarum Hungaricae, Tomus 48 (2—3), pp. 269—279 (1980)

MAGNETO-THERMOHALINE CONVECTION THROUGH POROUS MEDIUM

By

R. C. SHARMA and K. N. SHARMA

DEPARTMENT OF MATHEMATICS, HIMACHAL PRADESH UNIVERSITY, SIMLA-171005, INDIA

(Received 16. I. 1980)

The thermohaline convection in a layer of conducting fluid heated from below and subjected to a stable salinity gradient through porous medium is considered to include the effect of a uniform magnetic field. The salinity gradient and magnetic field are found to introduce oscillatory modes which were nonexistent in their absence. The medium permeability is found to have destabilizing effect on the system. The Rayleigh number is found to increase with the increase in stable salinity gradient as well as magnetic field parameters. The case of overstability is studied wherein the sufficient conditions for nonexistence of overstability are also found.

1. Introduction

The problem of thermohaline convection in a layer of fluid heated from below and subjected to a stable salinity gradient was investigated by VERONIS [5]. NIELD [3] considered the thermohaline convection in a horizontal layer of viscous fluid heated from below and salted from above.

There has been considerable interest in recent years in the study of the breakdown of the stability of a layer of fluid subject to a vertical temperature gradient in a porous medium and the possibility of convective flow. The stability of flow of a single component fluid through a porous medium taking into account the Darcy resistance has been studied by LAPWOOD [2] and WOODING [6]. The effect of the earth's magnetic field on the stability of such a flow is of interest in geophysics particularly in the study of the earth's core where the earth's mantle, which consists of conducting fluid, behaves like a porous medium which can become convectively unstable as a result of differential diffusion. Another application of the results of flow through a porous medium in the presence of a magnetic field lies in the study of the stability of a convective flow in the geothermal region. The problem of stability of a two component conducting fluid layer in the presence of magnetic field through a porous medium and subjected to a temperature gradient is of importance in geophysics, soil sciences and ground water hydrology etc. Conditions under which convective motions through porous medium are important in geophysics are usually far removed from the consideration of a single component fluid and rigid boundaries and therefore it is desirable to consider a two component fluid and free boundaries. In the case of a two component fluid buoyancy forces

can arise not only from density differences due to variations in temperature but also from those due to variations in solute concentrations. RUDRAIAH and PRABHAMANI [4] have studied the effect of thermal diffusion on the convective stability of a two component fluid in a porous medium.

In the present paper we study the thermohaline convection in a layer of conducting fluid heated and salted from below through porous medium in the presence of a uniform vertical magnetic field.

2. Perturbation equations

A layer of fluid of thickness d flowing through porous medium is heated from below so that the temperatures and salinities at the bottom surface $z = 0$ are T_0 and C_0 and at the upper surface $z = d$ are T_1 and C_1, respectively, z-axis being taken as vertical. A uniform vertical magnetic field $\mathbf{H}(0, 0, H)$ is embedded in the fluid and the boundaries are taken to be free as well as perfect conductors of both heat and salt. Then the equations governing the motion of a fluid flowing through a porous medium and following Boussinesq approximation are

$$\frac{\partial \mathbf{q}}{\partial t} + (\mathbf{q} \cdot \nabla)\,\mathbf{q} = -\frac{1}{\varrho_0}\nabla p - \frac{\nu}{k_1}\mathbf{q} + \left(1 + \frac{\delta\varrho}{\varrho_0}\right)\mathbf{g} + \frac{1}{4\pi\varrho_0}(\nabla \times \mathbf{H}) \times \mathbf{H}, \tag{1}$$

$$\nabla \cdot \mathbf{q} = 0, \tag{2}$$

$$\frac{\partial T}{\partial t} + (\mathbf{q} \cdot \nabla)\,T = \varkappa \nabla^2 T, \tag{3}$$

$$\frac{\partial C}{\partial t} + (\mathbf{q} \cdot \nabla)\,C = \varkappa' \nabla^2 C, \tag{4}$$

$$\nabla \cdot \mathbf{H} = 0, \tag{5}$$

$$\frac{\partial \mathbf{H}}{\partial t} = (\mathbf{H} \cdot \nabla)\,\mathbf{q} + \eta \nabla^2 \mathbf{H}, \tag{6}$$

where

$$\varrho = \varrho_0[1 - \alpha(T - T_0) + \alpha'(C - C_0)]. \tag{7}$$

Eqs. (1)—(4) express the conservation of momentum, mass, heat and solute. In writing Eqs. (1) and (2), use has been made of the Boussinesq approximation, i.e. density changes are disregarded in all terms except when they occur with gravity forces. Eqs. (5) and (6) express the Maxwell's equations. The equation of state (7) contains a thermal coefficient of expansion α and an analogous solvent coefficient α'. The suffix zero refers to values at the reference

level $z = 0$. We use Cartesian coordinates with the z-axis vertically upwards so that the porous medium lies between $z = 0$ and $z = d$. $\mathbf{q}(u, v, w)$, $\mathbf{g}(0, 0, -g)$ $\mathbf{H}(0, 0\ H)$, k_1, ϱ, p, T and C stand for velocity, gravitational acceleration, magnetic field, permeability of the medium (which has the dimension of length squared), density, pressure, temperature and solute mass concentration, respectively. The kinematic viscosity ν, the thermal diffusivity $\varkappa$, the solute diffusivity $\varkappa'$ and the electrical resistivity η are all assumed to be constant.

The steady state solution is

$$\mathbf{q} = 0,\ T = T_0 - \beta z,\ C = C_0 - \beta' z,\ \varrho = \varrho_0(1 + \alpha\beta z - \alpha'\beta' z), \tag{8}$$

where $\beta = \dfrac{T_0 - T_1}{d}$ and $\beta' = \dfrac{C_0 - C_1}{d}$ are the magnitudes of uniform temperature and concentration gradients. β and β' are both positive as the temperature and concentration decrease upwards.

We now consider a small perturbation on the steady state solution and let θ, γ, δp, $\mathbf{q}$, $\mathbf{h}$ and $\delta\varrho$ denote the perturbations in temperature, concentration, pressure, velocity, magnetic field and density, respectively, so that the change in density $\delta\varrho$, caused by the perturbations θ and γ in temperature and concentrations, is given by

$$\delta\varrho = -\varrho_0(\alpha\theta - \alpha'\gamma). \tag{9}$$

Then Eqs. (1)–(6) on linearization give

$$\frac{\partial \mathbf{q}}{\partial t} = -\frac{1}{\varrho_0}\nabla\delta p - \frac{\nu}{k_1}\mathbf{q} - \mathbf{g}(\alpha\theta - \alpha'\gamma) + \frac{1}{4\pi\varrho_0}(\nabla\times\mathbf{h})\times\mathbf{H}, \tag{10}$$

$$\nabla\cdot\mathbf{q} = 0, \tag{11}$$

$$\frac{\partial\theta}{\partial t} = \beta w + \varkappa\nabla^2\theta, \tag{12}$$

$$\frac{\partial\gamma}{\partial t} = \beta' w + \varkappa'\nabla^2\gamma, \tag{13}$$

$$\nabla\cdot\mathbf{h} = 0, \tag{14}$$

$$\frac{\partial\mathbf{h}}{\partial t} = (\mathbf{H}\cdot\nabla)\,\mathbf{q} + \eta\nabla^2\mathbf{h}. \tag{15}$$

We consider the case in which both the boundaries are free and the medium adjoining the fluid is a perfect conductor. The appropriate boundary conditions on velocity are $w = 0$ and $\dfrac{\partial^2 w}{\partial z^2} = 0$. If the temperature and concentration at a boundary are kept fixed, then there $\theta = \gamma = 0$. Also, the

medium adjoining the perfect conductor fluid, $\frac{\partial h_z}{\partial z} = 0$. Thus the boundary conditions appropriate to the problem are

$$w = \frac{\partial^2 w}{\partial z^2} = \theta = \gamma = \frac{\partial h_z}{\partial z} = 0 \quad \text{at} \quad z = 0 \text{ and } z = d. \tag{16}$$

Eqs. (10)—(15) give

$$\left(\frac{\partial}{\partial t} + \frac{\nu}{k_1}\right) \nabla^2 w - g\left(\frac{\partial^2}{\partial x^2} + \frac{\partial^2}{\partial y^2}\right)(\alpha\theta - \alpha'\gamma) - \frac{H}{4\pi\varrho_0} \nabla^2 \left(\frac{\partial hz}{\partial z}\right) = 0, \tag{17}$$

$$\left(\frac{\partial}{\partial t} - \varkappa \nabla^2\right) \theta = \beta w, \tag{18}$$

$$\left(\frac{\partial}{\partial t} - \chi' \nabla^2\right) \gamma = \beta' w, \tag{19}$$

$$\left(\frac{\partial}{\partial t} - \eta \nabla^2\right) h_z = H \frac{\partial w}{\partial z}. \tag{20}$$

3. Dispersion relation and discussion

Analyzing the disturbances into normal modes, we assume that the perturbation quantities are of the form

$$[w, \theta, \gamma, h_z] = [W(z), \Theta(z), \Gamma(z), K(z)] \exp(ik_x x + ik_y y + nt), \tag{21}$$

where k_x, k_y are horizontal wave numbers of the harmonic disturbance, $k^2 = k_x^2 + k_y^2$ and n is the growth rate which is, in general, a complex constant. Putting $a = kd$, $\sigma = \frac{nd^2}{\nu}$, $x|d = x^*$, $y|d = y^*$, $z|d = z^*$ and $D = d|dz^*$; Eqs.(17)—(20) in nondimensional form, using expression (21), become

$$\left(\sigma + \frac{1}{p_l}\right)(D^2 - a^2) W + \frac{gd^2}{\nu} a^2(\alpha\Theta - \alpha'\Gamma) - \frac{Hd}{4\pi\varrho_0\nu}(D^2 - a^2)\, DK = 0, \tag{22}$$

$$(D^2 - a^2 - p_1\sigma)\, \Theta = -\left(\frac{\beta d^2}{\varkappa}\right) W, \tag{23}$$

$$(D^2 - a^2 - q\sigma)\, \Gamma = -\left(\frac{\beta' d^2}{\varkappa'}\right) W, \tag{24}$$

$$(D^2 - a^2 - p_2\sigma)\, K = -\left(\frac{Hd}{\eta}\right) DW, \tag{25}$$

where $p_l = \frac{k_1}{d^2}$ is the dimensionless permeability, $p_1 = \frac{\nu}{\varkappa}$ is the Prandtl number, $p_2 = \frac{\nu}{n}$ is the magnetic Prandtl number and $q = \frac{\nu}{\varkappa'}$ is the Schmidt number. Operating Eq. (22) by $(D^2 - a^2 - p_1\sigma)(D^2 - a^2 - p_2\sigma)(D^2 - a^2 - q\sigma)$ and using (23)—(25), thus eliminating Θ, Γ and K, we obtain

$$\begin{aligned} Ra^2(D^2 - a^2 - p_2\sigma)\,(D^2 - a^2 - q\sigma)W = \left(\sigma + \frac{1}{p\eta}\right)(D^2 - a^2) \times \\ (D^2 - a^2 - p_1\sigma)\,(D^2 - a^2 - p_2\sigma)\,(D^2 - a^2 - q\sigma)W + \\ + Sa^2(D^2 - a^2 - p_1\sigma)\,(D^2 - a^2 - p_2\sigma)\,W \\ + Q(D^2 - a^2)\,(D^2 - a^2 - p_1\sigma)\,(D^2 - a^2 - q\sigma)\,D^2W, \end{aligned} \tag{26}$$

where $R = g\alpha\beta d^4/\nu\varkappa$ is the thermal Rayleigh number, $S = g\alpha'\beta' d^4/\nu\varkappa'$ is the analogous solute Rayleigh number and $Q = H^2d^2/4\pi\varrho_0\nu\eta$ is the Chandrasekhar number.

The boundary conditions appropriate for the problem are

$$W = D^2W = \Theta = \Gamma = DK = 0 \text{ at } z^* = 0 \text{ and } z^* = 1. \tag{27}$$

Dropping the stars for convenience and using (27), we can show that all the even order derivatives of W must vanish for $z = 0$ and $z = 1$ and hence the proper solution of Eq. (26) characterizing the lowest mode is

$$W = A \sin \pi z, \tag{28}$$

where A is a constant.

Substituting (28) in Eq. (26) and letting $x = a^2/\pi^2$, $P = \pi^2 p_l$, $R_1 = R/\pi^4$, $S_1 = S/\pi^4$, $Q_1 = Q/\pi^2$, we obtain the dispersion relation

$$\begin{aligned} R_1 = \frac{\left(\frac{\sigma}{\pi^2} + \frac{1}{P}\right)(1 + x)\left(1 + x + p_1\frac{\sigma}{\pi^2}\right)}{x} + S_1\frac{\left(1 + x + p_1\frac{\sigma}{\pi^2}\right)}{\left(1 + x + q\frac{\sigma}{\pi^2}\right)} \\ + Q_1\frac{(1 + x)\left(1 + x + p_1\frac{\sigma}{\pi^2}\right)}{x\left(1 + x + p_2\frac{\sigma}{\pi^2}\right)}. \end{aligned} \tag{29}$$

4. The oscillatory modes

In this Section, we examine the possibility of oscillatory modes, if any, on the stability problem due to the presence of salinity gradient and magnetic field. Multiplying Eq. (22) by W^*, the complex conjugate of W, integrating over the range of z, and making use of Eqs. (23)—(25) together with boundary conditions (27) we obtain

$$\left(\sigma+\frac{1}{p_l}\right) I_1+\frac{g\alpha'\varkappa' a^2}{\nu\beta'}(I_4+q\sigma^* I_5)+\frac{\eta}{4\pi\varrho_0\nu}(I_6+p_2\varrho^* I_7)=$$

$$=\frac{g\alpha\varkappa a^2}{\nu\beta}(I_2+p_1\sigma^* I_3), \tag{30}$$

where

$$\begin{aligned}
I_1 &= \int_0^1 (|DW|^2+a^2|W|^2)\,dz,\\
I_2 &= \int_0^1 (|D\Theta|^2+a^2|\Theta|^2)\,dz,\\
I_3 &= \int_0^1 |\Theta|^2\,dz,\\
I_4 &= \int_0^1 (|D\Gamma|^2+a^2|\Gamma|^2)\,dz,\\
I_5 &= \int_0^1 (|\Gamma|^2)\,dz,\\
I_6 &= \int_0^1 (|D^2K|^2+2a^2|DK|^2+a^4|K|^2)\,dz,\\
I_7 &= \int_0^1 (|DK|^2+a^2|K|^2)\,dz
\end{aligned} \tag{31}$$

which are all positive definite.

Substituting $\sigma=\sigma_r+i\sigma_i$ and then equating real and imaginary parts of Eq. (30), we obtain

$$\sigma_r\left[I_1+\frac{g\alpha'\varkappa' a^2}{\nu\beta'}qI_7+\frac{\eta}{4\pi\varrho_0\nu}p_2I_5-\frac{g\alpha\varkappa a^2}{\nu\beta}p_1I_3\right]=$$

$$=-\left[\frac{1}{p_l}I_1+\frac{g\,\alpha'\varkappa' a^2}{\nu\beta'}I_4-\frac{g\alpha\varkappa a^2}{\nu\beta}I_2+\frac{\eta}{4\pi\varrho_0\nu}I_6\right], \tag{32}$$

and

$$\sigma_i\left[I_1-\frac{g\alpha'\varkappa' a^2}{\nu\beta'}qI_5+\frac{g\alpha\varkappa a^2}{\nu\beta}p_1I_3-\frac{\eta}{4\pi\varrho_0\nu}p_2I_7\right]=0. \tag{33}$$

Eq. (33) yields that $\sigma_i = 0$ or $\sigma_i \neq 0$, which means that the modes may be nonoscillatory or oscillatory. In the absence of stable salinity gradient and magnetic field, Eq. (33) reduces to

$$\sigma_i \left[I_1 + \frac{g\alpha\varkappa a^2}{\nu\beta} p_1 I_3 \right] = 0 \tag{34}$$

and the terms in brackets are positive definite. Thus $\sigma_i = 0$, which means that oscillatory modes are not allowed and the principle of exchange of stabilities is satisfied (CHANDRASEKHAR [1], p. 26) in the absence of stable salinity gradient and magnetic field. This result is true for the porous as well as nonporous (CHANDRASEKHAR [1]) medium. The presence of each, the stable salinity gradient and the magnetic field, brings overstable oscillations (as σ_i may not be zero) which were nonexistent in their absence. Eq. (32) simply tells that σ_r may be positive as well as negative, i.e. there may be stability as well as instability in the presence of salinity gradient, magnetic field and porous medium which is also true in their absence.

5. The stationary convection

For the stationary convection, $\sigma = 0$ and Eq. (29) reduces to

$$R_1 = \frac{(1+x)^2}{xP} + \left(\frac{1+x}{x} \right) Q_1 + S_1. \tag{35}$$

To study the effects of salinity gradient, magnetic field and permeability of the medium on R_1, we examine the natures of $dR_1|dS_1$, $dR_1|dQ_1$, and $dR_1|dP$.

It follows from Eq. (35) that

$$\frac{dR_1}{dP} = -\frac{(1+x)^2}{xP^2}, \tag{36}$$

which is always negative. The medium permeability therefore has destablizing effect on the system. Eq. (35) yields

$$\frac{dR_1}{dS_1} = +1, \tag{37}$$

which is positive. This means that a stable salinity gradient (salted from below) has a stabilizing effect on the systems. If the system is heated from below

but salted from above (adverse concentration gradient), i.e. S_1 is negative, $dR_1|dS_1$ is negative which means that the adverse salinity gradient has a destabilizing effect on the system.

Eq. (35) also yields

$$\frac{dR_1}{dQ_1} = \frac{1+x}{x}, \tag{38}$$

which is positive. So the magnetic field has a stabilizing effect on the system.

The critical value of R_1, denoted by R_{1c} for the onset of instability, given by $dR_1|dx = 0$, is attained at the value of x given by

$$x = \sqrt{1 + PQ_1}. \tag{39}$$

Thus χ is independent of S_1 but depends on P and Q_1. Substituting this value of χ in (35) gives the critical Rayleigh number

$$R_{1C} = \frac{1}{P}[1 + \sqrt{1 + PQ_1}]^2 + S_1. \tag{40}$$

When $Q_1 = 0$ and $S_1 = 0$ (corresponding to hydrodynamic and absence of concentration gradient case), this reduces to LAPWOOD's [2] value

$$R_C = \frac{4\pi^2}{p_l}. \tag{41}$$

From (40) and (41) it is re-affirmed that the critical Rayleigh number increases with the increase in Q_1 (magnetic field parameter) and S_1 (stable concentration gradient parameter).

6. The overstable case

In this Section we consider the possibility of whether instability may occur as an overstability. Put $\sigma/\pi^2 = i\sigma_1$, it being remembered that σ may be complex. Since for overstability, we wish to determine the critical Rayleigh number for the onset of instability via a state of pure oscillations, it suffices to find conditions for which (29) will admit of solutions with σ_1 real. Eq. (29) becomes

$$R_1 = \frac{\left(i\sigma_1 + \frac{1}{P}\right)(1+x)(1+x+ip_1\sigma_1)}{x} + S_1\frac{(1+x+ip_1\sigma_1)}{(1+x+iq\sigma_1)} + \\ + Q_1\frac{(1+x)(1+x+ip_1\sigma_1)}{x(1+x+ip_2\sigma_1)}. \tag{42}$$

It follows from Eq. (42) that

$$\frac{dR_1}{dQ_1}=\left(\frac{1+x}{x}\right)\frac{1+x+ip_1\sigma_1}{1+x+ip_2\sigma_1}=\left(\frac{1+x}{x}\right)\frac{(1+x)^2+p_1p_2\sigma_1^2+i\sigma_1(1+x)(p_1-p_2)}{(1+x)^2+p_2^2\sigma_1^2}. \tag{43}$$

Equating real and imaginary parts of Eq. (43), we obtain

$$\frac{dR_1}{dQ_1}=\left(\frac{1+x}{x}\right)\frac{(1+x)^2+p_1p_2\sigma_1^2}{(1+x)^2+p_2^2\sigma_1^2} \tag{44}$$

and

$$p_1=p_2, \tag{45}$$

Substituting (45) in (44), we get

$$\frac{dR_1}{dQ_1}=\frac{1+x}{x}. \tag{46}$$

which is always positive. The magnetic field therefore has stabilizing effect on the system.

Eq. (42) yields

$$\frac{dR_1}{dS_1}=\frac{1+x+ip_1\sigma_1}{1+x+iq\sigma_1}=\frac{(1+x)^2+p_1q\sigma_1^2+i\sigma_1(1+x)(p_1-q)}{(1+x)^2+q^2\sigma_1^2}. \tag{47}$$

Equating real and imaginary parts of Eq. (47) and substituting $p_1=q$, the result of equating imaginary parts, in the result of equating real parts, we obtain

$$\frac{dR_1}{dS_1}=1, \tag{48}$$

which is positive. The stable salinity gradient therefore has stabilizing effect on the system.

It also follows from Eq. (42) that

$$\frac{dR_1}{dP}=-\frac{(1+x)(1+x+ip_1\sigma_1)}{xP^2}. \tag{49}$$

Equating real parts of Eq. (49), we get

$$\frac{dR_1}{dP}=-\frac{(1+x)^2}{x^2P}, \tag{50}$$

which is always negative. The permeabiliy of the medium has, therefore, destablizing effect on the system.

The real and imaginary parts of Eq. (42), when equated, give

$$R_1 x\{(1+x)^2 - p_2 q\sigma_1^2\} = S_1 x\{(1+x)^2 - p_1 p_2 \sigma_1^2\} + Q_1(1+x)^2 \times$$

$$\times\{(1+x)^2 - p_1 q\sigma_1^2\} + \frac{(1+x)^2}{P}[(1+x)^2 - p_1 p_2 \sigma_1^2 - q(p_1+p_2)\,\sigma_1^2]$$

$$- \sigma_1^2[q\{(1+x)^2 - p_1 p_2 \sigma_1^2\} + (1+x)^2(p_1+p_2)]\,(1+x), \tag{51}$$

and

$$R_1 x(p_2+q) = S_1 x(p_1+p_2) + Q_1(1+x)(p_1+q)$$

$$+ \frac{1}{P}[q\{(1+x)^2 - p_1 p_2 \sigma_1^2\} + (1+x)^2(p_1+p_2)]$$

$$+ (1+x)\,[(1+x)^2 - p_1 p_2 \sigma_1^2 - q(p_1+p_2)\,\sigma_1^2] \tag{52}$$

Eliminating R_1 between Eqs. (51) and (52), we obtain

$$p_2^2 q^2 \left(\frac{p_1}{P} + b\right) c^2 + \left[S_1(b-1)\,(p_1-q)\,p_2^2 + Q_1 q^2 b(p_1-p_2) + \right.$$

$$+ b^2\left(b + \frac{p_1}{P}\right)(p_2^2 + q^2)\Big] c + \Big[S_1 b^2(b-1)\,(p_1-q) +$$

$$\left. + Q_1 b^3(p_1-p_2) + b^4\left(b + \frac{p_1}{P}\right)\right] = 0, \tag{53}$$

where $1 + x = b$ and $\sigma_1^2 = c$. As σ_1 is real for overstability, the two values of c (or σ_1^2) are positive. Eq. (53) is quadratic in c and does not involve any of its roots to be positive if

$$p_1 > p_2 \text{ and } p_1 > q, \tag{54}$$

for then the coefficients of c^2, c and the constant term are all positive and there is no change of sign in Eq. (53).

(54) imply

$$\varkappa < \varkappa' \text{ and } \varkappa < \eta. \tag{55}$$

Thus if $\varkappa < \varkappa'$ and $\varkappa < \eta$ are satisfied, overstability is impossible and the principle of exchange of stabilities holds good. $\varkappa < \varkappa'$ and $\varkappa < \eta$ are, therefore, the sufficient conditions for the nonexistence of overstability, the violation of which does not necessarily involve occurrence of overstability.

In the absence of salinity gradient, the sufficient condition for nonexistence of overstability reduces to $\varkappa < \eta$ (CHANDRASEKHAR [1]), but the introduction of salinity gradient introduces an additional sufficient condition $\varkappa < \varkappa'$.

REFERENCES

1. S. CHANDRASEKHAR, Hydrodynamic and Hydromagnetic Stability, Oxford University Press, 1961.
2. E. R. LAPWOOD, Proc. Camb. Phil. Soc., **44**, 508, 1948.
3. D. A. NIELD, J. Fluid Mech., **29**, 545, 1967.
4. N. RUDRAIAH and P. R. PRABHAMANI, 5th International Heat Transfer Conference at Keidanrenkaikan Building, Tokyo, Sept. 3—Sept. 7, 79, 1974.
5. G. VERONIS, J. Marine Res., **23**, 1, 1965.
6. R. A. WOODING, J. Fluid Mech., **9**, 183, 1960.

Acta Physica Academiae Scientiarum Hungaricae, Tomus 48 (2—3), pp. 281—291 (1980)

DYNAMICAL ASPECTS OF THE FORMATION OF THE MESOMORPHIC STATE STRUCTURE

By

V. K. PERSHIN, VL. K. PERSHIN and L. A. FISHBEIN

URAL POLYTECHNICAL INSTITUTE, SVERDLOVSK, USSR

(Received in revised form 16. I. 1980)

In terms of the self-consistent phonon field method generalized with regard to the orientational degrees of freedom the dynamics of the formation of the mesomorphic state structure at the activation of the molecular crystal oscillations is studied. The reasons for the existence and for the stability of the partially ordered media with liquid-crystalline and plastic packing of the molecules are substantiated. The dependencies of the dynamical crystal characteristics versus temperature are calculated. From the analysis of the librational and translational anharmonicities evolution at the temperature alteration the energetic relations for the transition of the molecular crystal into the mesostate are established. It is shown that the anharmonic processes bound-up with different degrees of the molecules freedom give an essentially unequal contribution to the development of the dynamical instability of the system. The mutual correlation between the structural instability type, the molecular crystalline anisotropy coefficient and the molecular interaction anisotropy factor are investigated. The behaviour of the critical values as functions of the system anisotropy parameters is considered. Conclusions are drawn regarding the crystal lattice disarrangement in the pretransitional regions of liquid-crystalline and plastic mesogeneity.

1. Introduction

From the microscopic point of view phase transitions in ordered structures arise as a result of the instability of the collective particles excitations [1—3]. The detailed microscopic picture of the phase transition may be obtained on the basis of the analysis of the systems dynamics only [4—6].

The present paper is devoted to the development of the dynamical approach to the problem of the thermotropic mesomorphic state formation [7—11]. Due to the complexity of the molecular structure, packing, interaction and the steric effects, however, it is not possible to build up the successive theory of the molecular systems dynamics. Therefore for the establishment of the structural instability mechanisms and for their detailed investigation the elaboration of simple models is of a great importance. According to [7, 8] we shall consider a quasi-onedimensional molecular crystal whose particles have translational degrees of freedom along some direction in the space and perform angular oscillations in the perpendicular planes. For clearing up the role of the various types of the molecules movement in the structural instability origin and for the determination of the critical parameters of the molecular crystal in the high temperature limit it is necessary to undertake an analysis of the

self-consistent dynamical equations system which is obtained in [7] at the approximation of the nearest neighbours interaction:

$$kT/2 = x\Phi/4, \tag{1}$$

$$kT/2 = y^*R/4, \tag{2}$$

where $\langle \ldots \rangle$ is the statistical averaging; $\Phi = 2\partial^2\tilde{\Psi}/\partial\varphi^2$; $R = 2\partial^2\tilde{\Psi}/\partial l^2$ are pseudoharmonic lattice force constants; $\tilde{\Psi}(l, \varphi) = \langle \Psi(r, \psi) \rangle$ is the self-consistent interaction pair potential; T is the absolute temperature; k is the Boltzmann's constant; $x = \langle(\varphi_{j+1} - \varphi_j)^2\rangle$, $y^* = \langle(u_{j+1} - u_j)^2\rangle$ are the correlation functions of the relative librational and translational oscillations of the neighbouring molecules in the crystal; φ_j, u_j are the Heisenberg's operators of the displacement of the j-particle from its equilibrium state. In the left parts of the Eqs. (1) and (2) there are averaged kinetic energies related to a degree of freedom of the molecule, and the right parts are the virials of its translational and librational movement in the self-consistent field of the crystal. The Eqs. (1), (2) are true for the equilibrium molecular coordinates (l_0, φ_0) which are determined from the conditions

$$\partial\tilde{\Psi}/\partial l = 0, \quad \partial\tilde{\Psi}/\partial\varphi = 0. \tag{3}$$

The system of the Eqs. (1)—(3) allows to investigate the evolution of the molecular crystal state at the temperature alteration up to the stability limit.

2. Dynamical criteria for the type of the structural instability

The solutions of the system (1)—(3) correspond to the temperature range of the crystal state stability which is described in the developed approach only. The upper limit of this range T_c, is determined as the temperature of the dynamical instability of the lattice with respect to the propagation of the collective oscillations.

The mathematical analysis shows [10, 11] that when the librational and translational lattice sub-systems do not influence each other the system (1)—(3) disintegrates into two independent equations. Since in this trivial case the molecular lattice stability is lost over one of the degrees of freedom only we can judge unambiguously the character of the packing of the partially ordered phase. In the general case of bounded oscillating sub-systems the two parameters x and y^* become complex simultaneously beyond the instability point, T_c. It means that the crystal had lost its stability over both degrees of freedom of molecules reaching the same temperature point. Assuming the last statement only one cannot establish the type of the molecular ordering in the range

$T > T_c$. In this connection it should be noted that the whole complex of the phenomena which genetically determine the possible aggregation forms of the molecules beyond the instability point is created just in the crystalline state. Hence, if the crystalline state is described qualitatively correctly by the system of equations (1)—(3), it is possible on the basis of its investigation to establish the packing of the molecules in the new phase without any extra physical considerations.

The temperature of the dynamical instability, T_c, corresponds to the relative extremum of any of the virials of the molecular movement [9]. Then for the determination of the critical parameters (x_c, y_c^*, T_c) and assuming that the equilibrium angle φ_0 does not depend on temperature the system (1)—(3) should be added by the coupling equation [11] which is obtained by means of the Langrangian indeterminate factors method

$$(\Phi + x\partial\Phi/\partial x)\,(R + y^*\,\partial R/\partial y^*) = xy^* \cdot \partial R/\partial x \cdot \partial\Phi/\partial y^*.$$

In physical sense this means that though the loss of the lattice stability takes place over both molecular degrees of freedom simultaneously but at finite and nonzero librational ε_L- and translational ε_T-coupling energies at the critical point

$$\varepsilon_L(T_c) = x_{c_1}\Phi(x_{c_1}, y_c^*, l_{c_1})/4 - kT_c/2, \tag{4}$$

$$\varepsilon_T(T_c) = y_{c_2}^* R(x_c, y_{c_2}^*, l_{c_2})/4 - kT_c/2. \tag{5}$$

Parameters (x_{c_1}, l_{c_1}) and $(y_{c_2}^*, l_{c_2})$ are the solutions of the following systems of equations, respectively

$$\begin{cases} y^* = y_c^*, & \partial\widetilde{\Psi}/\partial l = 0, \\ (\Phi + x\partial\Phi/\partial x)\,\partial^2\widetilde{\Psi}/\partial l^2 & = x \cdot \partial\Phi/\partial l \cdot \partial^2\widetilde{\Psi}/\partial l\partial x, \end{cases} \tag{6}$$

$$\begin{cases} x = x_c, & \partial\widetilde{\Psi}/\partial l = 0, \\ (R + y^*\partial R/\partial y^*)\,\partial^2\widetilde{\Psi}/\partial l^2 = y^* \cdot \partial R/\partial l \cdot \partial^2\widetilde{\Psi}/\partial l\partial y^*. \end{cases} \tag{7}$$

The systems of equations (6), (7) and their roots have not any physical sense and are used as auxiliary ones in the calculation of coupling energies. The geometric interpretation of (6), (7) is that the intersections extremes of the translational and librational virials by the critical planes $x = x_c$, $y^* = y_c^*$ are approached at the points (x_{c_1}, l_{c_1}) and $(y_{c_2}^*, l_{c_2})$. Having obtained the values ε_L, ε_T one can write down the dynamical conditions of the realization of the various types of the structural transformations:

Crystal — liquid crystal (Cr—LC)

$$\varepsilon_L/\varepsilon_T \gg 1 \tag{8}$$

Crystal — plastic crystal (Cr—PC)

$$\varepsilon_L/\varepsilon_T \ll 1 \tag{9}$$

Crystal — disordered state (Cr—DS)

$$\varepsilon_L/\varepsilon_T \sim 1. \tag{10}$$

The relations (8)—(10) reflect the principle of the genetic coupling of the old and the new phase structures.

3. Self-consistent system of dynamical equations

The detailed study of the behaviour of the molecular crystal at the temperature variation is possible in the case only, if the intermolecular interaction potential Ψ is given. For the simplicity of calculation we shall introduce it in the additive pair interaction form [12, 13]

$$\Psi(r, \varphi) = \Psi_1(r) + \Psi_2(r, \varphi), \tag{11}$$

where r is the distance between the inertia centres of the molecules, φ is the mutual rotation angle of their long axes. Below we shall suppose that the function $\Psi_1(r)$ is introduced in the form of the Morse potential [4]

$$\Psi_1(r) = \varepsilon\{\exp[-2\alpha(r - r_0)] - 2\exp[-\alpha(r - r_0)]\}, \tag{12}$$

for which the conditions are realized $\partial\Psi_1(r_0)/\partial r = 0$, $\Psi_1(r_0) = -\varepsilon$. Besides we shall assume that the angular part of the interaction is given by the expression [14]

$$\Psi_2(r, \varphi) = -\eta \exp[-(r/a)^2] \cos 2\varphi, \tag{13}$$

where $\eta > 0$ is the dispersional interaction parameter; a is the quantity of order of the characteristic size of the molecule.

Calculating the self-consistent potential $\widetilde{\Psi}(l, \varphi)$ and the interaction constants, R, Φ we can write the system (1)—(3) in the form

$$t/2 = 2xQ/D, \tag{14}$$

$$t/2 = y\{d^2 \exp(-d^2 y)\ (2V^2 - V) + Q(1 - L/k^2 ND\}, \tag{15}$$

$$L = DNk^2 d \exp(-d^2 y)\ (V^2 - V)/Q, \tag{16}$$

$$\varphi_0 = 0.$$

Here the following designations are assumed:

$t = kT/\varepsilon$ is the relative temperature;

$k = a/r_0$ is the molecular crystalline anisotropy parameter;

$D = \varepsilon/\eta$ is the intermolecular interaction anisotropy parameter;

$L = l_0/r_0$ is the relative distance between the inertia centres of nearest molecules.

$$d = \alpha r_0,\ N = 1 + 2y/k^2,\ y = y^*/r_0^2,$$

$$Q = \exp\,(L^2/k^2N - 2x)\,N^{-1/2},\ V = \exp\,[-d(L-1) + 3d^2y/2].$$

The systems of equations (6) and (7) for the potential (12)—(14) are not shown here because of their complexity.

Now we can calculate the instability temperature with corresponding values of librational and translational coupling energies.

$$t_c = 4x_C Q_C/D, \tag{17}$$

$$\varepsilon_T/\varepsilon = y_{c_2}\{d^2 \exp\,(-d^2 y_{c_2})\,(2V_{c_2}^2 - V_{c_2}) + \\ + \exp\,[2(x_{c_2} - x_c)]\,Q_{c_2}(1 - L_{c_2}/k^2N_{c_2})/k^2N_{c_2}D\} - t_c/2, \tag{18}$$

$$\varepsilon_L/\varepsilon = 2x_{c_1}Q_{c_1}(N_{c_1}/N_c)^{1/2} \exp\,[(L_{c_1}/k)^2\,(1/N_{c_1} - 1/N_c)] - t_c/2. \tag{19}$$

Indices c, c_1 and c_2 mean that designated functions in (17)—(19) are calculated in critical (x_c, y_c) and auxiliary (x_{c_1}, L_{c_1}) (y_{c_2}, L_{c_2}) points, respectively.

4. Calculation techniques

The quantitative analysis of the contributions of the various types of the molecular movements into the origin of the instability of the crystalline state was carried out with the help of the computer. The expressions (14)—(16) are the system of three equations closed about the dynamical characteristics of the molecular crystal x, y, L. The latter are functions of the relative temperature, t, and depend also on the variables d, D, k as the parameters of the problem. Since $d \sim 6 \div 16$ [15, 4], then in all calculations the quantity d was fixed and arbitrarily assumed to be equal to 8. In each calculation cycle the relative temperature was assumed as an independent variable and the anisotropy parameters were assumed to be constant. With increasing t for $D, k = \text{const}$ the solutions $x(t)$, $y(t)$, $L(t)$ were determined by means of the method of successive approximations where for the initial values of y, L the known ones for the atomic crystal [16] were chosen. The system (14)—(16) had no roots while t reached some critical value t_c. The upper limit of the region of determination of the functions $x(t)$, $y(t)$, $L(t)$ was accepted as the system instability point. The critical values were calculated by the use of the expressions $x_c = x(t_c)$, $y_c = y(T_c)$, $L_c = L(t_c)$. The calculation was repeated with the

other fixed values of parameters k, D. We ought to note that since the relative temperature $t = kT/\varepsilon$ was changed independently and $d = \alpha r_0 = 8$ it was unobviously meant ε, $r_0 = \text{const}$. Hence, practically, the dynamical variables were determined as function of T at the different η- and α-values.

5. Results and discussion

Proceeding from (17)—(19) the dependences of the temperature, t_c, of the dynamical instability (Fig. 1a), of the virials $V_T = (\varepsilon_T/\varepsilon + t_c)$ and $V_L = (\varepsilon_L/\varepsilon + t_c)$ (Fig. 1b), of the ratio of the orientational and translational coupl-

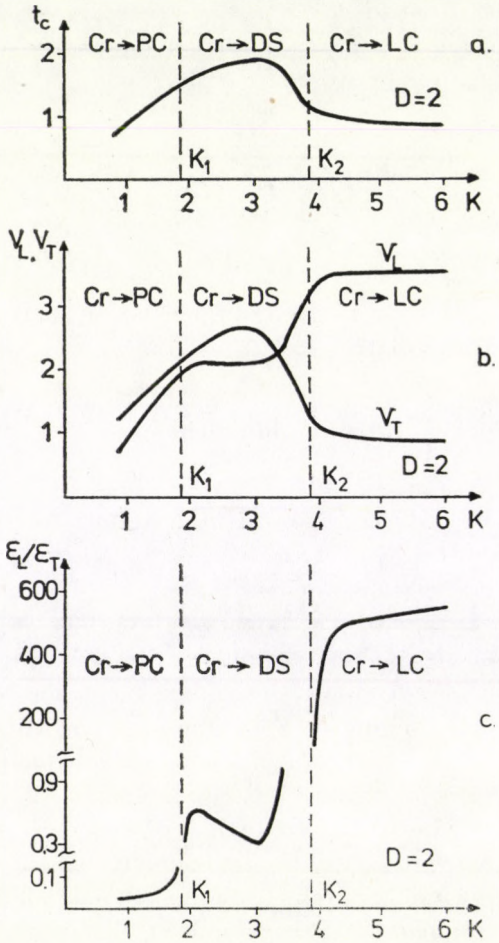

Fig. 1. Change of the dynamical instability temperature t_c (Fig. 1a) of the librational, V_L, and translational, V_T, virials (Fig. 1b) and of the ratio $\varepsilon_L/\varepsilon_T$ of the librational to the translational coupling energy at the critical point (Fig. 1c) versus the molecular crystalline anisotropy factor, k at $D = 2$

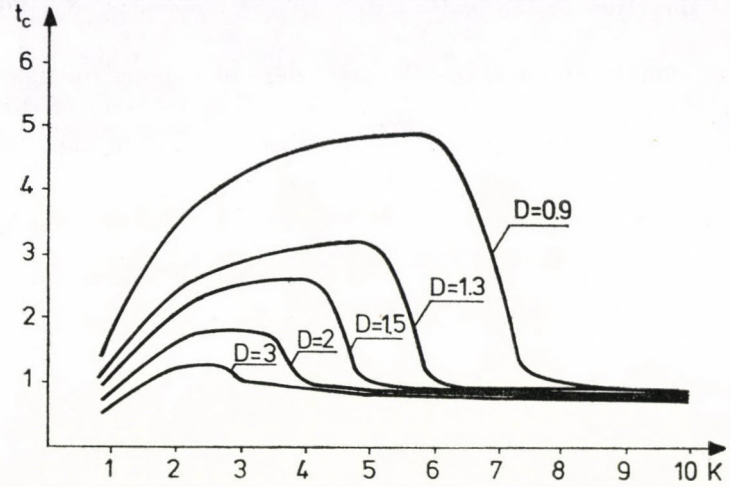

Fig. 2. Dependencies of the instability temperature, t_c, versus molecular-crystalline anisotropy factor, k, at different coefficients of the intermolecular interaction anisotropy D

ing energies $\varepsilon_L/\varepsilon_T$ (Fig. 1c) versus the anisotropy factor k at $D = 2$ are shown in Fig. 1. The dependencies $t_c(k)$, $V_T(k)$, $V_L(k)$ which are of interest in itself are supplementary at the construction of the function $\varepsilon_L(k)/\varepsilon_T(k)$. According to (8)—(10) the last ratio allows to identify the phase transition type. Actually in Fig. 1b one can distinguish three ranges of values of the anisotropy factor k with its own type of the instability of the crystalline state. In the range $0 < k < k_1$ the transformation Cr—PC occurs. The molecular system turns into the disordered state when the k-values satisfy the inequality $k_1 < k < k_2$. At $k > k_2$ transition into the liquid-crystalline state takes place ($\varepsilon_L/\varepsilon_T \gg 1$).

The curves shown in Fig. 2 reflect the alteration of the relative temperature of the dynamical instability with the increase of k at different values of the interaction anisotropy factor D. The analysis shows that at the increase of the anisotropy factor k the function t_c (k; D = const) rises in the range of the transition Cr—PC. It reaches the maximum value in the range of the structural re-arrangement Cr—DS and then decreases monotonously in the interval of the Cr—LC transformation. The qualitative interpretation of such a behaviour of $t_c(k)$ on the basis of the analysis of the curves $V_L(k)$ and $V_T(k)$ is given in [17]. In this connection we ought to note only that for any value of D there is always the interval $\delta k = |k_2 - k_1|$ whose reaching in the absence of external stresses does not give the possibility for the formation of a mesophase from the crystalline state in principle. Because of the bulky calculations we did not determine the boundary values of k_1 and k_2 at which the conditions of the transition Cr—DS became feasible. From the general considerations, however, one can infer that with increasing of D the values of k_1 and k_2 are transfer-

red in the direction of the lower values of the molecular crystalline anisotropy factors.

On the basis of the analysis of the dependencies $x_c(k)$, $y_c(k)$ and $L_c(k)$ shown in Fig. 3 one can draw conclusions on the character of the molecular mobility at different types of the structural instability of the molecular crystals. So, the raising of k results in a sharp increase of the orientational and in an insignificant decrease of the translational order in the range of the transition Cr—PC. The extreme values of the functions $x_c(k)$ and $y_c(k)$ in the interval $k_1 < k < k_2$ show that the largest disarrangement over both types of the molecules movement occurs in the region of the transition P—DS. At $k \approx k_2$ the orientational and the translational disarrangement decreases. In comparison with the transformation Dr—PC the transition into the liquid-crystalline state occurs at the significant stabilization of the orientational molecular movement and at the more developed translational oscillations. Contrary to it, the rotational type instability arises while the system approaches the strong orientational disorder in the pre-transitional state. We ought to note that the behaviour of the averaged distances between the inertia centres of the nearest molecules (Fig. 3c) is determined by the translational anharmonicities of the oscillations of molecules almost completely.

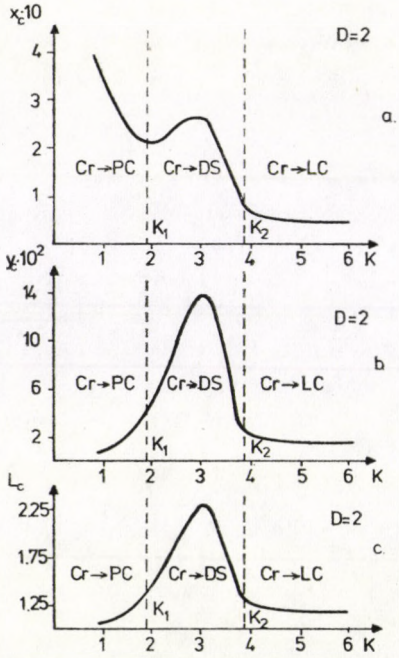

Fig. 3. Curves of the critical molecular crystal parameters x_c, y_c (Fig. 3a, b) and of the averaged distance, L_c, between the nearest neighbours at the instability point (Fig. 3c) in the regions of formation of the mesomorphic and disordered states

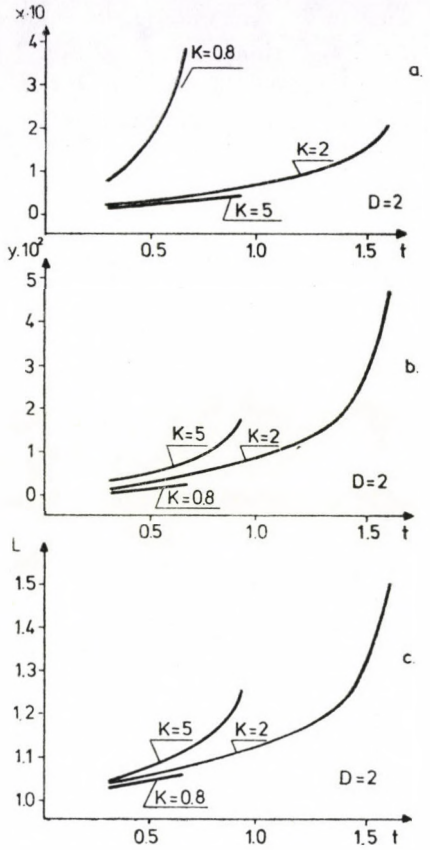

Fig. 4. Temperature dependencies of the dynamical lattice characteristics $x(t)$ (Fig. 4a), $y(t)$ (Fig. 4b), $L(t)$ (Fig. 4c) at $D = 2$ and at three values of $k = 0.8; 2; 5$

In Fig. 4 the results of the calculation of the dependencies $x(t)$, $y(t)$ and $L(t)$ for three anisotropy factor values $k = 0.8; 2; 5$ are presented. The latter ones correspond to the structural transitions Cr—PD, Cr—DS, Cr—LS, respectively. All the investigated dynamical variables change linearly in the range $T \ll T_c$ independently of the k-value. At the approach to T_c such a behaviour of the parameters x, y and L changes essentially and depends on the nature of the structural instability of the system. Actually the unlinear increase of the function $x(t)$ bound-up with the orientational molecules movement is observed in the range of the transition Cr—PC. Two other dependences change almost linearly up to the phase transition point. In contrast to this, at the transformation Cr—LC the direction of the temperature evolution of the crystalline state occurs in the way of the preferential development of the anharmonicity of the translational molecular oscillations. The latter is expressed in the unlinear behaviour of $y(t)$ and $L(t)$ in the pre-transitional state. In this

case x changes proportional to T almost along the whole range of the existence of the crystalline state. All functions shown in Fig. 4 change with essential unlinearity with the temperature in the pre-transitional transformation region if the phase transition of Cr—DS-type occurs in the system. Such a behaviour of the physical parameters is stipulated by the absence of the anisotropy in the temperature development of the translational and librational anharmonicities of the molecular oscillations. The anomalous growth of both the translational and librational fluctuations leads to the lattice destruction over the Cr—DS scheme.

6. Conclusions

1. The self-consistent phonon field method in terms of which the calculations are made is a mean-field approximation and cannot correctly describe the fluctuation range near the critical temperature. To be of qualitative character the results of the work allow the unambiguons interpretation of the correlation between the molecules mobility and the molecular crystalline structure with various types of the structural instability.

2. The anisotropy factor k used in the paper is related to the system of interacting particles with one long axis equal to a. Contrary to [17] this parameter is not bound up with the geometric shape of the particles only but is a characteristic both of the molecule and the crystal. In the case considered here the plastic and the liquid-crystalline states are formed by the absolutely anisotropic particles which differ in size only. Therefore, contrary to the existing opinion, it is necessary to accept that the geometric shape of the molecules is not a sufficient description of the molecular crystal ability to form the thermotropic mesophase of rotational or liquid-crystalline nature and it cannot be considered as an adequate phenomenological parameter of mesogeneous activity of the system. In the general case describing the structural instability of the molecular crystal it is necessary to account not only for the geometric shape of the molecules but also for their mutual arrangement about each other and about their crystallographic axis.

3. According to the mathematical analysis of the dynamical system of equations (14)—(16) its solutions become complex at the same temperature value, T_c. In physical sense this means that the crystal loses stability simultaneously over the translational and the librational movement of particles. However, from the consideration of the temperature dependences of x and y (Fig. 4) it follows that the anharmonic processes bound up with them contribute unequivalently to the structural instability of the system. The lattice disruption concerns mainly the oscillations of molecules whose dynamical characteristics have an essential unlinearity versus temperature in the pre-transitional range. The parameters corresponding to the stable movement of

the particles are changed almost linearly with the temperature up to the stability limit. On the basis of the analysis and the comparison of different dependencies of thermodynamical and dynamical experimental characteristics of the crystal versus temperature one can draw definite conclusions about the microscopic processes leading to structural lattice instability.

Acknowledgement

The authors should like to thank R. I. MINTZ, N. M. PLAKIDA and K. PARLINSKI for stimulating conversations about this work and for important comments on the manuscript.

REFERENCES

1. N. M. PLAKIDA and T. SIKLÓS, Acta Phys. Hung., **26**, 387, 1969; Phys. Lett. **26A**, 342, 1968.
2. T. SIKLÓS, Acta Phys. Hung., **34**, 327, 1973.
3. S. STAMENKOVIĆ, N. M. PLAKIDA, V. L. AKSIENOV and T. SIKLÓS, Acta Phys. Hung., **43**, 99, 1977.
4. N. M. PLAKIDA and T. SIKLÓS, Acta Phys. Hung., **45**, 37, 1978.
5. S. STAMENKOVIĆ, N. M. PLAKIDA, V. L. AKSIENOV and T. SIKLÓS, Phys. Rev., **B14**, 5080, 1976.
6. K. PARLINSKI, A. C. MITUS, R. SIKORA and T. WASIUTINSKI, J. Chem. Phys., **67**, 5366, 1977.
7. V. K. PERSHIN and V. S. ZHUKOV, Fiz. tverd. tela, **18**, 158, 1976.
8. R. I. MINTZ, V. S. ZHUKOV, V. K. PERSHIN and VL. K. PERSHIN, Fiz. tverd. tela, **19**, 1497, 1977.
9. V. K. PERSHIN and VL. K. PERSHIN, Ukr. fiz. zhurnal, **23**, 1388, 1978.
10. R. I. MINTZ, V. K. PERSHIN and VL. K. PERSHIN, Kristallografiya, **24**, 213, 1979.
11. V. K. PERSHIN and VL. K. PERSHIN, phys. stat sol. (b), **92**, 9, 1979.
12. K. KOBAYASHI, J. Phys. Soc. Jap., **29**, 1011, 1970.
13. W. L. MCMILLAN, Phys. Rev., **A8**, 1921, 1973.
14. S. CHAKRAVARTY and C.-W. WOO, Phys. Rev., **A11**, 713, 1975.
15. A. I. KITAJGORODSKI, Molecular crystals, Nauka, M., 1971, p. 199.
16. N. M. PLAKIDA and T. SIKLÓS, phys. stat. sol., **33**, 103, 1969; **33**, 113, 1969.
17. V. K. PERSHIN and VL. K. PERSHIN, Fiz. tverd. tela, **21**, 2292, 1979.

Acta Physica Academiae Scientiarum Hungaricae, Tomus 48 (2—3), pp. 293—296 (1980)

POLARIZABILITIES OF LIQUID CRYSTALS OF A SERIES OF 4-CYAN-PHENYL ESTERS OF 4′-*n*-ALKOXYCINNAMIC ACIDS

By

V. R. MURTHY and R. N. V. RANGA REDDY

MOLECULAR BIO-PHYSICS LABORATORY, DEPARTMENT OF PHYSICS,
S.V.U. AUTONOMOUS POST-GRADUATE CENTRE, ANANTAPUR-515 003, INDIA

(Received 16. I. 1980)

The mean polarizabilities of nematic liquid crystals of homologous series of 4-cyan-phenyl esters of 4′-n-alkoxycinnamic acids have been evaluated using a method due to Lippincot-δ-function potential model modified recently by MURTHY and REDDY [5]. The results are compared with α values obtained from Born's relation. The calculated values are in very good agreement with those obtained from Born's relation.

Introduction

Liquid crystals have attained special importance in recent times because of their multifarious applications. Their chemical, magnetic and optical properties have attracted the attention of many researchers especially in recent decades. The study of their optical properties such as circular dichroism, optical rotatory power and polarizabilities has made considerable progress and recent articles of LEBEDEV et al. [1] and CHANDRASEKHAR [2] give an account of the same. The polarizability is particularly useful in the sense that it gives an estimate of order parameter and helical content. The importance of polarizability for the stero-chemical problems of simple molecules has long been established and its application to the conformation of bio polymers has also been worked out by RAO et al [3] and MURTHY et al [4]. Recently, the spectroscopic studies of liquid crystals have been taken up in these laboratories [5] and the present investigation forms part of such studies. It deals with the evaluation of polarizabilities of liquid crystals for a homologous series of 4-cyan-phenyl esters of 4′-n-alkoxycinnamic acids, $C_nH_{2n+1}\ O-C_6H_4-CH=CH-$ $-COO-C_6H_4-CN$, represented by the first eight members ($n = 1-8$) by a method based on Lippincot-δ-function potential model. This potential model has been modified recently by MURTHY and REDDY, enabling its extension and applicability to liquid crystalline phase.

Method

The Lippincot-δ-function potential model is based on the quantum mechanical approach to the study of eigen state of the system and polarizability forms one of the fine criteria for testing the suitability of such wave functions. It gives an easy and fair reliability for the polarizability determination. Relevant equations to calculate the mean polarizability for liquid phase in terms of the parallel bond component ($\Sigma\alpha_{\|p}$), perpendicular bond contribution ($\Sigma 2\alpha_{\perp}$) and non bond region electron contribution ($\Sigma\alpha_{\|n}$) are given as

$$\alpha_l = 1/3(\Sigma\alpha_{\|p} + \Sigma\alpha_{\|n} + \Sigma 2\alpha_{\perp}), \tag{1}$$

where

$$\Sigma\alpha_{\|p} = \frac{4nA}{a_0}\left(\frac{R^2}{4} + \frac{1}{2C_R^2}\right)^2 \cdot \exp\left(\frac{-(x_1 - x_2)^2}{4}\right). \tag{2}$$

Here n is the bond order, A the δ function strength, R the bond length, x_1 and x_2 the Pauling's electro negativities of atoms A and B in the bond $A-B$. The values of A's and C_R's for various bonds are taken from [6] and [7].

$$\alpha_{\|n} = f_j \alpha_j. \tag{3}$$

Here f_j is the fraction of the non-bonded electrons of the jth atom and α_j is its atomic polarizability

$$\Sigma 2\alpha_{\perp} = n_{df}\left[\frac{x_j^2\,\alpha_j}{x_j^2}\right]. \tag{4}$$

Here n_{df} is the number of degrees of freedom given by the equation $n_{df} = = (3N - 2n_b)$, where N is the number of atoms and n_b is the number of bonds in the liquid crystal. n_{df} for the phenyl ring is taken to be 19.

In crystalline state, it is only the crystalline field whereas in liquid phase it is only the pure Brownian field that will act on the system. But in liquid crystalline phase, both fields will be acting on the system. The resultant effect due to these fields is to decrease the potential on the electron. In other words, the shielding on the electrons will be less thus contributing to more polarization. This behaviour is expressed empirically by using the equation

$$A_{LC} = A \exp\left[(T \sim T_C)/T_C\right], \tag{5}$$

where T is the temperature pertaining to the study of liquid crystal property and T_c is the mesomorphic temperature. This expression for A_{LC} is used in place of A in Eq. (2) for evaluating $\alpha_{\|p}$ and hence α.

Table I

Polarizabilities (X 10^{24} cm^3) of 4-cyan-phenyl esters of 4′-n-alkoxycinnamic acids

n	$\Sigma\alpha_{\|\|p}$	$\Sigma\alpha_{\|\|n}$	$\Sigma 2\alpha_{\perp}$	$m \times 10^3$	T_c °C	α calc.	α Born
1	71.43	1.48	34.95	1.110	162.0	35.78	35.10
2	76.73	1.48	35.62	1.040	161.5	37.75	37.394
3	80.44	1.48	36.30	1.067	147.0	39.21	39.406
4	84.95	1.48	36.98	1.000	144.0	40.94	41.137
5	88.43	1.48	37.68	1.077	133.0	42.30	42.528
6	93.62	1.48	38.38	0.960	134.0	44.28	44.442
7	97.54	1.48	39.08	1.067	127.0	45.79	46.033
8	102.97	1.48	39.80	0.963	129.0	47.85	48.080

Using Lorentz—Lorentz relation and considering the fact that the average refractivity does not depend very much on temperature we can write

$$\alpha = \alpha_l \left[1 - \frac{m}{\varrho_l} (T_C - T) \right]. \tag{6}$$

The details of the derivation of this expression are given in [5]. Here m is the slope of the ϱ versus T graph, and ϱ_l is the density of the liquid crystal in liquid phase, α_l is the mean polarizability in liquid phase obtained from the Lippincot-δ-function model and α is the mean polarizability in liquid crystalline phase. Using Eq. (6), the mean polarizability in liquid crystalline state is evaluated.

The bond lengths are taken from [9]. The values of $\Sigma\alpha_{\|p}$, $\Sigma\alpha_{\|n}$, $\Sigma 2\alpha_{\perp}$ and α are presented in Table I along with the values obtained from Born's relation taking the refractivity data from [8]. Very good agreement is found between these two values.

Acknowledgements

The authors thank Prof. S. V. SUBRAHMANYAM for his interest in this work. One of them (RNVR) thanks the Post Graduate Centre authorities for granting financial help in carrying out this work.

REFERENCES

1. V. I. LEBEDEV, C. I. MORDEROV and M. G. TOMILIN, Sov. J. Opt. Technol. (USA), **41**, 403, 1975.
2. S. CHANDRASEKHAR, Rep. Prog. Phys., **39**, 615, 1976.
3. B. P. RAO, V. R. MURTHY and D. V. SUBBAIAH, Ind. J. Bio Chem. and Bio Phys., **14**, 181, 1977.

4. V. R. MURTHY, Ind. J. Bio Chem. and Bio Phys., **16**, 32, 1979.
5. V. R. MURTHY, S. V. NAIDU and R. N. V. RANGA REDDY, Molecular crystals and liquid crystals (GB) (in press).
6. B. P. RAO and V. R. MURTHY, Curr. Sci., **41**, 15, 1972.
7. B. P. RAO, V. R. MURTHY and D. V. SUBBAIAH, Ind. J. Pure and Appl. Phys., **14**, 276, 1976.
8. V. A. GROZHIK and P. V. ADOMENAS, Opt. Spectrosc. (USSR), **44**, 602, 1978.
9. Handbook of Physics and Chemistry, Rubber Publishing Edition, 1979.

Acta Physica Academiae Scientiarum Hungaricae, Tomus 48 (2—3), pp. 297—302 (1980)

A MONTE CARLO CALCULATION OF SURFACE PROPERTIES OF WATER

By

B. BORŠTNIK, D. JANEŽIČ and A. AŽMAN

BORIS KIDRIČ INSTITUTE OF CHEMISTRY, LJUBLJANA, YUGOSLAVIA

(Received 17. I. 1980)

The Monte Carlo calculation on the liquid-vapour interface of water with 64 molecules and 10^6 configurations is reported. The density profile indicates the existence of rather low value of the surface thickness. The question whether the density profile is oscillatory or monotonous remains inconclusive. The results indicate that the molecules at the surface prefer the orientation with one hydrogen atom pointing towards the vapour phase. The surface energy results in a reasonable agreement with the experiment. The surface tension would need a much longer run to overcome the statistical fluctuations.

1. Introduction

The computer simulation of inhomogeneous systems such as liquid—vapour or liquid—crystal is mostly devoted to monoatomic systems [1, 2, 3]. The only calculation of surface properties of diatomic liquids is due to THOMPSON [4] and THOMPSON and GUBBINS [5]. In this work we would like to report the Monte Carlo simulation of the properties of liquid—vapour interface of water. The shape of the density profile, the width of the interface, surface ordering of molecules, surface energy and the surface tension were studied. The liquid water is a subject of several molecular dynamics and Monte Carlo simulations. The calculations were performed with different types of water—water pair potential. The structure and the molecular motion in bulk water is already well understood.

The water structure in the vicinity of ions was also studied [6]. Unfortunately, the studies of inhomogeneous systems such as liquid—vapour interface are very time-consuming, if one requires enough reliable results. Our results involve a high degree of uncertainty due to strong statistical fluctuations. One aim of this study was to use the information about the statistical fluctuations to get the impression about the number of configurations necessary to provide reliable results of surface properties.

2. Description of the calculation

The usual METROPOLIS Monte Carlo method was used [7]. BARSOTTI's computer program [8] was modified by adding the periodic boundary conditions in x and y directions. This means that our system had the form of a slab, as is the usual way of treating the liquid—vapour interfaces.

The system contained only 64 water molecules. We used the configuration interaction potential of MATSOUKA et al. [9] which was already tested in the Monte Carlo calculations on homogeneous liquid water systems [10, 11].

The potential was truncated at 6.44 Å which is slightly less than half of the dimension of the cell which is periodically repeated in xy plane. The tail of the truncated potential was neglected in the Monte Carlo run but it was taken into account later, when the results were analysed. After equilibration 10^6 configurations were generated. The fluctuation of the potential energy around a stationary value was taken as the criterion if the system is equilibrated. The temperature was taken to be 300 K.

The liquid—vapour density profile was set up as a histogram representing the probability distribution of the positions of the oxygen atoms along the x axis. Another question which is of interest concerns the orientational distribution of the water molecules at the liquid surface. We calculated at each value of the z coordinate the mean value of cos ϑ averaging over all molecules. ϑ is the angle between the molecular symmetry axis and z axis of fixed coordinate system

$$\langle \cos \vartheta(z) \rangle = \left[\sum_i \cos \vartheta_i(z_i, dz) \right] \Big/ dn(z_i, dz),$$

where the sum runs over dn (z_i, dz) molecules whose z coordinates of the oxygen atoms are found in the interval between z and $z + dz$.

The expression for the surface tension of molecular fluids was derived by GRAY and GUBBINS [12] where γ is expressed as the contribution of isotropic and anisotropic intermolecular forces. For the system where the potential is

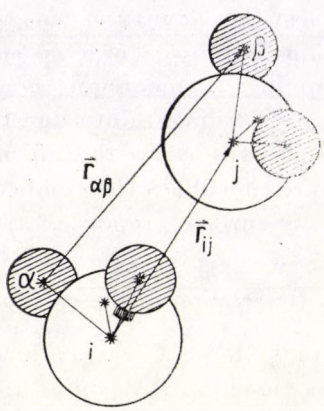

Fig. 1. Meaning of the symbols in Eqs. 1, 2 and 3. The vectors $\vec{r}_{\alpha\beta}$ connect all sites marked by asterisks

expressed as a sum of site—site interactions, an expression for γ can be derived in a way analogous with [12]:

$$\gamma = \frac{1}{2S}\left\langle \sum_{i>j}\sum_{\alpha,\beta} \frac{\partial V_{\alpha\beta}}{\partial r_{\alpha\beta}} \left(\frac{\vec{r}_{ij}\cdot\vec{r}_{\alpha\beta} - 3z_{ij}z_{\alpha\beta}}{r_{\alpha\beta}} \right) \right\rangle. \tag{1}$$

V is a site—site potential, α and β being the sites on the molecules i and j, respectively. $\vec{r}_{ij}$ is the vector connecting the centres of molecules i and j (Fig. 1)—in our case the oxygen—oxygen distance. Triangular brackets imply canonical averaging. S is the area of two free surfaces. To have better insight into the interplay of different contributions to γ we broke down the expression (1) into the contribution of isotropic and anisotropic forces [12] $\gamma = \gamma_R + \gamma_\vartheta$:

$$\gamma_R = \frac{1}{2S}\left\langle \sum_{i>j} \frac{x_{ij}^2 + y_{ij}^2 - 2z_{ij}^2}{r_{ij}^2} \sum_{\alpha,\beta} \frac{1}{r}\cdot\frac{\partial V_{\alpha\beta}}{\partial r_{\alpha\beta}} \vec{r}_{ij}\cdot\vec{r}_{\alpha\beta} \right\rangle, \tag{2}$$

$$\gamma_\vartheta = \frac{3}{2S}\left\langle \sum_{i>j}\sum_{\alpha,\beta} \frac{1}{r_{\alpha\beta}} \frac{\partial V_{\alpha\beta}}{\partial r_{\alpha\beta}} \left(\frac{z_{ij}^2}{r_{ij}^2}\vec{r}_{ij}\vec{r}_{\alpha\beta} - z_{ij}z_{\alpha\beta} \right) \right\rangle. \tag{3}$$

3. Results and discussion

The density profile is depicted in Fig. 2. The oscillations in the profile are of similar origin as in the case of the calculations on atomic Lennard—Jones system, where it was found that with a growing number of configurations

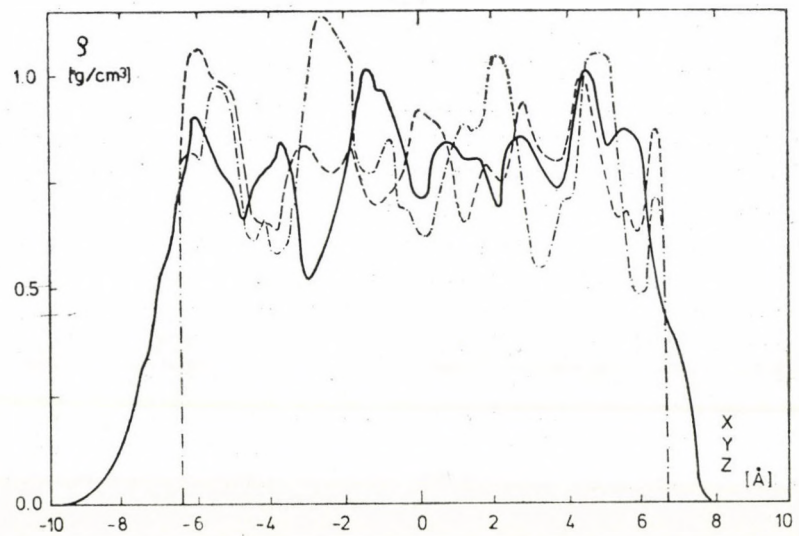

Fig. 2. The density profiles. Full line: $\varrho(z)$ — the profile perpendicular to the interface; dashed line: $\varrho(x)$; dash-dotted line: $\varrho(y)$

the oscillations vanish. In our case where the number of configurations is rather small (only 10^6) the values of the root mean square deviations from the average density $\Delta\varrho^{MC}_{r.m.s}$ are 0.11 g/cm³, 0.15 g/cm³ and 0.11 g/cm³ for ϱ_x, ϱ_y and ϱ_z, respectively.

If the moves of water molecules generated by the Monte Carlo procedure would be of random walk character then the estimated value $\Delta\varrho^{r.w.}_{r.m.s.}$ would be approximately equal to 0.015 g/cm³. The big difference between $\Delta\varrho^{MC}_{r.m.s.}$ and $\Delta\varrho^{r.w.}_{r.m.s.}$ is due to the persistence of certain configurations of water molecules, which contribute to the humps in the density profile. The water—water pair potential has deep minima expressed in terms of the thermal energy at the triple point in comparison with the Lennard—Jones potential and the smoothing process of the density profile is slower.

The value of the mean density is 0.805 g/cm³. We can compare this value with the results of OWICKI and SCHERAGA [13] who performed the isothermal isobaric (T, P, N) ensemble Monte Carlo calculation at 298 K and atmospheric pressure. Their calculation results in a 24% underestimate of density, which is close to our result. The underestimate of density (or unadequate value of the pressure in the usual (N, V, T) Monte Carlo calculation of LIE et al [10]) seems to be a peculiarity of the CI potential.

The surface thickness is less sensitive to the number of configurations than other surface properties. On the basis of Fig. 2 we can estimate the surface thickness to be approximately 2 Å. We can compare this value with the values of Lennard—Jones liquids [1] and with diatomic liquids [5], where the surface thickness, close to the triple point, ranges from 0.8 for chlorine to 1.6 for nitrogen and argon. If we express our value $d = 2$ Å in dimensionless units (taking $H_2O = 2.7$ Å as unit of length) we obtain $d = 0.74$. This means that in the case of water, the liquid vapour transition is accomplished in less than one molecular diameter. This result is in qualitative agreement with the results of LEKNER and HENDERSON who developed the theory which predicts the thickness of the liquid-vapour interface on the basis of experimental data such as surface tension, surface energy and bulk energy [13].

The orientational ordering of water molecules is depicted in Fig. 3. In the bulk region $\langle\cos\vartheta\rangle$ should vanish since all orientations are equally probable. However the fluctuations due to unsufficient averaging are appreciable, as can be seen in the Figure. The minimum at $z = -9$ Å and the maximum at $z = 8$ Å refer to the molecules at the surface. This means that the at surface the preferred orientation of the water molecules is the one in which one of the four tetrahedral hydrogen bonds are broken. This can be accomplished by those orientations of water molecules where one hydrogen atom points towards the gas phase.

The evaluation of surface energy u and surface tension γ was also attempted on the basis of Monte Carlo data. The surface energy was obtained by com-

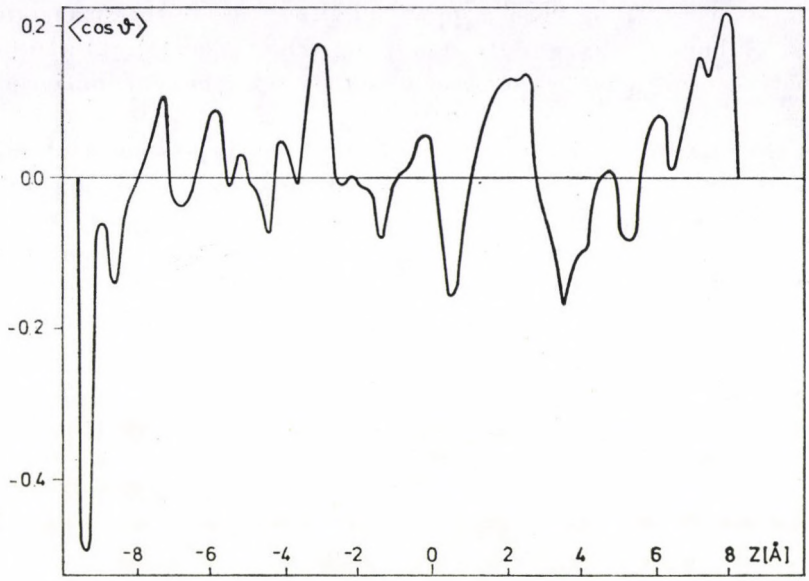

Fig. 3. z dependence of the average value of the projection of the unit vector along the molecule symmetry axis to the z axis

paring the potential energy of the slab with average potential energy of bulk water

$$u = [U_{\text{slab}}(N) - NU_{\text{bulk}}]/S. \tag{4}$$

$U_{\text{slab}}(N)$ is the potential energy of our system with 64 water molecules. Average potential energy per particle of the bulk was taken from [11] where the same number of molecules was treated with periodic boundary conditions. The corrections for neglected interactions were performed. The resulting value of the surface energy was 105 dyne/cm which can be compared with the experimental value [14] ($u = \gamma - Td\gamma/dT$) [15]): $u = 116$ dyne/cm.

Relatively good agreement with experiment was obtained for the surface energy which is a scalar quantity. The results of the surface tension, which is a vector quantity, are subjected to much greater extent to statistical fluctuations. The Eq. (2) can be interpreted as the sum of three terms. The terms with x_{ij}^2 and y_{ij}^2 represent the averaged contribution of the stress transmitted in x and y directions and the term with $2z_{ij}^2$ subtracts the contribution of internal pressure (the contribution of intramolecular forces (Eq. (2)), to obtain the surface tension.

In the bulk water the kinetic contribution and the contribution of intermolecular forces nearly cancel each other. Thus we can estimate the internal pressure to be approximately $p_{\text{int}} \approx \varrho kT \approx 1.4 \cdot 10^9$ dyne/cm^2.

This is a very strong "background" and to evaluate the surface tension one must evaluate the excess stress as it is given in Eqs. (1), (2) and (3). We evaluated independently the components of the stress (the contribution of central forces, Eq. (2) in x, y and z direction). Our results indicate that the Monte Carlo chain with 10^6 configurations performed on the system containing 64 water molecules does not provide enough data to evaluate the diagonal components of the stress tensor and the surface tension.

Partial results for the surface tension due to the subsequent segments of 30 000 configurations are scattered in the interval [−100, 100] (dyne/cm), the mean value being slightly positive. The contribution of the neglected interactions ($r_{00} > 6.44$ Å) to the surface tension is also highly uncertain. At these separations only electric multipole interactions survive. If the orientational and radial correlations are neglected, the contributions to the surface tension average out. If, on the other hand, the correlations at large separations are approximated by the factor $\exp(-U/kT)$, then the contribution to the surface tension is approximately 100 dyne/cm.

We can conclude that the Monte Carlo simulation of liquid—vapour interface of water is feasible. Some results can be obtained even with 10^6 configurations. To have overall reliable results one should perform a MC run with approximately 10^7 configurations which would require large amounts of computer time.

Acknowledgement

The authors thank Prof. E. CLEMENTI for sending us the computer program written by Dr. E. BARSOTTI. The financial support of Research Community of Slovenia is gratefully acknowledged.

REFERENCES

1. G. A. CHAPELLA, G. SAVILLE, S. M. THOMPSON and J. S. ROWLINSON, J. Chem. Soc. Faraday Trans. II **73**, 1133, 1977.
2. M. H. KALOS, J. K. PERCUS and M. RAO, J. Stat. Phys., **17**, 111, 1977.
3. A. J. C. LADD and L. V. WOODCOCK, Molec. Phys., **36**, 611, 1978.
4. S. M. THOMPSON, Faraday Dics. Chem. Soc., **66**, 107, 1978.
5. S. M. THOMPSON and K. E. GUBBINS, J. Chem. Phys., **70**, 4947. 1979.
6. E. CLEMENTI, Lecture Notes in Chemistry: Determination of Liquid Water Structure, Springer Verlag, 1976.
7. N. METROPOLIS, A. W. ROSENBLUTH, M. N. ROSENBLUTH, A. H. TELLER and E. TELLER, J. Chem. Phys., **21**, 1078, 1953.
8. R. BARSOTTI, Documentation of a Monte Carlo Program for Use in Statistical Mechanics Problems, Report N. 13/75, Montedison, Novara, 1975.
9. O. MATSOUKA, M. YOSHIMINE and E. CLEMENTI, J. Chem. Phys., **64**, 1351, 1976.
10. G. C. LIE, E. CLEMENTI and M. YOSHIMINE, J. Chem. Phys., **64**, 2314, 1976.
11. J. C. OWICKI and H. A. SCHERAGA, J. Am. Chem. Soc., **99**, 7403, 1977.
12. C. G. GRAY and K. E. GUBBINS, Molec. Phys., **30**, 179, 1975.
13. J. LEKNER and J. R. HENDERSON, Physica, **94A**, 545, 1978.
14. Handbook of Chemistry and Physics, R. C. Weast, ed., CRC Press, 1974.
15. C. A. CROXTON, Liquid State Physics — A Statistical Mechanical Introduction, Cambridge University Press, 1974.

Acta Physica Academiae Scientiarum Hungaricae, Tomus 48 (2—3), pp. 303—314 (1980)

FREE CONVECTION EFFECTS ON THE FLOW PAST AN ACCELERATED VERTICAL POROUS PLATE IN AN INCOMPRESSIBLE DISSIPATIVE FLUID WITH VARIABLE SUCTION OR INJECTION

By

N. G. KAFOUSIAS, A. A. RAPTIS and G. J. TZIVANIDIS

DEPARTMENT OF MECHANICS, UNIVERSITY OF IOANNINA, IOANNINA, GREECE

(Received 17. I. 1980)

An analysis of the effects of free convection currents on the flow field of an incompressible viscous dissipative fluid past an accelerated vertical porous plate is presented, when the fluid is subjected to a suction or injection with time-dependent velocity. Solution of the problem, in form of power series, is obtained and the expressions for the velocity field, temperature field and for their related quantities of skin friction and rate of heat transfer are given. The influence of the variable suction/injection velocity on the above quantities is shown graphically followed by a quantitative discussion.

1. Introduction

The significance of suction for the boundary layer control in the field of aerodynamics and space science is well recognized. It is often necessary to prevent separation of the boundary layer to reduce drag and attain high lift values. On the other hand, one of the important problems facing the engineers engaged in high-speed flow is the cooling of the surface to avoid structural failures as a result of frictional heating and other factors. We know the possibility of using injection at the wall to cool the body in a high-temperature fluid.

In recent years the problem of free convection past a moving surface has many technological applications as filtration processes, the drying of porous materials in textile industries and the saturation of porous materials by chemicals. The subject of this type of problems has attracted many authors in view not only of its own interest but also of its applications. SOUNDALGEKAR [5] studied the free convection flow past an impulsively started vertical impermeable plate when it is cooled or heated by the free convection currents. An extension of SOUNDALGEKAR's problem, when the fluid is subjected to a constant suction velocity through the porous plate, was obtained by KAFOUSIAS et al [4]. Recently GUPTA, POPP and SOUNDALGEKAR [1] investigated the unsteady flow and heat transfer in free convection flow past a vertical impermeable plate which is uniformly accelerated upwards in its own plane. Because

of the importance of suction/injection for the boundary layer control in the field of fluid mechanics, in this work we study the effects of free convection currents on the flow field of an incompressible viscous fluid past an infinite vertical porous plate, which is uniformly accelerated upwards in its own plane, when the fluid is subjected to a variable suction/injection velocity. It is assumed that this normal velocity of suction/injection at the porous plate varies as $t^{-1/2}$. We obtain solution of the problem in form of power series and give expressions for the velocity, temperature, skin friction and the rate of heat transfer. Their numerical results, for different values of the dimensionless parameters of the problem, are presented in a quantitative manner during the course of discussion.

2. Mathematical analysis

In this work we study the two dimensional unsteady flow and heat transfer in free convection flow of an incompressible viscous dissipative fluid, past a vertical porous flat plate which is uniformly accelerated upwards in its own plane. We take the x'-axis along the plate in the upward direction and the y'-axis normal to the plate. Initially, the fluid and the plate are at rest and at the same temperature T'_∞. But as $t' > 0$ the plate starts moving with velocity $u = ct'$, where c is a positive constant, in its own plane and its temperature is instantaneously raised or lowered to $T'_w (\gtrless T'_\infty)$ which is thereafter maintained constant. Under these assumptions the problem is described by Eqs. (1)—(3) and boundary conditions (4), respectively:

$$\frac{\partial v'}{\partial y'} = 0, \tag{1}$$

$$\frac{\partial u'}{\partial t'} + v' \frac{\partial u'}{\partial y'} = g_x \beta (T' - T'_\infty) + \nu \frac{\partial^2 u'}{\partial y'^2} \tag{2}$$

$$\frac{\partial T'}{\partial t'} + v' \frac{\partial T'}{\partial y'} = \frac{k}{\varrho c_P} \frac{\partial^2 T'}{\partial y'^2} + \frac{\nu}{c_P} \left(\frac{\partial u'}{\partial y'} \right)^2 \tag{3}$$

$$t' \leq 0 : u'(y', t') = 0, \; T'(y', t') = T'_\infty,$$

$$t' > 0 : \begin{cases} u'(0, t') = ct', \; T'(0, t') = T'_w, \\ u'(\infty, t') = 0, \; T'(\infty, t') = T'_\infty, \end{cases} \tag{4}$$

where u', v' are the velocity components in x' and y' direction, respectively, t' is the time, g_x the acceleration due to gravity, β the coefficient of volume expansion, T' the fluid temperature inside the thermal boundary layer, ν the

kinematic viscosity, ϱ the density, k the thermal conductivity and c_p the specific heat of the fluid at constant pressure.

From Eq. (1), we take

$$v' = -v_0(t') = -\alpha(\nu/t')^{1/2}, \tag{5}$$

where α represents the velocity of suction or injection at the porous plate according as $\alpha > 0$ or <0, respectively.

By use of the non-dimensional transformations

$$y = y'\left(\frac{c}{\nu^2}\right)^{1/3}, \qquad E = \frac{(\nu c)^{2/3}}{c_p(T'_w - T'_\infty)}, \text{ (Eckert number)}$$

$$t = t'\left(\frac{c^2}{\nu}\right)^{1/3}, \qquad G = \frac{1}{c}(T'_w - T'_\infty)\, g_x\beta, \text{ (Grashof number)}$$

$$u = \frac{u'}{(\nu c)^{1/3}}, \qquad T = \frac{T' - T'_\infty}{T'_w - T'_\infty},$$

$$P = \varrho\nu c_P/k, \text{ (Prandtl number)}$$

Eqs. (2) and (3) become

$$\frac{\partial u}{\partial t} - \alpha t^{-1/2}\frac{\partial u}{\partial y} = GT + \frac{\partial^2 u}{\partial y^2}, \tag{6}$$

$$P\frac{\partial T}{\partial t} - \alpha P t^{-1/2}\frac{\partial T}{\partial y} = \frac{\partial^2 T}{\partial y^2} + PE\left(\frac{\partial u}{\partial y}\right)^2, \tag{7}$$

and the boundary conditions (4) become

$$t \leq 0 : u(y, t) = 0,\ T(y, t) = 0,$$

$$t > 0: \begin{cases} u(0, t) = t & T(0, t) = 1, \\ u(\infty, t) = 0, & T(\infty, t) = 0. \end{cases} \tag{8}$$

It is known that the Eckert number E in incompressible fluids and in low speed flows is very small and hence we can expand the physical variables u and T as follows:

$$u(y, t) = u_0(y, t) + Eu_1(y, t) + \ldots,$$

$$T(y, t) = T_0(y, t) + ET_1(y, t) + \ldots \tag{9}$$

On substituting (9) in (6) and (7) and following standard procedure, we get

$$\frac{\partial u_0}{\partial t} - \alpha t^{-1/2} \frac{\partial u_0}{\partial y} = GT_0 + \frac{\partial^2 u_0}{\partial y^2}, \tag{10}$$

$$\frac{\partial u_1}{\partial t} - \alpha t^{-1/2} \frac{\partial u_1}{\partial y} = GT_1 + \frac{\partial^2 u_1}{\partial y^2}, \tag{11}$$

$$P \frac{\partial T_0}{\partial t} - \alpha P t^{-1/2} \frac{\partial T_0}{\partial y} = \frac{\partial^2 T_0}{\partial y^2}, \tag{12}$$

$$P \frac{\partial T_1}{\partial t} - \alpha P t^{-1/2} \frac{\partial T_1}{\partial y} = \frac{\partial^2 T_1}{\partial y^2} + P \left(\frac{\partial u_0}{\partial y} \right)^2 \tag{13}$$

and the initial and boundary conditions (8) become now

$$\begin{aligned} t \leq 0 &: u_0(y,t) = u_1(y,t) = 0,\ T_0(y,t) = T_1(y,t) = 0, \\ t > 0 &: \begin{cases} u_0(0,t) = t,\ u_1(0,t) = 0,\ u_0(\infty,t) = 0,\ u_1(\infty,t) = 0 \\ T_0(0,t) = 1,\ T_1(0,t) = 0,\ T_0(\infty,t) = 0,\ T_1(\infty,t) = 0. \end{cases} \end{aligned} \tag{14}$$

The Prandtl number P is a measure of the relative importance of viscosity and heat conductivity in the fluid. For most gases P is of unit order (for air $P = 0.71$), so that the velocity and the thermal boundary layers will be of the same order of thickness [2] and we will seek solution of our problem for this case. On the other hand during the initial stages of the development of the boundary layer on the porous plate the boundary layer is thin so that a solution of Eqs. (10)—(13) for small t can be obtained in the form

$$\begin{aligned} u_0 &= t f_0(\eta), \quad T_0 = g_0(\eta), \\ u_1 &= t^3 f_1(\eta), \quad T_1 = t^2 g_1(\eta), \end{aligned} \tag{15}$$

where $\eta = y/2t^{1/2}$. The functions f_i, g_i, $i = 0, 1$ are found to satisfy the following equations

$$f_0'' + 2(\eta + \alpha) f_0' - 4 f_0 = -4G g_0, \tag{16}$$

$$f_1'' + 2(\eta + \alpha) f_1' - 12 f_1 = -4G g_1, \tag{17}$$

$$g_0'' + 2(\eta + \alpha) g_0' = 0, \tag{18}$$

$$g_1'' + 2(\eta + \alpha) g_1' - 8 g_1 = -f_0', \tag{19}$$

where primes denote differentiations with respect to η. The corresponding boundary conditions become

$$\begin{aligned} f_0(0) = g_0(0) = 1,\ f_0(\infty) = g_0(\infty) = 0, \\ f_1(0) = g_1(0) = 0,\ f_1(\infty) = g_1(\infty) = 0. \end{aligned} \tag{20}$$

Thus the solutions of (16)—(19) in virtue of the boundary conditions (20) are

$$g_0(\eta) = \frac{Hh_0(\sqrt{2}\xi)}{Hh_0(\sqrt{2}\alpha)}, \tag{21}$$

$$f_0(\eta) = (1-G)\frac{Hh_2(\sqrt{2}\xi)}{Hh_2(\sqrt{2}\alpha)} + G\frac{Hh_0(\sqrt{2}\xi)}{Hh_0(\sqrt{2}\alpha)}, \tag{22}$$

$$\begin{aligned} g_1(\eta) = {} & G^2\frac{Hh_2^2(\sqrt{2}\alpha)}{Hh_0^2(\sqrt{2}\alpha)}\cdot\frac{Hh_4(\sqrt{2}\xi)}{Hh_4(\sqrt{2}\alpha)} + \frac{1}{2}\frac{Hh_4(\sqrt{2}\xi)}{Hh_4(\sqrt{2}\alpha)} + \\ & + G^2\frac{Hh_1^2(\sqrt{2}\alpha)}{Hh_0^2(\sqrt{2}\alpha)}\cdot\frac{Hh_4(\sqrt{2}\xi)}{Hh_4(\sqrt{2}\alpha)} + (1-G)\,G\frac{Hh_1(\sqrt{2}\alpha)}{Hh_0(\sqrt{2}\alpha)}\cdot \\ & \cdot\frac{Hh_3(\sqrt{2}\alpha)}{Hh_2(\sqrt{2}\alpha)}\cdot\frac{Hh_4(\sqrt{2}\xi)}{Hh_4(\sqrt{2}\alpha)} - G^2\frac{Hh_2^2(\sqrt{2}\xi)}{Hh_2^2(\sqrt{2}\alpha)} - \frac{(1-G)^2}{2}\cdot \\ & \cdot\frac{Hh_2^2(\sqrt{2}\xi)}{Hh_2^2(\sqrt{2}\alpha)} - \frac{G^2}{2}\cdot\frac{Hh_0^2(\sqrt{2}\xi)}{Hh_0^2(\sqrt{2}\alpha)} - G^2\cdot\frac{Hh_1^2(\sqrt{2}\xi)}{Hh_0^2(\sqrt{2}\alpha)} - \\ & - (1-G)G\cdot\frac{Hh_0(\sqrt{2}\xi)}{Hh_0(\sqrt{2}\alpha)}\cdot\frac{Hh_2(\sqrt{2}\xi)}{Hh_2(\sqrt{2}\alpha)} - (1-G)G\frac{Hh_1(\sqrt{2}\xi)}{Hh_0(\sqrt{2}\alpha)}\cdot \\ & \cdot\frac{Hh_3(\sqrt{2}\xi)}{Hh_2(\sqrt{2}\alpha)}, \end{aligned} \tag{23}$$

$$\begin{aligned} f_1(\eta) = {} & G\left[G^2\frac{Hh_2^2(\sqrt{2}\alpha)}{Hh_0^2(\sqrt{2}\alpha)} + \frac{1}{2} + G^2\frac{Hh_1^2(\sqrt{2}\alpha)}{Hh_0^2(\sqrt{2}\alpha)} + (1-G)\cdot G\cdot\frac{Hh_1(\sqrt{2}\alpha)}{Hh_0(\sqrt{2}\alpha)}\cdot\right. \\ & \left.\cdot\frac{Hh_3(\sqrt{2}\alpha)}{Hh_2(\sqrt{2}\alpha)}\right]\cdot\left[\frac{Hh_4(\sqrt{2}\xi)}{Hh_4(\sqrt{2}\alpha)} - \frac{Hh_6(\sqrt{2}\xi)}{Hh_6(\sqrt{2}\alpha)}\right] - G\left[G^2\frac{Hh_3^2(\sqrt{2}\alpha)}{Hh_0^2(\sqrt{2}\alpha)} + \right. \\ & + \frac{(1-G)^2}{2}\cdot\frac{Hh_3^2(\sqrt{2}\alpha)}{Hh_2^2(\sqrt{2}\alpha)} + \frac{G^2}{2}\left[\frac{Hh_1^2(\sqrt{2}\alpha)}{Hh_0^2(\sqrt{2}\alpha)} + 4\frac{Hh_2^2(\sqrt{2}\alpha)}{Hh_0^2(\sqrt{2}\alpha)} + \right. \\ & \left.\left. + 4\frac{Hh_3^2(\sqrt{2}\alpha)}{Hh_0^2(\sqrt{2}\alpha)}\right] + (1-G)G\left[2\frac{Hh_4(\sqrt{2}\alpha)}{Hh_0(\sqrt{2}\alpha)} + \frac{Hh_1(\sqrt{2}\alpha)}{Hh_0(\sqrt{2}\alpha)}\frac{Hh_3(\sqrt{2}\alpha)}{Hh_2(\sqrt{2}\alpha)}\right]\right]\cdot \\ & \cdot\frac{Hh_6(\sqrt{2}\xi)}{Hh_6(\sqrt{2}\alpha)} + G\left\{G^2\frac{Hh_3^2(\sqrt{2}\xi)}{Hh_0^2(\sqrt{2}\alpha)} + \frac{(1-G)^2}{2}\frac{Hh_3^2(\sqrt{2}\xi)}{Hh_2^2(\sqrt{2}\alpha)} + \frac{G^2}{2}\cdot\right. \end{aligned}$$

$$\cdot \frac{Hh_1^2(\sqrt{2}\xi)}{Hh_0^2(\sqrt{2}\alpha)} + 2G^2\left[\frac{Hh_2^2(\sqrt{2}\xi)}{Hh_0^2(\sqrt{2}\alpha)} + \frac{Hh_3^2(\sqrt{2}\xi)}{Hh_0^2(\sqrt{2}\alpha)}\right] + G(1-G)\frac{Hh_1(\sqrt{2}\xi)}{Hh_0(\sqrt{2}\alpha)} \cdot$$

$$\cdot \frac{Hh_3(\sqrt{2}\xi)}{Hh_2(\sqrt{2}\alpha)} + 2G(1-G)\frac{Hh_2(\sqrt{2}\xi)}{Hh_0(\sqrt{2}\alpha)} \cdot \frac{Hh_4(\sqrt{2}\xi)}{Hh_2(\sqrt{2}\alpha)}\Bigg\}, \tag{24}$$

where $\xi = \eta + \alpha$ and the function $Hh_n(\sqrt{2}\xi)$ is defined in JEFFREYS and JEFFREYS [3] and is related with the complementary error function (*erfc*) as in Appendix.

Once we know the velocity and temperature field it is important to calculate the skin friction and the rate of heat transfer which are given, in the dimensionless form, by the expressions (25) and (26), respectively

$$\tau_w = \frac{1}{2}t^{1/2}[f_0'(0) + Et^2 f_0'(0)], \tag{25}$$

and

$$h_w = -\frac{1}{2}t^{-1/2}[g_0'(0) + Et^2 g_1'(0)], \tag{26}$$

where

$$f_0'(0) = -\sqrt{2}\left\{(1-G)\frac{Hh_1(\sqrt{2}\alpha)}{Hh_2(\sqrt{2}\alpha)} + G\frac{Hh_{-1}(\sqrt{2}\alpha)}{Hh_0(\sqrt{2}\alpha)}\right\}, \tag{27}$$

$$f_1'(0) = -\sqrt{2}\,G\left\{G^2\frac{Hh_2^2(\sqrt{2}\alpha)}{Hh_0^2(\sqrt{2}\alpha)} + \frac{1}{2} + G^2\frac{Hh_1^2(\sqrt{2}\alpha)}{Hh_0^2(\sqrt{2}\alpha)} + \right.$$

$$\left. + (1-G)G\frac{Hh_1(\sqrt{2}\alpha)}{Hh_0(\sqrt{2}\alpha)}\frac{Hh_3(\sqrt{2}\alpha)}{Hh_2(\sqrt{2}\alpha)}\right\} \cdot \left[\frac{Hh_3(\sqrt{2}\alpha)}{Hh_4(\sqrt{2}\alpha)} - \right.$$

$$\left. - \frac{Hh_5(\sqrt{2}\alpha)}{Hh_6(\sqrt{2}\alpha)}\right] + \sqrt{2}G\left[G^2\frac{Hh_3^2(\sqrt{2}\alpha)}{Hh_0^2(\sqrt{2}\alpha)} + \frac{(1-G)^2}{2} \cdot \right.$$

$$\cdot \frac{Hh_3^2(\sqrt{2}\alpha)}{Hh_2^2(\sqrt{2}\alpha)} + \frac{G^2}{2}\left[\frac{Hh_1^2(\sqrt{2}\alpha)}{Hh_0^2(\sqrt{2}\alpha)} + 4\frac{Hh_2^2(\sqrt{2}\alpha)}{Hh_0^2(\sqrt{2}\alpha)} + \right.$$

$$\left. + 4\frac{Hh_3^2(\sqrt{2}\alpha)}{Hh_0^2(\sqrt{2}\alpha)}\right] + (1-G)G\left[2\frac{Hh_4(\sqrt{2}\alpha)}{Hh_0(\sqrt{2}\alpha)} + \right.$$

$$\left. + \frac{Hh_1(\sqrt{2}\alpha)}{Hh_0(\sqrt{2}\alpha)}\frac{Hh_3(\sqrt{2}\alpha)}{Hh_2(\sqrt{2}\alpha)}\right]\Bigg] \cdot \frac{Hh_5(\sqrt{2}\alpha)}{Hh_6(\sqrt{2}\alpha)} - \sqrt{2}G$$

$$\left\{2G^2\frac{Hh_3(\sqrt{2}\alpha)}{Hh_0(\sqrt{2}\alpha)}\frac{Hh_2(\sqrt{2}\alpha)}{Hh_0(\sqrt{2}\alpha)} + (1-G)^2\frac{Hh_3(\sqrt{2}\alpha)}{Hh_2(\sqrt{2}\alpha)} + \right.$$

$$+ G^2 \frac{Hh_1(\sqrt{2}\alpha)}{Hh_0(\sqrt{2}\alpha)} + 4G^2 \left[\frac{Hh_2(\sqrt{2}\alpha)}{Hh_0(\sqrt{2}\alpha)} \frac{Hh_1(\sqrt{2}\alpha)}{Hh_0(\sqrt{2}\alpha)} + \right.$$

$$+ \frac{Hh_3(\sqrt{2}\alpha)}{Hh_0(\sqrt{2}\alpha)} \frac{Hh_2(\sqrt{2}\alpha)}{Hh_0(\sqrt{2}\alpha)} + G(1-G) \left[\frac{Hh_3(\sqrt{2}\alpha)}{Hh_2(\sqrt{2}\alpha)} + \right.$$

$$\left. + \frac{Hh_1(\sqrt{2}\alpha)}{Hh_0(\sqrt{2}\alpha)} \right] + 2G(1-G) \left[\frac{Hh_1(\sqrt{2}\alpha)}{Hh_0(\sqrt{2}\alpha)} \frac{Hh_4(\sqrt{2}\alpha)}{Hh_2(\sqrt{2}\alpha)} + \right.$$

$$\left. \left. + \frac{Hh_3(\sqrt{2}\alpha)}{Hh_0(\sqrt{2}\alpha)} \right] \right\}, \tag{28}$$

$$g_0'(0) = -\sqrt{2} \frac{Hh_{-1}(\sqrt{2}\alpha)}{Hh_0(\sqrt{2}\alpha)}, \tag{29}$$

$$g_1'(0) = -\sqrt{2} \left\{ G^2 \frac{Hh_2^2(\sqrt{2}\alpha)}{Hh_0^2(\sqrt{2}\alpha)} \frac{Hh_3(\sqrt{2}\alpha)}{Hh_4(\sqrt{2}\alpha)} + \frac{1}{2} \frac{Hh_3(\sqrt{2}\alpha)}{Hh_4(\sqrt{2}\alpha)} + \right.$$

$$+ G^2 \frac{Hh_1^2(\sqrt{2}\alpha)}{Hh_0^2(\sqrt{2}\alpha)} \frac{Hh_3(\sqrt{2}\alpha)}{Hh_4(\sqrt{2}\alpha)} + (1-G)G \frac{Hh_1(\sqrt{2}\alpha)}{Hh_0(\sqrt{2}\alpha)} \cdot$$

$$\cdot \frac{Hh_3(\sqrt{2}\alpha)}{Hh_2(\sqrt{2}\alpha)} \frac{Hh_3(\sqrt{2}\alpha)}{Hh_4(\sqrt{2}\alpha)} - 2G^2 \frac{Hh_2(\sqrt{2}\alpha)}{Hh_0(\sqrt{2}\alpha)} \frac{Hh_1(\sqrt{2}\alpha)}{Hh_0(\sqrt{2}\alpha)} -$$

$$- (1-G)^2 \frac{Hh_1(\sqrt{2}\alpha)}{Hh_2(\sqrt{2}\alpha)} - G^2 \frac{Hh_{-1}(\sqrt{2}\alpha)}{Hh_0(\sqrt{2}\alpha)} -$$

$$- 2G^2 \frac{Hh_1(\sqrt{2}\alpha)}{Hh_0(\sqrt{2}\alpha)} - (1-G)G \left[\frac{Hh_{-1}(\sqrt{2}\alpha)}{Hh_0(\sqrt{2}\alpha)} + \frac{Hh_1(\sqrt{2}\alpha)}{Hh_2(\sqrt{2}\alpha)} \right] -$$

$$\left. - (1-G)G \left[\frac{Hh_3(\sqrt{2}\alpha)}{Hh_2(\sqrt{2}\alpha)} + \frac{Hh_1(\sqrt{2}\alpha)}{Hh_0(\sqrt{2}\alpha)} \right] \right\}. \tag{30}$$

3. Discussion

In order to point out the effects of suction/injection velocity on the flow field the following considerations are made. The Prandtl number P is taken as unity. In the expression $v' = -\alpha(v/t)^{1/2}$, α represents the velocity of suction or injection at the plate according as $\alpha > 0$ or $\alpha < 0$, respectively. The case $\alpha = 0$ corresponds in an impermeable plate. The Grashof number G, which represents here the effects of free convection currents, takes positive and

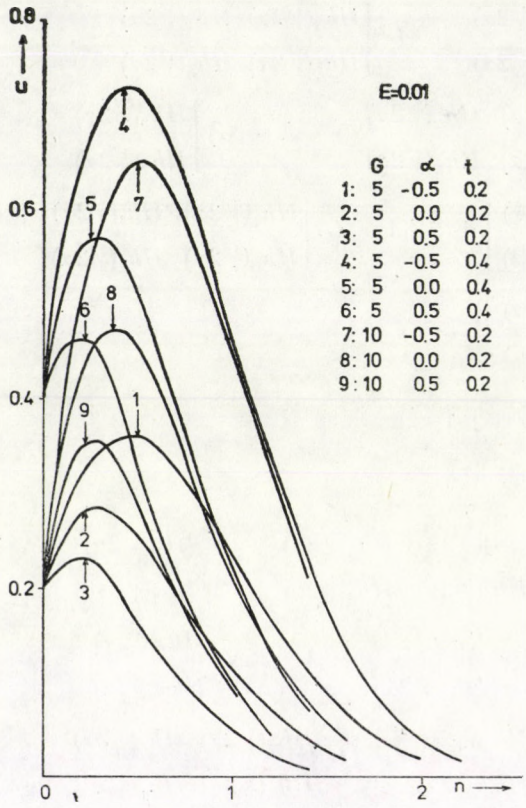

Fig. 1. Velocity profiles when the plate is being cooled ($G > 0$)

negative values. The case $G > 0$ (e.g. $T'_w > T'_\infty$) corresponds physically to an externally cooled porous plate, while the case $G < 0$ ($T'_w < T'_\infty$) corresponds to an externally heated one since the free convection currents are moving towards the plate. Then Eckert number E takes similar to that of G as it depends upon $T'_w - T'_\infty$. The numerical results obtained for various combinations of the dimensionless parameters, G, E, α and time t, are shown graphically in Figs. 1—3 while Table I gives the variations of skin friction and rate of heat transfer.

It is seen from Fig. 1 that the application of suction helps in reducing the dimensionless velocity when the plate is being cooled by the free convection currents. The converse holds in the case of injection. We also observe that as time t increases or owing to free convection currents (e.g. as G increases) the velocity increases but the influence of the suction or injection on the velocity field remains the same. Fig. 2 shows the variations of the velocity when the plate is being heated by the free convection currents. In the presence of the

plate being heated by the free convection currents, there exists a reverse type of flow and it is observed to be more fall in the velocity due to greater heating of the plate. This is more evident in the case of injection than in the case of suction.

The temperature profiles are shown in Fig. 3 for both $G, E \gtrless 0$. The fluid temperature T inside the thermal boundary layer is greater in the case of suction than in the case of injection in both cases $G, E > 0$ or $G, E < 0$. Greater cooling of the plate, in the presence of suction causes a rise in the fluid temperature.

Finally, Table I gives the variation of skin friction and rate of heat transfer for different values of the dimensionless parameters G, E and α and time t. We observe that when the plate is being cooled by the free convection currents application of suction helps in reducing the frictional drag from the plate while the opposite holds in the case of injection. However, the inverse phenomenon occurs when the plate is being heated by the free convection currents. For the case $G, E > 0$, as well as for the case $G, E < 0$ the rate of

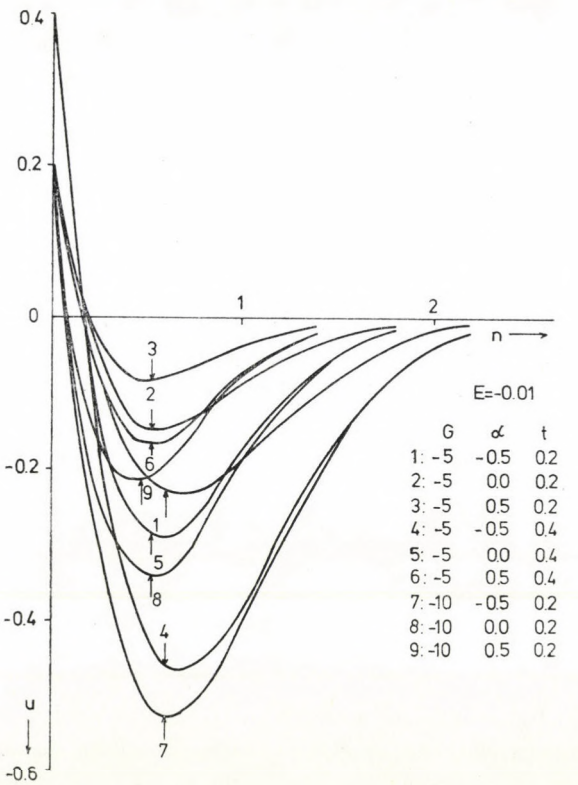

Fig.2. Velocity profiles when the plate is being heated ($G < 0$)

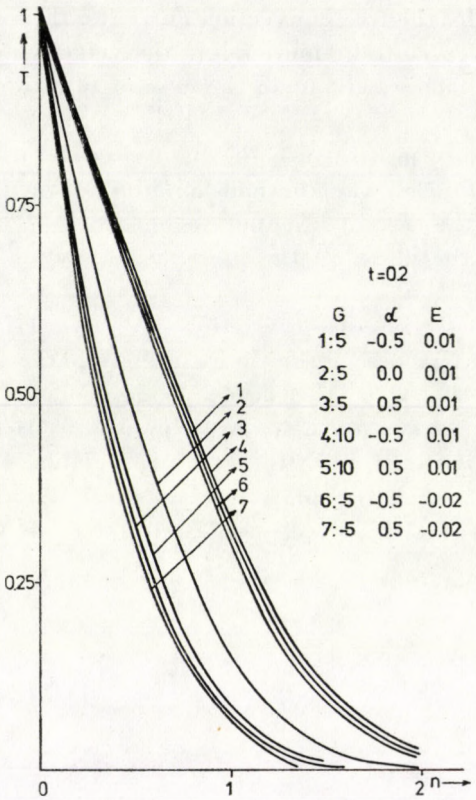

Fig. 3. Temperature profiles when the plate is being cooled or heated

heat transfer increases when the fluid is sucked through the porous plate and decreases when it is injected. Also, since the skin friction increases as the time t increases, the rate of heat transfer decreases.

4. Conclusions

In order to emphasize the influence of suction/injection on the flow field we summarize the important results as follows:

(i) Application of suction helps in reducing the velocity when the plate is being cooled by the free convection currents.

(ii) Due to greater heating of the plate there is a fall in the velocity and this fall is greater in the case of injection than that of suction.

(iii) For both cases (e.g. $G, E \gtrless 0$) the fluid temperature is greater in the case of suction than in the case of injection.

Table I

Variation of the skin friction and rate of heat trasnfer

	$\alpha = -0.5$				$\alpha = -0.0$				$\alpha = 0.5$			
	G	E/t	0.2	0.4	G	E/t	0.2	0.4	G	E/t	0.2	0.4
τ_w	5	0.01	0.931727	1.317896	5	0.01	0.756981	1.070712	5	0.01	0.503216	0.711816
	5	0.02	0.931782	1.318208	5	0.02	0.757023	1.070950	5	0.02	0.503254	0.712031
	10	0.01	2.258407	3.196418	10	0.01	2.018894	2.856795	10	0.01	1.644656	2.326949
	10	0.02	−2.259007	3.199816	10	0.02	2.019282	2.858992	10	0.02	1.644904	2.328355
	− 5	−0.01	−1.720402	2.432196	− 5	−0.01	−1.766045	−2.496938	− 5	−0.01	−1.779171	−2.515667
	− 5	−0.02	−1.720209	−2.431103	− 5	−0.02	−1.765897	−2.496102	− 5	−0.02	−1.779063	−2.515052
	−10	−0.01	−3.045577	−4.302206	−10	−0.01	−3.026948	−4.277310	−10	−0.01	−2.919978	−4.127217
	−10	−0.02	−3.044424	−4.295685	−10	−0.02	−3.026137	−4.272722	−10	−0.02	−2.919446	−4.124210
h_w	5	0.01	0.645396	0.454713	5	0.01	1.261131	0.890833	5	0.01	2.048791	1.448214
	5	0.02	0.644618	0.452512	5	0.02	1.260697	0.889605	5	0.02	2.048555	1.447549
	10	0.01	0.641406	0.443427	10	0.01	1.258491	0.883364	10	0.01	2.047323	1.444063
	10	0.02	0.636637	0.429939	10	0.02	1.255415	0.874666	10	0.02	2.045619	1.439245
	− 5	−0.01	0.649282	0.465705	− 5	−0.01	1.264347	0.899928	− 5	−0.01	2.051453	1.455744
	− 5	−0.02	0.652390	0.474496	− 5	−0.02	1.267128	0.907795	− 5	−0.02	2.053880	1.462608
	−10	−0.01	0.655602	0.483581	−10	−0.01	1.269335	0.914036	−10	−0.01	2.055112	1.466095
	−10	−0.02	0.665030	0.510247	−10	−0.02	1.277104	0.936011	−10	−0.02	2.061199	1.483310

(iv) Frictional drag from the plate decreases in the presence of suction and increases in the presence of injection.

(v) Application of injection helps in reducing the rate of heat transfer while the inverse phenomenon occurs in the case of suction.

Finally, it may be noted that when $\alpha = 0$, our results correspond with those of GUPTA, POPP and SOUNDALGEKAR [1] for an impermeable plate.

Appendix

$$\mathrm{Hh}_{-1}(\sqrt{2}\xi) = e^{-\xi^2},$$

$$\mathrm{Hh}_0(\sqrt{2}\xi) = \sqrt{\pi/2}\ \mathrm{erfc}\,(\xi),$$

$$\mathrm{Hh}_1(\sqrt{2}\xi) = e^{-\xi^2} - \sqrt{\pi}\xi\ \mathrm{erfc}\,(\xi),$$

$$\mathrm{Hh}_2(\sqrt{2}\xi) = 0.5[\sqrt{\pi/2}(1 + 2\xi^2)\ \mathrm{erfc}\,(\xi) - \sqrt{2}\xi\, e^{-\xi^2}],$$

$$\mathrm{Hh}_3(\sqrt{2}\xi) = \frac{1}{6}[2(1 + \xi^2)\, e^{-\xi^2} - \sqrt{\pi}\xi(3 + 2\xi^2)\ \mathrm{erfc}\,(\xi)],$$

$$\mathrm{Hh}_4(\sqrt{2}\xi) = \frac{1}{24}[\sqrt{\pi/2}\,(3 + 12\xi^2 + 4\xi^4)\ \mathrm{erfc}\,(\xi) - \sqrt{2}\,\xi(5 + 2\xi^2)\, e^{-\xi^2}],$$

$$\mathrm{Hh}_5(\sqrt{2}\xi) = \frac{1}{120}[(8 + 18\xi^2 + 4\xi^4)\, e^{-\xi^2} - \sqrt{\pi}\xi(15 + 20\xi^2 + 4\xi^4)\ \mathrm{erfc}\,(\xi)],$$

$$\mathrm{Hh}_6(\sqrt{2}\xi) = \frac{1}{720}[\sqrt{\pi/2}\,(15 + 90\xi^2 + 60\xi^4 + 8\xi^6)\ \mathrm{erfc}\,(\xi) - \sqrt{2}\,\xi(33 + 28\xi^2 + 4\xi^4)e^{-\xi^2}].$$

REFERENCES

1. A. S. GUPTA, I. POPP and V. M. SOUNDALGEKAR, Mécanique Appliquée, **24**, 561, 1979.
2. E. L. HOUGHTON and R. P. BOSWELL, Further Aerodynamics for Engineering Students, Edward Arnold (Publishers) Ltd., London, 1969, p. 252.
3. H. JEFFREYS and B. S. JEFFREYS, Methods of Mathematical Physics, Cambridge University Press, 1972 p. 622.
4. N. G. KAFOUSIAS, N. D. NANOUSIS and G. A. GEORGANTOPOULOS, Astroph. and Space Science, **64**, 391.
5. V. M. SOUNDALGEKAR, Journal of Heat Transfer, **99**, 343, 1977.

Acta Physica Academiae Scientiarum Hungaricae, Tomus 48 (2—3), pp. 315—321 (1980)

ЗАВИСИМОСТЬ СТРУКТУРЫ И СВОЙСТВ СЛОЕВ СЕЛЕНА ОТ ПЛОТНОСТИ ТОКА ЗАРЯДОВ В МОЛЕКУЛЯРНОМ ПОТОКЕ

П. Б. БАРНА, Л. ТОТ

ИНСТИТУТ ТЕХНИЧЕСКОЙ ФИЗИКИ ВЕНГЕРСКОЙ АН, БУДАПЕШТ, ВЕНГРИЯ

Б. ПЕТРЕТИС и Р. РИНКУНАС

ВИЛЬНЮССКИЙ ГОСУНИВЕРСИТЕТ им В. КАПСУКАСА, ВИЛЬНЮС, СССР

(Поступило 21. I. 1980)

Экспериментально показано, что полярность и плотность тока зарядов в молекулярном потоке селена существенно влияют на электрофотографические свойства и структуру слоев. Это влияние наибольше проявляется при температуре подложки во время напыления 323 ÷ 353 К, т.е. при температурах формирования кристаллического подслоя у подложки. Установлено, что отрицательный заряд в молекулярном потоке способствует образованию кристаллического подслоя, а положительный — замедляет процесс кристаллизации селена во время конденсации слоев. Полученные результаты объясняются зависимостью напряженности электростатического поля в слое от полярности и плотности тока зарядов в молекулярном потоке селена.

1. Введение

Физические свойства споев селена сильно зависят от ряда технологических условий их изготовления [1, 2]. К таким технологическим параметрам относятся температура подложки во время напыления ($T_п$), скорость конденсации вещества, давление остаточного газа в вакуумной камере, качество и концентрация примесей в исходном селене, природа подложки [3], а также режим термической обработки исходного вещества [4]. При изменении этих технологических условий изготовления слоев селена меняются их электрические и фотоэлектрические, в том числе и электрофотографические свойства, которые в некоторой степени обуславливаются фазовым составом слоев селена [5].

Известно [2], что в напыленных слоях селена на подогретой алюминиевой подложке больше 333 К создается сплошной кристаллический подслой у подложки, формирование кристаллического подслоя селена во время конденсации слоя в основном обуславливается термическим режимом напыления, но сильное влияние оказывает и природа подложки [3].

При термическом испарении вещества часть молекулярного потока ионизируется [6, 7]. За счет заряженных частиц конденсирующийся слой приобратает электрический заряд, который играет важную роль в процессе формирования слоя [8, 9]. На основе результатов измерений плотности тока зарядов при напылении некоторых металлов установлено, что 0,1—0,01% ато-

мов молекулярного потока ионизировано. Однако, следует полагать, что степень ионизации молекулярного потока зависит от технологических условий напыления, но таких данных фактически нет.

В ряде работ [10—12] показано, что электростатическое поле ускоряет процесс кристаллизации аморфного селена. Напряженность электрического поля в слое селена должна зависеть от знака и плотности зарядов в молекулярном потоке. Таким образом можно предположить, что фазовый состав слоев селена, а тем самым и их электрические свойства зависят от технологических условий напыления селена, влияющих на плотность и знак преобладающих зарядов в молекулярном потоке. Этим вопросам и посвещена данная работа.

2. Методика эксперимента

Плотность тока зарядов в молекулярном потоке селена определялась из непосредственных показаний электрометра, который был подключен к подложке слоя. Для создания стабильной плотности тока на путь молекулярного потока селена ставилась дополнительная вольфрамовая спираль, которая в зависимости от нужной плотности тока зарядов, нагревалась до температуры 773 ÷ 1173 К. Положительные или отрицательные заряды из молекулярного потока селена исключались создавая соответствующей полярности разность

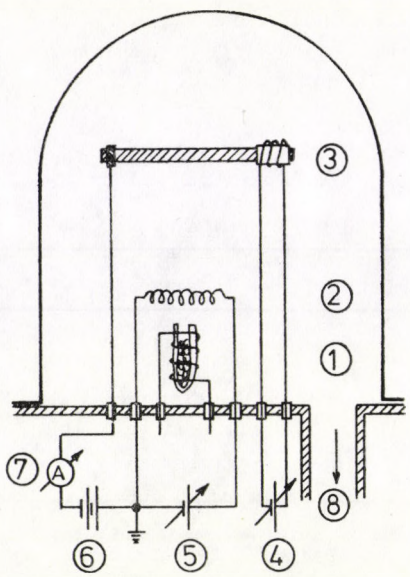

Рис. 1. Установка испарителя с ионизатором. Обозначения: 1 — источник, 2 — ионизатор, 3 — Al подложка, 4 — регулировка температуры подложки, 5 — регулировка температуры ионизатора, 6 — напряжение между ионизатором и подложкой, 7 — электрометр для измерения тока зарядов, 8 — диффузионной насос

потенциалов в несколько вольт (5 ÷ 20 В) между дополнительной спиралью, которая была основным источником зарядов, и подложкой (рис. 1). Напыление производилось одновременно на две подложки: на одной с положительными или отрицательными зарядами в молекулярном потоке, а на другую без зарядов. Кроме этого в подложках создавался температурный градиент, что позволило изучить влияние воздействия заряда на свойства и структуру слоев селена, изготовленных при разных температурах подложки. Температура подложки в одном конце поддерживалась 293 К, а в другом — 373 К. Испарение селена производилась из кварцевого тигля с косвенным нагревом. Скорость конденсации слоя была 17—33 нм. $С^{-1}$. Толщина слоя 35—50 мкм.

Электрофотографические свойства слоев селена исследовались с помощью специального электрометра с вибрирующим зондом, который обеспечивал разрешающую способность в несколько десятков микронов [13]. Потенциал зарядки и его кинетика в темноте измерялись в отдельных точках или при зондировании в направлении температурного градиента.

Структура слоев селена исследовалась путем электронной микроскопии на просвет ультратонких срезов поперечного сечения слоя [2], а также при помощи исследований поперечного излома массивных образцов в сканирующем микроскопе JSM-35.

3. Результаты

Проведенные исследования показали, что плотность тока зарядов в молекулярном потоке селена существенно зависит от температуры испаряемого вещества (рис. 2). При испарении селена в молекулярном потоке име-

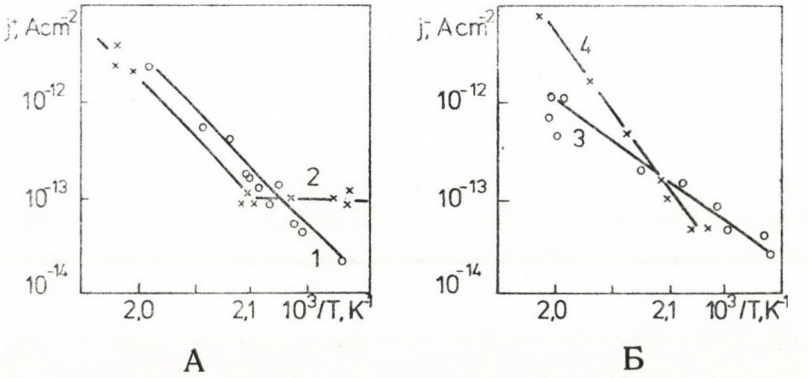

Рис. 2. Зависимость плотности тока положительных (А) и отрицательных (Б) зарядов в молекулярном потоке от температуры источника при испарении из испарителя прямого (1, 3) и косвенного (2, 4) нагрева

ются электроны (кривые 3,4) и положительные ионы (кривые 1,2), плотность тока которых можно менять в широком интервале ($10^{-14} \div 10^{-6}$ А. см$^{-2}$), меняя температуру испарителя или нагревательного элемента испарителя (в случае косвенного нагрева испарителя), конструкцию испарителя, напряженность и направление электрического поля в пространстве между испарителем и подложкой. Напр.: созданная разность потенциала в несколько вольт (2—4 В) между испарителем и подложкой меняет полярность тока зарядов в молекулярном потоке. Исследования распределения положительных ионов в вакуумной камере и зависимости плотности тока ионов от температуры ионизатора (нагретая вольфрамовая спираль) показали, что ионы образуются за счет поверхностной ионизации молекул, попадающих на нагретую поверхность [14, 15]. Используя это обстоятельство и зависимость плотности и полярности тока от напряженности электрического поля, в молекулярном потоке селена создавался желаемой плотности и полярности поток зарядов.

Опыты показали, что как ионы так и электроны в молекулярном потоке селена оказывают существенное влияние на электрофотографические свойств напыленных слоев селена. В характерных зависимостях электрофотографических параметров (предального потенциала зарядки, времени полуспада потенциала в темноте) от температуры подложки имеется сравнительно резкий перепад при $T_п = 323 \div 353$ К (рис. 3). Проведенные эксперименты показали, что температурный интервал изменения свойств напыленных слоев при увеличении плотности тока электронов в молекулярном потоке смещается к более низким температурам (кривая 1), а при увеличении пготности тока положительных ионов — в область более высоких температур (кривая 3).

Проведенные электрономикроскопические исследования структуры слоев селена показали, что полярность и плотность тока зарядов в молекулярном

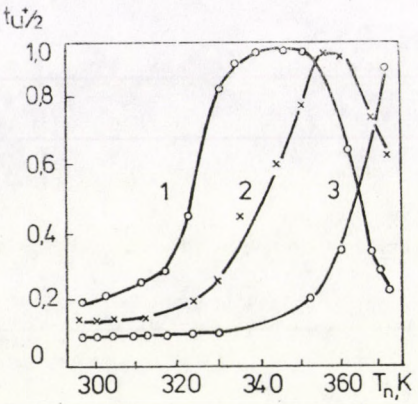

Рис. 3. Зависимость времени полуспада положительного потенциала зарядки от температуры подложки. При напылении селена плотность тока электронов (1) и положительных ионов (3) была 1—2. 10^{-7} А. см.$^{-2}$. (2) — плосткость тока зарядов в молекулярном потоке меньше 1.10^{-14} А.см$^{-2}$

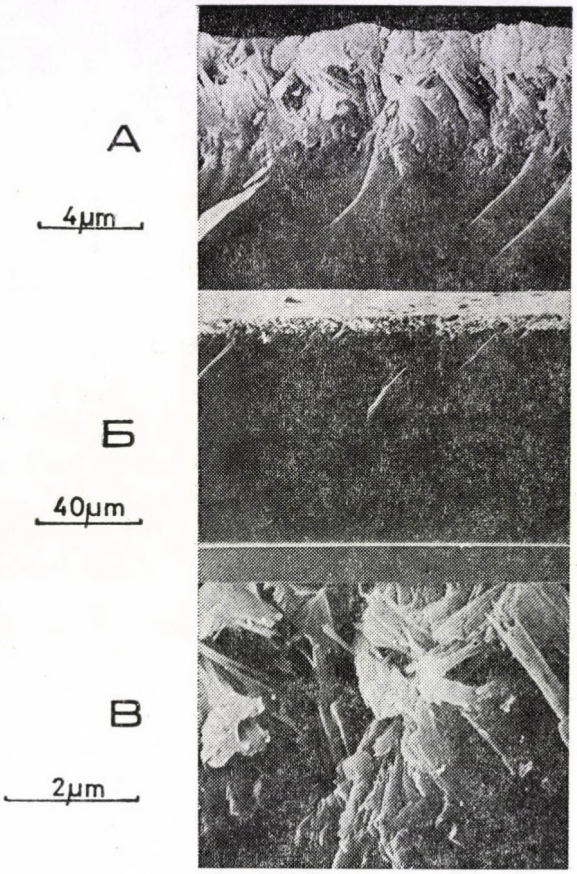

Рис. 4. Микрофотографии поперечного излома слоев селена

потоке сильно влияет на формирование кристаллического подслоя у подложки (рис. 4А). Кристаллическая фаза идентифицировалась при помощи электронографических исследований ультратонких срезов поперечного сечения слоя [2]. Толщина кристаллического подслоя и ее зависимость от плотности зарядов в молекулярном потоке определялась при помощи изучения излома поперечного сечения слоя в сканирующем микроскопе (рис. 4Б). Данная методика позволила получить некоторые сведения о морфологическом строении кристаллического подслоя. Из микрофотографии представленной на рис. 4В видно, что иглоподобные кристаллы селена переплетаются образуя волокнистую структуру. Можно предположить, что в процессе формирования кристаллического подслоя создаются микропоры. Толщина кристаллического подслоя селена у подложки быстро увеличивается с увеличением температуры подложки, а также зависит от полярности и плотности электрических зарядов в молекулярном потоке селена (рис. 5). Отрицательный заряд в мо-

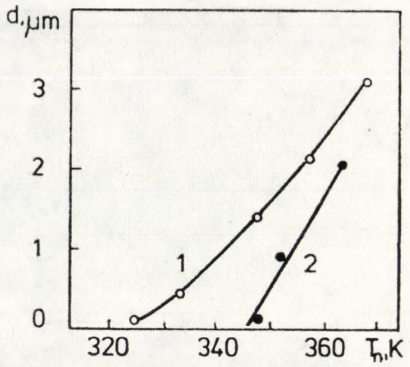

Рис. 5. Зависимость толщины кристаллического подслоя от температуры подложки. Обозначения и условия напыления слоев селена те же, как в рис. 2

лекулярном потоке способствует образованию кристаллического подслоя и он создается при более низких температурах подложки (кривая 1), чем в случае без зарядов в молекулярном потоке (кривая 2). Следует указать, что большая разница в толщине кристаллического подслоя наблюдается при сравнительно невысоких температурах подложки, т. е. когда толщина кристаллического подслоя не превышает 1 мкм. Положительные ионы в молекулярном потоке замедляют процесс кристаллизации селена.

4. Обсуждение результатов

Полученные экспериментальные результаты показали, что полярность и плотность тока зарядов в молекулярном потоке селена существенно влияют на свойства и структуру слоев. Это можно объяснить тем, что плотность зарядов меняет напряженность электростатического поля в слое селена во время его конденсации. Так как селен во время конденсации имеет сравнительно высокую температуру и большую вязкость, то под действием электрического поля происходит ориентация молекул селена, степень которой будет зависеть от напряженности поля. Это, безусловно, приведет к изменению структуры и кристаллизационной способности аморфной фазы селена. Наиболее благоприятные условия для кристаллизации селена во время конденсации слоев создаются у подложки. В области подложка-слой селена контактная разность потенциалов создает соответствующую напряженность электростатического поля. Это поле зависит от вещества подложки и внешнего электрического поля. Таким образом напряженность и направление электростатического поля в области подложка-слой селена будет зависить от полярности и плотности тока зарядов в молекулярном потоке селена. Поэтому можно предположить, что зависимость фазового состава слоев селена от плотности тока

зарядов при конденсации слоев обусловлена изменением электростатического поля в приконтактной области.

Известно [5], что кристаллический подслой селена у подложки слоев значительно уменьшает инжекцию электронов из подложки. Поэтому образование кристаллического подслоя селена (рис. 5) увеличивает время спада положительного потенциала зарядки в темноте (рис. 3). Однако, полностью объяснить зависимость электрофотографических параметров от плотности и полярности зарядов в молекулярном потоке изменением толщины кристаллического подслоя не удается. Напр.: установлено, что увеличение плотности положительных ионов при напылении селена увеличивает положительный остаточный потенциал при экспонировании сильнопоглощаемым светом, а также уменьшает предельный положительный потенциал зарядки. Поэтому предполагаем, что заряды в молекулярном потоке оказывают влияние и на формирование структуры аморфной фазы селена во всем объеме слоя.

Таким образом плотность и полярность тока зарядов в молекулярном потоке селена может быть использована для управления свойств и структуры слоев селена.

Авторы выражают свою благодарность Я. Лабару за помощь оказанную в исследованиях растровым электронным микроскопом.

ЛИТЕРАТУРА

1. P. H. Keck, J. Opt. Soc. Amer., **42**, 221, 1952.
2. E. Montrimas, B. Petretis, Phys. Stat. Sol. (a), **15**, 361, 1973.
3. B. Petretis, H. Rogass, A. Satas, Phys. Stat. Sol. (a), **20**, K3, 1975.
4. B. Petretis, A. V. Karaliunets, in "Amorphous Semiconductors" 76, edited by I. Kósa-Somogyi, Budapest, 1976, p. 295.
5. J. K. Viscakas, E. A. Montrimas, A. A. Satas, Lietuvos fizikos rinkinys, **8**, 831, 1968.
6. K. L. Chopra, J. Appl. Phys., **37**, 2249, 1966.
7. D. I. Kennedy, R. E. Hayes, R. W. Alsford, J. Appl. Phys., **38**, 1986, 1967.
8. K. L. Chopra, Thin Film Phenomena. McGraw-Hill Book Company Inc. New York, 1969.
9. J. F. Pócza, A. Barna, B. P. Barna, I. Pozsgai, G. Radnóczi, Proc. 6th Internl. Vacuum Congr. J. Appl. Phys. Suppl., **2**, 525, 1974.
10. Ш. А. Бэлан, И. Э. Болотов, З. И. Комарова, Изв. вузов, физика, **6**, 106, 1971.
11. И. Кх. Гэллэр, Б. Т. Коломич, А. И. Попов, Г. М. Балактар, Изв. Акад, Наук СССР, сер. Неорг. Матер., **8**, 1005, 1972.
12. Г. В. Абдуллаев, Д. Абдинов, Физика Селена, изд. «ЭЛМ», Баку, 1975, стр. 50.
13. A. Bodrovolskis, B. Petretis, S. Sakalauskas, V. Karpavicius, Lietuvos fizikos rinkinys, **15**, 811, 1975.
14. Э. Я. Зандберг, А. И. Ионов. Поверхностная ионизация. «Наука», Москва, 1969.
15. Л. Н. Добречов, Электронная и ионная эмиссия, Изд. техн.-теор. лит., Москва—Ленинград, 1952.

Acta Physica Academiae Scientiarum Hungaricae, Tomus 48 (2—3), pp. 323—331 (1980)

GENERAL FORM OF THE CENTRIFUGAL CORRECTIONS OF THE SPIN INTERACTIONS IN DIATOMIC MOLECULES

By

I. KOVÁCS

DEPARTMENT OF ATOMIC PHYSICS, TECHNICAL UNIVERSITY, 1521 BUDAPEST, HUNGARY

(Received 26. II. 1980)

General forms valid for terms of any type and multiplicity in diatomic molecules are obtained for the first and second correction terms of centrifugal distortions of the spin-orbit, spin-spin and spin-rotation interactions.

1. Introduction

The energy values of the multiplet states corresponding to Hund's case a) can be readily obtained from the separable wave equation including the diagonal terms of several interactions of the resultant spin momentum. By the omission of certain terms the wave equation may be separated into three parts: containing the electron coordinates, the rotational coordinates and the vibrational coordinate (internuclear distance), respectively. Energy values calculated from the wave equation in this way, however, did not correspond closely to the experimental results. This is understandable inasmuch as this limiting case practically means neglecting all interactions, with the exception of a few, due to the neglection of the off diagonal terms of several interactions. In the actual molecule, however, all interactions are operative to a greater or smaller extent. Results compatible with experimental findings can be obtained, however, if these energy values are used initially, i.e. those of the unperturbed system, and the off diagonal matrix elements of all interactions are taken into consideration by perturbation calculation. In this way we can obtain energies or term values intermediate between Hund's limiting cases. These intermediate values are capable of describing the gradual transition from one limiting case to another.

Although the term formulas so obtained show agreement with experiments in most of the observed multiplet terms, in some cases, especially in the case of hydrides, they cannot be applied successfully. The observed discrepancies usually consist in that the coupling constants apparently change with the rotational quantum number J and, in addition, the multiplet splitting deviates from the above mentioned multiplet term formulas.

If the rotating molecule is not a rigid rotator, then the centrifugal effect will influence the rotational energy and the energies of the spin interactions because the interaction constants obtained by the solution of the electronic part of the wave equation contain the internuclear distance as parameter and the latter increases with increasing rotation. This effect for the rotational energy and for special cases of the spin-orbit, spin-spin and spin-rotation interactions is already well known. Namely, for the spin interactions they have been calculated for doublet terms by KOVÁCS and VUJISIĆ [1], for triplet terms by KOVÁCS and EL AGRAB [2], for $^4\Sigma$ term by KOVÁCS and KORWAR [3]. In the following we are going to give the general form of the matrix elements of the centrifugal corrections of all the spin interactions valid for terms of any kind and multiplicity.

2. Theory of the centrifugal distortion of the spin interactions

If certain terms are omitted from the wave equation of a molecule

$$(\hat{H} - E)|\rangle = 0 \tag{1}$$

it can be solved by a wave function

$$|n, \Lambda, \Sigma\rangle|n, v\rangle|J, \Omega, M\rangle, \tag{2}$$

where $|n, \Lambda, \Sigma\rangle$ depends on the electron and the spin coordinates, $|n, v\rangle$ on the internuclear distance and $|J, \Omega, M\rangle$ on the rotational coordinates. Multiplying (1) by $\langle n, \Lambda, \Sigma|$ and integrating over the electron and spin coordinates we obtain

$$[\hat{H}_{\text{vibr}} + \hat{H}_{\text{rot}} + \hat{H}^s - (E - E_{\text{el}}(r))] \; |n, v\rangle|J, \Omega, M\rangle = 0. \tag{3}$$

Using a power series expansion about the $E_{\text{el}}(r_e)$ minimum energy to express the dependence of the electronic energy on the internuclear distance we get

$$E_{\text{el}}(r) = E_{\text{el}}(r_e) + \frac{1}{2} k r_e \, \xi^2 \tag{4}$$

and in a similar manner by a power series we obtain for the rotational Hamiltonian

$$H_{\text{rot}} = \bar{B}_e(1 - 2\xi + 3\xi^2) \, \hat{R}^2, \tag{5}$$

where

$$\xi = \frac{r - r_e}{r_e}, \quad \bar{B}_e = \frac{h^2}{8\pi^2 \mu r_e^2}, \quad k = 4\pi^2 c^2 \omega^2 \mu. \tag{6}$$

μ is the reduced mass, ω is the vibrational frequency, $\hat{R}$ is the operator of the angular momentum of nuclear rotation.

The spin part of the Hamiltonian of a diatomic molecule can be written

$$\hat{H}^S = \hat{H}^{SO} + \hat{H}^{SS} + \hat{H}^{SR}, \tag{7}$$

where $\hat{H}^{SO}$ is the spin-orbit, $\hat{H}^{SS}$ the spin-spin, and $\hat{H}^{SR}$ the spin-rotation interaction operator, which can be written as follows

$$\hat{H}^{SO} = \bar{A}(r)\,(\hat{L}\,\hat{S}), \tag{8a}$$

$$\hat{H}^{SS} = \bar{\varepsilon}(r)\,[3\hat{S}_z^2 - \hat{S}^2], \tag{8b}$$

$$\hat{H}^{SR} = \bar{\gamma}(r)\,(\hat{R}\,\hat{S}), \tag{8c}$$

where $\hat{L}$ and $\hat{S}$ are the operators of the resultant orbital and spin momentum, respectively, $\bar{A}(r)$, $\bar{\varepsilon}(r)$ and $\bar{\gamma}(r)$ are the spin-orbit, spin-spin, and spin-rotation coupling constants, respectively. Because of the radial dependence of the coupling coefficients the operators of the spin interactions must be completed with centrifugal correction terms. Owing to the dependence on the internuclear distance using a power-series expansion about the equilibrium distance r_e we obtain for the coefficients of (8a), (8b), (8c)

$$\bar{A}(r) = \bar{A}_0 + \bar{\alpha}_1\xi + \bar{\alpha}_2\xi^2, \tag{9a}$$

$$\bar{\varepsilon}(r) = \bar{\varepsilon} + \bar{\varepsilon}_1\xi + \bar{\varepsilon}_2\xi^2, \tag{9b}$$

$$\bar{\gamma}(r) = \bar{\gamma} + \bar{\gamma}_1\xi + \bar{\gamma}_2\xi^2, \tag{9c}$$

where

$$\bar{A}_0 = (\bar{A})_{r=r_e},\ \bar{\alpha}_1 = r_e\left(\frac{\partial\bar{A}}{\partial r}\right)_{r=r_e},\ \bar{\alpha}_2 = \frac{1}{2}r_e^2\left(\frac{\partial^2\bar{A}}{\partial r^2}\right)_{r=r_e} \tag{10}$$

and similar expressions are valid for the other coefficients.

To explain the rotational structure in the first approximation it is not necessary to take into account the vibrational motion and, consequently, the vibrational dependence. So apart from the vibrational motion in the rotating molecule the internuclear distance has to assume a value r such that the centrifugal force is cancelled by the restoring force $kr_e\xi$ generated by the slight displacement $r - r_e$ from the equilibrium position r_e. The expression of the centrifugal force

$$F_c = \frac{\mathbf{R}^2}{\mu r^3}, \tag{11}$$

where $\mathbf{R}$ is the rotational angular momentum of the molecule. Equating the centrifugal force to the restoring force, we obtain

$$kr_e\xi = \frac{\mathbf{R}^2}{\mu r^3}. \tag{12}$$

Substituting, in a first approximation, r_e for r, and $(h^2/4\pi^2)\hat{R}^2$ the appropriate operator for $\mathbf{R}^2$, we get for ξ

$$\xi \sim \frac{h^2\hat{R}^2}{4\pi^2\mu r_e^4 k}. \tag{13}$$

Putting Eq. (13) in (9a), (9b) and (9c) we obtain for (8a), (8b) and (8c)

$$\hat{H}^{SO} = (A_0 + A_1\hat{R}^2 + A_2\hat{R}^4)\,(\hat{L}\,\hat{S}), \tag{14a}$$

$$\hat{H}^{SS} = (\varepsilon + \tau\hat{R}^2 + \varrho\hat{R}^4)\,(3\hat{S}_z^2 - \hat{S}^2), \tag{14b}$$

$$\hat{H}^{SR} = (\gamma + \sigma\hat{R}^2 + \varphi\hat{R}^4)\,(\hat{R}\,\hat{S}), \tag{14c}$$

where all coefficients are measured in cm^{-1} units (divided by hc in (9) and neglecting all the accents above the symbols) and

$$A_1 = \beta\alpha_1; \quad \tau = \beta\varepsilon_1; \quad \varrho = \beta\gamma_1; \quad \beta = \frac{4B_e^2}{\omega^2}$$

$$A_2 = \beta^2\alpha_2; \quad \varrho = \beta^2\varepsilon_2; \quad \varphi = \beta^2\gamma_2; \quad B_e = \frac{h}{8\pi^2\mu c r_e^2}. \tag{15}$$

The values of the corresponding matrix elements of the $\hat{R}^2$, $\hat{R}^4$, $\hat{L}\hat{S}$, $3\hat{S}_z^2 - \hat{S}^2$, $\hat{R}\hat{S}$ operators can be found in [4]. Using these values for the calculation of the general form of the matrix of (14a), (14b) and (14c) due to the non-commutativity of the matrices separated by the brackets the form $\frac{1}{2}(\hat{A}\hat{B} + \hat{B}\hat{A})$ is to be used instead of the multiplication form $\hat{A}\hat{B}$. The explicit form of the matrix elements (14) valid for terms of any kind and multiplicity is as follows:

$$\langle \Lambda, \Sigma|\hat{H}^{SO}|\Lambda, \Sigma\rangle = A_0\Lambda\Sigma + A_1\langle \Lambda, \Sigma \mid \hat{R}^2(\hat{L}\,\hat{S}) \mid \Lambda, \Sigma\rangle + \\ + A_2\,\langle \Lambda, \Sigma|\hat{R}^4(\hat{L}\,\hat{S})\,|\Lambda, \Sigma\rangle, \tag{16a}$$

$$\langle \Lambda, \Sigma \mid \hat{H}^{SO} \mid \Lambda, \Sigma \pm 1\rangle = A_1\langle \Lambda, \Sigma \mid \hat{R}^2(\hat{L}\,\hat{S})\,\Lambda, \Sigma \pm 1\rangle + \\ + A_2\langle \Lambda, \Sigma\,|\hat{R}^4(\hat{L}\,\hat{S})|\Lambda, \Sigma \pm 1\rangle, \tag{17a}$$

$$\langle \Lambda, \Sigma \mid \hat{H}^{SO} \mid \Lambda, \Sigma \pm 2\rangle = A_2\langle \Lambda, \Sigma \mid \hat{R}^4(\hat{L}\,\hat{S}) \mid \Lambda, \Sigma \pm 2\rangle, \tag{18a}$$

where

$$\langle \Lambda, \Sigma \mid \hat{R}^2(\hat{L}\,\hat{S}) \mid \Lambda, \Sigma\rangle = \Lambda, \Sigma[f(J, \Omega) + f(S, \Sigma)], \tag{16b}$$

$$\langle \Lambda, \Sigma \mid \hat{R}^4(\hat{L}\,\hat{S}) \mid \Lambda, \Sigma\rangle = \Lambda\Sigma\{[f(J, \Omega) + f(S, \Sigma)]^2 + 2f(J, \Omega)f(S, \Sigma) + 2\Omega\Sigma\}, \tag{16c}$$

$$\langle \Lambda,\ \Sigma \,|\, \hat{R}^2(\hat{L}\,\hat{S}) \,|\, \Lambda, \Sigma \pm 1\rangle = \Lambda \left(\Sigma \pm \frac{1}{2}\right) [g_1(J, \Omega)\, g_1(S, \Sigma)]^{1/2}. \tag{17b}$$

$$\langle \Lambda, \Sigma \,|\, \hat{R}^4(\hat{L}\,\hat{S})|\, \Lambda, \Sigma \pm 1\rangle = 2\Lambda \left(\Sigma \pm \frac{1}{2}\right) [g_1(J, \Omega) + g_1(S, \Sigma) - 1]$$
$$[g_1(J, \Omega) g_1(S, \Sigma)]^{1/2}, \tag{17c}$$

$$\langle \Lambda, \Sigma|\hat{R}^4(\hat{L}\hat{S})|\Lambda, \Sigma \pm 2\rangle = \Lambda(\Sigma \pm 1)[g_1(J, \Omega)g_1(S, \Sigma)g_2(J, \Omega)g_2(S, \Sigma)]^{1/2} \tag{18b}$$

$$f(x, y) = x(x + 1) - y^2;\ g_1(x, y) = x(x + 1) - y(y \pm 1),$$
$$g_2(x, y) = g_1(x, y \pm 1) = x(x + 1) - (y \pm 1)(y \pm 2), \tag{19}$$

$$\langle \Lambda, \Sigma|\hat{H}^{SS}|\Lambda, \Sigma\rangle = \varepsilon[3\Sigma^2 - S(S + 1)] + \tau\langle \Lambda, \Sigma|\, \hat{R}^2(3\hat{S}_z^2 - \hat{S}^2)|\Lambda, \Sigma\rangle +$$
$$+ \varrho\langle \Lambda, \Sigma|\hat{R}^4(3\hat{S}_z^2 - \hat{S}^2)|\Lambda, \Sigma\rangle, \tag{20a}$$

$$\langle \Lambda, \Sigma|\hat{H}^{SS}|\Lambda, \Sigma \pm 1\rangle = \tau\langle \Lambda, \Sigma|\hat{R}^2(3\hat{S}_z^2 - \hat{S}^2)|\Lambda, \Sigma \pm 1\rangle +$$
$$+ \varrho\langle \Lambda, \Sigma|\hat{R}^4(3\hat{S}_z^2 - \hat{S}^2)|\Lambda, \Sigma \pm 1\rangle, \tag{21a}$$

$$\langle \Lambda, \Sigma|\hat{H}^{SS}|\Lambda, \Sigma \pm 2\rangle = \varrho\langle \Lambda, \Sigma|\hat{R}^4(3\hat{S}_z^2 - \hat{S}^2)|\Lambda, \Sigma \pm 2\rangle, \tag{22a}$$

where

$$\langle \Lambda, \Sigma \,|\, \hat{R}^2(3\hat{S}_z^2 - \hat{S}^2) \,|\, \Lambda, \Sigma\rangle = [3\Sigma^2 - S(S + 1)]\,[f(J, \Omega) + f(S, \Sigma)], \tag{20b}$$

$$\langle \Lambda, \Sigma|\hat{R}^4(3\hat{S}_z^2 - \hat{S}^2)|\Lambda, \Sigma\rangle = [3\Sigma^2 - S(S + 1)]\ \{[f(J, \Omega) + f(S, \Sigma)]^2 +$$
$$+ 2f(J, \Omega)f(S, \Sigma) + 2\Omega\Sigma\}, \tag{20c}$$

$$\langle \Lambda, \Sigma|\hat{R}^2(3\hat{S}_z^2 - \hat{S}^2)|\Lambda, \Sigma \pm 1\rangle = \left\{3\left[\left(\Sigma \pm \frac{1}{2}\right)^2 + \frac{1}{4}\right] - S(S + 1)\right\}$$
$$[g_1(J, \Omega)\, g_1(S, \Sigma)]^{1/2}, \tag{21b}$$

$$\langle \Lambda, \Sigma|\hat{R}^4(3\hat{S}_z^2 - \hat{S}^2)\,|\Lambda, \Sigma \pm 1\rangle = 2\left\{3\left[\left(\Sigma \pm \frac{1}{2}\right)^2 + \frac{1}{4}\right] - S(S + 1)\right\}$$
$$[g_1(J, \Omega) + g_1(S, \Sigma) - 1]\ [g_1(J, \Omega)\, g_1(S, \Sigma)]^{1/2}, \tag{21c}$$

$$\langle \Lambda, \Sigma|\hat{R}^4(3\hat{S}_z^2 - \hat{S}^2)|\Lambda, \Sigma \pm 2\rangle = \{3[(\Sigma \pm 1)^2 + 1] - S(S + 1)\}$$
$$[g_1(J, \Omega)\, g_1(S, \Sigma)\, g_2(J, \Omega)\, g_2(S, \Sigma)]^{1/2} \tag{22b}$$

and finally

$$\langle \Lambda, \Sigma|\hat{H}^{SR}|\Lambda, \Sigma\rangle = -\gamma f(S, \Sigma) + \sigma\langle \Lambda, \Sigma|\hat{R}^2(\hat{R}\,\hat{S})|\Lambda, \Sigma\rangle +$$
$$+ \varphi\langle \Lambda, \Sigma|\hat{R}^4(\hat{R}\,\hat{S})|\Lambda, \Sigma\rangle, \tag{23a}$$

$$\langle \Lambda, \Sigma|\hat{H}^{SR}|\Lambda, \Sigma \pm 1\rangle = -\frac{1}{2}\gamma[g_1(J, \Omega)\, g_1(S, \Sigma)]^{1/2} +$$

$$+ \sigma\langle \Lambda, \Sigma|\hat{R}^2(\hat{R}\,\hat{S})|\Lambda, \Sigma \pm 1\rangle + \varphi\langle \Lambda, \Sigma|\hat{R}^4(\hat{R}\,\hat{S})|\Lambda, \Sigma \pm 1\rangle, \tag{24a}$$

$$\langle \Lambda, \Sigma|\hat{H}^{SR}|\Lambda, \Sigma \pm 2\rangle = \sigma\langle \Lambda, \Sigma|\hat{R}^2(\hat{R}\,\hat{S})|\Lambda, \Sigma \pm 2\rangle +$$
$$+ \varphi\langle \Lambda, \Sigma|\hat{R}^4(\hat{R}\,\hat{S})|\Lambda, \Sigma \pm 2\rangle, \tag{25a}$$

$$\langle \Lambda, \Sigma|\hat{H}^{SR}|\Lambda, \Sigma \pm 3\rangle = \varphi\langle \Lambda\, \Sigma|\hat{R}^4(\hat{R}\,\hat{S})|\Omega, \Sigma \pm 3\rangle, \tag{26a}$$

where

$$\langle \Lambda, \Sigma|\hat{R}^2(\hat{R}\,\hat{S})|\Lambda, \Sigma)\rangle = -[f(S, \Sigma)^2 + 2f(J, \Omega)\, f(S, \Sigma) + \Omega\Sigma)], \tag{23b}$$

$$\langle \Lambda, \Sigma|\hat{R}^4(\hat{R}\,\hat{S})|\Lambda, \Sigma\rangle = -\{[f(J, \Omega)f(S, \Sigma) + \Omega\Sigma]\,[3f(J, \Omega) + 6f(S, \Sigma) - 2] +$$
$$+ [2\Omega^2 + f(S, \Sigma)^2]f(S, \Sigma) + \Sigma(2\Sigma + \Omega)f(J, \Omega)\}, \tag{23c}$$

$$\langle \Lambda, \Sigma|\hat{R}^2(\hat{R}\,\hat{S})|\Lambda, \Sigma \pm 1\rangle = -\frac{1}{2}\,[g_1(J, \Omega) + 3g_1(S, \Sigma) -$$
$$- 2][g_1(J, \Omega)\, g_1(S, \Sigma)]^{1/2}, \tag{24b}$$

$$\langle \Lambda, \Sigma|\hat{R}^4(\hat{R}\,\hat{S})|\Lambda, \Sigma \pm 1\rangle = -\frac{1}{2}\{[g_1(J, \Omega) + 5g_1(S, \Sigma) - 6] \times$$
$$\times [g_1(J, \Omega) + g_1(S, \Sigma)] + [3g_1(J, \Omega) - 4]g_1(S, \Sigma) +$$
$$+ (\Omega + \Sigma \pm 3)^2 + 8\Omega\Sigma - 1\}\,[g_1(J, \Omega)g_1(S, \Sigma)]^{1/2}, \tag{24c}$$

$$\langle \Lambda, \Sigma|\hat{R}^2(\hat{R}\,\hat{S})|\Lambda, \Sigma \pm 2\rangle = -\frac{1}{2}\,[g_1(J, \Omega)\, g_1(S, \Sigma)\, g_2(J, \Omega)\, g_2(S, \Sigma)]^{1/2}, \tag{25b}$$

$$\langle \Lambda, \Sigma|\hat{R}^4(\hat{R}\,\hat{S})|\Lambda, \Sigma \pm 2\rangle = -\frac{1}{2}\{2f(S, \Sigma \pm 1) + g_1(J, \Omega) +$$
$$+ g_1(S, \Sigma) + g_2(J, \Omega) + g_2(S, \Sigma) -$$
$$- 4\}\,[g_1(J, \Omega)\, g_1(S, \Sigma)g_2(J, \Omega)g_2(S, \Sigma)]^{1/2}, \tag{25c}$$

$$\langle \Lambda, \Sigma|\hat{R}^4(\hat{R}\,\hat{S})|\Lambda, \Sigma \pm 3\rangle = -\frac{1}{2}\,[g_1(J, \Omega)\, g_1(S, \Sigma)\, g_2(J, \Omega)$$
$$g_2(S, \Sigma)\, g_3(J, \Omega)\, g_3(S, \Sigma)]^{1/2}, \tag{26b}$$

where

$$g_3(x, y) = g_1(x, y \pm 2) = x(x + 1) - (y \pm 2)(y \pm 3). \tag{27}$$

The perturbation matrix is now composed of the perturbation matrices of a number of interactions which differ by orders of magnitude. In such cases

the most practical method is to select the largest of the interaction terms and diagonalize the matrix so obtained; the remainder of the weak perturbations can then be taken into account by the perturbation calculation as follows.

Let then $\hat{H} = \hat{H}' + \hat{\hat{H}}^p$, where $\hat{H}' = \hat{H}_0 + \hat{H}^p$ is the energy operator used at the first stage of the calculation; $\hat{H}_0$ is the operator of the separable wave equation ; $\hat{H}^p$ is the sum of the operators of the stronger perturbations, namely the terms neglected in the separation of the wave equation and the first term of (16a) ($A_0 \Lambda\Sigma$), whereas $\hat{\hat{H}}^p$ is the sum of the weak-perturbation operators, namely the remainder terms of (16a), $\hat{H}^{SS}$ and $\hat{H}^{SR}$. The eigenvalues $E' = S\hat{H}'S^{-1}$ of the $\hat{H}'$ operator are the well-known multiplet term formulas, whereas according to [4]

$$\bar{H}^p_N(J) = S_{\Lambda-S,N} \sum_{\Sigma=-S}^{+S} S_{\Lambda+\Sigma,N} \langle \Lambda, -S | \hat{\hat{H}}^p | \Lambda, \Sigma \rangle + S_{\Lambda-S+1,N} \times$$

$$\times \sum_{\Sigma=-S}^{+S} S_{\Lambda+\Sigma,N} \langle \Lambda, -S+1 | \hat{\hat{H}}^p | \Lambda, \Sigma \rangle + \ldots + S_{\Lambda+S,N} \sum_{\Sigma=-S}^{+S} S_{\Lambda+\Sigma,N} \langle \Lambda, +S | \hat{\hat{H}}^p | \Lambda, \Sigma \rangle \tag{28}$$

$$(N = J - S, J - S + 1, \ldots, J + S)$$

gives the deviations $S\hat{H}S^{-1} - E' = S\hat{\hat{H}}^pS^{-1}$ from the multiplet term formulas caused by the $\hat{\hat{H}}^p$ weak perturbations, in the present case by the centrifugal distortion of the spin-orbit interaction if $\hat{\hat{H}}^p = H^{SO} - A_0 \Lambda\Sigma$ and by the spin-spin interaction and spin-rotation interaction including its centrifugal distortions, if $\hat{\hat{H}}^p = \hat{H}^{SS}$ or $\hat{H}^{SR}$. The detailed form of the S transformation matrix elements which transform the H' energy operator into diagonal form, can be found for doublet, triplet and quartet states in the intermediate case between Hund's case a) and b) in [4], for quintet states in [5], for sextet states in [6], and for septet states in [7] in the Hund's case b). For Hund's case a), of course, (28) gives the diagonal part of the spin interactions, i.e. (16a), for the spin-orbit interaction (20a), for spin-spin interaction and (23a) for the spin-rotation interaction. Taken into account in this way the weak interactions contribute additively to the usual term formulas. Hence, they do not modify the formulas already established and the deviations stemming from them can be readily separated from the first stronger perturbation and from each other, too.

In Hund's case b), however, it is not necessary to use (28) containing the before mentioned S transformation matrices and the spin interaction matrices treated above. Applying the form of Hund's case b) of the spin interaction matrices given by [4] we get directly from (14a), (14b), (14c)

$$H^{S0}_N(N) = \Lambda^2[A_0 + A_1 f(N, \Lambda) + A_2 f(N, \Lambda)^2] \frac{C}{2f(N, 0)}, \tag{29a}$$

$$H_N^{SS}(N) = -2[\varepsilon + \tau f(N, \Lambda) + \varrho f(N, \Lambda)^2] \frac{\frac{3}{4}C(C+1) - f(N,0)f(S,0)}{(4f(N,0) - 3)f(N,0)} \times [f(N, \Lambda) - 2\Lambda^2], \tag{29b}$$

$$H_N^{SR}(N) = \frac{1}{2}[\gamma + \sigma f(N, \Lambda) + \varphi f(N, \Lambda)^2]\, C\, \frac{f(N, \Lambda)}{f(N, 0)}, \tag{29c}$$

where

$$C = f(J, 0) - f(N, 0) - f(S, 0) \tag{29d}$$

and $N = J - S, J - S + 1, \ldots, J + S$. These formulas are valid for terms of any kind and multiplicity in Hund's case b).

3. Application of the theory to the multiplet Σ terms ($\Lambda = 0$)

Taking into account that in most of the multiplet Σ terms, in general, the Hund's case b) form gives a good approximation we get for the multiplet term values

$$F_N(N) = v_0 + T_N(N) + H_N^{SS}(N) + H_N^{SR}(N), \tag{30}$$

where

$$T_N(N) = Bf(N, 0) - Df(N, 0)^2 \tag{31}$$

and the detailed form of the remainder terms can be obtained by substitution of $\Lambda = 0$ in (29b), (29c) and $N = J - S, J - S + 1, \ldots, J + S$ [8]. Owing to $\Lambda = 0$ in this case, of course, $H_N^{SO}(N)$ is equal to 0.

The experimental applications of (30) can be found in [8], namely for the $X^2\Sigma^+$ ground state of the HgH molecule, the $B^2\Sigma$ term of the YO molecule, the $A^3\Sigma^+$ term of the N_2 molecule and the $^4\Sigma^-$ term of the MnH molecule.

In case of Σ terms of triplet or higher multiplicity, however, especially when the coefficient of the spin-spin interaction ε is larger than the others, the Hund's case b) approximation is no longer sufficient.

In such a case one can start from Hund's case a) for all interactions in (20a) and (23a) and taking into account the off-diagonal matrix elements in (21a), (22a) and (24a), (25a), (26a) the complete secular determinant is to be solved. This is the situation in the cases of the $^3\Sigma$ term of the O_2 molecule [9] and of $^4\Sigma$ terms of the GeH and SnH molecules [10].

4. Application of the theory to the multiplet $\Pi, \Delta \ldots$ terms ($\Lambda > 0$)

The analytically closed formula was applied to the term values of the $^2\Delta$ state ($\Delta = 2$) of both the SnH and Sn molecules. In the case of doublet terms, of course, the spin-spin interaction is zero. It was found that, in the

case of SnH, it is sufficient to take into account only the first and second centrifugal corrections of the spin-orbit interaction without the centrifugal corrections of spin-rotation interaction, while in the case of SnD it was necessary to use the complete formula [1].

In the case of the $C^3\Delta$ state of TiO molecule after taking into account the centrifugal distortion of the spin-orbit and spin-spin interactions by (28) the observed and the theoretically expected change of the coupling constant shows good agreement [2]. It was not necessary to take into account here the spin-rotation interaction.

Finally, in the case of terms of higher than quartet multiplicity the perturbation method (28) cannot be applied because for lack of the analytically closed solutions the transformation matrix for intermediate case cannot be calculated explicitly. Therefore the matrix diagonalization can be carried out only in a purely numerical way by electronic computer. This is the situation among others in the case of the $^7\Pi$ state of MnH molecule. Taking into account the first centrifugal correction of the spin-spin and spin-rotation interactions the observed and calculated term values for the each of the seven components of the $^7\Pi$ term show good agreement [11].

REFERENCES

1. I. Kovács and B. Vujisić, J. Phys. B.: Atom Molec. Phys., **4**, 1123, 1971.
2. I. Kovács and M. I. M. El Agrab, Acta Phys. Hung., **42**, 67, 1977.
3. I. Kovács and V. M. Korwar, J. Phys. B.: Atom Molec. Phys., **4**, 759, 1971.
4. I. Kovács, Rotational Structure in the Spectra of Diatomic Molecules, Akadémiai Kiadó, Budapest and Adam Hilger Ltd., London, 1969.
5. I. Kovács and A. Grandpierre, Acta Phys. Hung., **43**, 319, 1977.
6. I. Kovács and I. Péczeli, Acta Phys. Hung., **43**, 293, 1977.
7. I. Kovács, I. Péczeli and A. Grandpierre, Acta Phys. Hung., **45**, 327, 1978.
8. I. Kovács, Acta Phys. Hung., **32**, 5, 1972.
9. M. Tinkham and M. W. P. Strandberg, Phys. Rev., **97**, 937, 1955.
10. I. Kovács and P. Pacher, J. Phys. B.: Atom Molec. Phys., **4**, 1633, 1971.
11. I. Kovács and P. Pacher, J. Phys. B.: Atom Molec. Phys., **8**, 796, 1975.

RECENSIONES

V. L. GINZBURG:

Theoretical Physics and Astrophysics

International Series in Natural Philosophy, Vol. 99. Translated by D. Ter Haar, Pergamon Press, Oxford—New York—Toronto—Sydney—Paris—Frankfurt

The topics of this textbook are based on a lecture course for students at the Physics and Astrophysics Department of the Moscow Physico-Technical Institute. The main aim is to present topics especially related to electrodynamics and to show some applications in various aspects of astrophysics.

Since the text includes conclusions drawn from a large number of papers the book closely resembles a monograph regarding its character. The 17 chapters treat among others charge particles interacting with photons, the radiations reaction of moving charge described by the Hamiltonian method, the rotation of a magnetic moment applied to astrophysics in case of pulsars, the discussion of the spectral distribution of radiation of accelerated moving charge, radiative losses when charge moves in a magnetic field, peculiarities and some applications in astrophysics of the synchrotron radiation, the limits of applicability of the theory.

In the second part of the book the phenomena of the electrodynamics of the continuous medium are investigated, viz.: Cerenkov effect, Doppler effect, transition radiation, superluminal radiation sources, reabsorption and radiative transfer, electrodynamics of media with spatial dispersion, dielectric permittivity and wave propagation in a plasma, the energy-momentum tensor in macroscopic electrodynamics, fluctuations in Van der Waals forces, scattering of waves in a medium.

The last three Chapters are very interesting and topical. The rapid progress in astronomy during the last three decades elucidates the reason why the mechanisms of X-ray and gamma emission, the analysis of the propagation and of the transformation of the chemical composition of the cosmic rays traversing interstellar space and neutrino physics have attracted the attention of astronomers. These Chapters are devoted to the processes occurring in the Universe which are restricted to the problems of so-called high-energy astrophysics.

The Chapter on cosmic ray astrophysics treats the model of the propagation of cosmic rays, the ionization energy losses, the beam instability and plasma effects in cosmic rays, the application of transfer equation in a special case.

The last two Chapters are devoted to the processes leading to the formation of X-rays and gamma-rays, X-ray brems-emission by plasma, the inverse Compton effect, Compton energy losses, X-ray synchrotron emission, the gamma radiation produced by cosmic ray component, a few examples of galaxies, the absorptions of X-rays and gamma-rays.

S. KANYÓ

G. DECONNINCK:

Introduction to Radioanalytical Physics

"Nuclear Methods" Vol. 1 Monograph Series of the Journal of Radioanalytical Chemistry and Radiochemical and Radioanalytical Letters, Editors: T. Braun and E. Bujdosó. Co-edition of Elsevier Scientific Publishing Company, Amsterdam, the Netherlands and Akadémiai Kiadó, The Publishing House of the Hungarian Academy of Sciences, Budapest, Hungary, 1978, pp. 242.

Methods involving nuclear radiations are worldwide accepted as useful analytical tools. Nuclear activation analysis and more specifically neutron activation analysis has been used almost since the beginning of the nuclear age. Consequently, a great deal of literature, in the

form of reviews and text books, already exists on the subject. Prompt nuclear reaction applications, however, are more recent and the subject is still in development. Professor DECONNINCK made very important contributions even to this subject. His book forms the basis of a complete course on modern nuclear analytical techniques using charged particles and photons excluding neutron activation.

Chapter 1 yields a description of the basic physical principles of nuclear reactions, namely, kinematics, reaction mechanisms and cross-sections. Chapter 2 is devoted to the discussion of the interaction of particle beams with matter. Beside the description of the slowing down process and the calculation of the energy straggling effects (which are essential in depth profile analysis) the charged particle induced characteristic X-rays used for elemental analysis is also discussed in this Chapter. Chapter 3 deals with the principles and applications of the backscattering of heavy charged particles, including the channeling effect. Different nuclear reactions leading to gamma-ray emission and the application of these reactions for surface and bulk analysis, depth profiling and trace analysis are discussed in Chapter 4.

Chapter 5 deals with the analysis by charged particle and neutron spectroscopy. The last Chapter is a general review giving the analytical techniques for all the elements from hydrogen to uranium. Typical applications to chemistry and biology are also described in this Chapter.

Typical examples and solved problems help in the comprehension of the text and make of this book a real tool for elemental analysis.

Z. SZŐKEFALVI-NAGY

P. RENNERT:

Einführung in die Quantenphysik

Mathematisch-Naturwissenschaftliche Bibliothek,
Band 65, BSB B.G. Teubner Verlagsgesellschaft, Leipzig, 1978

Es sind wohl mehr als fünfzig Jahre seit der stürmischen Entwicklung der Quantenmechanik vergangen und bekanntlicherweise erschien über die Quantentheorie in der Zwischenzeit eine praktisch unübersehbare Menge von Lehrbüchern verschiedenster wissenschaftlicher und didaktischer Zielsetzungen bzw. Qualitäten. Hat man demzufolge eine neue "Einführung" in der Hand, so öffnet man das Buch oft mit dem Vorurteil, dass auf diesem Gebiet heute kaum mehr etwas wesentlich neues oder interessantes beigetragen werden kann.

Das kleine Büchlein von Professor RENNERT (nur 195 Seiten in Kleinformat) ist in dieser Hinsicht eine sehr angenehme Überraschung und überzeugt den Leser, dass das oben erwähnte Vorurteil wieder einmal vollkommen unbegründet ist. Erfreulicherweise findet man hierbei eine solche "Einführung" in die Quantenphysik, die von den physikalischen und didaktischen Standpunkten aus äusserst sorgfältig durchdacht ist und den heutigen Bedürfnissen des technischen und naturwissenschaftlichen Hochschulunterrichts, der oft recht früh nötigen, einleitenden Vorlesungen sehr wohl entspricht.

Das Buch ist in vier Kapitel eingeteilt: 1. Experimentalle und theoretische Grundlagen der Quantenphysik, 2. Stationäre Zustände, 3. Darstellung und Zeitablauf physikalischer Grössen sowie 4. Das Wasserstoffatom.

Diese Aufteilung des Stoffes ist im Grunde genommen der konventionelle Weg. Der Unterschied zu vielen anderen Einteilungen liegt dementsprechend mehr an der Art und Weise wie der Inhalt dargestellt und bearbeitet wird.

Der Verfasser bespricht z. B. in diesem Buch auch die berühmten, alten Grundexperimente der Quantenphysik, wie es früher fast immer die Regel war, gibt aber zu gleicher Zeit auch derartige Vorbereitungen an, und behandelt den Text in solcher Weise, dass auch ein Leser mit der Vorausbildung des 3-ten oder 4-ten Semesters genügend vorbereitet wird um die sehr oft aus diesen Experimenten entwickelten, heutzutage wichtigen Untersuchungsmethoden zu verstehen. So werden z. B. die Photoelektronenspektroskopie, die Comptonspektroskopie, die LEED, sowie die Elektronenstrahlmikroanalyse schon im ersten Kapitel ziemlich gut verständlich behandelt.

Lobenswert ist, dass der Autor durchaus eine recht gleichmässige, hohe theoretische Darstellungsstufe beibehalten hat und mit den Grundlagen jenen Punkt erreichen konnte, nach denen der Leser bereits das Studium von fortgeschrittenen Büchern beginnen kann.

Das Buch ist in einem klaren, leicht verständlichen Stil, mit vielen, sehr eindeutigen Abbildungen und Tabellen geschrieben. Ein sehr gutes Lehrbuch für den Hochschulunterricht, ein Band von der berühmten Serie der Mathematisch-Naturwissenschaftlichen Bibliothek, herausgegeben mit der üblichen Sorgfalt der Verlagsgesellschaft Teubner.

J. ANTAL

W. HANDLE and H. KLEINPOPPEN:

Progress in Atomic Spectroscopy

Part A and Part B

Plenum Press, New York and London, 1978—79, 712 + 788 pages

The surge of activity over the last decades in the development of nonoptical spectroscopic methods has had a significant impact on the field of atomic spectroscopy. Spectroscopy has always been involved in research on atomic structure and the interaction of light and atoms, but modern atomic spectroscopy and its applications are now linked with many other branches of fundamental physics, including quantum electrodynamics, and through the study of leptonic interactions and models of weak neutral currents, particle physics.

Progress in Atomic Spectroscopy, *Part A* and *Part B*, summarize the most important methods and applications currently in use in this expanding technology The contributors examine the progress made in the study of the relationship between astrophysics and atomic spectroscopy, precision measurements of atomic structure, laser applications, and innovative methods such as X-ray, stored ion, and laser high-resolution spectroscopy. In addition, this comprehensive volume outlines the basic properties of atoms and perturbations, thus serving as a useful review of these subjects and a thorough introduction to atomic spectroscopy.

I. KOVÁCS
Department of Atomic Physics
Technical University, Budapest

Printed in Hungary

A kiadásért felel az Akadémiai Kiadó igazgatója — Műszaki szerkesztő: Botyánszky Pál
A kézirat kiadóba érkezett 1980 III. 12. A kézirat nyomdába érkezett: 1980. III. 17. — Terjedelem: 19,25 (A/5) ív, 59 ábra

80.8161 Akadémiai Nyomda, Budapest — Felelős vezető: Bernát György

NOTES TO CONTRIBUTORS

I. PAPERS will be considered for publication in Acta Physica Hungarica, only if they have not previously been published or submitted for publication elsewhere. They may be written in English, French, German or Russian.

Papers should be submitted to

Prof. I. Kovács, Editor
Department of Atomic Physics, Technical University
1521 Budapest, Budafoki út 8, Hungary

Papers may be either articles with abstracts or short communications. Both should be as concise as possible, articles in general not exceeding 25 typed pages, short communications 8 typed pages.

II. MANUSCRIPTS

1. Papers should be submitted in three copies.

2. The text of papers must be of high stylistic standard, requiring minor corrections only.

3. Manuscripts should be typed in double spacing on good quality paper, with generous margins.

4. The name of the author(s) and of the institutes where the work was carried out should appear on the first page of the manuscript.

5. Particular care should be taken with mathematical expressions. The following should be clearly distinguished, e.g. by underlining in different colours: special founts (italics, script, bold type, Greek, Gothic, etc.); capital and small letters; subscripts and superscripts, e.g. x_2, x^3; small *l* and 1; zero and capital O; in expressions written by hand: *e* and *l*, *n* and *u*, *v* and *v*, etc.

6. References should be numbered serially and listed at the end of the paper in the following form: J. Ise and W. D. Fretter, Phys. Rev., *76*, 933, 1949.

For books, please give the initials and family name of the author(s), title, name of publisher, place and year of publication, e.g.: J. C. Slater, Quantum Theory of Atomic Structures, I. McGraw-Hill Book Company, Inc., New York, 1960.

References should be given in the text in the following forms: Heisenberg [5] or [5].

7. Captions to illustrations should be listed on a separate sheet, not inserted in the text.

8. As per 1st January 1980 the use of SI units has been made compulsory for all publications issued in Hungary. Please note that in papers submitted to Acta Physica after that date all measures should be expressed in SI units.

III. ILLUSTRATIONS AND TABLES

1. Each paper should be accompanied by three sets of illustrations, one of which must be ready for the blockmaker. The other sets attached to the copies of the manuscript may be rough drawings in pencil or photocopies.
2. Illustrations must not be inserted in the text.
3. All illustrations should be identified in blue pencil by the author's name, abbreviated title of the paper and figure number.
4. Tables should be typed on separate pages and have captions describing their content. Clear wording of column heads is advisable. Tables should be numbered in Roman numerals (I, II, III, etc.).

IV. RETURN OF MATERIAL

Owing to high postage costs, the Editorial Office cannot undertake to return *all* material not accepted for any reason for publication. Of papers to be revised (for not being in conformity with the above Notes or other reasons) only *one* copy will be returned. Material rejected for lack of space or on account of the Referees' opinion will not be returned to authors outside Europe.

Reviews of the Hungarian Academy of Sciences are obtainable at the following addresses:

AUSTRALIA
C.B.D. LIBRARY AND SUBSCRIPTION SERVICE, Box 4886, G.P.O., *Sydney N.S.W. 2001*
COSMOS BOOKSHOP, 145 Acland Street, *St. Kilda (Melbourne), Victoria 3182*

AUSTRIA
GLOBUS, Höchstädtplatz 3, *1200 Wien XX*

BELGIUM
OFFICE INTERNATIONAL DE LIBRAIRIE, 30 Avenue Marnix, *1050 Bruxelles*
LIBRAIRIE DU MONDE ENTIER, 162 Rue du Midi, *1000 Bruxelles*

BULGARIA
HEMUS, Bulvar Ruszki 6, *Sofia*

CANADA
PANNONIA BOOKS, P.O. Box 1017, Postal Station "B", *Toronto, Ontario M5T 2T8*

CHINA
CNPICOR, Periodical Department, P.O. Box 50, *Peking*

CZECHOSLOVAKIA
MAD'ARSKÁ KULTURA, Národní třida 22, *115 66 Praha*
PNS DOVOZ TISKU, Vinohradská 46, *Praha 2*
PNS DOVOZ TLAČE, *Bratislava 2*

DENMARK
EJNAR MUNKSGAARD, Norregade 6, *1165 Copenhagen*

FINLAND
AKATEEMINEN KIRJAKAUPPA, P.O. Box 128, *SF-00101 Helsinki 10*

FRANCE
EUROPERIODIQUES S. A., 31 Avenue de Versailles, *78170 La Celle St.-Cloud*
LIBRAIRIE LAVOISIER, 11 rue Lavoisier, *75008 Paris*
OFFICE INTERNATIONAL DE DOCUMENTATION ET LIBRAIRIE, 48 rue Gay-Lussac, *75240 Paris Cedex 05*

GERMAN DEMOCRATIC REPUBLIC
HAUS DER UNGARISCHEN KULTUR, Karl-Liebknecht-Strasse 9, *DDR-102 Berlin*
DEUTSCHE POST ZEITUNGSVERTRIEBSAMT, Strasse der Pariser Kommüne 3—4, *DDR-104 Berlin*

GERMAN FEDERAL REPUBLIC
KUNST UND WISSEN ERICH BIEBER, Postfach *46, 7000 Stuttgart 1*

GREAT BRITAIN
BLACKWELL'S PERIODICALS DIVISION, Hythe Bridge Street, *Oxford OX1 2ET*
BUMPUS, HALDANE AND MAXWELL LTD., Cowper Works, *Olney*, Bucks *MK46 4BN*
COLLET'S HOLDINGS LTD., Denington Estate, *Wellingborough*, Northants *NN8 2QT*
W.M. DAWSON AND SONS LTD., Cannon House *Folkestone, Kent CT19 5EE*
H. K. LEWIS AND CO., 136 Gower Street, *London WCIE 6BS*

GREECE
KOSTARAKIS BROTHERS, International Booksellers, 2 Hippokratous Street, *Athens-143*

HOLLAND
MEULENHOFF-BRUNA B.V., Beulingstraat 2, *Amsterdam*
MARTINUS NIJHOFF B.V., Lange Voorhout 9—11, *Den Haag*
SWETS SUBSCRIPTION SERVICE, 347b Heereweg, *Lisse*

INDIA
ALLIED PUBLISHING PRIVATE LTD., 13/14 Asaf Ali Road, *New Delhi 110001*
150 B-6 Mount Road, *Madras 600002*
INTERNATIONAL BOOK HOUSE PVT. LTD., Madame Cama Road, *Bombay 400039*
THE STATE TRADING CORPORATION OF INDIA LTS, Books Import Division, Chandralok, 36 Janpath, *New Delhi 110001*

ITALY
EUGENIO CARLUCCI, P.O. Box 252, *70100 Bari*
INTERSCIENTIA, Via Mazzé 28, *10149 Torino*
LIBRERIA COMMISSIONARIA SANSONI, Via Lamarmora 45, *50121 Firenze*
SANTO VANASIA, Via M. Macchi 58, *20124 Milano*
D. E. A., Via Lima 28, *00198 Roma*

JAPAN
KINOKUNIYA BOOK-STORE CO. LTD., 17-7 Shinjuku-ku 3 chome, Shinjuku-ku, *Tokyo 160-91*
MARUZEN COMPANY LTD., Book Department, P.O. Box 5050 Tokyo International, *Tokyo 100-31*
NAUKA LTD. IMPORT DEPARTMENT, 2-30-19 Minami Ikebukuro, Toshima-ku, *Tokyo 171*

KOREA
CHULPANMUL, *Phenjan*

NORWAY
TANUM-CAMMERMEYER, Karl Johansgatan 41—43, *1000 Oslo*

POLAND
WĘGIERSKI INSTYTUT KULTURY, Marszałkowska 80, *Warszawa*
CKP I W ul. Towarowa 28 *00-958 Warsaw*

ROUMANIA
D. E. P., *Bucureşti*
ROMLIBRI, Str. Biserica Amzei 7, *Bucureşti*

SOVIET UNION
SOJUZPETCHATJ — IMPORT, *Moscow*
and the post offices in each town
MEZHDUNARODNAYA KNIGA, *Moscow G-200*

SPAIN
DIAZ DE SANTOS, Lagasca 95, *Madrid 6*

SWEDEN
ALMQVIST AND WIKSELL, Gamla Brogatan 26, *101 20 Stockholm*
GUMPERTS UNIVERSITETSBOKHANDEL AB, Box 346, *401 25 Göteborg 1*

SWITZERLAND
KARGER LIBRI AG, Petersgraben 31, *4011 Basel*

USA
EBSCO SUBSCRIPTION SERVICES, P.O. Box 1943, *Birmingham, Alabama 35201*
F. W. FAXON COMPANY, INC., 15 Southwest Park, *Westwood, Mass. 02090*
THE MOORE-COTTRELL SUBSCRIPTION AGENCIES, *North Cohocton, N. Y. 14868*
READ-MORE PUBLICATIONS, INC., 140 Cedar Street, *New York, N. Y. 10006*
STECHERT-MACMILLAN, INC., 7250 Westfield Avenue, *Pennsauken* N. J. 08110

VIETNAM
XUNHASABA, 32, Hai Ba Trung, *Hanoi*

YUGOSLAVIA
JUGOSLAVENSKA KNJIGA, Terazije 27, *Beograd*
FORUM, Vojvode Mišiča 1, *21000 Novi Sad*

Index: 26.022
Acta Phys. Hung. Tom. 48. No. 2—3. Budapest, 20. XI. 1980 HU-ISSN 0001-6705

ACTA PHYSICA

ACADEMIAE SCIENTIARUM HUNGARICAE

TOMUS XLVIII FASCICULUS 4

AKADÉMIAI KIADÓ, BUDAPEST

1980

ACTA PHYS. HUNG. APAHAQ 48 (4) 337—468 (1980)

ACTA PHYSICA

ACADEMIAE SCIENTIARUM HUNGARICAE

SZERKESZTI
KOVÁCS ISTVÁN

Az *Acta Physica* angol, német, francia vagy orosz nyelven közöl értekezéseket. Évente két kötetben, kötetenként 4—4 füzetben jelenik meg. Kéziratok a szerkesztőség címére (1521 Budapest XI., Budafoki út 8.) küldendők.

Megrendelhető a belföld számára az Akadémiai Kiadónál (1363 Budapest Pf. 24. Bankszámla 215-11488), a külföld számára pedig a „Kultura" Külkereskedelmi Vállalatnál (1389 Budapest 62, P.O.B. 149. Bankszámla 217-10990), vagy annak külföldi képviseleteinél.

The *Acta Physica* publish papers on physics in English, German, French or Russian, in issues making up two volumes per year. Distributor: "Kultura" Foreign Trading Company (1389 Budapest 62, P.O. Box 149) or its representatives abroad.

Die *Acta Physica* veröffentlichen Abhandlungen aus dem Bereich der Physik in deutscher, englischer, französischer oder russischer Sprache, in Heften, die jährlich zwei Bände bilden.

Bestellbar bei »Kultura« Außenhandelsunternehmen (1389 Budapest 62, Postfach 149) oder seinen Auslandsvertretungen.

Les *Acta Physica* publient des travaux du domaine de la physique en français, anglais, allemand ou russe, en fascicules qui forment deux volumes par an.

On peut s'abonner à l'Entreprise du Commerce Extérieur «Kultura» (1389 Budapest 62, P.O.B. 149) ou chez représentants à l'étranger.

«*Acta Physica*» публикуют трактаты из области физических наук на русском, немецком, английском и французском языках.

«*Acta Physica*» выходят отдельными выпусками, составляющими два тома в год.

Заказы принимает предприятие по внешней торговле «Kultura» (1389 Budapest 62, P.O.B. 149) или его заграничные представительства.

ACTA PHYSICA

ACADEMIAE SCIENTIARUM HUNGARICAE

TOMUS XLVIII FASCICULUS 4

AKADÉMIAI KIADÓ, BUDAPEST
1980

ACTA PHYS. HUNG.

INDEX

Acta Physica Academiae Scientiarum Hungaricae, Tomus 48 (4), pp. 337—348 (1980)

BACKSCATTERING SPECTRA OF MEDIUM ENERGY ELECTRONS

By

G. GERGELY, B. GRUZZA* and M. MENYHÁRD

RESEARCH INSTITUTE FOR TECHNICAL PHYSICS OF THE HUNGARIAN ACADEMY OF SCIENCES
H—1325 BUDAPEST, HUNGARY

(Received 14. I. 1980)

Backscattering spectra of medium energy electrons (1—10 keV) are very important in Auger electron spectroscopy. Backscattered electrons compose the background and contribute to the excitation of Auger transitions.

The $N(E)$ backscattering spectra were determined by an Auger spectrometer with a CMA analyzer operated in DC mode using an isolation amplifier system.

The $N(E)$ backscattering spectra of electrons were studied on graphite, Si, stainless steel, Ge, Mo, W and Au in the 0.7—3 keV range. The backscattering spectra are presented. Our main results can be summarized as follows:

— the backscattering coefficient r_B was determined by integrating $N(E)$ above 272 eV (effective for Auger excitation of low energy peaks);
— r_B is little affected by the primary energy E_p and strongly increasing with Z;
— the elastic peak $N(E_p)$ is decreasing with E_p and strongly increasing with Z;
— the distribution $N(E)$ exhibits a drastic change with Z, going from Fe to Si;
— the percentage of elastically reflected electrons was determined.

Introduction, definitions

Medium energy electrons ($E_p = 1—10$ keV) impinging on a solid produce secondaries. The $N(E)$ spectrum covers the entire energy spectrum below E_p. It contains several important but not clearly and uniformly defined domains as summarized below:

— According to the classical definition low energy electrons (in practice $E < 50$ eV) are called secondary electrons.
— In reality, however, the secondary electron cascade is extended far above 50 eV, reaching a minimum in $N(E)$ at E_{cp} (SICKAFUS [1]).
— The position of this E_{cp} is strongly affected by the solid target material and by E_p.
— Above E_{cp} $N(E)$ consists of rediffused primaries [1].
— In this paper all $N(E)$ electrons able to excite an Auger electron are called backscattered electrons [2—5]. In this respect the backscattering spectra are composed partly of the secondary cascade and of the rediffused electrons. Their low energy limit is determined by E_i (ionization energy of the Auger transition involved).

* Laboratoire de Microscopie et Diffraction Electronique à l'Université d'Aix-Marseille III., Faculté des Sciences et Techniques de Saint Jêrome, France.

— The upper limit of the backscattering spectra is $N(E_p)$, the elastic peak adjacent to the plasmon loss peaks.
— The small Auger peaks are superimposed on the continuous $N(E)$ background. Electrons of $E > E_i$ in the (backscattered) $N(E)$ spectrum are contributing in the excitation of Auger electrons [1]. Some part of the Auger electrons is elastically reflected from the substrate. These effects produce an apparent enhancement of Auger emission, characterized by a factor r_{BA}, denoted as backscattering factor in the literature of AES.
— The angular distribution of backscattered electrons is approximately Lambertian [6].
— The backscattering coefficient r_B is proportional to

$$r_B \sim \int_{Ei}^{Ep} N(E)dE \,. \tag{1}$$

The aim of this work is to supply more details on the $N(E)$ spectra of some materials for AES applications.

Backscattered electrons play an important role in the excitation of Auger electrons in the surface layer [2—5]. Backscattering spectra are important for the quantitative evaluation of Auger spectra. Recently instead of the $N'(E)$ derivative mode highly sensitive AES and SAM have used the $N(E)$ spectra [7—9]. The background compensation for AES requires the exact knowledge of $N(E)$ spectra. In spite of the importance of backscattering spectra, since the early work of STERNGLASS [10], not many new data have been published [11—15].

On the other hand, very rich literature has been published on the backscattering coefficient r_B, its variation with the atomic number Z and primary energy E_p, however, rather for the high energy ($E_p > 10$ keV) range, to mention only the classical work of EVERHART [16] and the more recent works of MCAFEE [17], DARLINGTON [15], LILJEQUIST [18] and NIEDRIG [19], quoting ample references.

Experimental method

The backscattering spectra were determined with a conventional Auger spectrometer working in the $6 \cdot 10^{-7}$—10^{-8} Pa pressure range. A Riber OPC 103 CMA analyzer was used operating in the usual derivative mode with a lock-in amplifier (KFKI model NV 255) for taking Auger spectra.

Further, another mode of operation was realized, coupling the CMA multiplier output to an Analog Devices model 272J isolation amplifier [9] and an amplifier system built by our Electronics Laboratory. The DC output of the CMA was recorded supplying the $EN(E)$ spectra. This method was applied for determining the $N(E)$ backscattering spectra. They were taken with

1—1.2 μA beam current, $\varnothing$ 50 μm electron beam. The beam current was monitored by a Faraday collector. In general, $N(E)$ spectra were taken at 2 and 3 keV but for some samples their variation with E_p was studied.

In most cases $N(E)$ spectra were taken from $E = 272$ eV (the C Auger peak), low energy limit being effective already for the excitation of Auger transitions in the 80—160 eV range (Si, P, S). The CMA multiplier voltage and the detector sensitivity level of the system were carefully kept constant.

6 samples were mounted on the sample holder. After each measurement, the $N(E)$ spectrum of a graphite reference standard sample was recorded. The reproducibility (including the elastic peak) of these spectra was better than 5%.

In each case $N(E)$ spectra were determined on 2 parallel samples. The same reproducibility was achieved on the various samples. In the vacuum chamber a PHI model 04-164 ion gun was applied.

The samples

Backscattering spectra were determined on flat polycrystalline samples: graphite (semiconductor grade), Si (polycrystal), stainless steel (Kor 5 Hungarian standard), Mo, W plates (Plansee), Au (evaporated film 1 μm in thickness).

For comparison with literature data some Si (111), Si (100) and Ge (111) single crystal surfaces were studied, too. The angular distribution of backscattered electrons obeys Lambert's law [6]. The $N(E)$ spectra were taken with normal incidence excitation. For the polycrystalline samples, the application of a CMA, sampling the backscattered electrons within 42°, is fully justified. A comparison of our $N(E)$ spectra with the few literature data available gave similar results even for single crystals [12, 14].

In the case of thick samples backscattering is little affected by the texture of the target [19]. For our polycrystalline samples this was negligible.

The samples were deoxidized, etched using the conventional chemical cleaning procedures and shortly after cleaning they were mounted in the vacuum chamber. After the conventional pumping (with a Vacuum Generators 210 l/s ion pump) and baking (200 °C) processes, atomically clean surfaces were prepared by argon ion bombardment (1 keV, 100 μA/cm^2). The clean surfaces were checked by AES.

Experimental results

The $N(E)$ backscattering spectra of graphite, Si (polycrystalline), stainless steel and Ge are presented in Fig. 1a, those of Mo, W and Au in Fig. 1b for $E_p \simeq 3$ keV. They are plotted in arbitrary units but all the spectra

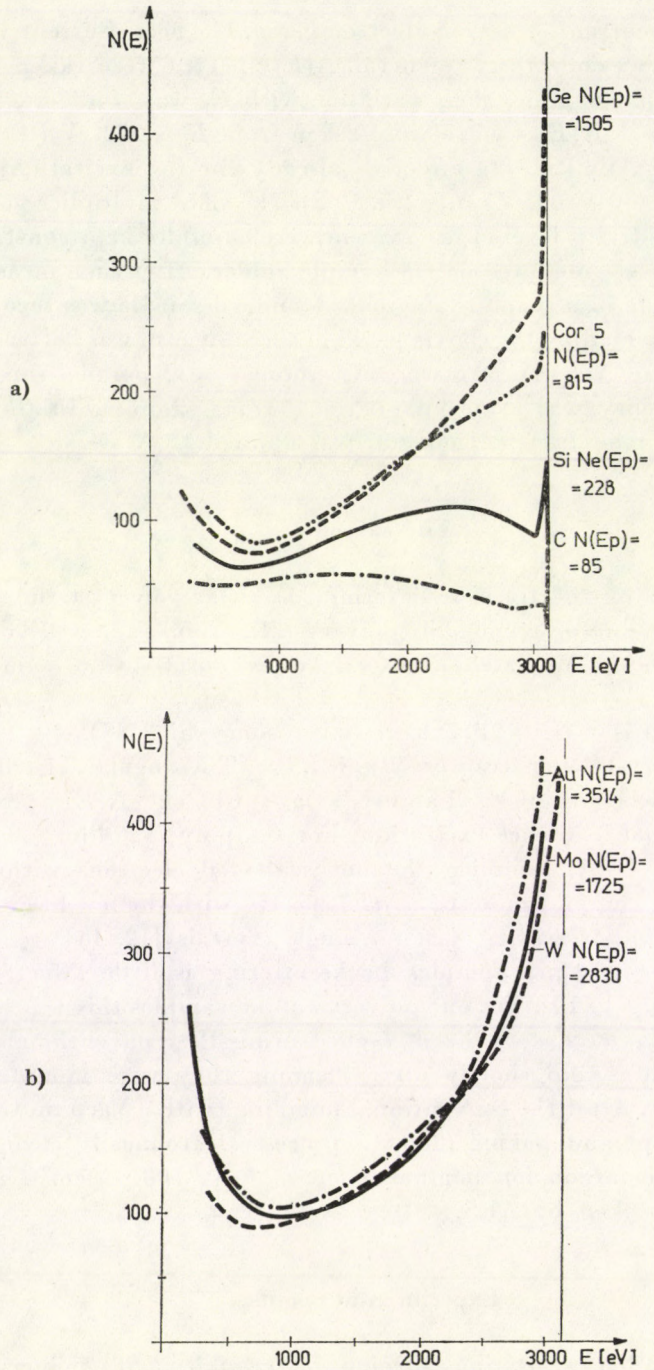

Fig. 1. Backscattering spectra, $N(E)$ in arbitrary units
a. Graphite, silicon, stainless steel and germanium
b. Molybdenum, tungsten and gold

on the same scale. The heights of elastic peaks $N(E_p)$ are indicated in the Figures. The spectra can be classified into three characteristic types, according to the atomic number Z:

The low atomic number elements C and Si exhibit a relatively low elastic peak followed by a high energy minimum (close to the plasmon loss range), a medium energy broad maximum, a second low energy minimum around $E_p \cong 800$ eV and the low energy cascade [1].

The high atomic number elements Mo, W and Au exhibit very big elastic peaks, followed by a broad rediffused electron [1] range, a single minimum at $E_{cp} \cong 1$ keV and a low energy cascade.

The medium Z samples, stainless steel and Ge exhibit some intermediary character but similar rather to the high Z elements. (The average Z value of our Kor 5 stainless steel is 26, corresponding to Fe).

The plasmon loss domain is not resolved in Figs. 1a and 1b. The fine structure around the elastic peak was determined on each sample. Some characteristic spectra are presented in the Figures: graphite in Fig. 2a, Si in Fig. 2b and W in Fig. 2c. The Figures exhibit a similar character. The main loss peaks observed are characteristic for the materials. They are composed by surface and volume plasmon losses and could be identified in most cases with literature data (e.g. [20] giving a comprehensive literature). The loss peaks are nearly equidistant, $\Delta E_{pl} = E_{pl_1} - E_{pl_2}$, etc. The most important information deduced from them is the magnitude of the dominant elementary loss process ΔE_{pl} of high energy primary electrons. The half width ΔE of elastic peaks corresponds to the resolution of the CMA.

The backscattering coefficient r_B was calculated by integrating the $N(E)$ spectra between 272 eV and E_p. Since the CMA measurements supply only the $N(E)$ distributions, the r_B data of McAfee [17] measured at $E_p = 3$ keV on C and Si were fitted to our results.

Table I

Some characteristic data of loss processes for $E_p \cong 3$ KeV

Material	ΔE_{pl} eV	$\frac{\Delta N(E_p)}{N_{be}}$	$\frac{\Delta N(E_{pl_1})}{N_{be}}$	$\frac{N(E_p)}{N(E_{pl_1})}$
Graphite	24. 27	5.3	2.2	4.3
Si (polycrystalline)	18	3	1.9	2.2
Stainless steel	22	4.15	1.3	16
Mo	25	5.3	1.6	6.4
W	26	6.2	1.8	6.7
Au	30	6.1	1.1	46

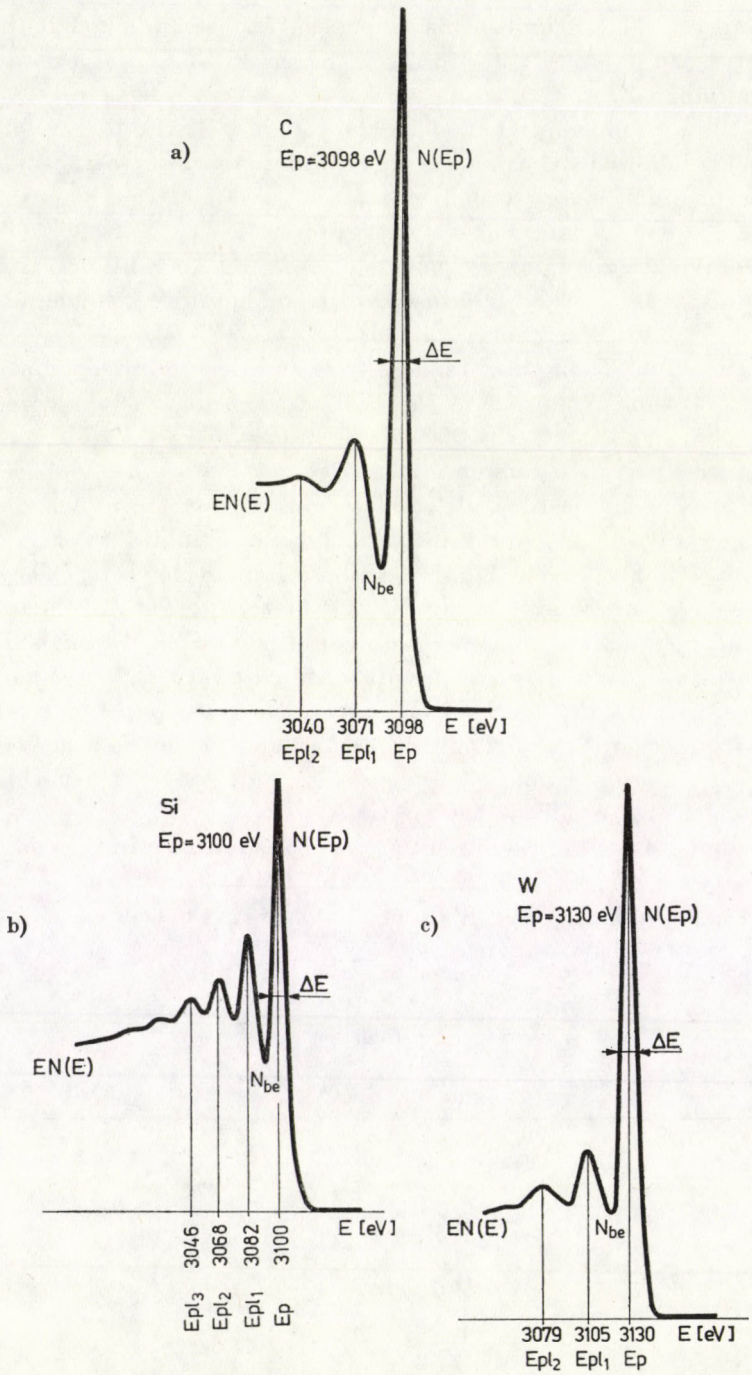

Fig. 2. The fine structure around the elastic peak
a. Graphite; *b.* Silicon; *c.* Tungsten

The other materials studied exhibited similar fine structures around their elastic peak. The high primary energy and the resolution of the CMA analyzer do not allow to determine finer details of the plasmon loss spectra, however, some data of interest are summarized in Table I. The minimum N_{be} lying between E_p and the first plasmon loss peak E_{pl_1} was in most cases identical with the continuous background of rediffused electrons. Only graphite exhibited a deeper minimum, Si and stainless steel showed little deviations. The reproducibility of $\Delta E_{pl} = E_p - E_{pl_1}$ plasmon losses was quite good as measured with different primary energies E_p.

The peak heights emerging from the background are:

$$\Delta N(E_p) = N(E_p) - N_{be}, \quad \Delta EN(E_{pl_1}) = N(E_{pl_1}) - N_{be}.$$

Our r_B data are similar to EVERHART's results [16] plotted in Fig. 3 containing our experimental points determined by Eq. (1). The spectra taken at $E_p = 2$ keV exhibit a similar character to those in Figs. 1 and 2, but with higher $N(E)$ values, producing approximately the same r_B values determined by integrating Eq. (1). The variation of the $N(E)$ spectra with E_p is shown in Fig. 4 for W. The backscattering coefficient deduced from the integrals is little affected by E_p. Some more details are presented on graphite in Fig. 5 indicating also the $N(272)$ C Auger peaks. The variation of r_B and $N(272)$

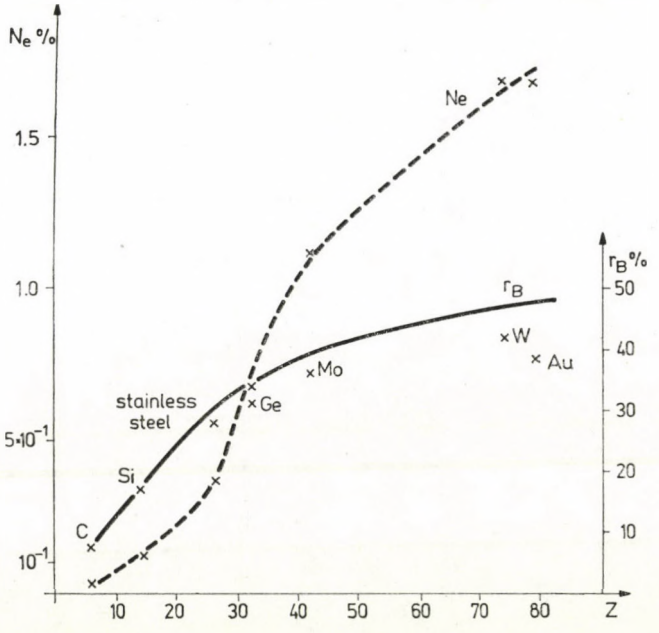

Fig. 3. The variation of r_B and N_e with atomic number

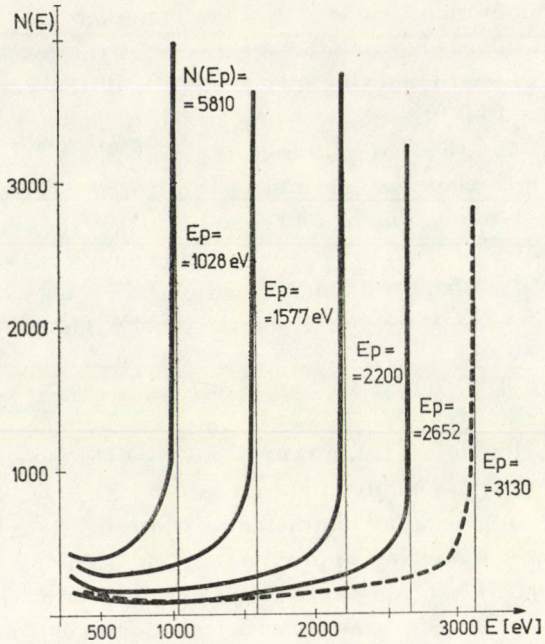

Fig. 4. The variation of $N(E)$ spectra with the primary energy for tungsten. $N(E)$ in arbitrary units but on the same scale as in Fig. 1b

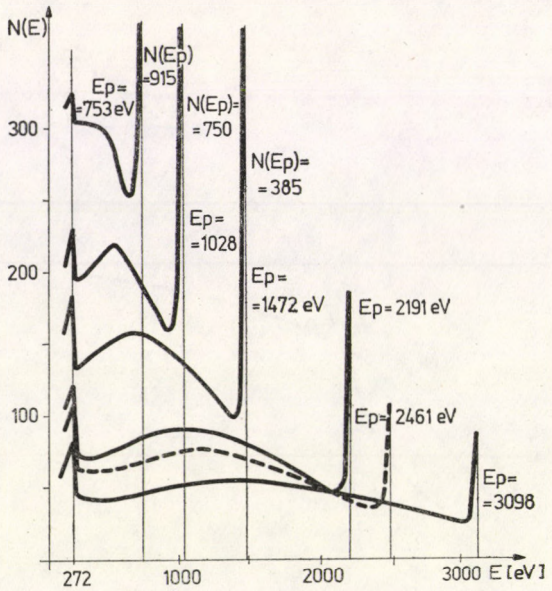

Fig. 5. The variation of $N(E)$ with E_p for graphite

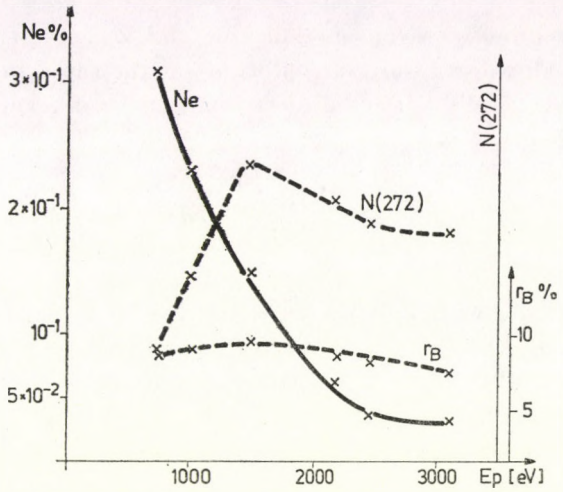

Fig. 6. The variation of the carbon Auger peak $N(272)$, N_e and r_B with E_p on graphite

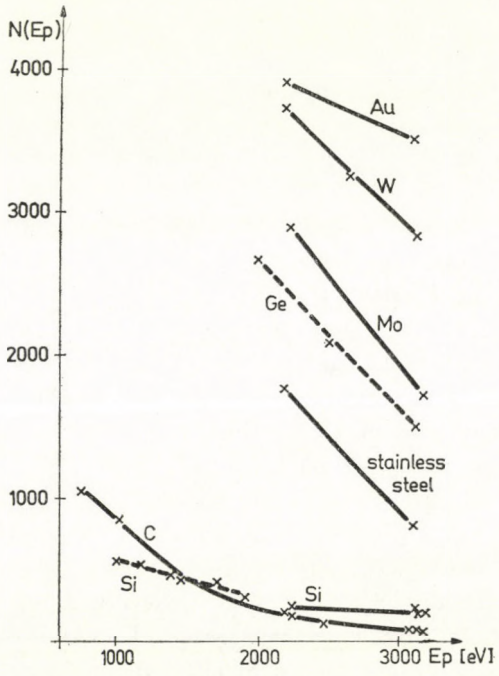

Fig. 7. The variation of the elastic peak $N(E_p)$ with E_p for various samples. $N(E_p)$ in arbitrary units but using the same scale as in Figs. 1. and 4. The dashed lines (– – –) for Ge and Si are taken from the literature [12, 14] but fitted to our experimental data

with E_p is shown in Fig. 6. The variation of the elastic peak $N(E_p)$ with E_p is presented in Fig. 7 for the samples studied. Data of Si and Ge are taken from NEAVE [12] and KENNEDY [14], resp. and fitted to our results. $N(E_p)$

is strongly decreasing with E_p especially for high Z elements as shown also in Fig. 5 for W. All these results are plotted on the same intensity scale. The percentage of elastically reflected electrons can be determined by Eq. (2) as

$$N_e = \frac{N(E_p)\,\Delta E}{\int_{272}^{Ep} N(E)\,dE} \quad . \tag{2}$$

The variation of N_e with Z is shown in Fig. 3 for $E_p = 3$ keV. N_e strongly decreases with E_p. Since r_B is little affected by E_p, a considerable rise of elastic reflection takes place at low energy excitation. This is shown in Fig. 6 for graphite, however, the effect becomes less pronounced with increasing Z.

Discussion

Let us compare the experimental data presented in the Figures and the Table with the few data available in the literature. The early work of STERNGLASS [10] used much higher E_p energies and did not resolve the elastic peak. But the broad maximum in the carbon spectrum was noticed by STERNGLASS and more recently also by DARLINGTON and COSSLETT [15]. Regarding the spectra of silicon studied by NEAVE and FOX [12], the smooth maximum between E_{cp} and E_p has been described. Their detailed study on the E_p dependence of the Si spectra shows similarity with our results on graphite and silicon too (omitting details). However , the $N(E_p)$ elastic peaks found by NEAVE above $E_p = 1{,}5$ keV seem to be surprizingly low, almost equal to the first plasmon peak. The broad maximum of backscattering spectra is a characteristic behaviour of low Z elements, noticed also on Al [10, 15] and Be films [13]. The $N(E)$ spectrum of Ge in Fig. 1a is analogous to that found by KENNEDY [14] and the spectrum of stainless steel in the same figure shows similarity to that of copper ($Z = 29$) described by GOTO [13].

Proceeding toward higher atomic numbers the predominance of the high energy rediffused domain and the strong increase of $N(E_p)$ is correlated with Z. This is valid also for N_e, the elastic reflection coefficient. However, the strong decrease of N_e with E_p on the same element is much more pregnant for low Z elements as found also on Si [12], Be and Cu [13].

The considerable change of the character of $N(E)$ spectra going from low Z (C, Si, etc.) to high atomic number elements shows the importance of Z in the backscattering process. The cascade tail below E_{cp} [1] does not exhibit this anomaly and can be explained with the present theories of secondary electron emission. On the other hand, the broad maximum found in the rediffused range of low Z elements was not explained in the literature, reaching

reasonable agreement with experimental data of r_B [16, 17]. In a similar way the authors are not aware of interpretation of the Z variation of $N(E_p)$ and N_e, and their strong increase with Z. Regarding the backscattering coefficient r_B i.e. the low energy limit of integration or the retarding voltage applied in the measurements are not unambigously defined in the literature.

VARMA [21] applied 50 V for retarding the low energy secondaries, whereas MCAFEE determined r_B under well defined conditions. In our Fig. 6 above 1,4 keV the backscattering coefficient of graphite decreases with E_p. This is in agreement with the results of VARMA and COSSLETT [15]. For lower E_p energies the apparent decrease of r_B is due to the 272 eV low energy limit of integration. The very strong rise and shift of $N(E)$ can be seen in the low energy excitation range of Fig. 5.

The constancy of r_B in the 1—3 keV range was described by MCAFEE [17] and KENNEDY [14] on several semiconductors. In practice our studies on samples covering a wide range of Z supplied similar results.

Finally, let us consider the plasmon loss data summarized in Table I. The position of the Et_1 plasmon loss peaks are in reasonable agreement with data published in the literature [20]. The peak ratios $N(E_p)/N(E_{pl})$ and $\Delta N(E_p)/\Delta N(E_{pl})$ give some information on the magnitude of plasmon loss process at the high primary energies used.

The r_B and $N(E)$ results described in this paper provide information on the r_{BA} backscattering excitation of Auger electrons [3—5], since it should be proportional to

$$r_{BA} \sim \int_{E_i}^{E_p} \sigma(E) \cdot N(E)\, dE\,. \tag{3}$$

These problems will be discussed in more detail in another paper.

Acknowledgement

The authors express their sincere thanks to Mr. K. NÉMETH for developing the CMA DC detector system used in our measurements.

REFERENCES

1. E. M. SICKAFUS, Phys. Rev. B., **16**, 1436, 1448, 1977.
   E. N. SICKAFUS and C. KUKLA, Phys. Rev. B., **19**, 4056, 1979.
2. H. E. BISHOP and J. C. RIVIÈRE, J. Appl. Phys., **40**, 1740, 1969.
3. T. E. GALLON, J. Phys. D. (Appl. Phys.), **5**, 822, 1972.
4. D. M. SMITH and T. E. GALLON, J. Phy. D. (Appl. Phys.), **7**, 151, 1974.
5. A. J. JABLONSKI, Surface Sci., **74**, 621, 1978; **87**, 539, 1979.
6. L. REIMER and G. PFEFFERKORN, Raster-Elektronenmikroskopie, Springer Berlin, 39, 1973.
   L. REIMER, W. PÖPPER and W. BRÖCKER, Scanning Electron Microscopy, I, 705, 1978.
7. A. BENNINGHOVEN, O. GANSCHOW, P. STEFFENS and L. WIEDMAN, J. Electron Spectrosc., **14**, 19, 1978.

8. C. Le Gressus, D. Massignon and R. Sopizet, Surface Sci., **68**, 338, 1977.
9. Bui Minh Duc and C. Jardin, Spéctrométrie Auger, 19—23 Mars 1979, Les Arcs (F), Le Vide, No. spécial, Mars 1979. 153.
Bui Minh Duc, C. Jardin, J. P. Gauthier and P. Michel, J. Phys. E., **12**, 43, 1979.
10. E. J. Sternglass, Phys. Rev., **95**, 545, 1954.
11. R. L. Gerlach and A. R. DuCharme, Surface Sci., **32**, 329, 1972.
12. J. H. Neave, C. T. Foxon and B. A. Joyce, Surface Sci., **29**, 411, 1972.
13. K. Goto, K. Ishikawa, T. Koshikawa and R. Shimizu, Surface Sci., **47**, 477, 1975.
14. A. J. Kennedy and H. W. Kalweit, K. Appl. Phys., **44**, 5301, 1973.
15. E. H. Darlington and V. E. Cosslett, J. Phys. D. (Appl. Phys.), **5**, 1969, 1972.
E. H. Darlington, J. Phys. D. (Appl. Phys.), **8**, 85, 1975.
16. T. E. Everhart, J. Appl. Phys., **31**, 1483, 1960.
17. W. S. McAfee, J. Appl. Phys., **47**, 1179, 1976.
18. D. Liljeouist, J. Phys. D. (Appl. Phys.), **11**, 839, 1978.
19. H. Niedrig, Scanning Electron Microscopy, I, 841, 1978.
20. D. Pines, Elementary Excitations is Solids, Benjamin, New York, 1964.
21. R. L. Verma, J. Phys. D. (Appl. Phys.), **10**, 1167, 1977.

Acta Physica Academiae Scientiarum Hungaricae, Tomus 48 (4), pp. 349—357 (1980)

ON THERMOHALINE-CONVECTIVE INSTABILITY WITH FINITE LARMOR RADIUS AND HALL EFFECTS

By

R. C. SHARMA and K. N. SHARMA

DEPARTMENT OF MATHEMATICS, HIMACHAL PRADESH UNIVERSITY, SIMLA-171005, INDIA

(Received 14. I. 1980)

Thermohaline-convective instability of a stellar atmosphere in the presence of a stable solute gradient is considered to include the effect due to Hall currents in the presence of a uniform vertical magnetic field. A criterion for monotonic instability is derived. The problem of thermohaline-convective instability is also considered to include finite Larmor radius effect. The criterion derived for monotonic instability is found to hold good in the presence of finite Larmor radius effect on thermohaline-convective instability.

1. Introduction

DEFOUW [2] has given a criterion that a stellar atmosphere is unstable if

$$D = \frac{1}{C_p}(L_T - \varrho\alpha L_\varrho) + K k^2 < 0\,, \tag{1}$$

where L is the heat-loss function (the energy lost minus the energy gained per gram per second) and ϱ, α, $\varkappa$, k, L_T, L_ϱ denote respectively the density, the coefficient of thermal expansion, the coefficient of thermometric conductivity, the wave number of the perturbation, the partial derivates of L with respect to temperature T, density ϱ; both evaluated in the equilibrium state. DEFOUW [2] has generalized the Schwarzschild criterion for convection to include departures from adiabatic motion and has shown that a thermally unstable atmosphere is also convectively unstable, irrespecstive of the atmospheric temperature gradient. 'Thermal-convective instability' is termed as the instability in which motions are driven by buoyancy forces of a thermally unstable atmosphere. In general, the instability due to inequality (1) may be either oscillatory or monotonic. DEFOUW [2] has also shown that inequality (1) is a sufficient condition for monotonic instability in the presence of magnetic field and rotation on thermal-convective instability.

The thermal instability problem, under varying assumptions of hydrodynamics and hydromagnetics, has been treated in detail by CHANDRASEKHAR [1]. VERONIS [8] has studied the problem of thermohaline convection in a

layer of fluid heated from below and subjected to a stable salinity gradient. The thermohaline convection in a horizontal layer of viscous fluid heated from below and salted from above has been considered by NIELD [3]. In the thermohaline-convective instability problem, buoyancy forces can arise not only from density differences due to variations in temperature but also from those due to variations in solute concentrations. The conditions under which convective motions are important in stellar atmospheres are usually far removed from the consideration of a single component fluid and rigid boundaries and therefore it is desirable to consider one gas component acted on by solute concentration gradient and free boundaries.

However, the Hall effects which are important for many cases of astrophysical interest, have not been included in the above studies. In many astrophysical situations such as the solar corona, interplanetary and interstellar plasmas, it is known that the approximation of zero Larmor radius is not valid. The effect of the finiteness of the ion Larmor radius which exhibits itself in the form of a magnetic viscosity in the fluid equations, on plasma instabilities have been studied by ROSENBLUTH et al [5] and ROBERTS and TAYLOR [4]. Keeping such astrophysical situations in mind, we consider the thermohaline-convective instability of a stellar atmosphere to include the effect due to Hall currents. The finite Larmor radius effects on thermohaline-convective instability of a stellar atmosphere are also studied.

2. Formulation of the problem

Consider an infinite orizontal fluid layer of thickness d heated from above and subjected to a stable solute concentration gradient so that the temperatures and concentrations at the bottom surface $z = 0$ are T_0 and C_0 and at the upper surface $z = d$ are T_1 and C_1, respectively, z-axis being taken as vertical. This layer is acted on by a uniform vertical magnetic field $\mathbf{H}(0, 0, H)$ and gravity force $\mathbf{g}(0, 0, -g)$. Let p, ϱ, T, C, $\mathbf{v}(u, v, \omega)$, g, α, α', N and e stand for pressure, density, temperature, solute concentration, velocity, gravitational acceleration, thermal coefficient of expansion, an analogous solvent coefficient, the electron number density and charge of an electron, respectively. The kinematic viscosity ν, the thermal diffusivity $\varkappa$ and the solute diffusivity $\varkappa'$ are each assumed to be constant. Then the hydromagnetic equations appropriate to the problem, following Boussinesq approximation, are

$$\frac{\partial \mathbf{v}}{\partial t} + (\mathbf{v} \cdot \nabla)\mathbf{v} = -\frac{1}{\varrho_0}\nabla p + \nu \nabla^2 \mathbf{v} + \mathbf{g}\left(1 + \frac{\delta\varrho}{\varrho_0}\right) + \frac{\mu_e}{4\pi\varrho_0}(\nabla \times \mathbf{H}) \times \mathbf{H}, \quad (2)$$

$$\nabla \cdot \mathbf{v} = 0, \quad (3)$$

$$\frac{\partial C}{\partial t} + (\mathbf{v} \cdot \nabla) C = \varkappa' \nabla^2 C, \tag{4}$$

$$\nabla \cdot \mathbf{H} = 0\,, \tag{5}$$

$$\frac{\partial \mathbf{H}}{\partial t} = (\mathbf{H} \cdot \nabla)\mathbf{v} + \eta \nabla^2 \mathbf{H} - \frac{1}{4\pi Ne} \nabla \times [(\nabla \times \mathbf{H}) \times \mathbf{H}]\,, \tag{6}$$

$$\varrho = \varrho_0 [1 - \alpha(T - T_0) + \alpha'(C - C_0)]\,, \tag{7}$$

where μ_e, η and $\delta\varrho$ denote respectively the magnetic permeability, the resistivity and the perturbation in density. The suffix zero refers to values at the reference level $z = 0$. Eqs. (2)—(4) express the conservation of momentum, mass and solute mass concentration, respectively. Eqs. (5) and (6) represent the Maxwell's equations and Eq. (7) represents the equation of state.

The steady state solution is

$$\mathbf{v} = 0,\ T = T_0 + \beta z,\ C = C_0 - \beta' z,\ \varrho = \varrho_0(1 - \alpha\beta z - \alpha'\beta' z), \tag{8}$$

where $\beta = \dfrac{T_1 - T_0}{d}$ and $\beta' = \dfrac{C_1 - C_0}{d}$ are the magnitudes of uniform temperature and concentration gradients. $\beta(= dT/dz)$ is positive as the temperature increases upwards whereas $\beta'(= -dC/dz)$ is positive as the concentration decreases upwards.

Consider a small perturbation on the steady state solution and let $\mathbf{v}$, $\delta\varrho$, δp, θ, γ and $\mathbf{h}(h_x, h_y, h_z)$ denote the perturbations in velocity, density, pressure, temperature, concentration and magnetic field, respectively, so that the change in density $\delta\varrho$, caused by the perturbations θ and γ in temperature and concentration, is given by

$$\delta\varrho = -\varrho_0 (\alpha\theta - \alpha' \gamma)\,. \tag{9}$$

Then Eqs. (2)—(6) on linearization give

$$\frac{\partial \mathbf{v}}{\partial t} = -\frac{1}{\varrho_0} \nabla \delta p + \nu \nabla^2 \mathbf{v} - \mathbf{g}(\alpha\theta - \alpha' \gamma) + \frac{\mu_e}{4\pi\varrho_0} (\nabla \times \mathbf{h}) \times \mathbf{H}, \tag{10}$$

$$\nabla \cdot \mathbf{v} = 0\,, \tag{11}$$

$$\frac{\partial \gamma}{\partial t} - \varkappa' \nabla^2 \gamma = \beta' \omega\,, \tag{12}$$

$$\nabla \cdot \mathbf{h} = 0\,, \tag{13}$$

$$\frac{\partial \mathbf{h}}{\partial t} = (\mathbf{H} \cdot \nabla)\mathbf{v} + \eta \nabla^2 \mathbf{h} - \frac{1}{4\pi Ne} \nabla \times [(\nabla \times \mathbf{h}) \times \mathbf{H}]\,. \tag{14}$$

The first law of thermodynamics may be written in the form

$$C_v \frac{dT}{dt} = -L + \frac{K}{\varrho} \nabla^2 T + \frac{p}{\varrho^2} \frac{d\varrho}{dt}, \tag{15}$$

where K, C_v and t denote, respectively, the thermal conductivity, the specific heat at constant volume and the time.

Following DEFOUW [2], the linearized perturbation form of Eq. (15) is

$$\frac{\partial \theta}{\partial t} + \frac{1}{C_p}(L_T - \varrho \alpha L_\varrho)\, \theta - \varkappa \nabla^2 \theta = -\left(\beta + \frac{g}{C_p}\right) \omega. \tag{16}$$

The density changes arise principally from thermal effects. Consider the case in which both boundaries are free as well as perfect conductors of both heat and solute concentration. The case of two free boundaries is the most appropriate for stellar atmospheres (SPIEGEL [6]). We also assume that the medium adjoining the fluid is electrically non-conducting. The boundary conditions appropriate for the problem are

$$\omega = \partial^2 \omega \,|\, \partial z^2 = \theta = \gamma = 0\,, \quad \frac{\partial \zeta}{\partial z} = 0\,,$$

$\xi = 0$ and $\mathbf{h}$ is continuous with an external vacuum field.

Here ζ and ξ denote, respectively, the z-components of vorticity and current density.

3. Dispersion relation and discussion

Analyzing in terms of normal modes, we seek solutions whose dependence on x, y, z and t is of the form

$$\exp\,[ik_x x + ik_y y + nt] \sin k_z z\,, \tag{17}$$

where n is the growth rate and $k_z = s\pi/d$, s being any integer and d is the thickness of the layer and $k = (k_x^2 + k_y^2 + k_z^2)^{1/2}$ is the wave number of the perturbation.

Eqs. (10)—(14) and (16) give

$$\frac{\partial}{\partial t} \nabla^2 \omega = g \left(\frac{\partial^2}{\partial x^2} + \frac{\partial^2}{\partial y^2}\right)(\alpha\theta - \alpha' \gamma) + \nu \nabla^4 \omega + \frac{\mu_e H}{4\pi \varrho_0} \nabla^2 \frac{\partial h_z}{\partial z}, \tag{18}$$

$$\frac{\partial \zeta}{\partial t} = \frac{\mu_e H}{4\pi \varrho_0} \frac{\partial \xi}{\partial z} + \nu \nabla^2 \zeta \,, \tag{19}$$

$$\frac{\partial h_z}{\partial t} = H \frac{\partial \omega}{\partial z} + \eta \nabla^2 h_z - \left(\frac{H}{4\pi Ne}\right) \frac{\partial \xi}{\partial z} \,, \tag{20}$$

$$\frac{\partial \xi}{\partial t} = H \frac{\partial \zeta}{\partial z} + \eta \nabla^2 \xi + \left(\frac{H}{4\pi Ne}\right) \nabla^2 \frac{\partial h_z}{\partial z} \,, \tag{21}$$

$$\left(\frac{\partial}{\partial t} + D\right) \theta = -\left(\beta + \frac{g}{C_p}\right) \omega \,, \tag{22}$$

$$\left(\frac{\partial}{\partial t} - \varkappa' \nabla^2\right) \gamma = \beta' \omega \,. \tag{23}$$

Eliminating θ, γ, h_z, ζ and ξ from Eqs. (18)—(23) and using (17), we obtain the dispersion relation

$$n^6 + A_5 n^5 + A_4 n^4 + A_3 n^3 + A_2 n^2 + A_1 n + A_0 = 0 \,, \tag{24}$$

where

$$\begin{aligned}
A_5 &= D + k^2(\varkappa' + 2\nu + 2\eta) \,, \\
A_4 &= k^4 \{\nu^2 + \eta^2 + 2\eta\varkappa' + 2\nu(\varkappa' + 2\eta)\} + k^2(\nu + \varkappa')D + \\
&\quad + k_z^2 \left\{2V^2 + k^2 \left(\frac{H}{4\pi Ne}\right)^2\right\} + k^2 D(\nu + 2\eta) + \Gamma \left(\beta + \frac{g}{C_p}\right) + \Gamma' \beta' \,, \\
A_3 &= P(D + k^2 \widetilde{\nu} + \varkappa') + k_z^2 V^2 (D + k^2 \overline{\nu + \varkappa' + \eta}) + \\
&\quad + \varkappa' k^2 \left\{k^2 D\nu + \Gamma \left(\beta + \frac{g}{C_p}\right)\right\} + \Gamma' \beta' D + \\
&\quad + \left\{\eta k^2 \left(\nu\eta k^4 + k_z^2 V^2\right) + \nu k^4 k_z^2 \left(\frac{H}{4\pi Ne}\right)^2\right\} + k^2 (\nu + 2\eta) Q \,, \\
A_2 &= \{D + k^2(\nu + \varkappa')\} \left\{\nu\eta^2 k^6 + \eta k^2 k_z^2 V^2 + \nu k^4 k_z^2 \left(\frac{H}{4\pi Ne}\right)^2\right\} + \\
&\quad + k_z^2 V^2 \{\nu\eta k^4 + k_z^2 V^2 + \varkappa' k^2 D + k^2(\nu + \eta)(D + \varkappa' k^2)\} + \\
&\quad + k^2 (\nu + 2\eta) \left\{(\nu\varkappa' k^4 + \Gamma' \beta') D + \varkappa' k^2 \Gamma \left(\beta + \frac{g}{C_p}\right)\right\} + PQ \,, \\
A_1 &= \left\{\nu\eta^2 k^6 + \eta k^2 k_z^2 V^2 + \nu k^4 k_z^2 \left(\frac{H}{4\pi Ne}\right)^2\right\} Q + \\
&\quad + P \left\{k^4 \varkappa' D(\nu + 1) + \varkappa' k^2 \Gamma \left(\beta + \frac{g}{C_p}\right) + \Gamma' \beta' D\right\} + \\
&\quad + k_z^2 V^2 \{\varkappa' k^4 D(\nu + \eta) + (\nu\eta k^4 + k_z^2 V^2)(D + \varkappa' k^2)\} \,,
\end{aligned} \tag{25}$$

$$A_0 = \left\{(v\varkappa' k^4 + \Gamma' \beta')D + \varkappa' k^2 \Gamma \left(\beta + \frac{g}{C_p}\right)\right\}\left[v\eta^2 k^6 + k_z^2 k^2 \left\{\eta V^2 + \right.\right.$$

$$\left.\left. + vk^2 \left(\frac{H}{4\pi Ne}\right)^2\right\}\right] + k_z^2 V^2 \varkappa' k^2 D(v\eta k^4 + k_z^2 V^2),$$

where

$$V^2 = \frac{\mu_e H^2}{4\pi \varrho_0}, \quad \Gamma = g\alpha \left(\frac{k_x + k_y^2}{k^2}\right) \text{ and } \Gamma' = g\alpha' \left(\frac{k_x^2 + k_y^2}{k^2}\right),$$

$$P = \eta^2 k^4 + 2v\eta k^4 + \left(\frac{H}{4\pi Ne}\right)^2 k_z^2 k^2 + k_z^2 V^2,$$

$$Q = vK' k^4 + k^2(v + \varkappa')D + \Gamma \left(\beta + \frac{g}{C_p}\right) + \Gamma' \beta',$$

when

$$D < 0 \text{ and } |(v\varkappa' k^4 + \Gamma' \beta')D| > \Gamma \left(\beta + \frac{g}{C_p}\right) \varkappa' k^2, \tag{26}$$

the constant term in Eq. (24) is negative. Eq. (24), therefore, involves one change of sign and hence contains one positive real root. The occurrence of positive root implies monotonic instability.

We thus obtain a criterion that the thermohaline-convective instability of a stellar atmosphere in the presence of stable solute concentration gradient and Hall currents is unstable if

$$D < 0 \text{ and } |(v\varkappa' k^4 + \Gamma' \beta')\, D| > \Gamma \left(\beta + \frac{g}{C_p}\right) \varkappa' k^2.$$

4. Finite Larmor radius effects

Here we consider an infinite horizontal plasma layer of thickness d heated from above and subjected to a stable solute concentration gradient so that the temperatures and concentrations at the bottom surface $z = 0$ are T_0 and C_0 and at the upper surface $z = d$ are T_1 and C_1, respectively, z-axis being taken as vertical. This layer is acted on by a uniform vertical magnetic field $\mathbf{H}(0, 0, H)$ and gravity force $\mathbf{g}(0, 0, -g)$. Let $\delta\mathbf{P}$ denote the perturbation in stress tensor $\mathbf{P}$. For the vertical magnetic field $\mathbf{H}(0, 0, H)$, the perturbation in stress tensor components $\delta\mathbf{P}$, taking into account the finite ion gyration (VANDAKUROV [7]), are

$$\delta P_{xx} = \delta p - \varrho v_0 \left(\frac{\partial u}{\partial y} + \frac{\partial v}{\partial x}\right), \quad \delta P_{xy} = \delta P_{yx} = \varrho v_0 \left(\frac{\partial u}{\partial x} - \frac{\partial v}{\partial y}\right),$$

$$\delta P_{xz} = \delta P_{zx} = -2\varrho\nu_0\left(\frac{\partial v}{\partial z} + \frac{\partial \omega}{\partial y}\right), \quad \delta P_{yy} = \delta p + \varrho\nu_0\left(\frac{\partial u}{\partial y} + \frac{\partial v}{\partial x}\right), \tag{27}$$

$$\delta P_{yz} = \delta P_{zy} = 2\varrho\nu_0\left(\frac{\partial \omega}{\partial x} + \frac{\partial u}{\partial z}\right), \quad \delta P_{zz} = \delta p.$$

In Eqs. (27), δp is the perturbation in the scalar part of the pressure and $\varrho\nu_0 = NT/4\omega_H$, where ω_H is the ion-gyration frequency, while N and T denote, respectively, the number density and temperature of the ions.

The linearized hydromagnetic perturbation equations, in the presence of finite Larmor radius effect, are

$$\frac{\partial \mathbf{v}}{\partial t} = -\frac{1}{\varrho_0}\nabla\delta\mathbf{P} + \nu\nabla^2\mathbf{v} - \mathbf{g}(\alpha\theta - \alpha'\gamma) + \frac{\mu_e}{4\pi\varrho_0}(\nabla\times\mathbf{h})\times\mathbf{H}, \tag{28}$$

$$\nabla\cdot\mathbf{v} = 0, \tag{29}$$

$$\nabla\cdot\mathbf{h} = 0, \tag{30}$$

$$\frac{\partial \mathbf{h}}{\partial t} = (\mathbf{H}\cdot\nabla)\mathbf{v} + \eta\nabla^2\mathbf{h}, \tag{31}$$

$$\frac{\partial \gamma}{\partial t} = \beta'\omega + \varkappa'\nabla^2\gamma. \tag{32}$$

Eqs. (28)—(32) and (16) with the help of (27) give

$$\frac{\partial}{\partial t}\nabla^2\omega = g\left(\frac{\partial^2}{\partial x^2} + \frac{\partial^2}{\partial y^2}\right)(\alpha\theta - \alpha'\gamma) + \nu\nabla^4\omega + \frac{\mu_e H}{4\pi\varrho_0}\nabla^2\frac{\partial h_z}{\partial z} + \nu_0\left(\nabla^2 - 3\frac{\partial^2}{\partial z^2}\right)\frac{\partial \zeta}{\partial z}, \tag{33}$$

$$\frac{\partial \zeta}{\partial t} = \nu\nabla^2\zeta + \frac{\mu_e H}{4\pi\varrho_0}\frac{\partial \xi}{\partial z} - \nu_0\left(\nabla^2 - 3\frac{\partial^2}{\partial z^2}\right)\frac{\partial \omega}{\partial z}, \tag{34}$$

$$\frac{\partial h_z}{\partial t} = H\frac{\partial \omega}{\partial z} + \eta\nabla^2 hz, \tag{35}$$

$$\frac{\partial \xi}{\partial t} = H\frac{\partial \zeta}{\partial z} + \eta\nabla^2\xi, \tag{36}$$

$$\left(\frac{\partial}{\partial t} + D\right)\theta = -\left(\beta + \frac{g}{C_p}\right)\omega, \tag{37}$$

$$\left(\frac{\partial}{\partial t} - \varkappa'\nabla^2\right)\gamma = \beta'\omega. \tag{38}$$

Eliminating $\theta, \gamma, \zeta, \xi$ and h_z from Eqs. (33)—(38) and using expression (17), we obtain the dispersion relation

$$n^6 + A_5' n^5 + A_4' n^4 + A_3' n^3 + A_2' n^2 + A_1' n + A_0' = 0\,, \tag{39}$$

where

$$\begin{aligned}
A_5' &= D + 2A + k^2 \varkappa',\\
A_4' &= G + A(D + k^2 \overline{\nu + \varkappa' + \eta}) + L + B,\\
A_3' &= M + AL + G(D + k^2 \overline{\nu + \varkappa' + \eta}) + B\,(D + k^2 \overline{\varkappa' + 2\eta}),\\
A_2' &= AM + N' + GL + B\,(\eta^2 k^4 + 2\varkappa' \eta k^4 + k^2 D \overline{\varkappa' + 2\eta})\,,\\
A_1' &= AN' + GM + B(\varkappa' \eta^2 k^6 + \eta k^4 D \overline{\eta + 2\varkappa'}),\\
A_0' &= GN' + B\varkappa' \eta^2 k^6 D\,,
\end{aligned} \tag{40}$$

and we have written

$$A = k^2(\nu + \eta),\ B = \{\nu_0(k^2 - 3k_z^2)\}^2 \frac{k_z^2}{k^2},\ G = \nu\eta k^4 + k_z^2 V^2,$$

$$L = k^4(\varkappa' \eta + \nu\varkappa' + \nu\eta) + k^2 D(\nu + \varkappa' + \eta) + k_z^2 V^2 + \Gamma\left(\beta + \frac{g}{C_p}\right) + \Gamma'\beta',$$

$$M = \nu\eta\varkappa' k^6 + Dk^4(\varkappa' \eta + \nu\varkappa' + \nu\eta) + k^2(\varkappa' + \eta)\,\Gamma\left(\beta + \frac{g}{C_p}\right) +$$

$$+ \Gamma'\beta'(D + \eta k^2) + k_z^2 V^2(D + \varkappa' k^2)$$

and

$$N' = \nu\eta\varkappa' k^6 D + \Gamma\left(\beta + \frac{g}{C_p}\right)\varkappa' \eta k^4 + \Gamma'\beta' \eta k^2 D + \varkappa' k^2 k_z^2 V^2 D.$$

When

$$D < 0 \quad \text{and} \quad |(\nu\varkappa' k^4 + \Gamma'\beta')D| > \Gamma\left(\beta + \frac{g}{C_p}\right)\varkappa' k^2\,,$$

the constant term in Eq. (39) is negative. The product of the roots must then be negative. Therefore at least one root of Eq. (39) is positive and one root is negative. The occurrence of positive root implies monotonic instability. (26), therefore, determines the criterion for monotonic instability.

We conclude therefore that the criterion for monotonic instability derived in the presence of Hall currents, also holds good in the presence of finite Larmor radius effect on thermohaline-convective instability of a stellar atmosphere.

REFERENCES

1. S. CHANDRASEKHAR, Hydrodynamic and Hydromagnetic Stability, Clarendon Press, Oxford, 1961.
2. R. J. DEFOUW, Astrophys. J., **160**, 659, 1970.
3. D. A. NIELD, J. Fluid Mech., **29**, 545, 1967.
4. K. V. ROBERTS and J. B. TAYLOR, Phys. Rev. Letters, **8**, 197, 1962.
5. M. N. ROSENBLUTH, K. KRALL and N. ROSTOKER, Nucl. Fusion Suppl., **1**, 143, 1962.
6. E. A. SPIEGEL, Astrophys. J., **141**, 1068, 1965.
7. J. V. VANDAKUROV, Prik. Mat. Mech. 1, **28**, 69, 1964.
8. G. VERONIS, J. Marine Res., **23**, 1, 1965.

Acta Physica Academiae Scientiarum Hungaricae, Tomus 48 (4), pp. 359—368 (1980)

UNSTEADY FORCED AND FREE CONVECTIVE MHD FLOW PAST AN INFINITE VERTICAL POROUS PLATE WITH CONSTANT SUCTION AND OSCILLATORY WALL TEMPERATURE

By

V. M. SOUNDALGEKAR

DEPARTMENT OF MATHEMATICS, INDIAN INSTITUTE OF TECHNOLOGY, POWAI, BOMBAY, INDIA

and

S. R. SHENDE

DEPARTMENT OF MATHEMATICS, WALCHAND COLLEGE OF ENGINEERING, SANGLI, INDIA

(Received 25. II. 1980)

A two-dimensional unsteady flow of a viscous, incompressible, electrically conducting fluid past an infinite vertical porous plate has been carried out under the following conditions: 1) constant suction at the plate; 2) the wall temperature oscillating in time about a non-zero mean; 3) constant free-stream; 4) transversely applied uniform magnetic field.

Approximate solutions to coupled non-linear equations governing the flow have been derived for the transient velocity, the transient temperature, the amplitude and phase of the skin friction and the rate of heat transfer. The velocity and the temperature have been shown on graphs and the numerical values of the amplitude and phase are entered in Tables. It has been observed that the amplitude of the skin friction and the rate of heat transfer decrease due to the application of the transverse magnetic field, but increase due to increasing the Grashof number.

1. Introduction

Oscillatory flows past bodies of semi-infinite nature were studied by MOORE [1], LIGHTHILL [2], LIN [3], STUART [4], etc. LIGHTHILL studied the small-amplitude phenomenon and LIN studied the finite-amplitude phenomenon. However, these studies are confined to horizontal bodies. The effects of free-stream oscillations on the flow past a vertical porous isothermal plate, on taking into account the free convection currents, were studied by SOUNDALGEKAR [5, 6]. In [5] the mean flow and in [6] the unsteady flow was studied. The effects of constant heat flux on the oscillatory flow past a vertical porous plate were studied by SOUNDALGEKAR and GUPTA [7]. But in many industrial applications, the plate temperature is found to be oscillating and the free-stream is uniform. Such a situation in case of a porous infinite plate has been recently studied by SOUNDALGEKAR [8].

The effects of a transversely applied magnetic field on the flow considered in [4] were studied by SURYAPRAKASH RAO [9] for an electrically conducting fluid whereas the MHD aspects of [5, 6] were studied by SOUNDALGEKAR [10, 11] and that of [7] by SOUNDALGEKAR and WAVRE [12]. It is now proposed to study the effects of a uniformly applied magnetic field on the unsteady flow

past an infinite vertical porous plate whose temperature oscillates in time about a constant mean temperature. In Section 2 the mathematical analysis is presented and in Section 3 the conclusions are set out.

2. Mathematical analysis

Consider the flow in the upward direction of an electrically conducting incompressible fluid. The x'-axis is taken along the plate in the direction of the flow and the y'-axis is taken normal to the plate. The magnetic field of uniform strength is assumed to be applied parallel to the y'-axis. Then as in [5, 6, 10, 11], under usual Bousinesq approximation, the flow can be shown to be governed by the following coupled non-linear equations:

Continuity equation:

$$\frac{\partial v'}{\partial y'} = 0 \,. \tag{1}$$

Momentum equation:

$$\frac{\partial u'}{\partial t'} + v' \frac{\partial u'_c}{\partial y'} = \frac{\partial U'}{\partial t'} + g\beta (T' - T'_\infty) + \nu \frac{\partial^2 u'}{\partial y'^2} - \frac{\sigma B_0^2}{\varrho} (U_0 - u'). \tag{2}$$

Energy equation:

$$\varrho' C_p \left(\frac{\partial T'}{\partial t'} + v' \frac{\partial T'}{\partial y'} \right) = k \frac{\partial^2 T'}{\partial y'^2} + \mu \left(\frac{\partial u'}{\partial y'} \right)^2 . \tag{3}$$

In Eqs. (2) and (3), the induced field is assumed to be neglected. All the physical variables have been defined in the Notation. For constant suction, Eq. (1) integrates to

$$v' = - v'_0 \,, \tag{4}$$

where v'_0 is the constant suction and the negative sign in (4) indicates that it is directed towards the plate.

The boundary conditions are

$$\begin{aligned} &u' = 0, \quad T' = T'_w + \varepsilon (T'_w - T'_\infty)\, e^{i\omega' t'} \quad \text{at} \quad y' = 0 \,, \\ &u' = U_0, \; T' = T'_\infty \qquad\qquad\qquad\quad \text{as} \quad y' \to \infty \,. \end{aligned} \tag{5}$$

Introducing the following non-dimensional quantities

$$\begin{gathered} y = y' v_0/\nu \,, \; t = t' v_0^2/4\nu \,, \; \omega = 4\nu\omega'/v_0^2 \,, \\ u = u'/U_0 \,, \; \theta = \frac{T' - T'_\infty}{T'_w - T'_\infty} \,, \; P = \frac{\mu C_p}{K} \,, \\ G = \frac{\nu g \beta (T'_w - T'_\infty)}{U_{00}^2} \,, \; E = \frac{U_0^2}{C_p (T'_w - T'_\infty)} \,, \; M = \frac{\sigma B_0^2 \nu}{\varrho v_0^2} \end{gathered} \tag{6}$$

in Eqs. (2), (3) and (5) and taking account of (4), we get

$$\frac{1}{4}\frac{\partial u}{\partial t} - \frac{\partial u}{\partial y} = G\theta + \frac{\partial^2 u}{\partial y^2} + M(1-u), \tag{7}$$

$$\frac{P}{4}\frac{\partial \theta}{\partial t} - P\frac{\partial \theta}{\partial y} = \frac{\partial^2 \theta}{\partial y^2} + PE\left(\frac{\partial u}{\partial y}\right)^2, \tag{8}$$

and the boundary conditions are

$$\begin{aligned} &u = 0,\ \theta = 1 + \varepsilon e^{i\omega t} && \text{at} \quad y = 0, \\ &u = 1,\ \theta = 0 && \text{as} \quad y \to \infty . \end{aligned} \tag{9}$$

To solve the coupled non-linear equations (7)—(8), we assume in the neighbourhood of the plate

$$\begin{aligned} u &= u_0 + \varepsilon\, e^{i\omega t} u_1, \\ \theta &= \theta_0 + \varepsilon\, e^{i\omega t} \theta_1, \end{aligned} \tag{10}$$

as $\varepsilon \ll 1$. Substituting (10) in Eqs. (7) and (8), equating the coefficients of different powers of ε, neglecting those of ε^2, we have the following set of coupled nonlinear equations:

$$u_0'' + u_0' - Mu_0 = -M - G\theta_0, \tag{11}$$

$$u_2'' + u_1' - \left(M + \frac{i\omega}{4}\right) u_1 = -G\theta_1, \tag{12}$$

$$\theta_0'' + P\theta_0' = -PEu_0'^2, \tag{13}$$

$$\theta_0'' + P\theta_1' - \frac{i\omega P}{4}\theta_1 = -2PEu_0' u_1' . \tag{14}$$

Here and henceforth, the primes denote differentiation with respect to y, and the boundary conditions are

$$\begin{aligned} &u_0 = 0,\ u_1 = 0,\ \theta_0 = 1,\ \theta_1 = 1 \quad \text{at} \quad y = 0, \\ &u_0 = 1,\ u_1 = 0,\ \theta_0 = 0,\ \theta_1 = 0 \quad \text{as} \quad y \to \infty. \end{aligned} \tag{15}$$

As the analytical solutions of Eqs. (11)—(14) are not possible, we again expand $u_0, u_1, \theta_0, \theta_1$ in powers of E, the Eckert number as for incompressible fluids, $E \ll 1$. Thus

$$\begin{aligned} &u_0 = u_{01} + Eu_{02},\ u_1 = u_{11} + Eu_{12}, \\ &\theta_0 = \theta_{01} + E\theta_{02},\ \theta_1 = \theta_{11} + E\theta_{12}. \end{aligned} \tag{16}$$

Substituting (16) in Eqs. (11)—(14), equating the coefficients of E, neglecting those of E^2, we get

$$u_{01}'' + u_{01}'' - Mu_{01} = -M - G\theta_{01}\,, \tag{17}$$

$$u_{02}'' + u_{02}'' - Mu_{02} = -G\theta_{02}\,, \tag{18}$$

$$u_{11}'' + u_{12}' - \left(M + \frac{i\omega}{4}\right) u_{11} = -G\theta_{11}\,, \tag{19}$$

$$u_{12}'' + u_{12}' - \left(M + \frac{i\omega}{4}\right) u_{12} = -G\theta_{12}\,, \tag{20}$$

$$\theta_{01}'' + p\theta_{01}' = 0\,, \tag{21}$$

$$\theta_{02}'' + P\theta_{02}' = -Pu_{01}'^2\,, \tag{22}$$

$$\theta_{11}'' + P\theta_{11}' - \frac{i\omega P}{4}\theta_{11} = 0\,, \tag{23}$$

$$\theta_{12}'' + P\theta_{12}' - \frac{i\omega P}{4}\theta_{12} = -2Pu_{01}'u_{11}' \tag{24}$$

and the corresponding boundary conditions are

$$\begin{aligned} &u_{01}(o) = 0,\ u_{02}(o) = 0,\ u_{11}(o) = 0,\ u_{12}(o) = 0\,,\\ &\theta_{01}(o) = 1,\ \theta_{02}(o) = 0,\ \theta_{11}(o) = 1,\ \theta_{12}(o) = 0\,,\\ &u_{01}(\infty) = 1,\ u_{02}(o) = 0,\ u_{11}(o) = 0,\ u_{12}(o) = 0\,,\\ &\theta_{01}(\infty) = 0, \theta_{02}(\infty) = 0, \theta_{11}(\infty) = 0, \theta_{12}(\infty) = 0\,. \end{aligned} \tag{25}$$

The solutions of these coupled linear equations (17)—(24), satisfying (25) are obtained and on substituting in (16), we get

$$\theta_0 = e^{-Py} + E\left[(a_1 - 1)^2 \frac{Pn^2}{a_2}(e^{-Py} - e^{2ny}) + \frac{Pa_1^2}{2}(e^{-Py} - e^{-2Py}) - \right.$$
$$\left. - \left\{\frac{2P^2 n}{n(P+n)} - (a_1 - 1)a_1\right\}(e^{-Py} - e^{-(P+n)y}\right], \tag{26}$$

$$a_1 = \frac{G}{P^2 - P - M}\,,\quad a_2 = 4n^2 - 2Pn\,,$$

$$\theta_1 = e^{-hy} + E\left[\frac{2a_1 Gn\,Pf}{a_3 a_4}(e^{-hy} - e^{-(n+f)y} - \frac{2a_1 Gn\,Ph}{a_4 a_5}(e^{-hy} - e^{-(n+h)y} - \right.$$
$$\left. - \frac{2a_1 GP^2 f}{a_3 a_4}(e^{-hy} - e^{-(P+f)y}) + \frac{2a_1 GP^2 h}{a_4 a_6}(e^{-hy} - e^{-(P+h)y})\right] \tag{27}$$

$$n = \frac{1+\sqrt{1+4M}}{2}, \quad h = \frac{P+\sqrt{P^2+i\omega P}}{2},$$

$$f = \frac{1+\sqrt{1+4\left(M+\frac{i\omega}{4}\right)}}{2},$$

$$a_3 = (P+f)^2 - P(P+f) - \frac{i\omega P}{4}, \quad a_4 = h^2 - h - \left(M+\frac{i\omega}{4}\right),$$

$$a_5 = (n+h)^2 - P(n+h) - \frac{i\omega P}{4}, \; a_6 = (P+h)^2 - P(P+h) - \frac{i\omega P}{4},$$

$$u_0 = 1 - e^{-ny} + a_1(e^{-ny} - e^{-Py}) + E\left[a_1\left\{\frac{n^2P(a_1-1)^2}{a_2} + \right.\right.$$

$$\left. + \frac{Pa_1^2}{2} - \frac{2a_1(a_1-1)nP^2}{n(P+n)}\right\}(e^{-ny} - e^{-Py}) -$$

$$- \frac{(a_1-1)^2Gn^2P}{a_2a_7}(e^{-ny} - e^{-2ny}) - \frac{a_1^2PG}{a_8}(e^{-ny} - e^{-2Py}) +$$

$$\left. + \frac{2a_1(a_1-1)nP^2G}{a_9n(P+n)}(e^{-ny} - e^{-(P+n)y})\right], \tag{28}$$

$$a_7 = 4n^2 - 2n - M, \; a_8 = 4P^2 - 2P - M,$$

$$a_9 = (P+n)^2 - (P+n) - M,$$

$$u_1 = \frac{G}{a_4}(e^{-fy} - e^{-hy}) + E\left[\frac{2PG^2}{a_4^2}\left\{(a_1-1)\left(\frac{nf}{a_{10}} - \frac{nh}{a_5}\right) - \right.\right.$$

$$- a_1\left(\frac{Pf}{a_3} - \frac{Ph}{a_6}\right)\left\}(e^{-fy} - e^{-hy}) - \right.$$

$$- \frac{2(a_1-1)G^2nPf}{(a_{10}-M)a_{10}a_4}(e^{-fy} - e^{-(n+f)y}) + \frac{2a_1G^2P^2f}{(a_3-M)a_3a_4} \times$$

$$\left. \times (e^{-fy} - e^{-(P+f)y}) - \frac{2a_1P^2hG^2}{(a_6-M)a_6a_4}(e^{-fy} - e^{-(P+h)y})\right], \tag{29}$$

where

$$a_{10} = (n+f)^2 - P(n+f) - \frac{i\omega P}{4}.$$

Substituting the values of u_0, u_1, θ_0, θ_1 from the above in Eq (10), we get the expressions for the velocity and temperature profiles. These can be written

in terms of the fluctuating parts of the velocity and the temperature as

$$u(y, t) = U_0(y) + \varepsilon(M_r \cos \omega t - M_i \sin \omega t), \tag{30}$$

$$\theta(y, t) = \theta_0(y) + \varepsilon(T_r \cos \omega t - T_i \sin \omega t), \tag{31}$$

where

$$M_r + iM_i = u_1, \quad T_r + iT_i = \theta_1 .$$

Hence the expressions for the transient velocity and the transient temperature for $\omega t = \pi/2$ are written as

$$\begin{aligned} u(y, \pi/2) &= u_0(y) - \varepsilon M_i, \\ \theta(y, \pi/2) &= \theta_0(y) - \varepsilon T_i . \end{aligned} \tag{32}$$

The transient velocity profiles and the transient temperature profiles are shown in Fig. 1 and Fig. 2, respectively. We observe from Fig. 1 that due to the application of magnetic field there is a considerable fall in the velocity. An increase in G, ω or E leads to a rise in the velocity whereas an increase in M leads to a fall in the velocity. We observe from Fig. 2 that due to the application of the magnetic field there is a fall in the transient temperature. An increase in ω or greater viscous dissipative heat causes a rise in θ whereas an increase in G leads to a fall in the value of θ.

It is now proposed to study the skin-friction. It is given by

$$\tau = \tau'/\varrho U_0 v_0 = \left.\frac{du}{dy}\right|_{y=0} = \left.\frac{du_0}{dy}\right|_{y=0} + \varepsilon e^{i\omega t} \left.\frac{du_1}{dy}\right|_{y=0} . \tag{33}$$

$\left.\frac{du_0}{dy}\right|_{y=0}$ represents the mean skin-friction and it has been discussed in [10]. From (33) and (29), we have

$$\begin{aligned} \left.\frac{du_1}{dy}\right|_{y=0} = \frac{G(h-f)}{a_4} + E\Bigg[\frac{2PG^2(h-f)}{a_4^2} \Bigg\{ (a_1 - 1)\left(\frac{nf}{a_{10}} - \frac{nh}{a_5}\right) - \\ - a_1\left(\frac{Ph}{a_3} - \frac{Ph}{a_6}\right)\Bigg\} - \frac{2(a_1 - 1) G^2 n^2 Pf}{a_0 a_4 (a_{10} - M} + \\ + \frac{2a_1 G^2 P^3 f}{[a_3 a_4 (a_3 - M)} - \frac{2a_1 P^2 h G^2 (P + h - f)}{a_4 a_6 (a_6 - M)}\Bigg] . \end{aligned} \tag{34}$$

We now study the amplitude and the phase of the skin friction. We express (33) in terms of the amplitude and phase as:

$$\tau = \left.\frac{du_0}{dy}\right|_{y=0} + \varepsilon|B| \cos(\omega t + \alpha), \tag{35}$$

where

$$B = B_r + iB_i = \left.\frac{du_1}{dy}\right|_{y=0} \tag{36}$$

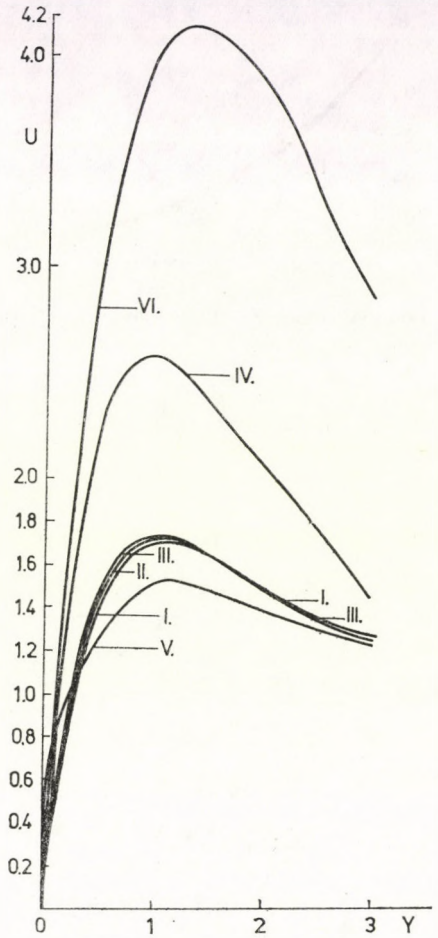

Fig. 1. Transient velocity profiles $\varepsilon = 0.2$, $\omega t = \pi/2$

M	G	E	ω	
2	5	0.01	5	I
2	5	0.01	10	II
2	5	0.02	5	III
2	10	0.01	5	IV
4	5	0.01	5	V
0	5	0.01	5	VI

and

$$\tan \alpha = B_i/B_r \, .$$

The numerical values of $|B|$ and $\tan \alpha$ are entered in Table I. We observe from this Table that the amplitude of the skin-friction decreases owing to the application of the magnetic field. An increase in ω leads to a decrease in the value of $|B|$. Under the action of the magnetic field, greater viscous

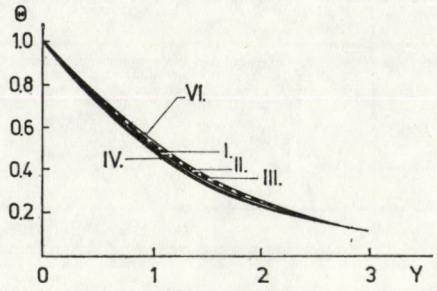

Fig. 2. Transient temperature profiles $\varepsilon = 0.2$, $\omega t\ \pi\ \pi/2$

M	G	E	ω	
2	5	0.01	5.0	I
2	5	0.01	10.0	II
2	5	0.02	5.0	III
2	10	0.01	5.0	IV
0	5	0.01	5.0	VI

Table I

Values of |B| and tan α, |Q| and tan β_1

M	G	E	ω	$\lvert B\rvert$	tan α	$\lvert Q\rvert$	tan β_1
0	5	0.01	5	2.5260	−0.94108	1.2483	0.63667
			10	1.7772	−0.98718	1.6229	0.70725
			15	1.4400	−1.0013	1.9142	0.74762
2	5	0.01	5	2.1239	−0.48531	1.2312	0.60291
			10	1.6639	−0.66274	1.6126	0.69635
			15	1.3965	−0.75672	1.9075	0.74196
2	5	0.02	5	2.1261	−0.48873	1.2258	0.62646
			10	1.6642	−0.66503	1.6134	0.70976
			15	1.3960	−0.75819	1.9097	0.75057
2	10	0.01	5	4.2587	−0.49361	1.2199	0.65518
2	10	0.01	10	3.3278	−0.66830	1.6164	0.72582
			15	2.7908	−0.76028	1.9123	0.76082
4	5	0.01	5	1.7822	−0.38444	1.2304	0.5951
			10	1.5022	−0.50326	1.6103	0.69341
			15	1.3120	−0.60435	1.9056	0.74073

dissipative heat or an increase in G leads to a rise in the value of $|B|$ whereas an increase in M leads to a fall in the value of $|B|$. The values of tan α being observed to be negative, we conclude that there is always a phaselag.

Knowing the temperature field, we now study the rate of heat transfer. It is given by

$$q' = -k\left(\frac{\partial u'}{\partial y'}\right)_{y'=0} \tag{37}$$

and in view of (6), (37) reduces to

$$q = -\frac{q'\nu}{k_0(T'_w - T'_\infty)} = \left.\frac{d\theta_0}{dy}\right|_{y=0} + \varepsilon e^{i\omega t}\left.\frac{d\theta_1}{dy}\right|_{y=0}. \tag{38}$$

Here, $\left.\frac{d\theta_0}{dy}\right|_{y=0}$ represents the mean rate of heat transfer and has been discussed in [10]. From (38) and (27), we get

$$\left.\frac{d\theta_1}{dy}\right|_{y=0} = -h + E\left[\frac{2a_1 Gn\, Pf}{a_3 a_4}(n+f-h) - \frac{2a_1 Gn^2 Ph}{a_4 a_5} - \right.$$
$$\left. - \frac{2a_1 GP^2 f}{a_3 a_4}(P+f-h) + \frac{2a_1 GP^3 h}{a_4 a_6}\right]. \tag{39}$$

We now express q in terms of the amplitude $|Q|$ and the phase of the rate of heat transfer. It is given by

$$q = \left.\frac{d\theta_0}{dy}\right|_{y=0} + \varepsilon|Q|\cos(\omega t + \beta_1), \tag{40}$$

where

$$Q = Q_r + iQ_i = \left.\frac{d\theta_1}{dy}\right|_{y=0} \tag{41}$$

and

$$\tan\beta_1 = Q_i/Q_r .$$

The numerical values of $|Q|$ and $\tan\beta_1$ are entered in Table I. We observe from Table I that due to the application of the magnetic field, there is a fall in the value of $|Q|$. An increase in G, M or E leads to a fall in the value of $|Q|$ but $|Q|$ increases due to a rise in the value of ω. There is always a phase-lead in case of the rate of heat transfer.

3. Conclusions

(1) Due to the application of the transverse magnetic field, there is a fall in the transient velocity and the transient temperature.
(2) An increase in ω or E leads to a rise in the transient velocity and temperature.

(3) An increase in G leads to a rise in the transient velocity and a fall in the transient temperature.

(4) Due to the application of the magnetic field, there is a fall in the value of $|B|$ and $|Q|$.

(5) An increase in ω leads to a fall in the value of $|B|$ and a rise in the value of $|Q|$.

(6) Greater viscous dissipative heat causes a rise in the value of $|B|$ and a fall in the value of $|Q|$.

(7) An increase in G leads to a rise in the value of $|B|$ and a fall in the value of $|Q|$ but there is a fall in the value of $|B|$ and $|Q|$ owing to a rise in M.

(8) There is a phase-lag in case of skin-friction and a phase-lead in case of the rate of heat transfer.

REFERENCES

1. F. K. MOORE, Unsteady laminar boundary layer flow, NACA TN 2471, 1951.
2. M. J. LIGHTHILL, Proc. Roy. Soc. (London), **A224**, 1, 1954.
3. C. C. LIN, Proc. 9th Intl. Congress of Applied Mech., **4**, 155, 1957.
4. J. T. STUART, Proc. Roy. Soc. (London), **A231**, 116, 1955.
5. V. M. SOUNDALGEKAR, Proc. Roy. Soc. (London), **A333**, 25, 1973.
6. V. M. SOUNDALGEKAR, **A333**, 37, 1973.
7. V. M. SOUNDALGEKAR and S. K. GUPTA, Iran J. Sci. and Tech., **6**, 11, 1977.
8. V. M. SOUNDALGEKAR, Unsteady forced and free convective flow past an infinite vertical porous plate with oscillatory wall temperature and constant suction, J. Astrophys. and Space Science, 1979 (accepted for publication).
9. U. S. RAO, Zeit. Angew. Math. Mech., **42**, 133, 1962.
10. V. M. SOUNDALGEKAR, J. Fluid Mech., **66**, 541, 1974.
11. V. M. SOUNDALGEKAR, Zeit. Angew. Math. Mech., **55**, 257, 1975.
12. V. M. SOUNDALGEKAR and P. D. WAVRE, Zeit. Angew. Math. Mech., **59**, 62, 1979.

Notation

$\|B\|$	amplitude of the skin-friction
B_0	magnetic field
C_p	specific heat at constant pressure
E	Eckert number
g	accelertaion due to gravity
G	Grashof number
k	thermal conductivity
M_r, M_i	fluctuating parts of the velocity profile
M	magnetic field parameter
P	Prandtl number
q'	rate of heat transfer
$\|Q\|$	amplitude of the rate of heat transfer
t'	dimensional time
t	dimensionless time
T'	temperature of the fluid
T'_w	temperature of the plate
T'_∞	temperature of the fluid in the free-stream
T_r, T_i	fluctuating parts of the temperature profile
u', v'	velocity components in the x', y'-directions
u	dimensionless velocity in the x-direction
U_0	free-stream velocity
u_0	mean velocity
v_0	suction velocity
x', y'	co-ordinate system
y	dimensionless co-ordinate normal to the wall
ω'	frequency
τ'	skin-friction
θ	dimensionless temperature
θ_0	mean temperature
$\varepsilon\theta_1$	amplitude of the temperature fluctuation
α	phase angle of the skin-friction
β_1	phase angle of the rate of heat transfer
ϱ'	density of the fluid
ϱ'_∞	density of the fluid in the free-stream
ν	kinematic viscosity
μ	viscosity
σ	electrical conductivity of the fluid
β	coefficient of volume expansion

Acta Physica Academiae Scientiarum Hungaricae, Tomus 48 (4), pp. 369—382 (1980)

SHOCKS AND WAVES IN THERMO-VISCOUS MFD WITH HIDDEN VARIABLES*

By

A. MORRO

DEPARTMENT OF MATHEMATICAL PHYSICS, 16132 GENOVA, ITALY

(Received 26. II. 1980)

The behaviour of heat conducting viscous fluids, acted on by a magnetic field, is described within the approximation of magnetofluiddynamics through a model accounting for heat conduction and viscosity via hidden variables. The constitutive equations adopted meet the restrictions imposed by the second law of thermodynamics and reduce to Navier-Stokes' and Fourier's laws in stationary processes. The foremost result of the paper is that, in general, such constitutive equations allow shock and wave propagation in thermo-viscous fluids. In particular, when the discontinuity fronts enter a region at equilibrium, the shock relations simplify to the standard shock relations of magnetofluiddynamics and the (acceleration) wave relations characterise waves which are the counterpart of the customary Alfvén waves and magnetoacoustic waves. Indeed, viscosity and heat conduction introduce quantitative differences but leave the propagation modes qualitatively unchanged.

1. Introduction

A systematic account for heat conduction and viscosity in magnetofluiddynamics (MFD) would be highly desirable on the basis of various arguments. To begin with note that heat conduction and viscosity are usually considered for the purpose of providing a description of the shock structure — see, e.g., [1], [2] §4.2.3. Also, on appealing to the law of increase of entropy, it is commonly asserted that the entropy of a fluid which has passed through a shock must exceed the initial entropy — [3] §82. Such an assertion appears to be obvious if irreversible phenomena, like heat conduction and viscosity, actually occur in the fluid. However, the existence of irreversible phenomena is in deep contrast with the customary energy balance equation as expressed by the vanishing of the material time derivative of the entropy. So in MFD, as well as in ordinary fluid dynamics, the fluid is regarded as viscous and heat conducting or inviscid and non-heat-conducting depending on the particular topic to hand.

The crux of the matter, which is at the bottom of this apparent contradiction, is that Navier—Stokes' law of viscosity and Fourier's law of heat con-

* Work performed under the auspices of the National Research Council (C.N.R. — G.N.F.M.), Italy.

duction rule out the possibility of wave propagation. This makes it unavoidable to assume that the fluid is inviscid and non-heat-conducting whenever wave propagation problems are concerned. Yet the achievement of a model of heat conduction and viscosity, compatible with wave propagation, would be the best way for removing the contradiction outlined above.

In relation to this subject in the last thirty years much research has been undertaken both in the classical and in the relativistic context — see, e.g. [4, 5] and references cited therein. Nevertheless, to my mind further research is in order because, on the one hand, the literature has been concerned almost only with the heat equation and, on the other hand, the models carried out appear to be not very handy for applications.

Recently, the problem of wave propagation in thermo-viscous materials has been faced by myself in [6] by supposing the material to be equipped with a suitable set of hidden variables [7, 9]. Following along the same lines, in this paper I attempt to produce a theory of thermo-viscous MFD which is both physically sound and formally not too complicated. In this connection it is a remarkable fact that a systematic use of the MFD approximation allows us to drop out the dependence of electric and magnetic quantities on the hidden variables. A further simplification is introduced by considering linear uncoupled evolution equations for the thermal and viscous hidden variables.

The plan of the paper is as follows. Accounting for the second law of thermodynamics via the Clausius—Duhem inequality, the full set of constitutive equations is gathered in Section 2. Then, on appealing to the noteworthy feature of hidden variables, whereby they are continuous across discontinuity fronts of the external variables, in Section 2 the jump relations for shocks — strong discontinuities — and waves — weak discontinuities — are derived. The shock relations become just those of standard MFD when the region ahead of the shock is held at equilibrium until the arrival of the front. In view of this I have elected to devote the subsequent section to the investigation of wave propagation only. Precisely, under the assumption that the region ahead has been at equilibrium, Section 4 exhibits the propagation condition and the propagation modes. The most outstanding results may be summarised by saying that two types of waves are possible, namely Alfvén-like waves and magnetoacoustic-like waves, while zero-speed waves occur only in the case of non-heat-conducting fluids. In general, it turns out that the effect of the hidden variables affect the value of the speeds but leave the propagation modes qualitatively unchanged.

The encouraging results obtained in this paper and the need for a model of viscosity in general relativity, outlined in Section 5, suggest to take over into the relativistic context the theory of thermo-viscous MFD. A preliminary relativistic counterpart concerning thermo-viscous fluiddynamics has been developed in [10].

2. Hidden variables. Constitutive equations

Throughout the domain of any field under consideration is $\mathcal{R}\times\mathbf{R}$, $\mathcal{R}$ being the simply-connected region occupied by the fluid in the present configuration and $\mathbf{R}$ the set of real numbers. The symbol ∇ stands for the spatial gradient while a superposed dot denotes the material time differentiation. As usual, ϱ is the mass density, $\mathbf{V}$ the velocity, $\mathbf{T}$ the Cauchy stress tensor, $\mathbf{D}$ the stretching tensor, e the internal energy density, $\mathbf{B}$ the magnetic induction, μ the magnetic permeability, and $\mathbf{H}$ the magnetic field. To adhere to the standard accounts of MFD the linear constitutive equation

$$\mathbf{B} = \mu\mathbf{H} \tag{2.1}$$

is assumed to be true. The symbol $\boldsymbol{\tau}$ denotes the magnetic stress tensor, that is

$$\boldsymbol{\tau} = \mu(\mathbf{H}\otimes\mathbf{H} - \frac{1}{2}H^2\mathbf{I})\,. \tag{2.2}$$

The electrical conductivity is supposed to be infinite. Accordingly, the balance laws for mass, momentum, energy, and magnetic field can be represented, respectively, by the differential equations

$$\begin{aligned}
&\dot{\varrho} + \varrho\nabla\cdot\mathbf{V} = 0\,,\\
&\varrho\dot{\mathbf{V}} = \nabla\cdot(\mathbf{T}+\boldsymbol{\tau}) + \varrho\mathbf{b}\,,\\
&\varrho\dot{e} = \mathbf{T}:\mathbf{D} - \nabla\cdot\mathbf{q} + \varrho r\,,\\
&\dot{\mathbf{B}} = (\mathbf{B}\cdot\nabla)\mathbf{V} - \mathbf{B}(\nabla\cdot\mathbf{V})\,,
\end{aligned} \tag{2.3}$$

where $\mathbf{b}$ is the mechanical body force, $\mathbf{q}$ the heat flux, r the heat supply, and $\mathbf{T}:\mathbf{D}$ is the trace of $\mathbf{TD}$. Moreover the field $\mathbf{B}$ must meet the condition

$$\nabla\cdot\mathbf{B} = 0\,. \tag{2.4}$$

By virtue of (2.1) and (2.2) the behaviour of the fluid is completely determined once the constitutive equations for $\mathbf{T}$, $\mathbf{q}$, e, and the specific entropy η are given. Now, to avoid the unpleasant feature of Navier—Stokes' and Fourier's laws, imagine the fluid to be equipped with a suitable set of hidden variables [6] but, meanwhile, assume that the constitutive Eqs. (2.1), (2.2) are left unchanged. Precisely, letting θ stand for the temperature, $\psi = e - \theta\eta$ the free energy, and $\boldsymbol{\sigma} = (\psi, \eta, \mathbf{T}, \mathbf{q})$ the set of response functions, we account for

the behaviour of the fluid through the $\mathbf{C}^2$ functions, $\boldsymbol{\sigma}$, $\mathbf{f}$ such that [1]

$$\boldsymbol{\sigma} = \boldsymbol{\sigma}(\theta, \varrho, \boldsymbol{\alpha}), \tag{2.5}$$

$$\dot{\boldsymbol{\alpha}} = \mathbf{f}(\theta, \varrho, \nabla\theta, \mathbf{D}, \boldsymbol{\alpha}), \tag{2.6}$$

$\boldsymbol{\alpha}$ being the set of hidden variables.

To adhere as close as possible to the standard theory of heat conduction and viscosity it is convenient to regard $\boldsymbol{\alpha}$ as consisting of a vector hidden variable $\boldsymbol{\alpha}_c \in \mathbf{R}^3$ and a tensor hidden variable $\boldsymbol{\alpha}_v \in \mathrm{Sym}\,(\mathbf{R}^3, \mathbf{R}^3)$ and besides to choose the function $\mathbf{f}$ so as to make (2.6) into the form

$$\begin{aligned} \dot{\boldsymbol{\alpha}}_c &= \frac{1}{\tau_c}(\nabla\theta - \boldsymbol{\alpha}_c), \\ \dot{\boldsymbol{\sigma}}_v &= \frac{1}{\tau_v}(\mathbf{D} - \boldsymbol{\alpha}_v), \end{aligned} \tag{2.7}$$

where τ_c, $\tau_v > 0$ play the role of relaxation times. If $\nabla\theta$, $\mathbf{D}$ are $\mathbf{C}^0$ functions on $[t_0, t]$ then the obvious solutions of Eqs. (2.7) are

$$\begin{aligned} \boldsymbol{\alpha}_c(t) &= \frac{1}{\tau_c}\int_{t_0}^{t} \exp\left(-(t-\zeta)/\tau_c\right)\nabla\theta(\zeta)\,d\zeta + \boldsymbol{\alpha}_c(t_0)\exp\left(-(t-t_0)/\tau_c\right), \\ \boldsymbol{\alpha}_v(t) &= \frac{1}{\tau_v}\int_{t_0}^{t} \exp\left(-(t-\zeta)/\tau_v\right)\mathbf{D}(\zeta)\,d\zeta + \boldsymbol{\alpha}_v(t_0)\exp\left(-(t-t_0)/\tau_v\right). \end{aligned} \tag{2.7$'$}$$

The response functions (2.5) are required to be compatible with the second law of thermodynamics. On assuming that such a law is expressed by the Clausius—Duhem inequality and accounting for the energy balance $(2.3)_3$ we take it that

$$-\varrho(\dot{\psi} + \eta\dot{\theta}) + \mathbf{T} : \mathbf{D} - \frac{1}{\theta}\mathbf{q}\cdot\nabla\theta \geq 0 \tag{2.8}$$

holds at any particle of the fluid for every set of histories θ, ϱ, $\nabla\theta \in \mathbf{C}^1(\mathbf{R})$ and $\mathbf{D} \in \mathbf{C}^0(\mathbf{R})$. More explicitly, (2.8) can be written as

$$\begin{aligned} -\varrho(\psi_\theta + \eta)\dot{\theta} + \left(\mathbf{T} + \varrho^2\psi_\varrho\mathbf{I} - \frac{\varrho}{\tau_v}\psi_{\alpha_v}\right) : \mathbf{D} - \left(\frac{1}{\theta}\mathbf{q} + \frac{\varrho}{\tau_c}\psi_{\alpha_c}\right)\cdot\nabla\theta + \\ + \varrho\left(\frac{1}{\tau_c}\psi_{\alpha_c}\cdot\boldsymbol{\alpha}_c + \frac{1}{\tau_v}\psi_{\alpha_v} : \boldsymbol{\alpha}_v\right) \geq 0\,, \end{aligned}$$

the subscripts $\theta, \varrho, \boldsymbol{\alpha}_c, \boldsymbol{\alpha}_v$ denoting partial derivatives. The solutions (2.7)$'$ make it evident the independence of $\boldsymbol{\alpha}_c(t), \boldsymbol{\alpha}_v(t)$ of the present values $\nabla\theta(t)$,

[1] As already remarked in previous papers [6, 11], the explicit dependence of $\boldsymbol{\sigma}$ on $\nabla\theta$ and $\mathbf{D}$ is not compatible with wave propagation.

$\mathbf{D}(t)$. Accordingly, accounting also for the arbitrariness of $\dot{\theta}(t)$, it follows that the Clausius—Duhem inequality holds if and only if

$$\eta_\theta = -\psi_\theta, \quad \mathbf{T} = -\varrho^2 \psi_\varrho \, \mathbf{I} + \frac{\varrho}{\tau_v} \psi_{\alpha_v}, \quad \mathbf{q} = -\frac{\theta \varrho}{\tau_c} \psi_{\alpha_c}, \tag{2.9}$$

$$\frac{1}{\tau_c} \psi_{\alpha_c} \cdot \alpha_c + \frac{1}{\tau_v} \psi_{\alpha_v} : \alpha_v \geqq 0. \tag{2.10}$$

So any free energy function $\psi(\theta, \varrho, \alpha_c, \alpha_v)$ consistent with (2.10) makes the response functions (2.9) identically compatible with the second law of thermodynamics. With a view to the purposes we have in mind, the simplest model accounting for hidden variables is obtained by choosing ψ in the form

$$\psi(\theta, \varrho, \alpha_c, \alpha_v) = \Psi(\theta, \varrho) + \frac{1}{\varrho} \left\{ \frac{\varkappa \tau_c}{2\theta} \alpha_c \cdot \alpha_c + \chi \tau_v \alpha_v : \alpha_v + \frac{1}{2} \lambda \tau_v (\mathbf{I} : \alpha_v)^2 \right\}, \tag{2.11}$$

Ψ being an arbitrary function. Observe that the function (2.11) meets the requirement (2.10) if and only if the non-vanishing parameters $\chi, \lambda, \varkappa$ are subject to the restrictions

$$\chi > 0, \quad 3\lambda + 2\chi \geqq 0, \quad \varkappa > 0. \tag{2.12}$$

Substitution of (2.11) into (2.9) yields

$$\eta = -\psi_\theta + \frac{\varkappa \tau_c}{2\varrho\theta^2} \alpha_c \cdot \alpha_c, \tag{2.13}$$

$$\mathbf{T} = -p\,\mathbf{I} + 2\chi \alpha_v + \lambda (\mathbf{I} : \alpha_v)\,\mathbf{I}, \quad \mathbf{q} = -\varkappa \alpha_c, \tag{2.14}$$

where $p = \varrho^2 \psi_\varrho$. The physical meaning of the parameters $\chi, \lambda, \varkappa$ is easily recognised by noting that if $\nabla\theta$ and $\mathbf{D}$ are constant in time we get

$$\lim_{t \to \infty} (\alpha_c(t), \alpha_v(t)) = (\nabla\theta, \mathbf{D}).$$

So in this instance, apart from an additive term in p containing quadratic invariants of the hidden variables, Eqs. (2.14) asymptotically become just the Navier—Stokes and Fourier constitutive equations. This assigns the meaning of viscosity coefficients to χ, λ and of thermal conductivity to $\varkappa$, thus making (2.12)'s to be the Stokes—Duhem and Fourier inequalities.

Before concluding this Section it is worth considering briefly a property of hidden variables which is essential to later developments.

Remark. For any fixed particle of the fluid, Eq. (2.6) is an ordinary differential equation governing the evolution of the hidden variables at that particle. Appealing to a well known theorem we assert that if $\mathbf{f}$ is continuous on $\pi := (\theta, \varrho, \nabla\theta, \mathbf{D})$ and Lipshitzian with respect to α then the initial value problem

$$\dot{\alpha} = \tilde{\mathbf{f}}(t, \alpha(t)), \quad \alpha(t_0)\alpha = \alpha_0,$$

being $\tilde{\mathbf{f}}(t, .) := \mathbf{f}(\pi(t), .)$, has a unique solution provided $\pi(t)$ is continuous with respect to t. This in turn emphasises that the solutions (2.7)′ of the particular problem (2.7) exist in $[t_0, t]$ whenever $\nabla\theta, \mathbf{D} \in \mathbf{C}^0[t_0, t]$.

Usually wave propagation is associated with a discontinuity of π. As a consequence we have to solve the problem of the prolongation of α across the time t corresponding to a discontinuity. On the other hand, motivated by the physical situation, we may consider the discontinuity of π as a limiting case of a continuous evolution of π in a suitably short time interval Δt around t. In this instance the relations (2.7)′ still apply and, furthermore, they imply that the change of α, no matter how π changes, tends to zero as Δt tends to zero. This argument warrants the prolongation by continuity of α across the discontinuity of π.

3. Shock and wave jump relations

Consider a surface $S(t)$ which divides the region $\mathcal{R}$ into the regions $\mathcal{R}^+$, $\mathcal{R}^-$ and forms a common boundary between them. The unit normal of the surface is directed towards $\mathcal{R}^-$. If $\xi(\cdot, \cdot)$ is any function such that $\xi(\cdot, t)$ is continuous within the regions $\mathcal{R}^+$ and $\mathcal{R}^-$, the symbols, ξ^+, ξ^- denote the limits of $\xi(\mathbf{y})$ as $\mathbf{y}$ approaches a point on S from paths entirely within the regions $\mathcal{R}^+$ and $\mathcal{R}^-$, respectively. The surface $S(t)$ is said to be singular with respect to $\xi(\cdot\ t)$ at time t if

$$\xi^-(t) - \xi^+(t) \neq 0 .$$

Henceforth we shall be concerned with two classes of singular surfaces, namely shock and wave fronts. In view of the continuity property of hidden variables outlined above, shock fronts are characterised as follows.

A singular surface $S(t)$ is said to be a shock front if (S1) the hidden variables α_c, α_v are continuous everywhere, (S2) the functions $\mathbf{V}, \theta, \varrho, \mathbf{H}, \dot{\alpha}_c, \dot{\alpha}_v, \nabla\alpha_c, \nabla\alpha_v$ and their derivatives of any order suffer jump discontinuities across $S(t)$ but are continuous functions everywhere else.

Denote by U the local speed of propagation [12] of the shock front and by $[\xi] = \xi^- - \xi^+$ the jump of any quantity ξ across the shock. Of course $[\mathbf{V} \cdot \mathbf{n}] \neq 0$ implies that also $[U] = -[\mathbf{V} \cdot \mathbf{n}]$ does not vanish. To determine the relations between the shock discontinuities it is convenient to introduce the ordered arrays

$$\varepsilon = (1, \mathbf{V}, e + V^2/2 + \mu H^2/2\varrho, \mathbf{H}/\varrho),$$

$$\varphi = (0, \mathbf{T} + \tau(\mathbf{T} + \tau)\mathbf{V} - \mathbf{q},\ \mathbf{V} \oplus \mathbf{H}),$$
$$\omega = (0, \mathbf{b}, \mathbf{b} \cdot \mathbf{V} + r,\ 0),$$

which allow the integral counterpart of (2.3) to be written as

$$\frac{d}{dt}\int_{\mathcal{V}} \varrho\varepsilon d\mathcal{V} = \int_{\partial\mathcal{V}} \boldsymbol{\varphi} \cdot \boldsymbol{\nu} dA + \int_{\mathcal{V}} \varrho\omega d\mathcal{V} \tag{3.1}$$

$\mathcal{V} \subset \mathcal{R}$ being an arbitrary simply-connected region in the present configuration of the fluid and $\boldsymbol{\nu}$ the unit outward normal to the boundary ∂v of v. If ω is bounded we can apply Kotchine's theorem to the balance equations (3.1). So, accounting also for the condition

$$\int_{\partial\mathcal{V}} \mathbf{H} \cdot \boldsymbol{\nu} dA = 0$$

and being $[\mathbf{q}] = \mathbf{0}$ because of $(2.14)_2$, the shock jump relations can be given the form

$$\begin{gathered} [\varrho U] = 0\,, \\ [\varrho U \mathbf{V}] + [\mathbf{T} + \boldsymbol{\tau}]\mathbf{n} = \mathbf{0}\,, \\ [\varrho U(e + V^2/2 + \mu H^2/2\varrho)] + [(\mathbf{T} + \boldsymbol{\tau})\mathbf{V}] \cdot \mathbf{n} = 0\,, \\ [U\mathbf{h}] + H_n[\mathbf{v}] = \mathbf{0}\,, \end{gathered} \tag{3.2}$$

where $\mathbf{h}$ and $\mathbf{v}$ are the parts of $\mathbf{H}$ and $\mathbf{V}$ orthogonal to $\mathbf{n}$ while the subscript n denotes the normal component. In writing $(3.2)_4$ we have omitted the correspondent normal component because it is an identity.

The Eqs. (3.2) should be contrasted with the analogous relations of MFD[2]. Observe first that, because of $(2.14)_1$, we have $[\mathbf{T}] = -[p]\mathbf{I}$. Also, letting

$$\Lambda = \frac{\varkappa\tau_c}{2\theta}\boldsymbol{\alpha}_c \cdot \boldsymbol{\alpha}_c + \chi\tau_v \boldsymbol{\alpha}_v : \boldsymbol{\alpha}_v + \frac{1}{2}\lambda\tau_v(\mathbf{I} : \boldsymbol{\alpha}_v)^2\,,$$

we can write $p = \varrho^2\psi_\varrho - \Lambda$ and then

$$[p] = [\varrho^2\psi_\varrho(\theta, \varrho)]\,.$$

This result shows that the shock relation $(2.2)_2$ is left unchanged by the introduction of the hidden variables. On the contrary, a new contribution arises in $(3.2)_3$ and it is due both to $\boldsymbol{\alpha}_c$ and to $\boldsymbol{\alpha}_v$; precisely we have the additional term

$$[\mathbf{TV}] \cdot \mathbf{n} + [\varrho^2\psi_\varrho V_n] = \Lambda[V_n] + 2\chi(\boldsymbol{\alpha}_v\mathbf{n}) \cdot [\mathbf{V}] + \lambda\mathbf{I} : \boldsymbol{\alpha}_v[V_n]\,. \tag{3.3}$$

[2] See, e.g. [2] § 1.3.3.

Look now at the wave jump relations. Owing to the prolongation by continuity of hidden variables across singular surfaces we can write the following definition.

A singular surface $S(t)$ is said to be a wave front if (W1) the functions $\mathbf{V}, \theta, \varrho, \mathbf{H}, \alpha_c, \alpha_v$ *are continuous everywhere, (W2) the derivatives* $\dot{\mathbf{V}}, \nabla\mathbf{V}, \dot{\theta}, \nabla\theta, \dot{\varrho}, \nabla\varrho, \dot{\mathbf{H}}, \nabla\mathbf{H}, \dot{\alpha}_c, \nabla\alpha_c, \dot{\alpha}_c, \nabla\alpha_v$ *and the derivatives of higher order suffer jump discontinuities across* $S(t)$ *but are continuous functions everywhere else.*

Denote by U also the local speed of propagation of the wave front and by $[\xi] = \xi^- - \xi^+$ the jump of any quantity ξ across the wave. If $[\xi] = 0$ Maxwell's theorem gives

$$[\nabla \xi] = [\nabla_n \xi]\,\mathbf{n} \tag{3.4}$$

while the kinematic compatibility condition yields

$$[\dot{\xi}] = -U\,[\nabla_n \xi]\,. \tag{3.5}$$

It is a consequence of (3.4) and (2.4) that

$$[\nabla_n H_n] = 0\,. \tag{3.6}$$

On assuming that the external contributions $\mathbf{b}, r$ are continuous, namely $[\mathbf{b}] = \mathbf{0}$ and $[r] = 0$, a straightforward application to (2.3) of (3.4) and (3.5) provides

$$\begin{aligned} -U[\nabla_n \varrho] + \varrho[\nabla_n V_n] &= 0\,, \\ -\varrho U[\nabla_n \mathbf{V}] + U^{-1}[\dot{\mathbf{T}} + \dot{\boldsymbol{\tau}}]\mathbf{n} &= 0\,, \\ -\varrho U[\nabla_n e] - (\mathbf{T}\mathbf{n})\cdot[\nabla_n \mathbf{V}] - U^{-1}[\dot{\mathbf{q}}]\cdot\mathbf{n} &= 0\,, \\ U[\nabla_n \mathbf{h}] + H_n[\nabla_n \mathbf{v}] - \mathbf{h}\,[\nabla_n V_n] &= \mathbf{0}\,, \end{aligned} \tag{3.7}$$

where, as usual, we have omitted the counterpart of the normal component of $(2.4)_4$ because it is an identity. To get a more explicit form of (3.7) note first that in view of (2.7), (2.14) it follows

$$\begin{aligned} [\mathbf{T}]\mathbf{n} = (Up_\theta + \varkappa\alpha_c\cdot\mathbf{n}/\theta)[\nabla_n\theta]\,\mathbf{n} + Up_\varrho\,[\nabla_n\varrho]\,\mathbf{n} + (\chi/\tau_v)\,[\nabla_n\mathbf{V}] + \\ + \big((\chi+\lambda)/\tau_v\big)\,[\nabla_n V_n]\,\mathbf{n} + 2\chi\,\{(\boldsymbol{\alpha}_v\mathbf{n})\cdot[\nabla_n\mathbf{V}]\}\,\mathbf{n} + \lambda\mathbf{I}:\boldsymbol{\alpha}_v[\nabla_n V_n]\,\mathbf{n}, \\ [\dot{\mathbf{q}}]\cdot\mathbf{n} = -(\varkappa/\tau_c)[\nabla_n\theta]\,. \end{aligned}$$

Moreover, on considering the definition (2.2) and accounting for (3.6) we find that

$$[\dot{\boldsymbol{\tau}}]\,\mathbf{n} = \mu U\,\{(\mathbf{h}\cdot[\nabla_n\mathbf{h}])\,\mathbf{n} - H_n[\nabla_n\mathbf{h}]\}\,.$$

Finally, a straightforward calculation yields

$$[\nabla_n e] = a_1[\nabla_n \theta] + a_2[\nabla_n \varrho] - (2\chi/\varrho U)(\boldsymbol{\alpha}_v \mathbf{n}) \cdot [\nabla_n \mathbf{V}] - (\lambda/\varrho U)\mathbf{I} : \boldsymbol{\alpha}_v [\nabla_n V_n],$$

where

$$a_1 = -\theta\psi_{\theta\theta} - (\varkappa\tau_c/\varrho\theta^2)\,\boldsymbol{\alpha}_c \cdot \boldsymbol{\alpha}_c - (2\varkappa/\varrho\theta U)\,\boldsymbol{\alpha}_c \cdot \mathbf{n},$$

$$a_2 = \psi_\varrho - \theta\psi_{\theta\varrho} - \Lambda/\varrho^2 .$$

Substitution of these results into (3.7) delivers

$$-U[\nabla_n \varrho] + \varrho\,[\nabla_n V_n] = 0\,,$$

$$\left(\frac{\chi}{U\tau_c} - \varrho U\right)[\nabla_n \mathbf{V}] + \left(p_\theta + \frac{\varkappa}{\theta U}\boldsymbol{\alpha}_c \cdot \mathbf{n}\right)[\nabla_n \theta]\,\mathbf{n} + p_\varrho[\nabla_n \varrho]\,\mathbf{n} + \frac{\chi+\lambda}{\tau_v}[\nabla_n V_n]\,\mathbf{n} +$$

$$+ U^{-1}\{2\chi(\boldsymbol{\alpha}_v \mathbf{n}) \cdot [\nabla_n \mathbf{V}] + \lambda\mathbf{I} : \boldsymbol{\alpha}_v[\nabla_n V_n]\}\,\mathbf{n} + \mu\{(\mathbf{h} \cdot [\nabla_n \mathbf{h}])\,\mathbf{n} - H_n[\nabla_n \mathbf{h}]\} = 0, \tag{3.8}$$

$$-\varrho U\left(a_1 - \frac{\varkappa}{\varrho U^2 \tau_c}\right)[\nabla_n \theta] - \varrho U a_2\,[\nabla_n \varrho] + p\,[\nabla_n V_n] = 0,$$

$$U\,[\nabla_n \mathbf{h}] + H_n\,[\nabla_n \mathbf{v}] - \mathbf{v}\,[\nabla_n V_n] = 0\,.$$

The systems of equations (3.2), (3.8) constitute the sought relations between the discontinuities at shock and wave fronts, respectively. For the sake of simplicity such relations are now investigated by supposing that the region ahead of the front has been at equilibrium until the arrival of the front, that is to say

$$\nabla\theta = (\nabla\theta)^+ = 0, \quad \mathbf{D} = \mathbf{D}^+ = 0,$$

in the region ahead. Then, according to (2.7)′, the hidden variables $\boldsymbol{\alpha}_c$, $\boldsymbol{\alpha}_v$ are identically zero until the arrival of the front. In this instance Eqs. (3.2) become just the standard shock relations for inviscid non-heat-conducting fluids[3]. That is why the next Section deals with the analysis of waves only.

4. Waves entering a region at equilibrium

The system (3.8) is a set of seven linear homogeneous equations in the seven unknowns $[\nabla_n \varrho]$, $[\nabla_n \mathbf{V}]$ (three), $[\nabla_n \theta]$, $[\nabla_n \mathbf{h}]$ (two), with the coefficients depending also on the hidden variables. If the region ahead of the wave

[3] Indeed, if $\boldsymbol{\alpha}_c = \mathbf{0}$ and $\boldsymbol{\alpha}_v = \mathbf{0}$ then the right hand side of (3.3) vanishes.

front has been at equilibrium until the arrival of the front, and hence $\alpha_c = 0$, $\alpha_v = 0$, then the system (3.8) simplifies to

$$
\begin{aligned}
&U[\nabla_n \varrho] - \varrho[\nabla_n V_n] = 0\,,\\
&p_\varrho[\nabla_n \varrho]\mathbf{n} + \left(\frac{\chi}{U\tau_v} - \varrho U\right)[\nabla_n \mathbf{V}] + \frac{\chi+\lambda}{U\tau_v}[\nabla_n V_n]\mathbf{n} +\\
&+ p_\theta[\nabla_n \theta]\mathbf{n} + \mu\{(\mathbf{h}\cdot[\nabla_n \mathbf{h}])\mathbf{n} - H_n[\nabla_n \mathbf{h}]\} = 0,\\
&U\eta_\varrho[\nabla_n \varrho] + U\left(\eta_\theta - \frac{\varkappa}{\varrho\theta U^2 \tau_c}\right)[\nabla_n \theta] = 0,\\
&-\mathbf{h}[\nabla_n V_n] + H_n[\nabla_n \mathbf{v}] + U[\nabla_n \mathbf{h}] = 0\,,
\end{aligned}
\tag{4.1}
$$

where the coefficients depend only on θ and ϱ. We are now in a position to establish whether, and how, waves can exist in the fluid to hand.

4.1 *Propagation condition*

The existence of waves is associated with the existence of non-trivial solutions of (4.1). To examine the possibility of non-trivial solutions it may be convenient to represent the vectors $[\nabla_n \mathbf{V}]$, $[\nabla_n \mathbf{h}]$ via their components with respect to a suitable basis; for instance $(n, \mathbf{h}/h, \mathbf{n}\wedge\mathbf{h}/h)$. So (4.1) acquires the form

$$\mathbf{M}\,\mathbf{z} = \mathbf{0},$$

where z is the ordered array consisting of the seven (scalar) unknown discontinuities while $\mathbf{M}$ is the 7×7 matrix to be derived from (4.1) Accordingly, non-trivial solutions of (4.1) are possible only if the equation

$$\det \mathbf{M} = 0 \tag{4.2}$$

holds. Letting

$$A = \varrho U^2 - \left(\frac{\chi}{\tau_v} + \mu H_n^2\right),$$

a tedious calculation shows that (4.2) can be given the form

$$U^{-1}A\{(c_1 U^2 - c_2 c_3)A - (U^2 - c_3)(A + \mu H_n^2)(A - \mu h^2)]\} = 0\,, \tag{4.3}$$

where

$$c_1 = \varrho\hat{p}_\varrho + (\chi + \lambda)/\tau_v,\quad c_2 = \varrho p_\varrho + (\chi + \lambda)/\tau_v,\quad c_3 = \varkappa/\varrho\theta\eta_\theta\tau_c\,,$$

and $\hat{p}_\varrho = p_\varrho - p_\theta\, \eta_\varrho/\eta_\theta$ is the derivative of p with respect to ϱ at constant entropy. It follows immediately from (4.3) that the solution $U = 0$, occurring in standard MFD, is allowed provided heat conduction is absent $-c_3 = 0$ if $\varkappa = 0$. Otherwise, only the values of U satisfying

$$A = 0 \tag{4.4}$$

or

$$(c_1 U^2 - c_2 c_3) A - (U^2 - c_3)(A + \mu H_n^2)(A - \mu h^2) = 0 \tag{4.5}$$

can be local speeds of propagation of waves.

The solution of (4.4), that is

$$U_A = \pm \left\{ \frac{1}{\varrho} \left(\frac{\chi}{\tau_v} + \mu H_n^2 \right) \right\}^{1/2}$$

accounts for waves with a speed which reduces to the usual Alfvén speed if the fluid is inviscid ($\chi = 0$) and to the speed of transverse waves in fluids [6] if $H_n = 0$. Moreover the speed of such waves turns out to be greater than the usual Alfvén speed because the coefficient of viscosity χ is strictly positive.

Besides being hardly suggestive, a detailed analysis of the solutions of (4.5) is rather cumbersome. In view of this confine our attention to situations making (4.5) into a simpler equation. First, suppose that the properties of the fluid allows us to disregard the effects of heat conduction against those of viscosity. Then, letting $\varkappa = 0$, (4.5) yields

$$2\varrho U^2 = \frac{2\chi}{\tau_v} + c_1 + \mu (h^2 + H_n^2) \pm \{(c_1 + \mu(h^2 - H_n^2))^2 + 4\mu^2 H_n^2 h^2\}^{1/2}, \tag{4.6}$$

whereby we have always two real roots, U_-, U_+ as it happens in MFD. Second, consider the opposite case ($\chi = 0$, $\lambda = 0$, $\varkappa \neq 0$) and, furthermore, suppose that $H_n = 0$. In this instance (4.5) provides

$$2\varrho U^2 = c_1 + \varrho c_3 + \mu h^2 \pm \{(c_1 + \varrho c_3 + \mu h^2)^2 - 4\varrho c_3 (c_2 + \mu h^2)\}^{1/2}. \tag{4.7}$$

Assume, as usual, that $p_\varrho > 0$, $\eta_\theta > 0$. So, owing to the Maxwell relation $p_\theta = -\varrho^2 \eta_\varrho$, we can write $\hat{p}_\varrho > p_\varrho > 0$ and hence $c_1 > c_2 > 0$. In such a case it is a simple matter to prove that $(c_1 + \varrho c_3 + \mu h^2)^2 - 4\varrho c_3 (c_2 + \mu h^2) > (c_1 - \varrho c_3 + \mu h^2)^2$ thereby showing that two real roots U_-, U_+ do exist. Of course, if we suppose that $\varkappa = 0$ then Eq. (4.7) gives the result $U_- = 0$.

To conclude the present analysis look at the propagation modes, expressed by suitable ordered arrays, z, corresponding to the wave speeds examined above.

4.2 *Propagation modes*

Bearing in mind the propagation modes of standard MFD, begin by considering waves with speed $U = 0$, that is to say waves carried along with the fluid. Such waves can exist only if $\varkappa = 0$; in this instance a glance to (4.1) allows us to infer that $[\nabla_n \mathbf{V}] = \mathbf{0}$. To evaluate the discontinuities $[\nabla_n \varrho]$, $[\nabla_n \theta]$, and $[\nabla_n \mathbf{h}]$ we substitute $(4.1)_1$ and $(4.1)_4$ into $(4.1)_2$ as though we had $U \neq 0$. Then, on taking the limit of $(4.1)_2$ as $U \to 0$ we find

$$[\nabla_n \mathbf{h}] = \frac{\chi}{\varrho(\chi + \mu H_n^2 \tau_v)} \mathbf{h} [\nabla_n \varrho],$$

$$[\nabla_n \theta] = -\frac{1}{p_\theta} \left(p_\varrho + \frac{2\chi + \lambda}{\varrho \tau_v} + \frac{\mu \chi h^2}{\varrho(\chi + \mu H_n^2 \tau_v)} \right) [\nabla_n \varrho] .$$

Of course, if $\chi = 0$, $\lambda = 0$ we achieve the usual entropy waves characterised by

$$[\nabla_n \mathbf{V}] = 0 , \quad [\nabla_n \theta] = -(p_\varrho / p_\theta)[\nabla_n \varrho] , \quad [\nabla_n \mathbf{h}] = 0 .$$

Examine now the propagation mode z_A correspondig to the speed $U = U_A$. A comparison between the transverse part of $(4.1)_2$ and $(4.1)_4$ leads to $[\nabla_n V_n] = 0$. Therefore Eqs. $(4.1)_{1,3}$ imply that $[\nabla_n \varrho] = 0$, $[\nabla_n \theta] = 0$, and then the normal component of $(4.1)_2$ delivers $\mathbf{h} \cdot [\nabla_n \mathbf{h}] = 0$. Hence it follows that $[\nabla_n \mathbf{h}] = \mathscr{A} \mathbf{n} \wedge \mathbf{h} / h$. To sum up, the propagation mode z_A with respect to the basis $(\mathbf{n}, \mathbf{h}/h, \mathbf{n} \wedge \mathbf{h}/h)$ is

$$z_A = \mathscr{A}(0, \ 0, \ 0, \ -U_A / H_n, \ 0, \ 0, \ 1) ,$$

whereby the peculiar properties of Alfvén waves described in MFD hold in the present theory as well. In view of this the term Alfvén wave for z_A appears to be quite legitimate.

The propagation modes associated with the speeds arising from (4.5) are generalisations of the customary magnetoacoustic waves. The only significant difference is that the non-vanishing discontinuities $[\nabla_n \varrho]$ and $[\nabla_n \theta]$ are related in such a way that the normal derivative of the entropy suffers a jump discontinuity across the front. Indeed, Eq. (4.1) yields

$$[\nabla_n \theta] = -\frac{\varrho \theta \tau_c U^2 \eta_\varrho}{\varrho \theta \tau_c U^2 \eta_\theta - \varkappa} [\nabla_n \varrho]$$

which reduces to $[\nabla_n \eta] = 0$ if $\varkappa = 0$. Looking now at Eqs. $(4.1)_{1,2,4}$ we find that

$$[\nabla_n V_n] = \frac{U}{\varrho} [\nabla_n \varrho] ,$$

$$[\nabla_n \mathbf{v}] = -\frac{\mu H_n U}{\varrho A}\mathbf{h}\,[\nabla_n \varrho],$$

$$[\nabla_n \mathbf{h}] = \frac{\varrho\tau_v U^2 - \chi}{\varrho\tau_v A}\mathbf{h}\,[\nabla_n \varrho].$$

The results so obtained are summarised by writing the corresponding array z_M as

$$z_M = [\nabla_n \varrho]\left(1, \frac{U}{\varrho}, -\frac{\mu H_n U}{\varrho A}h, 0, -\frac{\varrho\theta\tau_c U^2 \eta_\varrho}{\varrho\theta\tau_c U^2\ \eta_\theta - \varkappa}, \frac{\varrho\tau_v U^2 - \chi}{\varrho\tau_v A}h, 0\right).$$

5. Comments

The results gathered in this paper show how the hidden variable model of thermo-viscous MFD appears to be acceptable also in connection with wave propagation topics. Now, the availability of appropriate experimental results would allow us to check more rigorously the physical relevance of the model and, meanwhile, to determine the values of the phenomenological parameters τ_v, τ_c. For example, τ_v could be determined through a measure of the Alfvén speed U_A.

Besides the experimental aspect related to the present theory, I wish to emphasise the worthiness of a realistic generalisation of the hidden variable model both in fluiddynamics and in MFD. In this connection it is well known that the attempt to get more realistic astrophysical models has given rise to an increasing interest in topics concerning viscosity in General Relativity. For instance, MATZNER and MISNER [13, 14] developed an account of dissipative processes in anisotropic homogeneous cosmologies via neutrino viscosity. Also, radiative viscosity plays a central role in WEINBERG's investigation on the formation of galaxies in the early universe [15]. Further researches on viscosity effects in isotropic world models have been carried out by BELINSKII and KHALATNIKOV [16]. To all this we must add the unpleasant feature of the usual description of viscosity whereby it is unavoidably associated with conceptual difficulties in the Cauchy problem and rules out the possibility of wave propagation. That is why a relativistic generalisation of the present procedure would by highly desirable. This study is under way.

REFERENCES

1. A. G. KULIKOVSKII and G. A. LYUBIMOV, Sov. Phys. Dok., **4**, 1185, 1959/60.
2. H. CABANNES, Theoretical Magnetofluiddynamics, Academic Press, New York, 1970.
3. L. D. LANDAU and E. M. LIFSHITZ, Fluid Mechanics, Pergamon Press, Oxford, 1959.
4. G. MAUGIN, J. Phys. A, **7**, 465, 1974.

5. E. Massa and A. Morro, Ann. Inst. Henri Poincaré, **29**, 423, 1978.
6. A. Morro, Arch. Mech., **32**, 145, 1980.
7. B. D. Coleman and M. E. Gurtin, J. Chem. Phys., **47**, 597, 1967.
8. W. Kosinski and P. Perzyna, Arch. Mech., **24**, 629, 1972.
9. W. A. Day, Arch. Ratl Mech. Anal., **62**, 367, 1976.
10. F. Bampi and A. Morro, Acta Phys. Polon. B, **10**, 1081, 1979.
11. A. Morro, Arch. Mech., **32**, 193, 1980.
12. M. F. McCarthy, Continuum Physics II (A.C. Eringen ed.), Academic Press, New York, 1975.
13. R. A. Matzner and C. W. Misner, Ap. J. **171**, 415, 1972.
14. R. A. Matzner, Ap. J., **171**, 433, 1972.
15. S. Weinberg, Ap. J., **168**, 175, 1971.
16. V. A. Belinskii and I. M. Khalatnikov, Sov. Phys. JETP, **45**, 1, 1977.

Acta Physica Academiae Scientiarum Hungaricae, Tomus 48 (4), pp. 383—389 (1980)

CYLINDRICALLY SYMMETRIC EMPTY SPACE-TIME SOLUTIONS OF SEN—DUNN THEORY

By

A. R. ROY and B. CHATTERJEE

DEPARTMENT OF MATHEMATICS, INDIAN INSTITUTE OF TECHNOLOGY, KHARAGPUR-721302, INDIA

(Received 26. II. 1980)

A class of exact solutions is obtained for non-static cylindrically symmetric space-time of MARDER corresponding to vacuum field equations of a scalar-tensor theory of gravitation as proposed by SEN and DUNN. We observe that, given any solution of the vacuum field equations of Einstein's theory, it is possible to generate the solution of the corresponding field equations of the SEN—DUNN theory. The presence of the scalar-interaction function x^0 influences one of the parameters (viz. α) of the MARDER's metric. The solutions preserve the wave character as in Einstein's theory.

I. Introduction

In the scalar-tensor theory proposed by SEN and DUNN [1], a theory formally similar to Brans—Dicke theory, the scalar field is characterised by the function $x^0 = x^0(x^i)$, x^i being the co-ordinates in a four-dimensional Lyra manifold and the tensor field is identified with the metric tensor g_{ij} of the manifold. The study of such a theory with a view to examine how the presence of the scalar interaction function x^0, introduced into the theory to make it Machian, alters the mathematical and physical consequences of Einstein's theory, is essential. This would help in comparing the theories and decide between them against the observational values. The present paper is an attempt in this direction wherein the discussion is mostly mathematical with certain physical conclusions.

In their study SEN and DUNN [1] have obtained only a series type solution to the static vacuum field equations. Later HALFORD [2] considered the vacuum field equations corresponding to an isotropic metric and obtained an exact solution. REDDY [3] has established a result that an analogue of Birkhoff's theorem of Einstein theory exists in this new theory of gravitation also, provided that the scalar interaction function x^0 is independent of time.

As a first step towards a comparative study of the two theories (viz; Einstein's theory and SEN—DUNN theory), in this paper we obtain a class of exact solutions of the vacuum field equations of SEN—DUNN theory of gravitation corresponding to the general cylindrically symmetric metric of MARDER [4]. Because of the importance of the MARDER'S metric in the study

of cylindrical gravitational waves in Einstein's theory we consider this metric and observe that the presence of the scalar interaction function x^0 in SEN—DUNN theory still allows the solutions to possess a wave-like character, like in Einstein's theory.

II. Field equations and their solutions

We consider the general cylindrically symmetric metric (MARDER [4])

$$ds^2 = e^{2\alpha-2\beta}(dt^2 - d\varrho^2) - \varrho^2 e^{-2\beta} d\varphi^2 - e^{2\beta+2\nu} dz^2 , \tag{1}$$

where α, β, ν are functions of ϱ and t only and ϱ, φ, z, t correspond respectively to the coordinates x^1, x^2, x^3 and x^4. The field equations of SEN—DUNN theory [1] are given by

$$R_{ij} - \frac{1}{2} R g_{ij} = \frac{8\pi G}{(x^0)^2} T_{ij} + \frac{w}{(x^0)^2}\left[x_i^0 x_j^0 - \frac{1}{2} g_{ij}\, x^{0k} x_k^0\right], \tag{2}$$

where x^0 is the scalar interaction function, $w = 3/2$ and other symbols have their usual meaning as in Einstein theory. For the metric (1) the field equations (2) corresponding to the matter free region ($T_{ij} = 0$) finally take the form

$$-\nu_{44} + \alpha_1\nu_1 + \alpha_4\nu_4 - 2\beta_1\nu_1 - 2\beta_4\nu_4 - \beta_1^2 - \beta_4^2 - \nu_4^2 + \frac{\alpha_1}{\varrho} + \frac{\nu_1}{\varrho} = -\frac{w}{2}(h_1^2 + h_4^2) \tag{3}$$

$$\alpha_{11} - \alpha_{44} + \nu_{11} - \nu_{44} + 2\beta_1\nu_1 - 2\beta_4\nu_4 + \beta_1^2 - \beta_4^2 + \nu_1^2 - \nu_4^2 = \frac{w}{2}(h_1^2 - h_4^2), \tag{4}$$

$$\alpha_{11} - \alpha_{44} + 2\beta_{44} - 2\beta_{11} - 2\frac{\beta_1}{\varrho} + \beta_1^2 - \beta_4^2 = \frac{w}{2}(h_1^2 - h_4^2), \tag{5}$$

$$\nu_{11} - \alpha_1\nu_1 - \alpha_4\nu_4 + 2\beta_4\nu_4 + 2\beta_1\nu_1 + \beta_4^2 - \frac{\alpha_1}{\varrho} + \beta_1^2 + \nu_1^2 + \frac{\nu_1}{\varrho} = \frac{w}{2}(h_1^2 + h_4^2) \tag{6}$$

and

$$\nu_{14} + 2\beta_1\beta_4 - \alpha_1\nu_4 - \alpha_4\nu_1 + 2\beta_1\nu_4 + 2\beta_4\nu_1 - \frac{\alpha_4}{\varrho} + \nu_1\nu_4 = wh_1h_4, \tag{7}$$

where for convenience we have introduced an auxiliary function h defined by

$$x^0 = e^h . \tag{8}$$

Here, the subscripts 1 and 4 after an unknown function represent partial differentiation with respect to ϱ and t, respectively. From (4) and (5), we get the equation

$$\nu_{11} - \nu_{44} - 2\beta_{44} + 2\beta_{11} + 2\beta_1\nu_1 - 2\beta_4\nu_4 + 2\frac{\beta_1}{\varrho} + \nu_1^2 - \nu_4^2 = 0 \tag{9}$$

and (3) and (6) yield

$$\nu_{11} - \nu_{44} + \nu_1^2 - \nu_4^2 + 2\nu_1/\varrho = 0 . \tag{10}$$

Thus for the solution of the unknowns α, β, ν and x^0, we need only to solve the equations (3) ,(4), (7), (9) and (10). Eq. (10) possesses a solution in the form given by

$$\nu = \log(t + c) - \log(a\varrho) , \tag{11}$$

where a and c are arbitrary constants of integration. Using this value of ν (9) can be easily solved for β and we get

$$\beta = \log\varrho + b\varrho - \log(t + c) , \tag{12}$$

where b is an arbitrary constant of integration. With the values of β and ν so obtained, (3) (4) and (7) respectively assume the forms

$$\alpha_4 = -\frac{w}{2}(t + c)(h_1^2 + h_4^2) + b^2(t + c) - 1/(t + c), \tag{13}$$

$$\alpha_{11} - \alpha_{44} = \frac{w}{2}(h_1^2 - h_4^2) - b^2 - \frac{1}{\varrho^2} - \frac{1}{(t+c)^2} \tag{14}$$

and

$$\alpha_1 = -w(t + c)h_1h_4 + 1/\varrho . \tag{15}$$

It can now be easily verified that the condition of integrability of (13) and (15) viz: $\alpha_{41} = \alpha_{14}$ is satisfied only if it satisfies the differential equation

$$h_{44} - h_{11} + h_4/(t + c) = 0 . \tag{16}$$

Eq. (16) possesses a general solution in the form given by

$$h = [AJ_0\{k(t + c)\} + BY_0\{k(t + c)\}]\cos(k\varrho) , \tag{17}$$

where $J_0[k(t+c)]$ and $Y_0[k(t+c)]$ are Bessel's functions of order zero of first and second kind, respectively, and A, B are constants. As the irregular Bessel function $Y_0[k(x+t)]$ is not well-behaved, we exclude the part containing Y_0 by taking $B=0$ and consider the solution of (16) in the form

$$h = AJ_0\{k(t+c)\}\cos(k\varrho). \tag{18}$$

Using the value of h, (13) and (15) assume respectively the forms

$$\alpha_4 = b^2(t+c) - \frac{1}{(t+c)} - \frac{w}{2}(t+c)A^2k^2\left[\sin^2(k\varrho)(J_0\{k(t+c)\})^2 + \right.$$
$$\left. + \cos^2(k\varrho)(J_1\{k(t+c)\})^2\right] \tag{19}$$

and

$$\alpha_1 = \frac{wkA^2(t+c)}{2}J_0\{k(t+c)\}J_0'\{k(t+c)\}\sin 2k\varrho + \frac{1}{\varrho}. \tag{20}$$

Integrating (19) and (20) and using some standard results of Bessel's function we finally get α in the form

$$\alpha = \frac{b^2}{2}(t+c)^2 - \log(t+c) - \log\varrho - \frac{w}{4}A^2k^2(t+c)^2(J_1^2 - J_0J_0'') -$$
$$- \frac{w}{4}A^2k(t+c)J_0J_0'\cos(2k\varrho), \tag{21}$$

where $J_0 = J_0[k(t+c)]$.

The values of h and α given by (18) and (21) can be easily seen to satisfy the Eq. (14). Thus a nonstatic solution of the vacuum field equations is given by the set of equations (11), (12), (18) and (21) viz;

$$\alpha = \frac{b^2}{2}(t+c)^2 - \log(t+c) - \log\varrho - \frac{w}{4}A^2k^2(t+c)^2(J_1^2 - J_0J_0'') -$$
$$- \frac{w}{4}A^2k(t+c)J_0J_0'\cos(2k\varrho),$$

$$\beta = \log\varrho + b\varrho - \log(t+c), \tag{22}$$

$$\nu = \log(t+c) - \log(a\varrho)$$

and

$$x^0 = e^h = e^{AJ_0\{k(t+c)\}\cos(k\varrho)}.$$

III. Some more solutions

(i) When we consider the metric (1) to be static for which the metric parameters α, β and ν are functions of the radial coordinate ϱ only, the corresponding field equations are

$$\alpha_1\nu_1 - 2\beta_1\nu_1 - \beta_1^2 + \frac{\alpha_1}{\varrho} + \frac{\nu_1}{\varrho} = -\frac{w}{2}h_1^2\,, \tag{23}$$

$$\beta_{11} + \beta_1\nu_1 + \frac{\beta_1}{\varrho} - \frac{\nu_1}{\varrho} = 0\,, \tag{24}$$

$$\nu_{11} + \nu_1^2 + \frac{2\nu_1}{\varrho} = 0 \tag{25}$$

and

$$\alpha_{11} + \alpha_1\nu_1 + \frac{\alpha_1}{\varrho} - \frac{\nu_1}{\varrho} = 0\,. \tag{26}$$

The solution of the above field equations can easily be obtained as

$$\begin{aligned} \alpha &= m\log(b - a/\varrho) + (m+1)\log\varrho\,,\\ \beta &= n\log(b - a/\varrho) + (n+1)\log\varrho\,,\\ \nu &= \log(b - a/\varrho) \end{aligned} \tag{27}$$

and

$$x^0 = (b\varrho - a)^{\left\{\frac{2}{w}(n^2+2n-m)\right\}^{1/2}},$$

where a, b, m and n are arbitrary integrating constants.

(ii) When the scalar interaction function x^0 is dependent on time only and the metric parameters α, β, ν are functions of both ϱ and t, the solution of the corresponding field equations is given by

$$\begin{aligned} \alpha &= \log\varrho + \frac{b^2}{2}(t+c)^2 - \log(t+c)\left[\frac{wA^2}{2} + 1\right],\\ \beta &= \log\varrho + b\varrho - \log(t+c)\,,\\ \nu &= \log(t+c) - \log a\varrho \end{aligned} \tag{28}$$

and

$$h = A\log(t+c) + B\,,$$

where A, B and C are constants.

(iii) *Special case*: When we take $\alpha = -\nu$ the solution assumes the form

$$\begin{aligned} \alpha &= \log(a\varrho) - \log(t+c),\\ \beta &= \log\varrho + b\varrho - \log(t+c)\,,\\ \nu &= \log(t+c) - \log(a\varrho) \end{aligned} \tag{29}$$

and

$$x^0 = e^{\sqrt{2/w}\, b\varrho}.$$

When the scalar interaction function x^0 is assumed to be constant it is interesting to note that the general solution (22) obtained earlier satisfies the vacuum field equations for the metric (1) corresponding to the Einstein's theory. In fact, it has been observed that knowing a solution $(\alpha^0, \beta^0, \nu^0)$ of the vacuum field equations of the Einstein's theory for the metric (1), we can always construct a solution $(\alpha, \beta, \nu, x^0)$ of the corresponding field equations of SEN—DUNN theory as given by

$$\begin{aligned} \alpha &= \alpha^0 - \frac{w}{2}\int (t+c)\,(h_1^2 + h_4^2)\,dt - w\int (t+c)\,h_1 h_4\, d\varrho\,, \\ \beta &= \beta^0\,, \\ \nu &= \nu^0\,, \end{aligned} \tag{30}$$

where h is given by the solution of the equation $h_{44} - h_{11} + h_{4(t+c)} = 0$, which can always be obtained by a straightforward calculation.

It can be easily verified that the solutions obtained above do not reduce all the components of the Riemann curvature tensor R_{hijk} to zero. This implies that the cylindrical waves given by (1) in the SEN—DUNN theory produce real curvature in space. For the solution (22) the scalar field x^0 can be easily seen to be regular at the source.

IV. Discussion

(a) *Contribution of the scalar field towards the C-energy*

THORNE [5] has defined 'Cylindrical energy' (C-energy) for systems that remain invariant under rotation about and translation along a symmetry axis and under reflection in any plane containing the symmetry axis or perpendicular to it. The C-energy of such systems is defined by him in terms of a contravariant flux-vector P_l^i which satisfies the conservation law $P_{l\,;i}^{i} = 0$.

Within the framework of the general theory of relativity, in the region outside any material source the relation determining this C-energy (Eq. (9), [5]), for the metric (1) assumes the form

$$4\pi G E(\varrho, t) = \alpha - \frac{1}{2}\log\left[1 + \varrho^2 \nu'^2 + 2\varrho\nu' - \dot{\nu}^2\right], \tag{31}$$

where $E\,(\varrho, t)$ is expressed in terms on the generators of the system (Eq. (14) [5]) and it acts as a potential function from which the C-energy flux vector is calculated.

Using the same formula (31) for the vacuum space time of SEN—DUNN theory, we find for the solution (22), that E consists of a negative term which depends entirely on the scalar interaction function x^0. Thus, we may say that the scalar field of SEN—DUNN theory contributes negatively to the C-energy defined by THORNE [5]. This result is in agreement with the findings of HALFORD [6] that the scalar field of SEN—DUNN theory can be identified as Hoyle's creation field with negative energy. It may be mentioned in this connection that SINGH [7] has observed similar behaviour of the scalar field for his solution of vacuum space time equation of a cylindrically symmetric metric with two degrees of freedom.

(b) *Motion of a test particle*

The motion of a test particle in SEN—DUNN theory is governed by the equation

$$x^0 \ddot{x}^\mu + x^0 \begin{Bmatrix} \mu \\ \alpha\beta \end{Bmatrix} \dot{x}^\alpha \dot{x}^\beta + \frac{1}{2} x^0_{,\alpha} \dot{x}^\mu \dot{x}^\alpha + \frac{1}{2} g_{\alpha\beta} g^{\mu\nu} x^0_{,\nu} \dot{x}^\alpha \dot{x}^\beta = 0 . \tag{32}$$

Taking the initial motion to be radial only, from the equation (32) it can be easily seen that free particles will move according to the equation

$$x = f(t), \; y = \text{const. and } z = \text{const.},$$

where $f(t)$ is some function of t only.

Acknowledgement

The authors are thankful to Professor J. R. RAO for his interest and constant encouragement in their work.

REFERENCES

1. D. K. SEN and K. A. DUNN, J. Math. Phys. **12,** 578, 1971.
2. W. D. HALFORD, J. Math. Phys., **13,** 1699, 1972.
3. D. R. K. REDDY, J. Phys. A. Maths. Gen., **10,** 3, 1977.
4. L. MARDER, Proc. R. Soc. (London), **A244,** 524, 1958.
5. K. S. THORNE, Phys. Rev., **138,** B 251, 1965.
6. W. D. HALFORD, Aust. J. Phys., **23,** 863, 1970.
7. T. SINGH, Proc. Indian. Acad. Sci., **85** A, 2, 90, 1977.

Acta Physica Academiae Scientiarum Hungaricae, Tomus 48 (4), pp. 391—395 (1980)

THE GROUND STATES OF THE NUCLEIDE ^{44}Ti*

By

FRANKLIN R. RUEHL, Jr.

UNIVERSITY OF CALIFORNIA, LOS ANGELES, CALIFORNIA, USA

(Received 12. III. 1980]

Ground state binding energies and equilibrium harmonic oscillator energies are computed for the various ground state configurations of the doubly even nucleide ^{44}Ti. Employed for the study is a variational calculation carried out in a Cartesian harmonic oscillator basis of states employing a tripartite interaction potential composed of Wigner central forces coupled to Majorana exchange forces each having Gaussian radial dependence.

A determination is made of which of three possible shapes, spherically symmetric, prolate spheroidal, or asymmetric, represents the preferred ground state configuration of the nucleide.

1. Introduction

While numerous calculations of the ground state binding energies of the doubly even, closed-shell nucleides ^{40}Ca and ^{90}Zr have been carried out [1—5], such studies of the doubly even nucleide ^{44}Ti are not well represented in the literature.

Actually, the nucleide ^{44}Ti merits special attention because it is a naturally occurring isotope with a half-life of over 20 years in contrast to a nucleide such as ^{90}Zr which is purely a theoretical construct, not found in nature. As ^{44}Ti is the first nucleide to occupy the 2p—1f shell (another facet making it an interesting target of study), detailed calculations are required to determine its optimum ground state shape and corresponding binding and harmonic oscillator energies.

The specific interaction chosen for the present analysis consists of a trio of Majorana exchange forces plus Wigner central forces having Gaussian radial dependence. This is utilized in a series of simple restricted Hartree—Fock calculations. As no account is taken of the Coulomb repulsive energy, the resulting energies actually represent the binding energies (B.E.) minus the Coulomb repulsion.

Such calculations have enjoyed a reasonable degree of success [6, 7] when harmonic oscillator wave function bases have been coupled to the Gaussian interactions. Accordingly, the oscillator basis of states is employed herein. And, the corresponding equilibrium harmonic oscillator energy $\hbar\omega$ is determined

* Work supported in part by the National Science Foundation

through a minimization of the total internal energy where, of course, the kinetic energy of the centre of mass is deducted.

The nucleon configurations under analysis are discussed in Section 2. In Section 3, the interaction potential is briefly reviewed. The relevant energy equations are treated in Section 4, with specific results presented in Section 5. Finally, a summary is presented in Section 6.

2. The nucleon configurations

In a rectangular oscillator basis of states, the nucleon configuration of the nucleide ^{44}Ti can be viewed as the addition of a four-particle level $(n_x, n_y, n_z)^4$ to a completely filled ^{40}Ca core, with three degenerate levels equally possible for occupation : the level $(111)^4$, which gives rise to a spherically symmetric shape; the level $(300)^4$, which engenders a prolate spheroidal configuration; and the level $(210)^4$, which promotes a triaxial or asymmetric form.

Table I

Nucleon configurations for the 3 shapes of the nucleide ^{44}Ti

Configuration designation	Configuration
TI(S)	$(000)^4\ (100)^4\ (010)^4\ (001)^4\ (200)^4\ (020)^4\ (002)^4\ (110)^4\ (101)^4\ (011)^4\ (111)^4$
TI(P)	$(000)^4\ (100)^4\ (010)^4\ (001)^4\ (200)^4\ (020)^4\ (002)^4\ (110)^4\ (101)^4\ (011)^4\ (300)^4$
TI(A)	$(000)^4\ (100)^4\ (010)^4\ (001)^4\ (200)^4\ (020)^4\ (002)^4\ (110)^4\ (101)^4\ (011)^4\ (210)^4$

In Table I, the nucleon configurations are presented, with the designations TI(S), TI(P), and TI(A) signifying the symmetric, prolate, and asymmetric shapes, respectively.

3. The interaction

The nucleon—nucleon interaction potential employed is a tripartite one featuring short-, medium-, and long-range components consisting of a Wigner central force coupled to a Majorana exchange force, with each having Gaussian radial dependence, generated by the formula

$$V(\mathbf{r}) = \sum_{i=1}^{3} S_i \left[1 - M_i + M_i P_M\right] e^{r^2/\mu_i^2} \tag{1}$$

Here, $\mathbf{r} = \mathbf{r}_2 - \mathbf{r}_1$ is a relative radial coordinate, the parameters S are indices of strength, the parameters μ are range indicators, the quantities M are Majorana exchange coefficients, and P_M is the Majorana exchange operator.

The specific parameter set utilized in this study, designated in previous papers [7—9] as SB_6 and evolved from initial conditions on the B.E. and $\hbar\omega_{eq}$ of the nucleide ^{4}He and the B.E./A and the equilibrium Fermi momentum k_F, is defined by the following values: $\mu_1 = 0.5$ fm, $S_1 = 1630.0$ MeV, $M_1 = -5.27$, $\mu_2 = 1.0$ fm, $S_2 = -392.3$ MeV, $M_2 = -0.787$, $\mu_3 = 2.0$ fm, $S_3 = -1.8$ MeV and $M_3 = 6.273$.

4. The energy equations

Table II lists the equations for the ground state binding energies of the trio of configurations for the nucleide ^{44}Ti under investigation. Note that the

Table II

Equations for the ground state binding energies of the 3 nucleon configurations of ^{44}Ti in terms of the harmonic oscillator energies and potential energy matrix elements $V(n_x, n_y, n_z)$ as functions of relative quantum numbers for use in HF calculations

Configuration	Equation
TI(S)	$E = 68.25\,\hbar\omega + 153.375\,V(000) + 343.125\,V(100) + 95.635\,V(200) + 88.125\,V(110) + 108.75\,V(210) + 19.375\,V(111) + 50.625\,V(300) + 6.75\,V(400) + 27.0\,V(310) + 13.5\,V(220) + 16.875\,V(211) + 5.625\,V(311) + 7.5\,V(221) + 0.75\,V(222)$
TI(P)	$E = 26.75\,\hbar\omega_x + 41.5\,\hbar\omega_y + 154.5\,V(000) + 130.0\,V(100) + 211.25\,V(010) + 41.25\,V(200) + 53.25\,V(020) + 61.75\,V(110) + 26.0\,V(110) + 48.75\,V(210) + 33.75\,V(120) + 30.0\,V(012) + 15.0\,V(111) + 26.875\,V(300) + 30.0\,V(030) + 9.0\,V(400) + 4.5\,V(040) + 9.0\,V(310) + 4.5\,V(120) + 4.5\,V(013) + 6.75\,V(220) + 2.25\,V(022) + 4.5\,V(211) + 4.5\,V(121) + 6.25\,V(500) + 1.25\,V(320) + 5.0\,V(410) + 0.625\,V(311) + 1.875\,V(600)$
TI(A)	$E = 24.75\,\hbar\omega_x + 22.75\,\hbar\omega_y + 20.75\,\hbar\omega_z + 153.75\,V(000) + 123.125\,V(100) + 114.375\,V(010) + 105.0\,V(001) + 36.375\,V(200) + 32.25\,V(020) + 26.265\,V(002) + 32.375\,V(110) + 30.125\,V(101) + 27.875\,V(011) + 24.375\,V(210) + 19.375\,V(201) + 25.0\,V(120) + 16.25\,V(102) + 16.25\,V(021) + 15.625\,V(012) + 20.725\,V(111) + 24.375\,V(300) + 16.875\,V(030) + 15.0\,V(003) + 5.625\,V(400) + 2.25\,V(040) + 2.25\,V(004) + 5625\,V(310) + 3.375\,V(301) + 4.5\,V(130) + 2.25\,V(103) + 2.25\,V(013) + 2.25\,V(031) + 6.375\,V(220) + 2.625\,V(202) + 2.25\,V(022) + 4.15\,V(211) + 3.75\,V(121) + 3.0\,V(112) + 3.75\,V(410) + 3.75\,V(320) + 1.875\,V(230) + 3.75\,V(311) + 0.625\,V(221) + 0.25\,V(212) + 1.125\,V(420)$

axial and triaxial shapes may be treated as spherically symmetric by employing a single harmonic oscillator (with $\hbar\omega_x = \hbar\omega_y = \hbar\omega_z$), thereby allowing a check on the gain in B.E. in shifting from the spherical to the axial ($\hbar\omega_x \neq \hbar\omega_y \neq \hbar\omega_z$) and the triaxial ($\hbar\omega_x \neq \hbar\omega_y \neq \hbar\omega_z$) variations.

5. The results

Table III presents the binding energy and oscillator energy results for the shapes of the nucleide ^{44}Ti. With only a single oscillator varied, the symmetric state TI(S) appears to be most stable, with an average advantage of 10 MeV over the prolate state TI(P) and 12 MeV over the asymmetric state TI(A).

While the B.E. figures are in excellent agreement with experiment, the $\hbar\omega_{eq}$ values are higher by approximately 4 MeV. These results are to be expected, as the parameter set SB_6 was originally derived in part based on its accurate prediction of the ground state of the nucleide ^{40}Ca [7]. However, its forecasts of $\hbar\omega_{eq}$ values were characteristically higher than experiment.

Table III

Energy results for the three nucleon configurations of ^{44}Ti for spherically symmetric (S), axial or prolate (P), and triaxial or asymmetric (A) treatments. All energies are in MeV

Configuration	Quantity	Exp.	SB_6
TI(S)	B.E.(S)	470.9	443.5
	$\hbar\omega$(S)	9.7	13.6
TI(P)	B.E.(S)	470.9	435.1
	B.E.(P)	470.9	462.9
	$\hbar\omega$(S)	9.7	13.6
	$\hbar\omega_x$(P)		12.0
	$\hbar\omega_y$(P)		13.9
TI(A)	B.E.(S)	470.9	433.4
	B.E.(A)	470.9	460.3
	$\hbar\omega$(S)	9.7	13.6
	$\hbar\omega_x$(A)		12.0
	$\hbar\omega_y$(A)		13.0
	$\hbar\omega_z$(A)		15.0

With full-fledged oscillator variation along two and three axes, the prolate state TI(P) maintains a slight (3 MeV) advantage over the asymmetric configuration, and thus appears to represent the favored shape for the ground state of ^{44}Ti.

6. Conclusions

Utilizing a tripartite interaction potential, the preferred ground state shape for the nucleide ^{44}Ti appears to be the prolate spheroidal shape, although its B.E. advantage over the asymmetric shape is only approximately 3 MeV. Both configurations predominate over the spherically symmetric shape by 17—19 MeV.

While the B.E. predictions for the three shapes are within 8—27 MeV of the experimental value, the harmonic oscillator energy values are roughly 4 MeV higher than the corresponding laboratory figures.

REFERENCES

1. G. J. Stephenson, Jr. and M. K. Banerjee, Phys. Lett., **24B**, 209, 1967.
2. J. Bar-Touv and I. Kelson, Phys. Rev., **138**, B1035, 1965.
3. J. Bernier and M. Harvey, Nucl. Phys., **A94**, 593, 1967.
4. S. Das Gupta and M. Harvey, Nucl. Phys., **A94**, 602, 1967.
5. G. Ripka, Adv. Nucl. Phys., **1**, 183, 1968.
6. D. M. Brink and E. Boeker, Nucl. Phys., **A91**, 1, 1967.
7. F. R. Ruehl, Jr., Nucl. Phys., **A136**, 241, 1969.
8. F. R. Ruehl, Jr., Acta Phys. Hung., **30**, 283, 1971.
9. F. R. Ruehl, Jr., Acta Phys. Hung., **40**, 213, 1976.

Acta Physica Academiae Scientiarum Hungaricae, Tomus 48 (4), pp. 397–402 (1980)

SUR LE CARACTERE ANHARMONIQUE DE LA DILATATION THERMIQUE DES SOLIDES A HAUTE TEMPERATURE

Par

Y. THOMAS

INSTITUT DE RECHERCHES SCIENTIFIQUES ET TECHNIQUES, 49045 ANGERS CEDEX, FRANCE

(Reçu 18. III. 1980)

La méthode des perturbations au second ordre appliquée au modèle du solide d'Einstein, acceptable à haute température, permet de mettre en évidence une contribution anharmonique au coefficient de dilatation thermique en accord avec les résultats expérimentaux. On retrouve également les autres fonctions thermodynamiques classiques du solide.

Dans l'approximation harmonique, un solide constitué de N atomes identiques peut être considéré, à haute température, comme un ensemble de $3N$ oscillateurs linéaires, indépendants, de même fréquence, se comportant comme des bosons. Ce modèle ne rend pas compte de la dilatation.

En fait, lorsque la température s'élève, les oscillateurs deviennent anharmoniques, l'hamiltonien est perturbé: des termes supplémentaires apparaissent du fait des interactions phonons—phonons. La dilatation peut alors être mise en évidence. Si H_0 est l'hamiltonien classique:

$$H_0 = \frac{p^2}{2m} + \frac{ax^2}{2} = \frac{p^2}{2m} + \frac{m\omega_0^2 x^2}{2}$$

(p: impulsion, ω_0: fréquence angulaire de vibration, m: masse des atomes).

V_0 le potentiel perturbateur que nous écrivons:

$$V_0 = bx^3 + cx^4 \ll H_0$$

(a, b, c, étant des constantes) on peut calculer l'énergie dégénérée au second ordre [1]:

$$E = E_n + E_1 + E_2 = \hbar\omega_0 \left(n + \frac{1}{2}\right) + \frac{3}{2}\left(\frac{\hbar}{m\omega_0}\right)^2 c\left(n^2 + n + \frac{1}{2}\right) - \frac{15}{4}\left(\frac{1}{\hbar\omega_0}\right)$$
$$b^2\left(\frac{\hbar}{m\omega_0}\right)^3\left(n^2 + n + \frac{11}{30}\right).$$

E_n: représentant le spectre discret des valeurs propres équidistantes.

En reformulant d'une façon plus générale la théorie de la perturbation thermodynamique [2] et en l'appliquant à un oscillateur anharmonique on calcule l'énergie libre perturbée $F = -KT \log f$ qui sera prise au second ordre, f étant la fonction de partition perturbée $f = \sum_n e^{-\frac{E}{KT}}$ (F_0 et f_0 étant les valeurs correspondantes non perturbées):

$$F = F_0 + \frac{1}{f_0}\sum_n \exp\left(\frac{F_0 - E_n}{KT}\right)(E_1 + E_2) - \frac{1}{2KT}\sum_n \exp\left(\frac{F_0 - E_n}{KT}\right)(E_1)^2 + \\ + \frac{1}{2KT}\left[\sum_n \exp\left(\frac{F_0 - E_n}{KT}\right)E_1\right]^2 .$$

D'après Grüneisen, le coefficient de dilatation cubique β_0 du solide s'écrit en première approximation:

$$\beta_0 = \frac{\gamma\chi}{V} \cdot C_v \tag{1}$$

où β_0 est proportionnel à la chaleur spécifique à volume constant C_v (γ = constante de Grüneisen, χ = constante de compressibilité, V = volume spécifique).

A volume constant l'entropie du solide est:

$$S = \int_0^T \frac{C_v}{T} dT = R \frac{\partial}{\partial T}(T \log f_0) ,$$

$$\frac{C_v}{T} = R \frac{\partial^2}{\partial T^2}(T \log f_0) ,$$

il n'y a pas de travail fourni à l'extérieur du système, donc:

$$C_v = -T \frac{d^2}{dT^2}(F_0)$$

d'où pour un ensemble de $3N$ oscillateurs harmoniques:

$$\beta_0 = -\frac{\gamma\chi}{V} 4NT \frac{d^2}{dT^2}(F_0) . \tag{2}$$

A haute température pour des oscillateurs anharmoniques on aura:

$$\beta = -\frac{\gamma\chi}{V} 3NT \frac{d^2}{dT^2}(F) ,$$

$$\beta = -\frac{\gamma\chi}{V} 3NT \frac{d^2}{dT^2}\left[F_0 - \varepsilon \exp\left(F_0 - \frac{1}{2}\hbar\omega_0\right)\frac{1}{KT} \times \right.$$

$$\times \left\{\sum_n n^2 \exp\left(-n\frac{\hbar\omega_0}{KT}\right) + \sum_n n \exp\left(-n\frac{\hbar\omega_0}{KT}\right)\right\} +$$

$$\left. + \mu \exp\left(F_0 - \frac{1}{2}\hbar\omega_0\right)\frac{1}{KT}\sum_n \exp\left(-n\frac{\hbar\omega_0}{KT}\right)\right]$$

où:

$$\varepsilon = c\frac{3}{2}\left(\frac{\hbar}{m\omega_0}\right)^2 - \frac{15}{4}\left(\frac{1}{\hbar\omega_0}\right)b^2\left(\frac{\hbar}{m\omega_0}\right)^3,$$

et:

$$\mu = c\frac{3}{4}\left(\frac{\hbar}{m\omega_0}\right)^2 - \frac{11}{8}\left(\frac{1}{\hbar\omega_0}\right)b^2\left(\frac{\hbar}{m\omega_0}\right)^3.$$

Si l'on pose $\hbar\omega/KT = x$ (ω est la fréquence angulaire reliée à la température caractéristique d'Einstein θ_E par $\hbar\omega = K\theta_E$), il vient:

$$\beta = 3N\frac{\gamma\chi}{V}\left\{Kx^2\frac{e^x}{(e^x-1)^2} + 2\frac{\varepsilon}{T}\left[2x\frac{(e^x+e^{2x})}{(e^x-1)^3} - x^2\frac{(e^x+4e^{2x}+e^{3x})}{(e^x-1)^4}\right]\right\}.$$

A haute température on prend la limite des expressions en $x (x \ll 1)$:

$$\beta = 3N\frac{\gamma\chi}{V}\left\{K - \frac{4K^2T}{(\hbar\omega)^2}\left[c\frac{3}{2}\left(\frac{\hbar}{m\omega_0}\right)^2 - \frac{15}{4}\left(\frac{1}{\hbar\omega_0}\right)b^2\left(\frac{\hbar}{m\omega_0}\right)^3\right]\right\}.$$

Or:

$$\omega_0 = \sqrt{\frac{a}{m}},$$

$$\beta = 3N\frac{\gamma\chi}{V}K\left[1 + \left(\frac{15b^2}{a^3} - \frac{6c}{a^2}\right)KT\right].$$

Cette dernière expression met clairement en évidence la contribution de termes anharmoniques dans le coefficient de dilatation cubique d'un solide lorsque sa température s'élève: les calculs précédents ne sont valables que dans le domaine de convergence des développements, c'est-à-dire lorsque la température est suffisamment élevée (ce qui justifie l'emploi du modèle d'Einstein).

Lorsque le solide se dilate, la position d'un atome donné est modifiée de même que l'expression développée de son énergie potentielle (qu'on suppose invariante dans la suite des calculs). Soient $a/2, b, c$ les coefficients du développement en série de l'énergie potentielle non perturbée (correspondant à une dis-

tance interatomique r), soit dr le déplacement dû à la perturbation et x l'oscillation autour de cette nouvelle position. La distance entre les positions non perturbée et perturbée s'écrit $(x + dr)$ et, puisque l'énergie potentielle reste invariante, son développement dans la position initiale non perturbée s'écrit:

$$\frac{a}{2}(x + dr)^2 + b(x + dr)^3 + c(x + dr)^4 + \ldots$$

et dans la position perturbée:

$$\left(\frac{a + da}{2}\right) x^2 + (b + db)\, x^3 + (c + dc)\, x^4 + \ldots$$

d'où en identifiant:

$$\frac{da}{dr} = 6b, \quad \frac{db}{dr} = 4c, \ldots$$

Or $\nu = \frac{1}{2\pi}\left(\frac{a}{m}\right)^{1/2}$ est la fréquence phonique du solide d'où $\frac{1}{\nu}\frac{d\nu}{dr} = \frac{3b}{a}$.

D'après KITTEL [3] le déplacement moyen est: $\bar{x} = -3\,KT\,b/a^2$ et en tenant compte de la variation des fréquences phoniques, conséquence de la variation de volume, due à la dilatation:

$$-\frac{1}{\nu}\frac{d\nu}{dr} \cdot \frac{r}{r}\frac{\partial \bar{x}}{\partial T} = \frac{9b^2}{a^3} \cdot K.$$

Or:

$\gamma = -\frac{d \log \nu}{d \log V}$ et $\frac{1}{r}\frac{\partial \bar{x}}{\partial T} = \alpha_0$ coefficient de dilatation linéaire $(3\alpha_0 = \beta_0)$

il vient:

$$\gamma\beta_0 = \frac{9b^2}{a^3} \cdot K.$$

On retrouve ainsi le coefficient moyen de température des fréquences phoniques du solide que nous avons précédemment défini [4] et qui constitute donc bien une mesure de l'anharmonicité:

$$\beta = 3N\frac{\gamma\chi}{V}K\left[1 + \frac{9b^2}{a^3}K\left(\frac{5}{3} - \frac{2}{3}\frac{ac}{b^2}\right)T\right].$$

Si on pose:

$$\frac{5}{3} - \frac{2}{3}\frac{ac}{b^2} = B\,,$$

$$\beta = 3N\frac{\gamma\chi}{V}K\,[1 + \gamma\beta_0\,BT] = \beta_0\,[1 + \gamma\beta_0\,BT]\,.$$

Il y a donc, à haute température, apparition d'un terme en T proportionnel au coefficient moyen de température.

Cette formulation permet effectivement de rendre compte de résultats expérimentaux à haute température [5].

Il est intéressant de vérifier que l'on retrouve par cette méthode des perturbations les résultats classiques:

En s'arrêtant au premier terme du développement, à relativement basse température, l'oscillateur vibrant harmoniquement l'hamiltonien n'est pas perturbé de même que la fonction de partition f_0 et que l'énergie libre F_0, la formule (2) est valable:

$$\beta_0 = 3N\frac{\gamma\chi}{V}K\frac{\left(\frac{h\nu}{KT}\right)^2\exp\left(\frac{h\nu}{KT}\right)}{\left[\exp\left(\frac{h\nu}{KT}\right)-1\right]^2}$$

expression qui tend vers $\beta_0 = \frac{\gamma\chi}{V}C_v$ avec $C_v = 3NK$ quand la température s'élève. On retrouve l'équation (1), il n'y a pas de contribution anharmonique.

On retrouve les résultats classiques de Born et Brody [6], Schrödinger [7], Kittel [3], et Peierls [8] établis en supposant que les forces entre atomes n'obéissent plus exactement à la loi de Hooke et que le potentiel interatomique devient asymétrique. L'énergie totale d'un atome de masse m oscillant par agitation thermique, exprimée en fonction du moment p et du déplacement x de la position d'équilibre interatomique r, est:

$$E = \frac{p^2}{2m} + \frac{a}{2}x^2 + bx^3 + cx^4 + \ldots$$

d'où la fonction de partition au 2è ordre en KT:

$$f = \iint \exp\left(-\frac{E}{KT}\right)dx\,dp = \frac{2\pi}{\omega_0}\,KT\left[1 + \left(\frac{15\,b^2}{2a^3} - \frac{3c}{a^2}\right)KT\right]$$

connue par la mécanique statistique classique.

L'énergie interne par oscillateur:

$$U = KT + \frac{15b^2}{2a^3}(KT)^2 - \frac{3c}{a^2}(KT)^2$$

met en évidence les termes anharmoniques du second ordre qui apparaissent à haute température et s'ajoutent à l'énergie moyenne classique KT d'un oscillateur harmonique.

La chaleur spécifique par oscillateur:

$$C_v = K\left[1 + \left(\frac{15\,b^2}{a^3} - \frac{6c}{a^2}\right)KT\right]$$

montre l'addition à la constante de Dulong et Petit d'un terme anharmonique à haute température déjà mise en évidence par BORN et BRODY [6] et calculé par DAMKÖHLER [9] et LIEBFRIED [10]. Soit avec les notations précédentes:

$$C_v = K[1 + \gamma\beta_0 BT]$$

qui montre que la variation de la chaleur spécifique est un phénomène lié à la dilatation puisque les lois sont identiques. D'après la relation thermodynamique connue on a d'ailleurs:

$$C_p = C_v + \beta_0^2 \frac{VT}{\chi} = C_v[1 + \gamma\beta_0 T]$$

(C_p est la chaleur spécifique à pression constante).

On trouve donc au coefficient B près (dépendant de la forme du potentiel interatomique) que l'écart à la loi de Dulong et Petit à haute température est comparable à la différence entre C_p et C_v laquelle, on le sait, permet d'exprimer la dilatation.

REFERENCES

1. L. D. LANDAU et E. M. LIFCHITZ, Mécanique quantique, Editions Mir, Moscou, 1966, p. 162.
2. L. D. LANDAU et E. M. LIFCHITZ, Statistical Physics, Clarendon Press, Oxford, 1938, p. 93.
3. K. KITTEL, Introduction à la physique de l'état solide, Masson, Paris, 1958, p. 149.
4. G. GOUREAUX et Y. THOMAS, Compt. Rend. Acad. Sci. Paris, **265**, 1339, 1967.
5. Y. THOMAS, Physics Letters, **66 A**, 131, 1978.
6. M. BORN et M. BRODY, Z. Phys., **6** 132, 1921.
7. E. SCHRÖDINGER, Z. Phys., **11**, 170, 1922.
8. R. E. PEIERLS, Quantum Theory of Solids, Clarendon Press, Oxford, 1955, p. 34.
9. H. DAMKOHLER, Ann. d. Physik, **24**, 1, 1935.
10. G. LEIBFRIED, Hand. d. Physik, Springer Vlg., VII — 1, 274, 1955.

Acta Physica Academiae Scientiarum Hungaricae, Tomus 48 (4), pp. 403—408 (1980)

MÖSSBAUER EFFECT STUDY OF OXIDATION AND COORDINATION STATES OF IRON IN SOME SODIUM BORATE GLASSES

By

N. A. EISSA, A. M. SANAD, S. M. YOUSSEF, S. A. EL-HENAWII, S. SH. GOMAA

PHYSICS DEPARTMENT, FACULTY OF SCIENCE, AL-AZHAR UNIVERSITY, NASR-CITY, CAIRO, EGYPT

and

A. G. MOSTAFA

PHYSICS DEPARTMENT, FACULTY OF SCIENCE IN ASWAN, EGYPT

(Received in revised form 18. III. 1980)

A structural study of some sodium borate glasses containing iron was carried out applying ME spectroscopy. Both oxidation and coordination states of iron were investigated under the effect of gradual replacing of sodium carbonate by sodium nitrate in the glass batches.

The glasses were melted in porcelain crucibles using an electrically heated furnace at 1000 ± 10 °C, then were quenched on a steel plate at room temperature (R.T.). The ME source was 20 mCi radioactive Co-57 in chromium.

The obtained ME spectra indicated that at lower sodium nitrate content both Fe^{2+} and Fe^{3+} are present in these glasses. At moderate concentrations some Fe^{3+} ions were separated in a crystalline phase and the rest of the iron ions appeared as ferric ions in glassy state. At high sodium nitrate content only Fe^{3+} ions in glassy state were detected. The values of the ME parameters for all iron ions indicated that all of them are in the octahedral coordination state. The density measurements confirm the separation of a crystalline phase at moderate sodium nitrate content.

Introduction

Many studies dealing with the structure of iron ions in glass were previously published, from which the one by BATES [1] is of the greatest importance. He concluded that iron in glass exists in both ferrous and ferric states in equilibrium, as well as in a colloidal dispersed state. He pointed out also that the difficulty was to decide their coordination number. After the development of the Mössbauer effect spectroscopy it was successfully applied to investigate both oxidation and coordination states of iron ions in the glassy states [2].

From the data published in this field it was established that the change of coordination from six to four for either Fe^{3+} or Fe^{2+} ions would be expected to result in a decrease in isomer shift values [3]. The effect of the environment on the values of the ME parameters of iron ions in different glasses was known [4—6]. The behaviour of iron ions under the oxidation effect of chloride was also studied [7].

In the present work the Na_2CO_3 was replaced by $NaNO_3$ cation per cation in the glass batches to study the oxidation effect of NO_3 group on the structural states of iron in glasses.

Experimental

Chemically pure grade materials were melted in porcelain crucibles in order to obtain different glass samples according to the following formula:

$$16 \text{ mole } B_2O_3 + 4 \text{ mole } Na_2O + 1 \text{ mole } FeC_2O_4 \cdot 2H_2O.$$

In these glasses sodium oxide was supplied by sodium carbonate and/or sodium nitrate. This was achieved by the gradual replacing cation per cation of Na_2CO_3 by $NaNO_3$ in the glass batches. Table I presents the different amounts of Na_2O which were supplied by either Na_2CO_3 or $NaNO_3$.

Table I

The amounts of Na_2O which were supplied by either Na_2CO_3 or $NaNO_3$

Sample No.	1	2	3	4	5	6	7	8	9
Na_2CO_3 mole	4.0	3.5	3.0	2.5	2.0	1.5	1.0	0.5	0.0
$NaNO_3$ mole	0.0	0.5	1.0	1.5	2.0	2.5	3.0	3.5	4.0

The melting was carried out in an electric muffle furnace at about 1000 ± 10 °C for two hours. Melts were then quenched on a steel plate at room temperature.

A conventional Mössbauer spectrometer of the constant acceleration mode was used and the source was a 20 mCi Co-57 in Cr. The Mössbauer alsorbers were prepared in the form of powdered glass pressed between two thin sheets of aluminium in order to obtain homogeneous thickness of 10 mg per cm^2. All the Mössbauer measurements for these glasses were carried out at room temperature.

Archimedes method was applied to measure the densities of these samples.

Results and discussion

The change in the shape of the measured ME spectra as the sodium nitrate was increased in the glass batches can be easily observed in Figs. 1, 2 and 3. In the spectrum of the first sample it was observed that there are three resolved peaks and the peak in the high energy side had lower intensity than that in the low energy one. As the sodium nitrate began to be introduced in the glass batches and as its concentration was gradually increased, the intensity of the central peak increased while that in the high energy side decreased. When the

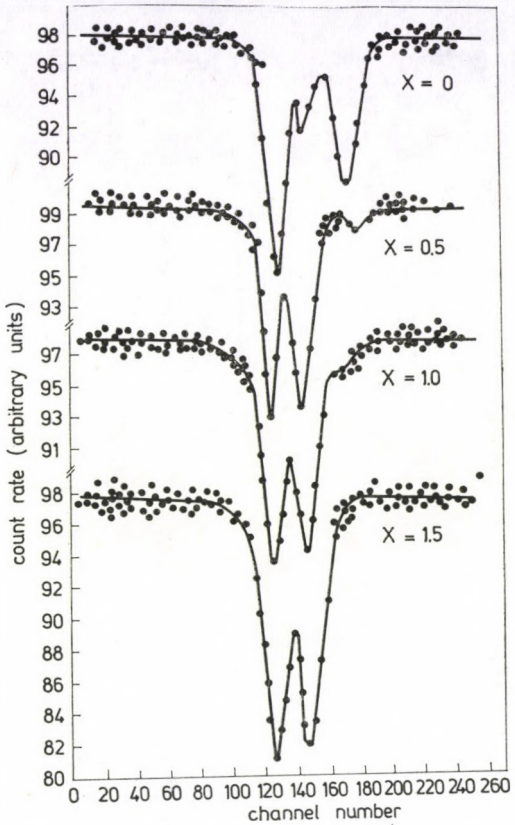

Fig. 1. ME spectra of samples 1, 2, 3 and 4 ($x = 0$, 0.5, 1.0, and 1.5 mole $NaNO_3$)

concentration of sodium nitrate reached 1.5 mole in the glass, the high energy side peak disappeared completely and the other two peaks appeared to be symmetric. Increasing the sodium nitrate by more than 1.5 mole a magnetic hyperfine splitting starts to appear in addition to the central doubles. As the sodium nitrate increased again just to 3 mole, the magnetic splitting disappeared.

The ME specra for the first three samples (Fig. 1) could be analyzed into two separated doublets A and B. Doublet A which has the greatest splitting energy represents the iron ions in the ferrous state, while doublet B represents the iron ions in the ferric state [4]. As the sodium nitrate was increased to 1.5 mole the doublet A completely disappeared. This means that both iron ions Fe^{2+} and Fe^{3+} present in these glasses were due to the reduction effect of the oxalate ions. The addition of the nitrate group oxidized the ferrous into ferric ions and at 1.5 mole of the nitrate content, all the ferrous ions present in these glasses were completely oxidized.

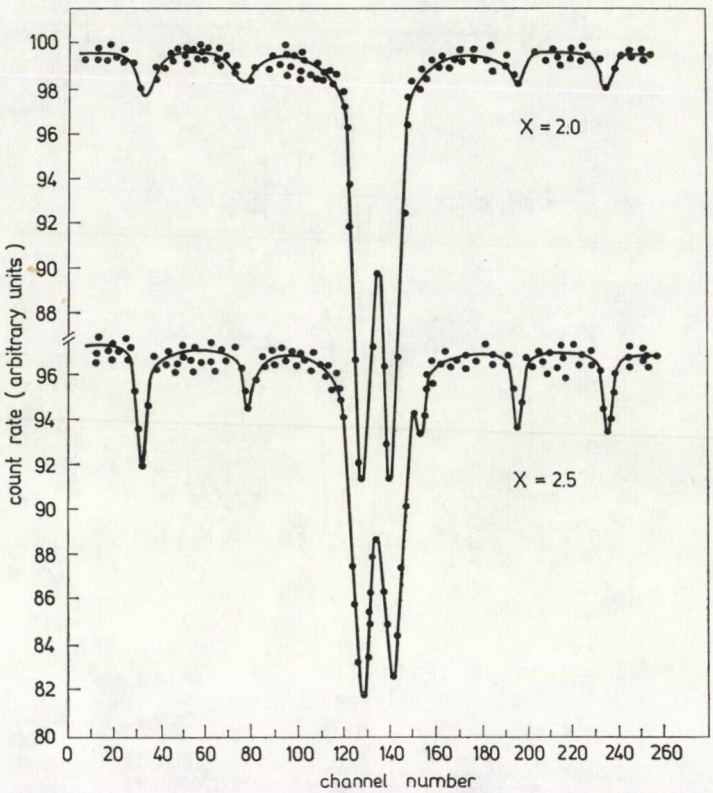

Fig. 2. ME spectra of samples 5 and 6 ($x = 2.0$ and 2.5 mole $NaNO_3$)

The magnetic hyperfine splitting which appeared in the following two samples (which contain 2 and 2.5 mole of sodium nitrate, respectively, Fig. 2) can be attributed to some precipitated Fe_2O_3. This could be concluded from ME parameters as presented in Table II. Such precipitation may be due to the fact that iron ions are slightly soluble in borate glasses [8].

Table II

ME parameters for the separated phases in sample No. 6 in mm/s

Isomer shift IS	Quadrouple splitting QS	Line width LW	Magnetic field KOe
0.20	0.35	0.75	517

The spectra of the last three samples (Fig. 3) indicated that all iron ions are in the ferric state in a pure glassy state.

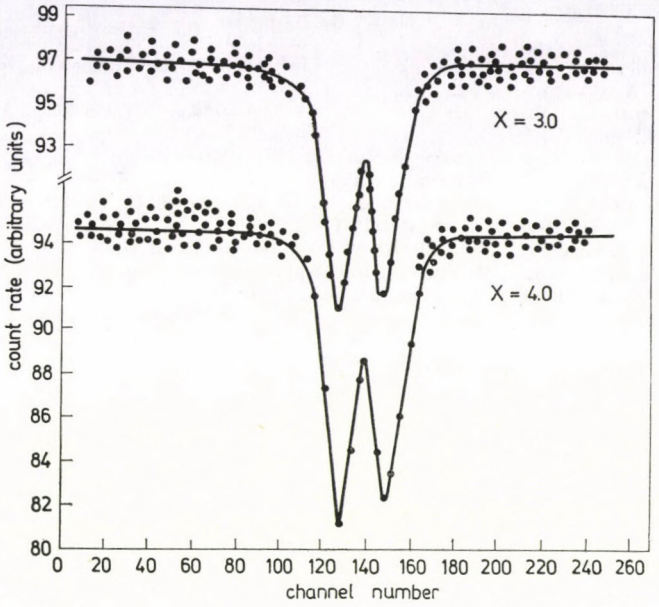

Fig. 3. ME spectra of samples 7 and 8 ($x = 3.0$ and 4.0 mole $NaNO_3$)

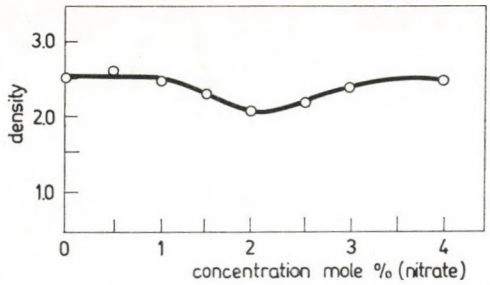

Fig. 4. Density measurements

All the (IS) and (QS) values for both iron ions in these glasses indicate that the preferable coordination state is the octahedral one [4].

The density measurements confirm the presence of a separated crystalline material in samples number 5 and 6. Fig. 4 shows that these two samples have smaller density values than the others. This may be due to the change of the structure into the compact one in these two glass samples.

It can be concluded that at lower sodium nitrate content both Fe^{2+} and Fe^{3+} ions were present in these glasses. Increasing its concentration some Fe^{3+} ions were separated in a magnetic ordered material and the rest of iron ions were detected in a pure glassy state as Fe^{3+} ions. At higher sodium nitrate content, it was found that all iron ions appeared as ferric ions in a glassy state.

REFERENCES

1. T. Bates, Modern Aspects of Vitreous State, Edited by I. D. Machenzi, Butterworth and Co. Ltd., Washington, 1962.
2. V. I. Goldanskii, The Mossbauer Effect and its Application in Chemistry, Academic Press, New York, 1964.
3. C. R. Kurkjian, J. Non-crystalline Solids, **3**, 157, 1970.
4. C. R. Kurkjian and D. N. Buchnan, Phys. Chem. Glass, **5**, 63, 1964.
5. A. A. Belyustin, Yu. M. Ostanevich, A. M. Pisarvskii, S. B. Tomilov, V. Bai-Shi and L. Cher, Soviet Phys. Solid State, **7**, 1163, 1965.
6. C. Harayama, J. G. Castle and M. Kuryama, Phys. Chem. Glasses, **9**, 109, 1968.
7. N. A. Eissa, A. M. Sanad, S. M. Youssef and A. G. Mostafa, Proceedings of the Mathematical and Physical Society of Egypt, **49**, 185, 1980.
8. C. R. Kurkjian and E. A. Sigety, in Proc. 7th Inter. Congress on Glass, Brussels, 1965.

Acta Physica Academiae Scientiarum Hungaricae, Tomus 48 (4), pp. 409—414 (1980)

AN EFFICIENT LABORATORY RAMAN SCATTERING SYSTEM*

By

Z. KONEFAŁ and J. SZCZEPAŃSKI

INSTITUTE OF PHYSICS, UNIVERSITY OF GDAŃSK, GDAŃSK, POLAND**

(Received 2. IV. 1980)

The apparatus consists of an UV-preionization nitrogen TEA laser (giving high peak power output), multipass Raman cell and spectrograph. The scattered Raman spectra of ordinary atmospheric air obtained using this apparatus are given as an example.

1. Introduction

The Raman scattering of incident radiation from gases, liquids, and solids has been of interest as a source of information on various materials, especially their molecular structure and chemical composition.

Recently, air and water pollution has become a worldwide problem. This necessitates the development of efficient methods for monitoring and measuring pollutants. For several years laser methods have been used in "in situ" measurements, applying the absorption, fluorescence, opto-acoustical Raman and Mie scattering techniques [1—5]. Raman scattering offers a unique and effective method for the analysis of molecular pollutants. The aim of this paper is to describe an apparatus for the laboratory detection of molecular pollutants in water and air.

2. Apparatus

a) *UV-preionization nitrogen TEA laser*

Laser power can be increased by increasing the volume or the pressure of the active medium. In electrical discharge laser scaling these quantities cause discharge instabilities, spatial nonuniformities of the optical medium and introduce a transition from a glow discharge to a discrete high-current arc. These effects seriously degrade the output energy and optical mode quality

* This work was supported under the Project No. 10.2 — 01.01.01.03

** Address: Instytut Fizyki, Uniwersytet Gdański 80—952 Gdańsk, ul. Wita Stwosza 57

of the laser. It has been shown [6, 7] that the double-discharge and electron beam preionizer increase the discharge stability. Double-discharge is used in N_2 lasers which operate at high pressure.

Fig. 1 shows the detailed construction of the N_2 laser used in the pollution apparatus. The 60 cm long laser discharge tube had a 1.0 cm electrode separation. The cross section of the superradiance radiation was 0.6×10 cm. The laser tube consists of two aluminium bars separated by plexiglass walls. Two copper tubes (I.D. of 0.4 cm) pressed into a slot of the aluminium bars provides water cooling for the laser tube. A front surface — aluminized mirror and feedback quartz window are sealed with O-rings, one at each end of the tube. In order to have a uniform gas flow in the laser tube, a special distribution system has been constructed. As is shown in Fig. 1, the nitrogen is distributed by many

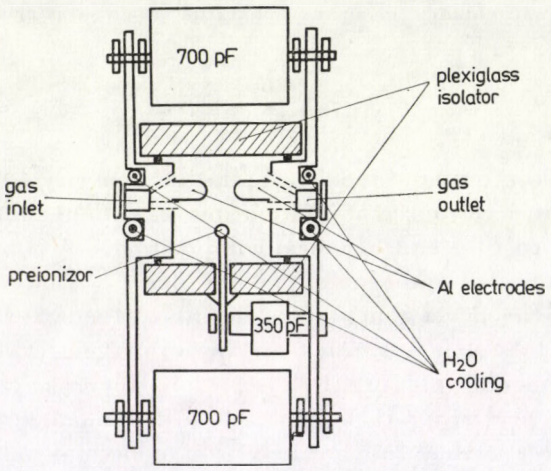

Fig. 1. Detailed construction of laser chamber

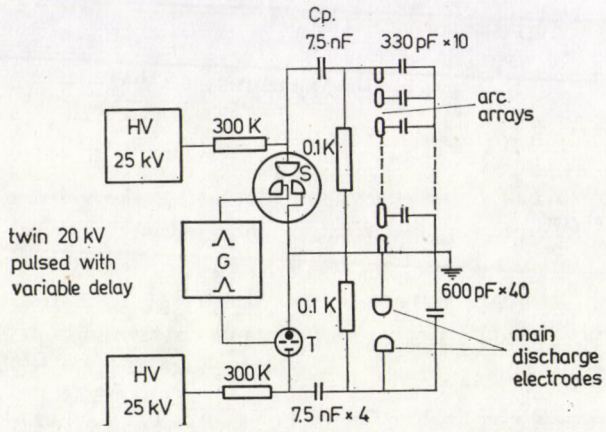

Fig. 2. The electric circuit of the UV-preionization laser

input holes in one of the aluminium electrodes. The entering gas flows across the discharge tube and exits around the other electrode where it is collected by an exhaust manifold. It has been tested that a sufficiently uniform gas flow is achieved with 100 inlet and exit holes of 2 mm diameter equally distributed on each electrode. In order to obtain high power output of the laser light it was necessary for a given pulse repetition to have a fairly high velocity of the

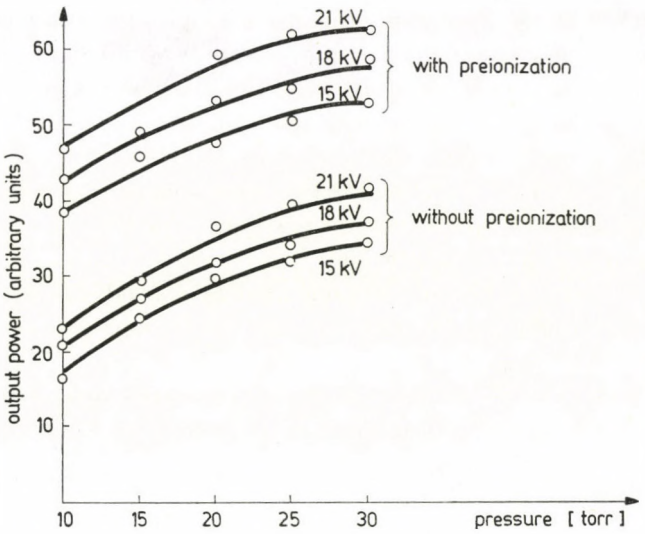

Fig. 3. Laser power versus nitrogen gas pressure at different charging voltages

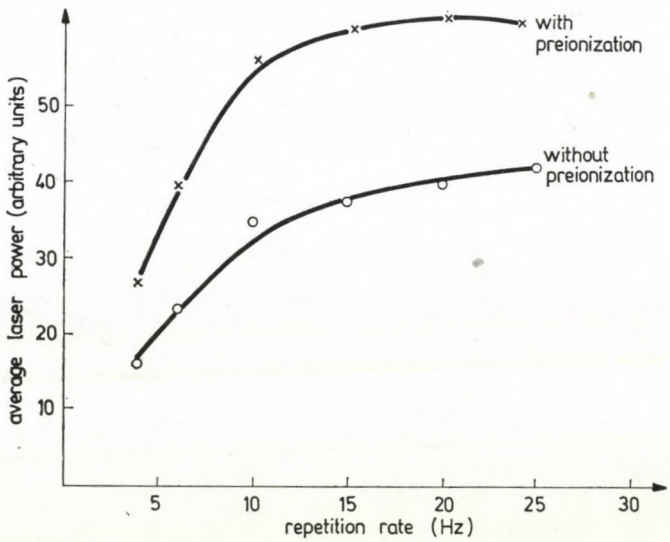

Fig. 4. Average laser output power versus pulse repetition rate

gas flow. This is required for the elimination of the residual ionization from the previous discharge pulse. If a few ions or a nonuniform distribution of ions appears in the discharge tube, the breakdown voltage of the gas decreases which results in a loss of laser output.

Fig. 2 gives the scheme of the electric circuit of the UV-preionization N_2 laser. The scheme consists of two circuits, i.e. the preionization and main discharge circuits. The preionization circuit involves the 7.5 nF storage capacitors (C_p), ten 330 pF dumping capacitors which are connected to the arc arrays as shown in Fig. 2 and the HV power supply which charges the preionizing electrodes through the 0.1 K resistance. The discharge is switched by means of a triggered pressurized hydrogen spark gap. The main discharge, supplied by another HV power feeder switched on by means of a thyratron gives the bright arc. The variable electronic delay allows control of the firing of the main discharge after the preionization process. Typically, the main discharge appears 12 μs after the preionization.

As can be seen in Fig. 3, for each applied voltage the preionization for which the high voltage was constant approximately doubles the output power of the laser.

Fig. 4 shows the dependence of the average laser output power vs pulse repetition rate. For slow N_2 flow through the discharge tube and 12 μs delay

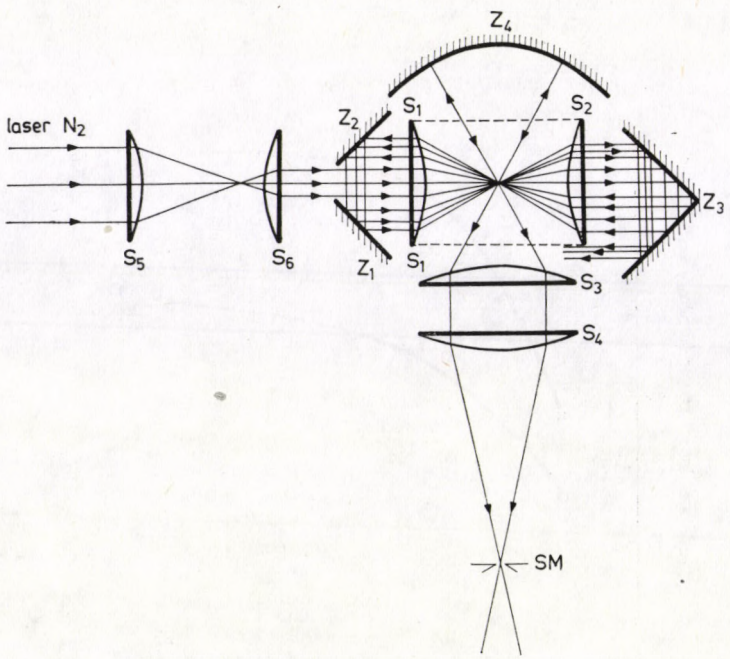

Fig. 5. The scheme of multipass Raman cell with the experimental setup of the Raman scattering experiment

of the main discharge the maximum laser power is obtained at 30 Hz. At higher velocities of gas flow the maximum value of laser power was obtained at higher repetition rates.

b) *Multipass Raman cell*

In order to increase the sensitivity of the apparatus a retroreflecting multipass cell has been used. Fig. 5 shows the scheme of the cell. The cell consists of a quartz tube (I.D. 2.5 cm) which has a length equal to the sum of the focal lengths of the two quartz lenses. This cell is surrounded by two retroreflecting mirror assemblies. One of the mirror assemblies is shifted from the optical axis. For such mounting the laser beam passes several times through the cell consisting of polluted gas before being reflected from the retroreflecting mirror assemblies. The laser beam, before entering the cell, passes a cylindrical lense beam expendor which changes the beam cross section from 0.6×10 mm to 0.2 mm $\times$ 10 mm.

The Raman scattered light is focused on the slit of the Hilger E 498 quartz spectrograph by two (S_3 and S_4) quartz lenses and by a parabolic reflecting mirror Z_4.

3. Results

Using the apparatus described above we obtained Raman spectra of polluted air which has been drawn from a street crossing (with heavy traffic). Fig. 6 shows this spectrum. The spectrum consists of the incident wave fre-

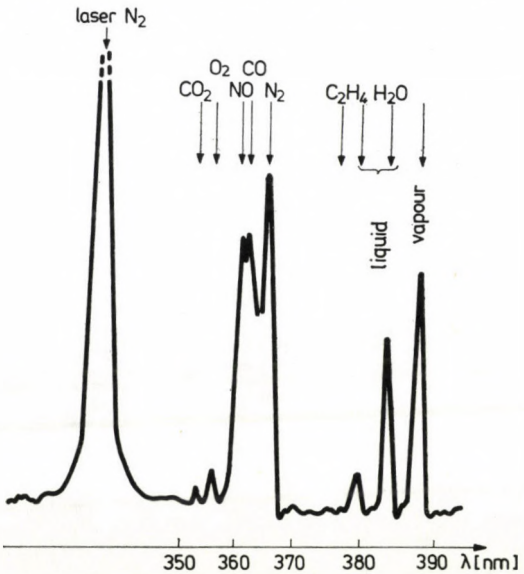

Fig. 6. The Raman scattering spectrum obtained from the polluted air drawn from the street crossing

quency ν_0 and series frequencies ν_r shifted toward lower values, i.e. the Stokes lines. The intensity of these Stokes lines is proportional to the concentration of each molecular pollutant. On the Figures the vertical arrows indicate the expected central wavelengths of the Q-branch of the vibrational-rotational Raman lines for each molecular species.

In our case the lines belong to the O_2, NO, CO, N_2, C_2H_4 and H_2O molecules.

Since the concentration of N_2 in the air does not depend on the concentration of the pollutants, it is convenient to evaluate the concentration of each molecular species relatively to N_2 [8].

REFERENCES

1. R. W. Terhune and J. E. Anderson, Optics Letters, **1**, 70, 1977.
2. R. Gerlach and N. M. Amer, Appl. Phys. Lett., **32**, 228, 1978.
3. S. M. Melfi, Appl. Optics, **11**, 1605, 1972.
4. J. Gelbwachs and M. Birnbaum, Appl. Optics, **12**, 2442, 1973.
5. I. J. Barton and J. F. Le Marshall, Optics Letters, **4**, 78, 1979.
6. Ing-Jiunn Ma, Tieh Chu Wang and Yuh Shuh Wang, J. Appl. Phys., **48**, 2515, 1977.
7. O. P. Indol, Appl. Phys. Lett., **22**, 95, 1973.
8. Laser Monitoring of the Atmosphere, Ed. by E. D. Hinkley, Springer-Verlag, Berlin, Heidelberg, New York, 1976.

Acta Physica Academiae Scientiarum Hungaricae, Tomus 48 (4), pp. 415—423 (1980)

NONSTATIC CYLINDRICALLY SYMMETRIC ZEL'DOVICH FLUID DISTRIBUTION

By

J. R. RAO, R. N. TIWARI and G. MOHANTY

DEPARTMENT OF MATHEMATICS, INDIAN INSTITUTE OF TECHNOLOGY, KHARAGPUR-721302, INDIA

(Received in revised form 15. IV. 1980)

The relations between some components of the metric tensor for the nonstatic cylindrically symmetric Einstein—Rosen metric and the electromagnetic potentials for the source free electromagnetic fields are obtained.These relations help to generate solutions for Zeldovich fluid distributions coupled with electromagnetic field from those of Zeldovich fluid solutions

I. Introduction

This study is an extension of the work of RAO et al [1] wherein they have obtained sets of exact solutions for nonstatic cylindrically symmetric fields. Here a class of solutions has been obtained for the nonstatic cylindrically symmetric Einstein—Rosen metric

$$ds^2 = e^{2\alpha-2\beta}(dt^2 - d\sigma\varrho^2) - \varrho^2 e^{-2\beta} d\Phi^2 - e^{2\beta} dz^2, \tag{1}$$

where α and β are functions of ϱ and t only and the coordinates ϱ, Φ, z, t correspond to x^1, x^2, x^3, x^4, respectively. This class of solutions is analogous to those obtained by WEYL [2], MAJUMDAR [3] and PAPAPETROU [4] (referred to as WMP class hereafter). WEYL [2] and BONNOR [5] have obtained the relation between the g_{44} component of the metric tensor and the electrostatic potential as

$$g_{44} = 4\pi\psi^2 + B\psi + A$$

(A and B are arbitrary constants) for axially symmteric metric, while MAJUMDAR [3] and PAPAPETROU [4] have established the same relation for generalised static metric

$$ds^2 = g_{ab}(x)\, dx^a\, dx^b + g_{44}\, dt^2, \ (a, b = 1, 2, 3, \ g_{44} < 0). \tag{2}$$

The corresponding problem for the cylindrically symmetric Einstein—Rosen metric in the case when only electromagnetic field in present has been investigated by MISRA and RADHAKRISHNA [6] and in the case of coupled zeromass

scalar and source free electromagnetic fields by TIWARI [7]. In both these papers the same WMP relations, viz.,

$$g_{33} = -\frac{k}{4\pi}\left(a + b\varphi - \frac{1}{2}\varphi^2\right)$$

and (3)

$$g_{22} = -\frac{k}{4\pi}\left(a + b\varphi - \frac{1}{2}\varphi^2\right)$$

have been obtained. Using relations (3) the above mentioned authors have obtained theorems which enable to generate the solutions of the WMP class stated earlier.

The problem investigated in these papers is an extension of the work of MISRA and RADHAKRISHNA [6] to the case of electromagnetic field coupled with perfect fluid. However, consistency of the field equations demands that the perfect fluid be restricted to Zeldovich fluid (with the equation of state, $w = p$ (Appendix).

It has been shown that the WMP relations, under certain mathematical restrictions, are not affected by the presence of Zeldovich fluid and remain the same as those obtained by MISRA and RADHAKRISHNA [6] and TIWARI [7]. These relations enable the construction of solutions fo the WMP class from those of the cylindrically symmetric Zeldovich fluid for the Einstein– Rosen metric.

II. Mathematical preliminaries

The Einstein field equations for charged perfect fluid with mass density w, pressure p, charge σ, four velocity u_i and the electromagnetic field tensor F_{ij} may be written as

$$G_{ij} \equiv R_{ij} - \frac{1}{2} g_{ij} R = -\frac{k}{4\pi}\left[-F_{is} F_{j.}^{s} + \frac{1}{4} g_{ij} F_{ab} F^{ab}\right] - \\ - \frac{k}{4\pi}\left[(w + p) u_i u_j - p g_{ij}\right], \tag{4}$$

$$u^i u_i = 1\,, \tag{5}$$

$$F_{ij} = A_{i,j} - A_{j,i}\,, \tag{6}$$

and

$$F^{ij}_{\ ,j} = -4\pi\sigma u^i\,, \tag{7}$$

where $K = 8\pi G (c = 1)$ is the gravitational constant and A_i is the electromagnetic four potential. A comma and a semicolon denote partial and covariant differentiations respectively. It can be shown along the lines of the work of

RAO et al [1], that for the metric (1), σ, F_{14}, F_{23} are identically zero and that the perfect fluid degenerates to the Zeldovich fluid viz., to the case when the proper density w equals the pressure p (Appendix). The rest of the components of F_{ij} can be derived from two independent potentials A_2 and A_3, of the four potential A_i. Denoting $A_2 = \varphi$ and $A_3 = \psi$, we get

$$F_{12} = -\varphi,\ F_{13} = -\psi,\ F_{24} = \varphi_4,\ F_{34} = \psi_4. \tag{8}$$

Here lower suffixes 1 and 4 after unknowns denote partial differentiation with respect to ϱ and t, respectively. Using (8), the field equations (4) to (7) for the metric (1) in comoving coordinates become

$$\beta_1^2 + \beta_4^2 - \frac{\alpha_1}{\varrho} = -\frac{k}{4\pi} e^{2\alpha-2\beta} p_i^i - \frac{k}{8\pi}\left[\frac{e^{2\beta}}{\varrho^2}(\varphi_1^2+\varphi_4^2)+[e^{-2\beta}(\psi_1^2+\psi_4^2)\right], \tag{9}$$

$$-\alpha_{11}+\alpha_{44}-\beta_1^2+\beta_4^2=-\frac{k}{4\pi}e^{2\alpha-2\beta}p-\frac{k}{8\pi}\left[\frac{e^{2\beta}}{\varrho^2}(\varphi_1^2-\varphi_4^2)-e^{-2\beta}(\psi_1^2-\psi_4^2)\right], \tag{10}$$

$$2\beta_{11}-2\beta_{44}-\alpha_{11}+\alpha_{44}-\beta_1^2+\beta_4^2+\frac{2}{\varrho}\beta_1 = -\frac{k}{4\pi}e^{2\alpha-2\beta}p + \\ +\frac{k}{8\pi}\left[\frac{e^{2\beta}}{\varrho^2}(\varphi_1^2-\varphi_4^2)-e^{-2\beta}(\psi_1^2-\psi_4^2)\right], \tag{11}$$

$$2\beta_1\beta_4 - \frac{\alpha_4}{\varrho} = -\frac{k}{4\pi}\left[\frac{e^{2\beta}}{\varrho^2}\varphi_1\varphi_4 + e^{-2\beta}\psi_1\psi_4\right], \tag{12}$$

$$w = p, \tag{13}$$

$$\varphi_1\psi_1 - \varphi_4\psi_4 = 0, \tag{14}$$

$$\varphi_{11} - \varphi_{44} - \frac{\varphi_1}{\varrho} = 2\beta_4\varphi_4 - 2\beta_1\varphi_1 \tag{15}$$

and

$$\psi_{11} - \psi_{44} + \frac{\psi_1}{\varrho} = 2\beta_1\psi_1 - 2\beta_4\psi_4. \tag{16}$$

III. WMP relation

Since the field equations are highly nonlinear, for the sake of mathematical convenience, we study the problem under the following two cases, viz.,

(i) $\varphi = 0,\ \psi \neq 0,$

(ii) $\varphi \neq 0,\ \psi = 0.$

Case (*i*) $\varphi = 0$, $\psi \neq 0$

The field equations for this case can be written as

$$\alpha_1 = \varrho\,(\alpha_{11} - \alpha_{44} + 2\beta_1^2) + \frac{k\varrho}{4\pi} e^{-2\beta} \psi_1^2 , \tag{17}$$

$$p(=w) = \frac{2\pi}{k} e^{-2\alpha+2\beta}\left[\alpha_{11} - \alpha_{44} - 2\beta_4^2 + \frac{\alpha_1}{\varrho} - \frac{k}{4\pi} e^{-2\beta}\psi_4^2\right], \tag{18}$$

$$\alpha_4 = 2\varrho\beta_1\beta_4 + \frac{k\varrho}{4\pi} e^{-2\beta}\psi_1\psi_4 , \tag{19}$$

$$\beta_{11}\beta_{44} + \frac{\beta_1}{\varrho} = -\frac{k}{8\pi} e^{-2\beta}(\psi_1^2 - \psi_4^2) \tag{20}$$

and

$$\psi_{11} - \psi_{44} + \frac{\psi_1}{\varrho} = 2\beta_1\psi_1 - 2\beta_4\psi_4 . \tag{21}$$

We now assume the metric potential β to be function of the electromagnetic potential ψ and the pressure p, i.e.,

$$\beta = \beta(\psi, p) . \tag{22}$$

Using (22), in Eq. (20) and (21), we get

$$\beta_{\psi\psi}(\psi_1^2 - \psi_4^2) + 2\beta_{\psi p}(\psi_1 p_1 - \psi_4 p_4) + \beta_\psi\left(\psi_{11} - \psi_{44} + \frac{\psi_1}{\varrho}\right) +$$

$$+ \beta_{pp}(p_1^2 - p_4^2) = -\frac{k}{8\pi} e^{-2\beta}(\psi_1^2 - \psi_4^2) , \tag{23}$$

$$\psi_{11} - \psi_{44} + \frac{\psi_1}{\varrho} = 2\beta_\psi(\psi_1^2 - \psi_4^2) + 2\beta_p(\psi_1 p_1 - \psi_4 p_4) , \tag{24}$$

where

$$\beta_p = \frac{\partial\beta}{\partial_p}, \quad \beta_{pp} = \frac{\partial^2\beta}{\partial p^2}, \quad \beta_\psi = \frac{\partial\beta}{\partial\psi}, \quad \beta_{\psi\psi} = \frac{\partial^2\beta}{\partial\psi^2} .$$

Further, substituting (24) in (23), we have

$$(\psi_1^2 - \psi_4^2)\left(\beta_{\psi\psi} + 2\beta_\psi^2 + \frac{k}{8\pi} e^{-2\beta}\right) + 2\,(\beta_{\psi p} + \beta_\psi\beta_p) \times$$

$$\times\,(\psi_1 p_1 - \psi_4 p_4) + \beta_{pp}(p_1^2 - p_4^2) = 0 . \tag{25}$$

When the gradient vectors of electromagnetic potential ψ and the pressure p are both null and mutually orthogonal, we have

$$g^{ij}\psi_i\psi_j = 0\,, \quad g^{ij}p_ip_j = 0\,, \quad g^{ij}\psi_i p_j = 0$$

which for the metric (1), become

$$(\psi_1^2 - \psi_4^2) = 0\,, \; (p_1^2 - p_4^2) = 0, \quad (\psi_1 p_1 - \psi_4 p_4) = 0\,.$$

In this case Eq. (25) is satisfied identically and thereby the corresponding WMP relation may or may not exist. Since $g^{ij}p_ip_j = 0$ implies that the constant pressure surfaces are characteristic surfaces, propagation of pressure gradient with the velocity of light ensues. As far as we know for various physical situations this is unlikely, and as such one may consider the solutions, for which $g^{ij}p_ip_j \neq 0$, as of interest. However, since our main aim is to establish a WMP relation, if exists, we assume

$$\beta_{\psi\psi} + 2\beta_\psi^2 + \frac{k}{8\pi}e^{-2\beta} = 0\,, \tag{26}$$

$$\beta_{\psi p} + \beta_\psi\beta_p = 0\,, \tag{27}$$

$$\beta_{pp} = 0\,. \tag{28}$$

It is obvious, that (25) is automatically satisfied by Eqs. (26), (27) and (28) irrespective of the conditions on ψ_i and p_i.

On integration, Eq. (28) gives

$$\beta = pf(\psi) + g(\psi)\,, \tag{29}$$

where f and g are arbitrary functions of ψ only.

Equations (29) and (27) together imply that β is a function of ψ only. Hence from (26), on integration, we get

$$-g_{33} = e^{2\beta} = \frac{k}{4\pi}\left(a + b\psi - \frac{1}{2}\psi^2\right), \tag{30}$$

where a and b are arbitrary constants. This is the required WMP relation in the case of coupled Zeldovich fluid and electromagnetic field and is of the same form as that obtained by MISRA and RADHAKRISHNA [6] for the case of Maxwell field and by TIWARI [7] for the case of coupled zeromass scalar and electromagnetic fields.

With the help of (30), Eqs. (20) and (21) become identical and reduce to

$$\psi_{11} - \psi_{44} + \psi_1/\varrho = \frac{(b-\psi)(\psi_1^2 - \psi_4^2)}{a + b\psi - \frac{1}{2}\psi^2} . \tag{31}$$

Hence, the values of α and $p = (w)$ can be obtained if we determine ψ from Eq. (31). We now consider the substitution

$$\int \frac{d\psi}{a + b\psi - \frac{1}{2}\psi^2} = \frac{2x}{\sqrt{2a + b^2}} \tag{32}$$

which when put in (31) yields

$$x_{11} - x_{44} + x_1/\varrho = 0 . \tag{33}$$

From Eq. (32), we get

$$\psi = b + \sqrt{2a + b^2}\, \tanh x . \tag{34}$$

Substituting (34) in Eq. (30), we obtain

$$e^{2\beta} = \frac{k}{4\pi}\left(a + \frac{b^2}{2}\right) \mathrm{Sech}^2 x . \tag{35}$$

With the help of Eqs. (30) and (32), the field equations (17) to (19) become

$$\bar{\alpha}_1 = \varrho(\bar{\alpha}_{11} - \bar{\alpha}_{44}) + 2\varrho x_1^2 . \tag{36}$$

$$\bar{p}(=\bar{w}) = \frac{2\pi}{k} e^{-2\bar{\alpha}+2x} [\bar{\alpha}_{11} - \bar{\alpha}_{44} + \alpha_1/\varrho - 2x_4^2] , \tag{37}$$

$$\bar{\alpha}_4 = 2\varrho x_1 x_4 , \tag{38}$$

where

$$\bar{p}(=\bar{w}) = \frac{2\pi}{k} \frac{(1+e^{2x})^2}{2a+b^2} p(=w), \quad \alpha = \bar{\alpha} .$$

It may be verified that the field equations (33) and (36) to (38) correspond to those for Zel'dovich fluid for the Einstein—Rosen metric given by

$$ds^2 = e^{2\bar{\alpha}-2x}(dt^2 - d\varrho^2) - \varrho^2 e^{-2x} d\Phi^{2x} - e^{2x} dz^2 . \tag{39}$$

Thus given any Zel'dovich fluid solutions for the metric (39), one can generate the corresponding solutions for the coupled Zel'dovich fluid and electromagnetic field using the relations (34) and (35).

Hence the following theorem:

Theorem: Given any $\{\bar{\alpha}, x, \bar{p}(=\bar{\omega})\}$ as the solution for Zeldovich fluid for cylindrically symmetric metric (39) one can always generate the corresponding coupled Zel'dovich fluid and source free electromagnetic solution $\{\alpha, \beta, \psi, p(=w)\}$ where

$$\alpha = \bar{\alpha}\,,$$

$$\beta = \frac{1}{2}\log\left[\frac{k}{4\pi}\left(a + \frac{b^2}{2}\right)\mathrm{Sech}^2\, x\right],$$

$$\psi = b + \sqrt{2a + b^2}\,\tanh x\,, \tag{40}$$

$$\frac{2\pi}{k}\,\frac{(1 + e^{2x})^2}{2a + b^2}\,p\,(=w) = \bar{p}\,(=\bar{w})\,.$$

Case (ii) $\varphi \neq 0$, $\psi = 0$

In this case the field equations take the form:

$$\alpha_1 = \varrho(\alpha_{11} - \alpha_{44} + 2\beta_1^2) + \frac{k}{4\pi}\,\frac{e^{2\beta}}{\varrho}\,\varphi_4^2\,, \tag{41}$$

$$p(=w) = \frac{2\pi}{k}\,e^{-2\alpha+2\beta}\left[\alpha_{11} - \alpha_{44} - 2\beta_4^2 + \frac{\alpha_1}{\varrho} - \frac{k}{4\pi}\,\frac{e^{2\beta}}{\varrho^2}\,\varphi_1^2\right], \tag{42}$$

$$\alpha_4 = 2\varrho\beta_1\,\beta_4 + \frac{k}{4\pi}\,\frac{e^{2\beta}}{\varrho}\,\varphi_1\,\varphi_4\,, \tag{43}$$

$$\beta_{11} - \beta_{44} + \frac{\beta_1}{\varrho} = \frac{k}{4\pi}\,\frac{e^{2\beta}}{\varrho^2}\,(\varphi_1^2 - \varphi_4^2)\,, \tag{44}$$

$$\varphi_{11} - \varphi_{44} - \frac{\varphi_1}{\varrho} = 2\beta_4\,\varphi_4 - 2\beta_1\,\varphi_1\,. \tag{45}$$

In order to establish the WMP relation in this case we consider

$$\varrho^2\,e^{-2\beta} \equiv W(\varrho, t)\,. \tag{46}$$

Substituting (46) in (44), we obtain

$$W_{11} - W_{44} + \frac{W_1}{\varrho} - \frac{W_1^2 - W_4^2}{W} = -\frac{k}{4\pi}\,(\varphi_1^2 - \varphi_4^2)\,. \tag{47}$$

With the help of (46), (45) yields

$$\varphi_{11} - \varphi_{44} + \frac{\varphi_1}{\varrho} = \frac{\varphi_1\,W_1 - \varphi_4\,W_4}{W}\,. \tag{48}$$

Following a similar procedure as in the previous case, we assume W to be function of φ and p. We get the following differential equations:

$$W_{\varphi\varphi} + \frac{k}{4\pi} = 0 \,, \tag{49}$$

$$W_{\varphi p} = \frac{W_\varphi W_p}{2W} \,, \tag{50}$$

$$W_{pp} = \frac{W_p^2}{W} \,. \tag{51}$$

It is clear from (50) and (51) that W can be taken as a function of φ only. Hence (49) gives

$$W = \frac{k}{4\pi}\left(a + b\varphi - \frac{1}{2}\varphi^2\right), \tag{52}$$

where a and b are arbitrary constants. Thus we get from (46)

$$-g_{22} = \varrho^2 e^{-2\beta} = \frac{k}{4\pi}\left(a + b\varphi - \frac{1}{2}\varphi^2\right). \tag{53}$$

This relation is analogous to that obtained by MISRA and RADHAKRISHNA [6] and TIWARI [7] between the metric component g_{22} and the electromagnetic potential φ. It is, however, difficult to establish a theorem for generating solutions in Case (ii) directly as in the Case (i). In order to overcome this difficulty, following PERJÉS [8], we use the substitutions $\frac{e^{2\beta}}{\varrho}\varphi_1 = \psi_4$ and $\frac{e^{2\beta}}{\varrho}\varphi_4 = \psi_1$ which take over the field equations of Case (ii) to those of Case (i) for which the generation theorem has already been established. The above substitutions are indeed dual constructions and hence form a solution with the same g_{ij} according to the theorem given by BONNOR [9].

Acknowledgement

The authors are thankful to the Referee whose comments have improved the presentation of the paper.

REFERENCES

1. J. R. RAO, R. N. TIWARI and G. MOHANTY (to be published).
2. H. WEYL, Ann. Physik, **54**, 117, 1917.
3. S. D. MAJUMDAR, Phys. Rev., **72**, 390, 1947.
4. A. PAPAPETROU, Proc. R. Ir. Acad., **A51**, 191, 1947.
5. W. B. BONNOR, Proc. Phys. Soc., (Lond.) **66**, 145, 1953.
6. M. MISRA and L. RADHAKRISHNA, Proc. Nat. Acad. Sci. India, Part **A28**, 632, 1962.
7. R. N. TIWARI, Indian J. Pure Appl. Math., **10(3)**, 339, 1979.
8. Z. PERJÉS, Il Nouvo. Cim., **45B**, 600, 1968.
9. W. B. BONNOR, Proc. Phys. Soc. (Lond.), **A67**, 225, 1954.

Appendix

In a comoving coordinate system [i.e. $u_1 = u_2 = u_3 = 0$, $u_4 = (g^{44})^{-1/2}$] the surviving field equations (4) for the metric (1) are

$$\beta_1^2 + \beta_4^2 - \frac{\alpha_1}{\varrho} = -\frac{k}{4\pi} e^{2\alpha-2\beta} p - \\ - \frac{k}{8\pi} e^{2\alpha-2\beta} [F_{12}F^{12} + F_{13}F^{13} + F_{14}F^{14} - F_{23}F^{23} - F_{24}F^{24} - F_{34}F^{34}], \quad \text{(A.1)}$$

$$\alpha_{44} - \alpha_{11} + \beta_4^2 - \beta_1^2 = -\frac{k}{4\pi} e^{2\alpha-2\beta} p - \frac{k}{8\pi} e^{2\alpha-2\beta} [F_{12}F^{12} + F_{23}F^{23} + \\ + F_{24}F^{24} - F_{13}F^{13} - F_{14}F^{14} - F_{34}F^{34}], \quad \text{(A.2)}$$

$$2\beta_{11} - 2\beta_{44} - \alpha_{11} + \alpha_{44} - \beta_1^2 + \beta_4^2 + \frac{2}{\varrho}\beta_1 = -\frac{k}{4\pi} e^{2\alpha-2\beta} p - \\ - \frac{k}{8\pi} e^{2\alpha-2\beta} [F_{13}F^{13} + F_{23}F^{23} + F_{34}F^{34} - F_{12}F^{12} - F_{14}F^{14} - F_{24}F^{24}], \quad \text{(A.3)}$$

$$\beta_1^2 + \beta_4^2 - \frac{\alpha_1}{\varrho} = -\frac{k}{4\pi} e^{2\alpha-2\beta} w + \frac{k}{8\pi} e^{2\alpha-2\beta} [F_{14}F^{14} + F_{24}F^{24} + F_{34}F^{34} - \\ - F_{12}F^{12} - F_{13}F^{13} - F_{23}F^{23}], \quad \text{(A.4)}$$

$$2\beta_1\beta_4 - \frac{\alpha_4}{\varrho} = \frac{k}{8\pi} e^{2\alpha-2\beta} [F_{12}F^{42} + F_{13}F^{43}], \quad \text{(A.5)}$$

$$F_{12}F^{13} + F_{24}F^{34} = 0. \quad \text{(A.6)}$$

From Eqs. (A.1) and (A.4), we get

$$(w - p) - g^{11}g^{44}F_{14}^2 + g^{22}g^{33}F_{23}^2 = 0. \quad \text{(A.7)}$$

Since for the metric (1), g^{11}, g^{22}, g^{33} are negative and g^{44} is positive and for known physical distributions $w \geq p$, the above equation implies

$$w = p, \quad F_{14} = 0 \quad \text{and} \quad F_{23} = 0. \quad \text{(A.8)}$$

Using (A.8) in Eq. (7), we have

$$\sigma = 0, \quad (\text{since } u_4 \neq 0). \quad \text{(A.9)}$$

Since w, p, and σ are invariants, the conclusions $w = p$ and $\sigma = 0$, even though deduced in comoving coordinate system, will hold in all coordinate systems as they are invariant equations.

Acta Physica Academiae Scientiarum Hungaricae. Tomus 48 (4), pp. 425—437 (1980)

ANOMALOUS PROPAGATION OF PROBABILITY IN QUANTUM MECHANICS*

By

H. E. WILHELM

DEPARTMENT OF ENGINEERING SCIENCES, UNIVERSITY OF FLORIDA, GAINESVILLE, FLORIDA 32611, USA

and

S. H. HONG

DEPARTMENT OF NUCLEAR ENGINEERING, SEOUL NATIONAL UNIVERSITY, SEOUL, KOREA

(Received in revised form 18. IV. 1980)

The initial-value problem of the force-free Schrödinger equation is solved in closed-form for initial wave functions which are constrained to a finite region of space and improper boundary conditions at infinity. It is shown that the wave function and probability density propagate with infinite speed into the space. This is explained mathematically to be due to the parabolic nature of the Schrödinger equation. It is concluded that the Schrödinger equation gives a qualitatively not quite satisfactory description of the (time-dependent) propagation of probability densities due to the occurrence of infinite propagation speeds.

Introduction

In general, transient processes are described by hyperbolic or quasi-hyperbolic equations, e.g., the (linear) Maxwell equations which determine the propagation of electromagnetic signals in vacuum or the (nonlinear) compressible hydrodynamic equations which determine the propagation of shock waves in gases. The parabolic equations for the diffusion of particles and heat are approximate equations assuming proportionality of fluxes and diffusion forces (disregarding the inertia of the molecules) which exhibit physical and mathematical deficiencies [1, 2]. From the physical point of view, the essential difference between hyperbolic and parabolic equations is that they propagate signals with finite and infinite speed, respectively [1, 2]. Since real processes propagate with finite speed, a proper physical description cannot be achieved by means of (quasi-) parabolic equations.

As a brief quantitative illustration to the nature of hyperbolic and parabolic solutions, consider the initial-value problems for the one-dimensional diffusion of particles concentrated initially in the plane $x = 0$ with a density $n(x, 0) = \overline{n}_0 \delta(x)$ based on [2]

i) Hyperbolic Diffusion Theory:

$$\partial^2 n/\partial t^2 + \tau^{-1} \partial n/\partial t = c^2 \partial^2 n/\partial x^2 ,$$

* Supported by the U.S. Office of Naval Research.

$$n(x, 0) = \bar{n}_0 \delta(x),$$
$$\partial n(x, 0)/\partial t = 0$$

and

ii) Parabolic Diffusion Theory:

$$\partial n/\partial t = D\partial^2 n/\partial x^2,$$
$$n(x, 0) = \bar{n}_0 \delta(x),$$
$$n(x, t) \to 0, \; |x| \to \infty,$$

where the diffusion coefficient (D), speed of sound (c), and momentum relaxation time (τ) are interrelated by $D = c^2\tau$. Case i) reduces to case ii) in the limit $\tau \to 0$, $c \to \infty$, such that $c^2\tau \to D$, $0 < D < \infty$. The corresponding solutions are:

$$\begin{aligned} n(x, t) = \frac{1}{2} \bar{n}_0 \exp(-t/2\tau) \{ & \delta(x - ct) + \delta(x + ct) + \\ & + (t/2\tau)[c^2 t^2 - x^2]^{-1/2} I_1([c^2 t^2 - x^2]^{1/2}/2c\tau) + \\ & + (1/2c\tau) I_0([c^2 t^2 - x^2]^{1/2}/2c\tau)\}, \quad |x| < ct, \\ & = 0, \qquad\qquad |x| > ct, \end{aligned} \tag{i}$$

and

$$n(x, t) = \bar{n}_0 (4\pi Dt)^{-1/2} \exp(-x^2/4Dt), \qquad |x| \leq \infty. \tag{ii}$$

It is seen that the hyperbolic solution (i) propagates the particles with a maximum, finite speed c such that discontinuous wave fronts exist at $x = \pm ct$ at any time $t < \infty$ and the initial discontinuity $n(x, 0) = \bar{n}_0 \delta(x)$ is moved with finite speed c symmetrically into the space $|x| < \infty$. On the other hand, the parabolic solution (ii) propagates particles with infinite speed, $c = \infty$, such that, at any time $t > 0$, a continuous particle distribution extends up to $|x| = \infty$ and the initial discontinuity is smoothed out quasi-instantaneously. By means of the asymptotic expansions for the modified Bessel functions $I_0(x)$ and $I_1(x)$ one can show that Eq. (i) reduces to Eq. (ii) in the limit $\tau \to 0$ with $c^2\tau \to D$ for all points $|x| < ct$, i.e. not for the space $|x| > ct$.

The common designation of the Schrödinger equation as a "wave equation" is misleading since it suggests a hyperbolic type. Even Schrödinger, in comparing his equation with the parabolic diffusion equation, states [3]: "In both cases, the differential equation is of first order in time, but the occurrence of the factor $\sqrt{-1}$ gives the wave equation a hyperbolic, or physically spoken, a reversible character, as distinguished from the parabolic- irreversible character of the Fokker-Planck equation." The mathematical type of the

time-dependent Schrödinger equation is determined by the coefficients of the spatial derivatives of second order [4], according to which it is a parabolic equation. A first attempt at hyperbolizing the Schrödinger equation by means of a pure mathematical approach [5] has lead to a wave equation with complex, energy-dependent coefficients, which reduces in limiting cases to the Lorentz and Galilei covariant equations of Klein—Gordon and Schrödinger, respectively.

In view of the parabolic nature of the time-dependent Schrödinger equation, "wave" functions $\psi = \psi(\mathbf{r}, t)$ and probability densities $\varrho = \psi\psi^*$, which are initially ($t = 0$) limited to a finite region in space, will spread quasi-instantaneously over the infinity of space after an arbitrary short time $t > 0$. In the following, we will discuss quantitatively the time and space dependent spreading of wave functions and probability densities based on the nonrelativistic Schrödinger equation. For this purpose, we will evaluate a basic Cauchy problem for the Schrödinger equation with the initial value limited to a finite region in space.

Initial-value problem

The spreading of ψ-waves has been analyzed based on an initial wave function which corresponds to a Gaussian probability density ("wave packet") [6]. Since this type of initial distribution ($t = 0$) extends from $x = -\infty$ to $x = +\infty$, all subsequent ($t > 0$) wave functions extend from $x = -\infty$ to $x = +\infty$, no matter whether these are described by a parabolic or hyperbolic wave equation.

In order to deduce a physically familiar, spatially limited initial condition for the wave function, consider first a particle of mass m which is constrained to the region $-a \leq x \leq +a$ by a potential $V(x) = 0$ for $|x| < a$ and $V(x) = \infty$ for $a < |x| < a + \Delta$, with $\Delta > 0$ (ideal one-dimensional box) [6]. The complex wave functions for the state n of the particle in the box are in dimensionless, normalized form [6]:

$$\psi_n(\xi, \tau) = e^{-i\varepsilon_n \tau} \cos \alpha_n \xi\,, \quad |\xi| < 1,\ n = 1, 3, 5, \ldots, \tag{1}$$

$$\psi_n(\xi, \tau) = e^{-i\varepsilon_n \tau} \sin \alpha_n \xi,\ \ |\xi| < 1,\ n = 2, 4, 6, \ldots, \tag{2}$$

where

$$\alpha_n = (\pi/2)n\,, \quad \varepsilon_n = \frac{1}{2}\alpha_n^2, \tag{3}$$

are the dimensionless eigenvalues and energy levels of the particle, respectively. The dimensionless (ψ, ξ, τ) and dimensional (Ψ, x, t) variables are interrelated by

$$\xi = x/a, \quad \tau = t/(ma^2/\hbar)\,, \quad \psi = a^{1/2}\Psi. \tag{4}$$

The solutions (1) and (2) represent symmetrical and asymmetrical "oscillations" of the complex wave function $\psi_n(\xi, \tau)$ with respect to the central plane $\xi = 0$. The probability density ϱ_n and velocity $\mathbf{v}_n$ fields of the box particle, however, are time-independent fields[7]

$$\varrho_n = \psi_n \psi_n^* = \cos^2 \alpha_n \xi\,, \quad |\xi| < 1, \quad n = 1, 3, 5, \ldots, \tag{5}$$

$$\varrho_n = \psi_n \psi_n^* = \sin^2 \alpha_n \xi\,, \quad |\xi| < 1, \quad n = 2, 4, 6, \ldots, \tag{6}$$

$$\mathbf{v}_n = (\hbar/m) \nabla \Phi_n = 0, \qquad |\xi| < 1, \quad \Phi_n = -i\varepsilon_n \tau\,. \tag{7}$$

If the potential walls $V(\xi = \pm 1 \pm 0) = \infty$, are removed at time $\tau = 0$, the particle will move out of the box $|\xi| < 1$, i.e. either to the left ($\xi < -1$) or to the right ($\xi > +1$) with equal probability, since the box geometry is symmetric with respect to the plane $\xi = 0$. This follows directly from the uncertainty principle, according to which the particle in the box has in state n a (dimensional) momentum uncertainty [7]

$$\pm \Delta p_n = \pm \frac{1}{2} \hbar (n\pi/2) a^{-1}. \tag{8}$$

The propagation of the wave function $\psi(\xi, \tau)$ out of the box $|\xi| < 1$ into the infinite space $|\xi| \leq \infty$ is described by the (dimensionless) initial-value problem for the force-free Schrödinger equation:

$$\frac{\partial \psi}{\partial \tau} = \frac{i}{2} \frac{\partial^2 \psi}{\partial \xi^2}\,, \tag{9}$$

$$\psi(\xi, 0) = \psi_n^0(\xi)\,, \tag{10}$$

$$\psi(\xi, \tau) \to 0\,, \quad |\xi| \to \infty\,, \tag{11}$$

where

$$\psi_n^0(\xi) = H(1 - |\xi|) \begin{matrix} \cos \alpha_n \xi \\ , \\ \sin \alpha_n \xi \end{matrix}, \quad n = \begin{matrix} 1, 3, 5, \ldots \\ \\ 2, 4, 6, \ldots \end{matrix} \tag{12}$$

and $H(1 - |\xi|) = 1$; 0 for $|\xi| < 1$; >1 (Heaviside function). Eqs. (9)—(11) represent a Cauchy problem for proper initial conditions (10), since only improper boundary conditions (11) exist.

The initial conditions have been assumed in the form of Eq. (12), in order to relate the initial state to the familiar physical situation of a particle in a box. It should be noted, however, that an initial value $\psi_n^0(\xi)$ could have been chosen, which is any arbitrary function of ξ, compatible with the uncertainty principle. For any initial condition different from Eq. (12), the calculations are analogous to those to be presented.

Analytical solution

The general solution of the initial-value problem (9)—(11) is represented by a Fourier integral for the space $|\xi| \leq \infty$. This approach gives, for an arbitrary initial condition $\psi_n^0(\xi)$, a solution of Eqs. (9)—(11) in the form:

$$\psi(\xi, \tau) = \int_{-\infty}^{+\infty} \psi_n^0(\xi') G(\xi, \xi', \tau) d\xi', \tag{13}$$

where

$$G(\xi, \xi', \tau) = (-i/2\pi\tau)^{1/2} e^{-i(\xi'-\xi)^2/2\tau} \tag{14}$$

is the Green's function of Eq. (9) for the improper boundary conditions (11). Substitution of the initial conditions (12) into Eq. (13) yields the solutions

$$\psi(\xi, \tau) = \frac{1}{2}(-i/2\pi\tau)^{1/2} \int_{-1}^{+1} (e^{+i\alpha_n\xi'} + e^{-i\alpha_n\xi'}) e^{i(\xi'-\xi)^2/2\tau} d\xi', \quad n = 1, 3, 5, \ldots, \tag{15}$$

$$\psi(\xi, \tau) = \frac{1}{2i}(-i/2\pi\tau)^{1/2} \int_{-1}^{+1} (e^{+i\alpha_n\xi'} - e^{-i\alpha_n\xi'}) e^{i(\xi'-\xi)^2/2\tau} d\xi', \quad n = 2, 4, 6, \ldots, \tag{16}$$

for the wave functions with symmetric ($n = 1, 3, 5, \ldots$) and asymmetric ($n = 2, 4, 6, \ldots$) initial values, respectively. The integrals in Eqs. (15)—(16) are

$$J_n^{\pm}(\xi) = \int_{-1}^{+1} e^{\pm i\alpha_n\xi' + i(\xi'-\xi)^2/2\tau} d\xi', \tag{17}$$

i.e.

$$J_n^{\pm}(\xi)/[\pi^{1/2}\tau^{1/2} e^{\pm i\alpha_n\xi - i\alpha_n^2\tau/2}] =$$
$$= C([1 - \xi \pm \alpha_n\tau]\pi^{-1/2}\tau^{-1/2}) + C([1 + \xi \mp \alpha_n\tau]\pi^{-1/2}\tau^{-1/2}) +$$
$$+ i\{S([1 - \xi \pm \alpha_n\tau]\pi^{-1/2}\tau^{-1/2}) + S([1 + \xi \mp \alpha_n\tau]\pi^{-1/2}\tau^{-1/2})\}, \tag{18}$$

where

$$C(z) = \int_0^z \cos\frac{\pi}{2}x^2 dx, \quad C(-z) = -C(+z), \tag{19}$$

$$S(z) = \int_0^z \sin\frac{\pi}{2}x^2 dx, \quad S(-z) = -S(+z), \tag{20}$$

are the Fresnel integrals which have the series representations [8],

$$C(z) = \cos\left(\frac{\pi}{2}z^2\right) \sum_{\nu=0}^{\infty} \frac{(-1)^\nu \pi^{2\nu}}{(1 \cdot 3 \ldots (4\nu+1))} z^{4\nu+1} +$$
$$+ \sin\left(\frac{\pi}{2}z^2\right) \sum_{\nu=0}^{\infty} \frac{(-1)^\nu \pi^{2\nu+1}}{1 \cdot 3 \ldots (4\nu+3)} z^{4\nu+3}, \tag{21}$$

$$S(z) = -\cos\left(\frac{\pi}{2}z^2\right)\sum_{\nu=0}^{\infty}\frac{(-1)^\nu\,\pi^{2\nu+1}}{1\cdot 3\ldots(4\nu+3)}z^{4\nu+3} + \\ + \sin\left(\frac{\pi}{2}z^2\right)\sum_{\nu=0}^{\infty}\frac{(-1)^\nu\,\pi^{2\nu}}{1\cdot 3\ldots(4\nu+1)}z^{4\nu+1}. \tag{22}$$

$C(z) \geq 0$ and $S(z) \geq 0$ are functions which oscillate with decreasing amplitude about their asymptotic values $C(\infty) = 1/2$ and $S(\infty) = 1/2$, respectively [8]. For a convenient representation, the final results are expressed in terms of the functions,

$$P_n(\xi,\tau) = C([1-\xi+\alpha_n\tau]\,\pi^{-1/2}\,\tau^{-1/2}) + C([1+\xi-\alpha_n\tau]\,\pi^{-1/2}\,\tau^{-1/2}), \tag{23}$$

$$Q_n(\xi,\tau) = C([1-\xi-\alpha_n\tau]\,\pi^{-1/2}\,\tau^{-1/2}) + C([1+\xi+\alpha_n\tau]\,\pi^{-1/2}\,\tau^{-1/2}), \tag{24}$$

$$M_n(\xi,\tau) = S([1-\xi+\alpha_n\tau]\,\pi^{-1/2}\,\tau^{-1/2}) + S([1+\xi-\alpha_n\tau]\,\pi^{-1/2}\,\tau^{-1/2}), \tag{25}$$

$$N_n(\xi,\tau) = S([1-\xi-\alpha_n\tau]\,\pi^{-1/2}\,\tau^{-1/2}) + S([1+\xi+\alpha_n\tau]\,\pi^{-1/2}\,\tau^{-1/2}), \tag{26}$$

which have the properties,

$$\begin{aligned} P_n(\xi,\tau=0),\ldots,N_n(\xi,\tau=0) &= 1\,, \qquad |\xi|<1\,,\\ &= 0\,, \qquad |\xi|>1\,, \end{aligned} \tag{27}$$

$$P_n(\xi=\infty,\tau),\ldots,N_n(\xi=\infty,\tau) = 0\,, \qquad 0\leq\tau<\infty\,, \tag{28}$$

and

$$P_n(\xi,\tau>0),\ldots,N_n(\xi,\tau>0) > 0, \qquad |\xi|<\infty\,. \tag{29}$$

Substitution of the integrals (18) into Eqs. (15) and (16) gives the closed-form solutions for the wave functions $\psi(\xi,\tau)$ and their probability densities $\varrho(\xi,\tau) = \psi\psi^*$ for the symmetrical ($n = 1, 3, 5, \ldots$) and asymmetrical ($n = 2, 4, 6, \ldots$) initial conditions, respectively:

$$\psi(\xi,\tau) = \frac{1}{2}(\mp i/2)^{1/2}\,e^{-i\alpha_n^2\tau/2}\quad\{e^{+i\alpha_n\xi}\,[P_n(\xi,\tau)+iM_n(\xi,\tau)]\pm \\ \pm e^{-i\alpha_n\xi}\,[Q_n(\xi,\tau)+iN_n(\xi,\tau)]\},\quad n = \begin{matrix}1,3,5,\ldots\\2,4,6,\ldots\end{matrix} \tag{30}$$

and

$$\varrho(\xi,\tau) = \frac{1}{8}[P_n(\xi,\tau)\mp Q_n(\xi,\tau)]^2 + \frac{1}{8}[M_n(\xi,\tau)\mp N_n(\xi,\tau)]^2 \pm \\ \pm\frac{1}{2}[P_n(\xi,\tau)N_n(\xi,\tau) - Q_n(\xi,\tau)\,M_n(\xi,\tau)]\sin\alpha_n\xi\cos\alpha_n\xi \pm \\ \pm\frac{1}{2}[P_n(\xi,\tau)\,Q_n(\xi,\tau)+M_n(\xi,\tau)\,N_n(\xi,\tau)]\cos^2\alpha_n\xi,\quad n = \begin{matrix}1,3,5,\ldots\\2,4,6,\ldots\end{matrix} \tag{31}$$

In Eqs. (30)—(31), the upper sign refers to the symmetrical initial values $\psi_n^0(\xi)$, $n = 1, 3, 5, \ldots$, and the lower sign refers to the asymmetrical initial values $\psi_n^0(\xi)$, $n = 2, 4, 6, \ldots$ [s. Eq. (12)].

By means of the discontinuous property (28) of the functions $P_n(\xi, \tau)$, $\ldots$, $N_n(\xi, \tau)$ it is readily demonstrated that the solutions (30) and (31) satisfy the initial conditions

$$\psi(\xi, \tau = 0) = \begin{matrix} \cos \alpha_n \xi \\ \sin \alpha_n \xi \end{matrix}, \quad |\xi| < 1,$$
$$= 0, \qquad |\xi| > 1, \tag{32}$$

$$\varrho(\xi, \tau = 0) = \begin{matrix} \cos^2 \alpha_n \xi \\ \sin^2 \alpha_n \xi \end{matrix}, \quad |\xi| < 1,$$
$$= 0, \qquad |\xi| > 1, \tag{33}$$

Finally, the solutions (30) and (31) satisfy the improper boundary conditions at $\xi = \infty$ in view of the limits (28) of the functions $P_n(\xi, \tau), \ldots, N_n(\xi, \tau)$

$$\psi(\xi, \tau) \to 0, \quad |\xi| \to \infty, \quad 0 \leq \tau < \infty, \tag{34}$$
$$\varrho(\xi, \tau) \to 0, \quad |\xi| \to \infty, \quad 0 \leq \tau < \infty. \tag{35}$$

Discussion

In view of the parabolic nature of the time-dependent Schrödinger equation (9), we expect that the signals $\psi(\xi, \tau)$ or $\varrho(\xi, \tau)$ propagate from the initial region $|\xi| < 1$ into the adjacent space $|\xi| > 1$ with infinite speed. Indeed, the solutions (30) and (31) demonstrate that $\psi(\xi, \tau)$ and $\varrho(\xi, \tau)$ extend, continuously, from $\xi = -\infty$ to $\xi = +\infty$ after any, no matter how short, time $\tau > 0$, i.e.

$$|\psi(\xi, \tau > 0)| \geq 0, \quad \varrho(\xi, \tau > 0) \geq 0, \quad \text{for} \quad |\xi| < \infty, \tag{36}$$

where the equal signs hold only for those points ξ where $|\psi(\xi, \tau)|$ and $\varrho(\xi, \tau)$ touch tangentially the ξ-axis. This means that the distributions $\psi(\xi, \tau)$ and $\varrho(\xi, \tau)$ spread quasi-instantaneously over the entire space $|\xi| \leq \infty$. Since physical phenomena can propagate only with finite speed, it must be concluded that the time-dependent Schrödinger equation provides a misleading and insufficient description of proper time-dependent microprocesses.

In the following illustrations, it is $\varrho(-\xi, \tau) = \varrho(+\xi, \tau)$ for symmetry reasons. Fig. 1 gives plots of the initial probability density $\varrho(\xi, 0)$ versus

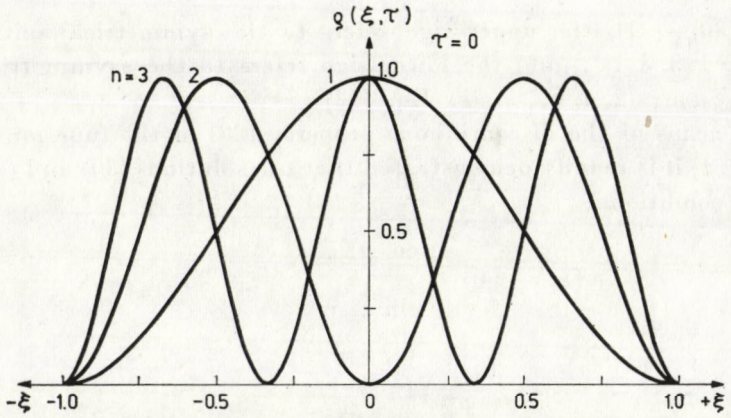

Fig. 1. $\varrho(\xi, \tau)$ versus ξ for $\tau = 0$ and $n = 1; 2; 3$

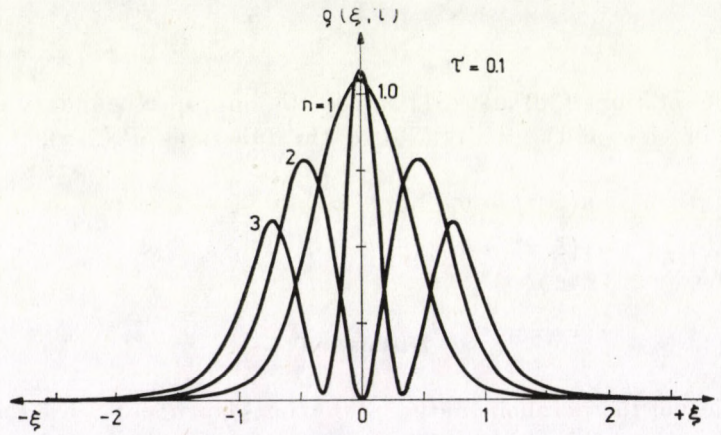

Fig. 2. $\varrho(\xi, \tau)$ versus ξ for $\tau = 10^{-1}$ and $n = 1; 2; 3$

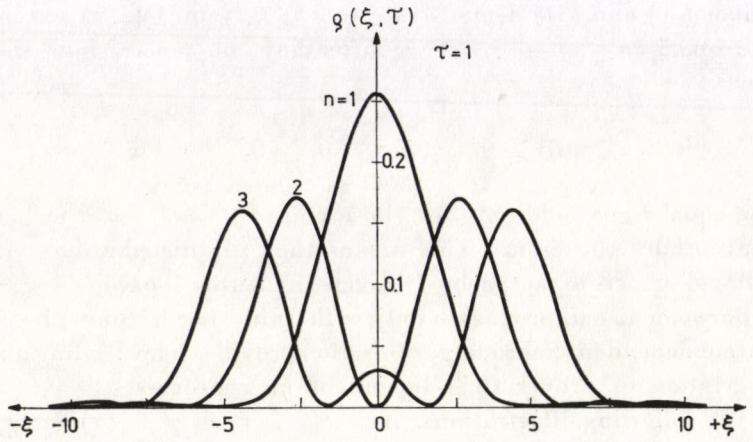

Fig. 3. $\varrho(\xi, \tau)$ versus ξ for $\tau = 10^{0}$ and $n = 1; 2; 3$

$|\xi| \geq 0$ for the states $n = 1, 2, 3$, which is non-zero only in the region $|\xi| < 1$, i.e. $\varrho(\xi, 0) = 0$ for $|\xi| \geq 1$.

Figs. 2—4 give the probability densities $\varrho(\xi, \tau)$ versus $|\xi| \geq 0$ for $n = 1, 2, 3$ at the times $\tau = 10^{-1}$, 10^{0}, and 10^{1}, respectively. In each case $\varrho(\xi, \tau)$ extends over the entire space $|\xi| \leq \infty$. In the case of the initial state $n = 1$, $\varrho(\xi, 0)$ has a single maximum which stays at $\xi = 0$, while the entire distribution $\varrho(\xi, \tau)$ diffuses into the space $|\xi| \leq \infty$ with decreasing height as time τ increases. In the case of the initial state $n = 2$, $\varrho(\xi, 0)$ has two maxima at $\xi = \pm 1/2$, which move with finite speed and decreasing height into the half-spaces $\xi < 0$ and $\xi > 0$, respectively, as time τ increases. In the case of the initial state $n = 3$, $\varrho(\xi, 0)$ has three maxima at $\xi = 0$ and $\xi = \pm 2/3$. With increasing time τ, the maximum at $\xi = 0$ remains at $\xi = 0$ and decreases

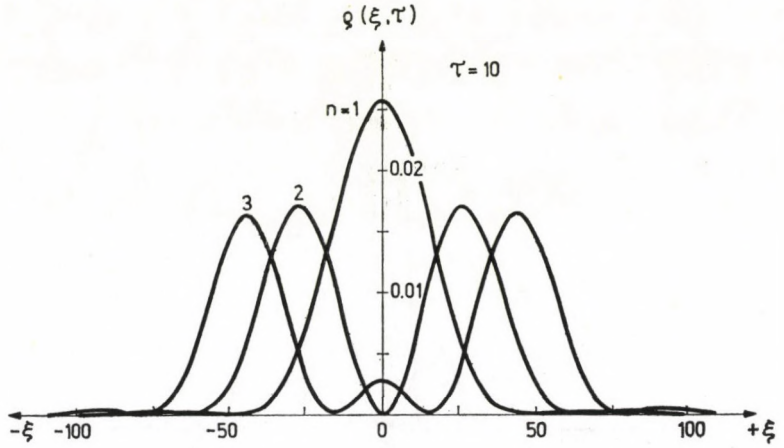

Fig. 4. $\varrho(\xi, \tau)$ versus ξ for $\tau = 10^{1}$ and $n = 1; 2; 3$

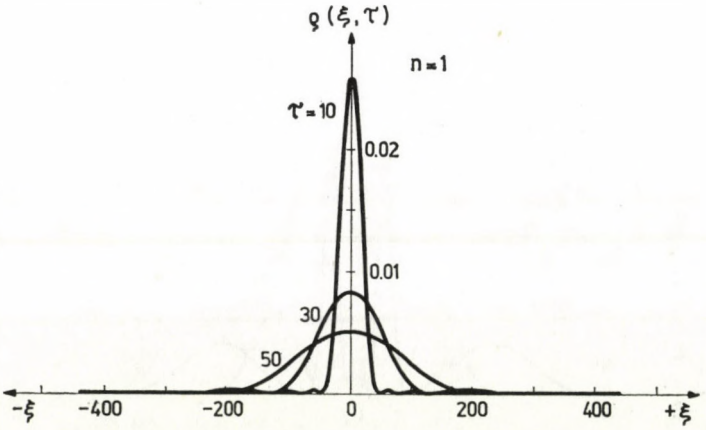

Fig. 5. $\varrho(\xi, \tau)$ versus ξ for $\tau = 10; 30; 50$ and $n = 1$

in amplitude, whereas the maxima initially at $\xi = \pm 2/3$ propagate with finite speed and decreasing amplitudes into the half-spaces $\xi < 0$ and $\xi > 0$, respectively. In addition to the main maxima present at $\tau \geq 0$, the distributions $\varrho(\xi, \tau)$ exhibit secondary maxima of relatively small amplitude at times $\tau > 0$. In each case, the diffusion of the probability distributions $\varrho(\xi, \tau)$ leaves the total probability conserved,

$$\int_{-\infty}^{+\infty} \varrho(\xi, \tau) d\xi = 1, \quad 0 \leq \tau \leq \infty \,. \tag{37}$$

Figs. 5—7 present the probability densities $\varrho(\xi, \tau)$ versus $|\xi| \geq 0$ at the successive times $\tau = 10$, 30, 50 for the initial states $n = 1, 2$, and 3, respectively. In each case, $\varrho(\xi, \tau)$ extends over the entire space $|\xi| \leq \infty$. Fig. 5 ($n = 1$) shows how the main maximum at $\xi = 0$ decreases and $\varrho(\xi, \tau)$

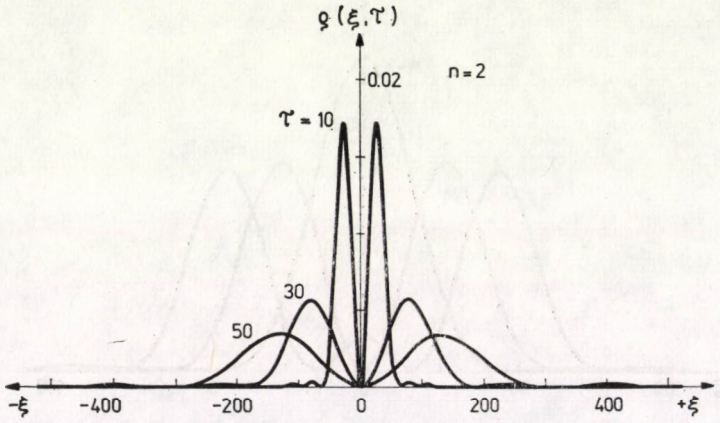

Fig. 6. $\varrho(\xi, \tau)$ versus ξ for $\tau = 10$; 30; 50 and $n = 2$

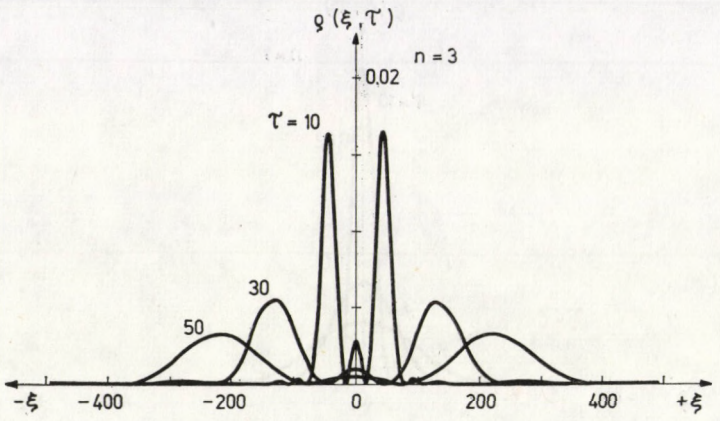

Fig. 7. $\varrho(\xi, \tau)$ versus ξ for $\tau = 10$; 30; 50 and $n = 3$

becomes flatter with increasing time τ. Fig. 6 ($n = 2$) shows the temporal decrease of the distribution $\varrho(\xi, \tau)$ with two main maxima, which propagate with decreasing height into the space $|\xi| > 0$ as time τ increases. Fig. 6 ($n = 3$) shows the temporal decrease of the distribution $\varrho(\xi, \tau)$ with three maxima. The two off-center maxima propagate with finite speed and decreasing amplitude into the space $|\xi| \leq \infty$, whereas the central maximum remains at $\xi = 0$ and loses rapidly in height as τ increases.

The dimensionless speed U_n with which the (main) off-center ($\xi \neq 0$) maxima of the probability distribution $\varrho(\xi, \tau)$ move into the space $|\xi| \leq \infty$ is by Eq. (31)

$$U_n = \frac{\Delta\xi}{\Delta\tau} = \frac{\pi}{2} n, \quad n = 2, 3, 4, \ldots . \tag{38}$$

Accordingly, at time τ the (main) off-center maxima of $\varrho(\xi, \tau)$ are in the half spaces $\xi < 0$ $(-)$ and $\xi > 0$ $(+)$ at the locations

$$\pm\hat{\xi} = \hat{\xi}_0(n) + \frac{\pi}{2} n\tau , \quad n = 2, 3, 4, \ldots , \tag{39}$$

where $\pm\hat{\xi}_0(n) \neq 0$ are the dimensionless positions of the off-center maxima at time $\tau = 0$. By Eq. (31), the value $\hat{\varrho}(\hat{\xi}, \tau)$ of the off-center maxima is independent of the state n at large times,

$$\hat{\varrho}(\hat{\xi}, \tau) \cong 1/2\pi\tau, \quad n = 2, 3, 4, \ldots, \quad \alpha_n \tau \gg 1 . \tag{40}$$

The value $\hat{\varrho}(0, \tau)$ of the central maxima is by Eq. (31) for arbitrary times,

$$\hat{\varrho}(0, \tau) = \frac{1}{2} [P_n^2(0, \tau) + M_n^2(0, \tau)], \quad n = 1, 3, 5, \ldots, \quad \tau \geq 0 , \tag{41}$$

i.e.

$$\hat{\varrho}(0, \tau) \cong 0, \quad n = 1, 3, 5, \ldots, \quad \alpha_n \tau \gg 1 \tag{42}$$

in the asymptotic approximation of Eq. (40). Eqs. (40) and (42) indicate that the central ($\hat{\xi} = 0$) maxima decay much faster than the off-center ($\hat{\xi} \neq 0$) maxima.

The characteristic (dimensional) time scale of the quantum mechanical diffusion process is by Eq. (4)

$$t_0 = ma^2/\hbar . \tag{43}$$

As a numerical illustration, it is noted that the characteristic length scale [Eq. (4)] is a $\sim 10^{-8}$ cm for microscopic systems and a $\sim 10^{0}$ cm for macro-

scopic systems. Hence, $t_0 \sim 10^{-16}$ s for a microscopic system and $t_0 \sim 10^0$ s for a macroscopic system in case of an electron or positron ($m = 9.108 \times \times 10^{-28}$ gm). The corresponding speeds with which the main maxima of $\varrho(\xi, \tau)$ propagate are $u_n \sim 10^8\ n$ cm/s for $a = 10^{-8}$ cm and $u_n \sim 10^0\ n$ cm/s for $a = 10^0$ cm by Eq. (38) where $n = 2, 3, 4, \ldots$. It is seen that u_n is nonrelativistic for microscopic β-particle systems with $n \leq 10$.

As main conclusions, it is noted that the time-dependent Schrödinger equation spreads quantum-mechanical probability with infinite speed over space, as typical for a partial differential equation of parabolic type. The time-dependent Schrödinger equation provides, therefore, a physically not quite correct description of transient microprocesses. Since the maxima of the probability density propagate with finite speed, the time-dependent Schrödinger equation describes transient microsystems in some approximation (similar to the parabolic equation for classical diffusion processes).

By transient quantum systems or processes we mean those which have a wave function

$$\psi(\mathbf{r}, t) = R(\mathbf{r}, t)\, e^{i\Phi(\mathbf{r}, t)} \tag{44}$$

of such $\mathbf{r}$ and t dependence that the density field ϱ and the velocity field $\mathbf{v}$ are time-dependent, where [7]

$$\varrho(\mathbf{r}, t) = R^2(\mathbf{r}, t), \quad \mathbf{v}(\mathbf{r}, t) = (\hbar/m)\, \nabla\Phi(\mathbf{r}, t)\,. \tag{45}$$

Improper time-dependent quantum systems have time-dependent wave functions of the form $\psi(\mathbf{r}, t) = R(\mathbf{r}) \exp[i\omega t + i\varphi(\mathbf{r})]$ so that $\varrho = R^2(\mathbf{r})$ and $\mathbf{v} = (h/m)\, \nabla\varphi(\mathbf{r})$ are time-independent. In the (nonlinear) hydrodynamic formulation of quantum mechanics, the fields $\varrho(\mathbf{r})$ and $\mathbf{v}(\mathbf{r})$ are obtained as solutions of the steady-state ($\partial/\partial t = 0$!) quantum hydrodynamic equations [7], whereas the steady-state Schrödinger equation with $\partial/\partial t = 0$ appears to have no physical meaning, i.e.

$$-(\hbar^2/2m)\, \nabla^2\psi + V(\mathbf{r})\, \psi = i\hbar\partial\psi/\partial t \neq 0\,, \tag{46}$$

where $V(\mathbf{r})$ is the potential energy. According to EINSTEIN [9] the complex (unreal) time-dependent wave function is nothing else but an ingeneous mathematical means for solving nonlinear steady-state quantum problems. Thus, for so-called quasi-stationary quantum systems (particle in box, hydrogen atom, harmonic oscillator, etc. [6]) with discrete energy eigenvalues, the Schrödinger equation gives (nonrelativistically) correct results, since the latter systems are true steady-state systems in the hydrodynamic picture of quantum mechanics [7].

Any space-time dependent function $f(x, t)$ satisfying the Dirichlet condition, including the probability density $\varrho(x, t)$, is representable as a Fourier integral in k or ω space,

$$f(x, t) = \int_{-\infty}^{+\infty} f_k(t)\, e^{ikx}\, dk\,, \tag{47}$$

or

$$f(x, t) = \int_{-\infty}^{+\infty} f_\omega(x)\, e^{i\omega t}\, d\omega\,. \tag{48}$$

From the occurrence of infinite wave numbers $k = \pm\infty$ and infinite frequencies $\omega = \pm\infty$ in Eqs. (47) and (48), respectively, it cannot be concluded that the signal $f(x, t)$ propagates with infinite speed. Whether the solution $f(x, t)$ propagates with finite or infinite speed depends on the type of partial differential equation $f(x, t)$ has to satisfy, e.g., the propagation speed is i) $c < \infty$ and ii) $c = \infty$ for hyperbolic and parabolic equations, respectively.

The Klein—Gordon and Dirac equations are hyperbolic and propagate wave signals $\psi(x, t)$ with the finite speed of light, c_0. However, because the former gives probability densities $\varrho(x, t) \lesseqgtr 0$ and the latter gives particle and antiparticle states $\varepsilon \gtreqless 0$, a simple one-particle probability interpretation of the wave function exists no longer. Thus the relativistic wave equations do not actually resolve the fundamental difficulty $c = \infty$ of the one-particle Schrödinger equation.

Within the hydrodynamic formulation of quantum mechanics [7], numerical solutions for transient probability densities were given by WEIMER and ASKAR [10—11]. The purpose of the present communication was to show quantitatively the paradoxial propagation of probability with infinite speed by solving analytically typical initial-value problems of the Schrödinger equation. The problem arose in connection with the short-time interaction of electrons in high density plasmas [12].

REFERENCES

1. L. D. LANDAU and E. M. LIFSCHITZ, Mechanics of Continuous Media, Pergamon, New York, 1953.
2. H. E. WILHELM and S. H. CHOI, J. Chem. Phys., **63**, 2119, 1975.
3. E. SCHRÖDINGER, S. Ber. Berlin Akad., 1930, p. 400.
4. A. SOMMERFELD, Partial Differential Equations of Mathematical Physics, Academic Press, New York, 1964.
5. F. BORGHESE, P. DENTI and T. RUGGERI, Int. J. Theor. Phys., **9**, 55, 1974.
6. L. I. SCHIFF, Quantum Mechanics, McGraw-Hill, New York, 1955.
7. L. JÁNOSSY and M. ZIEGLER, Acta Phys. Hung., **16**, 37, 1963.
8. M. ABRAMOWITZ and I. STEGUN, Handbook of Mathematical Functions, Dover, New York, 1965.
9. A. EINSTEIN, Letter to M. Born (1948).
10. J. H. WEIMER and A. ASKAR, J. Chem. Phys., **54**, 3534, 1971.
11. J. H. WEIMER and A. ASKAR, J. Chem. Phys., **54**, 1108, 1971.
12. R. BECKER and F. SAUTER, Quantum Theory of Atoms and Radiation / G. Teubner, Stuttgart, 1959.

Acta Physica Academiae Scientiarum Hungaricae, Tomus 48 (4), pp. 439—448 (1980)

POINCARÉ'S PRINCIPLE DETERMINES THE BEHAVIOUR OF MOVING PARTICLES AND CLOCKS

By

P.-A. IVERT

MATHEMATICAL INSTITUTE, RUHR UNIVERSITY, D-4630 BOCHUM, FRG

and

T. SJÖDIN

TONELLI MATHEMATICAL INSTITUTE, I-56100 PISA, ITALY

(Received 18. IV. 1980)

The behaviour of particles and clocks moving inertially in the physical vacuum is investigated. It is found that Poincaré's principle about the impossibility to detect absolute motion together with assumptions about the homogeneity of space and time and the isotropy of space leave only two possibilities open: *Either* all fundamental interactions are of ballistic nature and moving particles and clocks undergo no change of dimension respectively rate, *or* all fundamental interactions are of wavelike nature, no signal velocity higher than the common wave velocity c exists, moving particles undergo no transversal change of dimension but a contraction in the direction of motion by the factor $\sqrt{1 - w^2/c^2}$, and moving clocks are slowed down by the same factor.

1. Introduction

The purpose of the present paper is to derive the functions describing the behaviour of particles and clocks moving inertially with respect to the physical vacuum ("ether"). To this end we will, in addition to the usual assumptions about homogeneity of space and time and isotropy of space, use Poincaré's principle about the impossibility to detect absolute motion. From these assumptions we will arrive at two possibilities: either all fundamental interactions are of ballistic nature and moving particles undergo no change of dimensions and moving clocks no change of rate, or there exist waves in the ether, all these travel at the same velocity and moving particles undergo no transversal contraction but a contraction in the direction of motion given by the factor $\sqrt{1-w^2/c^2}$, and moving clocks are slowed down by the same factor. Here w denotes the velocity of the moving object and c the velocity of the waves in the ether. The possibility of signal velocities (in the ether) higher than the wave velocity c is ruled out.

Poincaré's principle is basic for our work. We therefore find convenient to state it explicitly in the form that we will use it:

Poincaré's Principle: It is impossible to detect motion with respect to the ether ("absolute motion"). In other words: there is no way for an inertial observer to ascertain if he is at rest with respect to the preferred system, or not.

This principle was probably first considered by POINCARÉ in 1895 (cf. KESWANI [1]). For the reader not acquainted to newer investigations in ether theory we refer to the work of PODLAHA [2]. See also SJÖDIN [3].

The plan of the paper is as follows: In Section Two we will deduce some fundamental identities for the above-mentioned functions. These identities will in the third Section be transformed into a system of ordinary differential equations, which will be solved. In Section Four a physical interpretation of a parameter characterizing the deduced functions will be given. The paper is ended with a conclusion and a discussion of the present work in connection with related work.

2. The basic relations

In this Section we will arrive at the point from which most authors depart, namely at the proposition that the functions determining the behaviour of moving particles and clocks as observed from an arbitrary inertial system S will have the same form as in the privileged system S_0. This we will do with the help of Poincaré's principle and assumptions about the homogeneity of space and time and the isotropy of space. In order to simplify the discussion somewhat, we will only consider a two-dimensional space. The extension to three dimensions presents no problem.

Our aim is to determine the factors Φ, ψ, and Ω, describing respectively the change of dimension of a moving particle in the direction of motion, the change of dimension in the transversal direction, and the change of rate of a moving clock. We may exploit our assumptions about the *homogeneity of space and time* in assuming Φ, Ψ, and Ω to be independent of the time and space coordinates. Sometimes [4] it is also assumed that these functions do not depend on whether the objects in question are accelerated or not. To minimize assumptions, we will not do this here. However, since we in the following never consider accelerated objects, we may suppress the possible dependence on acceleration and write $\Phi = \Phi(w)$, $\Psi = \Psi(w)$, $\Omega = \Omega(w)$, where w is the velocity with respect to S_0. From the assumption about the *isotropy of space* we may finally conclude $\Phi(w) = \Phi(|w|)$, $\Psi(w) = \Psi(|w|)$, and $\Omega(w) = \Omega(|w|)$. For technical reasons we assume that Φ, Ψ and Ω are continuously differentiable functions of one variable.

Up to now we have only been interested in one inertial system, namely the privileged system S_0. In order to apply Poincaré's principle we shall also consider other systems moving with respect to S_0. Let us introduce the inertial system S, moving at the velocity u along the positive x-axis of S_0. We assume the two systems to be oriented in the same way. In order to be able to relate observations in different inertial systems, we must choose units and synchronization in these in some appropriate way. Because of Poincaré's principle,

methods of synchronization and of units stipulation must be chosen, whose realization does not depend on the knowledge of absolute velocities. We choose units in S *preserving matter-geometry* [3], i.e. so that a rod at rest in S will have the same length when measured in S, as the same rod, resting in S_0, would have when measured in S_0. Likewise for a clock. We choose *natural synchronization* [3] in S. This means that if a clock is synchronized at one place and then moved at infinitesimal velocity (relatively to S) to another place, it will also there show the "right" time.*

As a help for determining the functions Φ, Ψ and Ω, we introduce the corresponding functions Φ_S, Ψ_S, and Ω_S, describing the apparent change of dimensions of moving particles and rates of moving clocks as observed in the system S. For technical reasons we will often use the notation $\Phi(u, v)$, $\Psi(u, v)$, and $\Omega(u, v)$ instead of $\Phi_S(v)$, $\Psi_S(v)$, and $\Omega_S(v)$. v is here the velocity of the moving object, as measured in S. We consider only the case of u and v parallel.

In general, the functions Φ_S, Ψ_S, and Ω_S will not necessarily be equal to Φ, Ψ, and Ω. It will, however, always be possible to express them in terms of these. To do this is our nearest task. At the end of the Section we will then find that the validity of Poincaré's principle implies that the functions $\Phi(u, v)$, $\Psi(u, v)$, and $\Omega(u, v)$ are independent of u.

We commence the investigation with the function Ψ_S. To this end we consider a particle moving at the velocity v along the positive x-axis in S. Its dimension in the transverse direction will then be $\Psi(u, v)L_0$, where L_0 is its dimension in the transverse direction when at rest in S. It is easy to convince oneself that the measurement of the transversal dimensions of a moving particle is independent of the chosen synchronization in S in the direction of motion. Because of this and of the fact that the synchronization in the transversal direction is the same in the two systems (natural synchronization has this effect when Ω is radial [3]), $\Psi(u, v)$ will only depend on the real dimension of the particle and the real length of the measuring-rods used in S. (By "real length" of a particle we understand its length as measured in S_0). Letting w denote the velocity of the particle with respect to S_0, we find

$$\Psi(u, v) = \Psi(u)^{-1}\Psi(w) , \tag{2.1}$$

where the factor $\Psi(w)$ is due to the real change of the transversal dimension of the particle and the factor $\Psi(u)^{-1}$ is due to the change of the measuring-rods used in S.

* This should not be understood as that clocks are moved at infinitesimal velocities, this being physically impossible, but in the following way: Two clocks, A and B, stationary in S, are synchronized if for every $\varepsilon > 0$ it is possible to move a third clock C, synchronized at A, at constant velocity on a straight line from A to B so slowly that the difference in readings between B and C at their coincidence is smaller than ε, and that this will hold for every clock moved slower than C. We remark that because of the form of Ω in our actual world ($\Omega = \sqrt{1 - w^2/c^2}$, $c = 3 \cdot 10^{10}$ cm/sec) even relatively high velocities give good approximations.

When determining $\Phi(u, v)$ we get the corresponding factor $\Phi(u)^{-1}\Phi(w)$ due to the real change of the longitudinal dimension of the particle and to the change of length of the measuring-rods in S, but also an additional factor depending on the chosen synchronization in S. In the process of computing this factor we will also find the transformation formula for velocities.

We consider two points x_1 and x_2 on the x-axis of $S(x_1 < x_2)$. The distance between these two points will be $(x_2 - x_1)\Phi(u)$ as measured in S_0. The fact that we have chosen natural synchronization in S implies that two clocks synchronized in S will in general not be synchronized when seen in S_0. We shall compute the discrepancy: Natural synchronization means that two resting clocks are synchronized if a third clock, when moved between them with infinitesimal velocity (as measured in S), indicates the same time as each of the two clocks at their respective coincidences. If a clock is sent from x_1 to x_2 with infinitesimal velocity (in S), we may denote its velocity in S_0 with $u + du$. The time, as measured in S_0, needed for the clock to cover the distance $x_2 - x_1$ is $(x_2 - x_1)\Phi(u)/du$; and hence, due to the difference in rate, $\Omega(u + du) - \Omega(u)$, compared with clocks at rest in S, the discrepancy will be:

$$(x_2 - x_1)\,\Phi(u)\,[\Omega(u + du) - \Omega(u)]/du = (x_2 - x_1)\,\Phi(u)\Omega'(u)\ .$$

Let us assume that when the front end of the moving particle passes x_1, the clock at x_1 indicates the time T_1, and when it passes x_2 the clock there indicates the time T_2. The time, as measured in S_0, needed for the particle to pass from x_1 to x_2 will then be given by the expression

$$[T_2 - T_1 - \Omega'(u)\,\Phi(u)(x_2 - x_1)]\,\Omega(u)^{-1}\,.$$

During this time the particle travels the distance

$$\Phi(u)\,(x_2 - x_1) + [T_2 - T_1 - \Omega'(u)\,\Phi(u)\,(x_2 - x_1)]\Omega(u)^{-1}u\ ,$$

and hence the velocity of the particle with respect to S_0 is given by

$$w = u + \frac{\Omega(u)\,\Phi(u)\,(x_2 - x_1)}{T_2 - T_1 - \Omega'(u)\Phi(u)(x_2 - x_1)}\ .$$

Since $x_2 - x_1 = (T_2 - T_1)v$, we thus obtain the velocity transformation formula

$$w - u = \frac{\Omega(u)\,\Phi(u)}{1 - \Omega'(u)\,\Phi(u)\,v}\,v\ . \tag{2.2}$$

This formula gives the relation between the velocity of a moving particle relative to S, as measured in S_0 and as measured in S. In the factor which

multiplies v we may interpret the components: $\Phi(u)$ is due to the change of length of the measuring-rods, $\Omega(u)$ to the change of rate of clocks and $1 - \Omega'(u)\Phi(u)v$ to the chosen synchronization.

The inverse of (2.2) is sometimes useful:

$$v = \frac{w - u}{\Omega(u)\Phi(u) + \Omega'(u)\Phi(u)(w - u)} . \tag{2.3}$$

In order to arrive at the expression for $\Phi(u, v)$, we express the time (as measured in S_0) needed for the particle to pass x_1 in two ways: computed in in S and divided by the change of rate factor $\Omega(u)$ it is $\frac{\Phi(u, v) L_0''}{\Omega(u) v}$, and in S_0 it is $\frac{\Phi(w) L_0''}{w - u}$. From the equality of these expressions we obtain:

$$\Phi(u, v) = \Phi(u)^{-1}\Phi(w)(1 - \Omega'(u)\Phi(u)v) . \tag{2.4}$$

An analogous reasoning, which is left to the reader, yields

$$\Omega(u, v) = \Omega(u)^{-1}\Omega(w)(1 - \Omega'(u)\Phi(u)v) . \tag{2.5}$$

We will now show how POINCARÉ's principle implies that the functions $\Phi(u, v)$, $\Psi(u, v)$, and $\Omega(u, v)$ are independent of u. This fact will in its turn enable us to calculate the functions Φ, Ψ, and Ω from the relations already deduced. We will perform the reasoning only for the function Φ, since it would be completely analogous for Ψ and Ω.

We have assumed that Φ and Ω are even functions. Hence, if measurements of the functions Φ_S and Ω_S would show that they are not even, motion of the inertial system S with respect to the ether could be inferred, in contradiction with *Poincaré's principle*. Thus $\Phi(u, v) = \Phi(u, -v)$ and $\Omega(u, v) = \Omega(u, -v)$. From (2.2) and (2.4) we immediately find

$$\Phi(-u, v) = \Phi(u, -v) = \Phi(u, v), \text{ whence } \frac{\partial}{\partial u}\Phi(u, v)\Big|_{u=0} = 0 .$$

Let us now consider, in addition to the system S, an inertial system S'. moving with the velocity u' (relatively S) along the positive x-axis of S. We introduce the function $\Phi_S(\cdot, \cdot)$, corresponding to $\Phi(\cdot, \cdot)$, but measured in S instead of in S_0. In virtue of the transformation formula (2.2) we have

$$\Phi_S(u', v) = \Phi\left(u + \frac{\Omega(u)\Phi(u)u'}{1 - \Omega'(u)\Phi(u)u'}, v\right),$$

and thus $\Phi_S(u', -v) = \Phi_S(u', v)$. By exactly the same reasoning as above we find the relation

$$\Phi_S(u', v) = \Phi_S\left(u' + \frac{\Omega_S(u')\,\Phi_S(u')v}{1 - \Omega'_S(u')\,\Phi_S(u')v}\right)\Phi_S(u')^{-1}\big(1 - \Omega'_S(u')\,\Phi_S(u')\,v\big),$$

which gives $\Phi_S(-u', v) = \Phi_S(u', -v) = \Phi_S(u', v)$. We therefore have

$$\frac{\partial}{\partial u'}\Phi_S(u', v)\bigg|_{u'=0} = 0, \quad \text{that is,} \quad \Omega(u)\,\Phi(u)\frac{\partial}{\partial u}\Phi(u, v) = 0,$$

and since we exclude the possibility $\Omega(u) = 0$ or $\Phi(u) = 0$, we find that $\Phi(u, v)$ must be independent of u. In other words, the functions Φ_S are the same for all inertial systems S. Likewise for Ψ_S and Ω_S. In the next Section we shall calculate these functions explicitly.

3. The differential equations

We have obtained the following identities:

$$\Phi(v) = \Phi\left(u + \frac{\Omega(u)\,\Phi(u)v}{1 - \Omega'(u)\Phi(u)v}\right)\Phi(u)^{-1}\big(1 - \Omega'(u)\,\Phi(u)\,v\big), \tag{3.1a}$$

$$\Psi(v) = \Psi\left(u + \frac{\Omega(u)\,\Phi(u)\,v}{1 - \Omega'(u)\,\Phi(u)v}\right)\Psi(u)^{-1}, \tag{3.1b}$$

$$\Omega(v) = \Omega\left(u + \frac{\Omega(u)\,\Phi(u)\,v}{1 - \Omega'(u)\,\Phi(u)v}\right)\Omega(u)^{-1}\big(1 - \Omega'(u)\,\Phi(u)v\big). \tag{3.1c}$$

Differenting (3.1a) and (3.1b) once and (3.1c) twice with respect to v, and setting $v = 0$, we find:

$$\begin{aligned}
\Phi'(0) &= \Phi'(u)\,\Omega(u) - \Omega'(u)\,\Phi(u)\,,\\
\Psi'(0) &= \Psi'(u)\,\Omega(u)\,\Phi(u)\,\Psi(u)^{-1}\,,\\
\Omega'(0) &= 0\,,\\
\Omega''(0) &= \Omega''(u)\,\Omega(u)\,\Phi(u)^2\,.
\end{aligned}$$

Setting $\Omega' = A$, this may be transformed into a first order system of ordinary differential equations:

$$\Phi'(u) = \frac{\alpha + A(u)\,\Phi(u)}{\Omega(u)}\,,$$

$$\begin{aligned} \Psi'(u) &= \frac{\beta\Psi(u)}{\Omega(u)\Phi(u)}, \\ \Omega'(u) &= A(u), \\ A'(u) &= \frac{\gamma}{\Omega(u)\Phi(u)^2}, \end{aligned} \tag{3.2}$$

with the initial conditions $\Phi(0) = \Psi(0) = \Omega(0) = 1$, $A(0) = 0$. It follows from the Picard—Lindelöf theorem (cf. e.g. [5]) that this system has exactly one solution with the given initial values. One easily verifies that this solution is given by

$$\Phi(u) = (1 - u/c_+)^{\frac{c_-}{c_+ + c_-}} (1 + u/c_-)^{\frac{c_+}{c_+ + c_-}},$$

$$\Psi(u) = (1 - u/c_+)^{\frac{k}{2}\frac{c_- - c_+}{c_+ + c_-}} (1 + u/c_-)^{\frac{k}{2}\frac{c_+ - c_-}{c_+ + c_-}},$$

$$\Omega(u) = (1 - u/c_+)^{\frac{c_+}{c_+ + c_-}} (1 + u/c_-)^{\frac{c_-}{c_+ + c_-}},$$

$$A(u) = -\frac{u}{c_+ c_-} (1 - u/c_+)^{\frac{-c_-}{c_+ + c_-}} (1 + u/c_-)^{\frac{-c_+}{c_+ + c_-}},$$

where c_+, c_-, and k are given by

$$\frac{1}{c^+} = -\frac{\alpha}{2} + \sqrt{\alpha^2/4 - \gamma}, \quad \frac{1}{c_-} = \frac{\alpha}{2} + \sqrt{\alpha^2/4 - \gamma}, \quad k = \frac{2c_+ c_-}{c_+ - c_-}\beta.$$

(In the case $\alpha^2 < 4\gamma$ these expressions are to be interpreted properly. The solution is defined in the maximal interval containing the origin but none of the points c_+ and c_-.)

In our case we have $\alpha = \Phi'(0) = 0$, $\beta = \Psi'(0) = 0$, and if we put $\gamma = \Omega''(0) = A'(0) = -c^{-2}$ our formulas specialize to $c_+ = c_- = c$,

$$\Phi(u) = \Omega(u) = (1 - u^2/c^2)^{1/2}, \quad (u) \equiv 1. \tag{3.3}$$

If $c^2 > 0$ this solution is defined on $(-|c|, |c|)$, otherwise on all of R.

4. Interpretation

Having derived the relations (3.3) it only remains to determine the sign of c^2 and to give it a physical interpretation. Depending on whether c^2 will be positive, negative or infinite, moving particles will undergo respectively contraction, dilatation or remain unchanged. Likewise for clocks.

We distinguish two cases depending on whether a limiting (signal) velocity (with respect to S_0) exists or not.

a) *No limiting velocity exists*

Having signals with arbitrary high velocities at our disposal, we would be able to establish "absolute" synchronization [3]. Since absolute and natural synchronization are equivalent in S_0 (this follows from $\Omega'(0) = 0$), the possibility to establish absolute synchronization in S implies that they must be equivalent also in S if *Poincaré's principle* is to be valid (otherwise absolute motion of S with respect to S_0 could be detected). Now, if absolute and natural synchronization are to be equivalent in all frames, our synchronization factor $1 - \Omega'(u)\Phi(u)v$ must equal one, i.e. $\Omega'(u) = 0$. In this case it follows from Eq. (3.3) that $\Phi = \Psi = \Omega = 1$. In this *Newtonian world* no waves in the ether are allowed. As was already remarked in [6, 3], this is the only world, where the concept of ether loses its meaning.

b) *A limiting velocity exists*

Denoting the limiting velocity with V_0 we make use of (2.3) and calculate the value, V, of the limiting velocity as measured in S:

$$V = \frac{1 - u/V_0}{1 - uV_0/c^2} V_0 \,. \tag{4.1}$$

It is easily seen that if V would depend on the "absolute" velocity u, knowledge of V in two different inertial systems and of their relative velocity would enable us to calculate u. This contradicts *Poincaré's principle*. Hence the only possibility is $V = V_0$, independently of u. But, as is easily seen by inserting $V = V_0$ in (4.1), this gives $V_0 = \pm c$, i.e. $c^2 > 0$.

This is our familiar *Lorentzian world*. Here waves in the ether are allowed, but they must *all* travel at the same velocity c. This velocity will at the same time be a limiting velocity and an invariant velocity.

We notice that the alternative $c^2 < 0$ is ruled out in any case. We may hence summarize this section by saying that *either* $\Phi = \Psi = \Omega \equiv 1$ and the world is totally ballistic, *or* $\Psi = 1$, $\Phi = \Omega = (1 - w^2/c^2)^{1/2}$ and all waves travel in the ether at the velocity c [3], that is the highest possible velocity as well as an invariant velocity (this later presupposing natural synchronization in all systems). *Experimentally* it has been shown that there exist waves in the ether [7].

5. Conclusion and discussion

From assumptions about the homogeneity of space and time, the isotropy of space and POINCARÉ's principle we have derived that $\Psi \equiv 1$ and $\Phi = \Omega = (1 - w^2/c^2)^{1/2}$, where $c^2 \in]0, \infty]$. Assuming the existence of waves in the ether, we may exclude $c^2 = \infty$ and identify c with the velocity of the waves in the ether. We have thus reached our goal, namely to prove that these our presuppositions determine the behaviour of inertially moving particles and clocks.

Finally, we would like to point out the essential features of our treatment as compared to related work. Contrary to many authors, we think that the substance of a theory of moving particles and clocks is contained in the proposition about the form of the functions Φ, Ψ, and Ω, and not in the transformation equations [8]. In order to motivate this point of view, we first call attention to the (trivial) fact that all physical phenomena can be described within *one* inertial system. Only if one wants to relate the descriptions within different systems, transformation equations are needed. Furthermore, knowing the form of the coordinate transformation, the form of the functions Φ, Ψ, and Ω may usually be deduced. The condition is, however, that the convention governing the choice of units and synchronization in different systems is known. Likewise the knowledge of the functions makes it an easy task to derive appropriate transformation equations (after having chosen the units and synchronization [3, 9]). We may summarize this in saying that different transformations may describe the same world and different worlds may be described by the same transformation, but to every world there belongs only one set of functions Φ, Ψ, and Ω.

Numerous derivations of the Lorentz transformation have appeared. These may be divided into essentially two groups, according as the concept of ether has been used or not. Most derivations belonging to the second group are based on either the principle of relativity (or the closely related group postulate) [10], the principle of constancy of light velocity [11], or both [12]. An exception worth mentioning is ROBERTSON [13], who obtained the transformation coefficients from an analysis of the Michelson—Morley, Kennedy—Thorndike, and Ives—Stilwell experiments.

There are also many derivations making use of the concept of ether [14, 8]. Contrary to most "relativistic" derivations, however, these are usually not based on some universal principle. This is one important reason why the "ether approach" has been much criticized [15]. In fact, as far as we know, our derivation is the first one from POINCARÉ's principle. (In [3], footnote p. 238, the transformation was derived from the condition that the one-way velocity of light (natural synchronization) be constant.) Beside other reasons for employing an ether approach, we finally want to point out that: POINCARÉ's

principle, in that it speaks about the possibility of certain measurements, is of purely physical nature, whereas Einstein's principle of relativity (and of course still more the group postulate), speaking about the form of laws, is of a more mathematical nature.

REFERENCES

1. G. H. KESWANI, Brit Journ. Phil. Science, **15,** 286, 1964.
2. M. F. PODLAHA, Ind. Journ. Theor. Phys., **22,** 73, 1974; **23,** 70, 1975; **25,** 37, 1977; **26,** 181, 189, 1978; **27,** 81, 1979; Brit. Journ. Phil. Science, **26,** 133, 1975; **27,** 261, 1976; M. F. PODLAHA, B. ALTHAUS and H. BAENSCH: Philosophia Naturalis, **16,** 315, 1977.
3. T. SJÖDIN, Il Nuovo Cimento, **51B,** 229, 1979.
4. M. F. PODLAHA and T. SJÖDIN, Lett. Nuovo Cimento, **20,** 593, 1977; Acta Phys. Hung., **48,** 69, 1980.
5. K. YOSIDA, Lectures on Differential Equations, 2nd ed., Wadsworth, Balmont, California, 1966.
6. M. F. PODLAHA, Some New Aspects of Relativity; Coordinate Frames, Physical Systems and the Ether, manuscript, 1977.
7. T. ALVÄGER, J. M. BAILEY, F. J. M. FARLEY, J. KJELLMAN and I. WALLIN, Arkiv för Fysik, **31,** 145, 1966.
8. H. E. IVES, Phil. Mag., **36,** 392, 1945.
9. T. SJÖDIN, On the Linearity of Certain Coordinate Transformations, Istituto di matematica "Tonelli", Pisa, Preprint, Oct. 1980.
10. P. FRANK and H. ROTHE, Ann. Physik, **34,** 825, 1911; M. V. LALAN, Bull. Soc. Math. France, **65,** 83, 1937; V. BERZI and V. GORINI, Journ. Math. Phys., **10,** 1518, 1969; G. SÜSSMANN, Z. Naturforsch., **24A,** 495, 1969.
11. E. C. ZEEMAN, Journ. Math. Phys., **5,** 490, 1964; H. J. BORCHERS and C. G. HEGERFELDT, Comm. Math. Phys., **28,** 259, 1972.
12. A. EINSTEIN, Ann. Physik, **17,** 891, 1905.
13. H. P. ROBERTSON, Rev. Mod. Phys., **21,** 378, 1949.
14. J. LARMOR: Aether and Matter, Ch. 11, Cambridge Univ. Press, Cambridge, 1900; H. POINCARÉ, Rend. Circ. Mat. Palermo, **21,** 129, 1906; M. F. PODLAHA and E. NAVRATIL, Rev. Acad. Cienc. Exactas Madrid, **61,** 555, 1967; H. A. LORENTZ, Proc. Acad. Sci. Amsterdam, **6,** 809, 1904.
15. M. VON LAUE, Das Relativitätsprinzip, §3, 19—20, Vieweg, Braunschweig, 1911: "A real, experimental decision between the extended theory of Lorentz and the theory of relativity is probably not to be gained at all, and that the former, in spite of this, has receded into the background is chiefly due to the fact that, close as it comes to the theory of relativity, it still lacks the great simple universal principle, the possession of which lends the theory of relativity, already in its present form, still in need of further development, an imposing appearance."

Acta Physica Academiae Scientiarum Hungaricae, Tomus 48 (4), pp. 449—460 (1980)

THE GREENHOUSE EFFECT OF THE CO_2 IN THE ATMOSPHERE

By

G. MARX

DEPARTMENT OF ATOMIC PHYSICS, ROLAND EÖTVÖS UNIVERSITY, BUDAPEST, HUNGARY

and

F. MISKOLCI

INSTITUTE FOR ATMOSPHERIC PHYSICS, BUDAPEST, HUNGARY

(Received 6. V. 1980)

The CO_2 is a polar molecule, having a strong absorption band in the region 450—870cm^{-1}. This is just the maximum intensity region for a black body radiation of $T = 288$ K, corresponding to the average surface temperature of the Earth. The consequence of the atmospheric CO_2 is a greenhouse effect, which is in the focus of recent interest. Taking the intensity and line width values for 2500 spectral lines of CO_2 into account, the atmospheric absorption has been calculated for different CO_2 concentrations. At higher concentrations the line shape has a considerable influence. The past and future climatic consequences are also discussed in some detail.

Introduction

The role of the CO_2 content in influencing the surface temperature of our home planet is a subject of recent discussions. Several estimations have been made in the last decades [1]. It has been agreed that a future doubling of the present 330 ppm atmospheric concentration of CO_2 may be expected due to the fast combustion of fossil fuels and to deforestation of tropical continents. According to the pioneering studies of MÖLLER [2] and others, this may result in an overall temperature increase of a few degrees. This has been considered by several authors to be alarming: it may cause a disappearance of the polar ice cap (i.e. a catastrophic rise of the sea level) and a shift of precipitation already in the coming century [3, 4]. The thermodynamics and evolution of the atmosphere and ocean is really worth understanding. It has been emphasized in an earlier note [5], that the past history of the atmosphere may serve as a testing ground for any predictive theory.

Biologists assume the existence of a reducing atmosphere in the era of the formation of oceans on the Earth. Geophysicists, on the other hand, deduce the composition of this early atmosphere from the present composition of volcanic gases (consisting mainly of CO_2 and H_2O). This is certainly a relevant question from the point of view of the origins of life, which appeared practically simultaneously with the formation of oceans, about 3.8 billion years ago [6]. There is a majority concensus, however, that for a considerable part of terrestrial history (between -3.5 billion and -0.75 billion years)

the main component of the atmosphere was CO_2. This was transformed into O_2 by spreading vegetation and into $CaCO_3$ by sea life and anorganic chemistry. The long CO_2 era on Earth resembled the present state of Mars and Venus. The calculated weight of terrestrial CO_2, bound now mainly in $CaCO_3$ and in organic compounds has been estimated to be about 100 atm [7], comparable to the present Venusian atmosphere. The planet Venus shows, however, a surface temperature of 500 °C. By making a simple estimation of the greenhouse effect RASOOL and De BERGH [8] concluded that the atmospheric CO_2 had never exceeded one tenth atm on Earth; the present material of the terrestrial atmosphere might be a consequence of recent outgasing from the crust.

On our home planet life has existed without interruptions in the past 3.8 billion years [6, 9]. This fact contains a very valuable message about this planet: the temperature of the world ocean did not exceed the boiling point of H_2O (100 °C) or the melting point of DNA (80 °C) in the last 3.5 billion years. The mean chemical composition of the atmosphere changed drastically from polar CO_2 to apolar O_2, N_2 compounds in the last 0.75 billion years. In order to understand the thermal stability on the surface of the Earth, in spite of these recent drastic changes, one has to study the atmospheric absorption of a thick CO_2 atmosphere (this will be made in the next Chapter), then one has to combine the calculated greenhouse effect with other long scale phenomena influencing the temperature (this will be made in the closing Chapter). The theoretical conclusions can be compared with the temperature history of Earth, deciphered by geophysical methods.

The atmospheric absorption of the 15μ CO_2 band

The intensity of the terrestrial radiation at a certain wave number in the infrared region of the emission spectrum can be given [10] as follows:

$$J_\nu = \varepsilon_\nu B_\nu(T_s)\,\tau_{\nu,s} + \int_{\tau_{\nu,s}}^{1} B_\nu(T(p))\,d\tau_\nu(T, p, u)\,. \tag{1}$$

Here $B_\nu(T)$ is the Planck radiation, ε_ν is the emissivity of the surface, p is the pressure, u is the optical mass of the absorbing gas, τ_ν is the transmissivity, ν is the wave number usually in cm^{-1}. The subscript "S" refers to surface values. On the right side of this equation the first term gives the radiation of the surface and the second term gives that of the atmosphere. Utilizing the fact that the mixing ratio of the CO_2 in the atmosphere along a vertical path of ray is constant, the transmission function takes this form:

$$\tau_{\nu,s} = \exp\left[-c\int_0^{p_0} K_\nu(p, T)\,dp\right], \tag{2}$$

where p_0 is the pressure at the surface, c is a constant depending only on the CO_2 concentration, and $K_\nu(p, T)$ is the absorption coefficient which is determined by a summation over all absorption lines in the band. The parameters of these lines were taken from the McCLATCHEY's absorption line compilation [11]. In the calculation 2500 strong lines of CO_2 were used. The integrated absorption over the whole band is given as

$$A = \int_{\nu_1}^{\nu_2} (1 - \tau_{\nu,S})\, d\nu \,. \tag{3}$$

ν_1 and ν_2 are the wave number limits, which were chosen so that the weakest absorption lines taken into account be farer than 50 cm^{-1} from the ν_1 or ν_2. In our case $\nu_1 = 450\ cm^{-1}$ and $\nu_2 = 870\ cm^{-1}$. If we are interested in percentage absorption of the outcoming radiation, we can define the average absorption $\bar{A}$:

$$\bar{A} = 1 - \int \tau_{\nu,S}\, B_\nu(T_S) d\nu / \int B_\nu(T_S)\, d\nu \,. \tag{4}$$

Here one has to integrate over the whole infrared spectrum. It is easy to calculate the value of $\bar{A}$ from the integrated values of $\tau_{\nu,S}$ over a suitable short wave number interval, because the Planck function is the slowly varying function of ν compared with $\tau_{\nu,S}$. The calculation of the average $\tau_{\nu,S}$ was made by a direct integration method for 0.1 cm^{-1} wide intervals between 450 cm^{-1} and 870 cm^{-1} and for the 1962 US Standard Atmosphere.

Here we do not want to go into the details of the direct integration method concerning the main characteristics of our calculation. We mention only two remarks:

The atmosphere was divided into plain-parallel isotherm layers, the transmittances through the whole atmosphere were computed by multiplying the values of each homogeneous layer. Test calculations, which were made by using the present CO_2 level, showed, that it was not worth dividing the atmosphere into many layers, because the accuracy of the transmittances did not increase. We divided the atmosphere into 16 isotherm layers permitting about 2% relative errors in the values of τ_ν. It is obvious that this error is negligible in the determination of the integrated absorption as a function of the CO_2 concentration. (Fig. 1 shows the dependence of this error on the height.)

The second remark is related to the line shape. Under atmospheric conditions, where the pressure broadening of the lines plays a dominant role, the Lorentz line shape is in general use. Experimental observations — which were recently confirmed theoretically [12] — showed, however, that the absorption at the far line wings decreases much faster than in the case of a Lorentz line shape. In this calculation we applied an exponential line shape function which was given by Benedict and Shilvermann empirically:

$$K_{\nu i} = K\nu_{i,L} \exp\left(-0.135\,|\Delta\nu_i|^{0.7}\right). \tag{5}$$

Here $\Delta\nu_i$ is the line width and $K_{\nu_i, L}$ is the Lorentz line shape function [1]. In each case when the values of $\Delta\nu_i$ were larger than 7 cm^{-1} this formula was used. In other cases the Lorentz or the Voigt profile was used according to the pressure and $\Delta\nu_i$. The Lorentz half width was supposed to be constant from line to line.

Before presenting the detailed results concerning the integrated absorption of the atmosphere we compare the atmospheric transmittances with those quoted in the literature. In DRAYSON's paper which is the most accurate from this point of view [13], the transmittances were averaged over 5 cm^{-1} wide intervals between the 500 cm^{-1} and 860 cm^{-1} wave numbers, and were given in tabulated form. DRAYSON's calculation was made for the US

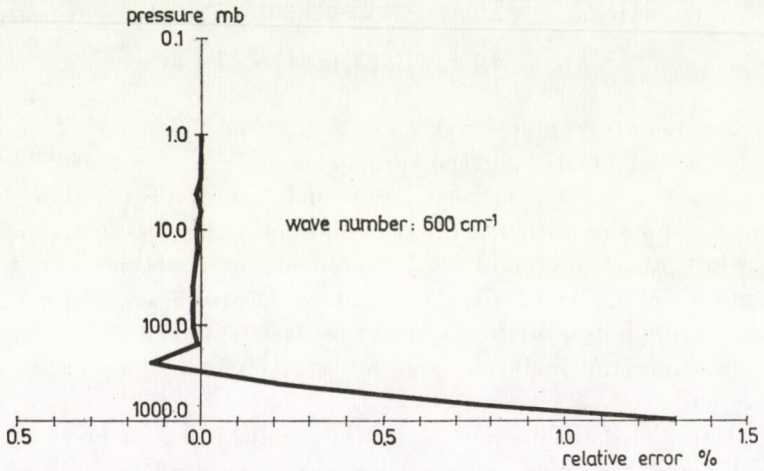

Fig. 1. Dependence of the relative errors of the transmittances on the height

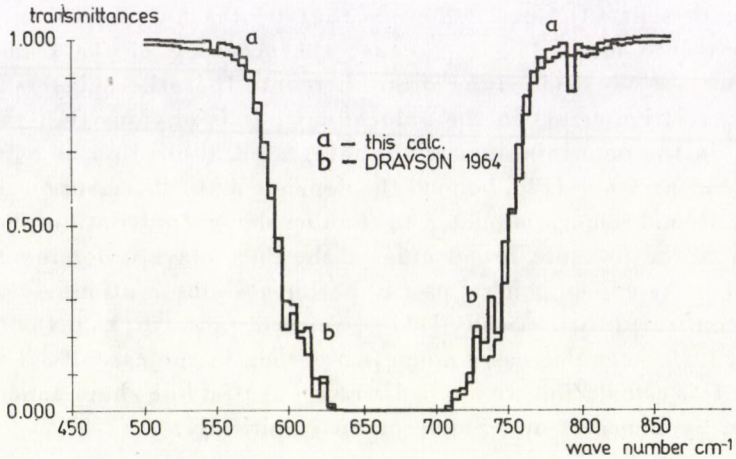

Fig. 2. Comparison of the transmittances calculated for the 1962 US standard atmosphere

Standard Atmosphere, too. Fig. 2 shows the comparison of transmittances, and the following Table I contains the calculated absorptions A for different pressure levels.

Table I

Integrated absorption values A as a function of atmospheric pressure levels

Pressure (mb)	DRAYSON (1960)	This calculation
1.0	$A =$ 1.45	$A =$ 1.93
10.0	8.10	9.90
100.0	52.48	57.66
1000.0	161.75	157.20

Though the transmittances show significant differences at certain wave numbers, the absorptions calculated by formula (3) are in good agreement. There are several possible reasons for the slight difference:

— The present calculation used 0.032% CO_2 by volume compared with 0.031 used by DRAYSON: this effect on the calculation is small.
— The line parameters used were not in full agreement.
— DRAYSON divided the atmosphere into 34 homogeneous layers.
— At the line wings the shape function was quite different.

In spite of the differences mentioned above we can regard the general agreement of the two calculations as an indication for the correctness of this method for the determination of the integrated absorption coefficients A and $\bar{A}$. Further on we computed the dependence of A and $\bar{A}$ on the CO_2 concentration and examined the effect of the variation of the temperature and the pressure.

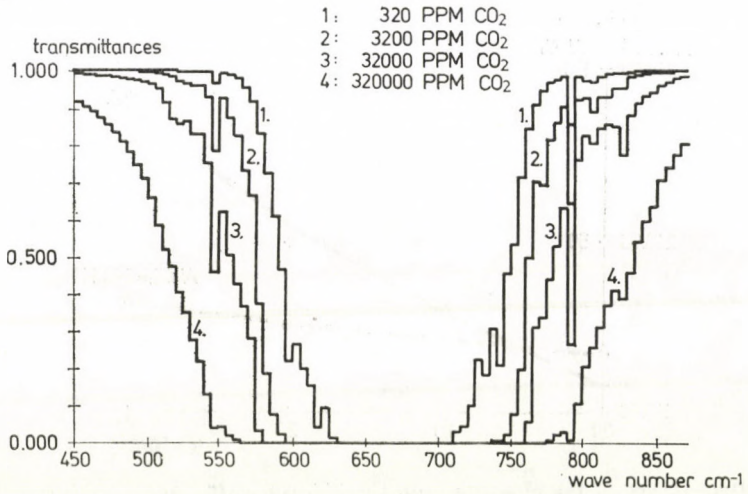

Fig. 3. Dependence of the transmittances on the CO_2 concentrations

In order to determine the concentration dependence the CO_2 concentration was increased 5, 10, 50, 100 and 1000 fold. The variation of the transmissivity can be seen in Fig. 3 and the variation of the absorption coefficients A and $\bar{A}$ in Fig. 4. In the case of $\bar{A}$ the integration limits were $\nu_1 = 10$ cm^{-1} and $\nu_2 = 2500$ cm^{-1}. It is clear from the curves of Fig. 4 that the integrated absorptions A and $\bar{A}$ depend on the concentration as a power function. To the points of A we fitted a power function by the least square method:

$$A = 156.13 \left(\frac{c}{c_0}\right)^{0.1016},$$

where $c_0 = 320$ ppm is the present CO_2 level and c is the concentration. The correlation coefficient was larger than 0.99.

The next important question is how the integrated absorption depends on pressure and temperature at high CO_2 level. The increase of the CO_2 concentration will result in the increase of the average molecular weight of the atmosphere and in consequence to that the increase of the surface pressure. This effect was taken into account only at the thousandfold CO_2 concentration. In this case the pressure value on the surface was 1261.0 mb, the atmosphere consisted of about 30% CO_2 and 70% N_2. We have examined the variation of the integrated absorption (DA) as a function of the variation of the surface pressure (DP). Fig. 5 shows that the relation in the examined region is linear. At 320 000 ppm CO_2 concentration the increase of the surface pressure produces the increase of A by 2.5 percent. It is likely that the effect of the pressure would be more important in a thicker atmosphere and at extreme high CO_2 concentrations.

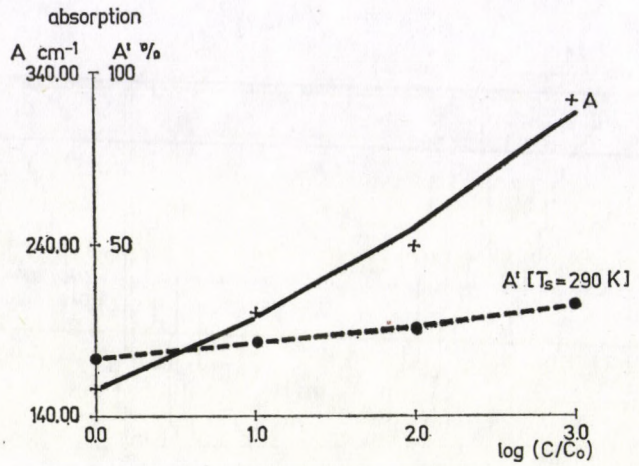

Fig. 4. Dependence of the absorption on the CO_2 concentration. C : CO_2 concentration; CO = 320 PPM

The variation of the absorption coefficient A at 320 000 ppm CO_2 concentration related to the variation of the average temperature of the atmosphere was also examined. Fig. 6 shows the results. As can be seen, increasing average temperature produces decreasing absorption. The explanation of this effect is that the intensity of the strong lines is in inverse ratio to the temperature and in the case of high CO_2 concentrations the absorption caused by the wings of the strong lines is dominating. Increasing the temperature of the atmosphere by + 45 degrees at each level the range of the variation of the integrated absorption A is about 2.5 percent. But in the case of the Earth this slight temperature dependence can be neglected as a consequence of the temperature stability of the planet.

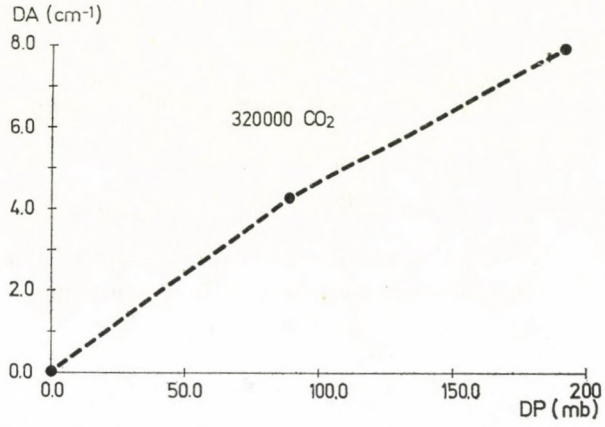

Fig. 5. Dependence of the absorption A on pressure. DP: Variation of the surface pressure. DA: Variation of the absorption A

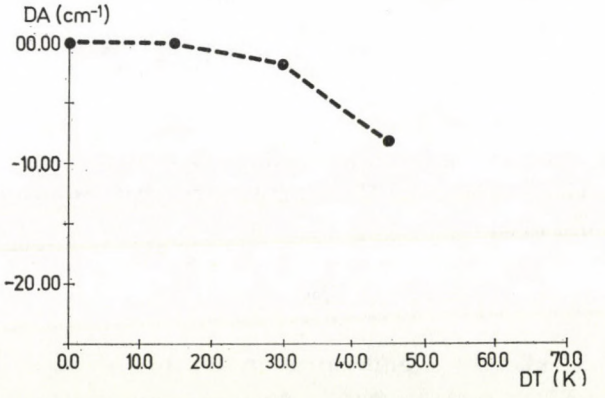

Fig. 6. Dependence of the absorption A on the temperature. DA: Variation of the absorption A. DT: Variation of the average temperature

Past and future greenhouse effects

The surface temperature of a naked inactive rotating planet is determined by the balance between solar heating and thermal radiation loss:

$$\pi R^2 (1 - a) S = 4\pi R^2 \sigma T_0^4 .$$

(Here R is the radius of the planet, S is the solar constant at the distance of the planet; a is the albedo, i.e. reflectivity and T_0 is the resulting planetary surface temperature.) At the Sun—Earth distance the present standard value of the solar constant is $S = 2$ cal/cm^2 min. So the average surface temperature can be calculated for different albedo values.

$T_0 =$	279 K	for $a =$ 0—
	272 K	10%
	264 K	20%
	255 K	30%
	245 K	40%
	236 K	50%
	221 K	60%

If the planet possesses an atmosphere with an effective transmittivity $\alpha <$ $< 100\%$, only a fraction of the thermal radiation escapes, consequently the equilibrium soil temperature T turns out to be higher:

$$\pi R^2 (1 - a) S = 4\pi R^2 \beta \sigma T^4 . \tag{6}$$

(Evidently β is averaged over the Planck distribution corresponding to T.) In order to obtain a first idea upon the CO_2 greenhouse effect, let us make use of the Eddington approximation [14,15], which relates the effective transmittivity β to the integrated atmospheric absorption $\bar{A}$ through the formula

$$\beta = \left[1 - \frac{3}{4} \ln (1 - \bar{A})\right]^{-1} . \tag{7}$$

(This formula assumes the isotropy of the soil radiation and the exponential absorption in the volume of the atmosphere. Evidently, a more realistic calculation would need to consider the cloud cover, the full radiation spectrum, the absorption of H_2O and O_3 as well and the dependence of the chemical composition on temperature. All these details may be the subjects of future study.)

Having calculated the concentration dependence of $\bar{A}$ (Fig. 4) one can compute the temperature increase, due to the presence of the CO_2 in the atmosphere, with the help of the formula (6).

The resulting T values are collected for different initial T_0 values in the following Table:

Table II

Average terrestrial surface temperature (T) as a function of atmospheric CO_2 concentration and average surface temperature of the naked Earth (T_0)

concentration (ppm)	280 K (T_0)	260 K (T_0)	240 K (T_0)	220 K (T_0)
0	289 K	268 K	248 K	227 K
320	291 K	270 K	250 K	229 K
3200	294 K	273 K	252 K	230 K
32000	300 K	279 K	258 K	236 K
3200000				

MÖLLER [2] predicted a temperature rise of about 2 °C for the doubling of the present CO_2 content, expected within hundred years. Our calculation using a more sophisticated spectroscopy, concluded in a more modest change of 0.5 °C. (It should be mentioned, however, that we restricted ourselves to the band 450—870 cm^{-1}, where the absorption was already almost complete. The "hot bands" at higher wave numbers may modify this result. The necessary extension of the computation is a task of the next future.)

The conclusion may be tested with the paleoclimatological evidence. The sudden drop of the atmospheric CO_2 content certainly produced a quick fall of temperature about 1—0.75 billion years ago. E.g. if the CO_2 concentration dropped from 32% to its present value, the transmissivity increased from 75% to 88%, corresponding to a temperature fall of 10—20 °C. This is the largest change, tolerated by the geochemical evidence [16]. (By measuring the isotopic ratio of oxygen in oceanic sediments, one can obtain the water temperature for different ages, as indicated in Fig. 7. There is a definite indi-

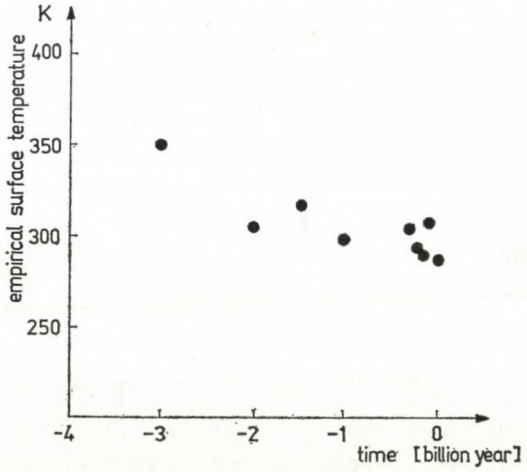

Fig. 7. Temperatures deduced from the isotopic composition of cherts. (KNAUTH—EPSTEIN, 1976)

cation of cooling in the last one billion year.) A more drastic temperature change such as suggested by the example of Venus, seems to be excluded empirically for our planet [17].

Concluding remarks on the thermal history of the Earth

Most geophysical calculations assume an invariable solar constant. But the standard solar model (even the nonconventional models) indicate $5 \pm 1\%$ increase in the solar luminosity per billion year [18]. (Decreased H concentration must be balanced by higher temperature in the Sun.) This means, that going back in time, the temperature must be decreased by 4 K in each billion year, taking into account the smaller solar luminosity. This helps to cool down the early hot greenhouse. The time dependence of the two effects are, however, completely different: the solar reactor warms up smoothly, the sudden disappearance of the CO_2 shield, on the other hand, results in a fast cooling in the last one billion years.

Another phenomenon, which might play an important role in the past, was the heat produced by the terrestrial radioactivity. An average heat producing power W per unit volume of the interior of the planet modifies the fundamental formula:

$$\frac{4\pi}{3} R^3 W(t) + \pi R^2 (1 - a) S(t) = 4\pi R^2 \sigma T^4 \beta \, .$$

The value of $W(t)$ is not known exactly, but it can be estimated. For simplicity, let us restrict ourselves to the ^{40}K decay. The present concentration is about 3g ^{40}K/ton crust material. If the ^{40}K were distributed uniformly inside the whole Earth, the energy produced by its radioactivity would correspond to 0.6 percent of the solar constant. But this is certainly an overestimation: the light elements are concentrated in the surface layers of the planet. The life time of ^{40}K is 1.28 billion years, thus at the formation of Earth the heat production of ^{40}K (and that of U and Th) did not exceed a few percent of the solar heating. The contribution of the radioelements did not have a large influence on the thermal household of Earth in the last 3.5 billion years. Only radioelements with lifetime considerably shorter than one billion years heated up the planet in the first billion years of it existence, but these nuclei quickly disappeared.

$W(t)$ might be significant at the beginning, but it had a half life smaller than one billion year and it became negligible after the formation of the planet.

Another early energy source for Earth was the tidal friction. The Moon was much nearer in the early era of the Solar System and the Earth rotated

faster. It is rather hard to estimate this effect [19], but it might have a significant contribution only in the first billion years, later it became negligible.

In Fig. 8. the time dependence of these effects are summarized. As we can see the power reaching the surface of the Earth did not decrease in the last three billion years. The observed slight temperature decrease can be explained only by the decreasing CO_2 content. The thermal stability of Earth (an ocean temperature between 270 K and 350 K in the past 3.8 billion years) still needs a more convincing explanation. The different effects have comple-

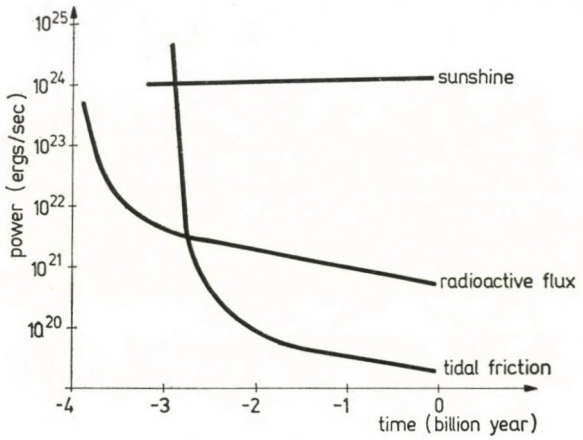

Fig. 8. Energies reaching the surface of earth

tely different time dependence, so the cancellation is still surprising. LOVELOCK and MARGULIS [20] assumed that the biological ecosystem of the Earth is a selfregulating organism, which takes care of itself, even by stabilizing the climate. This idea is far from being an elaborate quantitative theory, but let us remark: the only way by which the terrestrial life can influence the climate is the atmospheric CO_2 concentration. If mankind is interested in its past and in its future, one has to understand the working of this greenhouse in every detail.

REFERENCES

1. G. YAMAMOTO and T. SASAMORI, Calculation of the Absorption of the 15 micron CO_2 Band. Sci. Re, of Tohuku University **10**, No. 2, 1958.
2. F. MÖLLER, J. Geophysical Research, **68**, 3877, 1963.
3. J. WILLIAMS and W. HÄFELE, Acta Astronautica, **5**, 589, 1978.
4. A. HENDERSON-SELLERS, Computers and Geosciences, **4**, 319, 1978.
5. G. MARX, Acta Astronautica, **5**, 601, 1978.
6. H. D. PFLUG, Naturwissenschaften, **68**, 1979.
7. E. SZÁDECZKY-KARDOSS, Geonomy, Hungarian Academy Press, 1978.
8. S. I. RASOOL and C. DE BERGH, Nature, **226**, 1037, 1970.
9. C. SAGAN-MULLEN, Science, **177**, 177, 1972.
10. S. CHANDRASEHKAR, Radiative Transfer, Dover, New York.

11. R. A. McClatchey et al., Atmospheric Line Parameters Compilation AFCRL-TR-73-0096.
12. V. E. Zuev and V. V. Fomin: Consideration of Continuum Absorption in the Problems of Sounding from Outer Space XXI. Cospar, Innsbruck, 1978.
13. S. R. Drayson: Atmospheric Slant Path Transmission in the 15 micron CO_2 Band, Univ. Michigan, Technical Report 05863-3-T.
14. A. E. Ringwood, in Advances in Earth Science, edit. by P. M. Hurley, 1964.
15. H. D. Holland, in Petrologic Studies, edit. by A. E. Engel et al. 1962, p. 447.
16. Epstein—Knauth, Geochimica and Cosmochimica Acta, 1976.
17. T. M. L. Wigley, P. D. Jones and P. M. Kelly, Nature, **283**, 17, 1980.
18. M. J. Newman and R. T. Rood, On the Evolution of the Solar Constant. Orange Aid Preprint No. 585, Cal. Tech. Pasadena.
19. H. Turcottee, Icarus, **30**, 254, 1977.
20. J. Lovelock and L. Margulis, New Scientist, **65**, 391, 1978.

Acta Physica Academiae Scientiarum Hungaricae, Tomus 48 (4), pp. 461—464 (1980)

COMMUNICATIO BREVIS

STATIC BRANS—DICKE—MAXWELL FIELDS

By

A. BANERJEE*

INSTITUTO DE FISÍCA, U.F.R.J., ILHA DO FUNDAO, RIO DE JANEIRO, BRASIL

(Received in revised form 15. I. 1980)

Introduction

Recently TIWARI and RAO [1] obtained in the axially symmetric coupled Brans—Dicke—Maxwell field a relationship between g_{00}, the scalar field and the electric potential in a general situation, where both electric and magnetic fields are present. The assumptions made for the derivation of the above relation were that the magnetic potential is functionally related to the electric potential and that g_{00} is a function of the scalar field as well as the electric potential. We have generalised the result in the present note for a more general situation and have shown that the said relation holds not only in axial symmetry but also in all static coupled Brans—Dicke—Maxwell fields where g_{00} and the magnetic potential both are functionally related to the electric potential alone. It is shown that the scalar field ψ also then turns out automatically to be a function of the electric potential (RAYCHAUDHURI and BANDYOPADHYAY [2]). Moreover, the generalised WMP relation in Brans—Dicke theory in the presence of both electric and magnetic fields mentioned above is the only relation which follows from the field equations contrary to the comment of TIWARI and RAO that it is not the unique relation.

Derivation of the generalised Weyl—Majumdar—Papapetrou relation [3—5]

The line element for the static space time can be written as

$$ds^2 = e^{2U} dt^2 + e^{-2U} \gamma_{ij} dx^i dx^j \tag{1}$$

with U and γ_{ij} being functions of space coordinates only. In what follows a latin index is 1, 2 or 3 and a greek index is 1, 2, 3 or 4. The field equations in

* The author is on leave from Physics Department, Jadavpur University, Calcutta 700032, India.

Brans—Dicke theory (BRANS and DICKE [6]) in presence of electromagnetic field are

$$R_{\mu\nu} - \frac{1}{2} g_{\mu\nu} R = -\frac{8\pi}{\psi} \tau_{\mu\nu} - \frac{\omega}{\psi^2} \left(\psi_\mu \psi_\nu - \frac{1}{2} g_{\mu\nu} \psi_\alpha \psi^\alpha \right) - \frac{1}{\psi} (\psi_{\mu;\nu} - g_{\mu\nu} \Box \psi). \quad (2)$$

Also $\Box \psi = 0$ in the present case.

In the above $\tau_{\mu\nu}$ stands for the energy momentum tensor for the electromagnetic field and ψ stands for the scalar field. In view of $\Box \psi = 0$ and $\tau^\alpha_\alpha = 0$, the field equation (2) may also be written in the form

$$R^\mu_\nu = -\frac{8\pi}{\psi} \tau^\mu_\nu - \frac{\omega}{\psi^2} \psi^\mu \psi_\nu - \frac{1}{\psi} \psi^\mu{}_{;\nu}. \quad (3)$$

It is well known that

$$4\pi \tau_{\mu\nu} = -F_{\mu\alpha} F^\alpha_\nu + \frac{1}{4} g_{\mu\nu} \cdot F_{\alpha\beta} F^{\alpha\beta}, \quad (4)$$

where terms like $F_{\alpha\beta}$ stand for the electromagnetic field tensors. Now since for a static field $\psi_{,0} = 0$, one gets from (3) and (4) one of the field equations as

$$R^0_0 = -\frac{8\pi}{\psi} \tau^0_0 - \frac{1}{\psi} \psi^0_0 . \quad (5)$$

The electromagnetic field tensors may be said to be defined in terms of the scalar potentials ξ and η as

$$F_{0i} = \xi_{,i} \quad \text{and} \quad F^{ij} = e^{2U} \gamma^{-1/2} \epsilon^{ijk} \eta_{,k} . \quad (6)$$

In view of (4) and (6) (see HARRISON in the special case for $f_{,\alpha} = 0$ [7])

$$-8\pi \tau^0_0 = [\Delta_1(\xi) + \Delta_1(\eta)] \quad (7)$$

and Maxwell's equations are explicitly

$$\Delta_2(\xi) - 2\Delta_1(U, \xi) = 0 , \quad (8a)$$

$$\Delta_2(\eta) - 2\Delta_1(U, \eta) = 0 , \quad (8b)$$

where the notations mean

$$\Delta_1(F) = \gamma^{\alpha\beta} F_{,\alpha} F_{,\beta} , \quad \Delta_1(F, G) = \gamma^{\alpha\beta} F_{,\alpha} G_{,\beta} , \quad \Delta_2(F) = \gamma^{\alpha\beta} F_{;\alpha\beta}.$$

Maxwell's equations (8a) and (8b) may also be written in a different way as

$$(g^{00} g^{ij} \sqrt{-g}\, \xi_{,j})_{,i} = (g^{00} g^{ij} \sqrt{-g}\, \eta_{,j})_{,i} = 0\,. \tag{9}$$

Now if we assume that the magnetic potential η is functionally related to the electric potential ξ, Maxwell's equations immediately give

$$\frac{d^2 \eta}{d \xi^2} = 0$$

which reduces to the linear relationship

$$\eta = (\alpha \xi + \beta) \tag{10}$$

α and β being constants (PERJÉS [8]). Again since for a static metric

$$R_0^0 = \frac{1}{2\sqrt{-g}} (g^{00} g^{ij} \sqrt{-g}\, g_{00,j})_{,i} \text{ and } \psi_{,0} = 0. \tag{11}$$

One can obtain from (5), (7) and (11)

$$(g^{00} g^{ij} \sqrt{-g}\, g_{00,j})_{,i} + \frac{1}{\psi} \sqrt{-g}\, g^{00} g^{ij} g_{00,j} \psi_{,i} = \frac{2}{\psi} \sqrt{-g}\, g^{00} g^{ij} (\xi_i \xi_j + \eta_i \eta_j)\,. \tag{12}$$

Substituting the relation (10) in (12) and assuming that g_{00} is a function of only ξ we immediately get a relation

$$(g^{00} g^{ij} \sqrt{-g}\, g'_{00} \xi_j \psi)_{,i} = 2 \sqrt{-g}\, g^{00} g^{ij} (\alpha^2 + 1)\, \xi_{,i}\, \xi_{,j}, \tag{13}$$

where the constant α is the same as that in(10) and the symbol $'$ stands for $d/d\xi$.

In view of Maxwell's equations (9) the Eq. (13) further reduces to

$$g^{ij} \xi_{,j} \left[g'_{00} \psi - 2(\alpha^2 + 1)\xi\right]_{,i} = 0\,. \tag{14}$$

Following now the arguments put forward in the paper of RAYCHAUDHURI and BANDYOPADHYAY we may remark that for a finite source distribution $\nabla \xi$ cannot be orthogonal to $\nabla [g'_{00}\psi - 2(\alpha^2 + 1)\xi)$, the only other alternative to satisfy the Eq. (14) is that

$$g'_{00} \psi - 2 (\alpha^2 + 1) \xi = \text{const.} \tag{15}$$

which leads to the conclusion that ψ must be a function of the electric potential ξ. Again from $\Box \psi = 0$ we get

$$(g^{ij} \sqrt{-g}\, \psi_{,j})_{,i} = 0 \tag{16}$$

and in view of the fact that $\psi = \psi(\xi)$ and $g^{00}g_{00} = 1$ one can obtain using Maxwell's equations, the following result

$$g^{ij}\,\xi_{,j}(g_{00}\,\psi')_{,i} = 0 \tag{17}$$

which in turn yields

$$g_{00}\,\psi' = \text{const.} \tag{18}$$

Combining (15) and (16) one can finally obtain the relation

$$g_{00}\,\psi = (\alpha^2 + 1)\,\xi^2 + b\xi + c \tag{19}$$

b and c also being constants.

The relation (19) is a generalisation of the result of RAYCHAUDHURI and BANDYOPADHYAY and can be derived for any static coupled Brans—Dicke—Maxwell fields starting, however, with the assumption that both g_{00} and the magnetic potential are functions of only the electric potential.

Acknowledgement

The author acknowledges the financial support from F.I.N.E.P. of Brasil.

REFERENCES

1. P. P. RAO and R. . TIWARI, Acta. Phys. Hung., **45**, 285, 1978.
2. A. K. RAYCHAUDHURI and N. BANDYOPADHYAY, Prog. Theor. Phys., **59**, 414, 1978.
3. H. WEYL, Ann. d. Physik, **54**, 117, 1917.
4. S. D. MAJUMDAR, Phys. Rev., **72**, 390, 1947.
5. A. PAPAPETROU, Proc. Roy. Irish. Acad., **A51**, 191, 1947.
6. C. BRANS and R. H. DICKE, Phys. Rev., **124**, 925, 1961.
7. B. K. HARRISON, J. Math. Phys., **9**, 1744, 1968.
8. Z. PERJÉS, Acta. Phys. Hung., **25**, 393, 1968.

RECENSIONES

Synchrotron Radiation. Techniques and Applications

Edited by C. Kunz, Springer Verlag, Berlin, Heidelberg, New York, 1979, pp. 442

A monograph such as this book was missing very much in the rapidly developing field of the applications of synchrotron radiation. The number of measurement programs applying this radiation in atomic, molecular and solid-state physics as well as in biology is constantly growing. In KUNZ's book a chapter is devoted to each topic except the last one.

The vivid interest of the different branches of science in synchrotron radiation is due to the outstanding properties of this radiation originating from the synchrotron, an accelerator of electrons (or positrons) originally developed for research in nuclear and particle physics. Such properties are e.g. the continuous spectrum from the infrared through the vacuum-ultraviolet and soft X-radiations to the higher energy X-rays, linear and circular polarization, etc.

About half of the book is devoted to a review of the above mentioned applications. In addition to the properties of synchrotron radiation and the description of synchrotrons, the book also deals with the techniques and equipment required by applied research. One chapter deals with the theoretical aspects.

The book is very useful both as an introduction to the field for beginners and as handbook with useful tabulations for researchers actively working in the field.

D. BERÉNYI

B. K. AGARWAL: X-Ray Spectroscopy. An Introduction

Springer Verlag, Berlin, Heidelberg, New York, 1979, pp. 418

The monograph published in the Springer Series in Optical Sciences is intended as an introduction to the field and it is based on a one-year course for postgraduate students. However, with the useful tabulations at the end, it can be used as a handbook for active workers in the field, as well. Among the tables one can find the electronegativity scale, the K and L absorption edges, the electron distribution among the levels of free atoms, etc.

The book is divided into eight Chapters. Two of them deal with the two main types of X-rays (continuous and characteristic), three with the different interactions of X-rays with matter, two others with the experimental techniques. One Chapter treats the important application of X-rays for the study of chemical bonding. Unfortunately, there is no information in the book on X-ray fluorescence analytical techniques so important in contemporary instrumental analysis and industrial process control.

X-ray physics is a very interesting field of research not only from the point of view of applications. Recent results of e.g. muonic X-rays or EXAFS are also treated in the book. A comprehensive introduction to this field such as AGARWAL's is very useful and necessary. The value of the monograph is increased by a subject and an author index.

D. BERÉNYI

J. D. LAWSON: The Physics of Charged-Particle Beams

Clarendon Press, Oxford, 1977-1978. pp. 462

"Charged-particle beams are widely used in scientific, industrial, and even domestic apparatus", — the author writes in the introduction of the book. In fact, the role of charged-particle beams in our modern life is more and more important from the point of view of various applications, e.g. TV, the electron microscope and and different types of accelerators.

This is why so many good monographs and handbooks have been written on the various fields of applications as well as on the technical details of the equipment used.

The approach of this book is quite different. Here the physical features of charged-particle beams common in the diverse fields of applications are treated. One can find here the most important principles and concepts in handling and using charged-particle beams as e.g. emittance, stability criteria, wall-interactions, etc. No instrumental details are included, the whole approach is rather theoretical.

The material of the book is grouped into five Chapters beside the introduction, viz. on beam optics, on laminar and separately on non-laminar beams, on beams with scattering or dissipation and finally on different instabilities in beams. Every Chapter and Sub-chapter is headed by a special introduction. The book contains six Appendices, mainly with theoretical deductions of formulas used in the text, supplemented by a detailed list of references, a subject index and a list of symbols.

D. BERÉNYI

Theory of Magnetically Confined Plasmas

Proceedings of the Course held in Varenna, Italy, 1—10 September 1977, organized by the International School of Plasma Physics; edited by B. Coppi, T. Stringer, R. Pozzoli and E. Sindoni, J. P. Carnihan and G. G. Leotta; published for the Commission of the European Communities by Pergamon Press, Oxford 1979, pp. 513

The Varenna International School of Plasma Physics started in 1971 by giving the "Course on Instabilities and Confinement in Toroidal Plasmas", whose Proceedings were published by EURATOM.

The Course 1977 was devoted to the "Theory of Magnetically Confined Plasmas" and the Proceedings can be considered in some respects as an up-to-date review of a number of areas of thermonuclear plasma physics, including some data pertinent to the JET research.

The book consists of the directly reproduced script of the lectures, given by invited speakers, and discussions that followed them. Unfortunately, however, it was not possible to include all the Varenna recordings, because "of the poor quality of some tapes".

Contents: MHD theory (2 papers); transport phenomena and codes (3 papers, 2 extended abstracts only); modes and instabilities (3 papers, 1 summary only); new concepts (3 papers); heating (3 papers); alpha particles (1 paper); radiation (1 paper); experimental (1 paper). List of participants. Subject Index.

The Directors of the Course and of the Workshops were Prof. BRUNO COPPI and Prof. TED STRINGER. The number of participants was nearly 100, from the United States, France, Belgium, Germany, the United Kingdom, the Netherlands, Sweden, Japan, Switzerland, Austria, Denmark, Australia, the Soviet Union and Italy.

JÁNOS SZABÓ

WALTER THIRRING: Classical Field Theory

(A Course in Mathematical Physics 2.)
Springer-Verlag, New York, Wien, 1978, pp. 250

All the theoreticians who had read the first volume (Classical Dynamical Systems) of the Viennese Professor's book have been looking forward to the continuation with deep interest and curiosity. Now we have the second volume modest in size, which includes Maxwell's electrodynamics and Einstein's theory of the gravitational field. We enjoy the miracle of THIRRING's style once again: exactness, simplicity and elegance. All the essential problems of classical field theory are treated, from the electromagnetic field of an arbitrary charge distribution to the gravitational collapse, from the diffraction of electromagnetic waves to the necessity of singularity in the General Relativity. This means that this modest-looking textbook really includes theoretical electrodynamics and general relativity; it proves the statements with full mathematical rigour. The message of the author has been clearly presented and proven: exactness does not necessarily mean lengthy and tedious treatment.

Most textbooks of physics are made thick by the handwaving argumentation and wishful mathematics.

G. MARX

Plasma Physics and Controlled Nuclear Fusion Research 1978

Vols. 1—3, Seventh Conference Proceedings

International Atomic Energy Agency, Vienna, 1979
pp. 828 + 670 + 552

The three Volumes contain the papers presented at the Seventh IAEA Conference on Plasma Physics and Controlled Nuclear Fusion Research held at Innsbruck, 23—30 August, 1978. As is known this Conference was attended by about 500 specialist from 32 countries and discussed about 150 papers. The IAEA rendered an invaluable service to the fusion-world by the edition and publication of the conference papers so quickly and on a high technical level. This also must be considered as a sign showing the importance the promises fusion research represents in meeting the world's future energy requirements, and manifest the strategy of prompting close international collaboration among plasma and fusion physicists of all countries in this field.

The first Volume contains the papers of the tokamak experiments and tokamak theory sessions. The starting point of the first experiments session was devoted to the first ARTSIMOVICH memorical lecture — given by E. E. KINTNER (USA) — to commemorate the outstanding role ARTSIMOVICH's scientific activity and personality played in this field. The experimental papers report on injection, heating, instabilities, radiation, impurities, losses etc in different tokamaks. The theoretical papers treat questions of the general problems of stability in magnetic confinement, study of the nature of instabilities, transport properties, fluctuation phenomena, turbulence and report on different approaches of computational modelling.

The second Volume offers the material of the high beta, non-axisymmetric systems, open systems and plasma heating sessions.

The third Volume contains the sessions on inertial confinement (laser, electron and heavy ion beam procedures), on fundamental processes and new trends (Spheromak, cold blanquet system, large scale plasma simulation, relativistic electron beam ring) and on technology and reactor concepts.

The third Volume concludes with summary talks, on magnetic confinement experiments by C. M. BRAAMS (Netherlands), on magnetic-confinement theory by D. D. RYUTOV (USSR), on inertial confinement fusion by N. NISHIKAWA (Japan) and on reactor systems by R. W. CONN (USA).

I. ABONYI

Printed in Hungary

A kiadásért felel az Akadémiai Kiadó igazgatója — Műszaki szerkesztő: Botyánszky Pál
A kézirat a kiadóba érkezett: 1980. VI. 10. A kézirat nyomdába érkezett: 1980. VI. 19. — Terjedelem: 11,75 (A/5) ív, 37 ábra

81.8465 Akadémiai Nyomda, Budapest — Felelős vezető: Bernát György

NOTES TO CONTRIBUTORS

I. PAPERS will be considered for publication in Acta Physica Hungarica, only if they have not previously been published or submitted for publication elsewhere. They may be written in English, French, German or Russian.

Papers should be submitted to

Prof. I. Kovács, Editor
Department of Atomic Physics, Technical University
1521 Budapest, Budafoki út 8, Hungary

Papers may be either articles with abstracts or short communications. Both should be as concise as possible, articles in general not exceeding 25 typed pages, short communications 8 typed pages.

II. MANUSCRIPTS

1. Papers should be submitted in three copies.

2. The text of papers must be of high stylistic standard, requiring minor corrections only.

3. Manuscripts should be typed in double spacing on good quality paper, with generous margins.

4. The name of the author(s) and of the institutes where the work was carried out should appear on the first page of the manuscript.

5. Particular care should be taken with mathematical expressions. The following should be clearly distinguished, e.g. by underlining in different colours: special founts (italics, script, bold type, Greek, Gothic, etc.); capital and small letters; subscripts and superscripts, e.g. x_2, x^3; small l and 1; zero and capital O; in expressions written by hand: e and l, n and u, v and v, etc.

6. References should be numbered serially and listed at the end of the paper in the following form: J. Ise and W. D. Fretter, Phys. Rev., *76*, 933, 1949.

For books, please give the initials and family name of the author(s), title, name of publisher, place and year of publication, e.g.: J. C. Slater, Quantum Theory of Atomic Structures, I. McGraw-Hill Book Company, Inc., New York, 1960.

References should be given in the text in the following forms: Heisenberg [5] or [5].

7. Captions to illustrations should be listed on a separate sheet, not inserted in the text.

8. As per 1st January 1980 the use of SI units has been made compulsory for all publications issued in Hungary. Please note that in papers submitted to Acta Physica after that date all measures should be expressed in SI units.

III. ILLUSTRATIONS AND TABLES

1. Each paper should be accompanied by three sets of illustrations, one of which must be ready for the blockmaker. The other sets attached to the copies of the manuscript may be rough drawings in pencil or photocopies.

2. Illustrations must not be inserted in the text.

3. All illustrations should be identified in blue pencil by the author's name, abbreviated title of the paper and figure number.

4. Tables should be typed on separate pages and have captions describing their content. Clear wording of column heads is advisable. Tables should be numbered in Roman numerals (I, II, III, etc.).

IV. RETURN OF MATERIAL

Owing to high postage costs, the Editorial Office cannot undertake to return *all* material not accepted for any reason for publication. Of papers to be revised (for not being in conformity with the above Notes or other reasons) only *one* copy will be returned. Material rejected for lack of space or on account of the Referees' opinion will not be returned to authors outside Europe.

Reviews of the Hungarian Academy of Sciences are obtainable at the following addresses:

AUSTRALIA
C.B.D. LIBRARY AND SUBSCRIPTION SERVICE, Box 4886, G.P.O., *Sydney N.S.W. 2001*
COSMOS BOOKSHOP, 145 Acland Street, *St. Kilda (Melbourne), Victoria 3182*

AUSTRIA
GLOBUS, Höchstädtplatz 3, *1200 Wien XX*

BELGIUM
OFFICE INTERNATIONAL DE LIBRAIRIE, 30 Avenue Marnix, *1050 Bruxelles*
LIBRAIRIE DU MONDE ENTIER, 162 Rue du Midi, *1000 Bruxelles*

BULGARIA
HEMUS, Bulvar Ruszki 6, *Sofia*

CANADA
PANNONIA BOOKS, P.O. Box 1017, Postal Station "B", *Toronto, Ontario M5T 2T8*

CHINA
CNPICOR, Periodical Department, P.O. Box 50, *Peking*

CZECHOSLOVAKIA
MAD'ARSKÁ KULTURA, Národní třida 22, *115 66 Praha*
PNS DOVOZ TISKU, Vinohradská 46, *Praha 2*
PNS DOVOZ TLAČE, *Bratislava 2*

DENMARK
EJNAR MUNKSGAARD, Norregade 6, *1165 Copenhagen*

FINLAND
AKATEEMINEN KIRJAKAUPPA, P.O. Box 128, *SF-00101 Helsinki 10*

FRANCE
EUROPERIODIQUES S. A., 31 Avenue de Versailles, *78170 La Celle St.-Cloud*
LIBRAIRIE LAVOISIER, 11 rue Lavoisier, *75008 Paris*
OFFICE INTERNATIONAL DE DOCUMENTATION ET LIBRAIRIE, 48 rue Gay-Lussac, *75240 Paris Cedex 05*

GERMAN DEMOCRATIC REPUBLIC
HAUS DER UNGARISCHEN KULTUR, Karl-Liebknecht-Strasse 9, *DDR-102 Berlin*
DEUTSCHE POST ZEITUNGSVERTRIEBSAMT, Strasse der Pariser Kommüne 3—4, *DDR-104 Berlin*

GERMAN FEDERAL REPUBLIC
KUNST UND WISSEN ERICH BIEBER, Postfach *46, 7000 Stuttgart 1*

GREAT BRITAIN
BLACKWELL'S PERIODICALS DIVISION, Hythe Bridge Street, *Oxford OX1 2ET*
BUMPUS, HALDANE AND MAXWELL LTD., Cowper Works, *Olney*, Bucks *MK46 4BN*
COLLET'S HOLDINGS LTD., Denington Estate, *Wellingborough*, Northants *NN8 2QT*
W.M. DAWSON AND SONS LTD., Cannon House *Folkestone, Kent CT19 5EE*
H. K. LEWIS AND CO., 136 Gower Street, *London WC1E 6BS*

GREECE
KOSTARAKIS BROTHERS, International Booksellers, 2 Hippokratous Street, *Athens-143*

HOLLAND
MEULENHOFF-BRUNA B.V., Beulingstraat 2, *Amsterdam*
MARTINUS NIJHOFF B.V., Lange Voorhout 9—11, *Den Haag*
SWETS SUBSCRIPTION SERVICE, 347b Heereweg, *Lisse*

INDIA
ALLIED PUBLISHING PRIVATE LTD., 13/14 Asaf Ali Road, *New Delhi 110001*
150 B-6 Mount Road, *Madras 600002*
INTERNATIONAL BOOK HOUSE PVT. LTD., Madame Cama Road, *Bombay 400039*
THE STATE TRADING CORPORATION OF INDIA LTS, Books Import Division, Chandralok, 36 Janpath, *New Delhi 110001*

ITALY
EUGENIO CARLUCCI, P.O. Box 252, *70100 Bari*
INTERSCIENTIA, Via Mazzé 28, *10149 Torino*
LIBRERIA COMMISSIONARIA SANSONI, Via Lamarmora 45, *50121 Firenze*
SANTO VANASIA, Via M. Macchi 58, *20124 Milano*
D. E. A., Via Lima 28, *00198 Roma*

JAPAN
KINOKUNIYA BOOK-STORE CO. LTD., 17-7 Shinjuku-ku 3 chome, Shinjuku-ku, *Tokyo 160-91*
MARUZEN COMPANY LTD., Book Department, P.O. Box 5050 Tokyo International, *Tokyo 100-31*
NAUKA LTD. IMPORT DEPARTMENT, 2-30-19 Minami Ikebukuro, Toshima-ku, *Tokyo 171*

KOREA
CHULPANMUL, *Phenjan*

NORWAY
TANUM-CAMMERMEYER, Karl Johansgatan 41—43, *1000 Oslo*

POLAND
WĘGIERSKI INSTYTUT KULTURY, Marszałkowska 80, *Warszawa*
CKP I W ul. Towarowa 28 *00-958 Warsaw*

ROUMANIA
D. E. P., *Bucureşti*
ROMLIBRI, Str. Biserica Amzei 7, *Bucureşti*

SOVIET UNION
SOJUZPETCHATJ — IMPORT, *Moscow*
and the post offices in each town
MEZHDUNARODNAYA KNIGA, *Moscow G-200*

SPAIN
DIAZ DE SANTOS, Lagasca 95, *Madrid 6*

SWEDEN
ALMQVIST AND WIKSELL, Gamla Brogatan 26, *101 20 Stockholm*
GUMPERTS UNIVERSITETSBOKHANDEL AB, Box 346, *401 25 Göteborg 1*

SWITZERLAND
KARGER LIBRI AG, Petersgraben 31, *4011 Basel*

USA
EBSCO SUBSCRIPTION SERVICES, P.O. Box 1943, *Birmingham, Alabama 35201*
F. W. FAXON COMPANY, INC., 15 Southwest Park, *Westwood, Mass. 02090*
THE MOORE-COTTRELL SUBSCRIPTION AGENCIES, *North Cohocton, N. Y. 14868*
READ-MORE PUBLICATIONS, INC., 140 Cedar Street, *New York, N. Y. 10006*
STECHERT-MACMILLAN, INC., 7250 Westfield Avenue, *Pennsauken* N. J. 08110

VIETNAM
YXUNHASABA, 32, Hai Ba Trung, *Hanoi*

YUGOSLAVIA
JUGOSLAVENSKA KNJIGA, Terazije 27, *Beograd*
FORUM, Vojvode Mišiča 1, *21000 Novi Sad*

Index: 26.022
Acta Phys. Hung. Tom. 48. No. 4. Budapest, 30. I. 1981 HU-ISSN 0001-6705